

# **BULETINUL INSTITUTULUI POLITEHNIC DIN IAȘI**

**Publicat de  
UNIVERSITATEA TEHNICĂ "GH.ASACHI", IAȘI**

**Tomul LI (LV)**

**Fasc. 3**

**Secția**

**ȘTIINȚA ȘI INGINERIA  
MATERIALELOR**

**2005**

**President of the Editorial Board of Bulletin of the Polytechnic Institute**

**Prof. univ. dr. eng Nicolae Badea, Technical University “Gh. Asachi” Iași, Romania**  
Rector of Technical University “Gh. Asachi” of Iasi

**Editor-in-Chief of Bulletin of the Polytechnic Institute**

**Prof. univ. dr. eng Ion Giurma, Technical University “Gh. Asachi” Iași, Romania**  
Vice-Rector of Technical University “Gh. Asachi” of Iasi

**Managing Editor of Bulletin of the Polytechnic Institute**

**Prof. univ. dr. eng. Dan Gălușcă, Technical University “Gh. Asachi” Iași, Romania**  
Dean of the Faculty of Materials Science and Engineering

**Managing Editor of the *MATERIALS SCIENCE AND ENGINEERING***

**Assoc. prof. dr. eng. Iulian Ioniță, Technical University “Gh. Asachi” Iași, Romania**  
Scientific secretary of the Faculty of Materials Science and Engineering

**Editorial Board of the Section *MATERIALS SCIENCE AND ENGINEERING***

**Prof.univ.dr.eng. Yuri A. Burennikov, Vinnitsia State Technical University, Ukraine**

**Prof.univ.dr.eng. Borivoje Miškovič, Yugoslav Association of Metallurgical Engineers,  
Belgrad, Serbia-Montenegro**

**Prof.univ.dr.eng. Paolo Nanni, Universita degli Studi da Genova, Italy**

**Prof.univ.dr.eng. Strul Moisa, Ben-Gurion University of the Negev, Beer-Sheva, Israel**

**Prof.univ.dr.eng. Corneliu Munteanu, Technical University “Gh. Asachi” Iași,  
Romania**

**Prof.univ.dr.eng. Vasile Cojocaru-Filipiuc, Technical University “Gh. Asachi” Iași,  
Romania**

**Prof.univ.dr.eng. Constantin Baciu, Technical University “Gh. Asachi” Iași, Romania**

**Prof.univ.dr.eng. Luchian Zaharia, Technical University “Gh. Asachi” Iași, Romania**

**Prof.univ.dr.eng. Ioan Carcea, Technical University “Gh. Asachi” Iași, Romania**

**Prof.univ.dr.eng. Adrian Dima, Technical University “Gh. Asachi” Iași, Romania**

**Prof.univ.dr.eng. Ioan Alexandru, Technical University “Gh. Asachi” Iași, Romania**

**Assoc.prof.dr.eng. Leandru Gheorghe Bujoreanu, Technical University “Gh. Asachi”  
Iași, Romania**

**Assoc. prof.dr. eng. Ioan Rusu, Technical University “Gh. Asachi” Iași, Romania**

**Assoc. prof.dr. eng. Gheorghe Bădărău, Technical University “Gh. Asachi” Iași,  
Romania**

**Assoc. prof.dr. eng. Petrică Vizureanu, Technical University “Gh. Asachi” Iași,  
Romania**

**Editorial Secretary of the *MATERIALS SCIENCE AND ENGINEERING***

**Assoc.prof.dr.eng. Gheorghe Bădărău, Technical University “Gh. Asachi” Iași,  
Romania**

MATERIALS SCIENCE AND ENGINEERING

<b>CONTENTS</b>	
<b>ALEXANDRU I., ALEXANDRU A., BULANCEA V., GHEORGHIAN M.</b> – THE CHARACTERIZATION OF 6308 C3 RADIAL BEARINGS THERMALLY TREATED UNDER 0°C	1
<b>BÂCLEA A., DOBROVICI S., POTECAȘU O., POTECAȘU F., DRUGESCU E., CAZACU N.</b> – ASPECTS CONCERNING FLUIDIZED BED NITRIDING FOR ALLOYING STEEL WITH ALUMINIUM	7
<b>BIBIRE V., SUSAN M.</b> – THE POSSIBILITY OF STAMPING WITHOUT RIDGES THE MARKS OF “TOOTHED WHEEL” TYPE	13
<b>BUZAIANU A., CORBAN M., IONCEA A., CIUPITU I., TRUSCA R., NITA P., MANOLIU V.</b> – HIGH QUALITY PRODUCTS USED IN THE AIRSPACE INDUSTRY	19
<b>CĂLĂRAȘU D.</b> – CONTRIBUTIONS CONCERNING WAYS OF OBTAINING FERROFLUIDS	25
<b>CĂLĂRAȘU D.</b> – EXPERIMENTAL RESEARCHES ON THE MAGNETIC PROPERTIES SPECIFIC TO THE Fe <sub>3</sub> O <sub>4</sub> PARTICLES	29
<b>CANTEMIR D., BERTINI L., BEGHINI M., PAGLIARO M., CIOBANU O.</b> – TENSILE BEHAVIOUR OF A P355NL1 WELDED JOINT	33
<b>CAZACU N., DOBROVICI S., POTECAȘU O., DRUGESCU E., BÂCLEA A., SAVA L.</b> – SURFACE HARDENING OVER 38MoCrAl09 STEEL BY YAG:Nd PULSE LASER	41
<b>CIOBANU D., ȘOLTUZ D.V., NECULĂIASA V., HOPULELE I.</b> – RESEARCHES REGARDING THE WORK-HARDENING OF MACHINERY PARTS HARD EXPOSED TO WEAR OF EQUIPMENTS AND INSTALLATIONS FROM AGRICULTURE AND FOOD INDUSTRY THROUGH HARD ALLOY DEPOSITION	47
<b>CIOCAN A., BRATU F., NEGOIȚĂ D.</b> – STEEL GRIT, MATERIAL ACTIVE FOR CLEANING SURFACES	53
<b>CIOCÎLTEU ȘT.M., MIZUKAMI F., ONU P.</b> – A COMPARISON BETWEEN THE PROPERTIES OF SOME METAL LOADED SILICALITE-1 ZEOLITES	59
<b>CIUCĂ S., RUSET C., TÂRCOLEA M., GHERGHESCU I., GHEORGHIU-DOBRE A., SUCIU M.</b> – CATHODIC SPUTTERING – ESSENTIAL FACTOR IN PHASIC CONSTITUTION OF COMPOUND LAYER FORMED BY PLASMA NITRIDING	65
<b>CONSTANTINESCU S., MITOȘERIU O., RADU T., POPESCU M.</b> – CORRELATION BETWEEN MICROSTRUCTURE AND PROPERTIES OF SINTERED HARD ALLOYS	71

<b>CORĂBIERU P., CORĂBIERU A., ALEXANDRU I., VRABIE I. – THE INFLUENCE OF JOINING TEMPERATURE ON THE BIMETAL LAYER STRUCTURE AND CHARACTERISTICS</b>	77
<b>CORĂBIERU P., CORĂBIERU A., ALEXANDRU I., VRABIE I. – THE MANUFACTURING TECHNOLOGY FOR PRESS TOOLS THROUGH SUCCESSIVE ALLOYING AND ZONAL HEATING PROCESS BY CONTACT (ASPTZC)</b>	83
<b>BĂCLEA A., CAZACU N., DOBROVICI S., POTECAȘU F., DRUGESCU E., POTECAȘU O. – BEHAVIOR OF Rp3-HIGH SPEED STEEL ON SHORT TIME NITRIDING IN FLUIDIZED BED</b>	91
<b>CATARSCHI V., POROCH M., DANILA R., POROF I., CATARSCHI S. – EXPERIMENTAL RESEARCH ON THE APPLICATION OF THE NONCRACKING CONDITION WHEN HEATING MASSIVE STEEL HALF-FINISHED</b>	97
<b>COMANICI A. – NONCONDUCTIVE COATING THICKNESS MEASUREMENT USING EDDY CURRENT METHOD</b>	103
<b>COȘER N., CIOBANU D., ALEXANDRU I., HOPULELE I. – RESEARCHES REGARDING THE IMPROVEMENT OF ACTIVE SURFACE QUALITY OF COPPER ELECTRICAL CONTACTORS</b>	109
<b>COSER N., CIOBANU D., MIHAILOV V., ALEXANDRU I., ALEXANDRU A. – RESEARCHES REGARDING THE MASS TRANSFER AT SUPERFICIAL COATING AND ALLOYING WITH NOBLE METALS ON THE COPPER SUPPORT</b>	113
<b>DOBROVICI S., CAZACU N., POTECAȘU O., POTECAȘU F., BĂCLEA A., DRUGESCU E. – STEEL NITROCARBURIZING IN FLUIDIZED BED</b>	117
<b>DRUGESCU E., DOBROVICI S., POTECAȘU F, POTECAȘU O., CAZACU N., BĂCLEA A. – TEMPERATURE INFLUENCE OVER FLUIDIZED BED GASDYNAMICS FOR HEAT TREATMENTS</b>	123
<b>DULUCHEANU C., BĂNCESCU N., LUCA R. – ON THE BEHAVIOUR OF A DUAL-PHASE STEEL WITH 0,09% C AND 1,90% Mn IN THE CONDITIONS OF HERTZIAN CONTACT</b>	129
<b>GRIMBERG R., SAVIN A., STEIGMANN R., ANDREESCU A., BRUMA A. – ELECTROMAGNETIC EVALUATION OF NANOSTRUCTURED MATERIALS AND SOME MEMS DEVICES</b>	135
<b>IACOB E., RUSU I., DRUG O., MINEA L. – ASSESSMENT OF THE BIOCOMPATIBILITY OF DIFFERENT ALLOYS IN VITRO CELL CULTURE</b>	141
<b>ISTRATE L., CIOBANU D., ALEXANDRU I., CIOBANU B., ALEXANDRU A. – ASPECTS REGARDING THE SPECIFIC WEAR FORMS AT INDUSTRIAL TAPS</b>	143
<b>ITICESCU C., CĂRĂC G., MITOSERIU O. – INFLUENCE OF CeO<sub>2</sub> ON THE ELECTROLESS DEPOSITION OF THE COPPER COATINGS</b>	149
<b>GHENGHEA L.D., CIOBANU G., BOGDAN B. – TIG WELDING POOL CIRCUMSTANCES</b>	155
<b>LEIȚOIU B., ANTOHE M., MAREȘ M. – A IOSIPESCU THIN SPECIMEN SETTING VARIANT FOR SHEAR STUDY</b>	161
<b>MAREȘ M., LEIȚOIU B. – THE APPLICATION OF IOSIPESCU SHEAR TEST FOR ACCURATE DETERMINATION OF IN-PLANE SHEAR MODULUS, FOR METAL MATRIX COMPOSITES</b>	165

<b>MARKOS Z.</b> – RESEARCHES ABOUT THE STEEL SILICONIZING IN GAS MEDIUM AT LOW PRESSURE	173
<b>MARKOS Z.</b> – STUDY CONCERNING THE PROPERTYS OF DIFFUSION LAYERS AT BRONZE SILICONIZING	177
<b>BUZATU M., GHICA V.G., PÂRVAN I., DUMITRESCU D., IVĂNESCU S.</b> – DETERMINATIONS OF MECHANICAL TESTING AND CORROSION TESTS OF THE TITANIUM ALLOYS TI GRADE 2 AND TI GRADE 12	181
<b>MOCANU F., BARSANESCU P.D.</b> – SOME ASPECTS CONCERNING THE DURABILITY OF ADHESIVE JOINTS	187
<b>MOCANU F.</b> – THERMAL CHARACTERISTICS OF SINGLE LAP JOINTS UNDER STATIC LOADS	193
<b>MOCANU F.</b> – FRACTURE BEHAVIOUR IN EPOXY ADHESIVE JOINT WITH VARIOUS BOND THICKNESSES	199
<b>RUSU I., IACOB E.</b> – VORTEX GAS DRYING	203
<b>RUSU I.</b> – THE VORTEX EFFECT OF ENERGETICAL SEPARATION USED FOR THE DUST-GAS MIXTURES SEPARATION	207
<b>MOLDOVEANU V.V., BEJINARIU C., DRAGOI L., FLORESCU A.</b> – RESEARCH REGARDING THE BEHAVIOUR OF HYSTERETIC STEEL BARS ENERGY DISSIPATORS	211
<b>NEJNERU C., BERNEVIG M.A., HOPULELE I., CARABET R.</b> – RESEARCHES CONCERNING THE COOLING CHARACTERISTICS OF THE POWDER BACKING IN FLUIDIZED BED TIP SAND AND SALT MIXTURE BARBOTAGED WITH AIR	215
<b>NEJNERU C., GĂLUȘCĂ D.G., MIRON V., HOPULELE I.</b> – RESEARCHES CONCERNING THE COOLING CAPACITY OF THE HARDENING SYNTHETICALLY MEDIUMS: POLIALCHILENGLICOL (P.A.G. 15%)	223
<b>MOTOIU P., ROSSO M.</b> – EXPERIMENTAL RESEARCHES OF TITANIUM THERMICAL LAYERS OBTAINED BY PLASMA SPRAYING	229
<b>PREDESCU C., MATEI E., SOHACIU M.G., NICOLAE A.</b> – LABORATORY TECHNIQUE FOR ADVANCED REDUCING OF SOME POLLUTANTS FROM IRON AND STEEL WASTEWATERS	235
<b>SOLTANI R., SAMADI H., COYLE T.W.</b> – DEVELOPMENT OF ALTERNATIVE THERMAL BARRIER COATINGS FOR DIESEL ENGINES	243
<b>ROMAN M., BADILITA V., FIRESCU L., STOICIU F., MĂRGINEAN I., BRATU C.</b> – PRELIMINARY RESEARCHS ON METALURGICAL VALUE OF WASTES OF SECONDARY ALUMINIUM INDUSTRY	251
<b>FLOREA R.</b> – MICROSTRUCTURAL ASPECTS CONCERNING THE THERMOMECHANICAL TREATMENT APPLIED OF CHROMIUM HIGH ALLOYED STEELS	257
<b>TUDOR B., VASILIU A.</b> – RESEARCH AND STUDY REGARDING THE VARIATION OF SURFACE TENSION OF MOLTEN METALS AND ALLOYS WITH TEMPERATURE	261
<b>SUSAN M., ILIESCU V., DUMITRAS P., MANTU M., GLIGOR-PITICARI O.</b> – ON FORCE PARAMETERS AT EMPTY DRAWING OF THE TUBES WITH ULTRASONIC VIBRATIONS TRANSMITTED TO THE DIE ON THE DRAWING DIRECTION	267
<b>ILIESCU V., SUSAN M., MANTU M., MIRON V.</b> – ON CONTACT FRICTION AT DRAWING OF WIRES OF CYLINDRICAL SYMMETRY WITH ULTRASONICALLY VIBRATED DRAW PLATE	277

<b>TEODORESCU, R.</b> – THE TECHNOLOGY FOR HEAVY METALS FROM ELECTROPLATING SLUDGE VALORIFICATION, FOR ENVIRONMENT DEPOLLUTION	283
<b>SCOROBETIU L., CÂNDEA V.</b> – CUTTING OF GLASS PLATES THROUGH THERMO SHOCK	291
<b>COJOCARU M., TARCAN C., GOSTIN F.</b> – EXPERIMENTATIONS REGARDING THE KINETICS OF HIGH TEMPERATURE OXIDATION OF THE ALUMINUM NITRIDE	293

**ȘTIINȚA ȘI INGINERIA MATERIALELOR**

<b>CUPRINS</b>	
<b>ALEXANDRU I., ALEXANDRU A., BULANCEA V., GHEORGHIAN M.</b> – CARACTERIZAREA ELEMENTELOR DE RULMENȚI 6308C3 TRATATE SUB 0°C	1
<b>BÂCLEA A., DOBROVICI S., POTECAȘU O., POTECAȘU F., DRUGESCU E., CAZACU N.</b> – ASPECTE PRIVIND NITRURAREA ÎN PAT FLUIDIZAT A OȚELURILOR ALIATE CU ALUMINIU	7
<b>BIBIRE V., SUSAN M.</b> – POSIBILITATEA MATRIȚĂRIIFĂRĂ BAVURI A PIESELOR TIP “ROATĂ DINȚATĂ”	13
<b>BUZAIANU A., CORBAN M., IONCEA A., CIUPITU I., TRUSCA R., NITA P., MANOLIU V.</b> – PRODUSE DE ÎNALTĂ CALITATE UTILIZATE ÎN INDUSTRIA AEROSPAȚIALĂ	19
<b>CĂLĂRAȘU D.</b> – CONTRBUTII PRIVIND POSIBILITATI DE OBTINERE A FEROFUIDELOR	25
<b>CĂLĂRAȘU D.</b> – DETERMINAREA EXPERIMENTALĂ A UNOR MĂRIMI MAGNETICE CARACTERISTICE SISTEMELOR DE PARTICULE DIN $Fe_3O_4$	29
<b>CANTEMIR D., BERTINI L., BEGHINI M., PAGLIARO M.,CIOBANU O.</b> – COMPORTAMENTUL LA TRACȚIUNE AL UNEI IMBINARI SUDATE DIN OTEL P355NL1	33
<b>CAZACU N., DOBROVICI S., POTECAȘU O., DRUGESCU E., BÂCLEA A., SAVA L.</b> – DURIFICAREA SUPERFICIALĂ A OȚELULUI 38MoCrAl09 FOLOSIND LASERUL ÎN IMPULSURI YAG:Nd	41
<b>CIOBANU D., ȘOLTUZ D.V., NECULĂIASA V., HOPULELE I.</b> – CERCETARI PRIVIND DURIFICAREA ORGANELOR DE MARE SOLICITARE LA UZARE ALE MAȘINILOR ȘI INSTALAȚIILOR AGRICOLE ȘI DIN INDUSTRIA ALIMENTARĂ, PRIN DEPUNERI DE ALIAJE DURE	47
<b>CIOCAN A., BRATU F., NEGOIȚĂ D.</b> – GRITUL DE OTEL, MATERIAL ACTIV PENTRU CURATAREA SUPRAFETELOR	53
<b>CIOCÎLTEU ȘT.M., MIZUKAMI F., ONU P.</b> – COMPARAREA PROPRIETĂȚILOR UNOR PROBE DE SILICALIT 1 CONȚINÂND METALE	59
<b>CIUCĂ S., RUSET C., TÂRCOLEA M., GHERGHESCU I., GHEORGHIU-DOBRE A., SUCIU M.</b> – PULVERIZAREA CATODICĂ–FACTOR ESENȚIAL AL CONSTITUȚIEI FAZICE A STRATULUI ALIAT OBȚINUT PRIN NITRURARE ÎN PLASMĂ	65
<b>CONSTANTINESCU S., MITOȘERIU O., RADU T., POPESCU M.</b> – CORELAȚIA DINTRE MICROSTRUCTURA ȘI PROPRIETAȚILE ALIAJELOR DURE SINTERIZATE	71

<b>CORĂBIERU P., CORĂBIERU A., ALEXANDRU I., VRABIE I.</b> – INFLUENȚATEMPERATURII DE ÎMBINARE ASUPRA STRUCTURII STRATULUI DE BIMETAL ȘI CARACTERISTICILOR ACESTUIA	77
<b>CORĂBIERU P., CORĂBIERU A., ALEXANDRU I., VRABIE I.</b> – TEHNOLOGIA DE FABRICARE ASCULELOR DE PRESARE PRIN ALIERE SUCCESIVĂ ȘI ÎNCĂLZIRE ZONALĂ PRIN CONTACT (ASPTZC)	83
<b>BĂCLEA A., CAZACU N., DOBROVICI S., POTECAȘU F., DRUGESCU E., POTECAȘU O.</b> – COMPORTAREA OȚELULUI Rp3 LA NITRURAREA CU DURATE MICI ÎN STRAT FLUIDIZAT	91
<b>CATARSCHI V., POROCH M., DANILA R., POROF I., CATARSCHI S.</b> – CERCETĂRI EXPERIMENTALE PENTRU APLICAREA CONDIȚIEI DE NEFISURARE LA ÎNCĂLZIRE A SEMIFABRICATELOR MASIVE DIN OȚEL	97
<b>COMANICI A.</b> – MASURAREA GROSIMII STRATURILOR IZOLATOARE PRIN METODA EDDY CURRENT	103
<b>COȘER N., CIOBANU D., ALEXANDRU I., HOPULELE I.</b> – CERCETARI PRIVIND ÎMBUNATĂȚIREA CALITĂȚII SUPRAFETEI ACTIVE A CONTACTORILOR ELECTRICI DIN CUPRU	109
<b>COSER N., CIOBANU D., MIHAILOV V., ALEXANDRU I., ALEXANDRU A.</b> – CERCETARI PRIVIND TRANSFERUL DE MASA LA DEPUNEREA ȘI ALIEREA SUPERFICIALA CU METALE NOBILE PE SUPORT DE CUPRU	113
<b>DOBROVICI S., CAZACU N., POTECAȘU O., POTECAȘU F., BĂCLEA A., DRUGESCU E.</b> – NITROCARBURAREA ÎN STRAT FLUIDIZAT	117
<b>DRUGESCU E., DOBROVICI S., POTECAȘU F, POTECAȘU O., CAZACU N., BĂCLEA A.</b> – INFLUENȚA TEMPERATURII ASUPRA GAZODINAMICII PATULUI FLUIDIZAT DESTINAT TRATAMENTULUI TERMIC	123
<b>DULUCHEANU C., BĂNCESCU N., LUCA R.</b> – CERCETĂRI PRIVIND COMPORTAREA UNUI OȚEL BIFAZIC FERITO-MARTENSITIC CU 0,09% C ȘI 1,90% Mn LA CONTACT HERTZIAN	129
<b>GRIMBERG R., SAVIN A., STEIGMANN R., ANDREESCU A., BRUMA A.</b> – EVALUAREA ELECTROMAGNETICA A MATERIALELOR NANOSTRUCTURATE SI A UNOR REPERE MEMS	135
<b>IACOB E., RUSU I., DRUG O., MINEA L.</b> – EVALUAREA BIOCUMPATIBILITĂȚII UNOR ALIAJE ÎN CULTURI CELULARE IN VITRO	141
<b>ISTRATE L., CIOBANU D., ALEXANDRU I., CIOBANU B., ALEXANDRU A.</b> – ASPECTE PRIVIND FORMELE DE UZURA SPECIFICE ROBINETILOR INDUSTRIALI	143
<b>ITICESCU C., CĂRĂC G., MITOSERIU O.</b> – INFLUENȚA PARTICULELOR DE OXID DE CERIU IN DEPUNERILE DE CUPRU OBTINUTE PRIN METODA CHIMICĂ	149
<b>GHENGHEA L.D., CIOBANU G., BOGDAN B.</b> – CARACTERISTICI ALE BĂII DE SUDARE ÎN CAZUL METODEI TIG	155
<b>LEIȚOIU B., ANTOHE M., MAREȘ M.</b> – VARIANTA DE PRINDERE A EPRUVETELOR SUBTIRI TIP IOSIPESCU PENTRU STUDIUL FORFECARII	161
<b>MAREȘ M., LEIȚOIU B.</b> – CĂTEVA ASPECTE ALE APLICĂRII TESTULUI DE FORFECARE IOSIPESCU ÎN CAZUL UNOR MATERIALE COMPOZITE CU MATRICE METALICĂ	165
<b>MARKOS Z.</b> – CERCETĂRI CU PRIVIRE LA SILICIZAREA OȚELURILOR ÎN MEDIU GAZOS LA PRESIUNI JOASE	173

<b>MARKOS Z.</b> – STUDIUL PROPRIETĂȚILOR STRATURILOR DE DIFUZIE LA BRONZURILE SILICIZATE	177
<b>BUZATU M., GHICA V.G., PÂRVAN I., DUMITRESCU D., IVĂNESCU S.</b> – CARACTERISTICI DETERMINATE PRIN TESTE MECANICE ȘI DE COROZIUNE ALE ALIAJELOR DE TITAN TI GRADE 2 ȘI TITAN GRADE 12	181
<b>MOCANU F., BARSANESCU P.D.</b> – UNELE ASPECTE PRIVIND DURABILITATEA ÎMBINĂRILOR ADEZIVE	187
<b>MOCANU F.</b> – CARACTERISTICI TERMICE ALE ÎMBINĂRILOR ADEZIVE REALIZATE PRIN SIMPLĂ SUPRAPUNERE ÎN CONDIȚII DE SOLICITARE STATICĂ	193
<b>MOCANU F.</b> – COMPORTAREA ÎMBINĂRILOR REALIZATE CU ADEZIVI EPOXIDICI ÎN FUNCȚIE DE GROSIMEA LIPITURII	199
<b>RUSU I., IACOB E.</b> – USCAREA GAZELOR PRIN METODA VORTEX	203
<b>RUSU I.</b> – UTILIZAREA EFECTULUI TURBIONAR DE SEPARARE ENERGETICĂ LA SEPARAREA AMESTECURILOR PRAF-GAZ	207
<b>MOLDOVEANU V.V., BEJINARIU C., DRAGOI L., FLORESCU A.</b> – CERCETĂRI PRIVIND COMPORTAREA DISIPATORILOR HISTERETICI DIN BARE DE OȚEL	211
<b>NEJNERU C., BERNEVIG M.A., HOPULELE I., CARABET R.</b> – CERCETĂRI PRIVIND CARACTERISTICILE DE RĂCIRE ÎN PAT FLUIDIZAT A MEDIILOR PULVERULENTE TIP NISIP BARBOTAT CU AER	215
<b>NEJNERU C., GĂLUȘCĂ D.G., MIRON V., HOPULELE I.</b> – CERCETĂRI PRIVIND CAPACITATEA DE RĂCIRE A MEDIILOR SINTETICE DE CĂLIRE TIP POLIALCHILENGLICOL (P.A.G. 15%)	223
<b>MOȚOIU P., ROSSO M.</b> – CERCETĂRI EXPERIMENTALE DE OBTINERE TERMICĂ A STRATURILOR DE TITAN ÎN JET DE PLASMĂ	229
<b>PREDESCU C., MATEI E., SOHACIU M.G., NICOLAE A.</b> – TEHNICA DE LABORATOR PRIVIND REDUCEREA AVANSATĂ A UNOR POLUANȚI PREZENȚI ÎN APELE UZATE REZULTATE DIN SECTORUL SIDERURGIC	235
<b>SOLTANI R., SAMADI H., COYLE T.W.</b> – REALIZAREA UNEI BARIERE TERMICE ALTERNATIVE PENTRU MOTOARELE DIESEL	243
<b>ROMAN M., BADILITA V., FIRESCU L., STOICIU F., MĂRGINEAN I., BRATU C.</b> – CERCETĂRI PRELIMINARE ASUPRA VALORII METALURGICE A DEȘEURILOR DIN INDUSTRIA ALUMINIULUI SECUNDAR	251
<b>FLOREA R.</b> – ASPECTE MICROSTRUCTURALE PRIVIND APLICAREA TRATAMENTULUI TERMOMECHANIC OTELURILOR ÎNALT ALIATE CU CROM	257
<b>TUDOR B., VASILIU A.</b> – STUDII ȘI CERCETĂRI PRIVIND VARIATIA TENSIUNII SUPERFICIALE A METALELOR ȘI ALIAJELOR TOPITE, CU TEMPERATURA	261
<b>SUSAN M., ILIESCU V., DUMITRAS P., MANTU M., GLIGOR-PITICARI O.</b> – CONSIDERAȚII PRIVIND TRAGEREA TUBURILOR ÎN PREZENȚA VIBRAȚIILOR ULTRASONICE TRANSMISE DORNULUI PE DIRECȚIA TRAGERII	267
<b>ILIESCU V., SUSAN M., MANTU M., MIRON V.</b> – CONSIDERAȚII PRIVIND FRECAREA DE CONTACT LA TRAGEREA ÎN CÂMP ULTRASONOR A SÂRMELOR CU SIMETRIE CILINDRICĂ	277
<b>TEODORESCU, R.</b> – TEHNOLOGIE DE VALORIFICARE A UNOR METALE GRELE DIN NAMOLURI GALVANICE ÎN VEDEREA DEPOLUĂRII MEDIULUI	283

<b>SCOROBETIU L., CÂNDEA V. – TĂIEREA PLĂCILOR DIN STICLĂ PRIN TERMOȘOC</b>	291
<b>COJOCARU M., TARCAN C., GOSTIN F. – EXPERIMENTĂRI PRIVIND CINETICA OXIDĂRII LA TEMPERATURI ÎNALTE A NITRURII ALUMINIULUI</b>	293

## THE CHARACTERIZATION OF 6308 C3 RADIAL BEARINGS THERMALLY TREATED UNDER 0 °C

BY

IOAN ALEXANDRU, ADRIAN ALEXANDRU, VASILE BULANCEA,  
MIRELA GHEORGHIAN

**Abstract.** *The thermal treatment under 0°C of bearing elements, is an important way for decreasing the quantity of residual austenite and has a drastic influence on the increase of hardness, pitting wear resistance, dimensional stability, noise reduction, and finally increases the time of using of the bearings. The paper presents the experimental results concerning the characterization of bearing elements thermally treated at temperatures of -60°C*

**Keywords:** bearing, structure, residual austenite

### 1. INTRODUCTION

The Romanian bearings market is from the point of view of quality and prices in the middle group of main international producers, as: SKF, FAG, KOYO, ZKL, TAM, and NAKI.

In order to maintain an international market the URB bearings thermally (S.C. RULMENTI S.A. BARLAD) wants to produce bearings thermally treated under 0°C. The specialists from Technical University "Gh. Asachi" Iasi, were made experimental researches concerning the determination of some thermal treatments variants for the constructive elements of bearings.

It was studied the influences of temperatures of austenitising, of cooling under 0°C and of tempering on quantitative evolution of structural constituents: martensite, residual austenite and carbides.

The thermal treatment under 0°C decreases the quantity of residual austenite and increases carbides density with dimensions under 0,001 [mm]. The fact that the tempering applied after the thermal treatment under 0°C can be made at temperatures smaller than 170°C, in time of 90 minutes just for detension, makes possible the maintaining of a high hardness (62,5 ... 63 HRC) with a very small quantity of residual austenite.

The studied bearings are radials, with balls 6308 C3, for the industries of transportation auto and railways and similar domains.

### 2. EXPERIMENTAL PROCEDURE

On research were supposed samples (balls with  $\phi$  15x20 mm) of 6308 C3 bearing from RUL 1 steel with spectral determined chemical composition: 1,0% C; 0,28% Si; 0,37% Mn; 1,53% Cr; 0,04% Ni; 0,01% Mo; 0,08% Cu.

The steel austenitising for hardening were made in the domain of temperature 810...855<sup>0</sup>C.

Raceways having larger thickness that the internal and external rings were austenitised at higher temperatures to obtaining the same depth of hardening, Fig. 1.

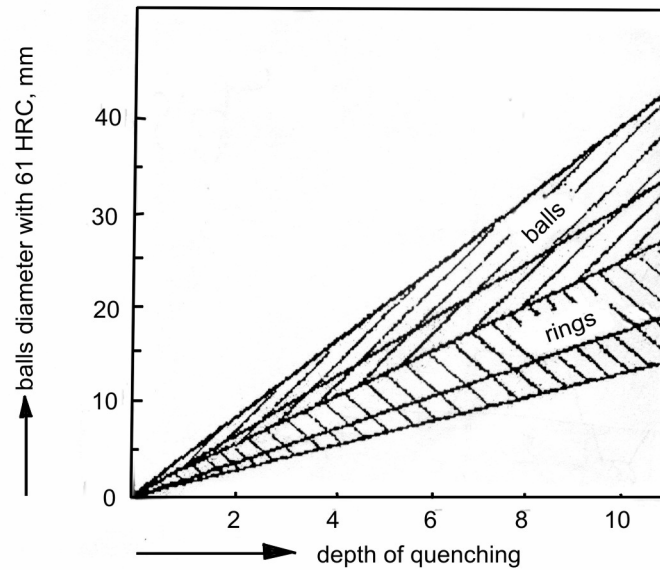


Fig.1 The dependence on depth of hardening of hardened balls and rings

The final thermal treatment which was applied to the constructive elements of bearings maded by RUL 1 steel is composed by a heating and a maintaining at 840<sup>0</sup>C in time of 54 minutes, oil cooling at 60<sup>0</sup>C, washing, cooling at -60<sup>0</sup>C, maintaining 60 minutes, tempering at 170<sup>0</sup>C and maintaining 1,5 h as is presented in Fig.2.

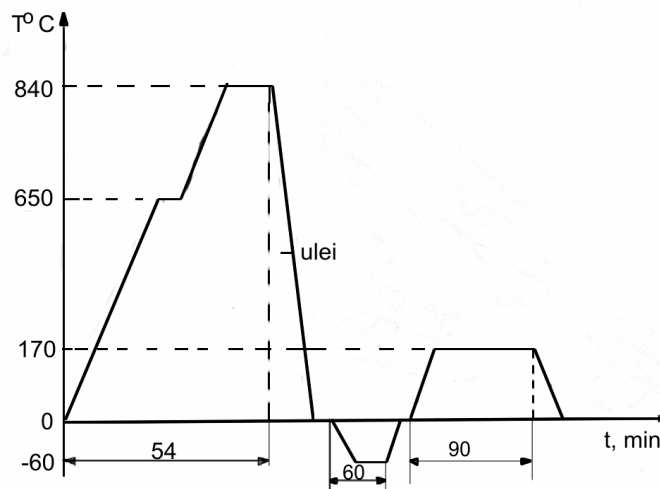


Fig. 2. The complex thermal treatment applied on RUL 1 steel

The thermally treated bearing elements were measured for dimension, shape, structure, vibration level, roughness and were quantitative and diffractografic analyzed.

### 3. EXPERIMENTAL RESULTS AND INTERPRETATION

The researches were maded on the constructive elements of the 3 bearings.

The measurements results are presented in table 1.

Table 1

No	Parameter	UM	Imposed	Measured										
				1			2			3				
1	Roughness of raceway –outer ring	μm	0.080	0.025			0.038			0.038				
2	Roughness of raceway-inner ring	μm	0.10	0.048			0.035			0.035				
3	Sphericity deviation of the balls	μm	0.50	0.20...0.25			0.08...0.013			0.08...0.24				
4	Roughness of the balls	μm	0.04	0.013...0.021			0.017...0.024			0.015...0.023				
5	Roundness of raceways-outer ring	μm	3	1.41			3.32			2.83				
6	Roundness of raceways-inner ring	μm	3	1.54			1.01			0.76				
7	Outer diameter	μm	-15	-10			-11			-10				
8	Inner diameter	μm	-12	-2			-2			0				
9	Width-outer ring	μm	-120	-23			-50			-46				
10	Width-inner ring	μm		-42			-28			-52				
11	Width variation-outer ring	μm	20	8			11			6				
12	Width variation-inner ring	μm		3			17			7				
13	Outer wearing out of round	μm	6	3			3			3				
14	Inner wearing out of round	μm		1			1			2				
15	Outer tapering	μm		1			1			1				
16	Inner tapering	μm		0			1			1				
17	Side run-out	μm	16	14			8			10				
18	Radial run-out of outer ring	μm	25	9			5			5				
19	Radial run-out of inner ring	μm	15	6			5			3				
20	Axial run-out of outer ring	μm	30	10			5			9				
21	Axial run-out of inner ring	μm	25	8			6			12				
22	Radial clearance	μm	15...33	27			26			22				
23	Residual magnetism	mT	0.30	0.22			0.38			0.55				
24	Vibration level KNT	VG/P/R	80/60	30/5			30/7			33/7				
25	Vibration level MGG 11C		A	B	C	A	B	C	A	B	C	A	B	C
			220	150	350	81	67.8	37.1	127.9	65.1	62.8	93.3	48.3	58.3
						95.4	82	39.9	103.8	66.1	36.3	96.3	49.9	54.5
26	Deviation of cross profile-outer ring	μm	3	0.961			1.396			0.824				
27	Deviation of cross profile-inner ring	μm		1.772			2.681			2.355				
28	Raceway radius-outer ring	mm	8...0.070	8.001			7.961			8				
29	Raceway radius-inner ring	mm	7.7+0.070	7.764			7.830			7.777				
30	Hardness-outer ring	HRC	61...64	61.5...62			61.5...62			61.5...62				
31	Hardness-inner ring	HRC		61.5...62.5			61.5...62.5			61.5...62				
32	Roughness-outer	μm	0.50	0.58			0.68			0.55				

33	Roughness-inner	$\mu\text{m}$	0.63		0.70	0.70	0.55			
34	Side roughness-outer ring	$\mu\text{m}$			0.40	0.48	0.54			
35	Side roughness-inner ring				0.50	0.45	0.38			
36	Tempering structure of outer ring		1...4				3			
37	Tempering structure of inner ring						3			
38	Carbide network-outer ring		max.3				0			
39	Carbide network-inner ring						0			
40	Decarburization-outer ring		without				0			
41	Decarburization-inner ring						0			
42	Raceway diameter		Outer ring	Inner ring	Outer ring	Inner ring	Outer ring	Inner ring	Outer ring	Inner ring
			80.081±0.015	49.919 -0.005 -0.0035	80.60	50.416	80.593	50.390	80.622	50.418
43	Residual austenite-inner ring	%	Max.16				5			
44	Residual austenite-outer ring						6			

The values obtained from measurements for each parameter were compared with the values from international standards. We can say that the majority of measured parameters are in the value domain imposed by standards.

The easy larger value at the 2 bearing for the vibration level P/R = 7 (the imposed values is 6) is accepted at this kind of bearings, because after assembling the vibrates level goes to normal rate. The easy larger values of the raceway compared with the imposed values (table 1, position 28, 29) have no influence concerning the quality of these bearings.

The exceeding of imposed limits for roughness (table 1, position 32 and 33) has no negative influence in bearings exploitation, because it depends on the precision of assembling surfaces. The different values for the raceways diameters (table 1, position 42) are normales because each producer choses the internal construction of his bearings. A curve with deviations from roundness of the raceways for outer rings is presented in Fig. 3.

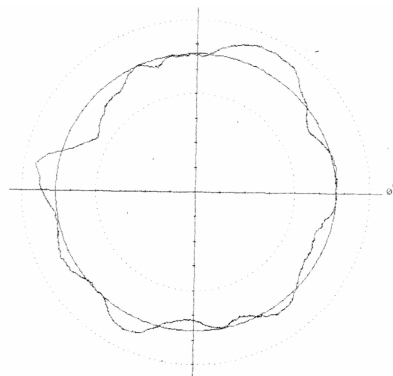


Fig. 3. Roundness deviation of the raceway for outer ring

The outer rings hardness is 61,5...62 HRC and inner rings is 61,5 ... 62,5 HRC, and the required values for hardness are 61...64 HRC.

The metallographical structures obtained on RUL 1 steel after and final treatment on prepared surfaces/Nital 2,5% 300:1) on a Neophot 21 microscope are formatted globulare perlite and carbides after annealing and by tempered martensite, carbides and residual austenite in small quantity after quenching and tempering Fig.4, a,b.

The steel not contain non-metallic inclusions.

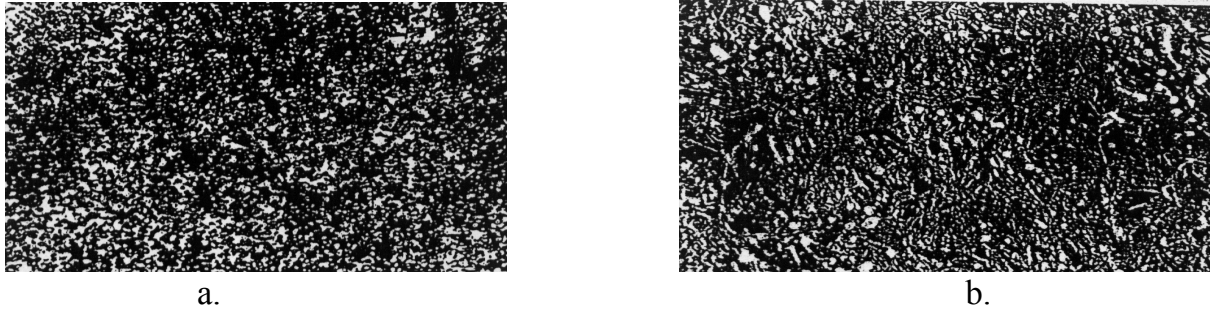


Fig. 4.a)Structure of annealing of RUL1 steel; b)Structure of quenching and tempering of RUL1 steel

The residual austenite determined on the thermally treated under 0°C steel from 3 bearing on inner ring has values of 5% which is very small in comparison with the maximum imposed value 16%.

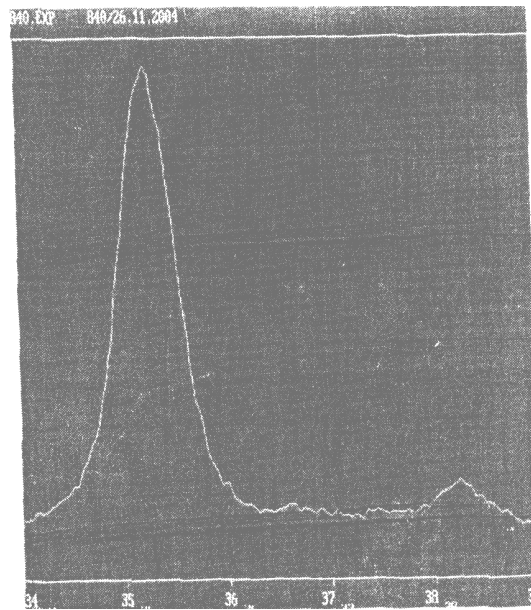


Fig.5. The diffractographic curve of RUL 1 steel thermally treated under 0°C

The steel from the studied bearings presents corrects structures of thermal treatments with small quantities of residual austenite and without carbides networks and without decarburised layers.

#### 4. CONCLUSIONS

- i) The 6308 C3 bearings are in according (constructive and as materials) with the international standards.
- ii) The small content of residual austenite in this steel structures make that this bearings to have a good behaviour in exploitation.

- iii) The studied bearings are in according with international standards from the point of view of vibration (noise) level and structure.

*Received April 15, 2005*

*Technical University "Gh.Asachi" Iasi*

#### REFERENCES

- /1/. Alexandru, I., Bulancea, V. *The Change of the Substructural Elements and the Redistribution of the Alloying Elements by Means of Cryotreatments in Alloy Tool Steel*. Congresul International de Tratamente Termice si Metalurgie Fizica, Budapesta, Ungaria, 1986.
- /2/. Andrean, H.O., *Precipitation of secondary carbides during tempering of HSS*. Int. HSS Conf. Leoben, 1990, Bohler.
- /3/. Alexandru, I., Bulancea, V. *Handbook of residual stress and distorsion of steel*. Cap. 26, Effect of cryogenic cooling on residual stress, Structure and Substructure.

#### CARACTERIZAREA ELEMENTELOR DE RULMENȚI 6308C3 TRATATE SUB 0°C

**Rezumat:** Tratamentele termice criogenice aplicate elementelor de rulmenti sunt o modalitate de a scadea cantitatea de austenita reziduala si au o influenta drastica asupra cresterii duritatii, rezistentei la uzura pitting, stabilitatii dimensionale, precum si asupra scaderii nivelului de zgomot si cresterii durabilitatii rulmentilor. Aceasta lucrare prezinta rezultatele experimentale privind caracterizarea elementelor de rulmenti tratate termic la temperaturi de -60°C.

## ASPECTS CONCERNING FLUIDIZED BED NITRIDING FOR ALLOYING STEEL WITH ALUMINIUM

BY

ADOLF BĂCLEA, SORIN DOBROVICI, OCTAVIAN POTECAȘU, FLORENTINA  
POTECAȘU, ELENA DRUGESCU, NELU CAZACU

**Abstract.** Nitriding is one of the most used treatments of steel machine parts. After nitriding treatment, superficial layers with special properties (high hardness) simultaneously with a reliable core which will offer to part exploiting exceptional properties (fatigue and wear resistance, tenacity). The paper is based by nitriding experiments made on a fluidized bed laboratory furnace. Fluidization was obtained in a steel refractory retort by solid granular (burned fire clay) and fluid (mixture of ammonia and nitrogen). Heating system is based by indirect electrical method. Heating transfer by furnace to retort is are high and is determinate by high value of heat transfer coefficient for fluidized bed. Anterior experiments fixed solid granulation and fluidization speed (by gas mixture debit). Nitriding processes was conduced by a classic experimental matrix (ammonia proportion is constant, nitriding time and nitriding temperature are variable). Results were investigated by: hardness HV5, micro-hardness HV0,05, microstructure and XRD. The results confirm nitriding process, media capacity for heat and mass transfer and a good behavior of 38MoCrAl09 steel.

**Keywords:** nitriding treatment, mechanical properties

### 1. INTRODUCTION

After nitriding treatment, superficial layer with special properties (high hardness) simultaneously with a reliable core which will offer to part exploiting exceptional properties (fatigue and wear resistance, tenacity). For increasing quality for treated machine parts, different techniques having a rapid developing, diversification and adaptability to product processes. Fluidized bed technology (FBT) offer an active media to thermochemical treatments at low investment costs, [0], [0]. For FBT applications with open furnace, technological costs for gases increase, [0]. Some limitations for shape parts are important too. Simple surfaces in vertical/axial positions are recommended for uniformity of treatments. Important mechanical gas solid processes (fluidized bed gasdynamics) having high influences over mass transfer and heat transfer processes is showing in Figure 1. High surfaces for solid/gas interfaces are an important characteristic for fluidized bed. Internal thermal transfer process between gas and granular solid

### 2. EXPERIMENTAL CONDITIONS

For nitriding in fluidized bed experiments we used a pilot furnace (Figure 2). Some important characteristics were:

- fluidized bed furnace (140mm diameter, H/D=1,2)
- heating technique: indirect electrical heater
- solid granular: burned fire clay with granulation: 0,010...0.016mm

- fluidization gas: mixture from ammonia (33%) and nitrogen (rest)
- Samples from 38MoCrAl09 steel (romanian standards, Table 1)
- experimental procedure: classical “full factorial” array with two factors and three level for each factor.

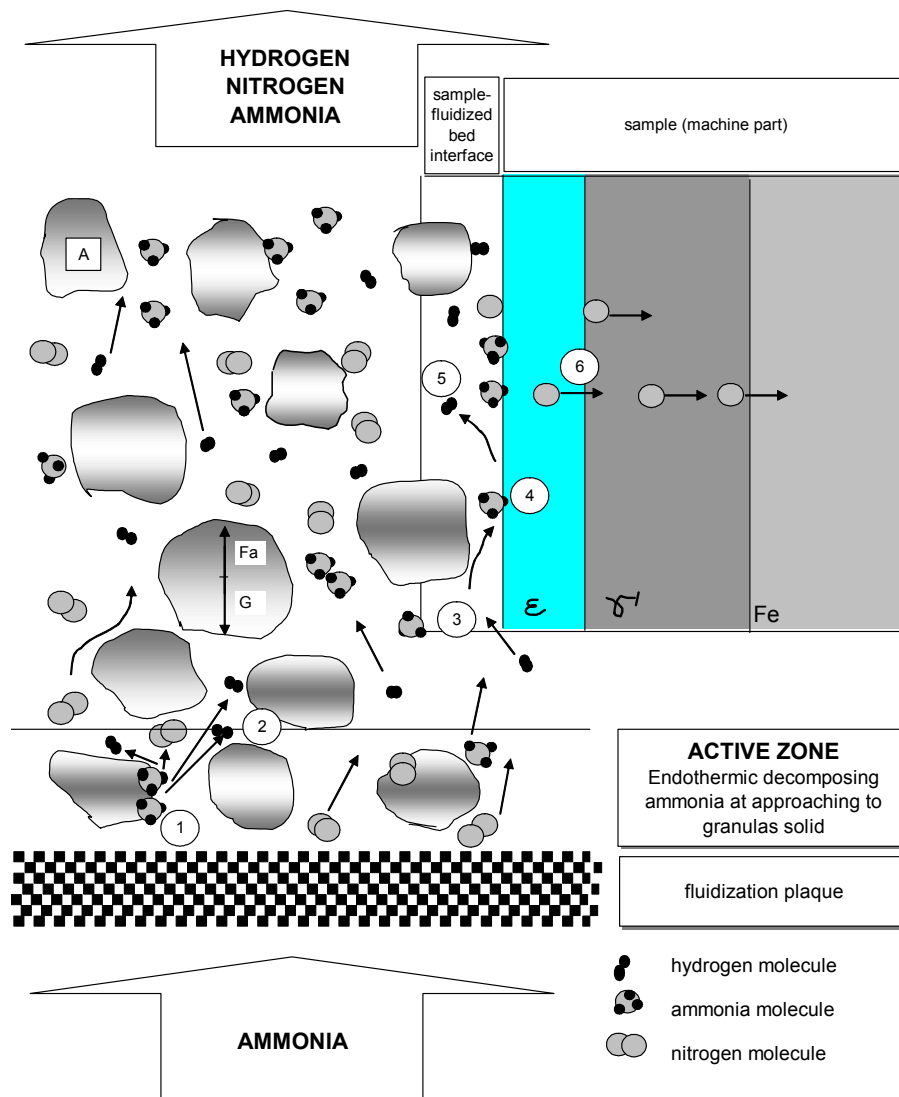


Figure 1. Representation of processes on fluidized bed nitriding: A-solid, G-weight, Fa- ascension force, 1- endothermic decomposing ammonia, 2-hydrogen molecule formation from atoms (similarity to nitrogen), 3-ammonia molecules approaching to surface, 4-endothermic decomposing ammonia, 5-hydrogen molecule formation from atoms, 6-nitrogen atoms diffuse into metal surface

Many factors having influence over nitriding process but nitriding temperature and nitriding time are presents for all nitriding technologies. Preliminary experiments fixing some important factors which come from fluidization. Fluidization was conduced by diagram pressure drop/velocity [0] but process repeatability is important. Gas mixture debit was constant for all nitriding regimes and visual observation was important for quality of fluidization.

Table 1. Chemical composition for 38MoCrAl09 steel (Romanian standard)

steel	C	Mn	P	S	Si	Mo	Cr	Ni	Al
38MoCrAl09	0,41	0,53	0,22	0,011	0,33	0,18	1,35	0,11	0,86

One of the most important factors influencing the quality of fluidization is the uniformity of gas flow across a constant pressure drop [0]. A drop pressure in fluidized bed was measured by “U” manometer. Samples had a disc shape and were immersed vertically in fluidized bed.



Figure 2. Image with nitriding furnace.

Table 2. Regimes for 38MoCrAl09 nitriding in fluidized bed

Exp. no.	Chemical composition of gas mixture	nitriding temperature	nitriding time
m.u.	%	°C	h
1	33%NH <sub>3</sub> +67%N <sub>2</sub>	520	1
2			2
3			3
4		550	1
5			2
6			3
7		580	1
8			2
9			3

### 3. RESULTS AND DISCUSSION

Results were investigated by: hardness HV<sub>5</sub>, micro-hardness HV<sub>0,05</sub>, microstructure and XRD.

For all 38MoCrAl09 steel samples, microstructures (Figure 3) showing nitriding layers. By increasing nitriding temperature and nitriding time a combination layer formation is present.

Hardness HV<sub>5</sub> measurements on the nitriding surfaces showing an appreciable increasing for all regimes. For 550°C and three hours hardness is over 1200 kgf/mm<sup>2</sup> (Figure 4). Total nitriding layer depth for all nitriding regimes by micrographic measurements is showing in Figure 5.

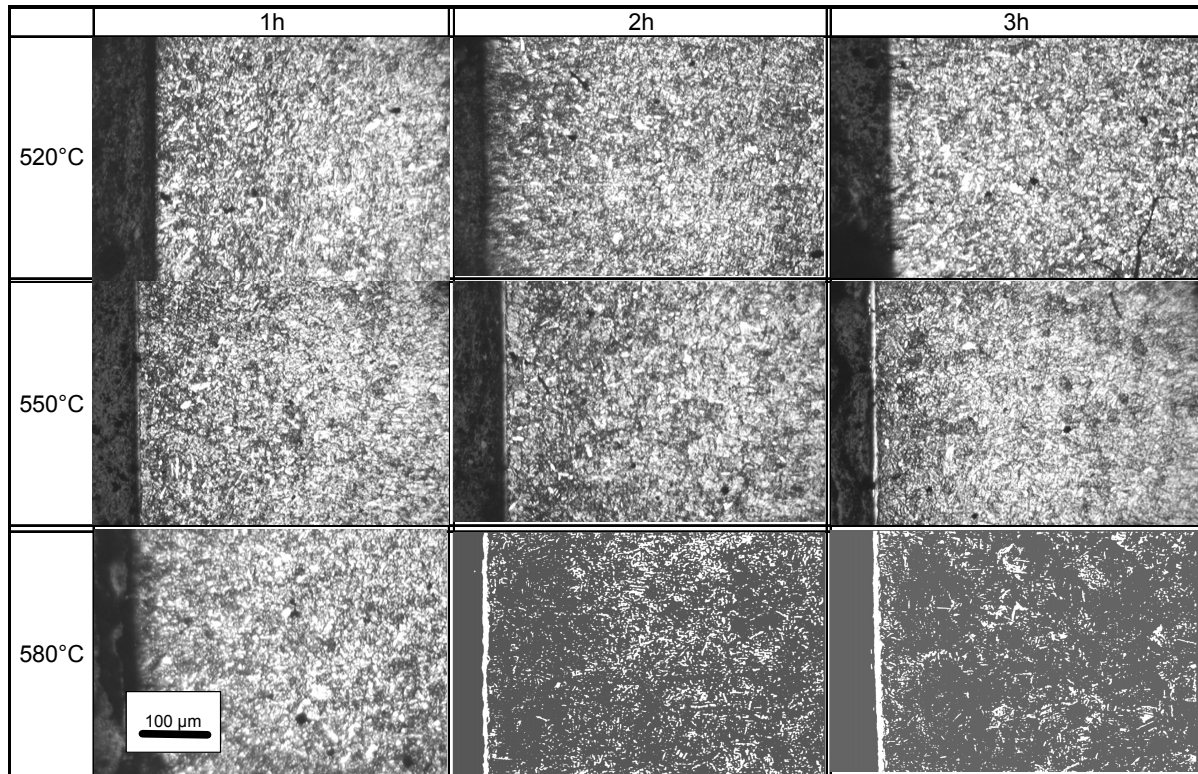


Figure 3. Micrographs of nitrided 38MoCrAl09 steel samples after experimental regimes [0].

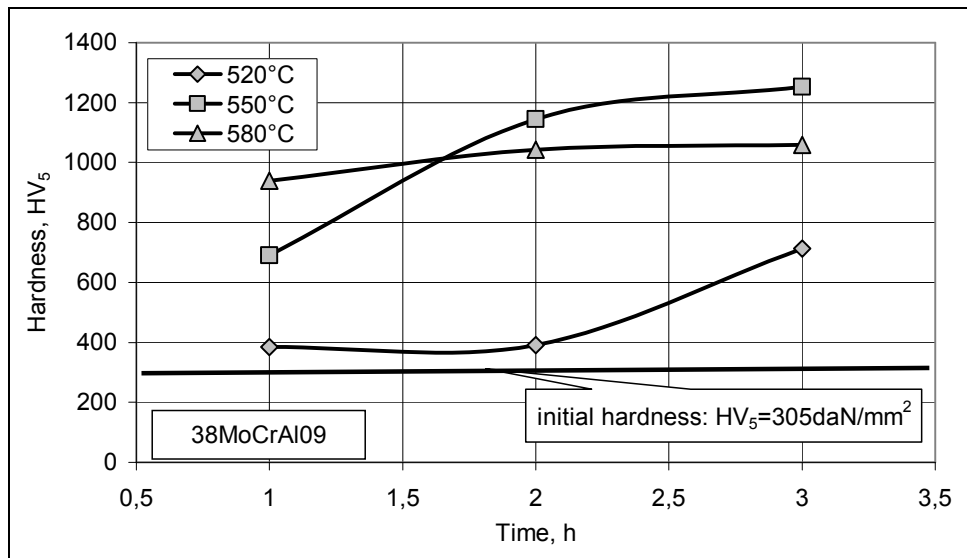


Figure 4. Hardness HV<sub>5</sub> on the nitriding surface for 38MoCrAl09 steel samples after nitriding in fluidized, [0].

For all 38MoCrAl09 steel samples, showing nitriding layers. a combination layer is present. By increasing nitriding temperature and nitriding time a combination layer is present and that increasing by . Diffusion layer has for three hour Hardness HV<sub>5</sub> measurements on the nitriding surfaces showing an appreciable increasing for all regimes. For 550°C nitriding temperature and three hours nitriding time hardness is over 1200 kgf/mm<sup>2</sup> (Figure 4). Total nitriding layer depth for all nitriding regimes by micrographic measurements is showing in Figure 5. Nitriding phases presence were investigate by XRD (DRON 3) and for 550°C for

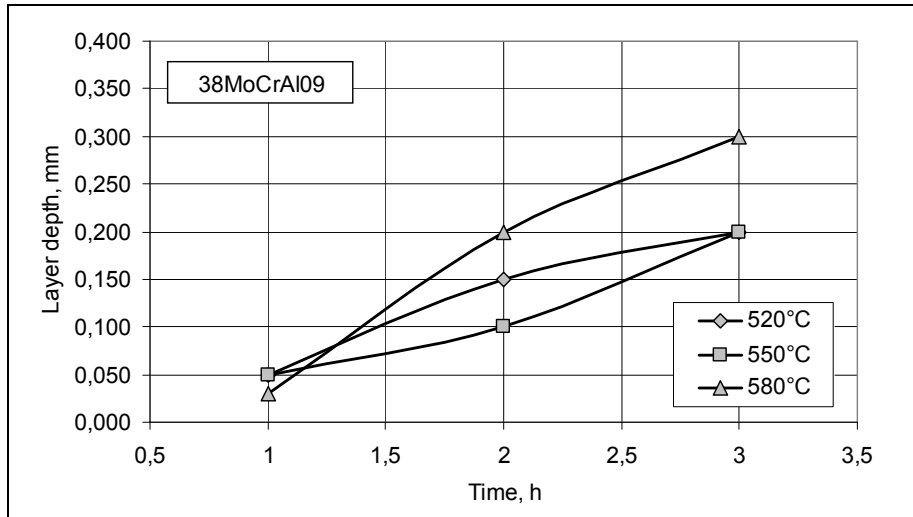


Figure 5. Total nitriding depth layer for 38MoCrAl 09 sample nitriding in fluidized bed for different temperature and time, [0].

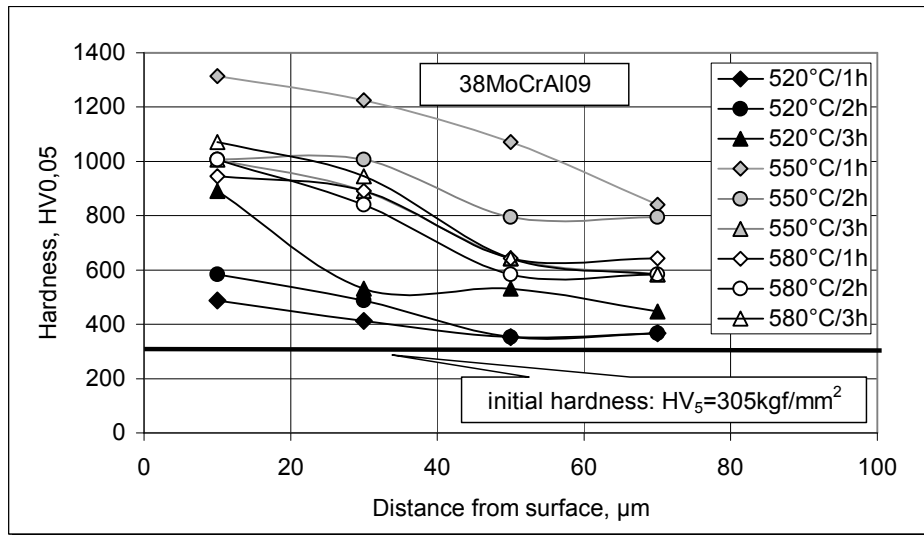


Figure 6. Microhardness HV0,05 for 38MoCrAl09 steel sample, [0].

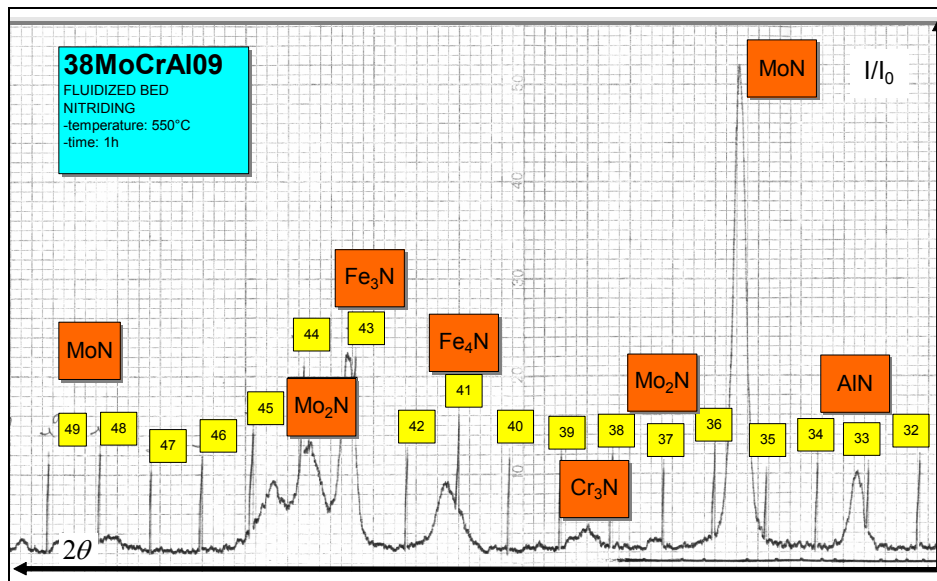


Figure 7. XRD diagram for 38MoCrAl09 steel

The nitriding temperature and one hour nitriding time the diagram is showing in Figure 7. The XRD investigation gives only the presence of phases, [0]. The steel has in chemical compositions Mo, Cr and Al that conducted to hard phases at nitrogen presence and temperature. Because fluidized bed having a high thermal and mass transfer coefficient the specific nitriding phases was formed for one hour nitriding time and 550°C nitriding temperature.

#### 4. CONCLUSIONS

The results investigated confirm nitriding process in fluidized bed, media capacity for heat and mass transfer and a good behavior of 38MoCrAl09 steel. Nitriding in fluidized bed process is characterized by a short time cycle (1...3h) because in experimental conditions we used an open furnace. The cooling process is shorter when comparing nitriding processes with other nitriding technologies and that increasing efficiency, [0]. The gas mixture after nitriding reactions containing hydrogen and rests of ammonia and that was burned in atmosphere at nonpolluting gasses (carbon dioxide and steam). For low alloyed steel with Cr, Mo and Al the hardness on surface (HV<sub>5</sub>) had 700... 1250 kgf/mm<sup>2</sup> for 550... 580°C and 1...3 hour nitriding time. By adequate selection of steel [0] and fluidization factors, nitriding in fluidized bed is characterized by a short total time of treatment that increases efficiency of process. Some limitation of part shapes and positions in fluidized bed are available for industrial applications.

Received May 3, 2005

"Dunărea de Jos" University Galați

#### REFERENCES

- /1/. Băclea, A., *Studii și cercetări privind implementarea nitrurării în strat fluidizat la ameliorarea proprietăților unor repere utilizate în construcții navale*, Teză de doctorat, Galați, 2004.
- /2/. Iacob, C., Vigier, P., *Transfert d'azote em lit fluidise: influence des parametres dynamiques du lit sur la nitruration d'un acier non allie*, ATTT 95 Internationaux de France du traitement thermique, Paris 21-23 juin 1995;
- /3/. Sagon-King, F., *ASM Handbook*, Vol. 4, Heat Treating, Fluidized-Bed Equipment, ASM International, Materials Park, OH 44073-0002, pages 484-491;
- /4/. Ivanuş Gh, etc., *Ingineria fluidizării*, Editura Tehnică, București, 1996;
- /5/. Kunii D., Levenspiel O, *Fluidization engineering*, John Wiley & Sons, Inc., New York, 1969;
- /6/. Convert F, *Analyse des couches de combination par diffraction X*, Traitements thermique, no. 352, 2004, pg.27
- /7/. Murry Guy, *Une nouvelle norme europeenne "Acier pour nitruration*, Traitement Thermique, nr.339, mai 2002, pag.30

#### ASPECTE PRIVIND NITRURAREA ÎN PAT FLUIDIZAT A OȚELURILOR ALIATE CU ALUMINIU

**Rezumat:** Nitrurarea este unul din cele mai utilizate tratamente termochimice, în construcția de mașini. După nitrurare se obține un strat superficial cu duritate ridicată și care alături de miezul pieselor de obicei tenace conduce la foarte bune proprietăți în exploatare (rezistență la oboseală și la uzură). Lucrarea se bazează pe experimentări de nitrurare în strat fluidizat realizate în condiții de laborator. Experimentările de nitrurare au fost conduse după o matrice experimentală clasică cu următorii factori: proporția de amoniac, durata nitrurării și temperatura de nitrurare. Rezultatele au fost investigate prin duritate HV<sub>5</sub>, microduritate HV<sub>0,05</sub>, analiză microstructurală și analiză de difracție cu raze X. Rezultatele confirmă realizarea procesului de nitrurare, capacitatea stratului fluidizat pentru a realiza transferul de masă și căldură și buna comportare a oțelului 38MoCrAl09 la nitrurarea în strat fluidizat.

## THE POSSIBILITY OF STAMPING WITHOUT RIDGES THE MARKS OF “TOOTHED WHEEL” TYPE

BY

VICTOR BIBIRE, MIHAI SUSAN

**Abstract.** The paper analyses the possibility of stamping without ridges the toothed wheels, by using a metallic ring (OSC) that undertakes the stress in the ridge and reduces the consumption of material (with up to 20%), i.e. for a lot of 10.000 pieces of alloy steel the material savings are of 1410 kg – the result of an economic calculation. The metallic ring was dimensioned for the internal pressure resulting in  $D_e = 129$  mm calculating at the same time the thermal tensions in the ring's walls that appear as a result of the difference in temperature.

**Keywords:** stamping, ridge duct, thermal tension

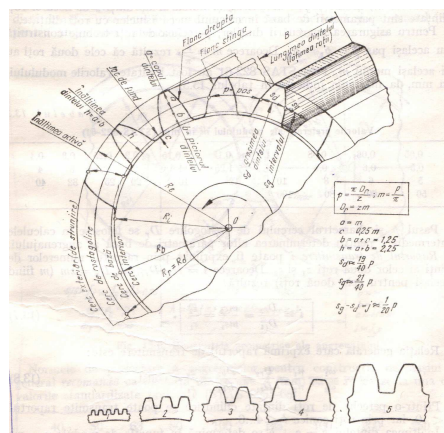
### 1. INTRODUCTION

Stamping as a method of processing by pressure has the widest applicability among the processing methods by plastic deformation of metals and alloys in the field of machine building. Thus, almost 70% of the parts used in machine building are obtained by stamping.

Transferring the mechanical power (P) and momentums (M) within a technical system type machine-tool, is based on the most often met mechanical movement, i.e. the rotating motion ensured by gears based on toothed wheels.

### 2. THE STATE OF STRESS

#### 2.1 – The fundamental geometrical parameters of a cylindrical toothed wheel



M, p, z,  $D_r$

Materials = alloy steel with cemented dental crown

## 2.2 – Mechanical stress in toothed wheels

Tooth deterioration:

- Tooth breaking:
  - static (overloads)
  - fatigue: bending  
contact (pitting)
- Deterioration of active surface of tooth flanks:
  - seizing
  - abrasive wear
  - plastic flow
  - thermal staining
  - exfoliation
  - interferences

The state of stress of the toothed wheels in a gear is variable and periodical.

- Bending fatigue – the main cause of toothed wheels destruction in a gear with the teeth flanks superficially hardened (HRC > 45)
- Contact fatigue – the main cause of teeth flanks destruction in toothed wheels with HB < 4500 MPa.
- Toothed wheels dimensioning – based on ensuring the criterion of bending strength.

$$m = \sqrt{y_f k F_t / \psi z_1 \sigma_{ai}}$$

- Gear durability – based on the verification of the resistance to contact pressure of toothed wheels.

$$\sigma_H = 151 \sqrt{(k F_t / \psi m^2 z_1) ((i+1)/i)} \leq \sigma_{ai}$$

## 2.3 Dimensioning of metallic ring on internal pressure

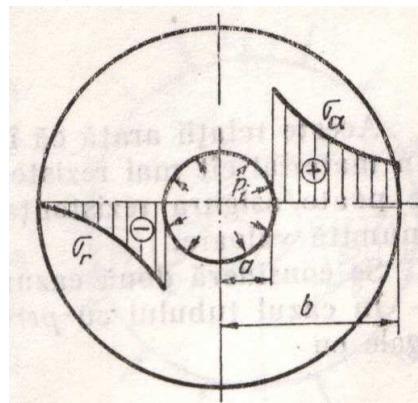
The metallic ring is considered as a tube with thick walls, stressed to bending – compression due to internal pressure, given by the material flow in the matrixes and to thermal tensions that appear between the ring's walls as a result of the difference in temperature between its walls.

$T_x$  = circular bending tensions

$T_r$  = radial compression tensions

The fundamental relation for dimensioning is:

$$b = a \sqrt{[\sigma_a + (1-k)p_i] / [\sigma_a - (1+k)p_i]}$$



The material of the metallic ring = OSC for plastic deformation (as the matrixes) 34M<sub>0</sub>CrNi15 STAS 3611.

In practice, the internal diameter of the metallic ring is considered  $D_i = 50 \text{ mm} = 5 \text{ cm}$ .

Maximum tension permissible  $\sigma = 300 \text{ [KN / cm}^2\text{]}$

From alloy steel nomograms it derives:  $p_i = 130 \text{ [KN / cm}^2\text{]}$

The force required for stamping by heading is:

$$F = p_i \times A = 60 \times \pi \times r_i^2 = 60 \times 3,14 \times 5^2 = 4710 \text{ [kN]}$$

- According to the theory of maximum normal tensions

$$b = a \sqrt{\sigma_a + p_i / \sigma_a - p_i} = 5 \sqrt{3/2} = 6,123 \text{ cm}$$

- According to the theory of maximum specific elongations

$$b = a \sqrt{\sigma_a + 0,7 p_i / \sigma_a - 1,3 p_i} = 5 \sqrt{57/37} = 6,205 \text{ cm}$$

- According to the theory of maximum tangential tensions

$$b = a \sqrt{\sigma_a / \sigma_a - 2 p_i} = 5 \sqrt{5/3} = 6,454 \text{ cm}$$

- According to the theory of the deformation energy

$$n = -v + \sqrt{v^2 - 1 + (\sigma_a/p_i)^2} = -0,3 + \sqrt{24,09} = 4,608$$

$$b = a \sqrt{n+1/n-1} = 6,233 \text{ cm}$$

- According to the theory of the form modifying energy

$$n = -k + \sqrt{k^2 - 1 + (\sigma_a/p_i)^2} = 4,524 \text{ cm}$$

$$b = a \sqrt{n+1/n-1} = 6,260 \text{ cm}$$

The theory of the biggest dimensions is adopted, in our case the theory of maximum tangential tensions.

$$b = r_e = 6,454 \text{ cm}; D_e = 129 \text{ mm}$$

## 2.4 Thermal stress

\* Calculus of thermal tensions in the metallic ring

As a result of uneven temperature, the effects of thermal tensions appearing in the metallic ring's walls overlap those caused by internal pressure  $p_i$ .

$T_i$  = the temperature on the inner surface of the metallic ring  $T_i = 1250^\circ\text{C}$

$T_e$  = the temperature on the outer surface of the metallic ring  $T_e = 850^\circ\text{C}$

$T$  = the difference in temperature between the metallic ring's walls  $T = T_i - T_e = 400^\circ\text{C}$

$E$  = Young's module  $E = 2,1 \times 10^6 \text{ dN/cm}^2$

$v$  = thermal constant  $v = 0,3$

$\alpha_0$  = linear thermal extension coefficient  $\alpha_0 = 12 \times 10^{-6}$

$T\alpha_i$  = circular thermal tension on the inner surface of the metallic ring

$T\alpha_e$  = circular thermal tension on the outer surface of the metallic ring

$$\sigma_{\alpha_i} = [(E\alpha_0 T)/3(1-v)][(a^2 + ab - 2b^2)/(b^2 - a^2)] = -4800 \times 26,038 / 16,654 = -7504,64 \text{ [KN/cm}^2\text{]}$$

$$\sigma_{\alpha_e} = [(E\alpha_0 T)/3(1-v)][(b^2 + ab - 2a^2)/(b^2 - a^2)] = 4800 \times 23,924 / 16,654 = 6895,35 \text{ [KN/cm}^2\text{]}$$

## 3. PROCESSING ADMIXTURES ON STAMPING

### 3.1 Processing admixtures

According to S.R. 7670 / 1 - 96 dimensional deviations may be:

- dimensional deviations that do not cross the separation plan: lengths, widths, ("l" length of the threshold)

- dimensional deviations from cross the separation plan: thickness, height, (“h” height of the threshold)

Two classes of stamping are provided:

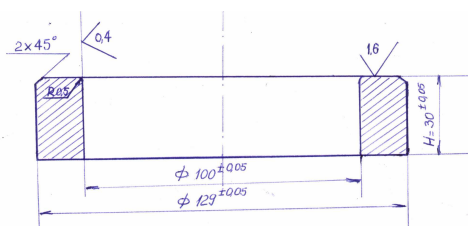
- F stamping class – normal tolerance is provided (stamping hammers)
- E stamping class – tolerance restricted to certain dimensions is provided (maxipress)

The maximum dimensions tolerances will apply, the plus (+) in the tolerance (T) is removed by ridge polishing by precision cut.

Cutting is performed based on the constant volume law, i.e. the parts in the lot are sorted out on mass units and not according to the H / D report.

Example:

Length  $l^{+3}_{-1,5}$  - +3 [mm] will be cut.



### 3.2 Technological explanations on the stamping process

Depending on the matrix's geometry and the flowing manner of material, stamping may be open or closed.

In the case of active ridge stamping, the material flows more towards the ridge duct and less towards the lower matrix, and in passive ridge stamping, the material flows with greater intensity in the lower matrix than the ridge duct. A constructive solution is offered by stamping with collective drain. In our case, we deal with a stamping by heading on maxipresses.

## 4. ECONOMIC CALCULUS

### 4.1 The calculus of losses due to ridge

The material flowing into the ridge plays a technological part, therefore it must be added to the material required for obtaining a stamped part.

The volume of material provided for the ridge depends on:

- the size of the ridge duct ( $h_1$ ,  $h_2$ ,  $b_1$ ,  $b_2$ )
- the complexity of the part.

$$V_b = C_b A_b P_b$$

$$m_b = \rho V_b \text{ [Kg]}$$

$C_b$  = coefficient of ridge duct filling

$A_b$  = the cross surface of the ridge duct

$P_b$  = average perimeter of the ridge

$\rho$  = steel density;  $\rho = 7,85 \text{ [Kg/dm}^3\text{]}$

Determination of height  $h_1$  ridge duct bridge (baffling area).

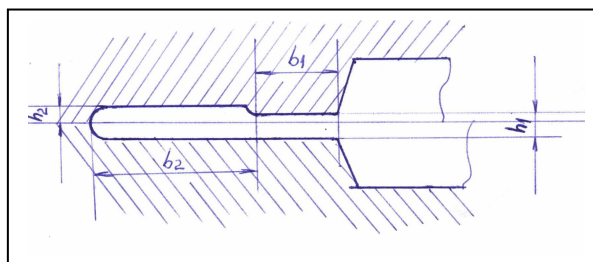
$$h_1 = 0,015 \sqrt{S_p}$$

$S_p$  = the surface of the stamped part at the level of the separation plan.

$$S_p = \pi r_e^2 = 3,14 \times 6,454^2 = 130,856 \text{ cm}^2$$

$$h_1 = 0,015 \sqrt{130,856} = 0,171 \text{ cm} = 1,71 \text{ mm} \cong 2 \text{ [mm]}$$

$$\begin{aligned} h_1 &= 2\text{mm} \\ h_2 &= 4\text{mm} \\ b_1 &= 9\text{mm} \\ b_2 &= 25\text{mm} \end{aligned}$$



For circular parts:

$$P_b = 2\pi[r_c + y_{(xG)}] = 2 \times 3,1415(6,454 + 11,72) = 2 \times 3,14 \times 18,174 = 114,18[\text{mm}]$$

$$Y_{(x)} = [h_1 b_1^2 / 2 + (h_2 + h_1 / 2)(b_1 + b_2 / 2)b_2] / h_1 b_1 + (h_2 + b_1 / 2)b_2 = 2703,5 / 230,5 = 11,72[\text{mm}]$$

$Y_{(xG)}$  = the position of the ridge duct's centroid determined by writing the above equation with static momentums in relation to the limit of the baffling threshold.

$$V_b = 0,7 \times A_b = b_1 b_2 = 225\text{mm}^2$$

$$225 \times 114,18 = 17983,35 \text{ mm}^3 = 0,017983\text{dm}^3$$

$$m_b = \rho V_b = 7,85 \times 0,017983 = 0,141[\text{Kg}]$$

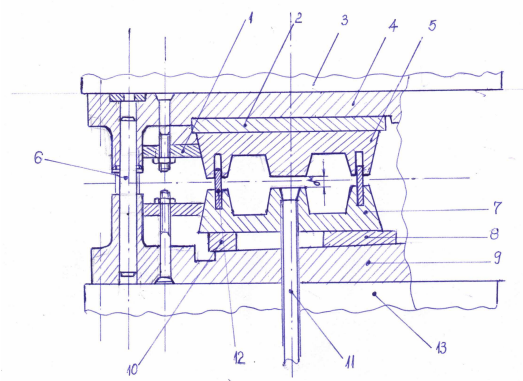
For a lot of 10.000 parts (cylindrical toothed wheels), the mass lost by removal of the ridge is:

$$M_{\text{lot}} = 10.000 \times 0,141 = 1.410 [\text{Kg}]$$

## 5. CONCLUSIONS

The possibility of stamping without ridge of the parts of "toothed wheel" type by using a metallic ring, of the ones presented above, ensures the following advantages to the classical solution, which also stands for the purpose of this paper, especially for open stamping of the parts in great series production:

- the ring takes over the ridge stress
- material saving resulting from ridge removal by cutting (for a lot of 10.000 pieces we save 1410 kg of steel)
- reduced labor and high productivity (work on parts – maxipresses)



Received April 5, 2005

Technical University "Gh.Asachi" Iasi

## REFERENCES

/1/. Susan, M., *Deformarea metalelor prin forjare*, Tehnopress Publishing House, Iași, 2002

- /2/. Chiriță, V., *Matrițarea la cald a metalelor și aliajelor*, Technical Publishing House, Bucharest, 1976
- /3/. Deutsh, I., *Rezistența materialelor*, E.D.P. Bucharest, 1979
- /4/. Gafițeanu, M., *Îndrumar de laborator - Organe de mașini*, I.P. Iași, 1985
- /5/. Popescu, V., *Tehnologia forjării*, E.D.P. Bucharest 1976
- /6/. Drăgan, I., *Tehnologia deformărilor plastice*, E.D.P. Bucharest, 1976
- /7/. Popescu, C., *Rezumat teză de doctorat "Cercetări privind rolul refulării în procesele tehnologice de forjare"*, Bucharest, 1995.

### **POSSIBILITATEA MATRIȚĂRII FĂRĂ BAVURI A PIESELOR TIP "ROATĂ DINȚATĂ"**

**Rezumat:** Prezenta lucrare studiază posibilitatea matrițării fără bavură pentru piesele tip "roată dințată" prin folosirea unui inel metalic (OSC) ce preia eforturile din bavură și reduce consumul de material (20%) datorită îndepărtării bavurii prin debitare. S-au prezentat parametrii geometrici de bază ai unei roți dințate ( $m$ ,  $p$ ,  $D_r$ ,  $z$ ), solicitările mecanice – oboseala de încovoiere și de contact, apoi s-a dimensionat inelul metalic la presiunea interioară rezultând  $D_e = 129\text{mm}$ . S-au calculat tensiunile termice din pereții inelului metalic datorită distribuției neuniforme a temperaturii în pereții acestuia. În final s-a efectuat un calcul economic, calculându-se volumul și masa bavurii, pentru un lot de 10.000 de piese rezultând o economie de 1410 Kg.

## HIGH QUALITY PRODUCTS USED IN THE AIRSPACE INDUSTRY

BY

A. BUZAIANU, M. CORBAN, A. IONCEA, I. CIUPITU, R. TRUSCA, P. NITA, V. MANOLIU\*

**Abstract.** *Manufacturing aircraft brakes is not a routine task. It calls a diverse range of disciplines, including: metallurgy, chemistry and mechanical engineering. It requires perfect process control. The exigent related the friction materials quality in what the loads and the speeds of use regards impose an increased life and a high safety level during exploitation. This fact implies an advanced understanding of the terminological phenomena, the extension of the specific material analyze and test types, and a new view on the design and production of the braking systems. The innovative strategy has proven successful for military and commercial brake systems and has allowed METAV-CD to develop brake design and system maintenance problems*

**Keywords:** *tribology, bimetallic materials, sintered metallo-ceramic material, airspace*

### 1. INTRODUCTION

The continuous improvement and diversification of the manufacturing technologies used for the friction couples made up of metallic-ceramic and bi-metallic disk require to verify after applying the braking tests and the satisfaction of the functional parameters.

A current research direction is the production of materials having improved a tribological characteristics used to the braking systems for special vehicles, aimed for the military end aircraft industries. For example the use of bimetallic components obtained by overcasting can reduce with up to 70% the consumption of the strategic metallic alloys, can increase the life and can reduce with up to about 40% the manufacturing costs. The results obtained on prototypes proved that the so-investigated materials could assure safe couple friction properties at speeds of over 23 m/s and improved resources.

### 2. METHODS AND EQUIPMENT TO EVALUATION OF MATERIALS

The SEM (Scanning Electron Microscopy) investigation provided detailed information about the morphological modification to the tribological couple. During our investigations a Philips SEM-515 electron microscope were used. To evaluate the tribological couple bimetallic- metallo-ceramic materials behavior at dry friction a testing machine was used equipped with a plane friction couple. The friction testing parameters were: the relative sliding speed:  $v = 23\text{m/s}$ ; normal loading on the sample ( $N = 4\text{daN}$ ;  $8\text{daN}$ ;  $12\text{daN}$ ); sample area:  $1\text{cm}^2$ .

### 3. RESULTS AND DISCUSSION

The modifications of the requirements related to the friction materials quality in what the operational loads and speeds regards made mandatory an increased life and

high safety degree. Presently, these requirements are assured by the new carbon-carbon composite, metallo-ceramic and bimetallic materials types (Fig1). The properties offered by the composition and the structure to the bimetallic and metallo-ceramic materials make possible their use up to 900-1000 °C and they should assure:

- sufficiently smooth braking;
- a high friction coefficient  $\langle \mu \rangle$  to be maintained at high temperature too;
- very good shock and vibration resistances;
- good heat absorption and dissipation capacity;
- relatively constant friction at variable speed and load.



Fig1 Bi-metallic and sintered friction components disks.

During exploitation a series of cast iron on steel support parts, as is the case of the friction bimetallic plates, suffer a dry friction process following which a weight loss is produced. The presence of a lubricant between the active friction coefficient (Fig.2) and doing so an increase loss by friction.

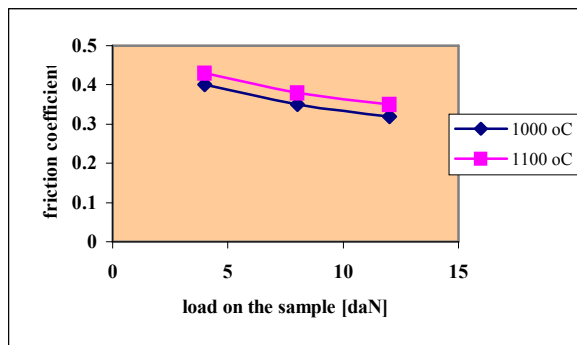


Fig.2 The variation of the friction coefficient at relative sliding speed  $v = 23\text{m/s}$

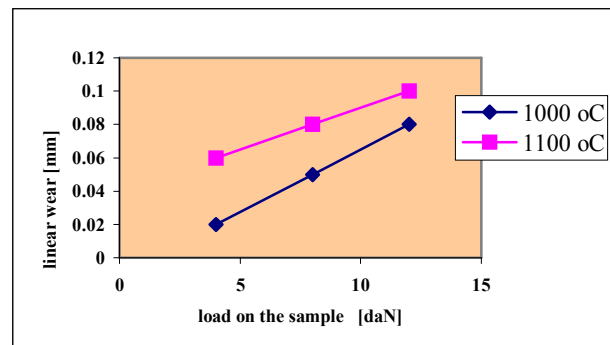


Fig.3 The variation of the linear wear at relative sliding speed  $v = 23\text{m/s}$

In the case of friction materials, the use of lamellar and compact graphite cast iron leads to some phenomena which decrease the wear (Fig3), diminish the deformation during the exploitation and increase the forces and the time of operation at instantaneous braking.

On the surface placed in the friction plane an increased carbon diffusion rate is recorded. The higher wear resistance of the cast iron as compared with steel is put primarily on the account of the microhardness increase brought by the pearlite. At the same time, a change of the ferrite lattice parameters is taking place due to the deformation produced during braking, simultaneously with the lubrication action

induced by the graphite. By analysing the cast iron abrasive wear [1] behaviour, a resistance increase was found along with the pearlite content increase, but nevertheless an important role is played by the graphite separation type (Fig4). Experimentally we found that for this type of application isolated graphite separations are recommended to be obtained.



Fig.4. Compact vermicular graphite separation type near the interface of the bimetallic plate



Fig.5. Quasillamellar graphite separation or star of the bimetallic plate (SEM x 100)

The appearance of the nest type or star type graphite (Fig5) in the cast iron structure accelerates the weight loss during braking. In all circumstances, amount pearlitic increase the  $\langle \mu \rangle$  and the finer it decrease the wear loss. Taking into account the main factors, which determine the thermal, shock resistance, it can be seen that the cast iron containing different graphite shapes presents advantages as well as disadvantages:

- the lamellar graphite cast iron possesses low thermal conductivity and low elastic modulus. This constitutes an advantage for the thermal shock resistance, but has low strength and elongation;

- the nodular graphite cast iron possesses high strength, an advantage for the thermal shock, but possesses low thermal conductivity and a high elastic modulus, a disadvantage for the thermal shock;

- the vermicular graphite cast irons are close to the nodular ones from the point of view of the strength and elongation and are similar to the lamellar graphite ones in what regards the thermal conductivity, which is an advantage for the thermal shock. The scanning electron microscope analysis of the vermicular graphite cast iron (Fig5) evidences the presence of the modifiers, as traces, in the graphite separations areas. At the ends of the graphite, the metal mass presents silicon segregation.

The geometry of the castings can have a great influence on the vermicular graphite characteristics. In the case of the "plate" type samples, as the trapezoidal bimetal part (Fig1). The dimensional characteristics of the graphite separations are essentially the same order of magnitude in the centre and at the surface. For the vermicular graphite cast iron, the graphitising annealing heat treatment leads to the removal of the free cementite and assures a complete ferrite structure. As the graphite compacting degree increases, the appearance of a supplementary porosity can be noticed due to the austenitic transformation.

It can easily be seen in the cast samples examined in the bimetal zone (Fig.6, Fig.7). SEM images show how the quasillamellar and vermicular graphite separations appeared in the whole area occupied by the cast iron, missing only in the interface zones. As compared to the primary structure of cast iron, after the heat treatment a

relative increase of the porosity is observed [2]. The phenomenon accompanying the graphitisation in the cast iron creates a compact graphite separation of about 20-100  $\mu\text{m}$ .



Fig.6 SEM bimetal interface of aircraft plate interface. (SEM x 100)



Fig.7 The diffusion zone of the bi-metallic plates (SEMx100)

The study of the bimetal interface area evidences vermicular graphite separation with an aspect ratio of 1/10. The examined samples are from the steel-cast iron in the contact zones. Using the Philips 515 electron microscope, the analyses evidenced a very good adherence of the two materials, no defect being detected along the joint.

**The sintered metal-ceramic friction materials** represent a complex mixes of metallic and non-metallic powder components. All these components act on the physic-mechanical and the technique-operational properties. Antithetical requirements as wear resistance and simultaneous high coefficient of friction show that sintered friction materials, in difference to materials of the mass powder metallurgy, are very complex in their structure. The sintered metal-ceramic friction materials represent a complex mixes of to nine metallic and non-metallic powder components. All these components act on the physic-mechanical and the technique-operational properties. In generally, the sintered composites friction materials (Fig8) must present the following characteristics: high storing and dissipation capacity of braking energy; high values of the friction coefficient ( $\mu$  0.25-0.50) and high operational stability; high temperature (400-700° C) stability.



Fig.8 Metallo-ceramic aeronautical breaks

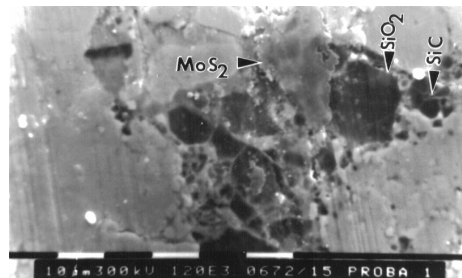


Fig.9 Micrography of the worn surface of the material sintered at 1000°C (SEMx150)

At the end of the tribological test, on the worn surfaces of the two samples a microstructure analysis was made using a SEM. The general aspect presents a heterogeneity material (Fig.9) having a plastically deformed matrix due to the action of the friction cast iron counterpart. The micrographs of the worn surface of the material sintered-presents a non-homogenous material having a plastically deformed matrix due to the action of the friction cast iron counterpart (Fig10).

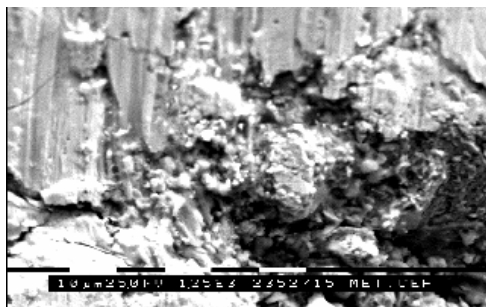


Fig.10 Metallo-ceramic material. Surface texture appearance. (SEM image x 1250)

The knowledge of the sub-critical crack length is a key to estimating for example the temperature dependence of the fracture toughness of materials. This allows us to understand that the mechanism of fracture change that is dependent not only on the condition of loading but also on crack growth when condition of the crack propagation.

The SEM is a very useful technique for their microstructural characterisation of metallo-ceramic materials: defects heterogeneity or bubbles. The general aspect presents a heterogeneity material having a plastically deformed matrix due to the action of the friction cast iron counterpart. Fig11 presents the micrographs of the worn surfaces of the material sintered at 1100°C .

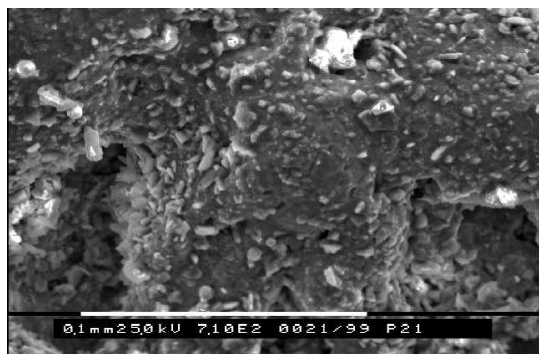


Fig11.Pore structure on material sintered (SEM x 1250)

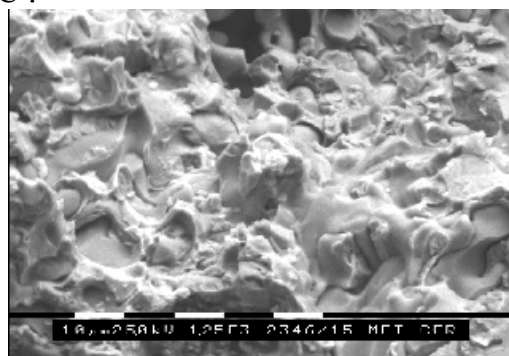


Fig12. Metallo-ceramic material homogeneity. (SEMx1250)

During liquid phase sintering a liquid phase coexists with a particulate solid at the sintering temperature. The liquid phase usually enhances the rate of interparticle bonding during sintering. Nevertheless the factors, which cannot be completely eliminated, are the microscopic level non-uniformity of this type material [3]. The physic-mechanical characteristics of the metallic matrix are strongly influenced by the structure (Fig11), achieved by this one during the sintering. Higher sintering temperatures make possible the embedding of greater quantities of mineral admixtures and dry lubricants. Defects in metallo-ceramic materials are numerous and existing a large experience. SEM/EDX allows a better determination of the defects tips: liquid-liquid immiscibility or phase separation. SEM- secondary electron images contain backscattered electron information show a difference of contrast between the components. This indicates a diffusion of heavy elements, especially iron, toward the crystallisation front, a diffusion which in fact promotes the nonomogeneity bulk. At the same time the microstructure of the main crystalline phase develops and produces a components leading to spherulitic crystallisation Fig.12.

#### 4. CONCLUSIONS:

This article shows how a comprehensive qualitative approach to quality evaluation of products used in the aerospace industry about electron microscopy. Structural analysis allows us to study such different tribological couple materials.

SEM fractography has been recognized as the most suitable analytical method not only to describe the structure of the fracture surface but to ascertain how the material had withstood mechanical and tribological tests. It is difficult to confine structural studies to one single method and it is necessary also to obtain quantitative parameters.

The results obtained proved that the materials thus investigated can ensure safe couple friction properties at speeds in excess of 23 m/s as well as an improved wear resistance potential.

*Received April 19, 2005*

METAV-C&D S.A., Bucharest

\* S.C.INCAS Research Aeronautical Institute, Bucharest

#### REFERENCES

- /1/. Buzaianu, A., Manoliu, V., *Bimetallic Materials for Special Application*; Materials Week European Congress on Advanced Materials, Processes and Applications", Munchen 2002
- /2/. Kwon S.J., Goo, B.C., *A study of friction and Wear Characteristic of brake Pads for Al MMC Disc*, Fracture and Strength of Solids, Vol.183, 2000, 1225-1230;
- /3/. Alov, N.V., Oskolokstad, K.V., *Surface Morphology Characterization using TXRF and SEM*, European Microscopy and Analysis, 81,5-7, 2003.

#### PRODUSE DE ÎNALTĂ CALITATE UTILIZATE ÎN INDUSTRIA AEROSPAȚIALĂ

**Rezumat:** Lucrarea face referire la cercetările autorilor privind realizarea frânelor pentru aeronave. Se explică o nouă strategie privind materialele utilizate în scopul amintit.

## CONTRIBUTIONS CONCERNING WAYS OF OBTAINING FERROFLUIDS

BY

DORU CĂLĂRAȘU

**Abstract.** *A good knowledge of the magnetic phenomena and properties of the systems of the magnetic particles utilized in the production of ferrofluids contribute essentially to the understanding of these special materials. The ferrofluids that contain magnetite are very spread and they are used to make ferrofluids on the basis of petrol, oils, kerosene, water, etc. and having a diversity of applications. That is why the study of the magnetite particles is well justified. The studies made on ferrofluids emphasized fluid-mechanical phenomena that lead to new solutions for problems of science and technology. Properties specific to magnetic fluids extend the area of their use in various applications for which conventional technical solutions are obsolete.*

**Keywords** *magnetic fluid, electro-hydraulic, magnetic property*

### 1. INTRODUCTION

Ferrofluids (magnetic liquids) are dispersions of subdomain magnetic particles in a basic liquid. Each colloidal particle in a magnetic fluid is a small permanent magnet that tends to align towards the magnetic field. Supposing that the particles are small, about 100 Å, the molecular thermal moving prevents their depositing. Besides, the particles are wrapped in order to prevent their magnetic interaction. Ferrofluids are perfectly soft from a magnetic point of view and they are nonmagnetic in the absence of an applied magnetic field. They show a magnetizing of saturation in the intense magnetic fields, without presenting a magnetic hysteresis. The viscosity of the magnetic fluids in the absence of the applied magnetic fields shows an ideal Newtonian behaviour without depending on the viscosity of the speed gradient. In a uniform magnetic field the viscosity tends to be non Newtonian.

The quality of the ferrofluids is dictated by the properties of the utilized colloids. This quality can be substantially improved if we choose a stabilizer that corresponds to the properties of the particles and the basic liquids. As a result, a good knowledge of the magnetic phenomena and properties of the systems of the magnetic particles utilized in the production of ferrofluids contribute essentially to the understanding of these special materials. The ferrofluids that contain magnetite are very spread and they are used to make ferrofluids on the basis of petrol, oils, kerosene, water, etc. and having a diversity of applications. That is why the study of the magnetite particles is well justified.

### 2. METHODS OF GETTING MAGNETIC COLLOIDS AND FERROFLUIDS

As a rule, any conductor or non-conductor liquid may constitute the base of a magnetic liquid. The stability of a magnetic liquid is assured by the reduced dimension

of the magnetizable particles ( $\text{Fe}_3\text{O}_4$ ,  $\gamma\text{-Fe}_2\text{O}_3$ , etc.) dispersed in a basic liquid, as the Brownian motion puts up resistance to the tendency of the particles to agglomerate and deposit.

In these conditions, the stability of the magnetic liquids is maintained through steric stabilization in organic media, electrostatic in watery media or through braking the development of particle germs in various alloys (e. g. mercury).

Papell in 1965 noticed that he could suspend between the poles of an electromagnet a colloidal suspension of magnetite stabilized with oleic acid and obtained an apparently continuous liquid with magnetic actions. J. L. Neuringer and R. E. Rosensweig called these colloids “ferrofluids”, a name that expresses the combination of magnetic properties.

As most solid magnetic inorganic substances are insoluble in common liquids and do not dissolve easily, coupling magnetic particles with the liquid phase is achieved by adding some adequate stabilization agents.

A typical compound of such a substance is the oleic acid,  $\text{C}_{17}\text{H}_{33}\text{-COOH}$ .

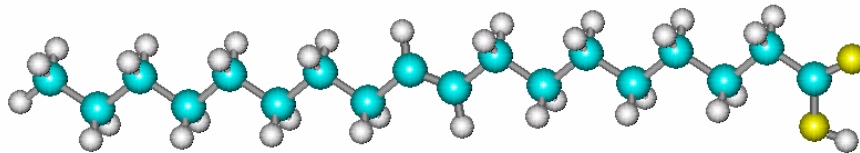


Fig.1 Oleic acid structure ( $\text{C}_{17}\text{H}_{33}\text{-COOH}$ )

The molecules of this acid contain the final polar group ( $-\text{COOH}$ ), which is absorbed by the surface of the particles and a part of the hydrocarbon which is similar to the medium of dispersion and so it can dissolve in this.

As concerns the very small particles, the cover of the stabilization agent is responsible for the suspension stability. In a well-prepared ferrofluid, the diameter of the particles is big enough.

In condition of knocking two particles, at a minimum distance of separation of  $2\delta$  between the surfaces, the thermal moving energy is bigger than the energy associated to London forces and the magnetic forces of interrelation between the particles.

If this fact is not realised, the forces among particles drive quickly to the agglomeration of the particles and to the separation of the solid phase.

For a ferrofluid the medium diameter  $D$  of the particles is always less than  $150\text{Å}$ , and the relation  $\delta/D$  is bigger than 0,2.

According to the base liquid nature and the dispersed magnetizable particles, there have been elaborated numerous methods that may help to prepare magnetic liquids, methods that have names associated to the way of obtaining fine magnetizable particles.

Mechanic dispersion method Stephen Papell prepared for the first time magnetic liquids by a mechanic method. He used a mixture made up of magnetizable powder, a basic liquid and a stabilizing agent, introduced in a ball-vibration grinder for over 1000 hours. After mixture centrifuging, Papell obtained a magnetic liquid with a density and a viscosity little different from the basic liquid and with strong magnetic properties.

S.E. Khalafalla and G.W. Reimers, to reduce the necessary grinding time, use adequate magnetic precursors. The magnetic liquid obtained by this method may be again concentrated by basis evaporation.

Electro-condensation method. The electro-condensation method is used by G. Bredig for obtaining colloidal suspensions. In a vessel filled with water, there are two Ag electrodes between which there is the powder of a metal that is dispersed. When firing the electric arch, vapours of metallic powders develop around the electrodes. In contact with the dispersion environment the temperature of which is low, vapours get condensed, forming very fine dispersed particles. These particles are dispersed and stabilized by using an adequate dispersant – stabilizing agent, obtaining a stable colloidal suspension. Using this dispersion method, Co, Fe, Ni could be dispersed in a series of alcohol, carbohydrate, polar and non-polar dispersion environments.

Method of electrodepositing. This method distinguished itself by the easiness of changing the physical-chemical and technological parameters of magnetic liquids. To obtain the fine magnetic particles of Fe-Ni, an electrolyte that contains Fe sulphate and Ni sulphate or a mixture of ammonium citrate and nickel may be used. By changing the quantities of ammonium citrate, particle composition may be premeditated.

Method of thermal decomposition This method was proposed by Thomas and his collaborators in 1965. Based on this method, metallic dispersions are prepared by the thermal decomposition of an organic-metallic compound in the presence of an inert solvent and of a polymer. Hees and Parker made a thorough study of this method. Magnetic liquids based on Fe or Ni have been obtained.

### 3. METHOD OF CHEMICAL PRECIPITATION WITH ULTRASONIC STABILIZATION

The method consists in precipitating the magnetite from bi-and trivalent iron salts, under the action of the hydroxide sodium or ammonium in excess.

We present the method by which magnetic liquids were obtained in the laboratory by this method. In glass bottles, the following solutions are prepared: 10.8 g  $\text{FeCl}_3 \cdot x \cdot 6\text{H}_2\text{O}$  in 300 ml distilled water and 5.6 g  $\text{FeSO}_4 \cdot x \cdot 7\text{H}_2\text{O}$  in 300 ml water are prepared. They are heated to 60° C, mixed and stirred forcefully, after which a solution of 10 g NaCl in 100 ml water is added at a constant flow. A black precipitate of magnetite amounting to about 4.6 g is deposited.



Fig.2 Obtained magnetite precipitate

The precipitate is then decanted, separated and washed with distilled water to remove any sodium salts. The washing is repeated with acetone until any trace of water is removed.

The obtained paste is washed with toluene so that the acetone is removed. In order to accelerate the process, there have been used ultrasounds that succeeded in breaking the clusters and a better cleaning of the particles. After that there has been added 2 ml of oleic acid and the mixture was warmed until 90-100°C to remove the toluene. The obtained paste together with 100 ml of kerosene was introduced in an ultrasound bath. In about half of hour we obtained a stable ferrofluid, the precipitated quantity being under 5%.

Subsequently, the liquid can be diluted by adding a base liquid or by removing

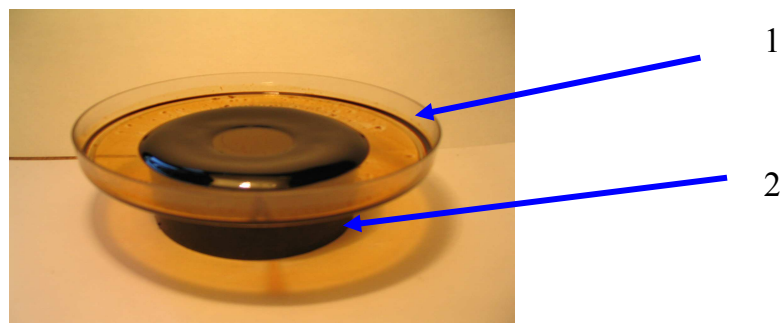


Fig.3 Ferrofluid in magnetic field; 1- a box with ferrofluid; 2- a permanent magnet

this (by evaporating). In this way, you can prepare magnetic liquids on different bases, and structures, according to the domain of utilization. By using ultrasounds you can obtain both a more efficient washing and a more rapid homogenization. The particles are presented from clustering and in this way they are more rapidly wrapped in the stabilizer agents. This method reduces substantially the time of preparation.

#### 4. CONCLUSIONS

- Methods and recipes of obtaining magnetic colloids and ferro-fluids are presented.
- A solution to obtain ferro-fluids by the method of chemical precipitation that reduces substantially the obtaining time is proposed.
- Colloidal magnetic particles were obtained from magnetite, perfectly soft from a magnetic perspective.
- By these particles, a ferro-fluid was prepared on kerosene basis.

Received April 26, 2005

Technical University "Gh.Asachi" Iasi

#### REFERENCES

- /1/. Luca. E. s.a.: *Ferrofluids and their Industrial Applications*, (in Romanian), Technical Publishing House, Bucharest, (1978).
- /2/. Bertotti G.: *Hysteresis in Magnetism*, Academic Press Inc. 1998 Science and Technology **63** (2003), p. 1105-1111.
- /3/. Odenbach S. *Ferrofluids - Magnetically Controlled Suspensions*, Colloids and Surfaces, A Physicochem Eng. Aspects, **217** (2003), p. 171-178.
- /4/. Călărașu D., Cotae C., Olaru R.: *Magnetic Fluid Brake*, Journal of Magnetism and Magnetic Materials, ELSEVIER SCIENCE, **201** (1999), p. 401-403.
- /5/. Cotae C., Baltag O., Olaru R., Călărașu D., Constandache D.: *The Study of a Magnetic Fluid Based Sensor*, Journal of Magnetism and Magnetic Materials, ELSEVIER SCIENCE, **201** (1999), p. 394-397.
- /6/. Olaru R., Sălceanu A., Călărașu D., Cotae C.: *Magnetic Fluid Actuator*, Sensors and Actuators, ELSEVIER SCIENCE, **81** (2000), p. 290-293.
- /7/. Călărașu D., Scurtu D.: *The Influence of the Exterior Magnetic Field on the Laminar Energy of the Magnetic Fields*, Meridian Engineering, U.T.M. Moldova Republic, (2002)

#### CONTRIBUTII PRIVIND POSIBILITATI DE OBTINERE A FEROFUIDELOR

**Rezumat:** O cunoaștere a fenomenelor și proprietăților magnetice ale sistemelor de particule *magnetice* utilizate la producerea ferrofluidelor contribuie în mod esențial la înțelegerea acestor materiale speciale. Ferrofluidele ce au în componență magnetita sunt unele din cele mai răspândite, realizându-se ferrofluide pe bază de petrol, uleiuri, cherosen, apă etc., cu aplicații diverse, de aceea studiul particulelor din magnetită este pe deplin justificat. Studiile făcute asupra ferrofluidelor evidentiază fenomene fluidomecanice care conduc la noi soluții în știința și tehnologie. Proprietățile specifice extind aria de utilizare a lor în diverse aplicații pentru care soluțiile convenționale sunt depășite.

## EXPERIMENTAL RESEARCHES ON THE MAGNETIC PROPERTIES SPECIFIC TO THE $\text{Fe}_3\text{O}_4$ PARTICLES

BY

DORU CĂLĂRAȘU

**Abstract.** *In order to describe the magnetic properties of the particles, there have been traced, by the help of a VSM magnetometer, calibrated with Ni, the hysteresis cycles for the magnetite nanoparticles obtained by the method of the chemical precipitation.*

**Keywords:** *magnetic fluid, electro-hydraulic, magnetic property*

### 1. VIBRATING SAMPLE MAGNETOMETER

The principle that lies at the basis of the magnetometer is that of the electromagnetic induction. The variation of the magnetic field through a helix produces the appearance of an electro-motor tension at its terminals. The sample, whose remanence magnetization has to be measured, is moved into a direction parallel with the coil axes.

There appears an electro-motor tension at its terminals. The amplitude of the tension is directly proportional with the magnetization of the sample.

The vibrations are transmitted by the help of the sample rod that is placed in a system of detection field coils. The electro-motor tension induced at the terminals of the detection field coil system is applied to the lock-in amplifier. This one has a maximum sensitivity of  $2 \times 10^{-12}$  V.

Its value is displayed through the amplification and synchronic detection.

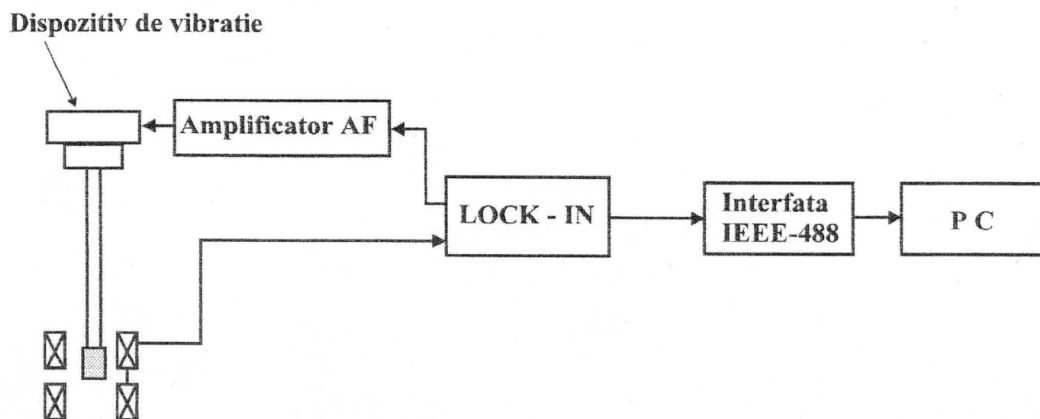


Fig. 1 The block scheme of the vibrating sample magnetometer

The lock-in amplifier is also equipped with an IEEE -488 interface that is connected to a PC. In this way there have been obtained and stored all the data. The analogue/numerical conversion of the signal to be measured is done on 16 bits with a sampling frequency of 256 kHz.

The detection coils constituted in pairs, are placed in front.

In accordance with the number of paired detection field coils and the orientation of these axes in space, the magnetometer can measure the components of the magnetic moment of the sample on one up to three axes.

To trace the magnetization curves, the vibrating magnetometer is used in combination with an electromagnet used to produce the continuous magnetic field and a Hall electrical sounder gaussmeter in order to measure the field (*Fig. 2*).

The sample and the detection field coils are placed between the polar pieces of an electromagnet supplied by a continuous current source that can be adjustably ordered.

The calculator transmits, by the help of a parallel circuit, to an 11 bits analogue digital convertor, the dimension of the current that has to be delivered by the source through the coils of the electromagnet. The source utilized is of a GE20024L type.

The magnetic field produced by the electromagnet is measured by the help of a gaussmeter with a Hall electrical sounder of VGM01 type.

The signal induced by the sample in the detector field coils is measured by the help of the lock-in amplifier and it is transmitted through one interface of the calculator. The measured value of the field, together with the value of the signal induced in the detection field coils, are graphically displayed and stored in a data folder.

In order to obtain a better precision of each value of the applied field there have been made 5 measurements of the sample magnetization. The final result is the arithmetical mean of the 5 results.

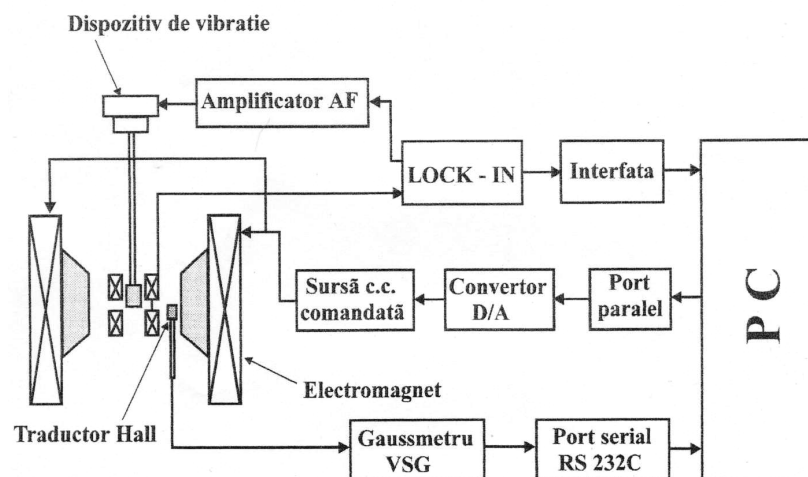


Fig. 2 The block scheme of the measurement device in which it is utilized a VSM magnetometer

You can see the magnetization curves for silicon, the magnetite powders dispersed in silicon and the pressed magnetite powders.

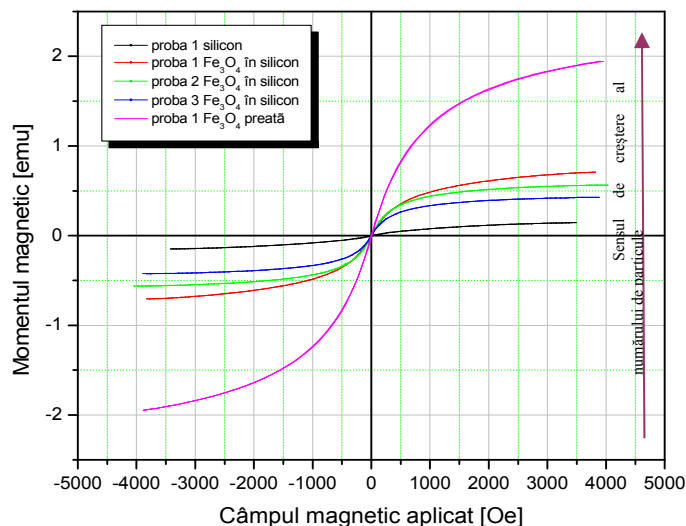


Fig. 3 Magnetization curves of the studied samples

As you can notice from the picture, the systems of particles don't show a magnetic hysteresis. The aspect of the curves shows a conduct of a supermagnetic type. For such a conduct you can calculate the maximum diameter of the particles.

So if you know the nature of the particles ( $\text{Fe}_3\text{O}_4$ ), the anisotropic energy has to be equal with the thermic energy:

$$KV_c = kT \quad (1)$$

in which  $K$  is the density of the anisotropic energy;  $k$  – Boltzman constant;  $T$  – the temperature of the sample;  $V_c$  – the critical volume under which we have a supermagnetic conduct. Thus, for the critical volume we have the following expression:

$$V_c = \frac{kT}{K} \quad (2)$$

Knowing that  $T = 300$  K and  $K = 10^4$  J/m<sup>3</sup>, we obtain, for the critical volume, the value:

$$V_c = 4,143 \cdot 10^{-25} \text{ m}^3 \quad (3)$$

If we admit that the shape of the particles is spherical, you can calculate the maximum diameter of the systems of particles.

$$V_c = \frac{4\pi \left(\frac{d_c}{2}\right)^3}{3} \quad (4)$$

The result is the critical diameter  $d_c = 9,25 \cdot 10^{-9} \text{ m}$ , so that the diameter of the particles has to be smaller than  $d_c$ .

If we take into consideration the volume of a particle equal to  $V_c$ , the number of particles in the volume submitted to magnetization can be determined from the magnetization curves.

Using the powders in an analogous way, there have been obtained ferro-fluids on the kerosene basis, through the chemical precipitation method with an ultrasonic stabilization.

## 2. CONCLUSIONS

There have been presented methods and detailed recipes used to obtain magnetic colloids and implicitly, the ferro-fluids.

It is proposed a solution to obtain ferro-fluids through the method of chemical precipitation, respectively “*chemical precipitation method with an ultrasonic stabilization*”, that reduces substantially the time necessary to obtain ferro-fluids.

There have been obtained colloidal magnetic particles of magnetite, perfectly soft from a magnetic point of view.

There have been presented the magnetization curves for silicon, magnetite powders dispersed in silicon and powders of pressed magnetite.

There has been prepared a ferro-fluid on kerosene basis.

Received April 26, 2005

Technical University “Gh.Asachi” Iasi

## REFERENCES

- /1/. Luca. E, s.a.: *Ferrofluids and their Industrial Applications*, (in Romanian), Technical Publishing House, Bucharest, (1978).
- /2/. Bertotti G.: *Hysteresis in Magnetism*, Academic Press Inc. 1998 Science and Technology **63** (2003), p. 1105-1111.
- /3/. Odenbach S. *Ferrofluids - Magnetically Controlled Suspensions*, Colloids and Surfaces, A Physicochem Eng. Aspects, **217** (2003), p. 171-178.
- /4/. Călărașu D., Cotae C., Olaru R.: *Magnetic Fluid Brake*, Journal of Magnetism and Magnetic Materials, ELSEVIER SCIENCE, **201** (1999), p. 401-403.
- /5/. Cotae C., Baltag O., Olaru R., Călărașu D., Constandache D.: *The Study of a Magnetic Fluid Based Sensor*, Journal of Magnetism and Magnetic Materials, ELSEVIER SCIENCE, **201** (1999), p. 394-397.
- /6/. Olaru R., Sălceanu A., Călărașu D., Cotae C.: *Magnetic Fluid Actuator*, Sensors and Actuators, ELSEVIER SCIENCE, **81** (2000), p. 290-293.
- /7/. Călărașu D., Scurtu D.: *The Influence of the Exterior Magnetic Field on the Laminar Energy of the Magnetic Fields*, Meridian Engineering, U.T.M. Moldova Republic, (2002)

## DETERMINAREA EXPERIMENTALĂ A UNOR MĂRIMI MAGNETICE CARACTERISTICE SISTEMELOR DE PARTICULE DIN $FE_3O_4$

**Rezumat:** Pentru o descriere a proprietăților magnetice a particulelor s-au trasat, cu ajutorul unui magnetometru de tip VSM, calibrat cu Ni, ciclurile de histerezis pentru nanoparticulele de magnetită obținute prin metoda precipitării chimice..

## TENSILE BEHAVIOUR OF A P355NL1 WELDED JOINT

BY

DORU CANTEMIR<sup>a,b</sup>, LEONARDO BERTINI<sup>b</sup>, MARCO BEGHINI<sup>b</sup>, MASSIMILIANO  
PAGLIARO<sup>c</sup> and OCTAVIAN CIOBANU<sup>d</sup>

**Abstract.** Carbon steel for pressure vessels P355NL1 is commonly used in fabrication of welded components for heat transfer equipment. Its temperature dependent properties have to be known in order to compute residual stress and distortion due to the welding process, by finite element method (FEM). To determine its mechanical properties, a series of hot tensile tests have been conducted for both, weld metal and base metal, using a Gleeble 3800 thermomechanical simulator. The tests and some results (yield strength, tensile strength, true fracture stress and reduction of area for various temperatures and on two material directions) are presented and discussed in this paper. The anisotropy of both, weld metal and base metal is evaluated, as well as the effect of welding on material properties.

**Keywords:** P355NL1 steel, hot tensile test, welding, temperature dependent mechanical properties, Gleeble 3800, material anisotropy

### 1. INTRODUCTION

Finite element simulation is a powerful method for computing residual stress and distortion due to welding [1, 2]. The prediction accuracy is considerably affected by material data employed, which must be considered as functions of temperature [3]. Unfortunately, for most of engineering materials, it is virtually impossible to find in literature or in commercially available databases their properties in the entire temperature range of interest.

In the frame of a study carried out at the Department of Mechanical, Nuclear and Production Engineering (DIMNP) of Pisa University, a welding experiment was conducted [4, 5]. Two plates were but-welded by manual shielded metal-arc welding with a heat input of about 0.75 kJ/mm, a preheating temperature of 250 °C and the maximum inter-pass temperature of 300 °C. A local post-weld heat treatment (PWHT) was performed, at 610 °C. After completion, a number of specimens were extracted from both, base metal (BM) and weld metal (WM) and tensile tested at various temperatures.

In this paper, the hot tensile tests are presented and some results are analyzed in order to evaluate the material anisotropy and the effects of welding on the mechanical properties. The characteristics considered are yield strength, tensile strength, true fracture stress and reduction of area. Their evolutions as function of temperature are plotted and compared for two material zones (WM and BM), on two perpendicular directions. For the third zone resulted after welding, the heat affected zone (HAZ), the quantity of material is too small to permit a proper tensile specimen extraction. A solution is to conduct welding simulations using Gleeble thermomechanical

simulator in order to obtain a specimen characteristic for the HAZ. However, in the present work the HAZ properties aren't investigated.

## 2. EXPERIMENTAL PROCEDURE

The material under study is hot rolled P355NL1 (according to EN-10028-3:92 specifications) carbon steel for pressure vessels, with the chemical composition shown in Table 1. It is commonly used in fabrication of welded components for heat exchangers and other equipments working under pressure.

Table 1 Chemical composition of P355NL1 steel (wt. %)

C	Si	Mn	P	S	Al	Cr	Cu	Mo	N	Nb	Ni	Ti	Fe
0.138	0.48	1.55	0.011	0.0004	0.041	0.032	0.016	0.009	0.0058	0.027	0.039	0.002	bal.

A number of 44 specimens with the geometry presented in Fig. 1 were extracted from the welded plates, according to Table 2. For the case of but-welded plates the welding process can be considered reasonable uniform, starting at a distance equal to plate thickness. In consequence, the specimens in the weld longitudinal direction (type B) were extracted at a distance from borders greater than the plate thickness, in order to avoid the welding start/end effects. In the case of specimens transversal to weld line (type A) the entire reduced section consists from weld metal. The specimens C and D were extracted from a zone of the base metal non-affected by PWHT.

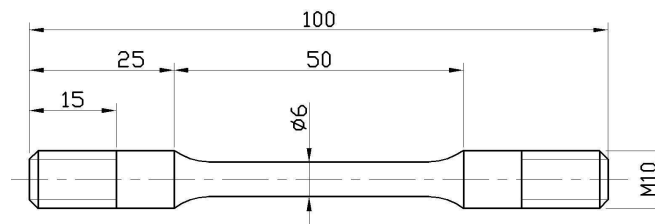


Fig. 1 Schematic drawing of tensile specimen

Table 2 Tensile specimens extraction

Specimen	Zone	Direction	Quantity
A	WM	transversal to weld line	15
B	WM	welding direction	7
C	BM	rolling direction	15
D	BM	transversal to rolling direction	7

Hot tensile tests have been conducted using Gleeble 3800, a state-of-the-art machine for dynamic thermal-mechanical testing of materials and physical simulation of processes. With its high-speed closed-loop heating system coupled with closed-loop mechanical systems, digitally controlled using appropriate software and digital signal processors, Gleeble is an excellent choice for these kind of tests. Its software is designed to prepare test programs, to provide digital closed-loop control of the thermal and mechanical systems and to collect data.

The specimens have been tested at temperatures ranging from 20°C to 1200°C, according to Table 3, where “x” indicates that a test was performed. Vacuum atmosphere about  $10^{-2}$  torr was maintained in the chamber to prevent oxidation of the

specimen and to minimize the heat convection which can cause a radial thermal gradient due to surface cooling [6].

Table 3 Hot tensile tests conducted and test temperatures

Test temperature (°C)	Specimen type			
	A	B	C	D
20	x	x	x	x
100	x		x	
200	x	x	x	x
300	x		x	
400	x	x	x	x
500	x		x	
600	x	x	x	x
700	x		x	
800	x	x	x	x
900	x		x	
1000	x	x	x	x
1100	x		x	
1200	x	x	x	x

The imposed testing cycle is schematized in Fig. 2. Specimens are heated up to testing temperature with a rate of 1°C/s, by direct resistance (Joule effect). Thanks to the high speed heating method of Gleeble system, the soak period needed to get uniform temperature in specimen calibrating zone is very short. A soak time of 1 minute was considered enough for the present tests, based on previous experience and measurements. This is much less with respect to the time needed when the specimen is heated using a furnace – not less than 20 minutes, according to ASTM standards [7]. After the soak period, specimens were tensile tested with a strain rate of 0.1 mm/s. Data acquisition frequency was 200 Hz.

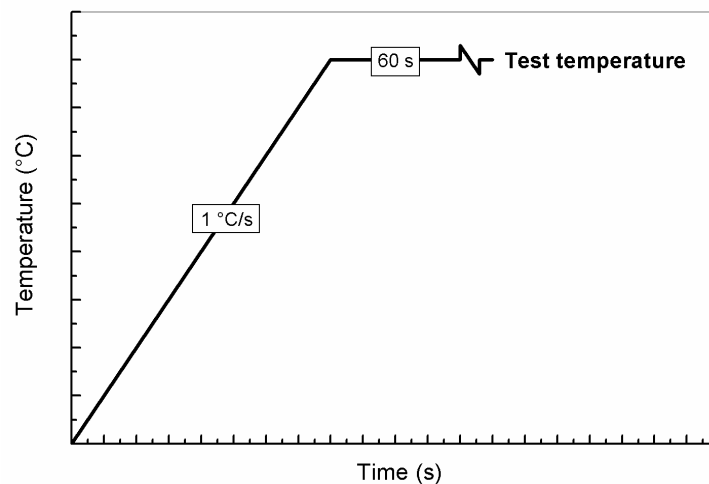


Fig. 2 Schematic of testing cycle

A thermocouple welded on the specimen central section was used for measurement and feedback control of specimen temperature. Alumel thermocouples were employed for testing temperatures smaller than 1000 °C, and platinum-rhodium

thermocouples for superior temperatures. The specimen elongation during tests was measured using a LVDT type transducer mounted between machine's jaws. Since the system used for specimen holding is very stiff compared to the stiffness of the specimen, the jaw-to-jaw measurements introduce little error in the elongation measurement. During heating and soak period the specimen was able to freely expand, it being automatically fixed right before the traction start.

The chamber, specimen, lengthwise strain transducer and thermocouple placed are shown in Fig. 3.

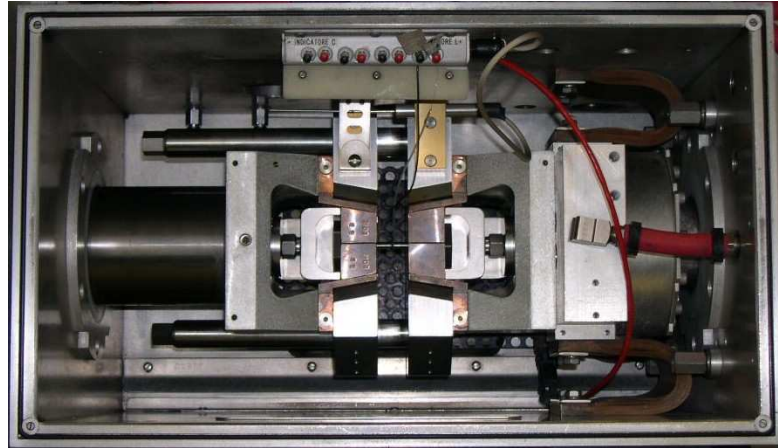


Fig. 3 Gleeble 3800 chamber with specimen gripped ready for testing

### 3. RESULTS AND DISCUSSION

The engineering stress-engineering strain curves, along other parameters, have been recorded by Gleeble in real time. From these curves, the yield strength and tensile strength were determined, according to ASTM standard [8]. The specimen's length and diameter were measured before and after test. Using the maximum load recorded by the machine,  $F_{\max}$ , and the ultimate cross-section area,  $A_u$ , measured on the specimen, the true fracture stress is computed using the relation:

$$\sigma_f = \frac{F_{\max}}{A_u} \quad (1)$$

Reduction of area is calculated using well known equation:

$$RA\% = \frac{A_0 - A_u}{A_0} \cdot 100 \quad (2)$$

where  $A_0$  is the specimen initial cross-section area.

#### 3.1 Material anisotropy

In order to evaluate the anisotropy of BM mechanical properties, the results obtained for the specimens extracted in the rolling direction and in the transversal one (C and D, respectively) are compared in Fig. 4 to Fig. 7.

As could be seen, the tensile strength and yield strength are practically the same in the both directions, while a quite big difference can be noted for the true fracture stress. Because the maximum load,  $F_{\max}$ , is quite similar for both directions, becomes clear that this discrepancy is caused by material ductility variation, visible in Fig. 7.

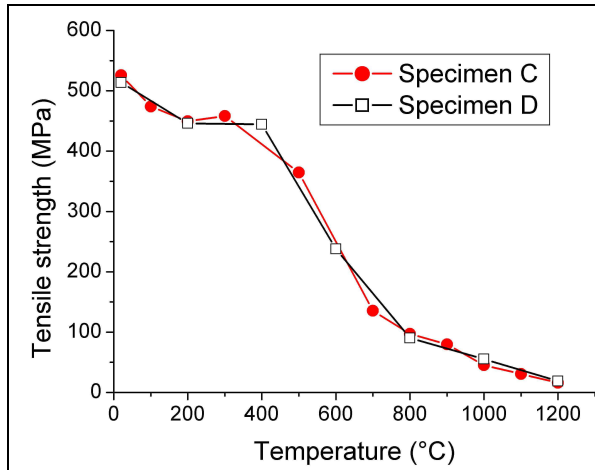


Fig. 4 Tensile strength of BM

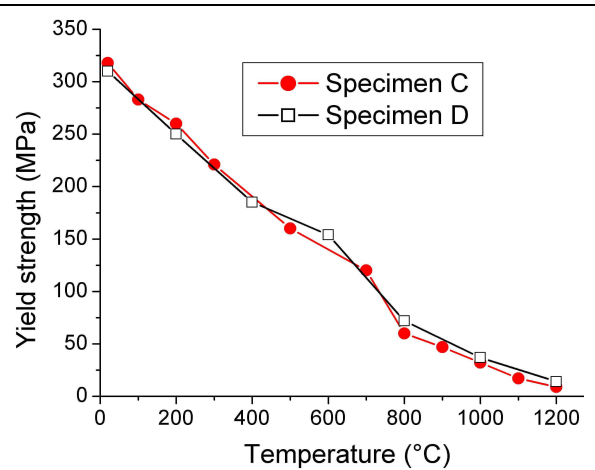


Fig. 5 Yield strength of BM

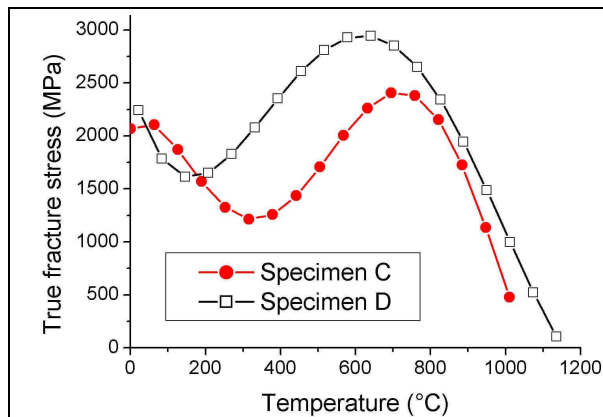


Fig. 6 True fracture stress of BM

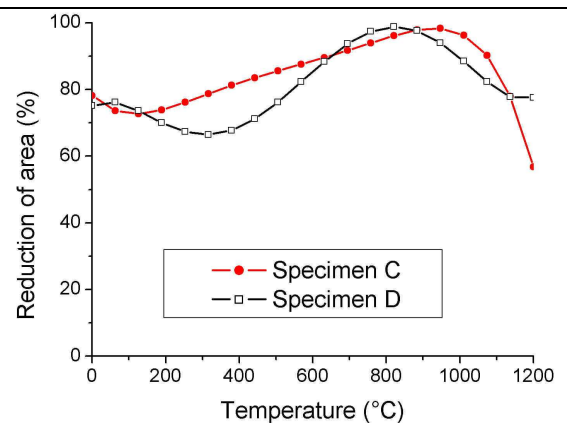


Fig. 7 Hot ductility curve for BM

To assess for WM anisotropy, the results obtained for the specimens extracted on welding direction and in the transversal one (B and A, respectively), are compared in Fig. 8 to Fig. 11. The yield strength is greater in the direction transversal to weld line, as well as the tensile strength (even if in the last case the difference is less visible). Still in this case, the material ductility varies for the two directions and, as a consequence, there is a variation of the true fracture stress.

Using tensile strength and yield strength, BM seems virtually isotropic but, when the true fracture stress is employed, the material anisotropy is obvious. In the case of WM, the material anisotropy is more evident. Considering these facts, seems reasonable to account for material anisotropy in a finite element welding model, by employing appropriate material models.

### 3.2 Welding effects

The welding effects on material's mechanical characteristics can be seen in Fig. 12 to Fig. 15. For temperatures less than 600-800 °C the WM has better yield strength than BM, but at superior temperatures the difference is very small. The same thing, although with little discrepancy, can be noted for the tensile strength variation.

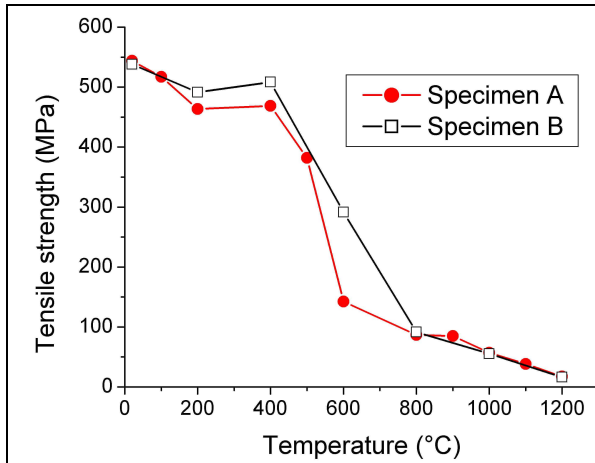


Fig. 8 Tensile strength of WM

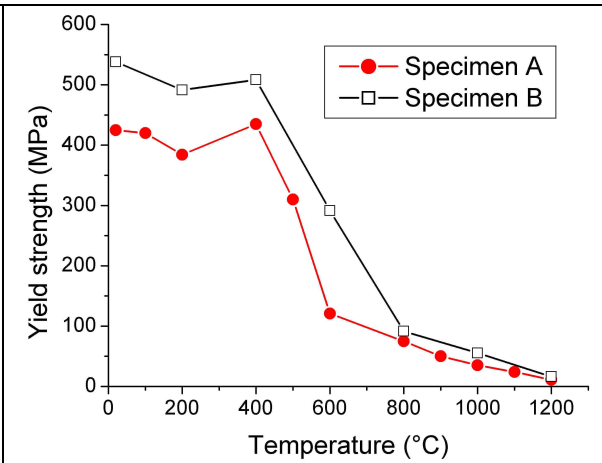


Fig. 9 Yield strength of WM

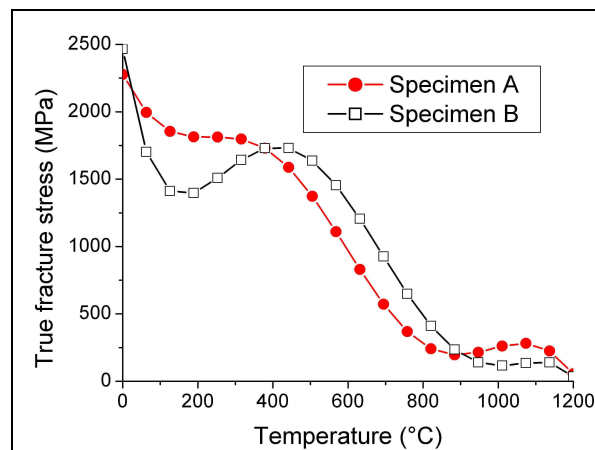


Fig. 10 True fracture stress of WM

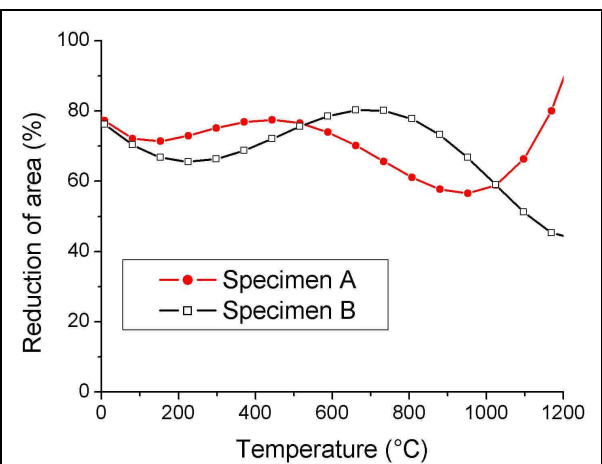


Fig. 11 Hot ductility curve for WM

A big difference can be observed between true fracture stresses of WM and BM (Fig. 14) as well as between reductions of area (Fig. 15). Because the finite element codes use the true stress-true strain curves for material data input, this variability of true fracture stress is important for welding modeling applications. Consequently, seems that in a finite element welding simulation one should use at least two different material models: one for BM and the other for WM. However, this is not the case for the majority of published work [1, 2]. A more in depth study is currently carried out in order to evaluate the influence of material parameters on the welding simulations results and is hoped that it will allow us to state a final conclusion regarding the opportunity of including WM material model, as well as the anisotropy of material properties.

#### 4. CONCLUSIONS

Hot tensile tests have been conducted on P355NL1 steel specimens, at temperatures ranging from 20°C to 1200°C. A comparison between BM and WM properties is done, as well as the estimation of mechanical properties anisotropy.

True fracture stress is proved to be a more sensitive parameter with respect to tensile strength and yield strength, showing clearer the material anisotropy.

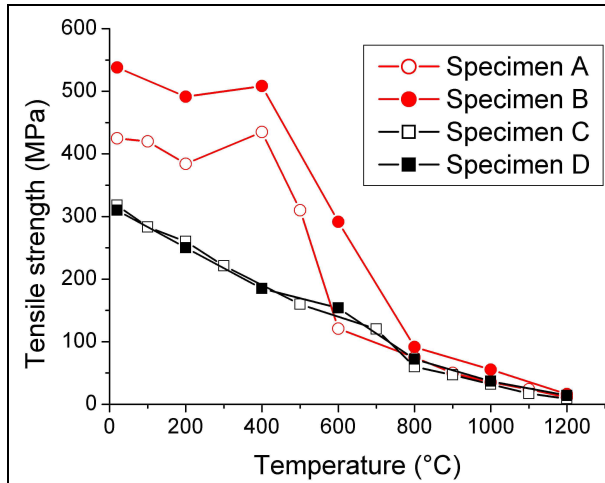


Fig. 12 Yield strength of WM and BM

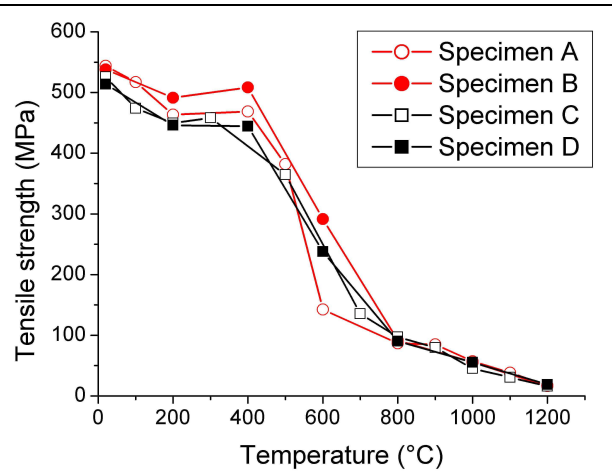


Fig. 13 Tensile strength of WM and BM

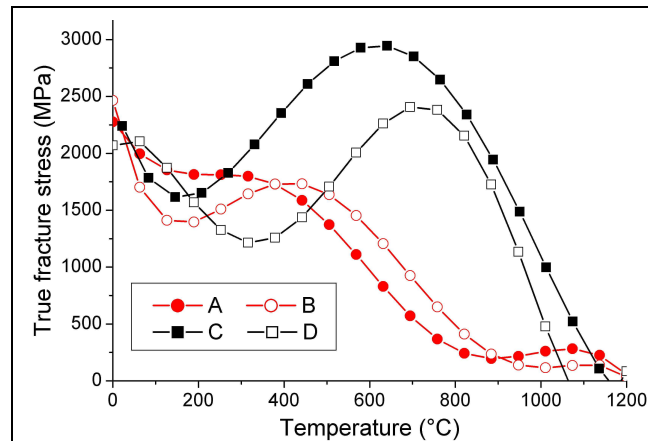


Fig. 14 True fracture stress for BM and WM

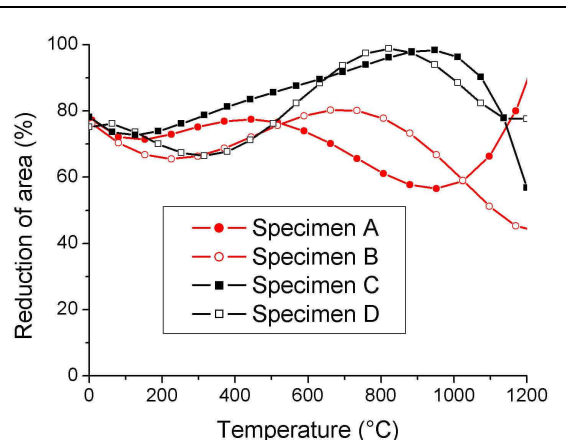


Fig. 15 Hot ductility curve for WM and BM

As expected, the WM properties are very different from BM properties. Consequently, this fact should be accounted for in a finite element welding model, as well as the anisotropy of both, WM and BM.

### Acknowledgements

We gratefully acknowledge specimens provided by GE Oil & Gas Nuovo Pignone, Massa, Italy. We thank Fabio Garelli for support in tests implementation. D. Cantemir acknowledges his Ph.D. grant from the University of Pisa, Italy.

Received April 20, 2005

<sup>a</sup>“Gh.Asachi” Technical University Iasi

<sup>b</sup>University of Pisa, Italy

<sup>c</sup>ILVA-Riva Group, Italy

<sup>d</sup>“Gr. T. Popa” University Iasi

### REFERENCES

/1/. Cantemir, D. - *Finite element modelling and simulation of welding - a state-of-the-art study*, Bul. Inst. Polit. Iasi, t. L(LIV), f. 6B, 2004, ISSN 1011-2855, 97-102

- /2/. Lindgren, L.-E. - *Finite element modelling and simulation of welding. Part 1-3*, J. Thermal Stresses, 24, 2001, 141-192; 195-231; 305-334
- /3/. Beghini, M., Bertini, L., Cantemir, D. - *A finite element procedure for assessment of a large tubesheet holes distortion due to welding*, 15<sup>th</sup> Italian ABAQUS User's Meeting, Bari, Italy, 2004
- /4/. Beghini, M., Bertini, L., Cantemir, D., Barbieri L., Spadaccini, F. - *Simulation of temperature evolution during multipass butt-welding of a large tubesheet*, in Advances in Experimental Mechanics, (C. Pappalettere, ed.), McGraw-Hill, Milano, 2004, ISBN 88 386 6273-8, 650
- /5/. Beghini, M., Bertini, L., Cantemir, D., Barbieri, L., Nicodemi, L., Spadaccini, F. - *Finite element thermal modelling of multipass welding of a perforated plate*, Bul. Inst. Polit. Iasi, t. L(LIV), f. 6B, 2004, ISSN 1011-2855, 91-96
- /6/. Seol, D.J. et al. - *High temperature behavior of carbon steel in the austenite and  $\delta$ -ferrite regions*, ISIJ International, 39, 1, 1999, 91-98
- /7/. ASTM Standard E21-03a, *Standard Test Methods for Elevated Temperature Tension Tests of Metallic Materials*, ASTM International, 2003
- /8/. ASTM Standard E 8m-95a, *Standard Test Methods for Tension Testing of Metallic Materials*, ASTM International, 1995

### COMPORTAMENTUL LA TRACTIUNE AL UNEI IMBINARI SUDATE DIN OTEL P355NL1

**Rezumat:** Otelul carbon pentru recipiente sub presiune P355NL1 este utilizat in mod frecvent in fabricarea reperelor sudate din componenta echipamentelor termice. Cunoasterea variatiei proprietatilor sale in functie de temperatura este esentiala atunci cand se doreste modelarea cu elemente finite a tensiunilor remanente si a deformatiilor rezultate in urma procesului de sudare. In aceasta lucrare sunt prezentate incercarile de tractiune la cald efectuate in vederea determinarii proprietatilor mecanice, atat ale materialului de baza cat si ale cordonului de sudura. Sunt incluse o serie de rezultate si se face o comparatie intre proprietile celor doua tipuri de material. Deasemenea, este evaluata anizotropia proprietatilor mecanice ale materialului de baza si ale sudurii.

## SURFACE HARDENING OVER 38MoCrAl09 STEEL BY YAG:Nd PULSE LASER

BY

NELU CAZACU, SORIN DOBROVICI, OCTAVIAN POTECAȘU, ELENA DRUGESCU,  
ADOLF BĂCLEA, LILIANA SAVA

**Abstract.** *Laser offers unique capabilities for high energy concentrations at small surfaces. Factors that have influences over interactions between laser beam and steel surfaces are very high control. Pulse laser YAG:Nd is usual used for cutting and welding. Paper is based by hardening experiments using KVANT 17 (YAG:Nd). pulse laser over 38MoCrAl09 steel. Results were investigated by hardness (HV5) macrographic and micrographic.*

**Keywords:** *laser, YAG:Nd, hardening, steel*

### 1. INTRODUCTION

Lasers have progressed from a laboratory curiosity to an industrial tool. Most of today's industrial lasers output infrared light in the form of a beam that is converted to heat energy when it interacts with a material being processed. Cutting and welding laser systems use highly focused beams having power densities in excess of  $106\text{W}/\text{cm}^2$  to quickly melt and vaporize metals. Because these two industrial applications total nearly 95% of all laser systems sold, the use of lasers for surface modification often is overlooked, 0. Superficial hardness is obtaining through beam energy distribution with low intensity for superficial heating of surface between melting point. The principal condition for process is energy uniform distribution over metallic material surface. That conduce to a uniform heating layer depth. Heating by power laser is characterized by high heating speed (pulse laser beam) from ambient temperature to austenitic domain. After heating laser beam is stopped (pause time) and heat from superficial layer is transmitted by material diffusivity to adjacent volumes with very high speed and a local quenching is realized. Cooling speed is higher by critical quenching speed that mean an autoquenching process and an exterior quenching media is unnecessary. The heat is loosed by thermal conductivity from heating layer to material core and cooling speed is approaching to  $1000^\circ\text{C}/\text{s}$ . Maximal temperature ( $^\circ\text{C}$ ) in superficial layer is given by relation:

$$T_{\max} = \frac{2F_0\sqrt{at}}{\lambda\sqrt{\pi}} \quad (1)$$

where:  $F_0$  – power density,  $\text{W}/\text{cm}^2$ ,  $a$  – thermal diffusivity,  $\text{cm}^2/\text{s}$ ,  $\lambda$  – thermal conductivity,  $\text{W}/^\circ\text{C}\cdot\text{cm}$ ;  $t$  – time, s. After surface heating by pulse laser is possible to obtaining a martensitic total transformations, but normally a quantity of residual austenite is present in microstructure. A cooling process is preferable to continue under  $0^\circ\text{C}$ .

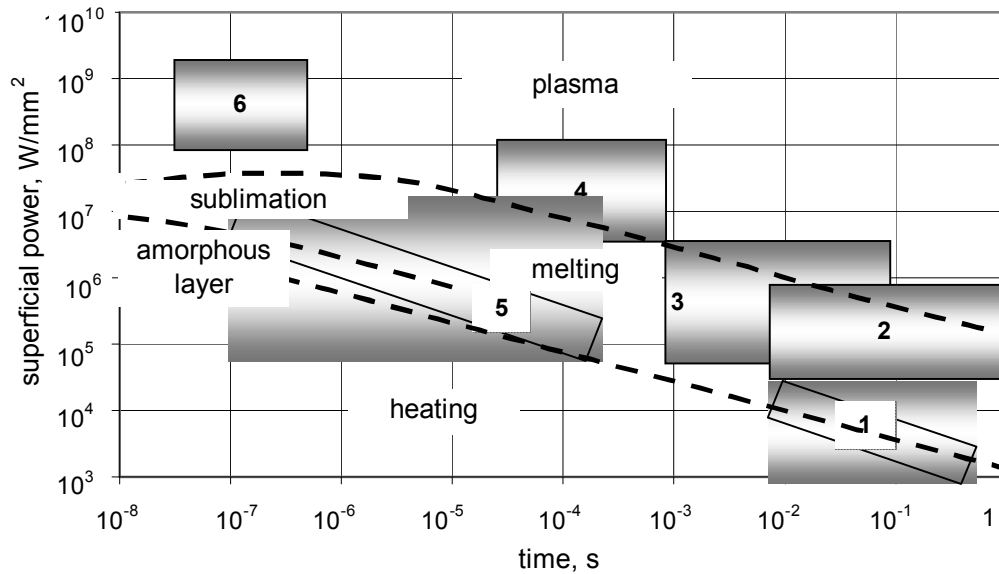


Figura 1. Basic processes and laser thermal applications in function of specific power and irradiation time: 1- superficial hardening, 2- alloying, 3- cutting and welding, 4-drilling, 5-glazing (amorphous layer) and superficial melting, 6- thermal pulse hardening, 0.

Table 1. Relative compare of different lasers used for heat treatments

Laser type	Wave length	Absorption efficiency	Initial cost	Operating cost	Expectede life
	nm				
CO2	10,6	Low	Low	Moderate	High
YAG:Nd	1,06	Moderate/High	High	High	High
HPDD	800	High	Moderate	Low	Low

Note: HPDD- high power direct diode

After surface heating by pulse laser is possible to obtaining a martensitic total transformations, but normally a quantity of residual austenite is present in microstructure. A cooling process is preferable to continue under 0°C. Laser hardening is characterized by:

Laser beam power increasing for a constant speed of part moving conduce to decreasing hardness

Speed and beam power are control factor for depth hardening layer and for incident interaction surface

Hardness obtaining by laser quenching is higher by furnace heating and liquid quenching. Laser hardening are easy optic controlled and depth of quenching layer is uniformly. Hardness is depending by thermal conductivity of material

Superficial hardening by YAG:Nd pulse laser are influenced by: steel hardenability (chemical composition), laser beam energy measured through accumulator supply of optical pumping system (at capacity battery connector), pulse frequency; focalization of laser beam at material surface (defocalisation)

## 2. EXPERIMENTAL CONDITIONS

Pulse laser KVANT 17 (made CIS) has a solid active media by YAG:Nd ( $Y_3Al_5O_{12}$ ). Some important characteristics are: active media dimensions diameter 6,3 mm și length 100 mm; wave length 1,06  $\mu\text{m}$  (IR); pulse time 2...5ms; pulse frequency 1...20 Hz; objective focal length 50 mm; surface diameter of interaction 0,3...1,3mm;

Table 2. Chemical composition for 38MoCrAl09

Steel	Chemical composition								
	C	Mn	P	S	Si	Mo	Cr	Ni	Al
38MoCrAl09	0,410	0,530	0,022	0,011	0,330	0,180	1,350	0,110	0,860

Table 3. Pulse laser (YAG:Nd) hardening experimental regimes

Experiment (sample)	Acumulator supply	Defocalization	Total pulse number	Pulse Frequency	Discharge current	Total time	Hardness HV <sub>5</sub> final
u.m.	V	mm	-	Hz	10 <sup>-6</sup> A	minute	daN/mm <sup>2</sup>
1	550	0	410	0,3	34-58	22	520
2	600	0	430	0,3	34-60	23	425
3	650	0	460	0,3	34-60	25	388
4	700	0	406	0,3	34-60	20	466
5	750	0	411	0,3	40-70	23	477
6	550	2,5	415	0,3	30-48	22	466
7	600	2,5	420	0,3	32-52	23	603
8	650	2,5	430	0,3	36-58	17	435
9	700	2,5	440	0,3	38-64	32	441
10	750	2,5	420	0,3	42-70	20	376
11	550	5	410	0,3	28-48	22	332
12	600	5	365	0,3	30-52	20	473
13	650	5	410	0,3	34-60	25	549
14	700	5	410	0,3	38-64	20	644
15	750	5	410	0,3	40-68	23	460
16	550	7,5	410	0,3	24-46	22	487
17							-
18	600	7,5	466	0,3	30-52	20	412
19	650	7,5	410	0,3	42-64	22	325
20	700	7,5	430	0,3	14-38	21	412
21	750	7,5	436	0,3	38-66	23	376
22	800	7,5	440	0,3	38-66	20	441
23	850	7,5	450	0,3	38-66	22	566
24	900	7,5	460	0,3	38-66	21	540
25	950	7,5	465	0,3	38-70	23	549
26	650	10	406	0,3	38-70	23	283
27	700	10	411	0,3	38-70	23	310
28	750	10	415	0,3	38-70	23	306
29	800	10	420	0,3	38-70	23	391
30	850	10	430	0,3	38-70	23	418
31	850	10	440	0,3	38-76	23	325
32	850	10	420	0,3	38-76	23	401
33	900	10	430	0,3	38-76	23	367
34	950	10	445	0,3	38-76	23	453
c1	800	5	440	0,3	40-76	26	418
c2	850	5	436	0,3	50-82	22	575
c3	900	5	422	0,3	54-88	21	371
c4	950	5	430	0,3	58-96	23	401
35							
36	800	0	410	0,3	44-74	20	603
37	850	0	430	0,3	48-80	22	644
38	900	0	460	0,3	52-86	23	655
39	950	0	406	0,3	52-86	21	-
40	800	2,5	415	0,3	44-76	24	-
41	850	2,5	420	0,3	46-80	20	441
42	900	2,5	430	0,3	50-92	23	353
43	950	2,5	440	0,3	64-100	24	623

pulse energy, min. 8J. For experiments was used 38MoCrAl09 steel with final heat treatments (quenching and tempering). Chemical composition is showing in Table 2. The experimental hardening regimes using YAG:Nd laser are in Table 3. No used additional sample surface painting and no additional cooling system for quenching.

### 3. RESULTS AND DISCUSSION

Hardening surface was investigated macroscopic, micrographic and by surface hardness. In Figure 1 and Figure 2 is showing micrographs with typical surface after laser hardening. A local melting is present and surface craters was formed because a high local energy was concentrated at the material surfaces (Figure 1). A normal surface hardening by laser beam is presented (Figure 2) when oxidizing surfaces appears at interactions surfaces with oxygen because the temperature is in austenitic domain.

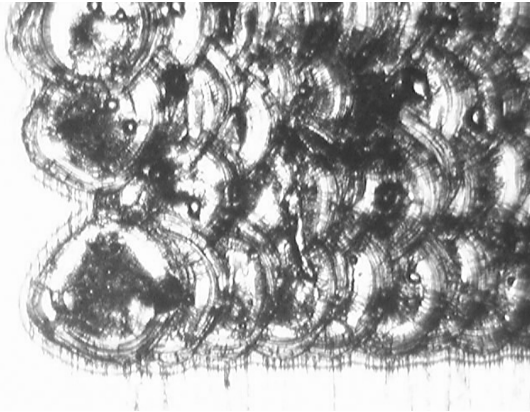


Figure 1. Surface sample 3 (magnitude 350x).

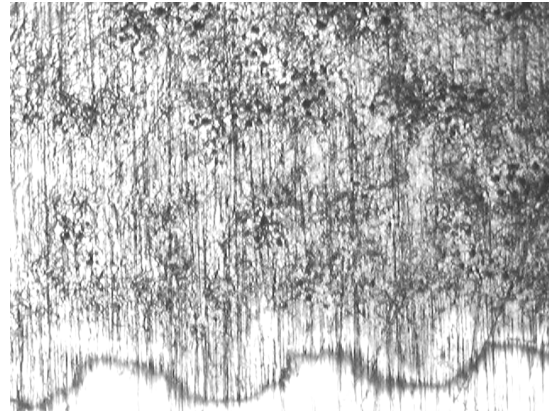


Figure 2. Surface sample 11 (magnitude 350x).

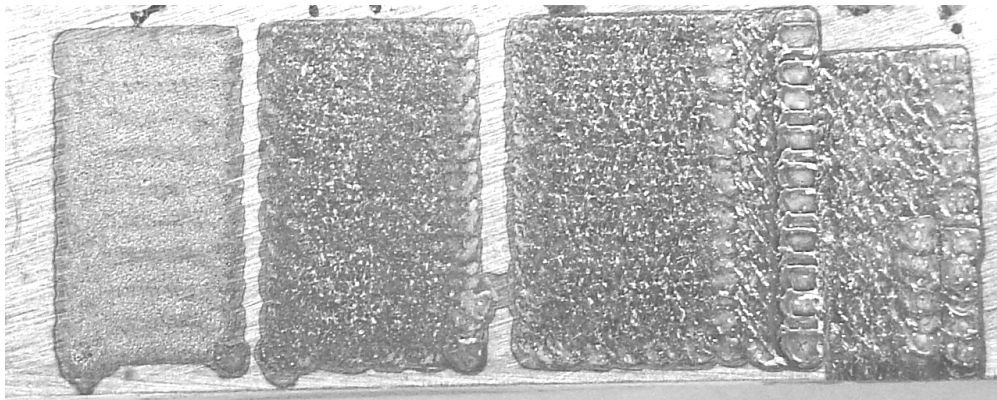


Figure 3. Surface macrograph (samples 18, 19, 20, 21).

Macrographs for different samples are showing in Figure 3.

Hardness increasing for all experimental regimes (Figure 4). For 0mm defocalisation hardness is higher over initial hardness  $300 \text{ daN/mm}^2$  between  $520 \text{ daN/mm}^2$  at 550V to  $650 \text{ daN/mm}^2$  at 900V. Hardness variation having a decreasing zone and a increasing zone. In a decreasing zone hardness having a linear decreasing with accumulator supply from  $520 \text{ daN/mm}^2$  to  $380 \text{ daN/mm}^2$ . Decreasing is a result of high energy localized on a minimum surface at focal distance of objective (50mm) and practical defocalisation is zero. The minimum surface is  $0,00785 \text{ mm}^2$ . Cooling capacity of material has a finite values and is determined by thermal conductivity of material. In a second stage hardness increasing because a cooling process from melt is present.

A similar situation appears for 7,5mm defocalisation. For 5mm defocalisation and 550V...700V surface hardness having a linear increasing from 320daN/mm<sup>2</sup> to 650daN/mm<sup>2</sup>. For 700V accumulation supply a maximum of hardness was obtaining, approx. 650daN/mm<sup>2</sup>. If accumulator supply increasing over 700V the energy of laser pulse beam increasing and hardness decreasing because local heating energy is higher and autoquenching time is too short. Over 800V local melting is present and hardness is difficult to measure (**Eroare! Fără sursă de referință.**). Surfaces are hardening by cooling from melt. A similar situation is for 2,5mm defocalisation.

For 10mm defocalisation hardness increasing only for 750V... 850V. defocalisation

Table 4. Results of hardness measurements over laser hardening surfaces

Experiment	Hardness, HV <sub>5</sub>				
	diagonal 1	HV <sub>5</sub>	diagonal 2	HV <sub>5</sub>	HV <sub>5m</sub>
mu	mm	daN/mm <sup>2</sup>	mm	daN/mm <sup>2</sup>	daN/mm <sup>2</sup>
1	0,153	396	0,12	644	520
2	0,142	460	0,154	391	425
3	0,162	353	0,148	423	388
4	0,140	473	0,142	460	466
5	0,142	460	0,137	494	477
6	0,141	466	0,141	466	466
7	0,124	603	0,124	603	603
8	0,146	435	0,146	435	435
9	0,145	441	0,145	441	441
10	0,157	376	0,157	376	376
11	0,167	332	0,167	332	332
12	0,140	473	0,140	473	473
13	0,130	549	0,130	549	549
14	0,120	644	0,120	644	644
15	0,142	460	0,142	460	460
16	0,138	487	0,138	487	487
17	-	-	-	-	-
18	0,150	412	0,150	412	412
19	0,169	325	0,169	325	325
20	0,150	412	0,150	412	412
21	0,157	376	0,157	376	376
22	0,145	441	0,145	441	441
23	0,128	566	0,128	566	566
24	0,131	540	0,131	540	540
25	0,130	549	0,130	549	549
26	0,181	283	0,181	283	283
27	0,173	310	0,173	310	310
28	0,174	306	0,174	306	306
29	0,154	391	0,154	391	391
30	0,149	418	0,149	418	418
31	0,169	325	0,169	325	325
32	0,152	401	0,152	401	401
33	0,159	367	0,159	367	367
34	0,143	453	0,143	453	453
c1	0,149	418	0,149	418	418
c2	0,127	575	0,127	575	575
c3	0,158	371	0,158	371	371
c4	0,152	401	0,152	401	401
36	0,124	603	0,124	603	603
37	0,120	644	0,120	644	644
38	0,119	655	0,119	655	655
39	-	-	-	-	-
40	-	-	-	-	-
41	0,145	441	0,145	441	441
42	0,162	353	0,162	353	353
43	0,122	623	0,122	623	623

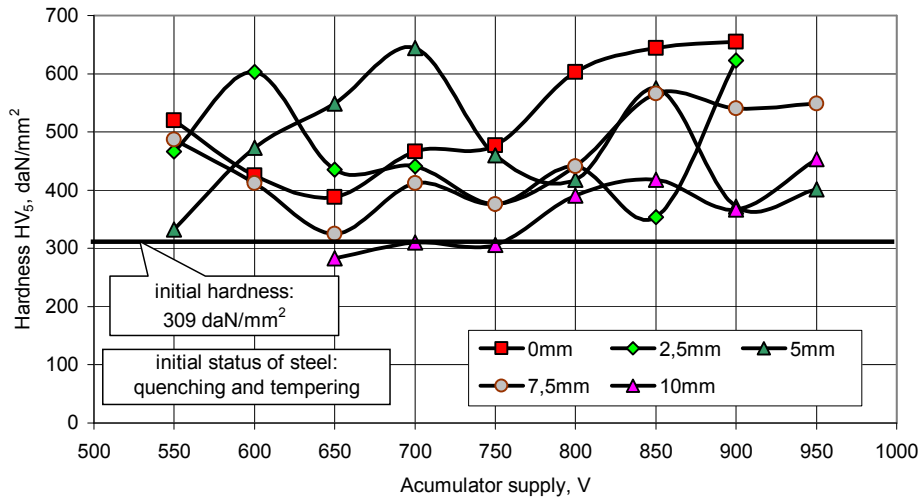


Figure 4. Hardness variations after pulse laser hardening for experimental regimes.

#### 4. CONCLUSIONS

The KVANT 17 pulse laser with solid active media (YAG:Nd) is normal dedicated for cutting and welding. By adapted a xy plotter conducted by computer, a small pieces are moving relative to laser beam. Interaction energy was controlled by defocalisation and indirect measurement of energy (capacitive accumulator supply).

Hardening surfaces by pulse laser YAG:Nd is possible to realized for small surfaces. For 38MoCrAl09 steel an increasing or hardness from 309 daN/mm<sup>2</sup> to 650 daN/mm<sup>2</sup> was obtaining in presented experimental condition.

Received May 5, 2005

"Dunărea de Jos" University Galați

#### REFERENCES

- /1/. Ganeev R.A, *Low-power laser hardening of steels*, Materials Processing Technology, Elsevier Pbs. No.121 (2002), pg. 414-419
- /2/. Popescu N, Gheorghe C, Popescu O, *Tratamente termice neconvenționale*, Editura tehnică, București 1990; (pag.223...245)
- /3/. Samoila C, Ionescu M.S, Drugă L, *Tehnologii și utilaje moderne de încălzire*, Editura Tehnică, București, 1986; (pag.291...360)
- /4/. Ursu I, Mihăilescu I.N, Prokhorov A.M, Konov V.I, *Interacțiunea radiației laser cu materialele*, Editura Academiei, București, 1986
- /5/. Donțu O, *Tehnologii de prelucrare cu laser*, Editura tehnică, București, 1985.
- /6/. Joel De Kock, Laser Machining Inc., Somerset, Wis, Lasers Offer Unique Heat Treating Capabilities Industrial Heating, Oct 2001

### DURIFICAREA SUPERFICIALĂ A OȚELULUI 38MoCrAl09 FOLOSIND LASERUL ÎN IMPULSURI YAG:Nd

**Rezumat:** Laserul oferă capacități unice pentru concentrarea de energii ridicate pe suprafețe mici. Factorii care influențează interacțiunea dintre radiația laser și suprafața unui material metalic (oțel călibil) pot fi controlați cu mare precizie. Laserul în impulsuri cu mediu solid YAG:Nd este utilizat în mod obișnuit pentru tăierea materialelor, în special a celor dure și extradure și pentru sudări de precizie a unor materiale mult diferite între ele. Lucrarea se bazează pe experimentările de durificare superficială utilizând instalația KVANT17 (laser în impulsuri cu mediu solid YAG:Nd) și efectuate asupra unor probe din oțel 38MoCrAl09. Rezultatele au fost investigate prin duritate Vickers (HV5), prin analiză microscopică și analiză microscopică..

**RESEARCHES REGARDING THE WORK-HARDENING OF MACHINERY  
PARTS HARD EXPOSED TO WEAR OF EQUIPMENTS AND  
INSTALLATIONS FROM AGRICULTURE AND FOOD INDUSTRY  
THROUGH HARD ALLOY DEPOSITION**

BY

**D. CIOBANU, D.V. ȘOLTUZ, V. NECULĂIASA, I. HOPULELE**

**Abstract.** *The paper presents some theoretical and experimental aspects from layers deposition domain with hard alloys (WCo8 and Ti15Co6) on OSC8M support, in view to increasing the durability of some cutting devices of equipments and installations from agriculture and food industry. Superficial work-hardening has realized using the method of deposition and alloying through electrical sparking with vibrator-electrode (DASE). Through this method can be obtained layers with thickness varying from tens microns to upper, with excellent adherence to support, respective high hardness and wear resistance, devoid the change of basic material structure.*

**Keywords:** *cutting devices, hard alloys, deposition, alloying, electrical sparking*

## **1. INTRODUCTION**

Equipments and installations from agriculture and food industry work in very difficult conditions, being under the influence both the mechanical stresses and the action of chemical factors, dependently by the nature of aggressive media in presence of those it working.

The active devices of these constructions are exposed to mechanical wear and corrosion, in the greater part of cases, or to mechano-chemical (tribocorrosion) wear, in which the mechanical and chemical effects can't be precisely separated [3].

In the battle with wear the first place must be occupied by knowledge and development of general theory of the materials resistances at wear. This theory is necessary for validation of constructive, technological and operation methods and means in the view to obtain a smaller wear. In the case of constructive solutions we understand also the quality of materials used, the thermal or thermo-chemical treatments applied, respective the hard alloys deposition methods for work-hardening of devices exposed to significant wear [1], [2] and [5].

A relative recent method for superficial work-hardening is the deposition and alloying through electrical sparking with vibrator-electrode (DASE). The principle of processing through electrical sparking consists in those that under the action of rectified pulsating current take place the material polar transferring from electrode (anode) to piece (cathode). The electrode material combines chemically with nitrogen and carbon from air, respective with carbon and other elements from cathode material. Thus, the electrode material forms on cathode a consistent superficial layer, very hard, resistant at wear and with excellent adherence to cathode material. At the same time in

superficial layer new formed appear the chemical complex compounds by kind of nitrides and carbonitrides, respective quenching structures [4].

In present, are frequently used the electrodes with metallic carbides from Cr, W and Ti. In general, are obtained the thickness of layers till to 50  $\mu\text{m}$ , with a density of layer till to 100%, with very great hardness (even over to 1100 HV) and a roughness by  $R_a = 3,2\div 14,8 \mu\text{m}$  [4].

## 2. MATERIALS AND METHODS

Researches investigate the superficial processing through periodical electrical sparking using electrodes from hard sintered carbides (WCo8 and Ti15Co6) of some probes by chisel steel, OSC8M hardened and tempered. The chemical composition of tested steel, determined with a BARD-DV6 optical emission spectrometer, is given in table 1.

Table 1

Material	Chemical composition, %									
	C	Mn	Si	P	S	Cr	Ni	Cu	Mo	Ti
OSC8M	0,85	0,56	0,26	0,03	0,025	0,2	0,15	-	-	-

The sparking has made on finished plate surfaces with  $20\times 15\times 7$  mm sides, which has been cleaning and degreasing in previous. The roughness of samples has been  $R_a = 50\dots 10\mu\text{m}$ .

The processing through electrical sparking has effectuated with ELITRON22 equipment, in manual regime, with three passing ( $t_{sp} = 1\text{min}/\text{cm}^2$ ) and with four work regimes, the work parameters are presented in table 2.

The analysis of samples has made on a normal section to new formed layer. This section has been grinding, polished and chemical attacked with 3% picric acid solution. The structural analysis of superficial layers obtained has made through optical metallographic microscopy with MC-9 microscope, in which has been installed a video chamber Philips.

The hardness measurements of layers obtained from investigations have effectuated with a PMT-3 hardness tester, using the follow relation:

$$M_{VH} = 1854,4 \cdot P/D^2 \text{ [daN/mm}^2\text{]},$$

in that  $P$  is the weight which press the diamante penetrometer [gf] and  $D$  is the diagonal of trace [ $\mu\text{m}$ ]. The normal load used for indentation has been by 50 gf.

The devices mentioned above are found in the endowment of Material Science and Engineering Faculty of Technical University "Gh Asachi" from Jassi.

## 3. RESULTS AND DISCUSSIONS

In figures 1 are shown the samples from chisel steel, OSC8M hardened and tempered, sparking with WCo8 and Ti15Co6 electrodes at four work regimes of ELITRON22 equipment.

Over the main structure, specific for quenched formed from martensite, residual austenite and primary and secondary carbides, can be observed the forming of a white layer of those characteristics depend evidently by sparking regime and by electrodes used.

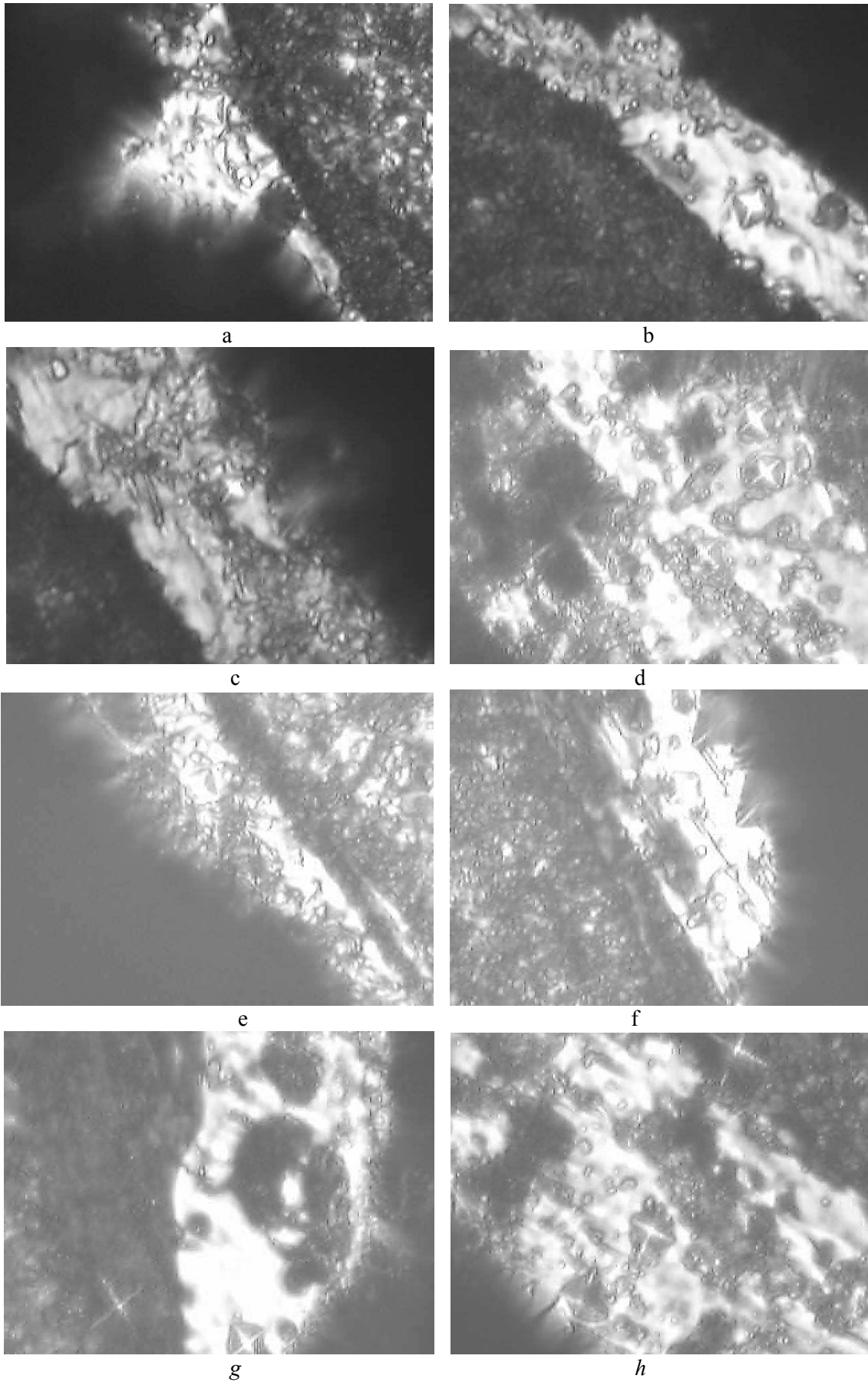


Fig. 1. Chisel steel, OSC8M, sparking with WCo8 (a - regime 1; b - regime 2; c - regime 3; d - regime 4) and Ti15Co6 (e - regime 1; f - regime 2; g - regime 3; h - regime 4) electrodes.  $\times 800:1$ .

The layer obtained with electrode from wolfram carbide and the first work regime, fig. 1 *a*, is thin, non-uniform and discontinue, but at sparkling with regimes 2 and 3 and the same electrode the layers obtained are more uniform, continue and with less pores, fig. 1 *b* and *c*. At sparkling with regime 4 and electrode of wolfram carbide the layers obtained are more substantial (thick), but present pores and cracks, fig. 1 *d*.

The layers obtained through superficial processing with electrode from titan carbide are much non-uniform and inhomogeneous (very porous), as a result to decomposition of titan carbide during the electrical sparkling and the deliverance of titan in layer, followed immediately by the oxidation of those. This phenomenon is more accentuated at processing with the regimes 3 and 4, fig. 1 *g* and *h*.

From micrographs presented can observe the presence under the white layer of a darkness domain (buffer zone), with fine structure, due to the modification of initial structure under the influence of thermal gradient formed during the electrical sparkling (similar with a tempering process).

The traces of hardness measurements, effectuated with 50 gf load, are little less on white layer obtained with electrode from wolfram carbides, which denotes that this have a hardness much great than to those of the layer obtained with electrode from titan carbide.

The obvious contour of microhardness indentations and the absence of cracks from near of those confirm the excellent adherence at the substrate of white layers formed.

The thickness and the hardness of superficial layers, respective of buffer layers obtained at the sparkling with WCo8 and Ti15Co6 electrodes and regimes 1-4 are shown in table 2.

Table 2

Sample	Material of sample	Material of electrode	Work regime	Microhardness $M_{HV50}$ /layer thickness, $\mu\text{m}$		
				White layer	Buffer layer	Base material
a	OSC8	WCo8	1 [0,5A]	142/19	642/13	672
b			2 [0,8 A]	159/27	591/21	672
c			3 [1,3 A]	1735/33	585/38	672
d			4 [1,8 A]	1887/43	580/50	672
e		Ti15Co6	1 [0,5A]	1332/14	630/11	672
f			2 [0,8 A]	1536/19	594/16	672
g			3 [1,3 A]	1685/28	581/31	672
h			4 [1,8 A]	1777/41	578/48	672

From data presented in table 2 can observe obvious that both the thickness and the hardness of layers obtained are influenced significantly by work regimes, appearing even a slight influence of the electrode material used.

At soft regimes by sparkling (regimes 1 and 2), when are not formed important buffer layers (13...21  $\mu\text{m}$  at the sparkling with WCo8 electrode and 11...16  $\mu\text{m}$  at the sparkling with Ti15Co6 electrode), the hardness modify suddenly, from little values of the basic structure till to values over the two times greater of white layer.

The greatest increasing of hardness of deposition layer, toward three times, has obtained at the sparkling with hard work regimes (regimes 3 and 4), and layers obtained have thickness much greater (33...43  $\mu\text{m}$  at the sparkling with WCo8 electrode and 28...41  $\mu\text{m}$  at the sparkling with Ti15Co6 electrode).

The processing with the WCo8 electrode conducts to greater values of layer hardness than in the case of Ti15Co6 electrode. Also, the hardness of buffer layer is much less than of basic material. This fact is caused by the elevated heating of material found under the white layer, forming structures by high tempering with lower hardness than the basic structure.

#### 4. CONCLUSIONS

From the analysis of presented data result the follow conclusions:

- As a result of deposition and microalloying of sample from chisel steel, OSC8M, with WCo8 and Ti15Co6 electrodes have obtained superficial layers with thickness varying from 14  $\mu\text{m}$  to 43  $\mu\text{m}$  and hardness just before at three times greater than of basic material, depending on work regimes and used electrode.
- 2. The sparkling with hard work regimes (regimes 3 and 4) lead at the obtaining of some layers with higher hardness, greater thickness and excellent adherence at the substrate, but the integrity of those it is in danger (the risk to appear pores and cracks in substrate, elevated roughness). In this case is recommended to apply a post-DASE processing that contributes at the improvement of deposition layers quality (smoothing with ultrasonic wave, laser and so on).
- 3. The application of DASE method for the obtaining of hard layers with very good adherence at substrate (with the keeping of characteristics of the basic material), on the active part of work elements (in special of cutting elements) of equipments from agriculture and food industry, lead at the increasing of the hardness and the wear resistance of those and consequently of their durability.

*Received April 26, 2005*

*Technical University "Gh.Asachi" Iasi*

#### REFERENCES

- /1/. Ciocîrdia C. și Gheorghe M., *Tehnologia construcției utilajului agricol*. București, E.D.P., 1979
- /2/. Ioancea L., *Mașini, utilaje și instalații în industria alimentară*. București, Ed. Ceres., 1986
- /3/. Neculăiaș V. și Țenu I., *Bazele cercetării experimentale a mașinilor și instalațiilor din agricultură și industria alimentară. Cercetări tribologice*. U. T. Iași., 1996
- /4/. Pop F., *Cercetări privind modificarea compoziției fazice a straturilor superficiale metalice obținute prin scânteie*. Teză de doctorat, Iași, 1998
- /4/. Tudor I., *Straturi rezistente la uzare prin abraziune. Tribologie*. Ploiești Ed. Universității, 2001
- /5/. \* \* \* , *Ustancova ELITRON22*. Chișinău, Academia Nauk, 1991

#### CERCETARI PRIVIND DURIFICAREA ORGANELOR DE MARE SOLICITARE LA UZARE ALE MAȘINILOR ȘI INSTALAȚIILOR AGRICOLE ȘI DIN INDUSTRIA ALIMENTARĂ, PRIN DEPUNERI DE ALIAJE DURE

**Rezumat:** Lucrarea prezintă câteva aspecte teoretice și experimentale în domeniul depunerii straturilor de aliaje dure (WCo8 și Ti15Co6) pe suport de OSC8M, în vederea creșterii durabilității unor organe de tăiere ale mașinilor și instalațiilor agricole și industria alimentară. Durificarea superficială s-a realizat utilizând procedeul

de depunere și aliere prin scânteie electrică (DASE) cu electrod vibrator. Utilizând acest procedeu se obțin straturi cu grosimi de la zeci de micrometri în sus, cu aderență , bună la suport, precum și duritate și rezistență la uzare ridicate, fără schimbarea structurii materialului de bază.

## STEEL GRIT, MATERIAL ACTIVE FOR CLEANING SURFACES

BY

ANIȘOARA CIOCAN, FELICIA BRATU, DANA NEGOIȚĂ

**Abstract.** *The grit is the abrasive material for the surface metal preparation in the shipbuilding and ship repair processes prior to application the coatings. This paper presented modification of the steel grit quality in the blasting process. The evolution of the particle shape, size was analyzed, in correlation with the resulting surface properties.*

**Keywords:** *cleaning agent, iron grit, surface metal preparation, ship repair processes*

### 1. INTRODUCTION

The studies focused on shipbuilding and ship repair processes include the first part of the researches about the wastes recycling.

Typical wastes generated from these operations include oils, coolants, lubricants and cleaning agents, various chemicals, paints and coatings, as well as abrasive material and dust from blasting, polishing and refinishing operations. By reducing the generation of these wastes at the source, or their recycling on or off site, will be benefit the marine yards by reducing disposal costs, and lowering the liabilities associated with hazardous waste disposal. The most part of these wastes is composed by the abrasive materials. Abrasive blasting is used in place of chemical stripping for removing paints. The most commonly used blasting media is sand and iron grit. This problem is very complex and this study is an introduction in this field, in order to solve a problem that is becoming critical not only for Romanian but also for European shipbuilding industry. Grit blasting is very pollutant, environmentally unaffordable, and is progressively being forbidden in the most environmental sensitive countries (mainly north Europe) only remaining in southern countries (Greece, Portugal, Spain). It is a clear trend to reduce the waste deposal until being definitively forbidden. The main objective is to develop a reliable and cost effective technology for coating removal capable to obtain a high quality surface preparation together with a reduction of waste and emissions to environment. It will be necessary to optimize the coating removal technologies, the cleaning installations, and original waste recycling systems.

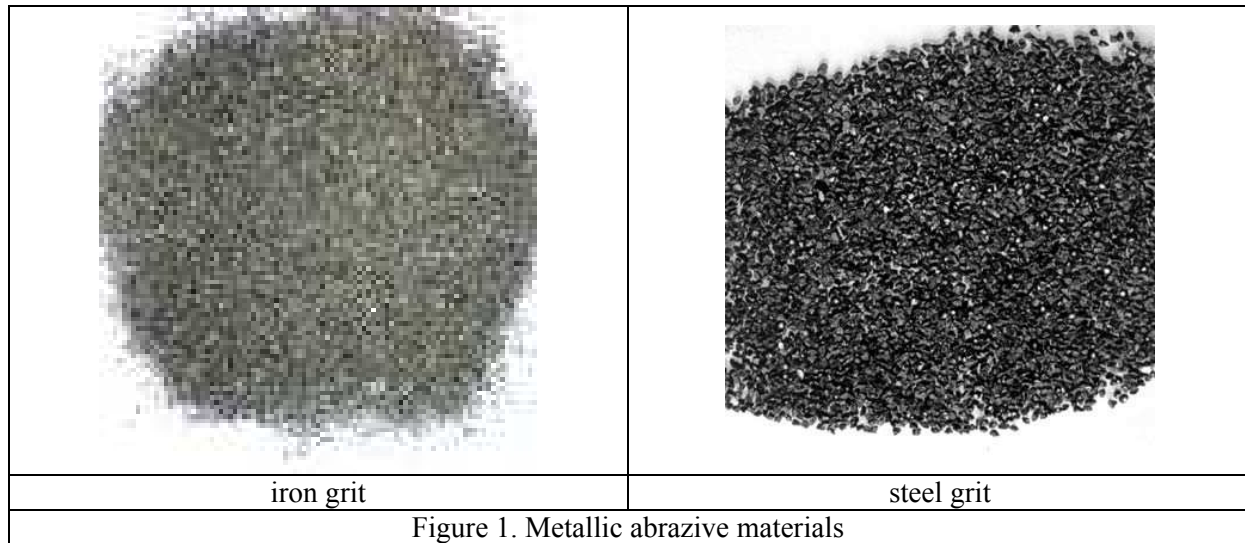
### 2. MATERIALS

Abrasive media used in the common Romanian shipyard, in the blasting operation is a mixture formed by metallic material and mineral abrasive.

Metallic abrasives are predominantly iron and steel abrasives (Figure 1).

Iron and steel abrasives come in two shapes: steel shot, which is round and steel grit, which is irregular to angular. In the studied situation, the iron grit is used for the

shipbuilding and ship repair processes in the blast cleaning stage for the removal of paint, rust, mill scale and other contaminants from steel surfaces. Mineral abrasives are hard and brittle, and thus are an excellent abrasive media. The sand is used in our mixtures. However, the sand due to the fracture in impact generates high amount of dust. Dust generating and abrasive breakdown at elevated nozzle pressures is a potential problem. In the cleaning operation, a mixture contains iron grit and sand is used. This mixture is reused during several cycles. The compressed air accelerates the media. Make-up abrasive material is typically added to compensate the loss caused by blasting process.



The technical data for several classes from iron grit material, named G, GP, GL and GH is shown in Table 1.

Moreover, the chemical composition limitations are given. The grit material used in studied mixtures is the grit GH. This grit has the high hardness and an angular form. These ensure the efficient cleaning process in order to obtain an uniform and smooth metal surface.

The grit granulation is variable. Virgin chilled iron grit is available in all standard grit sizes (Table 2). The sizes of the screens shall be in agreement with SAE J444. G80 was utilised in studied mixture.

Table 1. Standard iron grit characterization (GH)

Material		Chemical composition [%]					Hardness, [HV1]
Iron grit		C	Mn	Si	P	S	
Grit number	GP	0.75-	0.60-	0.60-	Max.	Max.	450-560
	GL	1.20	1.10	1.10	0,04	0,04	600-700
	GH						800-950

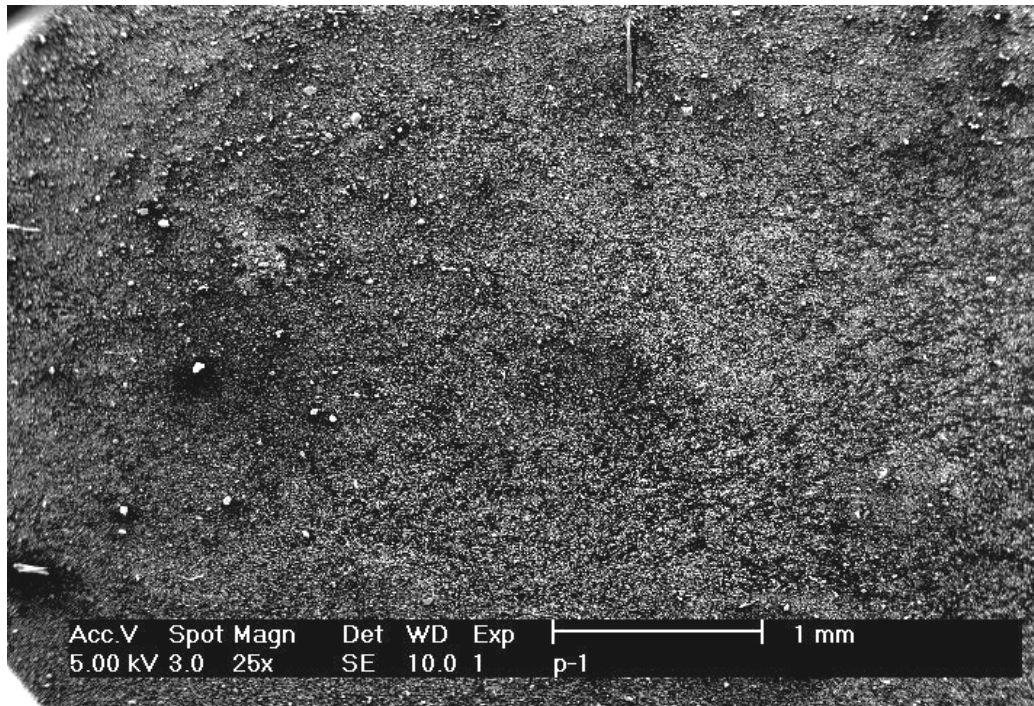
### 3. EXPERIMENTAL

In order to establish the recycling technology, the properties of the abrasive media must be studied. The chemical composition of the waste mixture (iron grit – sand) was determined. (Table 3). The shape of abrasive mixture particles is shown in figure 2 (at the different magnifications).

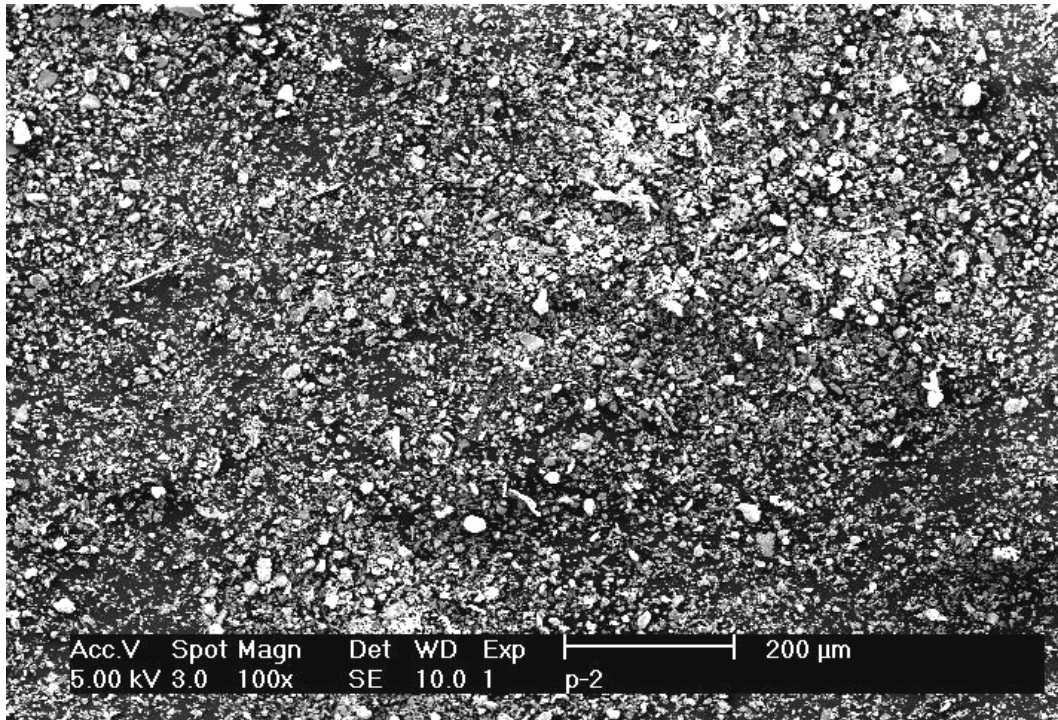


Table 3. Chemical composition of the waste mixture [%]

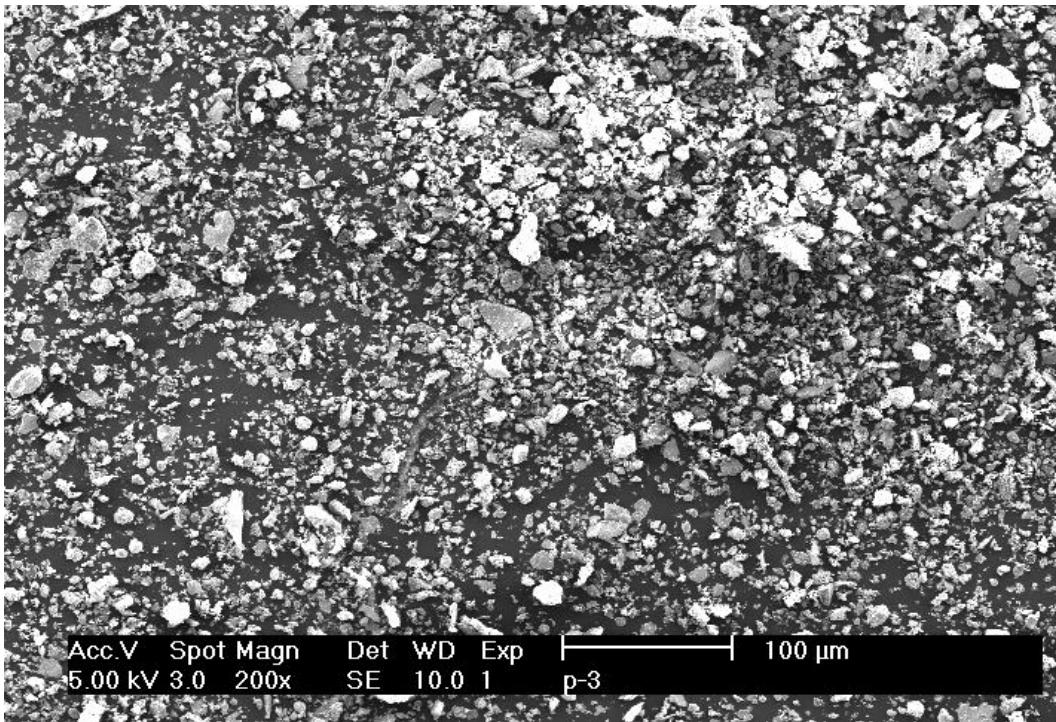
C	Mn	SiO <sub>2</sub>	S	P	CaO
0.16	0.28	41.78	0.70	0.014	6.72
MgO	Cr	V	Al <sub>2</sub> O <sub>3</sub>	Fe	P.C.
6.36	1.20	0.37	7.10	29.80	0.09



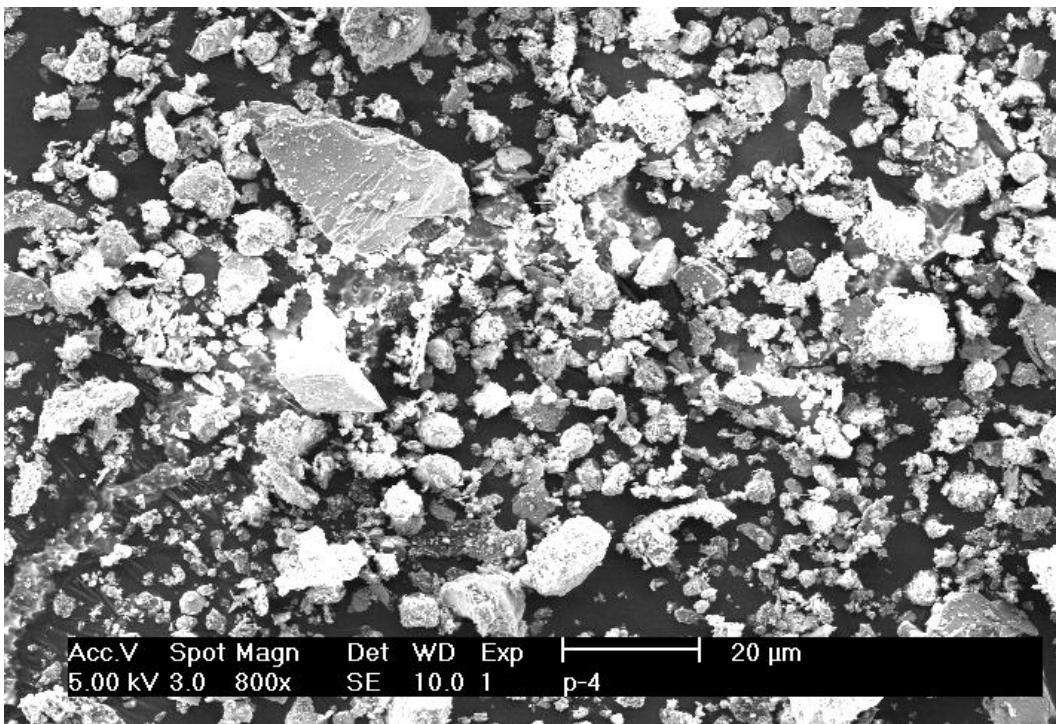
a. magnification 25



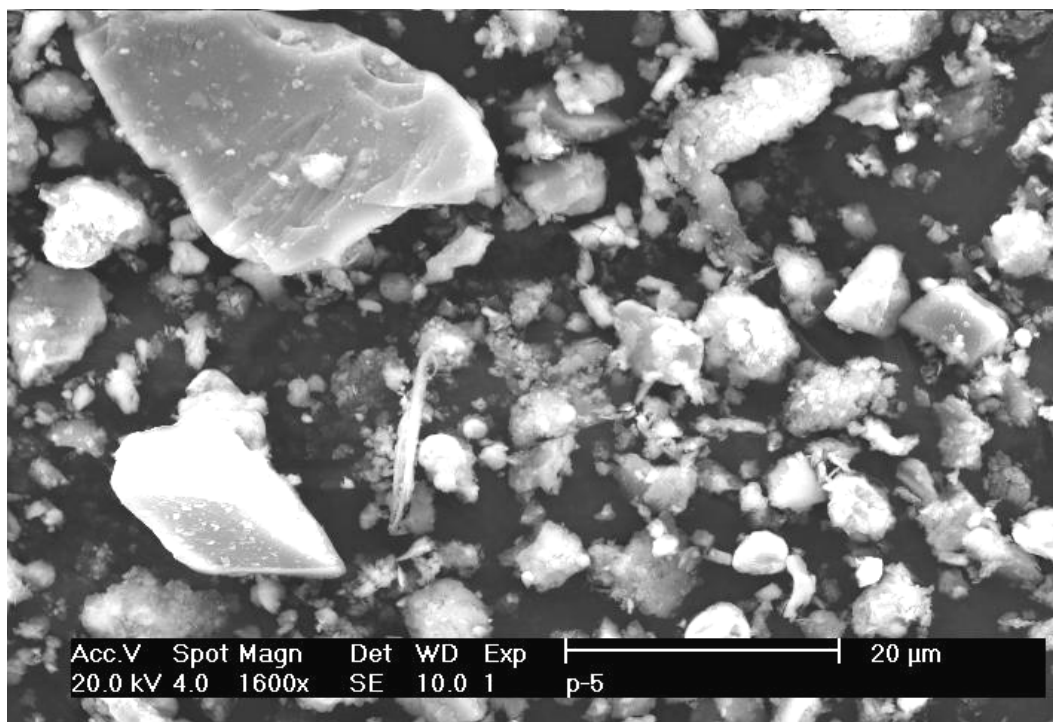
b. magnification 100



c. magnification 200



d. magnification 800



e. magnification 1600

Figure 2. The waste particles after the blasting process

#### 4. CONCLUSIONS

The iron grit is used for the shipbuilding and ship repair processes in the blast cleaning stage for the removal of paint, rust, mill scale and other contaminants from steel surfaces. The waste mixture of iron grit and sand after the blasting process was studied in this work. The biggest part of the studied waste is sand. Due to the fracture processes the most part of the sand becomes dust. This dust must be separated by the metallic part of the waste material. In the further work, dust and metallic part must be studied separately. In case of metallic waste, a more in depth analyses of the particles shapes and the iron combination is necessary.

Received May 5, 2005

"Dunărea de Jos" University Galați

#### REFERENCES

1. Ciocan, A., *Valorificarea Deseurilor*, Editor National Bucuresti, 2003
2. \* \* \*, *Guides to pollution prevention*, EPA /625/7-90/009, Cincinnati, USA, 1990

#### GRITUL DE OTEL, MATERIAL ACTIV PENTRU CURATAREA SUPRAFETELOR

**Rezumat:** Gritul este un material abraziv folosit pentru pregătirea suprafețelor în construcția navală și procesele de reparare premergătoare aplicării acoperirilor. Această lucrare prezintă modificarea calității gritului de oțel în timpul procesului de curățare. A fost analizată evoluția mărimei particulelor de grit corelată cu proprietățile suprafețelor.

## A COMPARISON BETWEEN THE PROPERTIES OF SOME METAL LOADED SILICALITE-1 ZEOLITES

BY

ȘTEFAN MARCEL CIOCÎLTEU\*, FUJIO MIZUKAMI\*\* and PETRU ONU\*

**Abstract.** *Cobalt, nickel and copper-containing silicalite 1 prepared by solid-state transformation and impregnation were characterized and compared using different techniques: XRD, ICP, SEM, TPR and BET. The influence of the preparation method has been studied in order to analyze the distribution of metal in the bulk zeolite. Data shows a greater dispersion and stability of metal loaded zeolites obtained by solid-state transformation compared with impregnated samples.*

**Keywords:** *silicalite, preparation methods, zeolite*

### 1. INTRODUCTION

Zeolite ZSM-5 has been reported to exhibit a great reaction selectivities and catalytic stabilities [1]. Modified ZSM-5 by incorporation of metals improves and enhanced its catalytic properties, in order to obtain catalyst for selective hydrocarbon conversion.

Metal loaded zeolites have recently received a great attention as catalytic materials, due to their activity in the decomposition and reduction of nitrogen oxide [2-4]. The incorporation transition of metals into the framework of molecular sieves can modify the catalytic acidity, thus affecting the activity and selectivity, comparatively with free-metal zeolite, leading to interesting catalytic properties. These solids are very complex due to the presence of two distinct phases, the crystalline one (zeolites) and the other than can be amorphous or crystalline (metal oxide), having different chemical composition and physico-chemical properties.

The objective of a preparation method is to distribute the active phase (metal) over the support in the most efficient way, highly dispersed in order to obtain a large specific area and maximum activity. The properties of the metal loaded zeolites are mainly determined by the preparation method and the nature of metal precursor compounds [5-7].

In the present work, the influence of the preparation method, solid-state transformation (SST) and impregnation (I), on three metal loaded zeolites and their influence on the textural properties of the obtained products are studied. The products were characterized by chemical analysis, powder X-ray diffraction, thermo-programmed reduction, scanning electronic microscopy and nitrogen adsorption. The comparison of two methods allows to obtain consistent results.

## 2. EXPERIMENTAL

### 2.1. Starting materials

The metal incorporation was carried out by two different methods: solid-state transformation [8, 9] and impregnation, each method using a metal nitrate compound as a metal source (Table 1). By impregnation method, zeolite silicalite 1 obtained by SST was mixed with a solution of metal nitrate at pH 4.8 using vacuum rotary evaporation. The samples were dried in air at 100 °C for 24 h.

After solid-state transformation and impregnation the samples were calcined at 500 °C for 20 h under air and subsequently reduced at 500 °C for 2h under hydrogen atmosphere (flow rate: 40 ml/min). The silicalite 1 was used in Na form.

### 2.2. Characterization

The purity of the crystalline products was ascertained by X-ray diffraction (MXP 18 diffractometer) and scanning electron microscopy (SEM HITACHI S-800). Chemical analyses were obtained by atomic absorption after acid digestion of solid, using a Thermo Jarrel Ash IRIS/AP. The nitrogen adsorption isotherms were obtained at liquid nitrogen temperature, using a Belsorp 36SP analyzer. For temperature-programmed reduction (TPR), 10 vol% H<sub>2</sub>-Ar was used as the reducing gas, with a flow rate of 30 ml min<sup>-1</sup> and the temperature of the sample bed was raised at a heating rate of 10 K min<sup>-1</sup>.

## 3. RESULTS AND DISCUSSIONS

### 3.1. X-ray diffraction

All the synthesized solids showed, by XRD spectra, the presence of highly crystalline MFI-type zeolitic structure with narrow and well-define peaks characteristic of a high structural order (Fig. 1). All samples synthesized by SST did not exhibit any characteristic metal oxide peaks after synthesis and calcination. Reductions bring in attention very weak metallic peaks for all SST samples. Normal decreases of XRD intensities are observed after calcination and reduction.

The behaviors of impregnated samples are different. The impregnated samples containing Co and Ni exhibit only weak oxide metallic peak after calcination, Co<sub>2</sub>O<sub>3</sub> respectively NiO. Both samples show the same weak peaks for the reduced metal after reduction. After impregnation, Cu impregnated sample show very strong XRD peak characteristic for Cu<sub>2</sub>(OH)<sub>3</sub>NO<sub>3</sub> and Cu<sub>2</sub>O. These peaks are replaced with very intense CuO peaks, after calcination, and Cu<sup>0</sup> after reduction. These data show that Cu impregnated samples exhibit a higher tendency to form big copper compounds aggregates, while for the samples with Co and Ni the dispersion of metal inside of bulk zeolite is higher comparative with copper samples. The shape of the XRD peak and the absence of very developed peaks due to the metal compounds (oxide or reduced metal) prove that the SST method allow to obtain metal loaded zeolites having a great dispersion at a high content of metal and the segregation absence of metal crystals.

### 3.2. Chemical composition and Crystal morphology

The amount of metal remained in the zeolite material (outside or inside of zeolite framework) remained around 12%wt after SST process. The morphology and crystal size of the samples have been studied by scanning electronic microscopy. Figure 2

shows the microphotographs of the following calcined samples: S 1, Co-S, Ni-S and Cu-S. Silicalite 1 adopted particle morphology of silicalite layers intergrowths to form nearly spherical crystals of ca. 0.7-20 nm [9]. The size and the shape of metal loaded zeolites samples are considerably changed by the presence of metal in initial mixture. Crystals show certain similarity in shape and size were observed. The shapes of crystals were hexagonal plate-like morphology with many intergrowths.

Table 1. Main characteristic of the synthesized samples

Samples	% Me (ICP)	XRD	Preparation method	Metal precursor compounds
S 1	-	SiMFI	SST	-
Co-S	11.3	SiMFI	SST	$\text{Co}(\text{NO}_3)_2 \cdot 6\text{H}_2\text{O}$
Ni-S	11.9	SiMFI	SST	$\text{Ni}(\text{NO}_3)_2 \cdot 6\text{H}_2\text{O}$
Cu-S	12.1	SiMFI	SST	$\text{Cu}(\text{NO}_3)_2 \cdot 3\text{H}_2\text{O}$
Co-I	12	SiMFI	Impregnation	$\text{Co}(\text{NO}_3)_2 \cdot 6\text{H}_2\text{O}$
Ni-I	12	SiMFI	Impregnation	$\text{Ni}(\text{NO}_3)_2 \cdot 6\text{H}_2\text{O}$
Cu-I	12	SiMFI	Impregnation	$\text{Cu}(\text{NO}_3)_2 \cdot 3\text{H}_2\text{O}$

Amorphous species or metal oxides, on the external surface of MeSiMFI samples, were also observed.

In alkaline medium, the pH can be higher, and more supersaturated reaction mixture are formed compared to in fluoride media [10] leading to more metastable phases which produce not well-formed crystals (Fig. 2).

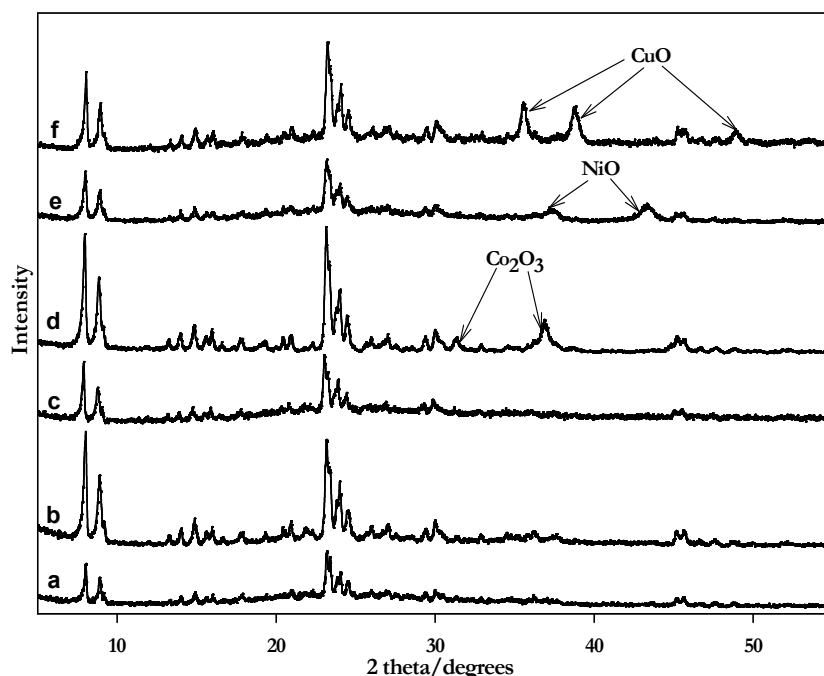


Fig. 1. XRD patterns of calcined samples: a) Co-S; b) Ni-S; c) Cu-S; d) Co-I; e) Ni-I; f) Cu-I.

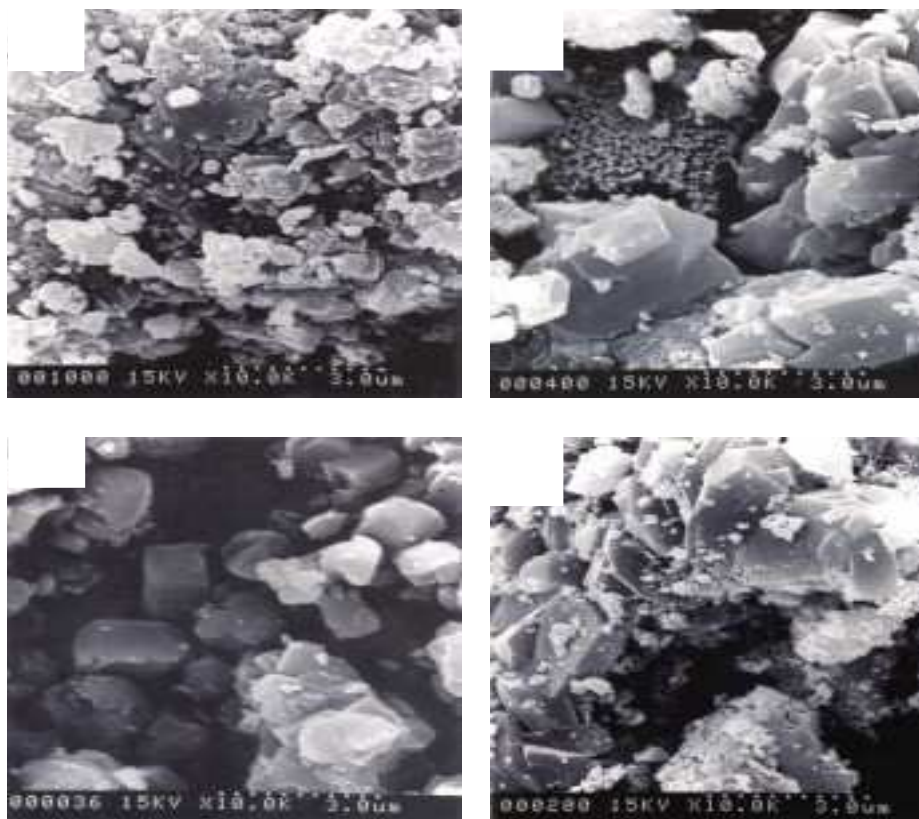


Fig. 2. Scanning electron microscopy photographs. a) S 1; b) Co-S; c) Ni-S; d) Cu-S.

### 3.3. TPR Data

Temperature programmed reduction of the catalyst was carried out to determine the differences in the reducibility of the metal loaded zeolites related to the location and dispersion of metals after the calcination step and the metal-support interaction depending on the differences between the TPR profiles of the samples. Figure 3 shows the TPR profiles of the samples prepared by SST and impregnation.

Calcined Co-S sample shows two broad peaks at 390 °C and 740 °C comparative with Co-I sample that shows only one peak at 450 °C. After calcination a part of Co ions or compounds positioned inside of channels or linked on the zeolite surface leave their position migrating outside zeolite surface forming  $\text{Co}_2\text{O}_3$ , which are reduced around 390 °C. Impregnation method provide Co ions situated in position quite easy reducible slighter above the reduction temperature of the first peak of SST sample. The low reduction temperature for SST sample vs. impregnated sample (450 °C) was due to the reduced dimension of  $\text{Co}_2\text{O}_3$  aggregates that are smaller comparative with  $\text{Co}_2\text{O}_3$  aggregates formed in the impregnated sample. The second peak of SST of Co-S shows that the SST process provides Co ions situated in heavy reducible positions.

For Ni-S and Ni-I samples the profile are quite different. The TPR profile of the Ni loaded sample by SST is characterized by a broad peak centered around 700 °C that appears at a higher temperature than that of Ni-I sample (290 °C respectively 325 °C). The differences in the sample TPR profiles as compared to that of SST sample indicates a bimodal nature of the fixed oxidic nickel. The higher reduction temperature

of Ni-S sample indicates a more complex and strong interactions between metal and zeolite structure. The shape of TPR pattern of the Ni-S sample supposes to be due to the existence of Ni compound with different environment.

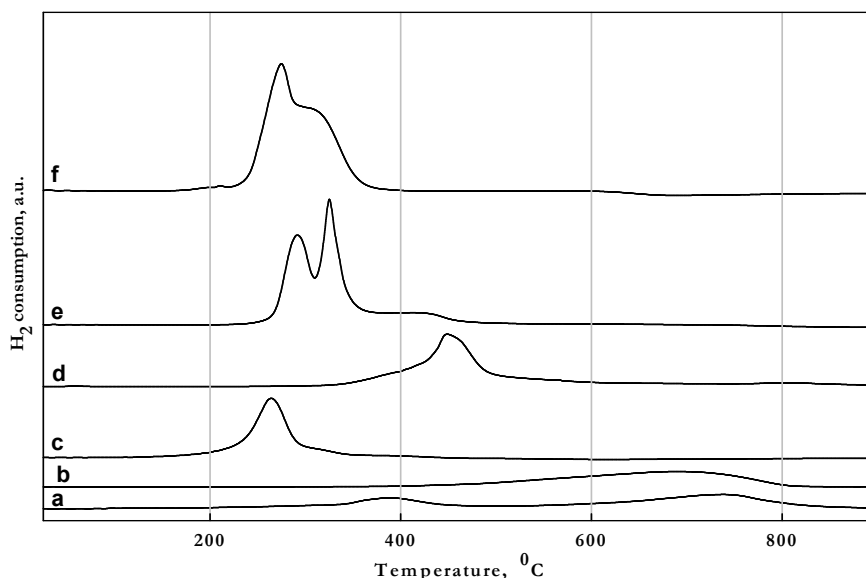


Fig. 3. H<sub>2</sub>-TPR profiles of calcined samples: a) Co-S; b) Ni-S; c) Cu-S; d) Co-I; e) Ni-I; f) Cu-I.

From H<sub>2</sub>-TPR data we can notice that the copper exhibit different environments. In case of the Cu-S sample, the sharp peak observed at 275 °C (Fig. 3) was attributed to Cu<sup>2+</sup> as dispersed undefined CuO species, reduced in one step process directly to Cu<sup>0</sup>. This peak is shifted at a slightly lower temperature comparative with impregnated sample. The shape, position and broadness of this peak, likely depending on the dispersion, reflecting the interaction of the CuO-oxidic like species with the zeolite matrix and existence of Cu<sup>2+</sup> species. The existence of oxocations is not valid because the color is not green and the reduction temperature is too high for reduction such of species. Like, nickel impregnated sample, copper impregnated sample indicate a bimodal nature of the fixed copper oxide (Fig. 3).

As can be seen the reduction temperature of cooper samples are quite similar. Among all analyzed samples the copper loaded samples (by SST and Impregnation) have the lowest reduction temperature, lees than 350 °C.

#### 4. CONCLUSIONS

The XRD analysis and the SEM data show that the SST samples have a good crystallinity a good dispersion of the metal in the zeolite bulk. Excess cobalt, nickel and copper are located on the outer surface of the zeolite in the oxide form: Co<sub>2</sub>O<sub>3</sub>, NiO and CuO. SST samples show a good distribution and complexe interaction with the zeolite structure.

Thus, low reduction temperature can be related to reduction of big particles or agglomerates of them and/or particles that interact weakly with zeolite. As the temperatures increases, the size of particles decreases and/or the interaction forces with

the support are higher. As it clearly can be seen, the techniques of incorporation has quite influence over its reducibility.

Received April 25, 2005

\*Technical University "Gh.Asachi" Iasi

\*\*National Institute of Advanced Industrial Science and Technology (AIST),  
AIST Tohoku, Japan

#### REFERENCES

- /1/. Martens, J.A., Parton, R., Uytterhoeven, L., Jacobs, P.L., Froment, G.F., *Appl.Catal.* 1991, 76, 95;
- /2/. Li, Y., Hall, W.K., *J.Catal.* 1991, 129,202;
- /3/. Lee, C.-Y., Choi, K.-Y., Ha, B.-H., *Appl.Catal.B*, 1994, 5, 7;
- /4/. Kharas, K.C.C., Liu.D.-J., Rabota, H.J., *Catal.Today*, 1995, 26, 129;
- /5/. Gil, A., Diaz, A., Gandia, L.M., Montes, M., *Appl.Catal. A* 1994,109, 167;
- /6/. Bartholomew, C.H., Panell, R.B., Butter, J.R., *J.Catal.* 1980, 65, 335;
- /7/. Satterfield, C.N., *Heterogenous Catalysis in Industrial Practice*, 2<sup>nd</sup> ed.; McGraw Hill, New York, 1991;
- /8/. M. Salou, Y. Kiyozumi, F. Mizukami, S. Niwa, M. Imamura and M. Haneda, *Stud. Surf. Sci. Catal.* 2001, 135, 335;
- /9/. M. Salou, Y. Kiyozumi, F. Mizukami, P. Nair, K. Maeda, S. Niwa, *J.Mater.Chem.* 1998, 8(9), 2125;
- /10/. J.L. Guth, H. Kessler J.M. Lamblin, J. Patarin, A. Siene, J.M. Chezeu, R.Wey, *ACS Symp.Ser.* 1989, 398, 176;

#### COMPARAREA PROPRIETĂȚILOR UNOR PROBE DE SILICALIT 1 CONȚINÂND METALE

**Rezumat:** S-au preparat probe de silicalite 1 conținând Co, Ni și Cu folosind două metode: transformarea în stare solidă și impregnare. Probele obținute au fost analizate prin difracție de raze X, compoziția elementară, microscopie electronică scanning și reducere programată cu hidrogen pentru a vedea influența metodei de preparare asupra capacității de reducere a speciilor metalice din zeolit și a gradului de dispersie a acestora în masa de zeolit.

## CATHODIC SPUTTERING – ESSENTIAL FACTOR IN PHASIC CONSTITUTION OF COMPOUND LAYER FORMED BY PLASMA NITRIDING

BY

SORIN CIUCĂ<sup>1</sup>, CRISTIAN RUSET<sup>2</sup>, MIHAI TÂRCOLEA<sup>1</sup>, IOANA GHERGHESCU<sup>1</sup>,  
ALEXANDRA GHEORGHIU-DOBRE<sup>1</sup>, MARCEL SUCIU<sup>3</sup>

**Abstract.** *Sputtering process – specific for plasma treatments – plays an important role in formation and developing of the hard surface layers. In this respect, our paper presents some investigations on the sputtering process occurring under specific conditions of plasma nitriding. Using an adequate experimental arrangement, the sputtering rate has been determined as a function of treatment parameters, especially gas composition, working pressure and discharge voltage. Depending on these factors, the sputtering rate varies in the range of 0.02-0.12  $\mu\text{m/h}$ . It has been found that the compound layer is not always a  $\gamma'$  –  $\text{Fe}_4\text{N}$  monophasic structure. Depending on sputtering rate, e.g. treatment parameters, a dual  $\gamma'$  and  $\epsilon$  –  $\text{Fe}_{2-3}(\text{N,C})$  structure can be obtained. The sputtered material has been analysed as well. The results show that the phase constitution is similar to that of the compound layer. All these data could be very useful in conceiving a computer program, able to predict the performances of a plasma nitrided material.*

**Keywords:** *plasma nitriding, sputtering rate, compound layer, XRD analysis, computer program*

### 1. INTRODUCTION

The sputtering phenomenon – as a specific process for plasma surface treatments – plays an important role in formation and developing of hard surface layers, particularly for the plasma nitrided compound layer.

The aim of this paper is to investigate the sputtering process under plasma nitriding conditions and to provide real experimental information regarding the sputtering process. The chemical composition of the substrate material, the process parameters and the sputtering rate will represent important data for the development of a mathematical model able to predict the plasma nitriding results. Thus, investigations were performed in order to determine the influence of the process parameters on the sputtering rate and to establish its correlation with the phase composition of the compound layer. The structure of the sputtered material during plasma nitriding was also investigated.

### 2. EXPERIMENTAL METHOD

The experimental arrangement devised for measuring the sputtering rate is shown in Fig. 1.

The cathode (1), which is a rod ( $\text{Ø}20 \times 380$  mm) made of OLC45 (C45) plain carbon steel, is surrounded by five hollow cylinders ( $\text{Ø}80 \times 70$  mm) made of stainless steel plate with a thickness of 0.35 mm. These cylinders are acting as the anode and

collect the sputtered material from the cathode. By weighing the cylinders BEFORE and AFTER the treatment, the sputtering rate at the cathode surface was calculated.

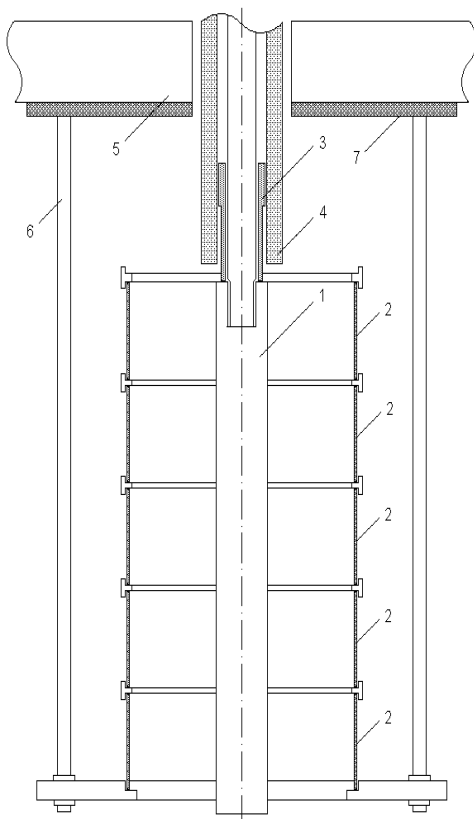


Fig. 1. Experimental set-up for measuring the sputtering rates: (1) cathode; (2) cylindrical anodes; (3) cathode support; (4) insulated ceramics; (5) top lid of the treatment chamber; (6) anode support rods; (7) metallic support.

It was supposed that the collected material was  $\gamma'$  -  $\text{Fe}_4\text{N}$  with a density of  $6.8 \text{ g/cm}^3$ . Approximately equal amounts of material have been collected by each of those five cylinders, proving the uniformity of the sputtering process along the cathode rod.

The hypothesis concerning the nature of the sputtered material was confirmed by another set of experiments using a device presented in Fig. 2.

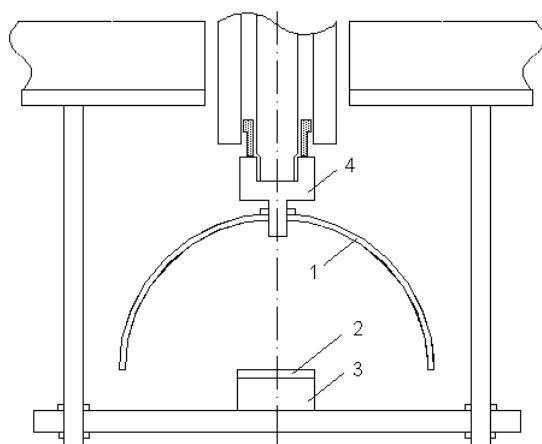


Fig. 2. Experimental set-up for establishing the nature of the sputtered material: (1) hemispherical cathode; (2) copper disc (anode); (3) sample support; (4) cathode support.

The material sputtered from the hemispherical cathode (1) is collected by the copper disc (2) and analyzed by XRD. Due to the low values of the sputtering rate, the process time was between 30 and 60h in order to obtain a significant amount of powder material, able to be analyzed. The main process parameters which have been modified were the total pressure, correlated with the discharge voltage (in order to keep constant the temperature of the cathode), and the gas composition. The partial

pressures of nitrogen and hydrogen were measured using a quadrupole mass spectrometer.

The chemical composition of the compound layers (depth profiles of the carbon and nitrogen) has been analyzed by the glow discharge optical spectrometry method (GDS).

### 3. RESULTS AND DISCUSSION

The influence of the working pressure on the sputtering rate is shown in Fig. 3.

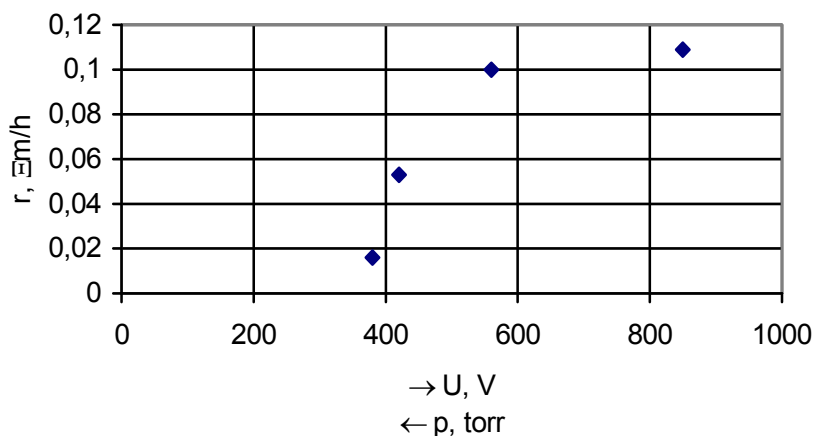


Fig. 3. The influence of the working pressure on the sputtering rate.

For low pressure values ( $p < 5.8$  Torr) the sputtering rate does not change significantly, while for high values ( $p > 5.8$  Torr) this rate drops drastically from 0.12 to 0.02  $\mu\text{m/h}$ . This is due to a decrease of the ion and fast neutral energy, determined by the reduction of the discharge voltage and of the mean free path.

A similar effect can be noticed when the gas composition is changed (Fig. 4).

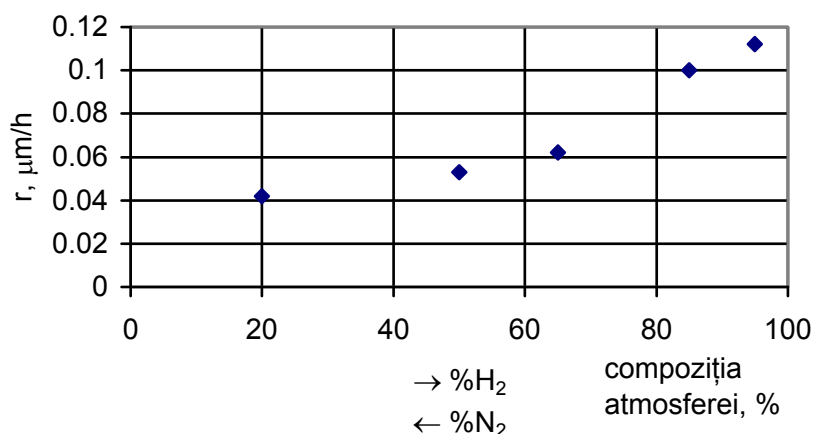


Fig. 4. The influence of the gas composition on the sputtering rate.

When the hydrogen percentage of the atmosphere in the treatment chamber decreases from 95 to 20%, the sputtering rate decreases from 0.13 to 0.05  $\mu\text{m/h}$ . This

is the consequence of the discharge voltage reduction which occurs when the nitrogen percentage in the processing atmosphere is increased.

It is established in Refs. [3,5] that the sputtering is directly responsible for the decarburization process which occurs during the process of plasma nitriding. Consequently, when the treatment parameters are set for a high sputtering rate, the decarburization is so intense that a very low carbon concentration is reached at the cathode surface, and according to the Fe-N-C phase diagram [6], a  $\gamma'$ -Fe<sub>4</sub>N mono-phase compound layer is formed. If the plasma nitriding is performed at high pressure, or with a high nitrogen percentage in the treatment atmosphere, the sputtering rate is too low to produce the necessary level of decarburization and consequently a significant amount of  $\epsilon$ -Fe<sub>2-3</sub>(N,C) phase is produced along with the  $\gamma'$ -Fe<sub>4</sub>N.

The XRD diagram of a OLC45 (C45) sample which was plasma-nitrided for 4h at 550°C and a pressure of 8.0 Torr, shows clearly a dual  $\gamma' + \epsilon$  structure of the compound layer (Fig 5). The working gas composition was 25% N<sub>2</sub> + 75% H<sub>2</sub>.

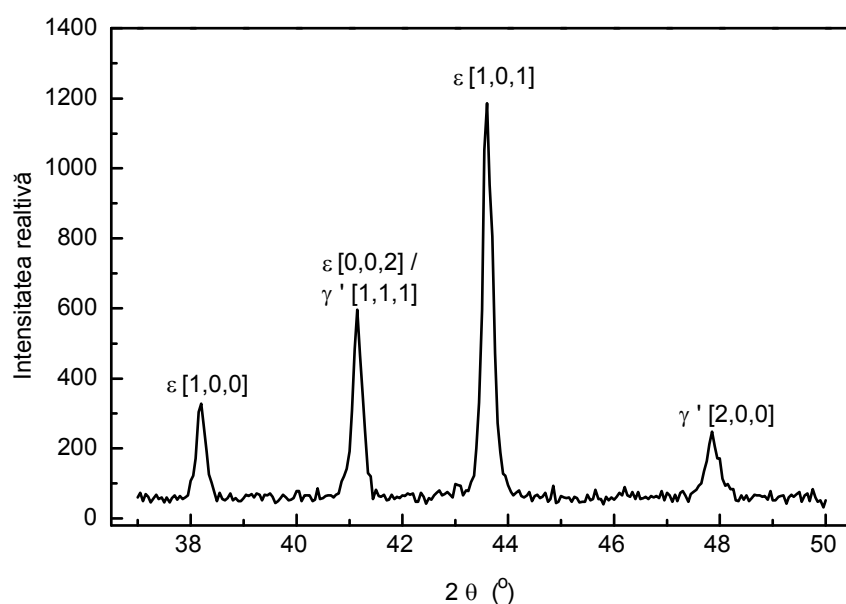


Fig. 5. XRD pattern ( $\lambda_{\text{CuK}\alpha}=1.54 \text{ \AA}$ ) of OLC45 (C45) sample plasma-nitrided at  $T=550^\circ\text{C}$ ,  $t=4\text{h}$ ,  $p=8 \text{ Torr}$  in a 25%N<sub>2</sub>+75%H<sub>2</sub> gas mixture.

The influence of the gas composition on the structure of the compound layer, together with the depth profile of nitrogen and carbon concentrations, is shown in Figs. 6 and 7.

A direct correlation between the carbon profile within the compound layer and its structure can be seen. Therefore, an important decarburizing effect appears when the treatment atmosphere contains 25% N<sub>2</sub> + 75% H<sub>2</sub>. In this way, the carbon concentration at the surface is below the limit-value (e.g. 0.45% C) (Fig. 6a). As a consequence, the structure of the compound layer (Fig. 6b) is almost mono-phase ( $\gamma'$ ). Increasing the nitrogen concentration level (80% N<sub>2</sub> + 20% H<sub>2</sub>) the sputtering rate and decarburization phenomenon drop even more (Fig. 7a). The carbon atoms cannot be removed from the surface and they participate in the formation of the  $\epsilon$ -Fe<sub>2-3</sub>(N,C) phase (Fig. 7b). The influence of the pressure on the sputtering rates seems to be

stronger than that of the nitrogen. This is shown in Figs. 3 and 4 and confirmed by the XRD patterns in Figs. 5 and 7b. In the first case the  $\epsilon$ -phase is dominant, while in the second the  $\gamma'$  is dominant.

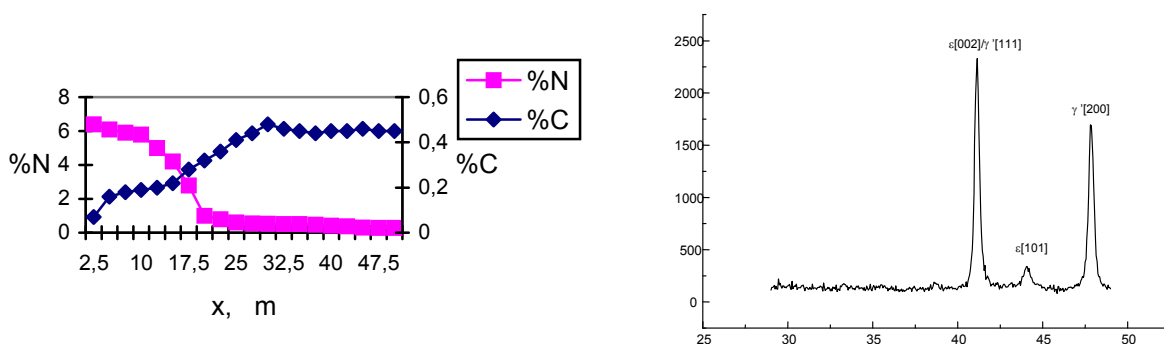


Fig. 6. Nitrogen and carbon profiles (a) and XRD pattern for OLC45 (C45) plasma-nitrided sample in a 25%N<sub>2</sub>+75%H<sub>2</sub> gas mixture (T=570°C, t=8h).

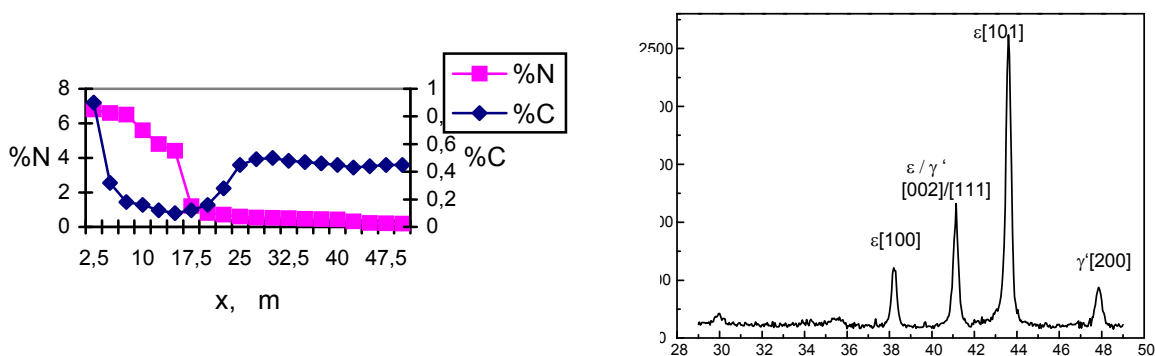


Fig. 7. Nitrogen and carbon profiles (a) and XRD pattern for OLC45 (C45) plasma-nitrided sample in a 80%N<sub>2</sub>+20%H<sub>2</sub> gas mixture (T=570°C, t=8h).

Using the experimental set-up presented in Fig 2, the powder material (sputtered under plasma nitriding conditions) has been investigated also. The XRD pattern is shown in Fig. 8.

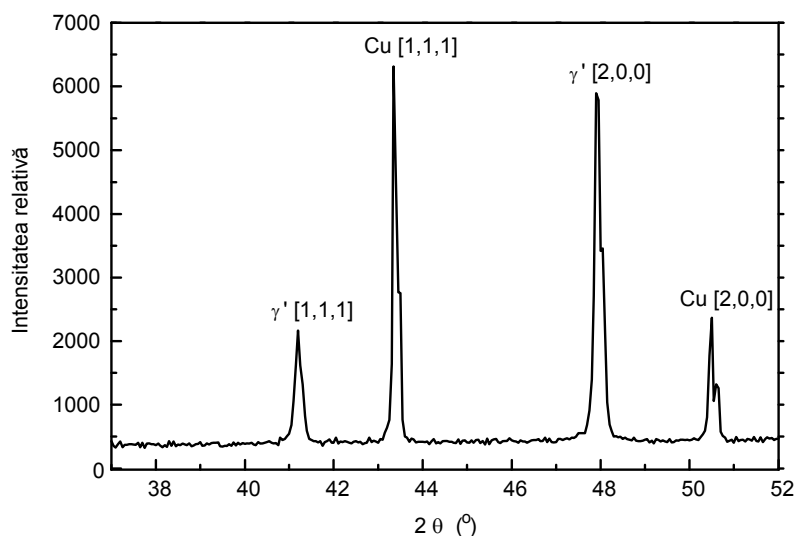


Fig. 8. XRD pattern of the sputtered material, collected on the copper anode (T=550°C, t=30h, p=1.5 Torr, 25% N<sub>2</sub>+75%H<sub>2</sub> gas mixture)

The phase constitution of the material collected on the copper anode is mono-phase  $\gamma'$ . The deposited layer is very thin, so the data of the copper substrate is collected also. No  $\alpha$ -Fe could be detected. This means that the material from the cathode surface ( $\gamma'$ -Fe<sub>4</sub>N) has been transferred to the anode by the sputtering phenomenon with the same structure.

#### 4. CONCLUSIONS

- The sputtering process has a direct influence on the decarburization phenomenon frequently observed in plasma-nitrided steels. It, along with other process parameters, has an important contribution in the phase constitution of the compound layers.
- The sputtering rate, a very efficient process parameter, is influenced by the pressure value (also directly associated with the discharge voltage), hence by the chemical composition of the atmosphere. The obtained data are very useful in finding the answers of the chemo-phase interface processes which occur during the plasma surface treatments.
- For low-pressure and high-voltage nitriding conditions, the resulted sputtered material has a  $\gamma'$ -Fe<sub>4</sub>N mono-phase structure. The experimental results have shown that the deposited material has the same structure as the compound layer formed in nitrided material.

Received April 21, 2005

<sup>1</sup> Polytechnic University of Bucharest

<sup>2</sup> INFLPR, Bucharest – Măgurele

<sup>3</sup> S.C. Romtub S.A., Bucharest

#### REFERENCES

- /1/. I. Wells, W. Strydom, *Sputtering and Deposition of cathode material during plasma nitriding*. „Surface Engineering“, 1986, vol. 2, nr. 4, pag. 263-268.
- /2/. C. Ruset, A. Bloyce, T. Bell, *Plasma nitrocarburising with nitrogen, hydrogen and hydrogen sulphide gas mixtures*. „Surface Engineering 1995“, vol. 11, no. 4, pag. 81-89.
- /3/. B. Edenhofer, *Conditions de formation et propriétés de nouvelles couches de combinaison obtenues par nitruration ionique d'aciers*. Traitement thermique, 140, 1979, pag. 47-59.
- /4/. Wolfgang Rudolf, *Nitruration et nitrocarburisation au plasma*. Traitement thermique, 253, 1992, pag. 77-84.
- /5/. Klumper-Westkamp H., Hoffman F, Mayr P., *Capteur de nitruration et formation de la couche blanche*. Traitement thermique, 240, 1990, pag. 43-51.
- /6/. J. Slicke, L. Sproge, J. Ågren, *Nitrocarburizing and the ternary Fe-C-N phase diagram*. „Scandinavian Journal of Metallurgy“ nr. 17, 1989, pag. 33-34.

#### PULVERIZAREA CATODICĂ–FACTOR ESENȚIAL AL CONSTITUȚIEI FAZICE A STRATULUI ALIAT OBȚINUT PRIN NITRURARE ÎN PLASMĂ

**Rezumat:** Procesul de pulverizare catodică este specific tratamentelor în plasmă și are un rol important în formarea straturilor superficiale dure. În acest sens lucrarea noastră prezintă câteva rezultate experimentale legate de condițiile specifice ale procesului de pulverizare din timpul nitrurării în plasmă.

## CORRELATION BETWEEN MICROSTRUCTURE AND PROPERTIES OF SINTERED HARD ALLOYS

BY

STELA CONSTANTINESCU, OLGA MITOȘERIU, TAMARA RADU, MARIA POPESCU

**Abstract.** *Unlike the TiC or TaC alloys, the simple WC-Co alloys with the same cobalt content are much more resistant to bending and breaking and feature improved electrical and heat conductivity. The oxidation resistance of the simple WC-Co alloys is considerably lower which results in a pregnant tendency for chip welding and low resistance.*

*The max values taken by the bending ultimate strength are reached at Co 20 - 25 % and suddenly decrease with high Co contents. At these compositions there are no contact bonds among the carbons, the carbon crystals being individual and surrounded by the Co metallic mass.*

*Due to over-heating and granulation growth by re-crystallization an acute decrease in the bending ultimate strength occurs. Under or de-carburated materials also containing fragile phases  $\eta$ , feature poor ultimate strength.*

*Hardness is affected by micro-porosity, granulation of WC phase, purity and composition, extent of homogenization of the liquid and carbons.*

*The excessively high sintering temperature results in a lower density which further negatively affects the mechanical strength.*

*The magnetic saturation increases with higher Co contents; it is worth mentioning that bigger grain alloys have a force considerably lower than that of fine grain ones.*

**Keywords:** *oxidation resistance, improved electrical, heat conductivity, hardness, density, porosity, alloys*

### 1. INTRODUCTION

The alloys mainly used for short chip material cutting ( cast iron, porcelain, etc) are alloys of WC-Co type, in some cases with small additions of other carbons. The same compositions but of different granulometric classes are also used for pieces exposed to wear ( wire drawing, moulds, etc) .

The higher performance of the WC-Co alloys in short chip machining applications is accounted for by its very good heat conductivity which is 2-3 times higher than that of fast steels

The alloys WC-Co, WC-TiC-Co, are mainly used for short chip material cutting and wear-resistant piece applications [1, 2] .

The hard-alloys producers can resort to a wide range of possibilities to achieve variation of the properties of a WC-Co composition and thus they can adapt their products to the particular types of tools they may choose to manufacture .

The present metallography technique allows for a correct identification and evaluation of hard sintered carbons structures. The metallography approach is an indispensable method of investigation and control in industry .

## 2. RESEARCHES AND EXPERIMENTAL RESULTS

When evaluate the structure of the hard sintered carbons structures by metallography method, the distinction is made between the metallographic aspect of the WC-Co , WC-TiC-Co by WC-TiC-TaC-(Nb)C-Co alloys. Particular attention is paid to the distribution of the sintering binder , namely the cobalt, to see the correlation between the alloy properties and cobalt content

In the case of two alloys having the same cobalt content but different WC granulations .it is found that a harder alloys involved finer granulations while milder alloys implies rough granulations.

The cobalt, which takes the form of very fine inclusions with alloys 5% Co and 95% WC , is much more agglomerated between the WC crystals along with a slight porosity .

Fig 1 illustrates the metallographic structure of the alloy containing 6% Co and 94 % WC and average granulation. The basic constituent , WC, is under recrystallization form, called  $\alpha_2$  which structurally stable crystals under triangle prismatic shapes of rectangular bases.

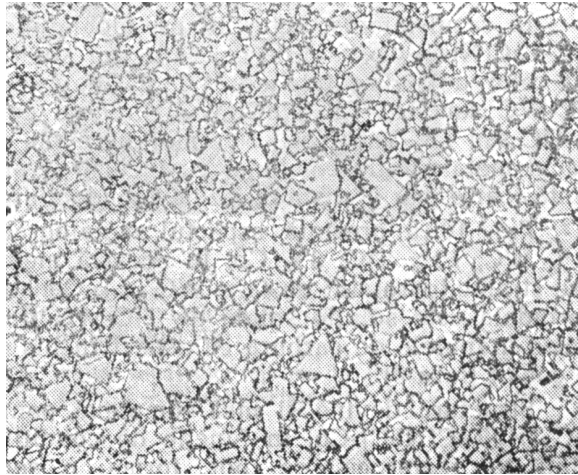


Figure 1. The metallographic aspect of the alloy containing 6% Co and 94 % WC , x1500, sol.KOH-K<sub>3</sub> (Fe(CN)<sub>6</sub>)

As to hardness, there is a tight correlation between the Co content and the WC-Co alloys produced under identical conditions. As shown in fig. 2, hardness decreases with the increase in the cobalt content.

The sintering temperature and the exposure time along with the type of grinding and mixture homogenizing can decisively affect the sintered metallic carbons alloys.

Hardness reaches max values with the optimum sintering temperature and then it decreases as a result of carbon recrystallization and alloy super-sintering. An excessive sintering time, even if the temperature is optimum, has the same effect ie lower hardness. The WC-Co alloy density depends on the Co content and the extent of sintering. Fig 3 shows the density variation depending on Co content in the alloy; it implies that the real measured density takes values within 0,5 - 3%, under the theoretical calculated values. This may be accounted for by the residual porosity

which is the result of a normal sintering process because of insufficient mixture homogenizing or slight low-or high carburizing which may occur with sintering [3,4].

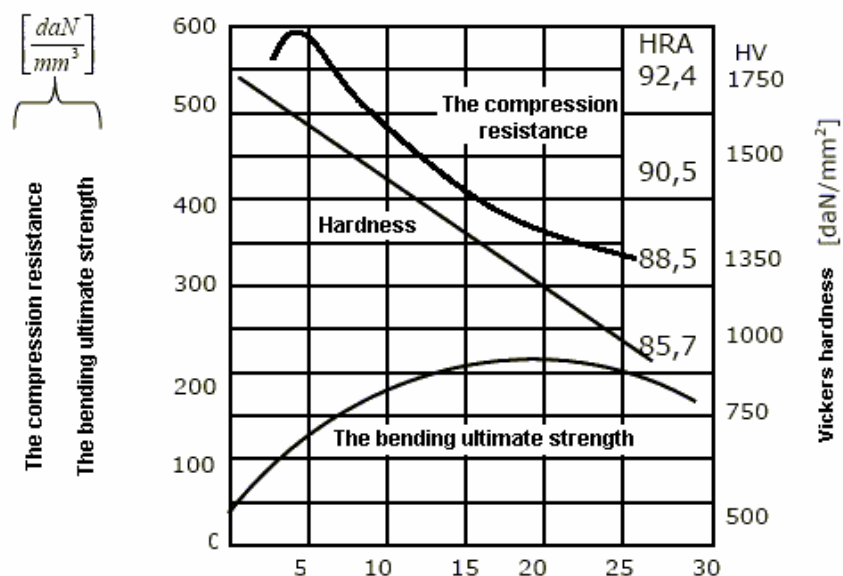


Figure 2. Variation of hardness, breaking and bending resistance and compression resistance of the alloys WC-Co, influenced by the Co content.

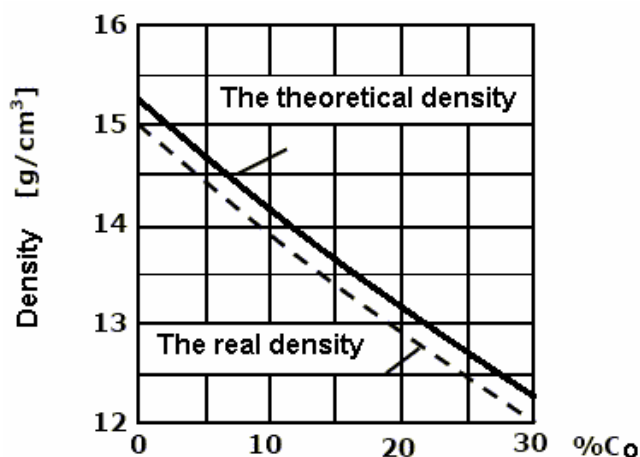


Figure 3. Alloy density vs Co content

As to the density variation, the specific pressure for pressing the compressed pieces has a lower influence while the sintering conditions, such as the sintering temperature and its being kept at lower values, play a decisive role in determining density (fig 4).

Modern methods such as hot pressing or hot iso-static pressing, allow for reaching densities identical to the calculated ones [5].

The breaking/bending strength of the WC-Co alloys increases with the cobalt content but the relation is not linear (Fig 2), [6]. The increase in the breaking/bending strength takes place also in the alloys having more than 20% Co provided these are sintered under special conditions (protected against carburizing). With alloys of 10% Co no permanent deformations of the material can be noticed during the breaking strength test, while they are quite obvious with Co contents higher than 20%.

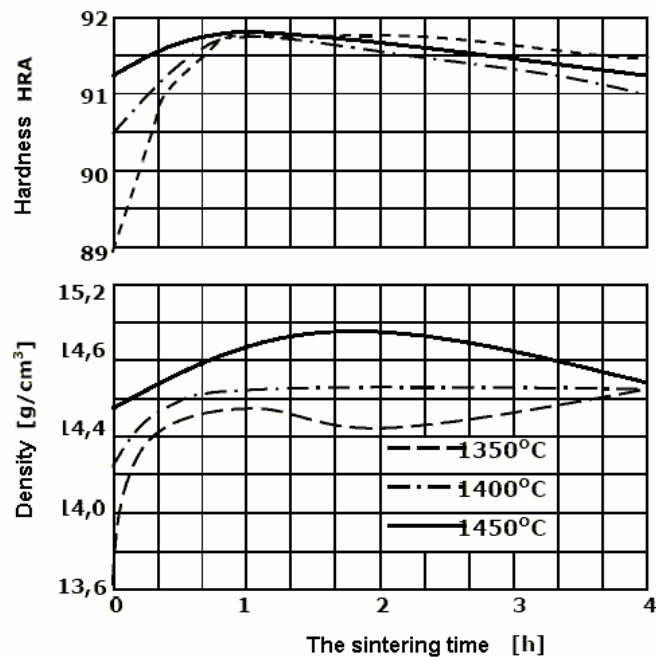


Figure 4. The effect of the sintering temperature and time on the WC-Co alloy containing 6% Co density and hardness

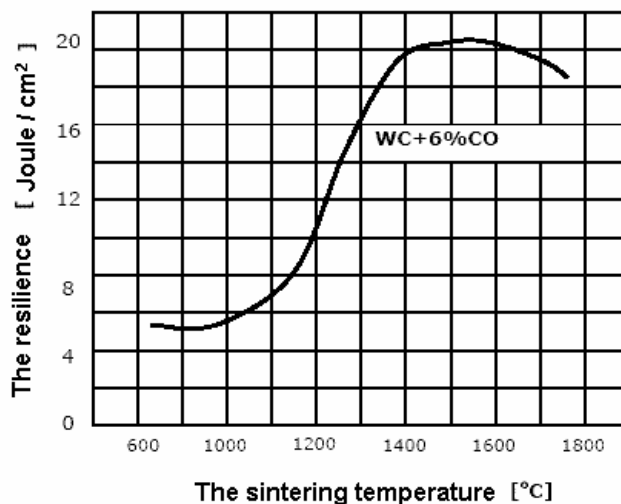


Figure 5. Chock resistance variation vs temperature on the WC-Co alloy containing 6% Co

The compression resistance of the WC-Co alloys, as shown in fig 2 increases with the Co content and then significantly decreases after 4% limit is exceeded .[7,8]

The resilience or impact resistance of the metallic sintered carbon alloy is a measure of the mechanical chock resistance. Chock resistance variation vs. temperature is illustrated in fig 5. The values of this curve have been determined on groove-free samples, 6x6 mm cross section, leaning against seats 40 mm distance apart. The curve shape reaches a peak at the optimum alloy –sintering temperature.[9]

The elongation strength is quite difficult to determine for such a fragile material like the hard sintered carbon alloy All the composition WC-Co containing up to 10% Co show no permanent deformation of the material. It can however be noticed elastic deformations, without plastic deformations, immediately after breaking alloys containing more than 25 % can feature a measurable elongation, [10]

The WC -Co alloy elasticity module is interesting for applications involving elastic strain. As shown in fig 6, the elasticity module decreases with the Co content.

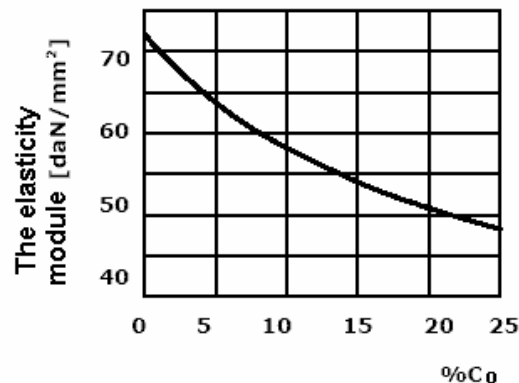


Figure 6. Elasticity module variation with Co content for WC-Co alloy

As regards the magnetic properties of the WC-Co alloys, magnetization upon saturation is related to the Co content ( the phase  $\eta$  - double Co and W carbon) and the force acting upon it strongly depends on sintering extent and the grain size. Thus the magnetic measurements can be of use in quality control, [11]

The scope of application of WC-Co alloys is a consequence of their properties as shown below:

Group I- 97% WC- 3% Co and 95,5% WC – 4,5% Co has the following scope of application: cutting of graphite , ceramics and other metallic materials, grinding, accuracy drilling of cast iron, non ferrous material machining, drawing machines .

Group II- 94,5% WC – 5,5% Co and 93,5% WC – 6,5% Co is used for:

a) global granulation sorts ( cast iron processing, non- ferrous materials and alloys, synthetic and plastic materials, sensors for wear resistance tools and pieces requiring no high tenacity , drawing machines .

b) fine granulation (machining of gray cast iron, mild cast iron, steels of ultimate strength higher than 175 daN/ mm<sup>2</sup>, bronze, Si alloys, drawing machines .

Group III – 91% WC – 9% Co , 89% WC – 11% Co , 87% WC – 13% Co used for machining wood , synthetic resin , easy machining of steels, brass and bronze grinding ,plates for agriculture tools, wear pieces calling for high tenacity.

Group IV – 85% WC – 15% Co , 80% WC – 20% Co , 75% WC – 25% Co , 70% WC – 30% Co used for: wear resistant parts calling for high tenacity ( cutting tools etc. ) .

### 3. CONCLUSIONS

Hardness is affected by micro-porosity , granulation of WC phase , purity and composition , extent of homogenization of the liquid and carbons.

The excessively high sintering temperature results in a lower density which further negatively affects the mechanical strength. The max values taken by the bending ultimate strength are reached at Co 20 - 25 % and suddenly decrease with high Co contents At theses compositions there are no contact bonds among the carbons, the carbon crystals being individual and surrounded by the Co metallic mass. Due to over- heating and granulation growth by re-crystallization an acute decrease in the bending ultimate strength occurs. Under or de-carburated materials also containing fragile phases  $\eta$  , feature poor ultimate strength .

The compression resistance first increases with the Co content then considerably decreases after the Co 4% is exceeded. The resilience of a Co 6% alloy increases with temperature and reaches a max value at 1600°C. The elongation vs compression resistance ratio is estimated as 1: 3 while the elongation resistance vs ultimate strength ratio is three times higher than that of steel. The magnetic saturation increases with higher Co contents; it is worth mentioning that bigger grain alloys have a force considerably lower than that of fine grain ones.

Received April 28, 2005

"Dunărea de Jos" University Galați

#### REFERENCES

- /1/. Mitoșeriu O. , Constantinescu S. , Radu T. ,ș.a. , *Modern methods to perform the properties of metal materials* , Universitatea „ Dunărea de Jos „ din Galați , 1998 ;
- /2/. Drugescu E.: *Thermiques treatment* , Didact. și Pedag., Publishing House , București, 1998;
- /3/. Constantinescu S. , Radu T., *Modern methods to perform thin layers*, Romanian Metallurgical Foundation Scientific. Publishing House , București , 2003;
- /4/. Constantinescu S.: *Metals properties and physical control methods*, Didact și Pedag. Publishing House , București , 2004;
- /5/. Constantinescu S.: *Destructive and nondestructive tests of metals*, Evrika Publishing House , Galați, 2000 ;
- /6/. Constantinescu S., Drugescu E. : *Studies on Mechanism and Kinetics of Phase Transformation in Superficial Layers Using Unconventional Procedures*. Research Contract no. 5005, Galati, 1995, p.53;
- /7/. Constantinescu S., Drugescu E., Radu T. : *Practical application of AE of the different grades of steel*. “ *Proceedings of the 25<sup>th</sup> European Conference on Acoustion Emission Testing* “ EWGAE 2002 “ Prague Czech Republic , 11 –13 september, 2002 , p. 135
- /8/. Constantinescu S. : *Influence of manufacturing process on chemical and structural homogeneity of welded pipe sheets for tanks and vessels working under pressure*. “ *Proceeding of the International Conference on Advances in Materials and Processing Technologies*, september 18 – 21 , Leganes, Madrid, Spain, 2001 , p.57 ;
- /9/. Constantinescu S., Drugescu E ,Radu T. : *The coating on the steel support* , 2003 *European Congress and Exhibition on Advanced Materials and Processes*, 1-5 sept., Lausanne, Switzerland, 2003 , p. 59, paper F4-456 . 2003
- /10/. Knauschner A. , *Elektrochemische Metallabscheidung*, Oberflächenveredeln und Plattierent von Mettalen, Leipzig, 1988, pag.61-119;
- /11/. Morosanu C.E. , *Chemical vapour deposition thin layers*, Ed.Tehnică, Bucuresti, 1981;

#### CORELAȚIA DINTRE MICROSTRUCTURA ȘI PROPRIETAȚILE ALIAJELOR DURE SINTERIZATE

**Rezumat:** Aliajele simple WC – Co cu același conținut de cobalt , față de aliajele conținând TiC sau TaC( NbC) , prezintă o mai ridicată tenacitate și rezistență la rupere la încovoiere ca și o mai bună conductibilitate electrică și termică. Rezistența la oxidare a aliajelor simple WC – Co este considerabil mai mică și aceasta conduce la o pronunțată tendință de sudare a așchii și respectiv o rezistență scăzută .Valorile maxime ale rezistenței de rupere la încovoiere sunt atinse la 20 – 25% Co și descresc brusc pentru conținuturi de Co înalte . La aceste compoziții , legăturile în punctele de contact între carburi numai există, cristalele de carbură apărând în structura metalografică sub formă individuală și fiind înconjurate de masa metalică a liantului – cobalt. Datorită supraîncălzirii și creșterii granulației prin recristalizare , are loc o pronunțată scădere a rezistenței la rupere prin încovoiere . Materialele subcarburate sau decarburate , conținând și faze fragile  $\eta$  , prezintă de asemenea o rezistență la rupere slabă. Duritatea este afectată de microporozitate , de granulația fazei WC , puritate și compoziție , grad de omogenizare a lichidului și al carburilor. Temperatura excesiv de înaltă de sinterizare conduce la o reducere a densității , care are un efect nefavorabil asupra rezistenței mecanice. Saturația magnetică crește cu creșterea conținutului de cobalt și , de asemenea , este de remarcat că aliajele cu granulație mai mare au forța coercitivă considerabil mai joasă decât cele cu granulație fină la aceleași compoziții .

## THE INFLUENCE OF JOINING TEMPERATURE ON THE BIMETAL LAYER STRUCTURE AND CHARACTERISTICS

BY

PETRICĂ CORĂBIERU<sup>1</sup>, ANIȘOARA CORĂBIERU<sup>1</sup>, IOAN ALEXANDRU<sup>2</sup>, IOAN VRABIE<sup>1</sup>

**Abstract.** *The thermal treatment at negative temperatures is an efficient and convenient modern thermal processing that, correctly applied in the technological operations, determines important increases in the exploitation properties of the alloyed and highly alloyed steel tools. The author's latest investigations on the influence of the cryogenic thermal treatments applied to highly alloyed steels from the high speed steels (HSS) on the mosaic blocks size and dislocations density are presented.*

**Keywords:** *bimetal bushes*

### 1. INTRODUCTION

The originality of this manufacturing process for steel-bronze bimetal bushes by immersion and vertical centrifugation (ICV) consists in its complete national novelty. The ICV process contributes at elimination of some operations and equipment which are required for the pre-heating, handling of liquid metal, casting in classical centrifugal machines, and extraction. The ICV process allows full automation, crossing and overlaying of the production processes – the deposition one and the bar and parts casting.

### 2. THE EXPERIMENTAL TECHNOLOGICAL PRINCIPLE

The technological experimental principle for execution of steel-bronze bimetallic bushes consists of the immersion of the steel core in the bronze bath, lifting the core out of the bath until about half its height and its spinning with an appropriate angular speed required for the deposition to take place. The centrifugal force that appears by spinning of the core in the bronze bath determines the repartition of bronze on the walls of the core steel, the adherence of the bronze layer and the diffusion of the atoms at the steel-bronze interface, thus creating the inter-phase zone. The principle schema of executing bimetallic bushes by vertical centrifuging is presented in fig. 1. The steel bush is immersed in the bronze bath and its spinning begins.

In the beginning time of the deposition process, the melted bronze does not have a uniform angular speed in all its layers, but gradually this speed gets uniformed and becomes equal to the angular speed of the steel core. In these conditions the spinning movement is stabilised and we can say that the spinning melted bronze finds itself in a relative rest situation, the space form of the free surface being a rotational paraboloid. After the stabilising of the spinning movement, the bush is gradually lifted up so that,

when the optimal deposition speed is reached, the bush is immersed only a hint in the bronze dip.

## 2. The experimental equipment for execution of bimetallic products by ICV

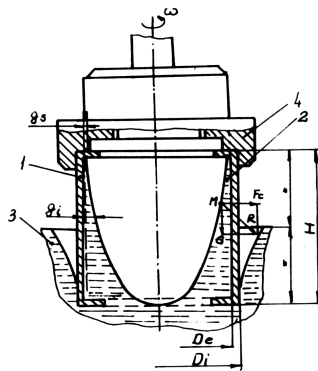
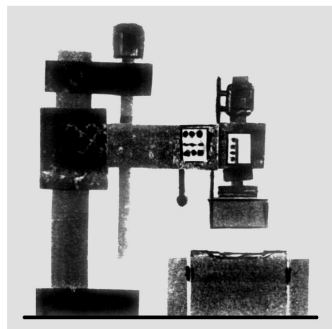


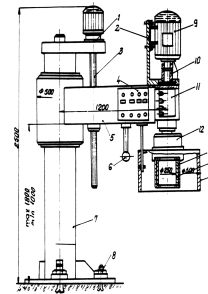
Figure 1: Principle scheme of the ICV process

1. Steel core; 2. The bronze layer distributed on the core walls; 3. The bronze bath; 4. Fastening chucks.

The experimental installation, designed and built for the execution of bimetallics by ICV is found in the TF department of the FORTUS S.A. Iași. The designed and built MC is the main equipment of the installation for execution of bimetallic bushes. The MC ensures the displacement of the steel core to each and every working point of the installation, executes the immersion of the bush core in the IDP, in the CTI, and in IR, as well as the spinning movement of the bush in the bronze bath in view of executing the deposition by ICV. In figure 2, the MC and its designed principle scheme are presented.



a



b

Figure 2. The machine for centrifuging MC

- a. the machine for vertical centrifuging for execution of bimetallics by ICV; b. the principle scheme of the designed and built MC; 1. Motor reduction gear for vertical movement; 2. Support for electric dc engine; 3. Screw-nut mechanism for vertical movement; 4. Control panel; 5. Folding arm; 6. Handle; 7. Guide column; 8. Foundation screws; 9. Dc engine; 10. Coupling; 11. Main shaft; 12. Mechanic lathe; 13. Steel bush; 14. Deposited bronze layer; 15. Sliding cylindrical guard.

## 3. THE INFLUENCE OF THE JOINING TEMPERATURE AS A METALLURGIC FACTOR ON THE CHARACTERISTICS AND STRUCTURE OF THE BIMETALS OBTAINED BY ICV

In order to outline the influence of the joining temperature a series of parameters have been held constant, and assessments were made for different values of the joining temperature. The parameters that were held constant in the experiments were: the dimensions of the basic half-finished  $\Phi 140 \times 8$ , OLT 35; the deposited bronze

layer: upper thickness  $G_s = 4$  mm; lower thickness  $G_i = 12$  mm; final thickness after working  $G_0 = 4$  mm; length of the steel core  $L = 140$  mm; duration of the joining process = duration of holding at the regimen angular speed = 90 s; the angular speed: 500 r.p.m.

During our experiments, 24 bimetallic bushes were executed: OLT35 – CuSn10 = 8 bimetallic bushes; OLT35 – CuAl19T = 8 bimetallic bushes; OLT35 – CuSn4Zn4Pb17 = 8 bimetallic bushes. From the experimentally obtained bushes, we took samples for execution of the test bars required for testing the bend resistance ( $L = 130$  mm,  $l = 10$  mm, diameter of the rod  $d = 3$  a = 30 mm, length of the joining area subject to bending  $l' = \pi(d+a/2)/2 = 54$  mm), of test bars for assessing the shearing disassembly resistance – specific adherence (area of the surface subject to shearing disassembly  $A = 1.5 g_s = 48$  sq.mm), and test bars for assessing the traction resistance.

The graphical analysis of the performed assessments within the experiments is shown in figure 3 – 5. The micro-structures of the joining areas of the experimented bimetallics are shown in figure 6 – 8.

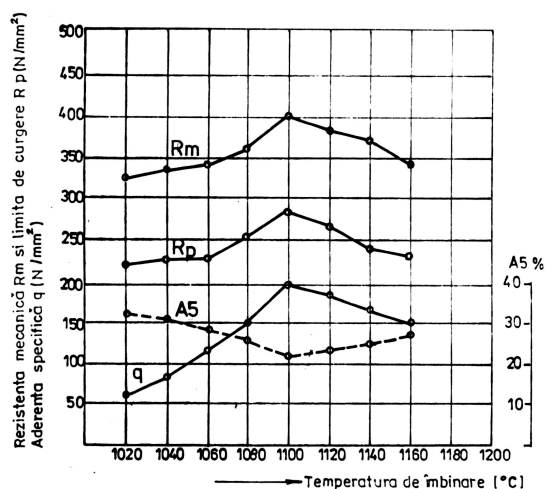


Figure 3. Influence of the joining temperature on the characteristics of the bimetal OLT35 – CuSn10

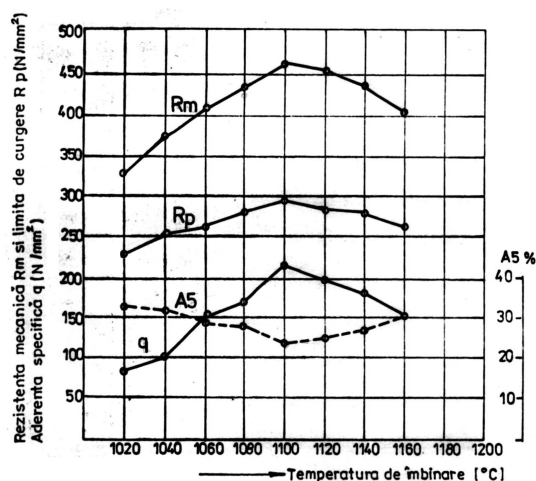


Figure 4. Influence of the joining temperature on the characteristics of the bimetal OLT35 – CuAl19T

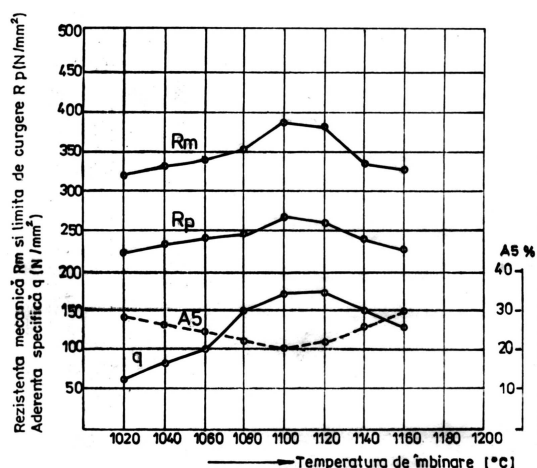


Figure 5. Influence of the joining temperature on the characteristics of the bimetal OLT35 – CuSn4Zn4Pb17

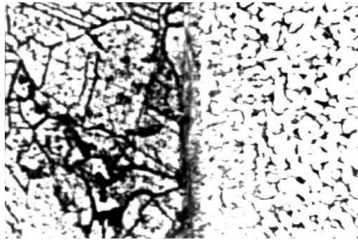
SD ZI MB

Figure 6. OLT35 – CuSn10 ( $T_{\text{join}} = 1120^{\circ}\text{C}$ )SD (deposited bronze layer) – s.s. $\alpha$  polyhedral with macles

MB (base material – steel) – ferrite – pearlite with homogenous and iso-axial grains

ZI (joining area) – passage area; the fully dissolved oxides; chemical bonds by element diffusion

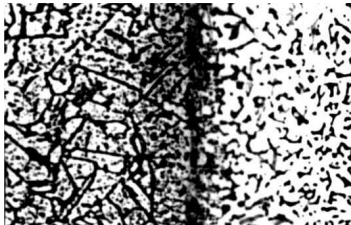
SD ZI MB

Figure 7. OLT35 – CuAl9T ( $T_{\text{join}} = 1160^{\circ}\text{C}$ )SD polyhedral s.s. $\alpha$ 

MB ferrite + pearlite

ZI passage area; the oxides are dissolved

SD ZI MB

Figure 8. OLT35 – CuSn4Zn4Pb17 ( $T_{\text{join}} = 1140^{\circ}\text{C}$ )

SD homogenous structure with small grains

MB ferrite – pearlite

ZI passage area; the oxides are dissolved; chemical compounds of the steel core, OLT35

#### 4. CONCLUSIONS

At joining temperatures  $T_{\text{join}} = T_{\text{melt1}} + 100^{\circ}\text{C}$  there is an optimal correspondence between the main characteristics:  $R_m$  and  $R_p$  have high values;  $A_5$  is lower; the specific adherence reaches values  $q > 170 \text{ N/sq.mm}$  that correspond to hard joints.

- At joining temperatures  $T_{\text{join}} > T_{\text{melt1}} + 100^{\circ}\text{C}$  the mechanical characteristics  $R_m$  and  $R_p$  decrease and the specific adherence diminishes towards  $150 \text{ N/sq.mm}$  corresponding to medium joints
- The joining temperature does not significantly afflict the thickness of deposited bronze layer

- The influence of the joining temperature on the structure of steel-bronze bimetallic joint comprises the following aspects:

a)  $T_{\text{melt1}} < T_{\text{join}} < T_{\text{melt1}} + 100\text{ }^{\circ}\text{C}$

Areas where partial blending of alloys occurs, and joining knots appear; areas where oxides are held in singular places between layers and areas where they are crashed and transformed in single spherical particles; concentration of defects in the nearby of the joint limit; alternating areas of joining knots and cohesion bridges; the area close to the steel is enriched in Pb, thus leading to intermediate lead structures in the bronze.

b)  $T_{\text{join}} = T_{\text{melt1}} + 100\text{ }^{\circ}\text{C}$

- Transitional areas on the whole interface; the oxides are completely dissolved
- Chemical bonds (the atoms of C and Fe have diffused in the bronze)

c)  $T_{\text{join}} > T_{\text{melt1}} + 100\text{ }^{\circ}\text{C}$

- Alternating areas of joining bridges and interface transitional areas;
- Isolated spherical oxides
- Cu diffuses in the steel and C and Fe in the bronze
- Chemical and structural irregularities in the nearby of the joining area;
- The zone close to the steel gets rich in Pb.

Received April 19, 2005

<sup>1</sup> PRESUM PROIECT Sh.C. Iași

<sup>2</sup> Technical University "Gh.Asachi" Iasi

#### REFERENCES

- /1/. Alexandru I., Corăbieru Petrică, Vasilescu Dan – *Contribuții privind influența factorilor metalurgici asupra caracteristicilor și structurii straturilor bimetalice*, First International Congress in Materials Science and Engineering, nov., 1994, Iași, Buletinul Institutului Politehnic Iași, Tomul XL (XLIV), Fasc. 1-2, vol.1, pag.511-518
- /2/. Corăbieru Petrică ș.a.- *Cercetări privind realizarea tehnologiei de obținere a semifabricatelor multistrat de tipul barelor, lamelelor, cuzineților, tamburilor și recipientelor rotunde prin procedee de depunere, stratificare și îmbinare, folosind metode gravitaționale prin imersie în medii izoterme*, Contract de cercetare științifică nr. C166 –B1/1996, S.C. Presum Proiect S.A. Iași, Beneficiar MCT București
- /3/. Corăbieru Petrică, Alexandru Ioan, Vasilescu Dan – *Tehnologie de obținere a bimetalelor oțel-bronz*, Conferința Internațională de Optimizarea Proiectării și a Tehnologiilor de Prelucrare în Construcția de Mașini, oct., 1995, Bacău, Buletinul Sesiunii Științifice, Academia Română, Filiala Iași, Vol.2, TSTM –1, 1995, pag. 358-362
- /4/. Corăbieru Anișoara, ș.a.– *Cilindri bimetali fabricați prin asamblări ax- tăblie din turnare*. Editura Tehnopress, Iași, 2004, ISBN 973-702-020-0
- /5/. Corăbieru Petrică, ș.a., - *Bimetale fabricate prin imersie și centrifugare verticală*. Editura Tehnopress, Iași, 2004, ISBN 973-702-048-0.

#### INFLUENȚATEMPERATURII DE ÎMBINARE ASUPRA STRUCTURII STRATULUI DE BIMETAL I CARACTERISTICILOR ACESTUIA

**Rezumat:** Tratatamentul termic la temperaturi negative este un eficient și convenabil proces termic modern care, aplicat corect în cadrul operațiilor tehnologice, determină creșteri importante ale proprietăților de exploatare ale sculelor realizate din oțeluri aliate și înalt aliate. Sunt prezentate ultimele cercetări ale autorului asupra influenței

tratamentului termic criogenic aplicat oțelurilor înalt aliate din categoria oțelurilor rapide (HSS) asupra mărimii blocurilor mozaic și densității de dislocații.

## THE MANUFACTURING TECHNOLOGY FOR PRESS TOOLS THROUGH SUCCESSIVE ALLOYING AND ZONAL HEATING PROCESS BY CONTACT (ASPTZC)

BY

PETRICĂ CORĂBIERU<sup>1</sup>, ANIȘOARA CORĂBIERU<sup>1</sup>, IOAN ALEXANDRU<sup>2</sup>, IOAN VRABIE<sup>1</sup>

**Abstract.** *ASPTZC method is formed from two main phases:*

- *successive alloying - direct achieved from casting through interaction of the liquid steel with the alloying layers which are deposited on the casting form walls. These alloy layers were obtained using alloying pastes which contain graphite, FeV, FeMo, FeCr, electrolytic Ni, diluent and binders;*
- *zonal heating process through contact – it is made on a simple PTZC installation using treatment cyclograms, which were established before, depending on the material of the pneumatic and calibration tools which are treated, composition and structure of the superficial layers obtained after the first phase AS*

**Keywords:** *successive alloying, zonal heating processes*

### 1. INTRODUCTION

ASPTZC is a modern manufacturing method for the achievement of tools with soft and tenacious core and hard superficial layers, which are resistant at all loading.

The thickness of the superficial layer is usual small comparative with the base material which assumes the majority of loading during the tools working. Comparative with the usual versions the pneumatic and calibration tools manufacturing through ASPTZC method assures a substantial reduction of the costs and all special properties of the work surfaces are respected. All this reasons justifies the growth of industry interest for the using of superficial hardened tools like a characteristic of the modern economical development.

### 2. SUGGESTED TECHNICAL SOLUTION – SUCCESSIVE ALLOYING AND ZONAL HEATING PROCESSING BY CONTACT

The suggested process for manufacturing of tools is new in Romania because it is obtained through successive alloying and zonal heating processing by contact.

ASPTZC method is formed from two main phases:

- successive alloying - direct achieved from casting through interaction of the liquid steel with the alloying layers, which are deposited on the casting form walls. These alloy layers were obtained using alloying pastes which contain graphite, FeV, FeMo, FeCr, electrolytic Ni, diluent and binders;
- zonal heating process through contact – it is made on a simple PTZC installation using treatment cyclograms, before established, depending on the material of the

pneumatic and calibration tools which are treated, composition and structure of the superficial layers obtained after the first phase AS.

The successive alloying replace the classic version of manufacturing for the tools from alloy steels with a more simplified version like phases and technological operations; it is based on casted steels that are cured in liquid phase through a new method which can be achieved on the installations from firms with metallurgic profile like S.C.FORTUS S.A. IAȘI. This method offers the advantage that the steel has a low manufacturing price and the high mechanical-physical characteristics are obtained through the diffusion of the carbide alloy elements (V, W, Cr) from the alloy pastes which are deposited on the cast form cavity surface for the tool. The durability of tools, which are obtained through ASPTZC, is comparative with the durability obtained through classic versions, respectively from alloy steels through one-piece method.

The science purpose is to obtain tools with a superficial layer which is resistant at composed loading: contact pressure, compression, wear, endurance and heating-mechanical composed alternative shocks.

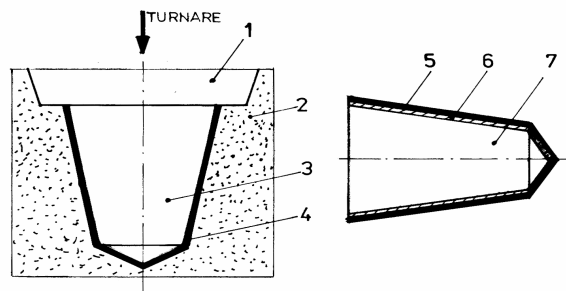


Fig.1 The principle scheme of the AS - superficial successive alloying - direct from the tool casting.

1. Casting feeder cavity; 2. Casting form;
3. Casting form cavity; 4. Alloying paste layer;
5. Successive alloying superficial layer; 6. Transition intermediate layer; 7. Tool core.

The method principle is described in figure 1.

The performances which are obtained through AS are comparative with the results obtained through the casting of high alloy steels.

The zonal heating processing by contact consists in using of Joule-Lenz effect which is produced by continuous or alternative current of 50 Hz frequency through the contact resistance from pressing of a copper electrode roll on the tool surface. The heat quantity is distributed between roll and tool, but the superficial layer absorbs

the most important part of heat. In a very short time a volume from the tool superficial layer arrives the austenite range. The current density proportional decreases with the square of distance to the core of processed tool. The heating of tool superficial layer is a gradual heating in spiral and the majority of tools have a cylinder shape or cylinder portions. This method has the following particularities:

- the appearance of a cold superficial layer (fig. 2a);
- the forming of auto-tempered strips in spiral (fig. 2b).

The temperature that must be maintained for the roll and superficial layer is 450° C and so the heat is continuous send to the tool core and roll

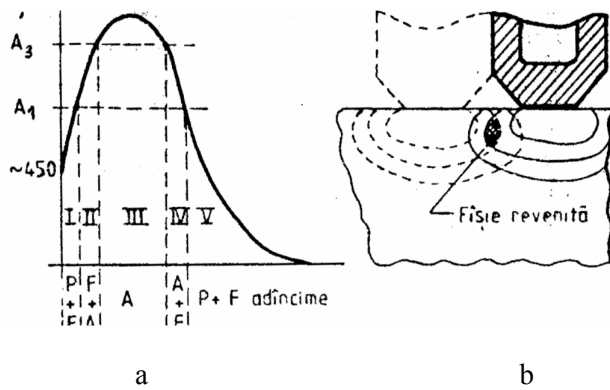


Fig. 2. The temperature variation in the tool superficial layer depth. a – zones which appear in the superficial layer at heating; b – the mode how appear the auto-tempered strips in spiral after cooling.

The temperature in the depth of tool superficial layer varies after a diagram which has five zones: - zone I under-heated (under  $A_1$ ); - zone II intercriticalheated; - zone III: heated over  $A_3$ ; - zone IV intercriticalheated; - zone V temperature under  $A_1$ . Because there are these five heating zones the hardened structure is nonuniform and it has three distinct portions:

- section I with initial structure (zone I and zone V);
- section II - incomplete hardened (zone II and zone IV);
- section III - complete hardened (zone III).

The existence of zone I represents an advantage because it is avoided the overheating, but it is a disadvantage the necessity of processing for removing of zone I and zone II which are soft.

The auto-tempered strips appear because the roll creates a thermal field which partial overlaps over the already hardened strips.

The method novelty consists in the following aspects:

- in the first phase it is achieved ,direct from casting, the successive alloying (AS) of the tools active superficial layers; the tools superficial layers are enriched with alloy elements Cr, Ni, V, Mo while the carbon content grows until 0,6%;
- in the second phase it is achieved the zonal heating process by contact (PTZC) which consists in two phenomenons:
  - the martensite hardening (structural transformation of phase); it is obtained a hard martensite-sorbite structure;
  - the forming of the hard chemical compounds in the superficial layer: hard carbides of Cr, Ni, V, Mo (chemical transformations).

### 3. EXPERIMENTS

For the selection of the optimal version for the casting-forming process, heating treatments, paste formula and technological parameters were studied many versions.

#### 3.1. Forming-casting versions which were experimented

The low alloy hypoeutectoid steel, which is used for the experiments, was smelted in the induction electrical furnace with a capacity of 100kg. It was selected the indirect method for the casting because it has the following advantages comparative with the direct method: the thermal stress of the forms is more low; it assures a complete filling with a suitable speed; the surface quality is better; the tools (tests) can be placed very easy in a horizontal position and so the obtained structures are uniform.

The forming was achieved with cores, which were prepared from forming mixture with reinforced silicate with CO<sub>2</sub>. It were experimented three forming versions which are simplified presented in figure no. 3.

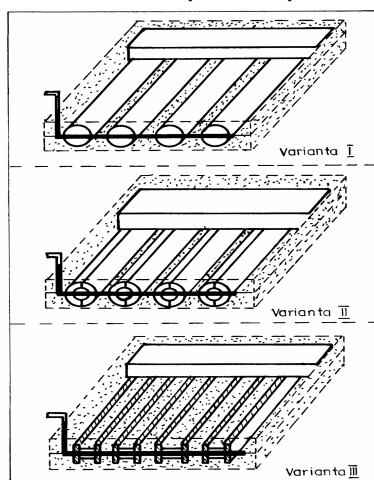


Figure 3. Version I – Forms with circular cross section  
Version II – Forms with semicircular cores  
Version III – Forms with I cores

After drying, on every core was applied a hardening paste layer. The drying and lubricating process was twice repeated.

### 3.2. Versions of hardening pastes which are used at the tools alloying

The method for preparing of hardening paste and the precisely establishment of the chemical composition represent some of the most important aspects of the hardening process. The reconnaissance and the obtained results on the tests prove that the researches must be achieved on three casting pastes. When the paste is applied on the active surface of the core, a mass is transported through diffusion at contact from metal-liquid-paste and so it is achieved the micro-alloying with Mn, V, Ni, Cr, Mo on a depth of a 2,5 mm.

In table 1 are presented the main component elements for three paste versions.

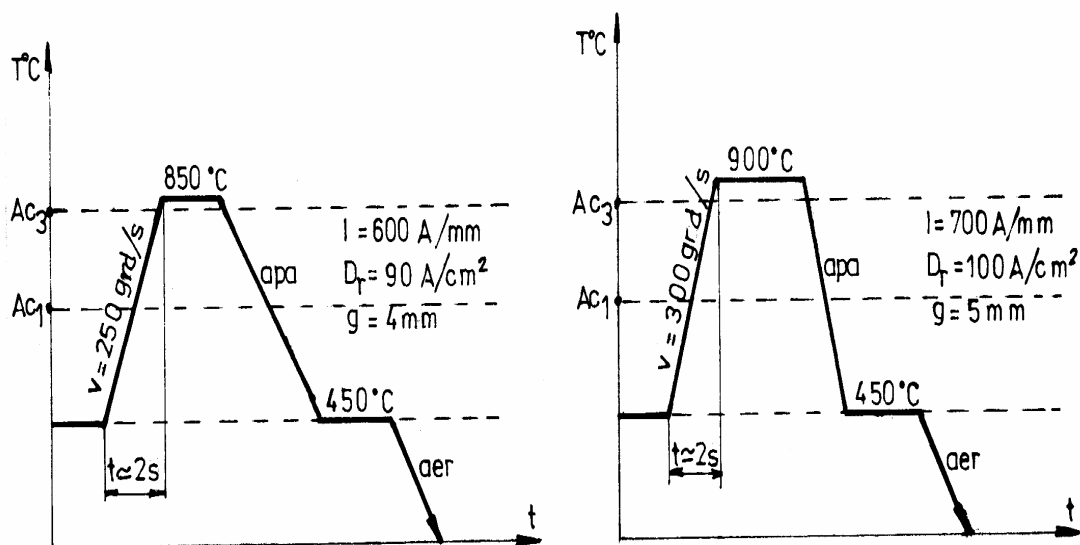
Table 1. Paste types

Paste notation	Main elements
Type A	Graphite + FeV + FeMo
Type B	Graphite + FeV + FeMo + Ni (electrolitic)
Type C	Graphite + FeV + FeMo + Ni + FeCr

The layer depth, of paste which is applied through brushing on the active surfaces of the core, is about 1,5-2 mm. For every paste formula was obtained different depths and superficial layer structures, which determine different behaviours of the tools during working. The determination of the best paste formula was achieved depending on the layer aspect, carbon and alloying elements content which is absorbed by the tools, the achieved hardening and other aspects which influence the tool behaviour in tests.

### 3.3. Zonal heating processes by contact which were experimented

After casting, cooling and knock-out the tools were zonal heating processed by contact. For the improvment of the tools machinability it must be cured like in figure 4, where are presented two cyclograms for the PTZC versions.



Version 1 PTZC

Version 2 PTZC

Figure 4 – Cyclograms for PTZC versions

This cyclogram of heating treatment had good results because it was achieved very easy and the study of other version wasn't necessary.

#### 4. ANALYSIS OF THE LABORATORY EXPERIMENTS RESULTS

The laboratory experiments which consisted in hardness tests, chemical and metallic analysis were made on 12 samples. The laboratory experiments results are presented in table 2.

Table2. Laboratory experiments results

Test sample	Carbon content	Carbon content on				Core hardening HRC	Layer depth
P1	0,2	0,4	0,3	0,25	50	35	2,5
P2	0,2	0,56	0,4	0,3	55	30	3
P3	0,2	0,5	0,4	0,25	50	35	2,5
P4	0,22	0,58	0,45	0,35	55	30	3
P5	0,22	0,6	0,4	0,3	60	30	3
P6	0,22	0,55	0,42	0,25	55	30	2,5
P7	0,25	0,61	0,43	0,32	60	30	3
P8	0,25	0,56	0,38	0,24	50	35	2,5
P9	0,25	0,62	0,45	0,35	60	30	3
P10	0,26	0,61	0,43	0,32	60	30	3
P11	0,26	0,6	0,4	0,33	60	38	3
P12	0,26	0,61	0,43	0,37	60	38	3,5

Sample 1 – charge no.1- carbon from core: 0,2%; - carbon from superficial layer: 0,4%; - carbon at depth of 1,5 mm: 0,3%; - carbon at depth of 2,5mm: 0,25%; - superficial layer depth: 2,5mm; - layer hardening: 50 HRC; - core hardening: 35 HRC; - geometrical configuration: ● 50mm; - L= 200mm; - casting version:I; - paste type: A; - PTZC version: 1; - structure: nital 2,5% attack, 100:1

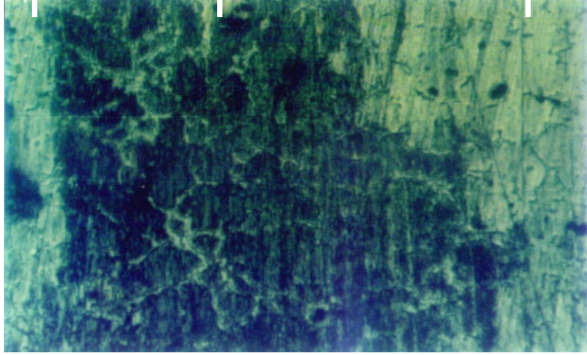


Figure 5. Sample 1 micrograph from charge 1, paste A, version 1 PTZC

1-superficial layer (martensite structure with complex carbides, acicular cementite);  
2-transition zone (transition sorbite-pearlite structure); 3- core (gross ferrite+pearlite).

Sample 2 – charge no.1- carbon from core: 0,2%; - carbon from superficial layer: 0,56%; - carbon at depth of 1,5 mm: 0,4%; - carbon at depth of 2,5mm: 0,35%; - superficial layer depth: 3mm; - layer hardening: 55 HRC; - core hardening: 30 HRC; - geometrical configuration: ● 50mm; - L= 200mm; - casting version:I; - paste type: A; - PTZC version: 1; - structure: nital 2,5% attack, 100:1

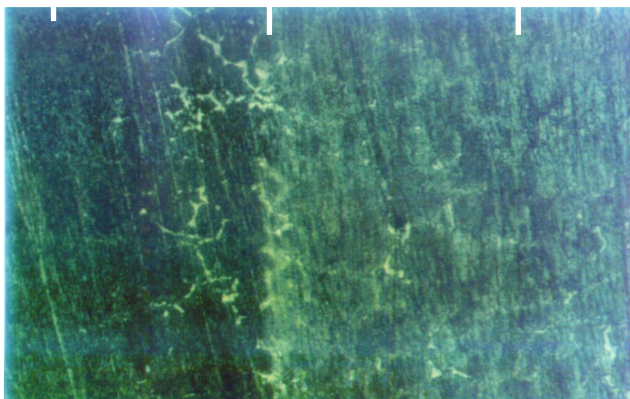


Figure 6. Sample 2 micrograph from charge 1, paste A, version 1 PTZC

1-superficial layer (martensite structure with complex carbides, acicular cementite); homogeneous layer with adequate depth; 2-transition zone (transition sorbite-pearlite structure); 3 – core (gross ferrite+pearlite).

Sample 3 – charge no.1- carbon from core: 0,2%; - carbon from superficial layer: 0,5%; - carbon at depth of 1,5 mm: 0,4%; - carbon at depth of 2,5mm: 0,25%; - superficial layer depth: 2,5mm; - layer hardening: 50 HRC; - core hardening: 35 HRC;

- geometrical configuration: ● 50mm; - L= 200mm; - casting version:I; - paste type: A; - PTZC version: 1; - structure: nital 2,5% attack, 100:1

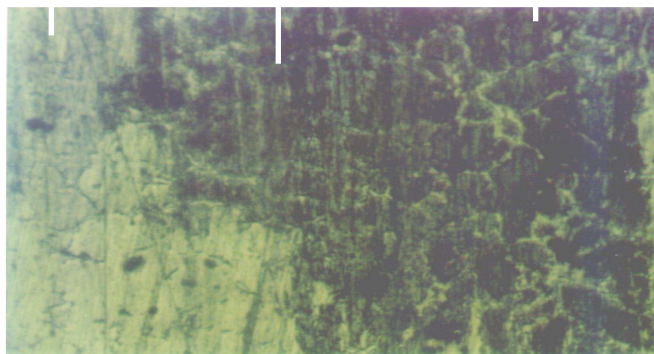


Figure 7. Sample 3 micrograph from charge 1, paste A, version 1 PTZC

1-superficial layer (martensite structure with complex carbides, acicular cementite); homogeneous layer on depth; 2- transition zone (transition sorbite-pearlite structure); 3 – core (gross ferrite+pearlite).

## 5. CONCLUSIONS

After experiments it were obtained the following optimal values for every technological parameter:

- Carbon content in core:	minim 0,2%; maximal 0,26%
- Carbon content in superficial layer:	minim 0,4%; maximal 0,62%
- Carbon content at 1,5mm depth:	minim 0,3%; maximal 0,45%
- Carbon content at 2,5mm depth:	minim 0,25%; maximal 0,37%
- Superficial layer hardening:	minim 50HRC; maximal 60HRC
- Core hardening	minim 30HRC; maximal 38HRC
- Superficial layer depth	minim 2,5mm; maximal 3,5mm
- Casting temperature	minim 1150° C; maximal 1600° C
- Temperature in superficial layer during PTZC process	minim 850° C; maximal 900° C
- Heating speed during PTZC process	minim 250° C/s; maximal 300° C/s
- Electric current intensity/roll breadth during PTZC process	minim 600A/mm; maximal 700A/mm
- Current density in superficial layer during PTZC process	minim 90A/cm <sup>2</sup> ; maximal 100A/cm <sup>2</sup>
- Layer heating depth	minim 4mm; maximal 5mm
- Maintenance temperature of superficial layer during PTZC process	450° C

The best results for the technological parameters were obtained when it were used the following:

- casting version no.II – forms with semicircular cores;
- casting version no. III – forms with type I cores;
- C paste type : graphite + FeV + FeMo + FeCr + electrolytic Ni;
- PTZC version no.2

Received April 19, 2005

<sup>1</sup> PRESUM PROIECT Sh.C. Iași

<sup>2</sup> Technical University "Gh.Asachi" Iasi

/1/. Corăbieru P., Alexandru I., Vasilescu D., *Durificarea și alierea superficială a sculelor perforatoare*, Revista Academiei, 1995, vol.1 TSTM – 1, pag.123- 127, 1995.

/2/. Vasilescu D., Alexandru I., Corăbieru P., *Durificarea și alierea superficială a oțelurilor prin încălzire directă în medii conductive electric*, Revista Academiei ,vol 2. TSTM-1, pag. 347-352, 1995.

/3/. Corăbieru A., *Cercetări privind realizarea tehnologiei de obținere a sculelor de calibrare și pneumatice- ASPTZC-* Contract Cercetare Științifică – nr. 1888/2003- Programul Relansin SC Presum Proiect SA Iași.

/4/. Alexandru I., Corăbieru A., Corăbieru P., *Cercetări privind realizarea tehnologiei de obținere a sculelor de calibrare și pneumatice prin alieri succesive, prelucrări termice zonale prin contact (ASPTZC)-* Revista Cercetări Metalurgice și de Noi Materiale, vol XII nr.3/2004, pag. 11-24, ISSN 1221-5503

/5/. Corăbieru P. ș.a, *Materiale pentru scule de deformare plastică. Procedee de prelucrare termică*. Editura Tehnopress, Iași, 2004, ISBN 973-702-049-9

#### TEHNOLOGIA DE FABRICARE ASCULELOR DE PRESARE PRIN ALIERE SUCCESIVĂ ȘI ÎNCĂLZIRE ZONALĂ PRIN CONTACT (ASPTZC)

**Rezumat:** Metoda ASPTZC are două faze principale:

- aliere succesivă – obținută după turnare prin interacțiunea dintre oțelul lichid și straturile de aliere ce sunt depuse pe pereții formei de turnare. Aceste straturi de aliere se obțin prin intermediul a diverse paste de aliere ce conțin grafit, FeV, FeMo, FeCr, Ni electrolitic, diluanți, lianți ;
- proces de încălzire locală prin contact – se realizează pe o instalație simplă tip PTZC prin folosirea ciclogramelor de tratament de termic stabilite în prealabil, funcție de materialul sculelor pneumatice și de calibrare care vor fi tratate, compoziția și structura straturilor superficiale ce trebuie obținute după prima fază AS

## BEHAVIOR OF Rp3-HIGH SPEED STEEL ON SHORT TIME NITRIDING IN FLUIDIZED BED

BY

ADOLF BÂCLEA, NELU CAZACU, SORIN DOBROVICI, FLORENTINA POTECAȘU,  
ELENA DRUGESCU, OCTAVIAN POTECAȘU

**Abstract.** *For steel nitriding, treatment time is a important factor. Gas and plasma nitriding are usual method to increase surface properties by nitriding. A close retort is used. Total time for treatment are higher because are necessary transition time for heating and cooling. Fluidized bed offer a short time for heating and cooling because furnace having an open retort. Work paper is based by nitriding experiments by experimental fluidized bed furnace. A gas mixture of ammonia and nitrogen was used. For samples were used HSS (Rp3) . Results were investigated micrographic, surface hardness test (HV5) and micro hardness (HV0,05)*

**Keywords:** *nitriding, fluidized bed, HSS, Rp3, short cycle*

### 1. INTRODUCTION

High speed steel (HSS) having a good properties for cutting tools (resistance, hardness, wear resistance, thermal stability) and these properties is determined by chemical compositions (high quantity of alloying elements) and specific heat treatments. A carbon presence in chemical compositions of steel is necessary to a high quantity of complex metallic carbides dispersed in metallic matrix. For these properties HSS are actually used for many other applications: tools for die press forging, extrusion tools and hydraulic parts. For all tools is important hardness over surfaces and surface porosity to maintaining wear agent for a long time that increasing using time of tool. Some thermochemical treatments are used for increased hardness and surface profile control (nitrocarburizing, nitriding). The paper is based by nitriding in fluidized bed experiments. Some goals are following by thermochemical treatments:

- higher values of superficial hardness
- stability at high working temperature
- corrosion resistance
- decreasing values for friction coefficient
- increasing durability

Nitriding treatments of HSS is based by subcritical values of treatment temperature that conduced to low values of inside transformation in material. The treatments is localised at surfaces and a new hard complex with fine distribution is possible to appear before nitrogen diffused in material and alloying elements. Using a fluidized bed technology a short time for nitriding treatment is obtaining and a supplementary hardness appear because secondary brittle by  $Fe_4N$  fine dispersed in metallic grain is avoided

## 2. EXPERIMENTS

Base of experiments are intense chemical activity of fluidized bed made by granular solid (0,10...0,16mm, burned clay) and mixed gas from ammonia (33%) and nitrogen, 0. Working with open chamber make a reduced total nitriding time because samples is take off after nitriding time (1h, 2h and 3h) and was cooling in air. That procedure has a normal benefits by reducing total time of treatments and by eliminate a  $Fe_4N$  precipitates that decreasing hardness, 0. Nitriding in fluidized bed experiments were made on laboratory conditions and nitriding furnace is showing in Figure 1. For experiments was used samples from Rp3 steel (Table 1). For all experiments a constant debit for mixed gases was used.

Table 1. Chemical composition for Rp3 (HSS - T1-AISI, STAS 7382/90).

C	Mn	Si	Cr	W	Mo	V	Co
0,7...0,8	max.0,45	0,30...0,40	3,62...4,40	17,5...19,5	max.0,60	1,0...1,4	-



Figure 1. Fluidized bed laboratory installation

## 3. RESULTS AND DISCUSSION

For Rp3 steel samples micrographic analysis is showing in Figure 2. For etching was used *royal water*. Micrographs showing a nitriding layers for all regimes, that are depending with nitriding time and nitriding temperature. Depth layer measurements on micrographs is showing in Figure 3. Hardness measured on the nitriding surface is the most important properties after nitriding treatments.

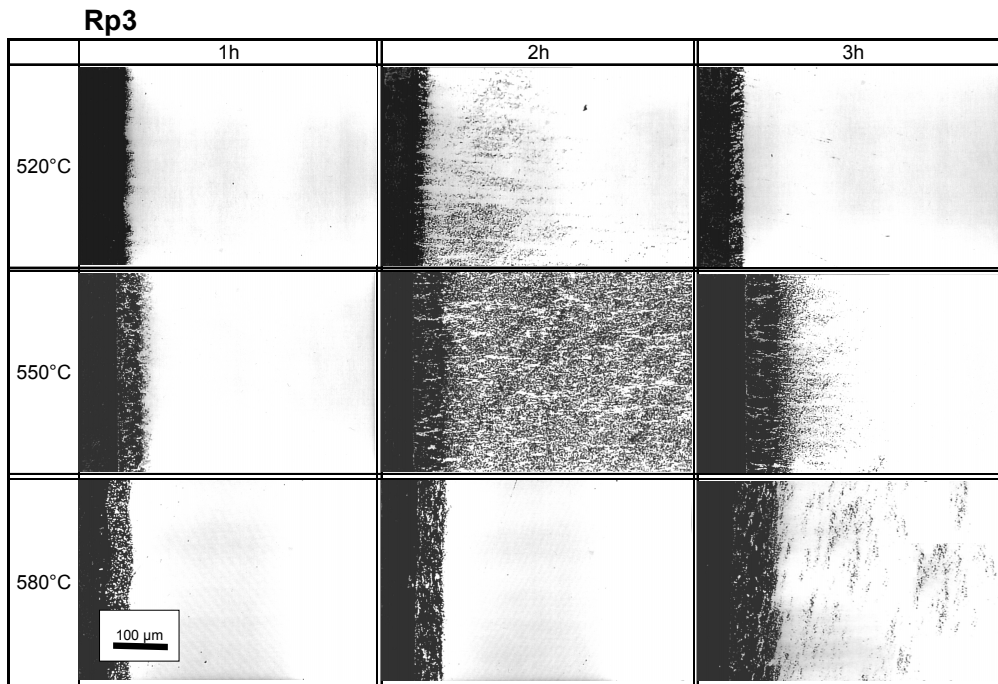


Figure 2. Micrographs for Rp3 steel samples after fluidized bed nitriding.

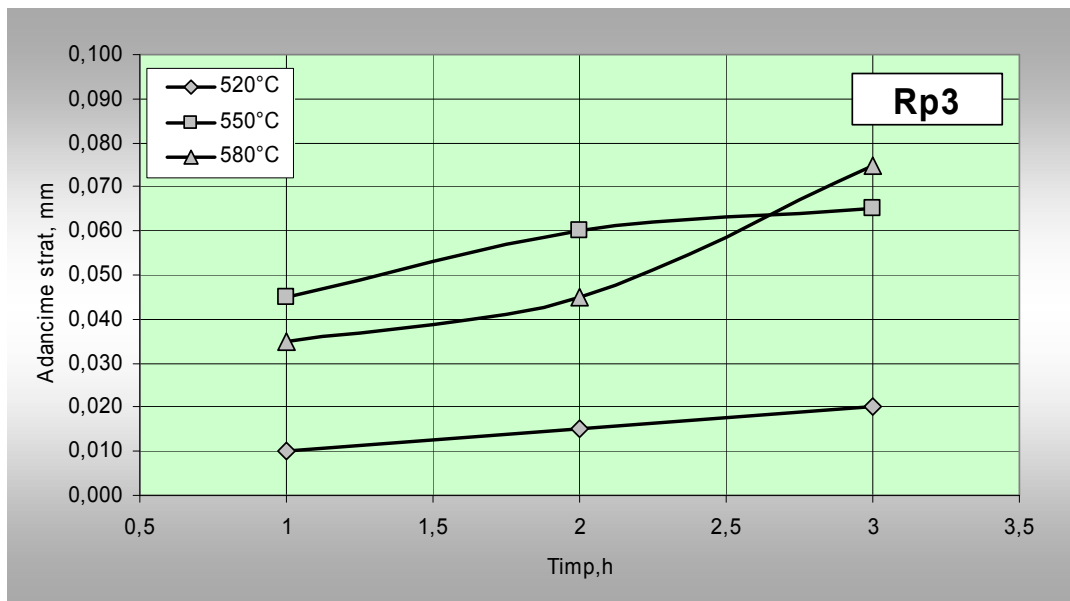


Figure 3. Nitriding layer depth variations with nitriding time and nitriding temperature

The hardness after nitriding in fluidized bed is showing in Figure 4 (Vickers TPP-2, CIS, with load 5kgf). Hardness increase with high values for nitriding temperature 550° C and 580°C, and for short nitriding time (maximum 3h). Chemical and thermal activity of fluidized bed media are important for reducing time of treatments. After treatment the samples was immediately take of that conduced to main-taining a hardness at high values, eliminated a secondary embrittlement of nitriding layer by  $Fe_4N$  ( $\gamma'$ ) acicular separation. Microhardness was measured by nitriding section (metallographic samples) PMT-3 (CIS) microhardness tester with 50g load (0,050kgf). A cross section profile of hardness was determined using microhardness and this profile is in concordance with superficial hardness and micrographs.

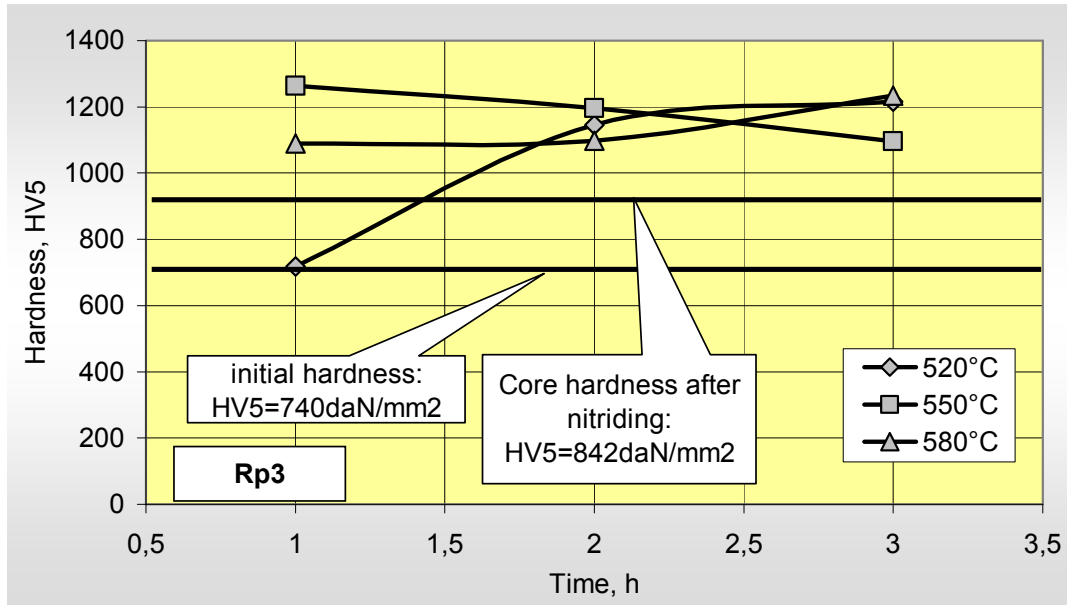


Figure 4. Hardness HV<sub>5</sub> after fluidized bed nitriding in function of nitriding temperature and nitriding time.

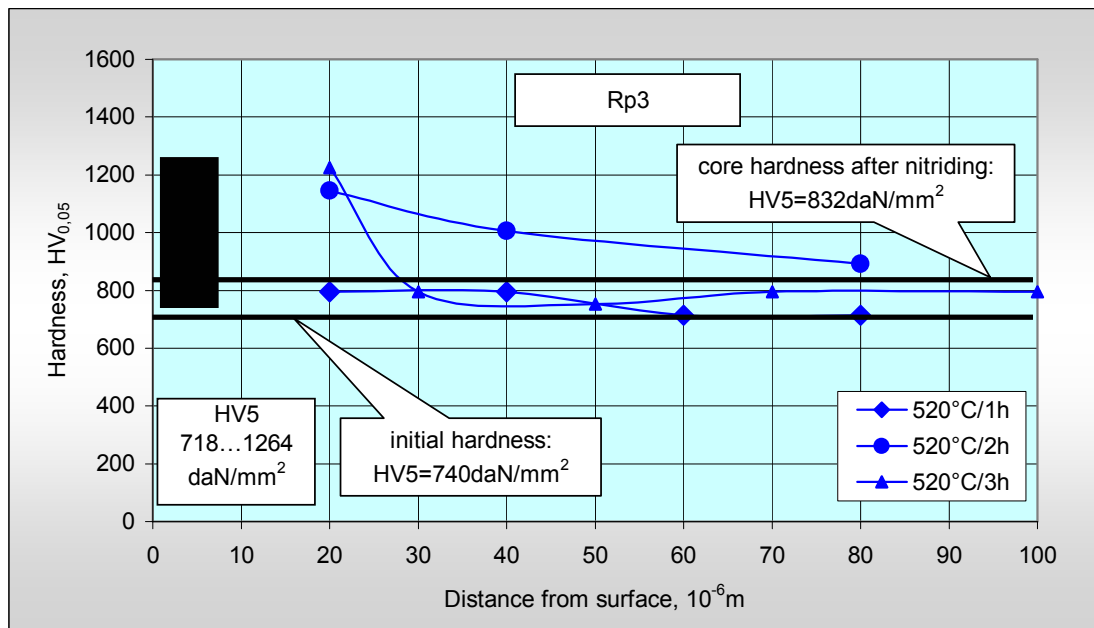


Figure 5. Micro hardness for Rp3 samples after fluidized bed nitriding at 520°C.

Microhardness was measured by nitriding section (metallographic samples) PMT-3 (CIS) microhardness tester with 50g load (0,050kgf). A cross section profile of hardness was determined using microhardness and this profile is in concordance with superficial hardness and micrographs.

#### 4. CONCLUSIONS

The Rp3 steel (HSS) having high quantity of alloying elements in chemical compositions. A very hardness metallic carbides dispersed in base matrix material. By nitriding a supplementary quantity of hard and thermal stable nitrides were dispersed by nitrogen diffused from nitriding media and by alloying elements from steel. A

supplementary hardness increasing is associated by a superficial porosity increasing, and all conducted to a good behaviour of tools in cutting process.

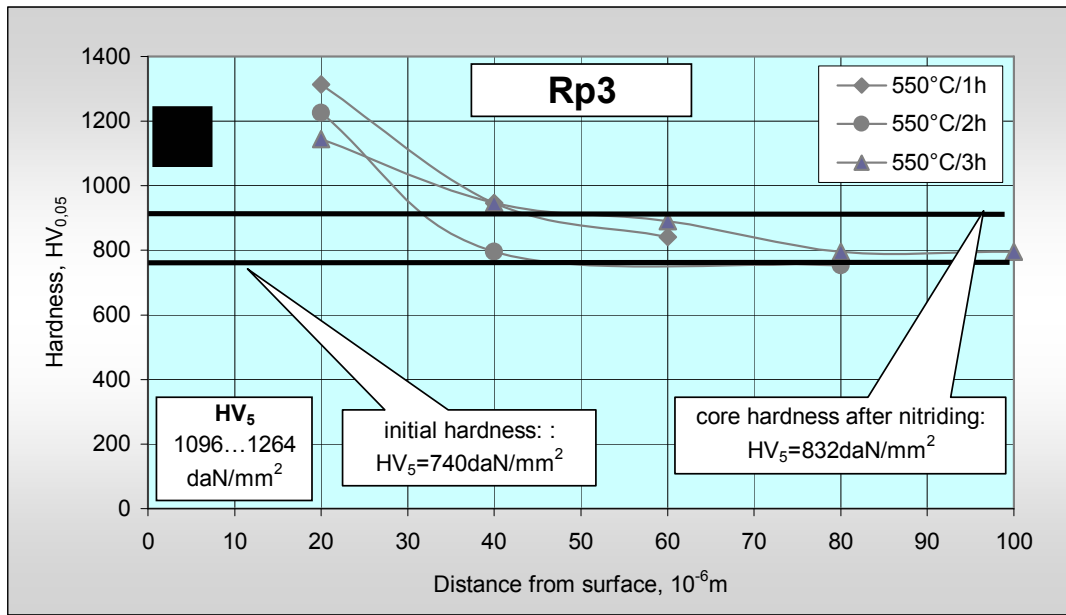


Figure 6 Micro hardness for Rp3 samples after fluidized bed nitriding at 550°C.

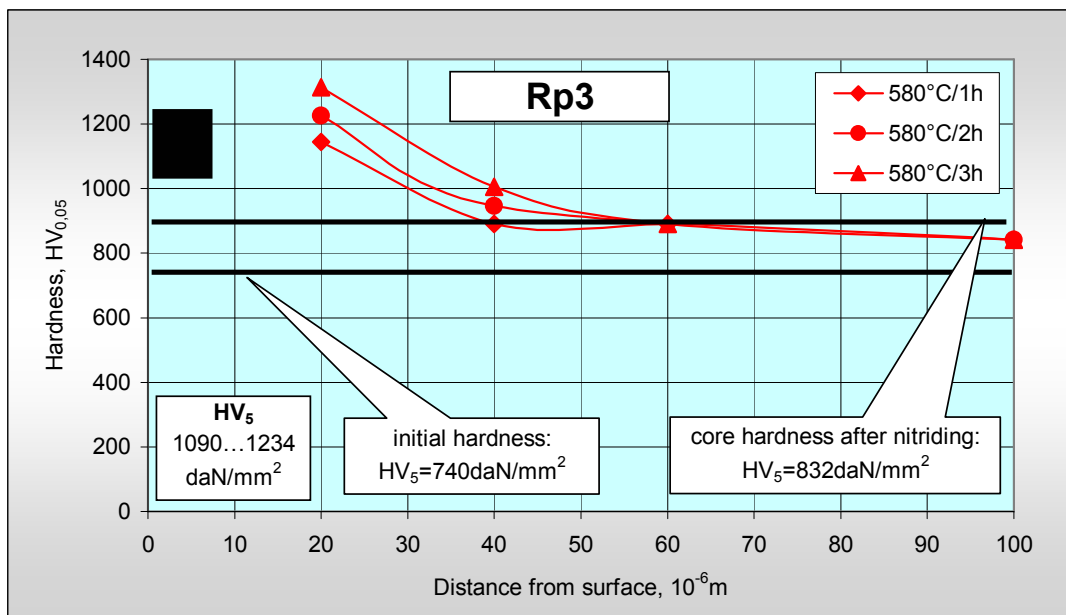


Figure 7. Micro hardness for Rp3 samples after fluidized bed nitriding at 580°C.

After nitriding in fluidized bed superficial hardness increasing with 250...400daN/mm<sup>2</sup>. The most higher value of hardness, 1234daN/mm<sup>2</sup> is obtaining at 580°C nitriding temperature and 3h for nitriding time. Microhardness (HV<sub>0.05</sub>- 50 grams load) measured by metallographic sections showing a decreasing profile for hardness in sections. A secondary increasing of hardness is present in core of samples. Micrographs showing a structure with only a diffusion layer. An oxide layer is present on the surface of samples. It appears because the samples are taken out in air from fluidized bed at nitriding temperature and oxidation is present. The depth layer

measured metallographic is depending by time and temperature. In fluidized bed conditions the total time of treatments is decreasing. The furnace is at working temperature and is simple to introducing another parts to nitriding. The total efficiency of installations increasing when compare with ion nitriding and gas nitriding where heating and cooling represents higher values of time in correlation with effective nitriding time.

Fluidized bed nitriding is a favourable applications of internal and external fluidizations properties. High values of thermal conductivity an acceptable values of mass diffusivity are internal properties that determine high values for mass and thermal global coefficient of transfer. The nitriding surface having an apart gray nuance of colour because a thin ferrous oxide layer is present after nitriding when samples is cooling in air at atmosphere temperature.

Applications of fluidized nitriding thermochemical treatments for Rp3 steel is recommended to be at third tempering regimes for material.

Received May 6, 2005

"Dunărea de Jos" University Galați

#### REFERENCES

- /1/. Băclea,A., *Some aspects concerning fluidized bed nitriding*, Proceeding of the MOC'40 Seminar, Odessa, 26-27 April 2001, pg.145;
- /2/. Kunii,D., Levenspiel,O, *Fluidization engineering*, John Wiley & Sons, Inc., New York, 1969;
- /3/. Băclea.A., Drugescu.E., Cazacu.N., Dobrovici.S., "Some aspects concerning the nitriding steels in fluidized bed", International Conference On Advances in Material and Processing Technologies, AMPT01, Leganes, Madrid, Spania, 18-21 Septembrie, 2001, Proceedings of The International Conference on Advanced Processing Technologies AMPT'01, vol. I, pag.131.
- /4/. Ivanuş Gh, Todea I., Pop Al, Nicola S, Damian Gh, *Ingineria fluidizării*, Editura Tehnică, Bucureşti, 1996;
- /5/. Drugescu E, Udvuleanu A, *Metalurgie fizică și tratamente termice*, Lucrări de laborator, Universitatea din Galați, 1981;
- /6/. Drugescu E, Udvuleanu A, Dobrovici S, *Tratamente termice. Lucrări de laborator*, Universitatea din Galați, 1985;
- /7/. Carțiș,I.Gh.,*Tratamente termice. Tehnologie și utilaje*, Editura Facla, Timișoara,1982
- /8/. Florian,E., Dulamiță,T., *Tratamente termice și termochimice*, Editura Didactică și Pedagogică, București,1982
- /9/. Murry Guy, *Une nouvelle norme europeenne "Acier pour nitruration"*, Traitement Thermique, nr.339, mai 2002, pag.30
- /10/. \* \* \* , Revista Tratamente termice și ingineria suprafețelor (ATTIS), Vol II, nr.1/2002, pag 39...40
- /11/. Dulamiță. T., *Producerea si utilizarea atmosferelor controlate pentru tratamente termice*, Editura Tehnica, București 1976;
- /12/. \* \* \* ,Revista Tratamente termice și ingineria suprafețelor (ATTIS),Vol II,nr.1/2002, pag 39-40
- /13/. Vermeșan,G., *Tratamente termice. Indrumător*, pag.167÷180, Editura Dacia Cluj Napoca, 1987;

#### COMPORTAREA OȚELULUI Rp3 LA NITRURAREA CU DURATE MICI ÎN STRAT FLUIDIZAT

**Rezumat:** Pentru tratamentul de nitrurare timpul este un factor important. La nitrurarea ionică și cea în gaz este folosită o retortă ceea ce face ca durata totală a tratamentului să crească pentru a se putea realiza încălzirea și răcirea. Utilizarea stratului fluidizat cu retortă deschisă face ca durata totală a tratamentului să scadă. Lucrarea se bazează pe experimentări de nitrurare în strat fluidizat efectuate pe probe din oțel Rp3. Rezultatele au fost investigate prin analiză metalografică, duritate pe suprafață și microduritate în secțiune.

## EXPERIMENTAL RESEARCH ON THE APPLICATION OF THE NONCRACKING CONDITION WHEN HEATING MASSIVE STEEL HALF- FINISHED

BY

VASILE CATARSCHI, MIHAELA POROCH, RADU DANILA, IOAN POROF,  
SMARANDA CATARSCHI

**Abstract.** *For the purpose of avoiding heating creaking of massive steel half-finished, one states a condition that leads to a diminishment of the metal heating speed down to those values where the metal does not creak. This condition mainly depends on the amount of the temperature difference between the surface and the core of the heated half-finished, and is valid until the temperature in the metal core reaches above approximately 550°C. In this research, we assessed the values of the breaking resistance and of the flow limit for several temperatures, in view of comparing these values with the amount of thermal stress of the respective materials, so as to rectify the heating speed*

**Keywords:** *massive steel, noncracking conditions*

### 1. THEORETICAL ISSUES

In view of heating massive steel half-finished, such as of cylindrical equivalent shape with equivalent radius  $R$ , and also in view of avoiding their creaking while heating, one endorsed the following creaking check condition [2, 3, 4]:

$$R_{Tn} = \frac{\beta \cdot E}{1 - \mu} \cdot (T_{\text{surf},n} - T_{\text{centr},n}) \leq (R_r - R_{Tr})|_{T_{\text{centr},n}} \quad (1)$$

where:  $R_{Tn}$  - the amount of thermal stress when heating steel after  $n$  time laps from the initial phase of heating.

$T_{\text{surf},n}$  - the surface temperature after  $n$  time laps of heating;

$T_{\text{centr},n}$  - the core temperature after  $n$  time laps of heating;

$R_r$  - the breaking resistance of the steel at the  $T_{cn}$  temperature;

$R_{tn}$  - the amount of remaining thermal stress in the steel.

The determination of some PC assisted modern heating technologies for heating the massive steel products (ingots, mill rolls etc.) in view of the plastic deformation, is based on mathematical modeling of the heat exchange within the metal. The analytical method used in this respect is based on the sum of Bessel – Fourier infinite sequences (Heiligenstaedt Method) and Biot, Fourier dimensionless criteria, criterion of surface  $\Phi_s$  and of centre  $\Phi_c$  [3, 5].

The determination of surface  $T_{\text{surf},n}$  and of  $T_{\text{centr},n}$  centre temperatures for a heated cylindrical ingot with equivalent radius  $R$ , for the heating mode  $T_{\text{fum},n} = \text{const.}$ , in the conditions when the initial thermal gradient is  $\Delta T_0 \neq 0$ , the following relations

are given:

$$T_{s.n} = T_{cupt0} + (T_{s.0} - T_{cupt0}) \sum_{n=1}^{\infty} M_n J_0(z_n) e^{-z_n^2 F_0} \quad (2)$$

$$T_{c.n} = T_{cupt.0} + (T_{s.0} - T_{cupt.0}) \sum_{n=1}^{\infty} M_n e^{-z_n^2 F_0} - \Delta T_0 \sum_{n=1}^{\infty} W_n e^{-z_n^2 F_0} \quad (3)$$

where:  $M_n = \frac{2J_1(z_n)}{z_n [J_0^2(z_n) + J_1^2(z_n)]}$  and  $W_n = \frac{4J_2(z_n)}{z_n^2 [J_0^2(z_n) + J_1^2(z_n)]}$  (4)

$J_0(z_n)$ ;  $J_1(z_n)$ ;  $J_2(z_n)$  – Bessel function of 0; 1; 2 order and argument  $z_n$ ;

$$J_0(z_n) / J_1(z_n) = z_n / (hR) \quad (5)$$

$z_n = m_n R$  are the solutions of the transcendent equation (4) for  $n = 1, 2, \dots, \infty$ .

$R$  – equivalent radius of the mill roll, in mm;

$h = \frac{\alpha}{\lambda}$  - the relative coefficient of thermal transfer of the steel;

$\alpha$  - heat passing coefficient at the surface of the metal;

$\lambda$  - thermal conductivity coefficient at the surface in the metal;

$F_0 = \frac{a \cdot \tau}{R^2}$  - Fourier's criterion of metal heating;

$a = \frac{\lambda}{c \cdot \gamma}$  - thermal diffusivity coefficient of the steel;

$c$  – specific heat of heated steel;

$\tau$  - heating time, in hours;

$\gamma$  - specific weight of the metal, depending on its chemical composition;

$hR = Bi$  – Biot's criterion of the metal heating;

$\Delta T_0 = T_{surf.0} - T_{centr.0}$  – initial thermal gradient of metal heating.

According to [1], for the purpose of outlining the maximum value the remaining thermal stresses (cooling stresses) in a steel ingot can reach, such an ingot was cut off immediately after air solidification – cooling. Then the remaining thermal stress was measured for a layer of 0.37m diameter, coming out with a value of approximately 250 MPa, when the admissible breaking resistance was of 800 MPa. It is from these experiments that one can see that the amount of remaining thermal stress accounts for about 30% of the pull breaking resistance for the respective steel.

One can thus write:

$$R_{Tr} = \frac{\beta \cdot E}{1 - \mu} \cdot \Delta T \leq 0.30 R_r \quad (6)$$

or

$$R_{Tr} \leq 0.30 \cdot R_r \quad (7)$$

where:  $\Delta T = T_{surf.} - T_{centr.}$  - the thermal gradient within the metal.

It results therefore that the amount of thermal heating stress must fulfil the following creaking checkup condition, according to the equation (1) and (7).

$$R_{Tn} \leq 0.70 \cdot R_r |_{T_{centr.n}} \quad (8)$$

The condition (8) is set for each time lap of steel heating, when the breaking resistance is measured according to the experimental data at the temperature  $T_{cn}$ .

Creacking checkup is performed until the temperature  $T_{cn}$  reaches over  $550^\circ\text{C}$  (the elastic range) for most of the carbon and low-allied steels.

In such case that the condition (8) is not met while heating, comes out that the thermal gradient  $\Delta T$  is too high and needs to be lowered. This diminishment of the thermal gradient  $\Delta T$  is performed according to the endorsed heating regimen by the following methods:

- a) In case one considers the heating regimen with constant furnace temperature ( $T_{furn.} = \text{constant}$ ), one shall lower the furnace temperature in decrements of  $\Delta t = 30^\circ\text{C}$ , and then resume the calculation of metal temperatures, until the condition (8) is met, by using the following relation:

$$T_{furn.n} = T_{furn.0} - 30 \quad [^\circ\text{C}] \quad (9)$$

- b) In case one considers the heating regimen with constant increasing speed of the furnace temperature:

$$T_{furn.n} = T_{furn.0} + w_0 \cdot \sum_{i=1}^n \Delta\tau_i \quad n = 1, 2, 3, \dots, \infty \quad [^\circ\text{C}] \quad (10)$$

the amount of the heating speed  $w_0$  is diminished in decrements of 10% per hour and then the calculation of metal temperatures shall be resumed until they fit in the condition (8), by using the following relation:

$$T_{furn.n} = T_{furn.0} + (w_0 - 10) \cdot \sum_{i=1}^n \Delta\tau_i \quad n = 1, 2, 3, \dots, \infty \quad [^\circ\text{C}] \quad (11)$$

## 2. EQUIPMENT USED FOR EXPERIMENTAL ASSESSMENT.

The installation of equipment for heating steel test bars in view of assessing the breaking resistance  $R_r$  and the flow limit  $R_c$  for different temperatures consists of (figure 1):

- The cylindrical wall (1) of the vertical electric furnace;
- Resistors (2) made of silicon carbide bars;
- Thermal insulation (3) made of ceramic fibres;
- A central tube (4) made of refractory steel for the protection of the resistors;
- Half-lids (upper and lower) (5) for closing the cylindrical enclosure (1);
- Thermocouple (6) PtRh-Pt (10%) for measuring the temperature of the test bar being heated;
- Mobile rack (7) for taking the furnace to the traction testing machine, on the rails (8).
- Electrical wiring (9) for commanding and controlling the heating of  $\Phi 10\text{mm}$  steel test bars.

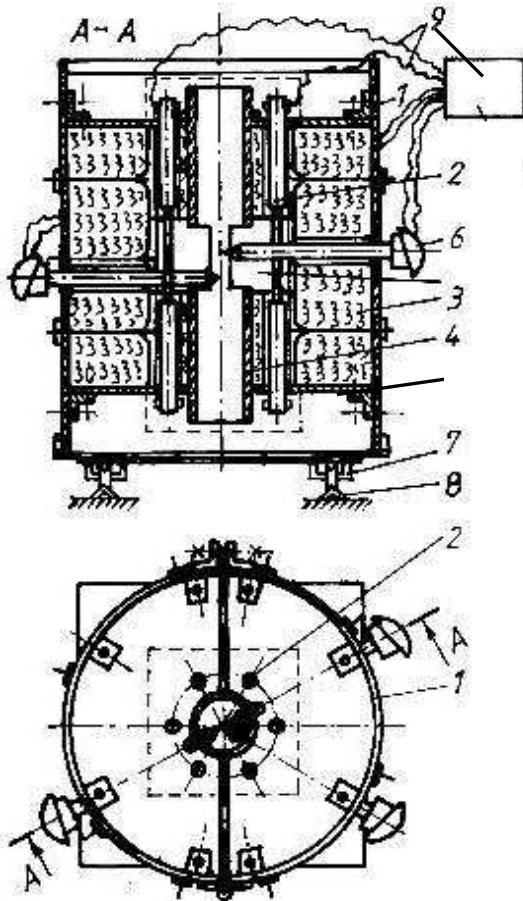


Figure 1: Test bar heating equipment.

breaking resistance and the flow limit, using standardized test bars, having the gauge diameter of 10 mm.

### 3. EXPERIMENTAL ASSESSMENTS

The experimental assessments were performed on both the equipment shown in figure 1 and the traction test machine from Technical University of Iassy, and another traction test machine type Wolpert with integrated furnace, from S.C. PETROTUB S.A. Roman. The experimental tests were performed on a number of 5 test bars for each temperature, and one then had those test values averaged (as shown in table 1 and table 3).

From the analysis of the data in table 1 and figure 2 one can see the influence of the alloy elements, molybdenum respectively, on the relevant characteristics ( $R_{p0.2}$  and of course  $R_m$ ).

The tests that were performed at PETROTUB SA Roman on steels used for pipes required in the nuclear energetic industry (Cernavodă Nuclear Power Plant), pertain to the following steel brands: TP 304L, SA106 gr. A, SA 106 gr. B and SA 106 gr. C, whose chemical composition is shown in table 2.

The average diameters of the ingots used are within 450 – 650 mm and their mass range from 3 to 6 tons.

The furnace is composed of two half-cylindrical halves that join together by hinges and tightening elements with screws. One has added an extra 6 mm asbestos layer between the thermal insulation made of ceramic fibres (withstanding up to 1250°C) and the walls (1). The resistors (2) are inserted in 6 tubes of refractory fire clay, windowed only towards the test bar heating chamber, in the test bar area. The three thermocouples (6) are put in guidance pipes of refractory steel. The central tube (4) is windowed on two opposite sides, along the test bar heating chamber. The thermocouples were paired before their assembly, in order to issue minimal reading differences.

The above described equipment was used for experimental laboratory tests on the traction test machine (still under the influence of temperature), type ZDM 500kN, made in Germany, from the Department of Material Resistance within the “Gh. Asachi” Technical University Iassy. The tests were performed at constant temperatures in 100°C increments up to 600°C, both for the

Table 1 Mechanical characteristics of certain types of steel

Temp.[ <sup>0</sup> C]	20	100	200	300	400	500	600
	R <sub>p0,2</sub> /R <sub>m</sub> [daN/mm <sup>2</sup> ]						
OLC45	36,0 / 63,0	34,0 / 61,0	33,0 / 70,0	26,5 / 73,0	23,5 / 57,5	20,0 / 38,0	12,0 / 24,0
34MoCr11	48,0 / 67,0	45,0 / 63,0	43,0 / 62,0	40,0 / 60,0	40,0 / 56,0	36,0 / 45,0	23,0 / 26,0
34MoCrNi15	54,5 / 76,5	48,2 / 73,5	44,5 / 69,5	42,3 / 66,0	41,0 / 61,0	32,5 / 42,5	18,5 / 24,5
42MoCr11	52,5 / 69,0	48,5 / 65,0	46,0 / 64,0	44,0 / 62,0	43,5 / 58,0	40,0 / 47,0	26,0 / 28,0
OLC10	26,0 / 43,0	21,0 / 41,0	23,0 / 49,0	18,5 / 52,0	17,0 / 38,0	16,0 / 26,0	9,0 / 11,0
13Cr130	41,0 / 62,0	39,0 / 57,0	38,0 / 54,0	38,0 / 53,0	38,0 / 50,0	28,5 / 37,0	18,0 / 23,0
K460	46,0 / 70,5	37,5 / 65,0	34,0 / 74,0	26,9 / 76,5	24,8 / 59,0	22,0 / 41,0	13,5 / 25,0

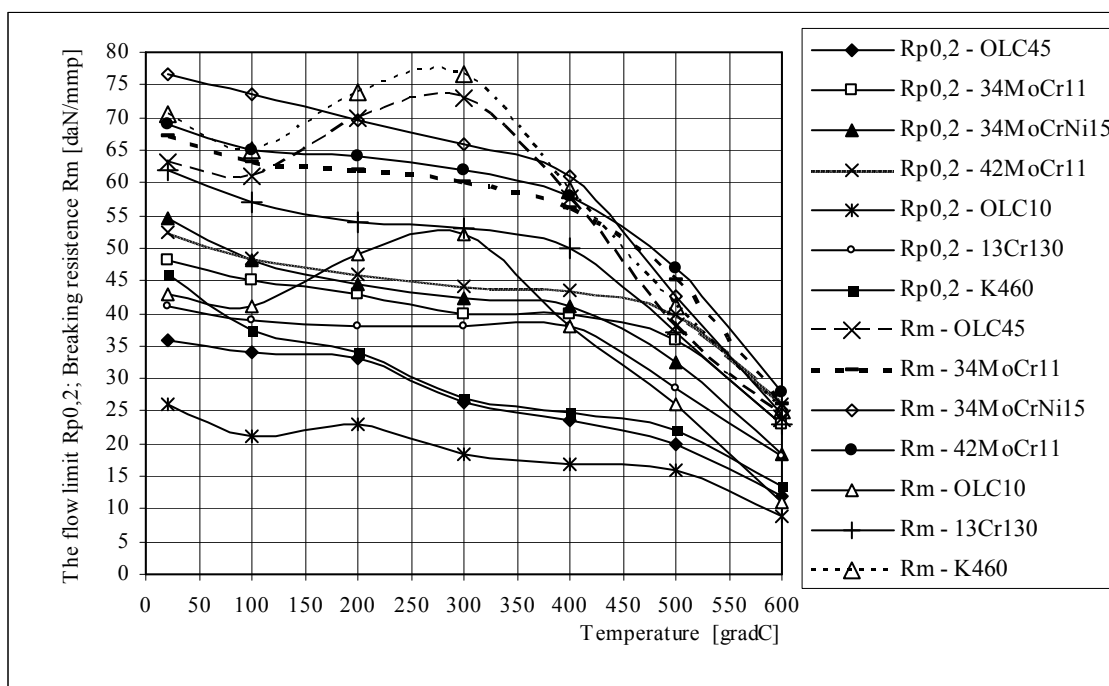
Figure 2 The flow limit  $R_{p0,2}$  and breaking resistance  $R_r$  for 7 brands of steel

Table 2 Chemical compositions of certain brands of steel

Nr. Ord	Steel mark	Chemical compositions, [%]							STAS or Norms
		C	Mn	Si	S	P	Cr, Ni	V	
1	TP 304 L	0.035	< 2.0	< 0.75	< 0.030	< 0.040	Cr: 18- 20% Ni: 8 -13%	Max. 0.1	ASTM53
2	SA 106 gr. A	0.25	0.29 – 0.96	< 0.10	< 0.058	< 0.048	-	-	ASTM 106
3	SA 106 gr. B	0.30	0.29 – 1.06	< 0.10	< 0.058	< 0.048	-	Max. 0.1	
4	SA 106 gr. C	0.35	0.29 – 1.06	< 0.10	< 0.058	< 0.048	-	-	

#### 4. CONCLUSION

The assessed amounts for the breaking resistance  $R_r$  are used as comparison factors for the internal stresses that occur while heating massive steel half-finished, in view of plastic working, initially loaded cold to the furnace.

This comparison is made by mean of a creaking checkup condition for the steel being heated, which is applied in the elastic temperature range (0 ... 550°C), by diminishment of the  $\Delta T$  thermal gradient in the metal.

Table 3 Mechanical characteristics of certain types of steel

Steel mark Temp [°C]	TP 304 L		SA 106 gr. A, gr. B, gr. C	
	R <sub>p0,2</sub> [daN/mm <sup>2</sup> ]	R <sub>m</sub> [daN/mm <sup>2</sup> ]	R <sub>p0,2</sub> [daN/mm <sup>2</sup> ]	R <sub>m</sub> [daN/mm <sup>2</sup> ]
38	17,00	48,50	24,10	41,4
93	14,68	45,64	22,01	41,4
149	13,17	41,99	21,39	41,4
204	12,06	40,33	20,70	41,4
260	11,24	39,85	19,53	41,4
316	10,69	39,30	17,87	41,4
343	10,48	39,02	17,52	41,4
371	10,27	38,75	17,38	41,4
399	10,13	38,54	16,83	40,95
427	9,93	38,27	16,08	38,00
454	9,79	37,64	15,52	34,60
482	9,58	37,16	15,32	30,75
510	9,38	35,85	14,77	27,30
538	9,17	35,02	13,45	23,78

The diminishment of the  $\Delta T$  thermal gradient is achieved by lowering the heating speed for the metal (hence by lowering the furnace maintenance temperature or by diminishing the constant heating speed of the furnace).

The assessed values for the flow limit  $R_c$  can be used in a plastic working checkup condition, during the steel heating process in the furnace.

Out coming results from the laboratory tests lead to the avoidance of heating rejects, these results being fully comparable to other similar tests shown in the specialty literature.

Received May 6, 2005

Technical University "Gh.Asachi" Iasi

#### REFERENCES

- /1/. Samoilovici, Iu. A, Timospolskii, V. I. - *Nagrev stali: Spravocinic posobie*. Vizaia scola.. Minsk, 1990.
- /2/. Nemzer, G. G. - *Teplovie protessi proizvodstva crupnih pocovoc*. Masinostroenie, Lningrad, 1979.
- /3/. Catarschi, V. - *Contribution considering the computer designed technologies for steel ingots heating in INCFOR programs*. METALURGIA INTERNATIONAL, nr.4/2004, ISSN 1582-2214, pag.8-13.
- /4/. Catarschi, V. - *Manufacturing Engineering of the Forged Mill Rolls for Rolled Products from SC FORTUS S.A. Iasi*. METALURGIA INTERNATIONAL, Nr.5/2004, ISSN 1582-2214, p.27-34.
- /5/. Roman, E., Maeder - *Programming in Mathematics*. Addison Wesley Publishing Company, Redwood City, California, U.S.A., 1991.

#### CERCETĂRI EXPERIMENTALE PENTRU APLICAREA CONDIȚIEI DE NEFISURARE LA ÎNCĂLZIRE A SEMIFABRICATELOR MASIVE DIN OȚEL

**Rezumat:** În vederea evitării fisurării la încălzire a semifabricatelor masive din oțel, se pune o condiție care determină reducerea vitezei de încălzire a metalului până la valori comparabile cu cele la care metalul nu fisurează. Această condiție depinde în principal de mărimea diferenței de temperatură dintre suprafața și centrul semifabricatului încălzit și se manifestă până când temperatura metalului în centru depășește cca. 550°C. În lucrarea prezentă se determină valorile rezistenței la rupere și ale limitei de curgere la diferite temperaturi, pentru câteva mărci de oțel, în vederea comparării acestor valori cu mărimea tensiunilor termice ale materialelor respective și a corectării vitezei de încălzire /1/, /2/, /3/.

## NONCONDUCTIVE COATING THICKNESS MEASUREMENT USING EDDY CURRENT METHOD

BY

ADRIAN COMANICI

**Abstract.** For coating thickness measuring it is used specialized devices based on Eddy Current (EC) or Ultrasonic method only for metallic or for nonmetallic layers, deposited on magnetic or nonmagnetic base metals. This paper presents a measurement method for nonconductive coating thickness (NCT), deposited on magnetic and on nonmagnetic metals, using a single multifrequency EC. device. This method is required in nondestructive tests (NDT) for thickness measurements of deposited layers which are: paints, sealants, adhesives, teflon, polymers, etc. This device is portable, so we can use it to perform many other types of controls in the same locations such are: sorting metallic alloys, conductivity tests, defectoscopic tests, the thickness and corrosion level of parts measurement (for pipelines and pressure vessels usually), the quality and homogeneity of heat treating, electrodepositing thickness layers measurement on magnetic and nonmagnetic base metal. This kind of tests can be performed in laboratory location, in production location, or in working condition, on finite pieces, pipelines, pressure containers, metallic constructions, chemical installations, etc.

**Keywords:** eddy current method, coating thickness measuring, nondestructive tests

### 1. INTRODUCTION

For NCT measurements deposited on metallic materials, was performed two programmes. For nonferrous base metal, we have the programme number 1 and for steel base metal the programme number 2. As a guideline of these programmes was the principle of strong dependence between the distance coil – pieces and the regression lines length in normalized impedances diagram, at “lift-off” (LO) processe time. Due measurements tests we have used D16 aluminium alloy and 30HGSA tempered and annealed steel, as base metals. The calibration of method was performed by nonconductive standard sheet with 6, 8, 30, 50 and 100 microns thickness. The results of these tests were used for graphical diagrams construction, to show the linear corelation between the depth (thickness) of nonconductive coating in microns, and the spot extension during LO, in oscilloscope RCT.divisions.

For NCT measurement and for microns transformation of RCT divisions it is necessary to:

- coupling the surface probe-type coil applied;
- put the device “ON”;
- recall the right program from the memory after the base metal kind: magnetic or nonferromagnetic;
- perform an LO on the nude area of base metal (without nonconductive coating), for finding zero level; If this area does not exist, we must try to test a reference piece made by the same material of the same wall thickness, in the same heat treating situation;

- perform LO on the test area, on the paint coating for example, and measure the difference between this and zero level, on oscilloscope RCT divisions, “N div” notation; we can use for this purpose the right side barr level as long as the probe is in contact with the part;
- using the diagram we can find the corresponding value of the “N div”, in microns depth.

**2. DEVICE SET UP**

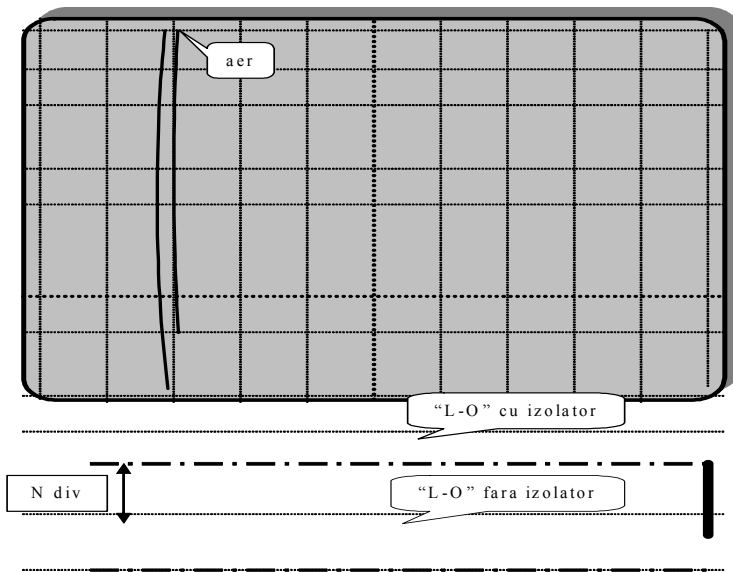
**Programme 1.** It is used for the NCT measuring deposited layers on aluminim and aluminium alloys surfaces, in corelation with the figure1 diagram. For example, if the oscilloscope RCT evaluation is N=2,0 divisions, the NCT of paint layer is 150 microns, on the D16 alloy.

**PROGRAM : 1**

**Tip sonda: SP-100**  
**Tensiune: LOW**  
**FILTRE: trecejos:100Hz**  
**trece-sus: 0 Hz**

**Frecventa: 100 kHz**  
**Faza: 297°**  
**Pozitie nul: oriz. 53**

**vert. 255**  
**Amplificare: oriz. 55 dB**  
**vert. 55 dB**



**PH 53 V 255 F 100**  
**GH 55 V 55 P 297 P**

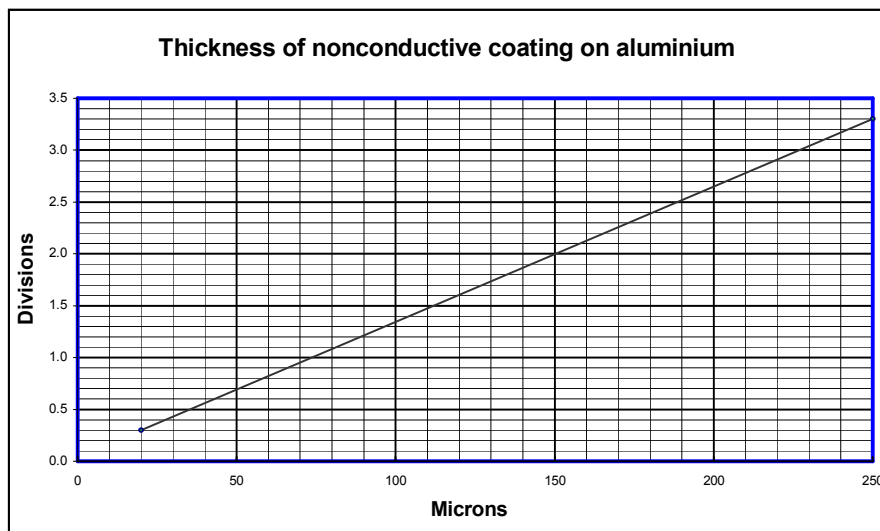
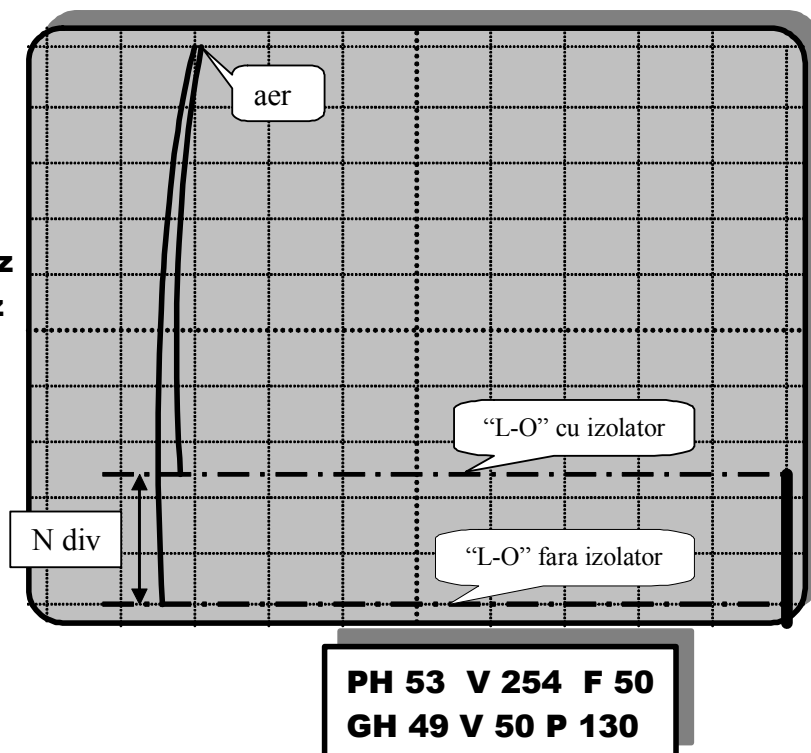


Figure 1

**PROGRAM: 2**

**Tip sonda: SP-100**  
**Tensiune: MID**  
**FILTRE trece-jos 100Hz**  
**trece-sus 0 Hz**

**Frecventa: 50 kHz**  
**Faza: 130°**  
**Pozitie nul: oriz.: 53**  
**vert.: 254**  
**Amplificare: oriz.: 49,5dB**  
**vert.: 50,6dB**



**Programme 2.** It is used for the NCT measuring deposited layers on steel 30 HGSA in accordance with the figure 2 diagram. At these materials the electrical conductivity function " $\sigma$ ", is very strong affected by the magnetic permeability " $\mu_r$ " level. For this reason if we want to measure the NCT deposited layer on others steels than 30HGSA, we have to take some cautions:

- adjust the coil frequency for an vertical LO spot line;
- adjust the phase angle for a linear LO finish line, without left or right traces;
- adjust the vertical amplifier level such as the finish point of LO to be on the horizontal lines of oscilloscope RCT division;
- must establish the new zero level by LO on the nude base metal;
- use standard NCT sheet for recalibrate the linear diagram on figure 2.

For example, if we read on the RCT the diference value  $N=2,5$  divisions, on diagram we find the thickness of paint film 200 microns deposited on the 30HGSA steel.

### 3. INSTRUMENT AND ACCESORIES

The tests were performed using a multifrequency programable device "NORTEC 19" STAVELEY INSTITUTION, with 100 Hz ..... 3 MHz frequency range, vertical and horizontal amplification between 0 and 90 dB, with 0,375 dB steps, RCT oscilloscope by 256 x 256 points and 5 ½ " diagonal, the phase angle can be rotate between 0 and 360 degrees. Operations system and accesories includes a large number of surfaces absolute coil probes, but the best results were obtaines using the nominal frequency coil of 100 kHz. The internal memory may store 50 different analysis programmes, and 2 video memory for RCT oscilloscope.

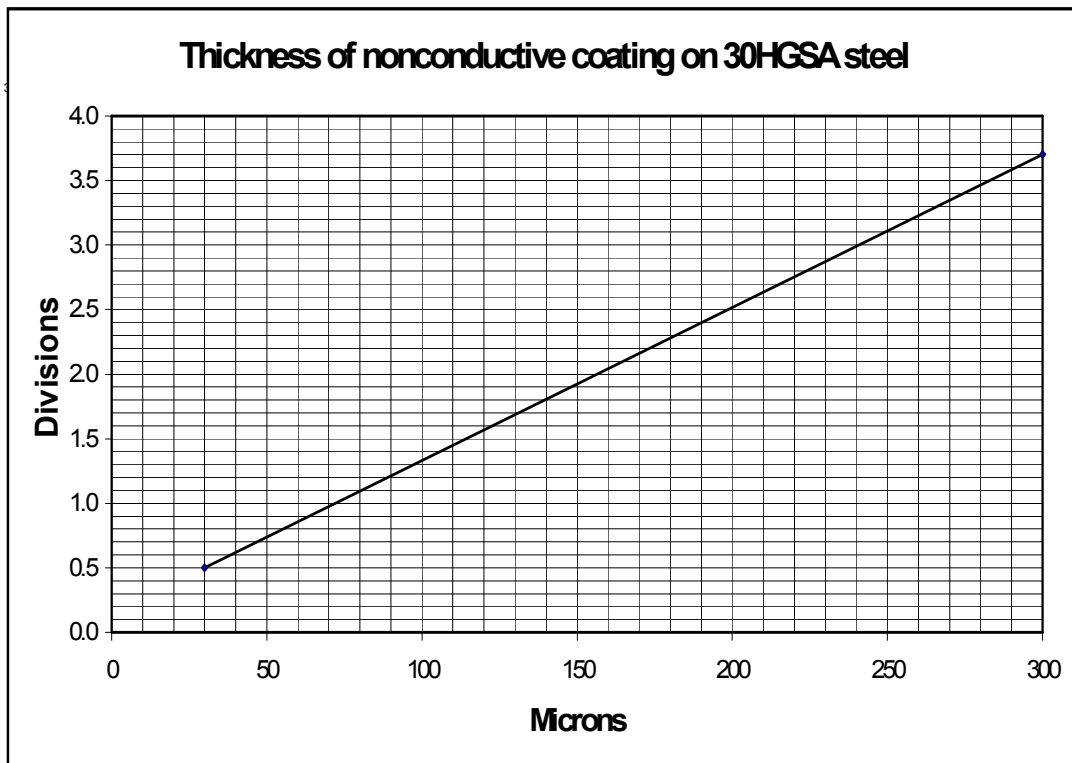


Figure 2



#### 4. CONCLUSIONS

This method is simple and faster than others, very useful especially in the field, excepted the recalibration condition in the case of steel base metal. This method is required in nondestructive tests (NDT) for thickness measurements of deposited layers which are: paints, sealants, adhesives, teflon, polymers, etc.

This device is portable, so we can use it to perform many others type of controls in the same locations such are: sorting metallic alloys, conductivity tests, defectoscopic tests, the thickness and corrosion level of parts measurement (for pipelines and pressure vessels usually), the quality and homogeneity of heat treating, inspection of welds, electrodepositing thickness layers measurement on magnetic and nonmagnetic base metal.

This kind of tests may be performed in laboratory location, in production location, on field laboratory in working condition, on finite pieces, pipelines, pressure containers, metallic constructions, chemical installations, etc.

*Received May 6, 2005*

*SC AEROSTAR SA, Bacau*

#### REFERENCES

- /1/. STAS 10785-76, *Defectoscopie cu curenti turbionari. Terminologie.*
- /2/. NORTEC 19 - *User instructions.*
- /3/. ASTM E 268 *Terminology Relating to Electromagnetic Testing.*
- /4/. ASTM E 376-89 *Standard Practice for Measuring Coating Thickness by Magnetic-Field or Eddy-Current (Electromagnetic) Test Methods.*
- /5/. ASTM B 244 *Test Method for Measurement of Thickness of Anodic Coatings on Nonmagnetic Basis Metals with Eddy-Current Instruments.*
- /6/. ASTM D 1400 *Test Method for Nondestructive Measurement of Dry Film Thickness of Nonconductive Coatings Applied to a Nonferrous Base Metal.*
- /7/. ASTM G 12 *Test Method for Nondestructive Measurement of Film Thickness of Pipeline Coatings on Steel.*
- /8/. ASTM E 1316-94 *Standard Terminology for Nondestructive Examinations.*
- /9/. ISO 2178 *Nonmagnetic Coatings on Magnetic Substrate – Measurement of Coating Thickness – Magnetic Method.*
- /10/. \* \* \* - *Handbook of nondestructive testing*, vol. 17. ASM International

#### MASURAREA GROSIMII STRATURILOR IZOLATOARE PRIN METODA EDDY CURRENT

**Rezumat:** Problema masurarii grosimilor straturilor, se rezolva prin utilizarea unor aparate specializate care folosesc ultrasunete sau curenti turbionari, diversificate in functie de natura stratului depus (metalic sau nemetalic) si a suportului (magnetic, nemagnetic sau nemetal). In aceasta lucrare se prezinta o metoda de masurare a grosimii straturilor izolatoare (GSI), depuse atat pe suport feromagnetic cat si neferomagnetic, folosind un aparat portabil, universal, prin curenti turbionari (CT), multifrecventa. Aceasta metoda prezinta interes acolo unde se cere masurarea nedistructiva a GSI, care pot fi dupa caz: grunduri, vopsele, teflon, ermetice, adezivi sau PVC. Aparatul fiind universal, permite realizarea succesiva si a altor tipuri de controale NDT, cum ar fi: sortarea metalelor, masurarea conductivitatii, masurarea straturilor metalice depuse electrogalvanic, defectoscopie, masurarea grosimii pieselor. Aceste controale pot fi realizate in laborator, in spatiile productive, servind la

monitorizarea proceselor respective, sau in teren, pe utilajele si instalatiile aflate in exploatare, servind la verificari de fiabilitate si mentenanta..

## RESEARCHES REGARDING THE IMPROVEMENT OF ACTIVE SURFACE QUALITY OF COPPER ELECTRICAL CONTACTORS

BY

N. COȘER, D. CIOBANU, I. ALEXANDRU, I. HOPULELE

**Abstract.** *In this paper are presented some theoretical and experimental aspects by layers deposition domain from noble metals on the copper support with the objective to the durability increasing of copper electrical contactors. The deposition method what have been used is a relative recent proceeding, named deposition and alloying through electrical sparkling with vibrator-electrode (DASE). Using this method obtain layers with thickness from ten millimeters to upper, with good adherence at support, high hardness and wear resistance..*

**Keywords:** *electrical contactor, alloying, deposition, electrical sparkling.*

### 1. INTRODUCTION

Taken in consideration the tendency to increase of electrical, electrotechnical and electronical products volume from year to year are imposed a sever regime to economy the noble metals or alloys of these metals used to the realization of electrical contactors from commutational systems from mentioned products.

A way to economy of noble metals is the replacement of monolithic contact used in almost cases, fig. 1 *a*, with a layer from noble metal, which can be deposited using classical methods or relative recent proceeding, named deposition and alloying through electrical sparkling (DASE), fig. 1 *b* [1], [2]. The main property of electrical contacts is the contact resistance, which depends by contact pressure, electrical conductivity and compression resistance of material from that the contact is realized.

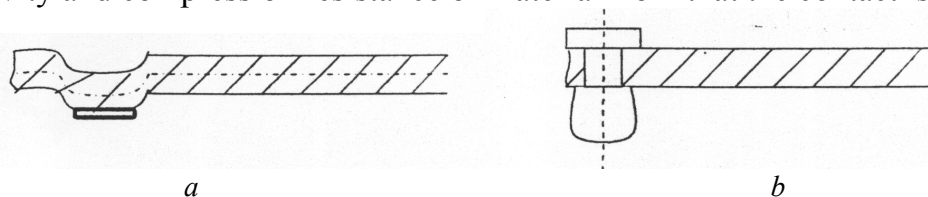


Fig. 1. Types by electrical contacts: a) electrical contact obtained through DASE and stamping;  
b) electrical contact obtained by stamping.

Electrolytic, thermal deposition or through noble metals soldering on electrical conductors by copper is not efficient due to the small resistance at wear of active surface of contactors, because the noble metals thus deposited are soft [2].

DASE is characterized by the following particularities:

- can be effectuated local layers deposition with thickness by micrometers order, without protection of the whole surfaces;

- high hardness, good wear resistance and excellent adherence to the support of deposited layer;
- DASE technology is simple to use, the equipment have a small dimensions and is transportable.

## 2 MATERIALS AND METHODS

In present paper are exposed to superficial microalloying samples from copper, the deposition have been realized with silver and platinum electrodes.

The processing through electrical sparking have effectuated in manual regime with EFI-10M device (0.7...1.2 A middle current;  $t_{sp} = 1 \text{ min/cm}^2$ ), using II ( $I = 0.8 \text{ A}$ ) and III work regimes ( $I = 1.5 \text{ A}$ ). The device is found in the endowment of Applied Physics Institute of Science Academy from Moldova Republic.

The samples analyses have been realized on a normal section on deposited layer. The polished, glazed and chemical exposed with 20% ferric chloride solution. Structural analysis of superficial layers obtained in experiments have been made through optical metallographic microscopy with MC-9 microscope, on which have been installed a video chamber Philips. For microhardness measures have been used a PMT-3 hardness tester. The last devices are found in laboratory of Material Science and Engineering Faculty of Technical University Gh Asachi from Jassi.

## 3 RESULTS AND DISCUSSIONS

In figures 2 and 3 are shown the microstructure of copper samples with silver and platinum deposition and alloying layer.

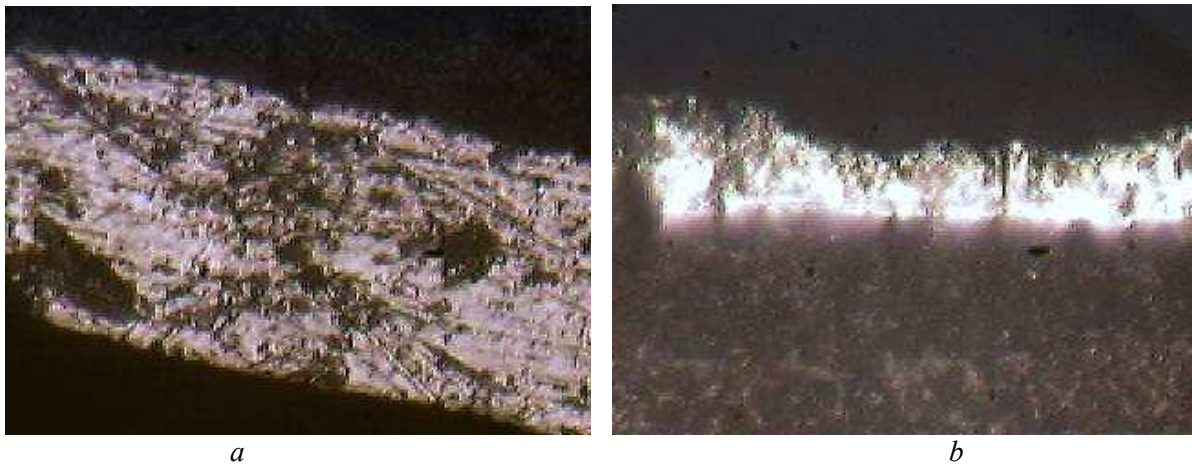


Fig 2. Structural microphotography for copper samples sparking with silver electrode:  
a) regime II; b) regime III; attack with 20% ferric chloride; 1x600, 1x400

From figure 2 can observe that white layer formed at sparking with silver electrode and regime II is uniform, without cracks and with excellent consistence (small number of pores). At sparking with regime III ( $I = 0.8 \text{ A}$ ), the layer has 26.26  $\mu\text{m}$  thicknesses and the diffusion area has 16...20  $\mu\text{m}$ . The upper values obtain for regime III ( $I = 1.5 \text{ A}$ ), respective 29.35  $\mu\text{m}$  for deposited layer and 18...30  $\mu\text{m}$  for diffusion layer, table 1.



Fig 3. Structural microphotography for copper samples sparking with platinum electrode: a) regime II; b) regime III; attack with 20% ferric chloride; 1x400; 1x200.

The layer obtained through sparking with platinum electrode is very thin ( $6.57 \mu\text{m}$  with regime II and  $8.187 \mu\text{m}$  with regime III), irregular and inhomogeneous (very porous), and transition zone can't be observed, fig. 3. The defects are more accentuated in the case of using of work regime III.

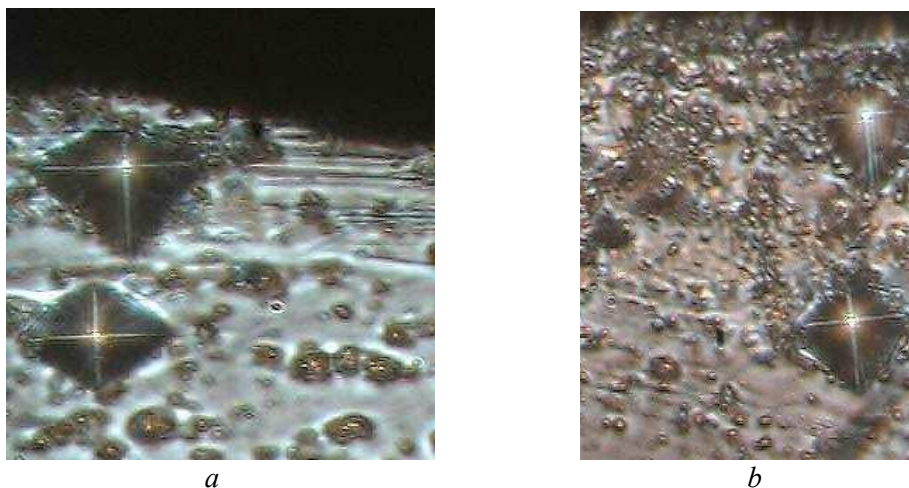


Fig. 4. Structural microphotography for copper samples sparking with silver electrode (a) and platinum electrode (b) and work regime II, not chemical attacked, with indentation microhardness; 1x800.

From figure 4 are observed distinct contour of indentation microhardness. Can remark also the absence of cracks closed to this. That certifies the excellent adherence at the substrate of white layers formed through electrical sparking with platinum electrode or silver electrode. The indentation from samples sparking with platinum electrode, fig. 4 *b*, has the diagonals much less than of those from samples sparking with silver electrode, fig 4 *a*. Result that the layer obtained in the first case have a greater hardness.

The thickness of deposited and alloying layers with platinum and silver electrodes, the work regimes II and III, respective the microhardness measured upon these layers are presented in table 1.

From table 1 can observe that the white layer obtained on sparking with platinum electrode is much hard than those obtained with silver electrode. Also, the

thickness of deposited and alloyed layers with platinum electrode is much thin that those obtained with silver electrode. This phenomenon can be explained through the fact that the melting temperature of platinum is greater than those of silver, such as the platinum electrode will erode less and the eroded and transferred mass on cathode (piece) will be much lower to the end of processing. From platinum and silver electrode sparking can be observed a little growth of hardness with processing regime, due to thermal effect of sparking processing over the layer material.

Table 1

Material of sample	Electrode material	Work regime	Microhardness MHV20/thickness, $\mu\text{m}$		
			Deposit layer	Diffusion zone	Base material
Copper	Silver	II	150,67/26,26	111,06/-18	67
		III	191,77/29,35	185,2/-24	
		II	201/6,67	-	
		III	242/8,187	-	

#### 4 CONCLUSIONS

From the analyses of presented data result the following conclusions:

1. Through microalloying with silver electrodes have been obtained substantial growth of deposited layer hardness, till to 3 times, which dependent and by the work used regime, and the adherence at the substrate of deposited layers is excellent.
2. The sparking with work regime III and platinum and silver electrodes is much less recommended due to deficient structures of white layer obtained. In this case is recommended to apply the post-DASE processing that contributes at the improvement of deposition layers quality (smoothing with ultrasonic wave, laser and so on).
3. The utilization of DASE method for deposition of thin layers by silver, on the active part of electrical contactors by copper, lead at the improvement of those hardness and implicitly to the increasing of wear resistance (with maintain of electrical characteristics) and so of their durability.

Received April 26, 2005

Technical University "Gh.Asachi" Iasi

#### REFERENCES

- /1/. Alexandru I., Carcea I., Pop F., Baciu C., Alexandru Adr., 1993, *Argintarea contactorilor din Cu prin scânteiere cu electrod vibrator*, Sesiunea de comunicări, Univ. "Dunărea de Jos" Galați.
- /2/. Anastasov T., Belopitov N., 1975, *Vozmojnosti zamena monolitnâh contactov iz blagorodnâh metalov solem metalla, nanesenâm âlectroiscovâm sposobâm*. *Âlectriceschie contactî M.Nauca*, 68-72.
- /3/. Coșer N., 2004, *Cercetări experimentale privind obținerea contactorilor electrice prin depunere și aliere prin scânteii electrice*, Referat nr. 3, Iași.
- /4/. Lazarencu B. R., ș.a., 1974, *Nanesenie kontaknâh materialov electriscovâm sposobom*. *Âlectronia obrabotka metalov*, nr.5, 25-30
- /5/. Mihailov V. V., Ghitlevici A. E., ș.a., 1985, *Sposob nanesenia pokrîtii I ustroistvo delea ego usoștvenie*, Opubl.V. B.I., nr. 15, SSSR.

#### CERCETARI PRIVIND ÎMBUNĂȚIREA CALITĂȚII SUPRAFETEI ACTIVE A CONTACTORILOR ELECTRICE DIN CUPRU

**Rezumat:** În lucrare sunt prezentate câteva aspecte teoretice și experimentale în domeniul depunerii straturilor din metale nobile pe suport de cupru în vederea creșterii durabilității contactorilor electrice din cupru. Ca metodă de depunere s-a utilizat un procedeu relativ nou și anume, depunerea și alierea prin scânteiere electrică cu electrod vibrator (DASE). Utilizând acest procedeu se obțin straturi cu grosimi de la zeci de milimetri în sus, cu aderență bună la suport, precum și duritate și rezistență la uzură ridicată..

## RESEARCHES REGARDING THE MASS TRANSFER AT SUPERFICIAL COATING AND ALLOYING WITH NOBLE METALS ON THE COPPER SUPPORT

BY

N. COSER, D. CIOBANU, V. MIHAILOV\*, I. ALEXANDRU, A. ALEXANDRU

**Abstract.** *Present paper shows some theoretical and experimental aspects from the domain of layers coating with noble metals on the copper support, using deposition and alloying method through electrical sparkingling (DASE) with vibrator-electrode. Erosive processes at DASE are estimated by the magnitude of electrical erosion and by mass transfer of the anode material on the cathode. This characteristic determines the process productivity or the rise intensity of the coating layer thickness on cathode (piece).*

**Keywords:** *mass transfer, coating, microalloying, noble metals, electrical sparkingling*

### 1. INTRODUCTION

Superior using of noble metals in products, as electrical contactors from communication systems of electrical and electronic devices and so forth, achieve through application of the high efficient technology by coating of layers from these metals.

Electrolytic, thermal coating or through noble metals soldering on electrical conductors by copper is not efficient due to the great failures of these metals determined by whole coating of the contactor surface, without to be necessary [1].

In the last period are imposed a relative recent method by coating named superficial deposition and alloying through electrical sparkingling (DASE). This method has at base the phenomenon of inverse electrical erosion and polar transfer of anodic material (electrode) on cathode (the piece subject to processing) in gaseous media [4]. The electrical erosion phenomenon and the material polar transferring between electrodes are processes practically inseparable in time. From this cause the simultaneous analysis of these processes characteristics can offer a complete image about the sparkingling process dynamics and the superficial layer formation on cathode or about the process productivity [3], [4].

### 2. MATERIALS AND METHODS

In present paper the plain surfaces of some samples by pure copper are exposed to superficial microalloying, which beforehand have been subjected to rectification, cleaning and degreasing. The samples have square forms with 1 cm side. For the microalloying have using silver and platinum electrodes.

The processing through electrical sparkingling are effectuated in manual regime with EFI-10M device (0.7...1.2 A middle current;  $t_{sp} = 1 \dots 8 \text{ min/cm}^2$ ), using II and III

work regimes ( $I = 0.8 \text{ A}$  and  $I = 1.5 \text{ A}$ ). The device is found in the endowment of Applied Physics Institute of Science Academy from Moldova Republic.

From energetic point to view the superficial processing regimes through electrical sparking can be grouped in [4]:

- Soft regime, when  $W_i < 1 \text{ J}$ ;
- Hard or severe regime, when  $W_i > 1 \dots 2 \text{ J}$ .

Using DASE have effectuated investigations on the mass transfer of the anode material to cathode for each electrodes and work regimes. The mass modifications have evaluated by weighing of samples with an analytical balances with 0.001g precision. Summing the differences between measured masses before and after every minutes of sparking both for anode ( $\Delta y_a$ ) and for cathode ( $\Delta y_c$ ) has obtained the contribution of the coatings at the mass increasing of cathode and the anode erosion.

The quantity of eroded material which deposes on cathode in time unity is calculated with the relation:

$$k = \frac{\Delta y_c}{\Delta y_a}, (\%) \quad (1)$$

### 3. RESULTS AND DISCUSSIONS

The variations of mass growths of cathode and the erosion of anode related to the duration of sparking process, work regimes and used electrodes are in fig. 1 - 5.

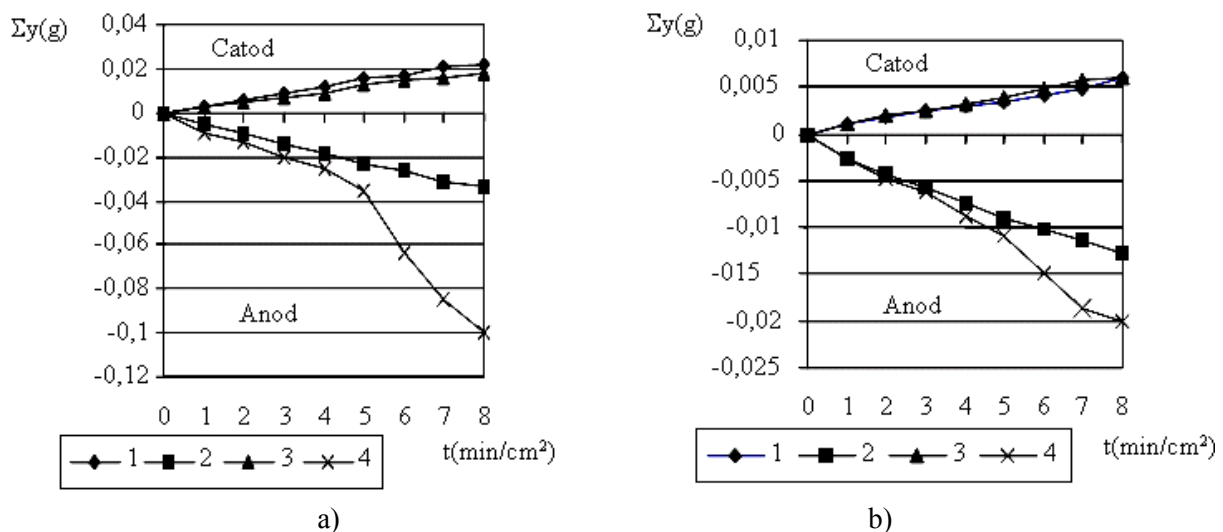


Fig. 1. Variation of mass growth of copper cathode related to processing time for different work regimes: a) 1, 2 – regime II; 3, 4 – regime III (silver electrode); b) 1, 2 – regime II; 3, 4 – regime III (platinum electrode).

The dynamics of superficial layers formations on the cathode are characterized through the maximum intensity of mass transfer from the anode to the cathode, in special, in the first periods of the process development, but it reduce gradually with the increasing of time processing [4].

At the sparking with silver electrode, fig. 1 *a*, can be observed that through the increasing of time processing increase continuously the cathode mass and the anode erosion. The both attain the maximal value in the first minutes of sparking, after that the transfer of eroded material diminishes for the sparking case with the regime III or maintain nearly constant for the regime II.

The same process takes place at sparking with platinum electrode, fig. 1 *b*. In both used regimes the anode erosion and the transfer of eroded material at cathode are produced with less intensity. Also ascertain a little growth in the regime III.

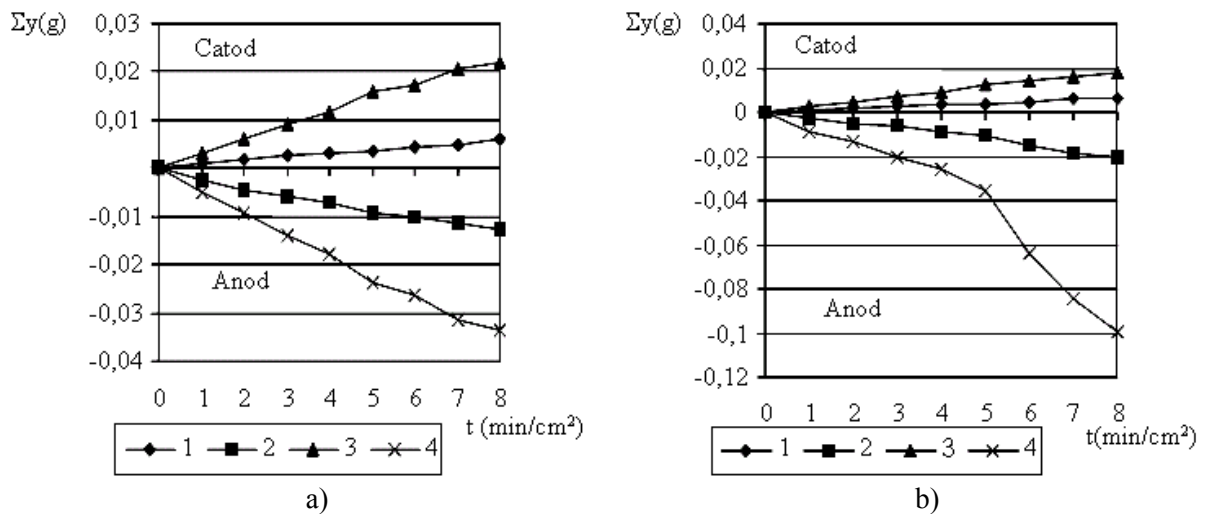


Fig. 2. Variation of mass growth of copper cathode related with time processing for different anodes: a) 1, 2 – platinum electrode; 3, 4 – silver electrode (regime II); b) 1, 2 – platinum electrode; 3, 4 – silver electrode (regime III).

The intensity of the eroded material transfer in the first minutes of the sparking process with the same work regime depend both the material properties of the anode and of the cathode [4]. From figure 2 can say that at the sparking with the same work regime the increasing in weight of cathode depend quantitatively by the magnitude of the anode erosion, which depends by thermo-physical properties of anode (electrode).

At the sparking with soft or weak work regimes (regime II), using either platinum electrodes or silver electrodes, the increasing in weight of cathode is nearly constant during the processing period.

In the case of using of hard work regimes (regime III), after a processing time (some 5 minutes), are found a reduction of the intensity of material transfer from the electrode to cathode, more accentuated at the sparking with silver electrode. In this case, the mass transfer is replaced by an erosion process of the layer already deposited, which maintain nearly constant the cathode mass.

For every kind of electrode material and used work regime have established experimentally the optimal length of processing time, also the optimal discharge energy thus as the quantity of transferred material from anode to cathode to be maximum.

The optimal periods for processing with platinum electrodes are 6 minutes for sparking in regime II, when on the cathode depose 80% from eroded material, and 3 minutes at processing with regime III, when on cathode depose 50%. At the processing with silver electrode the optimal periods for processing are 5 minutes for sparking with regime II, when on the cathode depose 75% from eroded material, and 4 minutes for regime III, when on the cathode depose 39.98% from eroded material, fig. 3 *a*.

Middle quantity of eroded and deposited material on cathode ( $\bar{k}$ ) after 8 minutes by processing is 49.12% for regime II and 32.38% for regime III at the sparking with platinum electrode, 63.5% for regime II and 25.64% for regime III at the sparking with silver electrode, fig. 3 *b*.

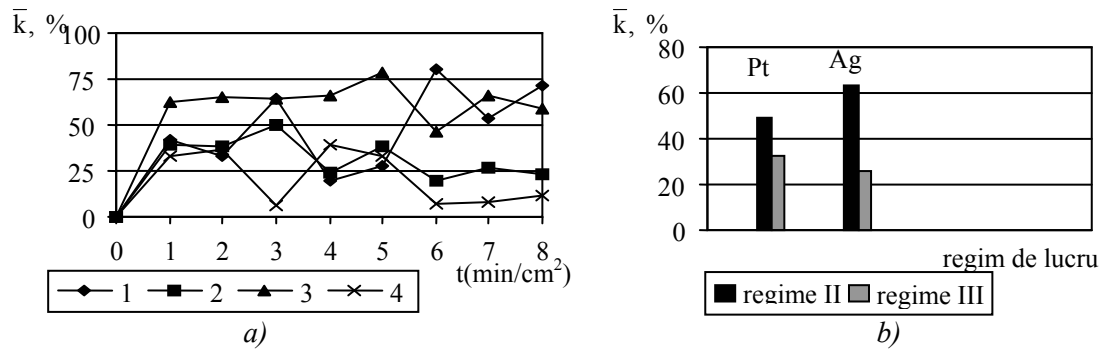


Fig. 3. Percentage variation of eroded mass deposited on cathode related with deposition time (a) and work regime (b); 1, 2 – platinum (regime II and III); 3, 4 silver (regime II and III).

#### 4. CONCLUSIONS

After the analyses of experimental data find the following aspects:

1. The intensity of material transfer from anode to cathode is highest in the first 2...3 minutes of the processing, after that begins to diminish nearly constant, due to the apparition of inverse erosion phenomenon when a part of deposited material on the cathode is pulverized in the interstice its depose on anode or its oxidize. The inverse erosion phenomenon is much intense in the case of regime III and silver electrode.
2. At the deposition and alloying through electrical sparking of copper samples, using platinum electrodes and regime III or silver electrodes and regime II, in function also by qualitative require and thickness of layer which follow to be obtained, the quantity of eroded and deposited material on the cathode have recorded the greatest values.
3. These depositions present the advantage that are realized with a lower consumption by noble metals, in comparison with classical deposition methods, and layers obtained have a good adherence on the substrate.
4. As application domains remember the following: for reduction of the contact resistances of the contacts surfaces from electrical engines and commutation equipments, for the reconditioning of contact surfaces of the high power circuit breakers and for similar commutation equipments.

Received April 26, 2005

Technical University "Gh.Asachi" Iasi  
\*Technical University Chisinau

#### REFERENCES

- /1/. Alexandru I., Carcea I., Baciuc C., Pop F., Alexandru Adrian, 1993, *Argintarea contactorilor din Cu prin scânteiere cu electrod vibrator*. Sesiune de comunicări, Univ. "Dunărea de Jos" Galați.
- /2/. Coșer N., 2004, *Cercetări experimentale privind obținerea contactorilor electrice prin depunere și aliere prin scânteie electrică*, Referat nr.3, Iași
- /3/. Lazarenco B. R., Mihailov V. V., Ghitlevici A. E., ș.a., 1978, *Lazernoie vozdeistvie na pokrîtia polucenîe electroiskrovîm metodom*. Ālectronaia obrabotka metalov, nr.3, 24-25.
- /4/. Nihailov V. V., Ghitlevici A. E., Tarcovkii N. I., 1995, *Electricescoie legirovanie metaliceschih pokrîtii*, Chișinău, Știința.

#### CERCETARI PRIVIND TRANSFERUL DE MASA LA DEPUNEREA SI ALIEREA SUPERFICIALA CU METALE NOBILE PE SUPORT DE CUPRU

**Rezumat:** Lucrarea prezintă câteva aspecte teoretice și experimentale în domeniul depunerii stratului din metale nobile pe suport de cupru, utilizând metoda de depunere și aliere prin scânteiere electrică (DASE) cu electrod vibrator. Procesele erozive la (DASE) se estimează prin mărimea eroziunii electrice și a transferului de masă a materialului anodului pe catod. Această caracteristică determină productivitatea procesului sau intensitatea creșterii grosimii stratului depus pe catod (piesă).

## STEEL NITROCARBURIZING IN FLUIDIZED BED

BY

SORIN DOBROVICI, NELU CAZACU, OCTAVIAN POTECAȘU, FLORENTINA  
POTECAȘU, ADOLF BĂCLEA, ELENA DRUGESCU

**Abstract.** *Paper is based by nitrocarburizing experiments made on pilot installation. For experiments were used different samples of steel at different nitrocarburizing regimes. Influence factors were: temperature and ammonia concentration. Treatment time had a constant value 2h30min. Influences of factors was investigated by: samples mass modifications, surface structure (micrograph), layer depth to all samples and hardness HV5 on the surface. The results confirm possibility to use fluidized bed like nitrocarburizing media and good behavior of steel*

**Keywords:** *nitrocarburizing, fluidized bed, steel*

### 1. INTRODUCTION

After nitriding, nitrocarburizing became the most usual treatments for pieces at lower temperature. Nitrocarburizing and oxynitrocarburizing became alternative technologies for parts of car industries. After this thermochemical treatment a surface layer with properties approaching at nitriding treatment is obtained, [0]. If a post oxidation is used to obtaining a  $Fe_3O_4$  superficial a porous layer, which increases corrosion resistance of parts. Porous layer offer a good adherence for different sealant that conduce to one order increasing for a corrosion resistance. For efficiency of nitrocarburizing treatment evolution shows tendencies for quality and low costs. A complex processes are performed in fluidized bed. Gasses (ammonia and methane in different proportion) in active zone, near over separation plaque, are thermal decomposing in contact with hot solid granular. The homogeneous reactions are possible to continue on the high of bed, but equilibrium is established at higher uniform regimes temperatures. A secondary stage is for heterogeneous reactions at surface samples, with adsorption of nitrogen and carbon atoms. As results of these two stage of reactions chemical compositions of gasses having major modifying: hydrogen and nitrogen and rests of methane and ammonia. These gasses produced normal fluidizations in bed and that maintaining a normal and a constant gas dynamics for constant properties of fluidized bed. A fluidized bed technology (FBT) for heat and thermo chemical treatments offers a low costs for investments and an acceptable quality [0]. The most important characteristics of fluidized bed are influenced by: chemical compositions of fluidization gas through physical gas properties and the solid granular properties (physical characteristics, shape, dimension).

High values for heat and mass transfer coefficient conduce to shorter treatment time and this technology may have applications for small enterprises and for small series of pieces.

## 2. EXPERIMENTAL CONDITIONS

Nitrocarburizing was made on the pilot conditions (Figure 1). The fluidized bed furnace has minimal conditions for nitrocarburizing. The furnace working up to 1000°C and a various gas mixtures is possible to use for different heat and thermochemical treatments. Fluidized beds are made from burned clay and a gas mixture by methane and ammonia, with different proportion of methane. Nitrocarburizing in fluidized bed is based by repeatability of process, [0]. The nitrocarburizing media was made in fluidized bed. In this case the internal and external properties of fluidized bed are important for treatment, because a large exchange surface is formed between fluidized bed and parts (samples).

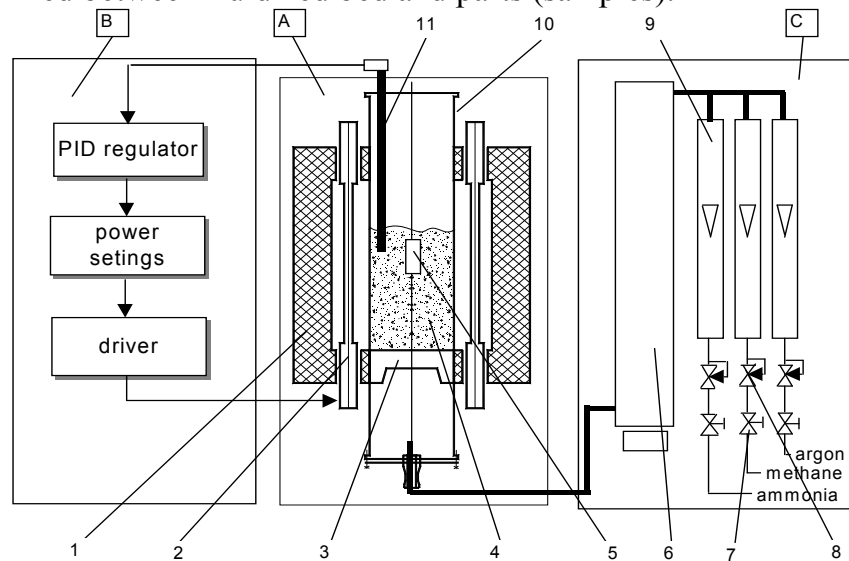


Figure 1. Schematic representation of fluidized bed furnace: B-automatization unit, A- furnace unit, C- gas unit, 1-isolation, 2-resistors, 3-fluidization plaque, 4-fluidized bed, 5-samples, 6-silicogel column, 7-valves, 8-gas regulators, 9-rotameters, 10-fluidized bed furnace, 11-K thermocouple

Table 1. Chemical composition for steel used in experimnts

Steel	Chemical composition, %.							
	C	Mn	Si	P	S	Cu	Cr	Ti
21TiMnCr12	0,20	0,95	0,28	0,014	0,016	-	1,05	0,06
18MnCr10	0,18	1,05	0,22	0,035	0,035	-	1,05	-
40Cr10	0,40	0,65	0,27	-	-	-	1,00	-

Table 2. Critical points for steels used in experiments

No.	Steel	Ac1	Ac3
m.u.	-	°C	°C
1	21TiMnCr12	740	840
2	18MnCr10	765	838
3	40Cr10	743	782

Table 3. Nitrocarburising in fluidized bed regimes

No.	Temperature	Time	gas composition
	°C	h, min	%
1	550	2h30min	25% ammonia + 75% methane
2			15% ammonia + 85% methane
3			5% ammonia + 95% methane

After fluidization, at outlet from furnace, gases were burned. For nitrocarburizing experiments three steels with 1%Cr were used: 21TiMnCr12, 18MnCr10 and 40Cr10 (Romanian standards). Chemical compositions are showing in Table 1. The critical points for transformation for all steels are showing in Table 2. For all steels nitrocarburizing are a sub critical treatments, that's have not influence over core structure and properties. Because ammonia is more expensive gas the proportion was varied between 5 and 25%, and the influence of ammonia proportion over experiments was studied (Table 3).

Table 4. Hardness measurements on the nitrocarburizing surface

steel	ammonia contents (rest methane)	HV <sub>5</sub>
m.u.	%	kgf/mm <sup>2</sup>
21TiMnCr12	5	667
	15	752
	25	655
18MnCr10	5	524
	15	623
	25	549
40Cr10	5	655
	15	713
	25	677

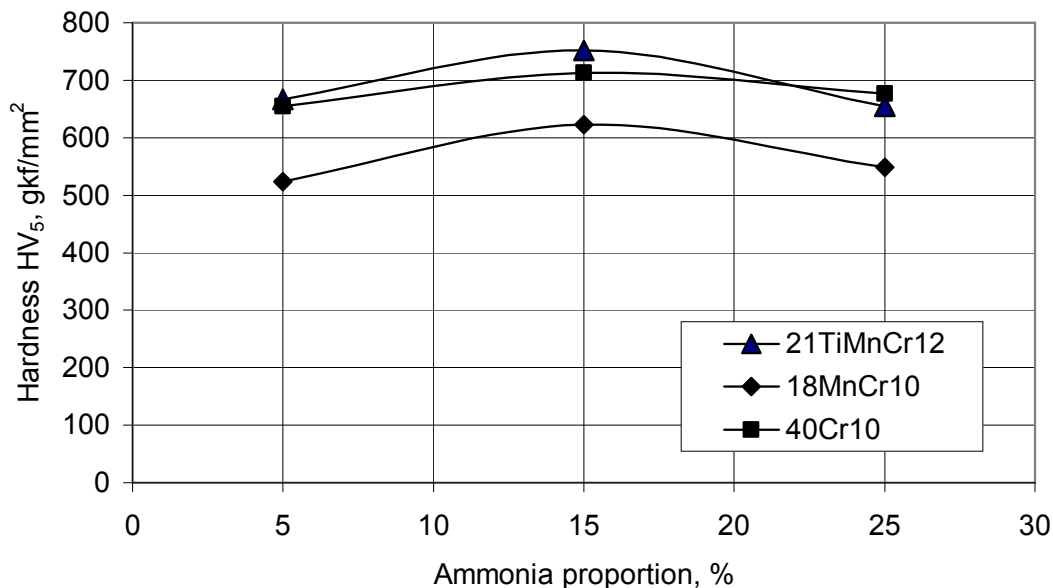


Figure 2 Hardness on the nitrocarburizing surface.

### 3. RESULTS

The hardness on the surfaces is the technological properties that are usual determined. All steel having in chemical compositions approximate 1%Cr. That conduced to hard combinations at temperature and nitrogen presence in surface. As a normal result for all samples hardness (HV<sub>5</sub>) having higher values (Table 4, Figure 2). For 15% ammonia contents in gas mixture for fluidization a maximum values were obtaining for all samples. Measurements of layer thickness for all nitrocarburizing

samples are showing in Figure 3. A normal increasing of layer depth by ammonia proportion is presence to all steel samples, but having different behaviour. The structure and properties of nitrocarburizing layer is determined by chemical compositions that conduced to particular behaviour of each steel samples.

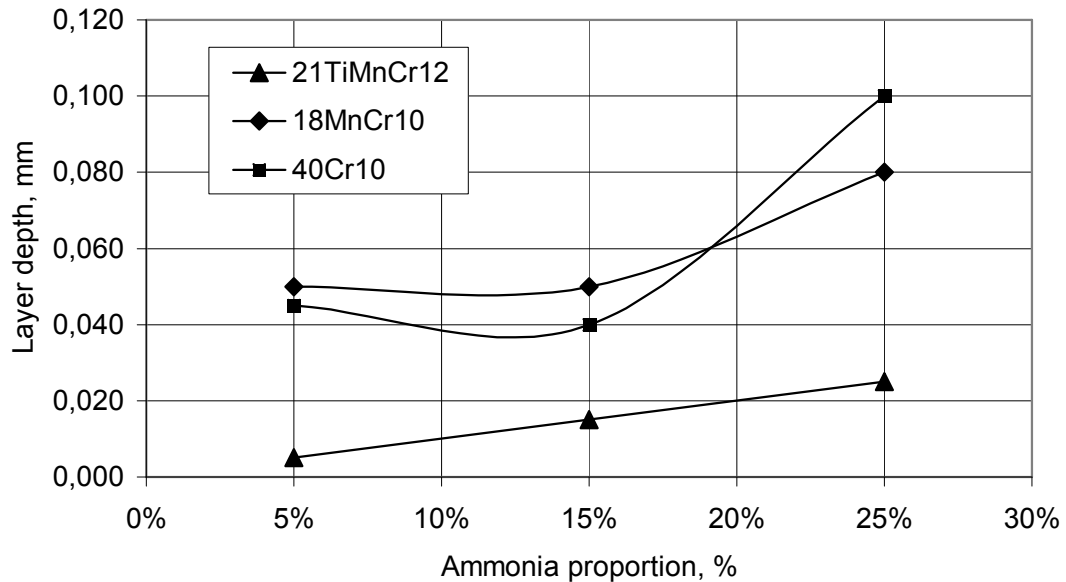


Figure 3. Nitrocarburizing layer variation with ammonia proportion

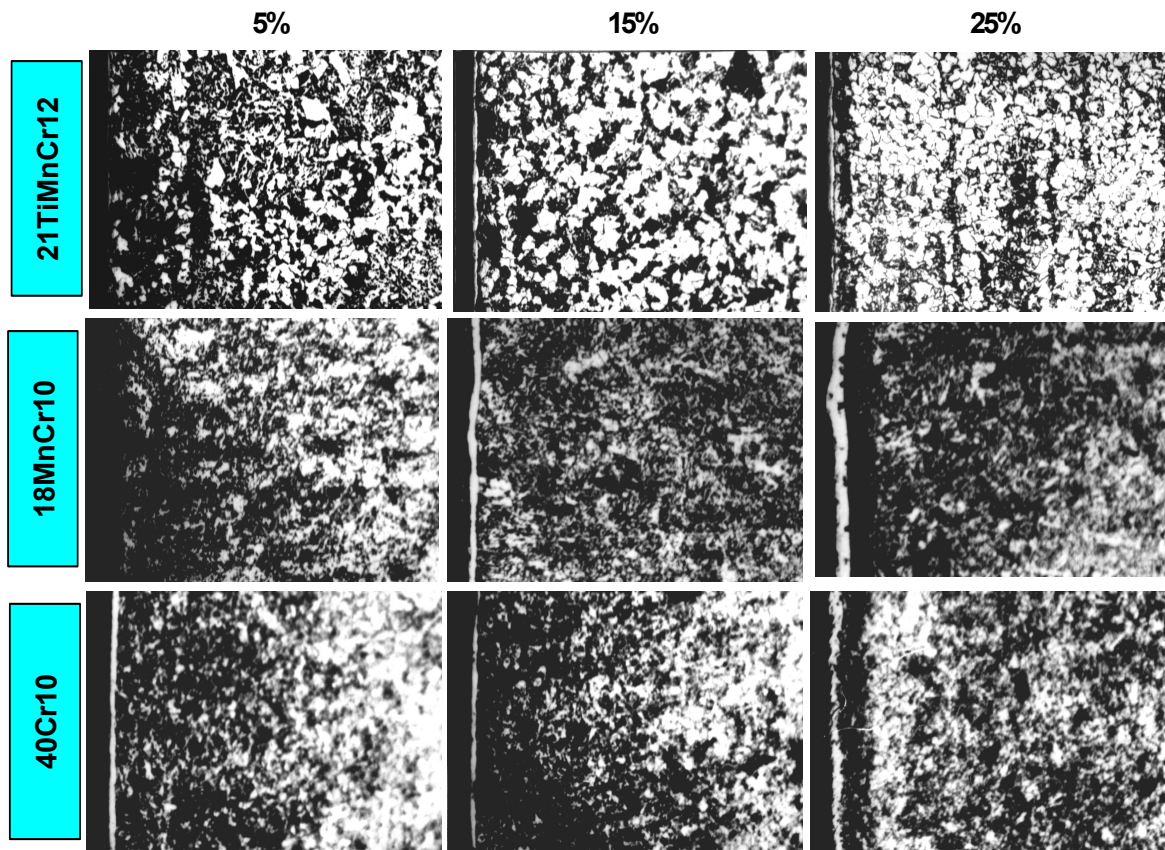


Figure 4. Representative microstructure for nitrocarburizing in fluidized bed layers

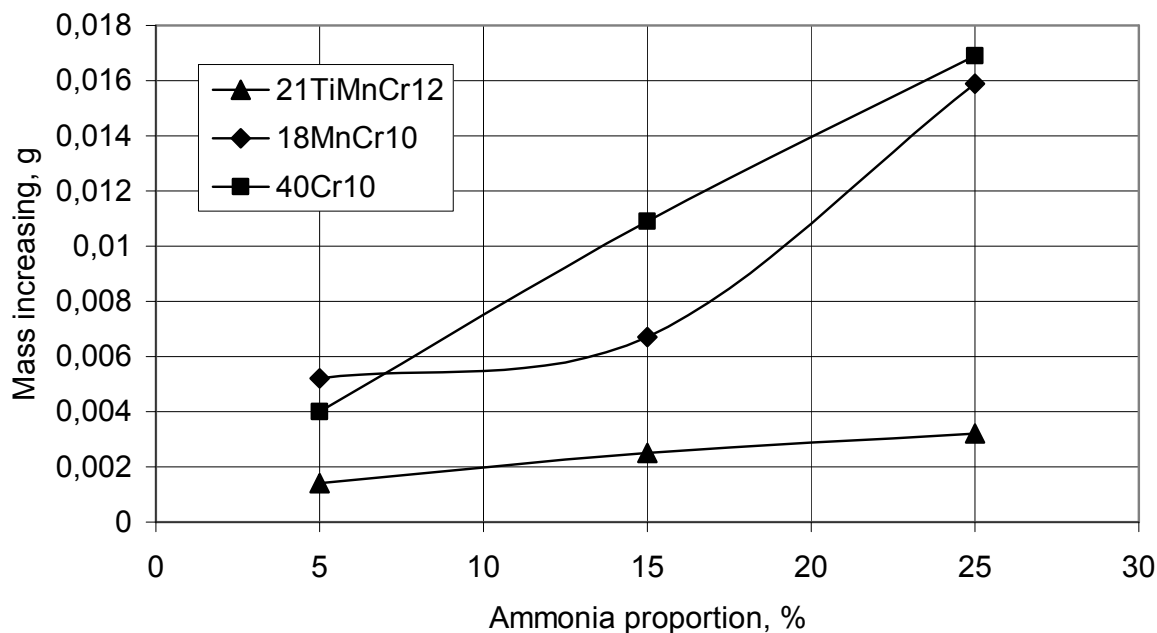


Figure 5. Mass increasing of nitrocarburizing samples

For all steel samples representative microstructures are showing in Figure 4. Combination layer has a normal increasing with ammonia proportion. Mass increasing for all steel samples was calculated by difference between final mass and initial mass, when the samples having identical shape and identical dimensions. The results are showing in Figure 5. Increasing of ammonia proportions in initial fluidization gas mixture conducted to mass increasing to all samples

#### 4. CONCLUSIONS

Nitrocarburizing experiments made in fluidized bed over the samples from 1% Cr steels confirm fluidized bed capacity for mass transfer at higher temperature. Nitrocarburizing layer was formed for all regimes, and structures and properties of layer is depending by ammonia proportion in initial gas mixture. A maximum values for hardness is in 720...750 kgf/mm<sup>2</sup> interval, which is higher values for 150min nitrocarburizing time at 550°C temperature. A shorter treatment time is the most important characteristics of fluidized bed technology.

Received May 6, 2005

"Dunărea de Jos" University Galați

#### REFERENCES

1. Dulcy M., Gantois M., *Principe de base de la cementation et de la carbo-nitruration*, Traitements thermique No.289, 1996, p.46-54
2. Roland A, *Oxicad (R) NT en four a tapis, Nitrocarburisation Oxidation Trempe*, Traitement thermique No.346/Avr 2003, pg.37
3. Willing R, Faulkner C, *Nouvelle facon d'utiliser le bain de sel en nitrocarburisation*, Traitement thermique No.333/ Aou-Sep 2001, pg.33
4. Beguin Cl, Crevoiserat O, *Controle des processus de nitruration et de nitrocarburisation gazeuses avec la sonde Datanit*, Traitement thermique No.352/Janv-Fevr 2004, pg.33

### NITROCARBURAREA ÎN STRAT FLUIDIZAT

**Rezumat:** Lucrarea are la bază experimentările de nitrocarburaire în strat fluidizat efectuate pe o instalație pilot. Pentru experimentări au fost folosite probe din diferite mărci de oțeluri. S-au realizat diferite regimuri de nitrocarburaire. Factorii de influență considerați au fost: temperatura de nitrocarburaire, proporția de amoniac. Durata tratamentului a fost constantă la 2h30min. Influența factorilor a fost investigată prin: modificarea de masă a probelor, micrografii, adâncime strat, duritate HV5 pe suprafața tratată. Rezultatele confirmă posibilitatea utilizării straturilor fluidizate ca mediu de nitrocarburaire la durate mici de tratament și buna comportare a oțelului ales la acest tratament

## TEMPERATURE INFLUENCE OVER FLUIDIZED BED GASDYNAMICS FOR HEAT TREATMENTS

BY

ELENA DRUGESCU, SORIN DOBROVICI, FLORENTINA POTECAȘU,  
OCTAVIAN POTECAȘU, NELU CAZACU, ADOLF BĂCLEA

**Abstract.** *Temperature is the most important factor for heat treatments of steels. If a fluidized bed is used for heating media, the uniformity of temperature is highest. But temperature having a direct influence over fluidized bed gas dynamics Internal mass and heat transfer and external transfer processes are depending direct or indirect by temperature. For fluidized bed technology (FBT) drop pressure is the most important technological control factor. The paper is based by fluidized bed experiments for temperature influence over drop pressure of fluidized bed*

**Keywords:** *fluidized bed, drop-pressure, heat treatment*

### 1. INTRODUCTION

Heat treatment is used to change mechanical properties based by changing of microstructure, and residual stress state 0. For example, a T6 heat treatment would be used to increase the strength and hardness of a part by precipitation hardening. The process starts by heating the part to near its solidus temperature of approximately 540 C, which varies between specific alloys. The part is allowed to soak at this temperature for a time to dissolve the soluble phases. Subsequent quenching locks these phases within the matrix, resulting in a supersaturated solution. An aging process follows where the part is held at a comparatively low temperature to form finely dispersed strengthening precipitates. The quality of this process is affected by many factors, but four significant issues are: how close the part can be brought to its solidus temperature; the repeatability of the heat treatment cycle from part to part and batch to batch; the uniformity of the heating and cooling processes; and the rate of heating and cooling. The effect of this process is to improve the properties of the material for the end user, such as optimizing strength, hardness, elongation or machinability. The use of newly developed fluidized-bed technology 0 offers several improvements over current heat treating methods. Heat transfer rates can be an order of magnitude faster than those seen in air ovens. Fluidized bed line heat treatment makes possible important energy saving. Parts can be put in heat treatment before they have fully cooled from casting. Since the parts have fully solidified but are still hot, less energy is needed to heat the parts to solution temperature.

The other possibility this rapid heat transfer offers is short cycle heat treating. In independent testing using the fluidized-bed system, A356 aluminum alloy parts were solution heat treated to 555 C, and peak tensile and elongation properties were achieved in as little as a 30-minute heat-treating cycle (including heating and soak time).

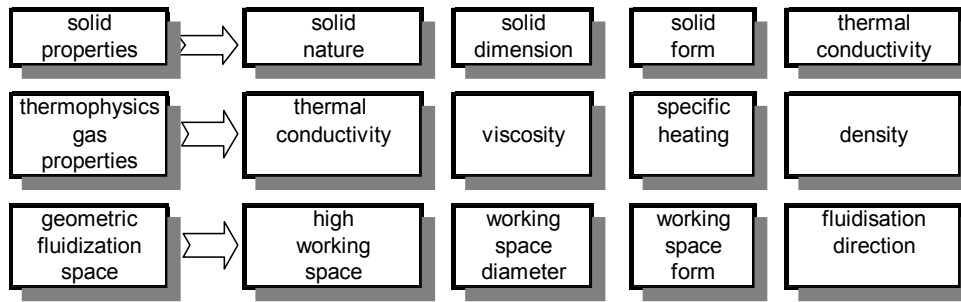


Fig. 1. Factors influence over fluidization, [0].

Table 1. Fluidization speed influence over drop pressure, for different temperature (granular solid quartz sand, 0,10...0,16 mm (G1), dry air at 20°C, initial high of granular bed: H=25 mm, initial bed diameter: D=49mm)

no	debit l/h	speed m/s	d <sub>p</sub> , mm H <sub>2</sub> O, at temperature, °C								
			100	200	300	400	500	600	700	800	900
0	0	0	0	0	0	0	0	0	0	0	0
1	59,91	0,002	15	22	25	25	40	44	42	48	56
2	134,48	0,005	32	44	50	50	56	62	62	72	90
3	209,05	0,008	48	52	58	60	70	80	86	98	120
4	283,62	0,011	56	62	72	80	90	106	108	122	140
5	358,19	0,014	64	70	80	90	100	120	124	138	160
6	432,76	0,017	70	80	85	100	110	138	134	148	170
7	507,33	0,020	80	88	92	105	118	146	142	162	180
8	581,90	0,022	84	92	102	110	120	152	148	168	190
9	656,47	0,025	92	102	108	120	130	160	168	188	200
10	731,04	0,028	100	108	118	130	140	170	178		205
11	805,61	0,031	110	120	128	140	148	180	190		
12	880,18	0,034	118	130	138	150	156	184	200		
13	954,75	0,037	128	140	144	158	170	192	210		
14	1029,32	0,040	140	150	158	170	180	205	220		
15	1103,89	0,043	150	160	170	182	195	220	235		
16	1178,46	0,045	164	170	180	200	205	245			
17	1253,03	0,048	176	180	190		220				
18	1327,60	0,051	190	194	205						
19	1402,17	0,054	200	210							
20	1476,74	0,057	210	245							

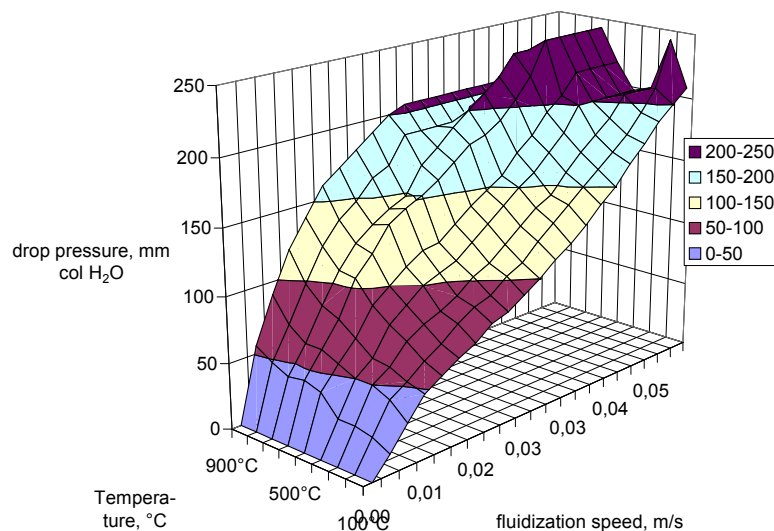


Fig. 2. Temperature influence over drop pressure for different fluidization speed for D = 50 mm, H = 25 mm, 0.



By comparison, over four hours of soak time alone is prescribed in a conventional air furnace [3]. The microstructures from these tests showed much more rapid coarsening kinetics and spheroidization of eutectic silicon particles in the samples heated in the fluidized bed. Improved product quality because of tightened temperature control is one of the most significant benefits to this fluidized-bed heat-treating process. The entire process chamber can have a very precision controlled temperature. This causes the fluidized bed to heat parts more uniformly than conventional systems

Every exposed surface of each part (internal and external) is in direct contact with the fluidizing media, and all of the media is at the same temperature. This uniformity results in true repeatability between components in the process: every part sees the exact same heating profile. Distortions associated with this phenomenon are reduced. In addition, the quench rate can be very precisely fine tuned because of the excellent temperature control in the bed. The fluidized bed also is used in the aging process. The same qualities that make a fluidized bed ideal for solutionizing (rapid heat transfer, process uniformity, and the ability to perform the process in line) also apply to the aging process. Process times can be shortened, and the quality of the end results can be improved compared with conventional aging. Again, the parts all see identical thermal cycles and so repeatability, and therefore quality, is enhanced. Using the fluidized bed in all three phases of solution heat treatment allows the processing time to be shortened by hours (total reduction in process time depends on the process in question) and the process made completely automated. After the parts are loaded in the system, they are conveyed through the solution bed and then automatically transferred to the quench bed. When quenching is complete this

Transfer is repeated as the parts move into the aging bed; after aging, the parts are placed in an unloading station. All of these transfers occur automatically. Some characteristic of fluidized bed are attractive for applications for heat and thermochemical treatments: high uniformity of temperature, higher mass transfer coefficient, higher heat transfer coefficient, thermal mobility. For fluidized bed applications in heat and thermochemical treatments of steels the influence factors are grouping like in Fig. 1.

Many years fluidization having a major problem in absence of mathematic model because too many factors having influence over internal and external processes and is difficult to correlate them. The DA and DA&C systems adapted to PC solve problems by adequate software. Temperature is one of factors that having higher influence over fluidization for heat treatments because having double influence: direct (heat treatment factor) and indirect, over solid properties, gas properties and fluidized bed properties.

1. Influence over granular solid properties with temperature: specific heat, heat conductivity
2. Influence over thermo-physics properties of gases: heat conductivity, cinematic viscosity, dynamic viscosity, density

### **EXPERIMENTAL CONDITIONS**

Temperature influence over fluidized gasdynamics was studied in conditions for high temperature heat treatments:

- fluidized bed ceramics chamber diameter:  $d=49...50$  mm;
- initial high of bed:  $H_i= 25, 50, 75$  mm;
- fluidization gas: dry air
- temperature air (inlet):  $20^\circ\text{C}$ ;
- granular solid: quartz sand:  $0,10...0,16$  mm

Drop pressure in fluidized bed was determined ( $d_p$ ) because are principal control factor for technological applications. The temperature influence over drop pressure was considered from 20 to  $900^\circ\text{C}$ .

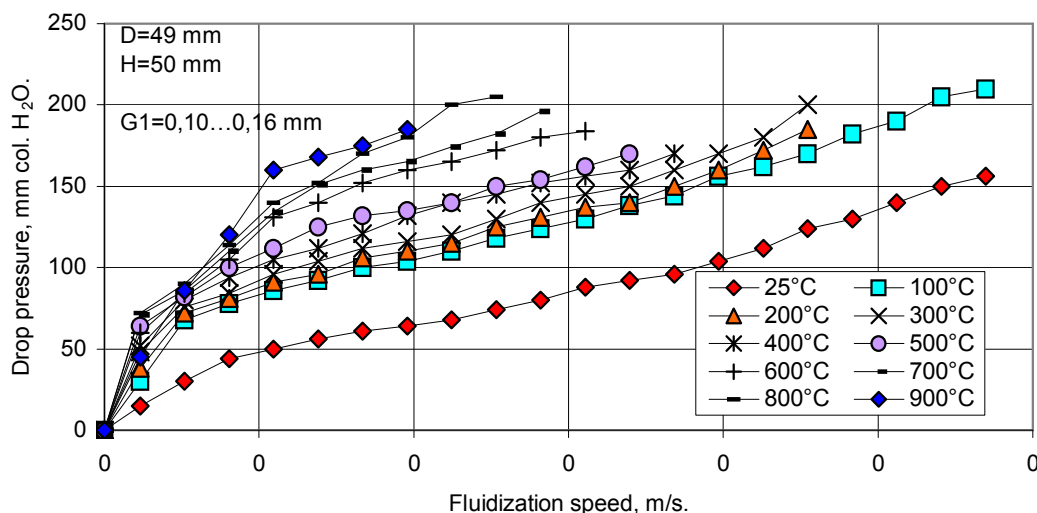


Fig. 3. Temperature influence over drop pressure for different fluidization speed for  $D=50$  mm,  $H=50$  mm, 0.

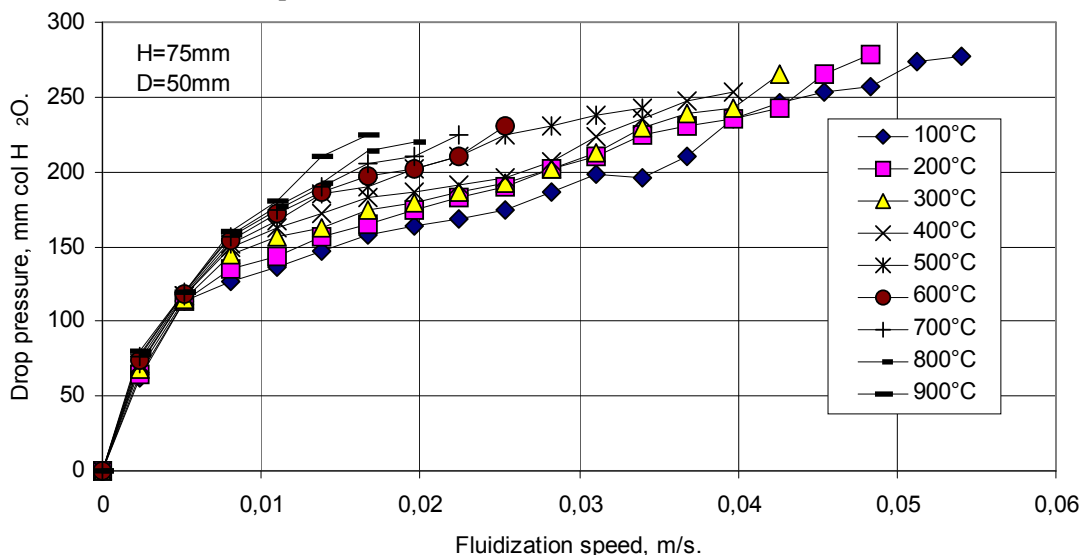


Fig. 4. Temperature influence over drop pressure for different fluidization speed for  $D=75$  mm,  $H=50$  mm, 0.

## RESULTS AND CONCLUSIONS

From initial grouping of influence factor for heat treatments in fluidized bed (Fig. 1) some factors was selected for experiments: temperature, fluidization speed and initial high of granular bed. Drop pressure was measured for different initial high of granular bed and fluidization speed. Fluidization speed increasing at maximal values

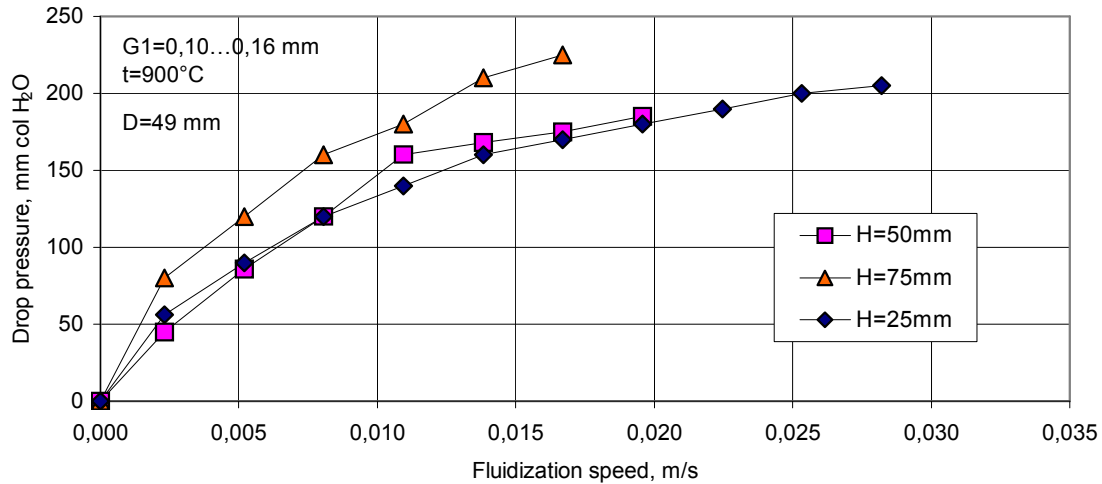


Fig. 5. Fluidization speed influence over drop pressure in fluidized bed for same solid granular for the same diameter and different initial bed high, 0.

and drop pressure having a nonlinear increasing: (Table 3, Fig. 4). At the same initial geometry of granular bed (H, D) and fluidization speed, drop pressure on fluidization bed increasing with temperature.

For a stable fluidization drop pressure was maintaining at constant values. At the same temperature drop pressure increasing with high of solid granular bed and fluidization speed (Fig. 5). Drop pressure is very common method for fluidization control (unique when superior surface of bed isn't visible). Result confirm complex influences of: temperature, fluidization speed and geometry of initial bed over bed drop pressure and important remarque that any modification in factor values (inclusive parts) will be considered in developing heat treatments and thermochemical treatment process.

Received May 6, 2005

"Dunărea de Jos" University Galați

#### REFERENCES

- /1/. Cazacu N., *Researches concerning fluidized bed heat treatment technology for pieces*, Doctoral thesys, University "Dunarea de Jos" of Galati, 2000;
- /2/. David Dingmann and Greg Handzel, *Short-Cycle Solution Heat Treatment In a Modern Fluidized Bed Technomics LLC*, Plymouth, Minn., Industrial Heating, august 2003
- /3/. Kunii. D., Levenspiel O., *Fluidization engineering*, p. .265...301, John Wiley&Sons Inc., 1969;
- /4/. Sagon-King, F, *Fluidized-Bed Equipment*, ASM Handbook, Vol. 4, Heat Treating, ASM International, Materials Park, OH 44073-0002, pages 484-491
- /5/. Samoila C, Ionescu M.S, Drugă L, *Tehnologii și utilaje moderne de încălzire*, Editura Tehnică, București, 1986

#### INFLUENȚA TEMPERATURII ASUPRA GAZODINAMICII PATULUI FLUIDIZAT DESTINAT TRATAMENTULUI TERMIC

**Rezumat:** Temperatura este cel mai important factor pentru tratamentele termice și termochimice. Dacă straturile fluidizate sunt folosite ca medii de încălzire, atunci se obține o uniformitate mare de temperatură. Temperatura influențează direct și dinamica curgerii gazelor. De asemeni transferul de masă și energie intern și extern depind de temperatură. Pentru Aplicațiile tehnologice ale fluidizării (FBT) căderea de presiune în strat este cel mai important factor de control tehnologic al fluidizării. Lucrarea se bazează pe experimente în care s-a urmărit influența temperaturii asupra căderii de presiune în stratul fluidizat.

## ON THE BEHAVIOUR OF A DUAL-PHASE STEEL WITH 0,09% C AND 1,90% Mn IN THE CONDITIONS OF HERTZIAN CONTACT

BY

CONSTANTIN DULUCHEANU, NICOLAI BĂNCESCU, REMUS LUCA

**Abstract.** *This article presents the research performed on the behaviour of the dual-phase steel with 0.09% C and 1.90% Mn in conditions of hertzian contact. The ferrite-martensite structure was obtained by intercritical quenching by heating at 740° C and cooling in water, oil and oil activated in ultrasonic field. The experiments were performed on a special installation with 4 work places and lasted 30 minutes for each specimen. For comparison, similar experiments were performed on specimens made by plain-carbon steel (OLC 45), subjected to a hardening and tempering heat treatment.*

**Keywords:** *dual-phase steel, ferrite-martensite structure, intercritical quenching, hertzian contact*

### 1. INTRODUCTION

Scientific and technical progress was possible due to new material usage. Dual-phase ferrite-martensite steels also belong to new material category which are defined as low-alloy steels having a structure made up by a soft tough ferrite matrix wherein martensite and a small amount of residual austenite are homogeneously scattered.

The superiority of these materials as compared to other steels is determined by the possibility of obtaining a high combination between the resistance properties and plasticity ones, fact which allows the achievement of complex mould castings with high mechanical resistance. This set of mechanical properties made possible the use of dual-phase ferrite-martensite steels in many fields such as the automotive industry and assembling component part industry.

Quenching at intercritical range of temperatures ( $\alpha + \gamma$ ) represents the main method of dual-phase steel production, the structure obtained by applying this method is influenced by both the chemical composition of steel and applied technology of intercritical heat treatment. At the same time, the physical, mechanical and technological properties certainly depend on the quantity ratio and structural component morphology resulting from the heat working process.

### 2. RESEARCH METHODOLOGY

An alloy of 0,09% C, 1,90% Mn, 0,06% Si, 0,10% Cr, 0,09% Ni, 0,03% Mo, 0,012% Al, 0,15% Cu, 0,019% P, 0,01% S (codified as DPS) was used in view of achieving the object of research theme, a material produced and worked by rolling at S.C. "Wire Industry" S.A. Campia Turzii. The chemical composition of material was determined by spectral analysis at S.C. "SIDEX" S.A. Galati.

In heat treatment technology it is extremely important to know the critical points  $A_{c1}$  and  $A_{c3}$ , as the successful performance of these heat treatments depends

on the correctness of these data. For this reason, alloy in question was subjected to a thermodifferential analysis that was achieved at the “Faculty of Metallurgy and Material Science” within “Dunarea de Jos” University in Galati, thus obtaining the critical points  $A_{c_1}$  and  $A_{c_3}$  as follows:

$$A_{c_1} = 702 \text{ } ^\circ\text{C}$$

$$A_{c_3} = 837 \text{ } ^\circ\text{C}$$

Roll specimens of 12 x 15 mm were used in order to determine the behaviour of dual-phase steel (DPS) in conditions of hertzian contact and they were subjected to the variants of heat treatment as shown in table 1:

Table 1. Technology variants of heat treatment.

Code	Technological parameters of intercritical quenching		
	Heating temperature ( $T_c$ ) [ $^\circ\text{C}$ ]	Holding time ( $t_m$ ) [min]	Cooling medium
$C_W^{740}$	740	30	W - Water ( $T_a = 20 \text{ } ^\circ\text{C}$ )
$C_O^{740}$	740	30	O - Oil TT 25 ( $T_u = 40 \text{ } ^\circ\text{C}$ )
$C_{US}^{740}$	740	30	US - Oil TT25 in ultrasonic field ( $f = 40,4 \text{ KHz}$ , $I = 2 \text{ W/dm}^2$ , $T_u = 40 \text{ } ^\circ\text{C}$ )

The cooling behaviour of DPS alloy in the three quenching mediums as shown in table 1 (water, oil, oil activated in ultrasonic field) was previously analysed, using in this view a plant existing in the Heat Treatment Laboratory at “Stefan cel Mare” University, a plant that allows the marking of cooling curves into temperature-time coordinates.

The quality evaluation of intercritical heat treatment was achieved by optical metallographic examination and diffractometrical analysis by using a DRON-3M tester at the “Dunarea de Jos” University in Galati. The martensite, ferrite and residual austenite quantities and the carbon content dissolved into martensite and its tetragonal degree were determined.

Tests concerning the behaviour in conditions of hertzian contact were carried out by using a machine made in Heat Treatment Laboratory, with four working places, that provides 3000 contact is plane-ball, using 10 mm, being heat treated in classical conditions. The plant provides a medium speed of ball  $u = 5\text{m/s}$ , a maximum hertzian pressure  $P_o = 2176 \text{ MPa}$ , and contact spot dimensions resulting from the calculation of  $a = b = 0,0659 \text{ mm}$ .

### 3. TEST RESULTS

The cooling times for different conveniently chosen temperature ranges were obtained from the diagrams of temperature time co-ordinates marked on the plant for behaviour analysis of cooling materials in different mediums and the cooling speeds (at same ranges) were calculated using the following ratio:

$$v_r = \frac{\Delta T}{\Delta t}, [^{\circ}\text{C/s}]$$

where:  $\Delta T$  is the temperature range,  $\Delta t$  - the cooling time in considered range of temperatures. A soft made by Microsoft (USA) was used in order to analyze the experimental data, the obtained results are shown in figure 1.

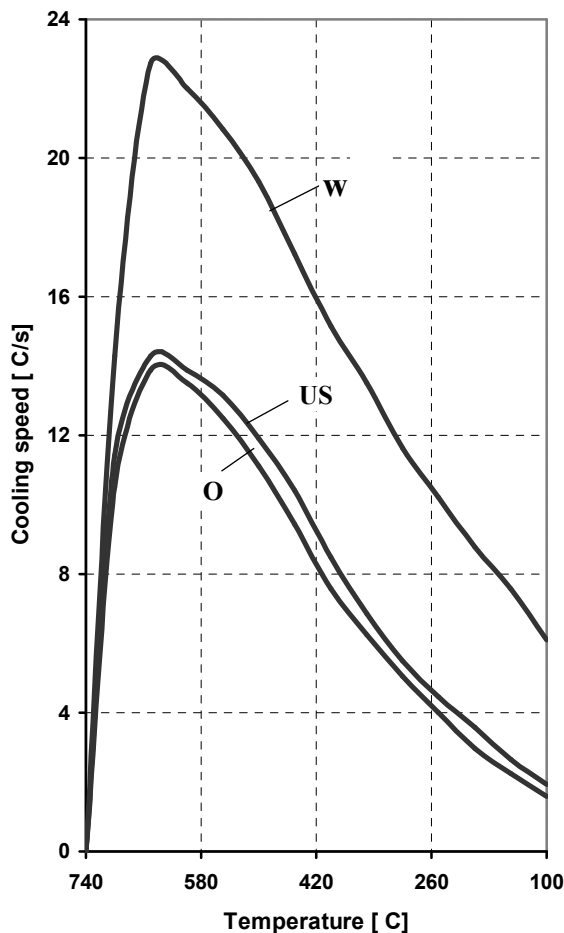


Figure 1. Cooling speed variation depending on temperature:  
W – water; O – oil; US - oil in ultrasonic field.

Quantitative analysis of metallographic components carried out in view of studying the heat treatment effect upon dual-phase steel structure was performed by linear segment method. Moreover, specially prepared specimens were also subjected to X-ray analysis, this analysis was carried out by using a  $\text{MoK}_\alpha$  radiation diffractometer. Mention must be made that the initial metallographic structure of specimens consisted of 74% ferrite and 26% perlite.

The results of metallographic quantitative analysis and those of X-ray analysis are shown in table 2.

Tests regarding the behaviour of dual-phase steel in conditions of hertzian contact were carried out in 30 minutes for each set of specimens. The tests were achieved by using 20 specimens for each variant of heat treatment as shown in table 1. After the experiments have ceased, the contact impressions from each specimen subjected to test were measured.

Table 2. The quantitative and X-ray analysis results of structure.

Heat treatment conditions	$Q_M$ [%]	$Q_F$ [%]	$Q_{A rez}$ [%]	$C_M$ [%]	c/a
$C_W^{740}$	25,10	73,60	1,30	0,338	1,0158
$C_O^{740}$	21,80	76,50	1,70	0,305	1,0142
$C_{US}^{740}$	23,40	75,60	< 1,00	0,313	1,0146

Note:  $Q_M$  - martensite quantity;  $Q_F$  - ferrite quantity;  $Q_{A rez}$  - residual quantity of austenite;  $C_M$  - carbon percent in martensite; c/a - tetragonal degree of martensite.

Before carrying out these tests, the specimens were subjected to Brinell hardness test ( $F = 187,5$  daN,  $D = 25$  mm).

For comparison, similar tests were carried out on carbon steel specimens of high quality, type OLC 45, where the specimens were subjected to a quenching and tempering heat treatment.

The performed test results are shown in table 3 and figures 2 - 5.

Table 3. Test results in conditions of hertzian contact.

Material	Heat treatment	HB Hardness [daN/mm <sup>2</sup> ]	Diameter of contact impression, [mm]
Dual-phase steel	$C_W^{740}$	371	2,067
Dual-phase steel	$C_O^{740}$	322	2,367
Dual-phase steel	$C_{US}^{740}$	345	2,155
OLC 45 steel	Quenching and tempering	286	2,637

#### 4. CONCLUSIONS

1. The cooling for DPS steel in cooling oil activated in ultrasonic field were slightly close to those performed in oil, being higher in the range of temperatures 600 - 250 °C (the field of temperatures specific to perlitic transformation).

2. The intercritical quenching by heating at 740 °C and cooling in the three different mediums (water, oil, oil activated in ultrasonic field) provided a structure confirming the definition given by specialized literature as regarding the dual-phase ferrite-martensite steel ( $Q_M = 21,80 - 25,10\%$ ). The resulting ferrite-martensite structures were influenced by the technological parameters of intercritical quenching.

3. The dimensions of contact impressions on the specimens of dual-phase steel were between 2,067 mm and 2,367 mm.

4. The size of contact impressions was influenced by the applied technology of intercritical heat treatment and therefore by the resulting structure of ferrite-martensite. The diameter of these impressions decreased with increasing of martensite content and with carbon content dissolved into martensite.

5. The results obtained for dual-phase steel were superior to those determined on carbon steel OLC 45

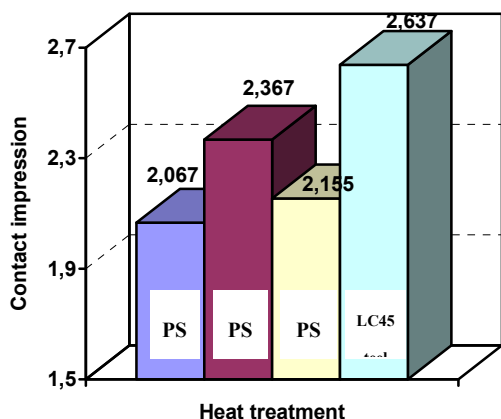


Figure 2. Heat treatment effect on contact impression.

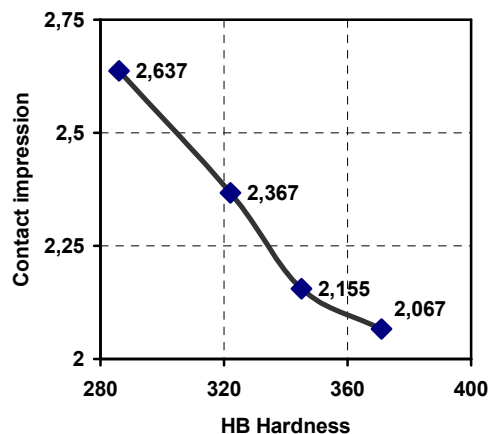


Figure 3. HB Hardness effect on contact impression.

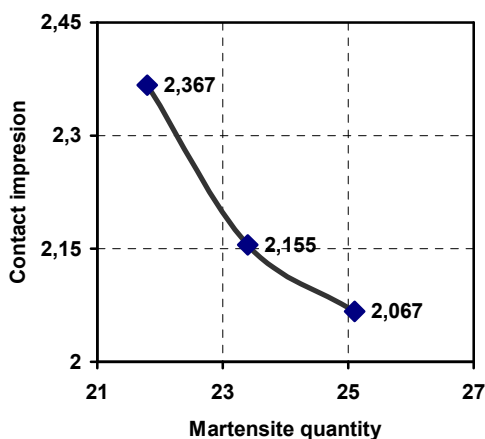


Figure 4. Effect of martensite quantity from dual-phase steel structure on contact impression.

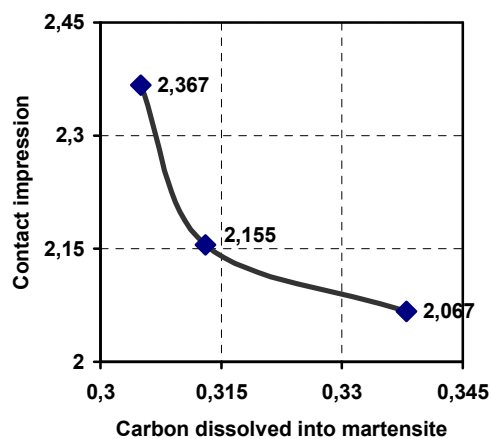


Figure 5. Effect of carbon content dissolved into martensite of dual-phase steel structure on contact impression.

Received May 4, 2005

„Stefan cel Mare” University, Suceava

#### REFERENCES

- /1/. Bancescu, N., Gramaticu, M., Crudu, I., Dulucianu, C., „*Quenching in Ultrasonic Field-An Increasing Modality of Hertzian Contact Durability*”, Magazine „Machine Engineering”, nr. 1-2, page 55-57, 1996.
- /2/. Dulucianu, C., “*Contributions Regarding the Physical, Mechanical and Technological Properties of Dual-phase Ferrite-Martensite Steels*”; Doctorate Thesis, Galati, 1999.
- /3/. Dulucianu, C., Bancescu, N., Gramaticu, M., „*Technological Parameter Effect of Intercritical Heat Treatment upon the Structure and Mechanical Properties o Dual-phase Steel*”, University Annals, „Dunarea de Jos”, Galati, ISSN 1453-083X, Number IX, Addition to volume XVI (XXI), page 352-359, 1998.

**CERCETĂRI PRIVIND COMPORTAREA UNUI OȚEL BIFAZIC FERITO-MARTENSITIC  
CU 0,09% C ȘI 1,90% Mn LA CONTACT HERTZIAN**

**Rezumat:** În articol sunt prezentate cercetările realizate pentru determinarea comportării unui oțel bifazic cu 0,09% C și 1,90% Mn la contact hertzian. Structura ferito-martensitică a fost obținută prin călire intercritică (încălzire la 740 °C și răcire în apă, ulei, ulei în câmp ultrasonor). Încercările s-au efectuat pe o instalație cu patru posturi de lucru care asigură 3000 contacte/min.; contactul a fost de tip bilă-plan, iar durata încercării de 30 minute pentru fiecare lot de probe. Pentru comparație, încercări similare au fost efectuate și pe probe din oțel OLC 45, probe ce au fost supuse unui tratament termic de îmbunătățire.

## ELECTROMAGNETIC EVALUATION OF NANOSTRUCTURED MATERIALS AND SOME MEMS DEVICES

BY

R.GRIMBERG\*, ADRIANA SAVIN\*, ROZINA STEIGMANN\*, A.ANDREESCU\*,  
ALINA BRUMA\*\*

**Abstract.** *This paper presents the method to evaluate the defects in nanotubes made from stainless steel 304 hard. The nanotubes are made for medical purpose, thus they should be tested before usage. The probability of detection (POD) was 98% for 98% reliability coefficient..*

**Keywords:** *nanomaterials, MEMS, microsensors, POD*

### 1. INTRODUCTION

Due to superior properties, nanostructured materials with electric and/or magnetic conductive have started to be used at large scale in different domains. To assure the quality of finite products, the materials and devices should be nondestructive tested.

In this paper, the usage of eddy current microsensor for special application is presented: the control of tubes made from stainless steel 304 hard with  $\Phi 226 \times 32 \mu\text{m}$ , intended for special catheters, using encircling transducer [1]

*Heraeus Materials – Medical Components Division, Switzerland*, has made the tubes and MEMS devices.

The dimension of controlled objects as well as those of the defects imposes the usage of high control frequency, about  $\sim 5\text{MHz}$ .

In the case of the tubes, the minimum perceptible defect, at 98% probability of detection (POD), for 98% reliability coefficient was a slot with  $25 \times 5 \times 10 \mu\text{m}$  [2]

### 2. EXPERIMENTAL SET-UP

The studied samples were two samples tubes with outer diameter (OD) 0.350 mm; inner diameter (ID) 0.260mm, presented in Figure 1. They are made from Stainless steel AISI 304, denoted S1 and S2. The lengths of samples are: S1- 1490mm, S2 - 1491mm.

The experimental conditions were selected as [3]:

**Examination method:** Eddy current with encircled differential send-receiver transducer  
**Control equipment:** SFT 6000N – SOFRATEST – France  
**Transducers:** Made at Nondestructive Testing Department – National Institute of R&D for Technical Physics, Iasi, ROMANIA

**Control conditions:**

Frequency - 4MHz

Injection – 10Vpp

Gain – 65

Phase - 169°

Low pass filter with cut-off: 20Hz

After optimal parameters determination, the phase was adjusted so that the noise due to tube vibration shall be projected on one of the channels. The eventually defect indications are visualized on the second channel.

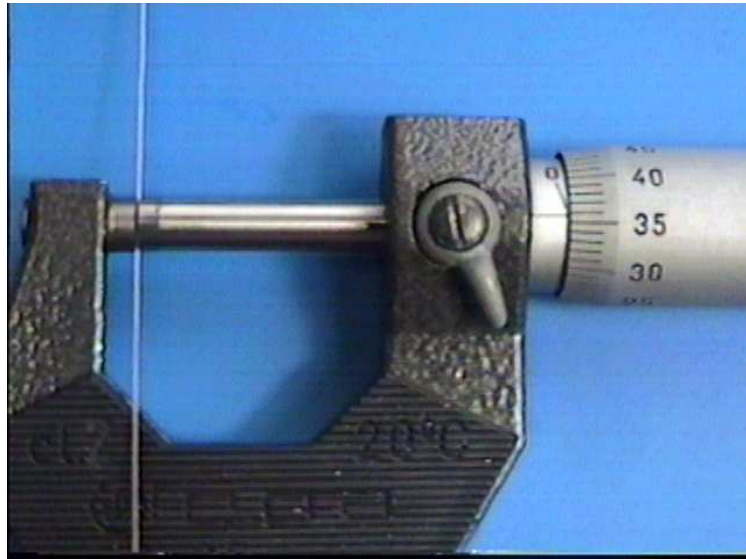


Fig.1. The studied sample

### 3. MAGNETIZATION ANALYSIS

The magnetization test shows that the both samples are magnetized at the ends. The remnant magnetization measurements were made with a magnetometer with flux-gate probe, self commuting [4]. The measurements of the remnant induction were made with the transducer closer to protection jacket of samples.

Sample S1:

- The induction was modified between 1.9 $\mu$ T at the ends of tube and 0.1 $\mu$ T at 40mm distance from the ends.

Sample S2:

- The induction was modified between 1.8 $\mu$ T at the ends of tube and 0.1 $\mu$ T at 40mm distance from the ends.

The existence of remnant magnetization shows that the material presents ferromagnetic properties, therefore a relative magnetic permeability bigger than 1. Due to high frequency, this value didn't influence the results of the control, for eddy current control, the tubes shall not be magnetized to saturation.

### 4. CONTROL RESULTS

The projection of the vibration noise on the one of the channels is presented in Figure 2. It is observed that the other channel is slightly influenced by the noise [5].

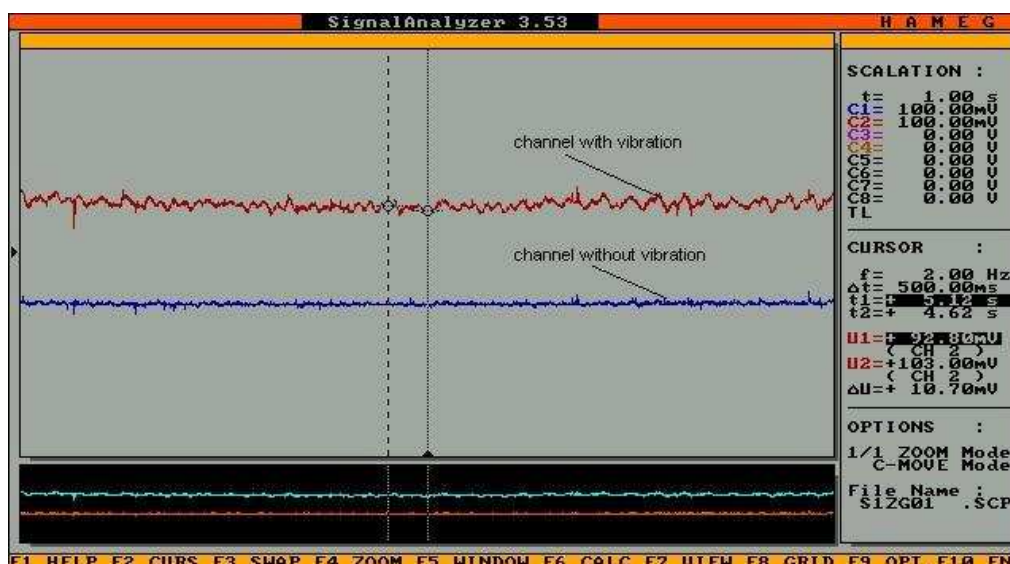


Fig.2. Noise due to vibration of the tube in the interior of transducer

### 5. SAMPLE 1 EXAMINATION

In Figure 3 is presented the results of examination for the region 100mm - 656mm of the sample S1. In this region, the existence of a visible material discontinuity is observed on the marked channel, that didn't contain the vibration noise. The position of discontinuity is between 610mm and 640mm from the beginning of tube.

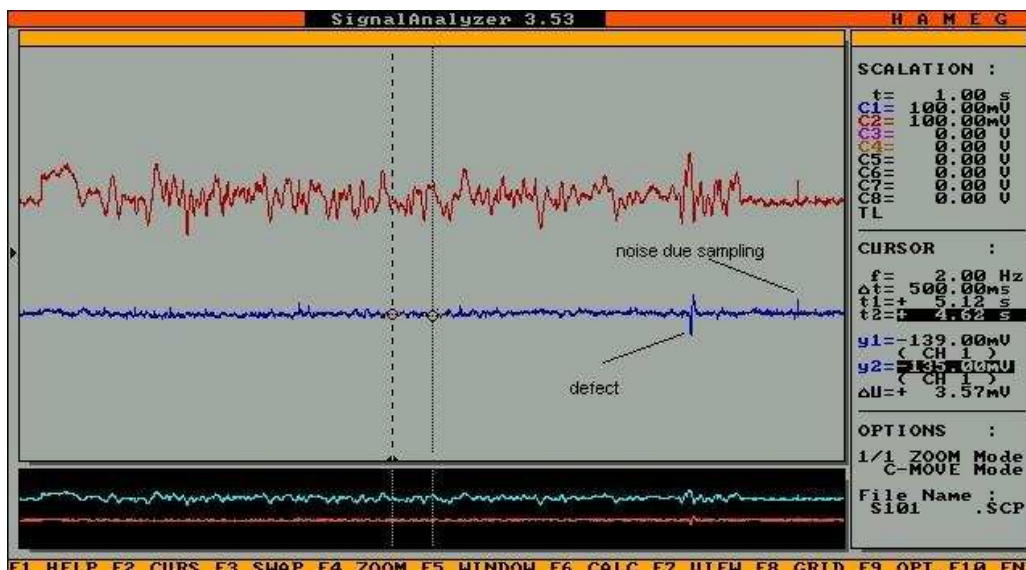


Fig. 3. Signal for the first region of sample S1.

For signal to noise report evaluation, the amplitude of the signal due to the discontinuity was measured and the maximum amplitude of the noise on the channel on which the measurements were made, was estimated.

10 displacements were made, with the tube rotated with randomly angle.

The results of the control are presented in Table 1.

Table 1. The results of sample S1 control.

No.crt.	Signal amplitude [mVpp]	Noise amplitude [mVpp]	Signal to noise ratio
1	107	4	26.75
2	96	6	16
3	969	5	19.2
4	104	4	26
5	85	6	14.17
6	93	4	23.25
7	100	6	16.67
8	111	7	15.86
9	103	5	20.6
10	100	3	33.3

Below, the statistic data analysis for the results from Table 1 is presented:

- Average of signal's amplitude [mVpp]: 99.5
- Standard deviation of signal's amplitude [mVpp]: 7.44
- Average amplitude of noise amplitude [mVpp]: 5
- Standard deviation of noise's amplitude [mVpp] 1.247
- Signal to noise ratio: 21.18
- Standard deviation of signal to noise ratio: 6.09

In Figure 4 is presented the result of examination for the region 656mm-1490mm. It is observed that on this region the tube didn't present discontinuities.

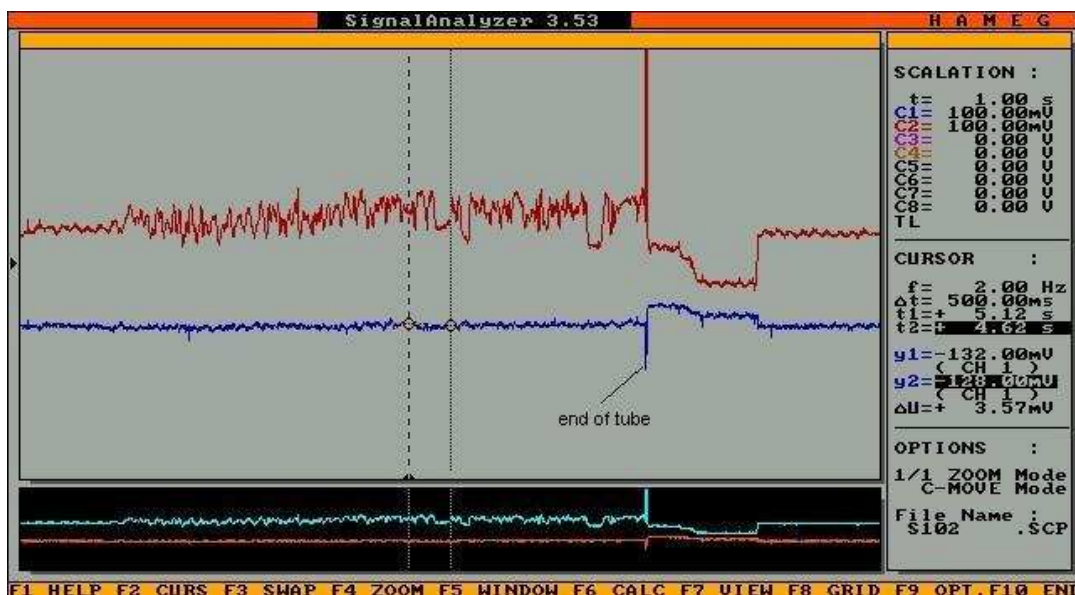


Fig4. Signal for the second region of sample S1.

## 6. SAMPLE 2 EXAMINATION

The parameters of the control were kept. Because the signal due to defect on sample S2 has amplitude smaller, the representation scale was increased so that the signal should be clearly visible.

In Figure 5 is presented the examination result for the region 100mm-700mm. In this region weren't discontinuities.

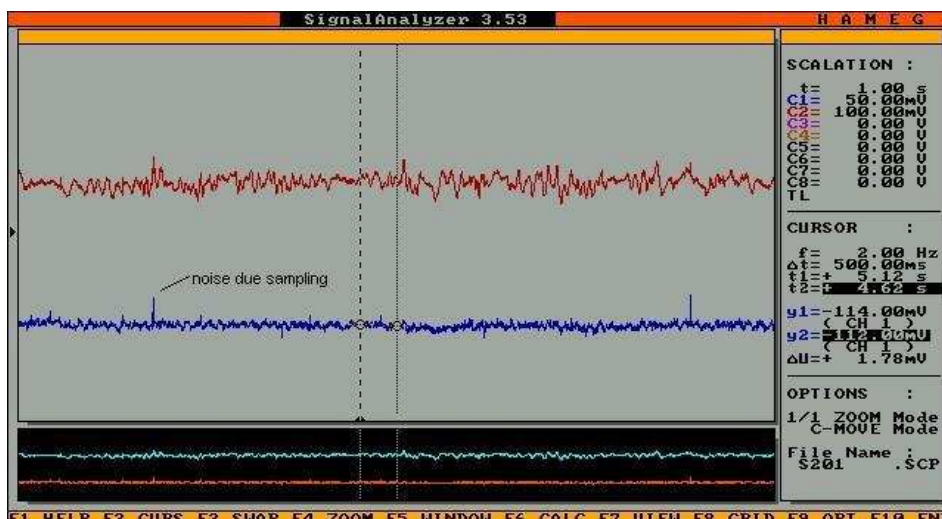


Fig 5. Signal for the first region of sample S2.

In Figure 6 is presented the results for the region 700mm-1491mm.

The existence of a defect localized between the blue markers at 1093mm-1125mm it is observed.

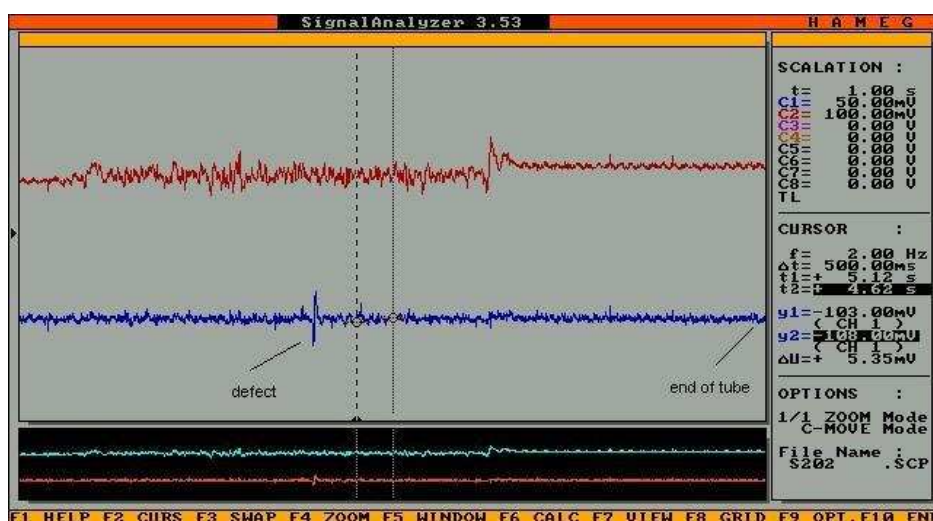


Fig6. Signal for the second region of sample S2.

10 displacements were made, with the tube rotated with randomly angle. The results are presented in Table 2.

Table 2. The results of sample S2 control.

No.crt.	Signal amplitude [mVpp]	Noise amplitude [mVpp]	Signal to noise ratio
1	67.7	4	16.925
2	62.1	4	15.525
3	67.9	5	13.58
4	60.7	6	10.116
5	63.8	4	15.95
6	60.7	4	15.175
7	60	5	12
8	55.2	6	9.2
9	54.8	4	13.7
10	69.1	6	11.516

Below, the statistic data analysis for the results from Table 2 is presented:

- Average of signal's amplitude [mVpp]: 62.2
  - Standard deviation of signal's amplitude [mVpp]: 4.75
  - Average amplitude of noise amplitude [mVpp]: 4.8
  - Standard deviation of noise's amplitude [mVpp] 0.87
  - Signal to noise ratio: 13.37
- Standard deviation of signal to noise ratio: 2.6

## 7. CONCLUSION

The sample S1 present one defect localized in the region 610mm -640mm (exactly between the two blue markers on the tube). The defect was emphasized with  $21.18 \pm 6.09$  signal to noise ratio. The eddy current control standards (example being those for nuclear power plants – ASME code, Sect. V, Art.8 +App. I and App. II) shown that defects that presents signal to noise ratio  $\geq 3$  can be emphasized. Due to high value of signal to noise ratio (in most unfavourable case being 14), we consider that the defect on sample S1 is clearly visible.

The sample S2 presents a defect localized in the region 1093mm-1125mm (in the region between the blue markers). The defect was emphasized with  $13.37 \pm 2.6$  signal to noise ratio, higher that those imposed by standards. The high value of signal to noise ratio (in most unfavourable case being 9.2) we consider the defect on sample S2 is clearly visible.

## Acknowledgements

This paper was partially support by Romanian Ministry of Education and Research, under CNCSIS Grant No. 982/2004.

Received April 28, 2005

\* Nat. Inst. of Research and Development for Technical Physics Iasi

\*\* University "Al.I.Cuza" Iasi

## REFERENCES

- /1/. R. Grimberg, D.Premel, E.Radu, A.Savin, *Calculation of the Electromagnetic Field Created by an Arbitrary Current Source in the Presence of a Conducting Cylinder with Material Discontinuities*, Studies in Applied Electromagnetics and Mechanics 18 Non-Linear Electromagnetic System, Paolo Di Barba and Antonio Savini(Eds) IOS Press,( 2000), 153-156
- /2/. MG Silk, AM Stonenham, JA Temple, *The reliability of nondestructive inspection*, Adam Hilger Eds., 1987
- /3/. R. Grimberg, D. Premel, A. Savin, R. Steigmann, D.D.Sandu, D.Placko, *Eddy current detection of long subsurface discontinuities*, *Systemes et microsystemes pour la caracterisation*, C2I 2001, vol.2, Hermes Science, p.279-286
- /4/. Jack Blitz, *Electrical and Magnetic Methods of Nondestructive Testing*, Adam Hilger Eds NY , 1991, ISBN 0 7503 0148 1
- /5/. \* \* \* , *Fundamentals of industrial control Practical Guides for measurement and control* Instrument society of America, CL Albert, DA Coggan Eds, 1996

## EVALUAREA ELECTROMAGNETICA A MATERIALELOR NANOSTRUCTURATE SI A UNOR REPERE MEMS

**Rezumat:** Aceasta lucrare prezinta metoda de evaluare nedistructiva a defectelor in nanotuburi realizate din otel inoxidabil 304. Nanotuburile sunt realizate in scop medical, de aceea ele trebuiesc testate inainte de utilizare. Probabilitatea de detectie a fost 98% pentru un coeficient de incredere de 98%.

## ASSESSMENT OF THE BIOCOMPATIBILITY OF DIFFERENT ALLOYS IN VITRO CELL CULTURE

BY

EMIL IACOB\*, IOAN RUSU\*\*, OANA DRUG\*\*\*, LUMINITA MINEA\*\*\*

**Abstract.** *Advanced technological development have resulted in rapid progress towards human prothesis. The compatibility of various materials with human tissues is a very important parameter to relation between organism-prothesis to prevent rejection and other undesirable problems. We study the biocompatibility of different alloys including Ni-Ti, and the effect of surface treatments on attachment and growth of epithelial cells.*  
**Keywords:** *Ni-Ti shape memory alloys; biocompatibility; nickel alloys; titanium alloys cell adhesion; surface treatments; epithelium*

### 1. INTRODUCTION

The biocompatibility of metallic alloys is critical to the success of many orthopedic therapies. Corrosion resistance and the immune response of the body to wear debris products ultimately determine the performance of these devices. The establishment of quantitative tests of biocompatibility is an important issue for biomaterials development.

### 2. MATERIALS AND METHODS

The biocompatibility of nickel-titanium alloys was investigated by single-culture experiments on functionally graded samples with a stepwise change in composition from pure nickel to pure titanium, including an Ni-Ti shape memory alloy for a 50:50 mixture. This approach permitted a considerable decrease of experimental resources by simultaneously studying a full variation of composition. The results indicate a good biocompatibility for a nickel content up to about 50%. The cells used in the biocompatibility studies comprised osteoblast-like osteosarcoma cells (SAOS-2, MG-63), kidney monkey cells (BSC-01), and murine fibroblasts (3T3).

To study the effect of surface treatments on attachment and growth of epithelial cells, rat palatal epithelial cells were cultured on various implant materials. The implant surfaces were treated by different procedures. The possible influence of these treatments on the attachment percentage and growth rate of the cells, and the effect of these surfaces on monolayer formation and barrier integrity was studied.

The results of the experiments demonstrate no significant relation between surface treatment and the behaviour of rat palatal epithelial cells cultured on the various kinds of substrates relevant for implants.

Tests have been made using samples from each material, samples that were put into direct contact with the cell culture for a week in special sterility conditions. There

have been used witnesses for sterility cellular viability and toxicity. The cellular line has been tested previously testing the stability, the multiplying potential and the dynamics of the development in the early and belated stages of evolution. The used methodology comprised: a direct microscopic examination and in phasic contrast on samples fixed and Giemsa colored; the cells counting, the determination of mitotic index of the cellular density on the surface support.

Also there have been made checkings on the presence of bacteria contaminants, fungi, and viruses both inside the culture itself and inside the solutions, media and ingredients.

Received May 4, 2005

\*University of Medicine and Pharmacy "Gr.T.Popa" Iasi

\*\*Technical University "Gh. Asachi" Iasi

\*\*\*Institute of Public Health Iasi,

#### REFERENCES

- /1/. C.Voiculescu – Cultura celulara in diagnosticul virozelor umane; Ed. Medicala; Bucuresti 1976
- /2/. E.Iacob, C.Durnea – Experienta laboratorului de virusologie al I.S.P. Iasi in domeniul culturilor celulare; A XXXII a Ses. St. Anuala a ISP Iasi, 7-8 mai 1998.
- /3/. Paul J. – Cell and Tissue Culture; E&S Livingstone Ltd. Edinburgh, London, 1970.
- /4/. Rubin H. – Growth Control in Cell Cultures – CIBA Foundation, London, 1971
- /5/. O.Zavate, N. Cajal – Enterovirusuri nepoliomielitice – Ed. Academiei Romane; Bucuresti, 1983
- /6/. J. P. C. M. van der Waerden and K. de Groot – Biomaterials vol.10 1989
- /7/. A Quaroni, J Wands, RL Trelstad and KJ Isselbacher – The Journal of Cell Biology vol. 80. 1079.
- /8/. Xing-He Weng, Klaus W. Beyenbach, and Andrea Quaroni - *Am J Physiol Gastrointest Liver Physiol* 288: G705-G717, 2005.

#### EVALUAREA BIOCOMPATIBILITĂȚII UNOR ALIAJE ÎN CULTURI CELULARE IN VITRO

**Rezumat:** A fost studiată biocompatibilitatea unor aliaje metalice continind diverse procente de nichel si titan pe diverse tipuri de culturi celulare. S-a constatat, ca si in alte studii anterioare, ca exista o buna biocompatibilitate, pina la un continut de nichel de 50% in aliajele cercetate.

## ASPECTS REGARDING THE SPECIFIC WEAR FORMS AT INDUSTRIAL TAPS

BY

L. ISTRATE, D. CIOBANU, I. ALEXANDRU, B. CIOBANU, A. ALEXANDRU

**Abstract.** *Elimination or control of wear, either cavitation erosion or cavitation abrasion or hidroabrasion wear, presents a great importance in work of machines elements, in direct contact with mobile fluids, like as the industrial taps. This phenomenon can produce serial specific effects that can modify fundamentally the characteristics of machines and installations in that the liquid is used as work agent. Apparition, development and cavitation effects in some constructive kinds by industrial taps present a real importance. In this direction are presented some aspects regarding the specific wear forms at industrial taps with application in cavitation erosion [2].*

**Keywords:** *erosion, cavitation, taps*

### 1. INTRODUCTION

Control device or closing device used in hydropower engineering, hydrotechnics constructions and, in general, in hydromechanics are improper named taps [1]. In fact they are grouped in the following categories: *valves*, which are inserted inside of networks and pipelines, at pressure intake ports, bottom discharges and so on; *gates*, which are installed at barrages, at discharge ports, water chamber with free level and so on; taps, which attend the installations of those technological processes impose hard work conditions regarding to pressure, temperature, hydromechanical stresses and montage technology [1].

The erosion process is present in all these elements above mentioned. Special importances present the valves and taps, because only in their case appear exceptional regimes to atypical work due to the prominent roles played by these organs inside of installation wherein they are set. The valves and taps rarely are completely closed or opened. They find in intermediate work positions. In function with require purpose these positions are changed by user. Thus appear different work situations, which are impossible to determine from designing stage.

Through definition the erosion represent a progressive losing of material as result of mechanical interaction between material surfaces and a fluid, a fluid mixture or with particles contained by a fluid.

In development of erosion process are distinguish three phases:

- *initial periods*, wherein the erosion are produced quickly till when are attained a certain equilibrium state;
- *normal periods of operation*, wherein the erosion is slow, near uniform, in limits which provide the respecting of conditions imposed;
- *critical periods*, wherein the erosion is very quickly and the pieces are in danger.

In the case of metallic materials the main forms of erosion are: uniform erosion, punctiform erosion, erosion with crevasse generation, corrosion-erosion and erosion through cavitation.

The cavitation are produced when the work pressure of fluid diminish under vapor pressure generated the bubble development, collapse of those with formation of microjets, which have a brutal impact with the surface of metallic material and even the destruction of those [6].

The spectacular effect of cavitation is that of the solid materials destruction. This phenomenon have been observed first time to the propelling screw, after that at hydraulic turbine, pumps, taps, valves and so forth.

## 2. EVALUATION CRITERIA OF MATERIAL RESISTANCE AT CAVITATION

The material resistance at cavitation is, in general, known and their capacity to absorption of energy in cavitational process for the breaking of a given volume. The evaluation and choosing of material corresponding with their resistance at cavitation are based on the follow criteria to comparison [5]:

- the curves of volume or gravimetric losses relative to time,  $\Delta V = f(t)$  or  $\Delta G = f(t)$ , respective the middle depth penetration  $MDP = f(t)$ ;
- the curves which indicate the cavitational erosion rate relative to time:

$$\frac{\Delta(\Delta V)}{\Delta t} = f(t) \quad \text{or} \quad \frac{\Delta(\Delta G)}{\Delta t} = f(t) \quad \text{and} \quad MDPR = f(t);$$

- the derivate parameters from characteristic erosion curves like as the incubation periods, time necessary for obtaining of given volume or gravimetric losses, respective of certain medium depth penetration, the maximum erosion speed, the speed of cavitational erosion corresponding to stationary domain.

Neither one from these criteria, definite by a singular parameter, have not been accepted in unanimous mode for the arranged of materials under the aspect of the resistance at cavitation. At the classification of this problem have contributed, in great measure, the results of ASTM Round Robin Test rapport [4], which present the curves of volume and gravimetric losses relative to time, respective the cavitational parameters obtained in 12 laboratories from USA, France and England for three materials. The experimental materials have been 6061-T 6511 aluminum, 319 stainless steel and commercial pure nickel [4]. From the ASTM Round Robin Test rapport and another comparative analysis result a great diversity of  $\Delta V$  and  $\Delta G$  parameters, for that not exist yet an accord between divers specialists and beneficiaries regarding to the operation with a certain parameter or some criteria of cavitational erosion.

## 3. THE ROLE OF CAVITATION IN EROSION PROCESS OF SOME KINDS BY INDUSTRIAL TAPS

In the case of taps, the erosion phenomenon of material from which is they realized it's much less complicated [2]. The more important factors that lead at the initiation and development of erosion are the following:

- *The fluid which cross the tap.* This can be gaseous or liquid. In the case of liquids, the erosion depends in great measure by pH, liquid viscosity (if this contain solid particle in suspension or not) and superficial tension.

- *The using mode of tap.* If this is used dynamically (with frequently closed and opened) or statically (with maintained in certain positions for obtaining of given or imposed fluxes).

- *The tap geometry.* This represents a very important factor, sometimes decisively. From the designing stage, in general, can be avoided the apparition of walls, curvatures or cavities which can create the premises of development of the cavitation phenomenon [4].

The process of cavitation erosion, fig. 1 [5]: tap geometry→work conditions→ cavitation apparition→cavitation development→apparition of cavitation streams→ interaction fluid/solid→isolate impacts→incubation period→material losses.

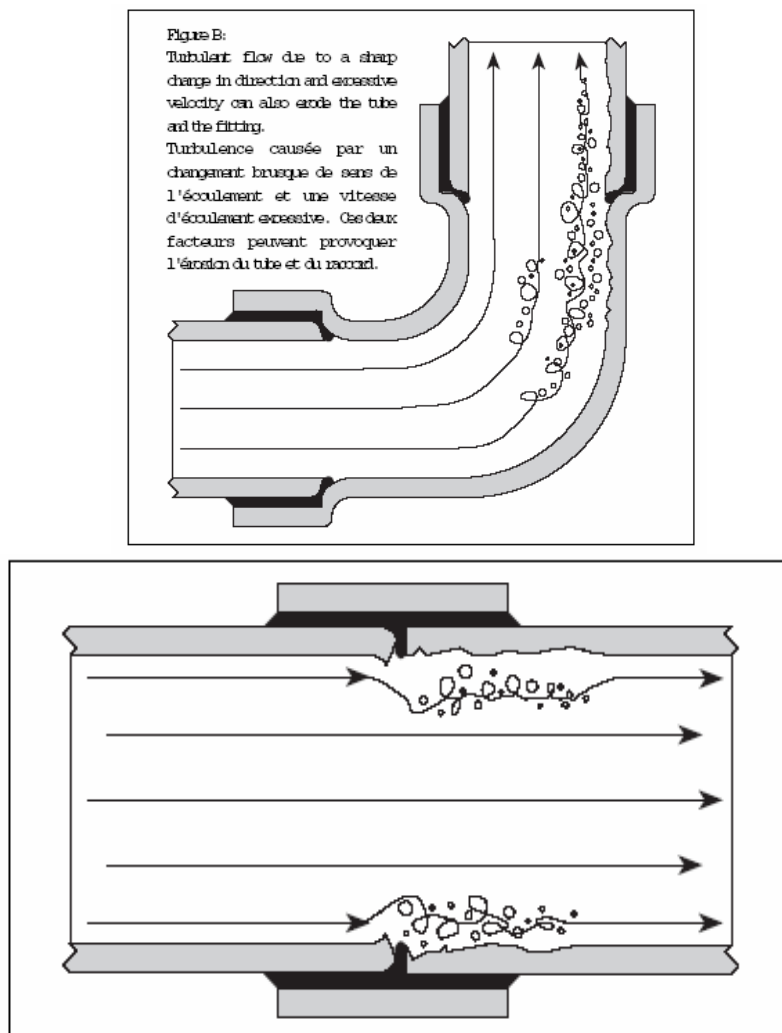


Fig. 1. The erosion process through cavitation.

Anton I. [2] has study the evolution of erosion process through cavitation, time by 40 hours, of a conical screw-down valve used in hydraulic systems for flow regulation or pressure control, fig. 2.

The destruction by cavitation of conical valve, after a certain function time, can be observed through the presence of characteristic pinches. These pinches which appear on the valve surface, attaining after a operation by 40 hours at a maximum diameter by 4 mm, show that the collapse of cavitation bubbles have take place in downstream to contraction section of current vein.

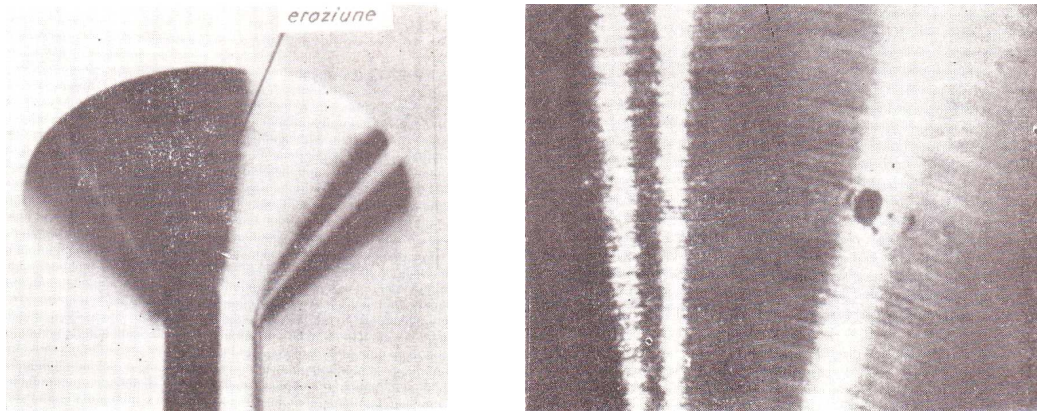


Fig. 2 Cavitation erosion on a conical valve.

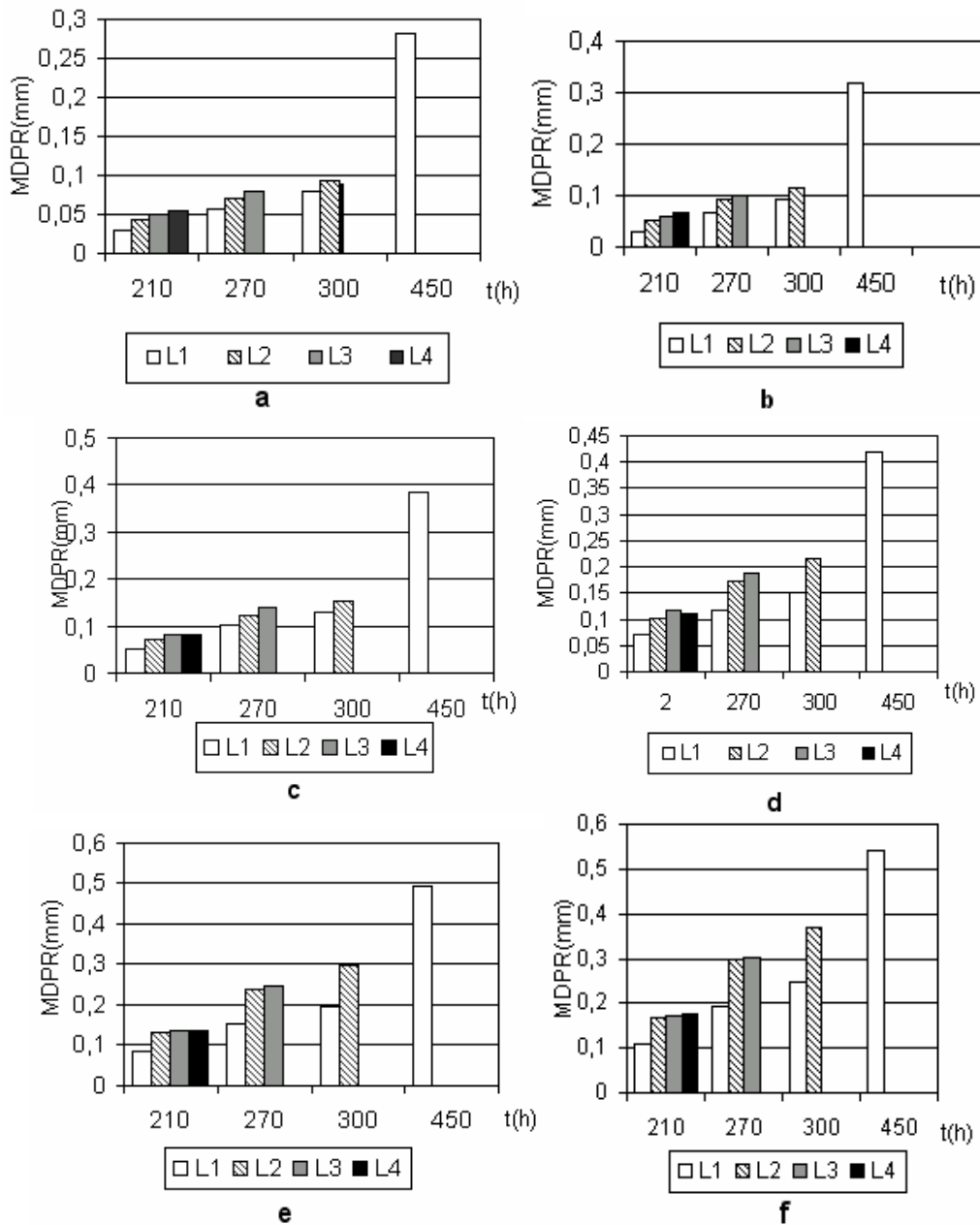


Fig. 3. The variation diagrams of medium depth penetration relative to time of tested samples: a) E1 (Ra = 16 μm); b) E2 (Ra = 20 μm); c) E3 (Ra = 25 μm); d) E4 (Ra = 32 μm); e) E5 (Ra = 67 μm); f) E6 (Ra = 104 μm).

These investigations regarding the cavitation erosion, which have led only to the conclusion that construction of conical valves must use special steels, are not completed and therefore require the carrying on the research.

An investigation of the influence of microgeometry parameters of contact surfaces over the cavitation – abrasive erosion have also been effected by Ciobanu [3], using an experimental installation formed by a turning disc, a fluid jet with or without abrasive material and samples from OLC45, the metallic surfaces having the different roughness. Used the experimental data contained in [3] have obtained the graphic representation of MDPR relative to time, fig. 3 a – f.

From these graphics can be observed the increasing of MDPR (accentuation of wear process) simultaneous with the reduction of the distance between the nozzle of injector and the surface of sample ( $L_1 = 80$  mm,  $\mu = 0$ ;  $L_2 = 60$  mm,  $\mu = 0$ ;  $L_3 = 40$  mm,  $\mu = 0$ ;  $L_4 = 40$  mm,  $\mu = 3$  kg/m<sup>3</sup>), respectively the catalytic role of the cavitation wear process, which have it the solid particle found in suspension in experimental liquid media ( $\mu = 3$  kg/m<sup>3</sup>).

#### 4. CONCLUSIONS

With all that in this domain exists a vast informative material both from the operation of hydraulic machines and regulating elements of those (valves, taps, regulators and so forth) and from research effected, are not formed an accord on the mechanism of cavitation destruction.

The process of cavitation destruction is dominant in the case of regulating elements and this is very complex, because involves two basic and distinct aspects, but which reciprocal interfere. The one depends by hydrodynamical character, specific to cavitation phenomenon, and another regard the physico-mechanical character, specific to the loading and destruction of solid material through fatigue.

The cavitation destruction observed in exploitation of hydraulic machines and of regulating elements of those is considered to be the result of actions of many mechanisms that coexist during the cavitation process. This aspect makes difficult much more the problem of cavitation destruction.

Additional data which can confirm or negate the relative existing theories of cavitation destruction of industrial taps have a great importance.

*Received April 26, 2005*

*Technical University "Gh.Asachi" Iasi*

#### REFERENCES

- /1/. Alexandru F. și Necula S., 1963, *Conducte și armături*, București, Editura Tehnică.
- /2/. Anton, I., 1984, *Cavitația*. Vol. I și II, București, Editura Academiei R.S.R.
- /3/. Ciobanu B., 2003, *Cercetări privind influența parametrilor microgeometriei suprafețelor active asupra performanțelor mașinilor hidraulice*. Teză de doctorat, Universitatea Tehnică Gh Asachi Iași.
- /4/. Hammit F.G. and Chao C., 1970, Round robin test with vibratory cavitation and liquid impact facilities of 6061-T6511 aluminum alloy, 316 Stainless steel and commercially pure nickel. ASTM, Material Research and Standards, vol. 10 (10).
- /5/. Lecoffre Y., 1998, A method evaluate cavitation erosion in valves. Third International Symposium on Cavitation, France.
- /6/. Șoltuz D. V., Neculăiaș V. and Țenu I., 2004, *Appearance forms of mechano-chemical wear at machines and installations from food industry*. Buletinul Institutului Politehnic Iași, Tomul L(LIV), Fascicola Vc, Secția Construcția de Mașini, 951-957.

### ASPECTE PRIVIND FORMELE DE UZURA SPECIFICE ROBINETILOR INDUSTRIALI

**Rezumat:** Eliminarea sau controlul fenomenelor de uzare, fie că este vorba de eroziune cavitațională, cavitațional-abrazivă, hidroabrazivă, prezintă o importanță majoră în funcționarea unor piese de mașini, în contact direct cu lichidele în mișcare, cum este și cazul robinetilor industriali, acest fenomen putând produce o serie de efecte specifice ce pot modifica esențial caracteristicile mașinilor și instalațiilor în care lichidul este folosit ca agent de lucru. Apariția, dezvoltarea și efectele cavitației în unele tipuri constructive de robineti industriali prezintă un real interes. În această direcție sunt prezentate unele aspecte privind formele de uzură specifice robinetilor industriali cu aplicație în eroziunea cavitațională.

## INFLUENCE OF CeO<sub>2</sub> ON THE ELECTROLESS DEPOSITION OF THE COPPER COATINGS

BY

CĂTĂLINA ITICESCU, GETA CÂRÂC, OLGA MITOSERIU

**Abstract.** *The study presents the influence of the CeO<sub>2</sub> particles as dispersed phase in the copper coatings. The coatings were obtained by electroless plating from copper sulphate electrolyte with formaldehyde as reducing agent. The CeO<sub>2</sub> particles of 1 μm were added in the electrolyte with a concentration between 5-50g/L.. Surface morphology and composition were studied by light and scanning electron microscopy (SEM) and EDAX analysis. The Vickers microhardness was measured on cross section. The results have shown that CeO<sub>2</sub> particles in solution or embedded in a small amount in the copper matrix have an influence on the structure and properties of the coatings. The coatings displayed changes in structure and mechanical properties (roughness, microhardness) in comparison with the pure copper coatings.*

**Keywords:** *copper, cerium oxide, electroless plating, structure, roughness, microhardness*

### 1. INTRODUCTION

Electroless plating is a chemical reduction process, which depends on the catalytic reduction of a metallic ion from an aqueous solution containing a reducing agent, without the use of electrical energy. During the past decades electroless plating has gained popularity due to its ability to produce coatings that possessed excellent corrosion, wear and abrasion resistance [1].

Among the variety of metals that can be plated using this method. Electroless deposition is a feasible and inexpensive method to obtain metal coatings. This technique has the advantage of low cost of tools and materials, low processing temperature, high quality material and high throughput of the process. Many parameters are involved in the electroless deposition process, including nature of electrolyte, pH, bath temperature, degree of agitation of the solutions, substrate and counter electrode geometry and material and presence of additives in the electrolyte (as shown in [2]).

Advantages of electroless plating include excellent uniformity, bulk processing capability and ability to produce unique catalytic coatings. The main disadvantages of electroless deposition are lower deposition rate and a larger amount of produced waste comparing to electroplating.

We have been successful in obtaining of copper coatings using a copper sulphate electrolyte and formaldehyde as reducing agent. By added of CeO<sub>2</sub> particles during electroless deposition of the copper, composite coatings with interesting properties can be produced. The properties of such coatings are dependent on the nature of the particles embedded.

## 2. EXPERIMENTAL PROCEDURES

The coatings of copper by electroless were obtained. The electrolyte was a copper sulphate with the following composition:  $\text{CuSO}_4 \cdot 5\text{H}_2\text{O}$ -30g/L;  $\text{Na}_2\text{CO}_3$  anh.-12g/L; Na and K tartrat -150g/L, NaOH-50g/L, EDTA - 6g/l [3]. Carbon steel as support was used. The formaldehyde (37%) was used as reducing agent and its amount was varied between 15-45 g/L HCHO. For avoided the surfaces passivity the electrolyte was refreshed at 60 each minutes. The optimal concentration of reducing agent was obtained. The pH of the electrolyte was raised to within the optimum range of 12 to 13.5. The codeposition experiments were performed in a larges glasses (1000 mL). Time of deposition was 300 minutes. The temperature of work was room temperature.

In the electrolyte were added particles of  $\text{CeO}_2$  as dispersed phase with a particles size of  $\sim 1\mu\text{m}$  and a concentration between 5 and 50 g/L. To keep the particles in suspension, the electrolyte was magnetically stirred at 500 rev/min. The modification of the electrolyte pH was not observed when added the particles.

Copper chemical deposits from electrolyte with and without particles in suspension were tested by optical microscopy on cross section. Surface morphology and composition were studied by scanning electron microscopy (SEM) with an X-ray analyzer (EDXS) from Leo Instruments. The Vickers microhardness was measured on the cross section of layers using a microhardness analyzer of Buehler (micromat 1). Additionally the surface roughness was measured applying a Hommel tester.

The results are compared with pure copper coatings to understand the effects of particles dispersed on the microstructure and roughness of composite coatings during the electroless crystallization.

## 3. RESULTS AND DISCUSSIONS

### 3.1. Structural aspects and composition

The better copper deposits were obtained using a copper sulphate electrolyte with 38,5 g/L  $\text{CH}_2\text{O}$ . When the concentration of reducing agent increases the rate of copper deposits is smaller, because the passivity phenomenon is faster. The  $\text{CH}_2\text{O}/\text{Cu}^{2+}$  ratio decreases for 15 g/L  $\text{CH}_2\text{O}$  in electrolyte. This may be caused by the formation of the Cu(I) complex which induce a passivity phenomenon. The reduction of copper takes place in the first part of the process:  $\text{Cu}^{2+} + 1\text{e}^- \rightarrow \text{Cu}^+$ . The rate of copper deposition increases with the number increase of the reductible ions in solution and the content of the formaldehyde [4].

There were obtained thin layers of the copper deposition with a thickness between 3-20  $\mu\text{m}$ . The aspect of layers is not completely uniform and this fact can be explained by destruction of metallic support during the preparation of samples for optical analyses. Samples were tested also by electronic microscopy (SEM) (Fig.1).

The presence of  $\text{CeO}_2$  particles affects the mechanism of the copper reduction by electroless plating [5]. The particles of dispersed phases were embedded in the copper deposits in a very small amount. The results of the investigations confirm that  $\text{CeO}_2$  was embedded into copper matrix by electroless plating. The EDXS analysis in point of  $\text{CeO}_2$  also indicated the presence of copper (Table 1, Fig. 2).

From experimental date it observed that the growth amount of  $\text{CeO}_2$  in deposit with the amount of oxide in the electroless solution (Fig.3).

### 3.2. Characteristics properties

#### 3.2.1. Microhardness

The Vickers microhardness ( $HV_{0.025}$ ) of coatings in the copper matrix was studied. The presence of dispersed phases in the electrolyte and coatings modifies the microhardness of layers and this fact can be correlated with the amount of dispersed phase in the deposit. Figure 3 shows the results obtained for the copper coatings with  $CeO_2$  particles in electrolyte. The amount of  $CeO_2$  in the electrolyte influences the microhardness of the coatings [6].

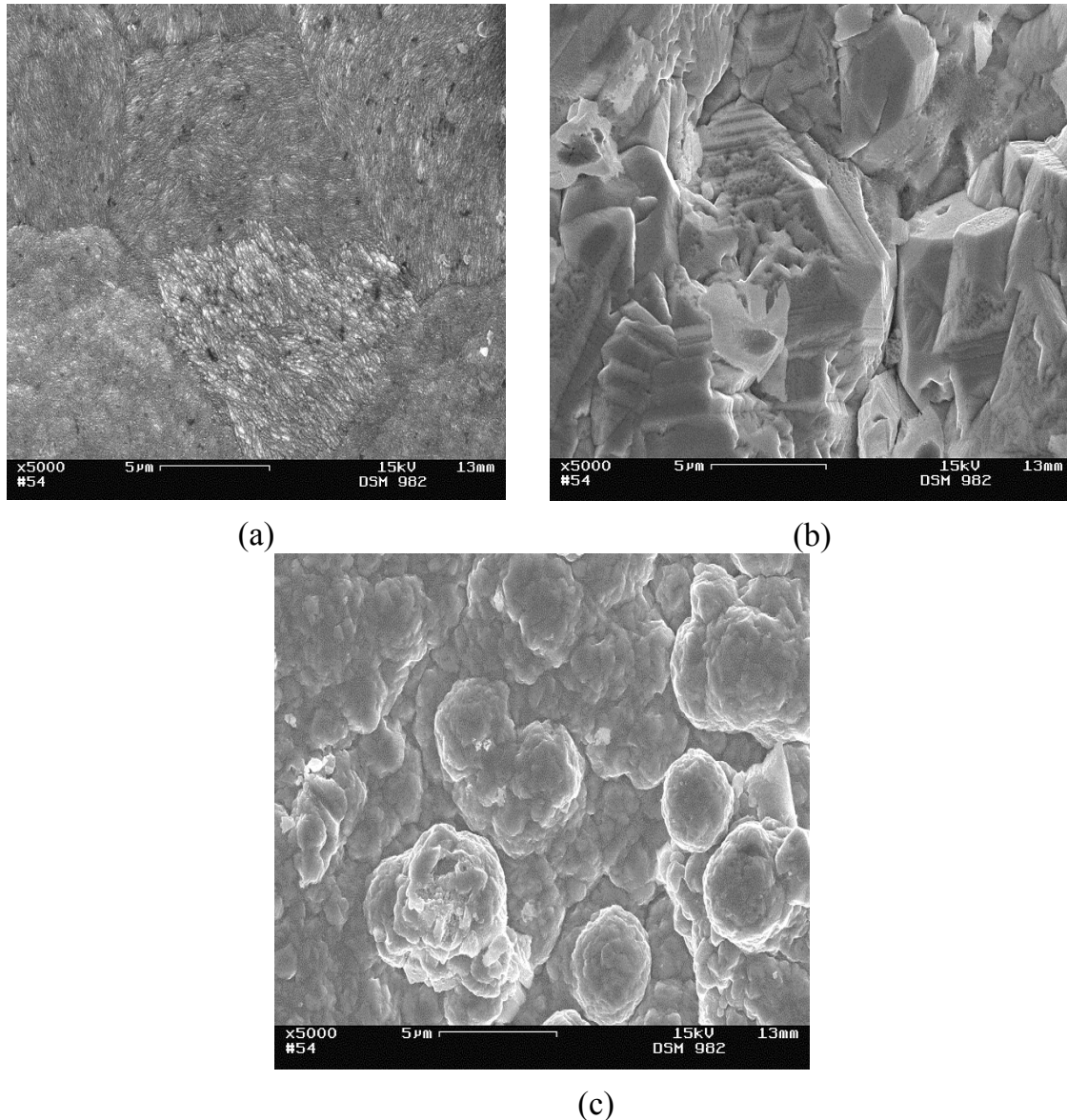


Fig.1. SEM micrographs of Cu- $CeO_2$  coatings  
a) pure Cu; b) 10g/L  $CeO_2$  in electrolyte ; c) 50g/L  $CeO_2$  in electrolyte

Table 1. EDXS analysis for the Cu- $CeO_2$  coatings:

1) Electrolyte with 5g/L  $CeO_2$ :

Element	Atom-%	Weight-%	Error(±)	Norm%
Cu	41.92	9.73	1.09	43.19
Ce	20.74	10.61	0.64	47.12
O	37.34	2.18	0.16	9.69
Total:	100.0	22.52		100.00

2) Electrolyte with 10g/L CeO<sub>2</sub>:

Element	Atom-%	Weight-%	Error(±)	Norm%
Cu	9.41	2.67	0.69	10.26
Ce	30.48	19.05	0.76	73.25
O	60.10	4.29	16.49	
Total	100.00	26.00		100.00

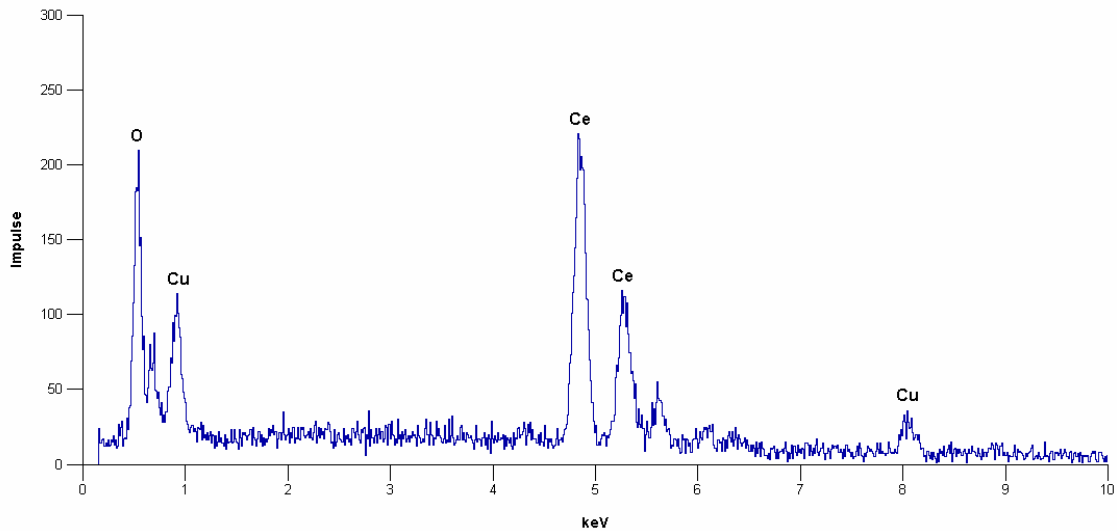


Fig.2. EDXS analysis on CeO<sub>2</sub> particles embedded in the copper matrix

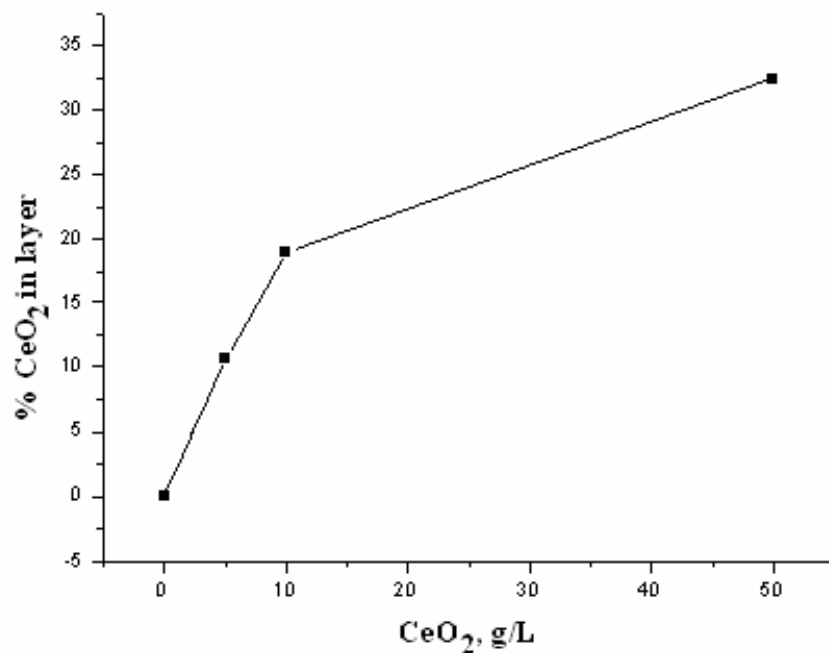


Fig.3. Influence of CeO<sub>2</sub> amount in electrolyte and layer

The microhardness of the coatings obtained with 5g/L and 10 g/L CeO<sub>2</sub> in electrolyte has increased smaller in comparison with that of the copper deposits without particles in the electrolyte. A decreasing in the microhardness of the layers obtained with 50 g/L CeO<sub>2</sub> in the electrolyte was observed. The dispersed phase content in a larger amount of electrolyte modifies the metal electroless deposition process (Fig.4).

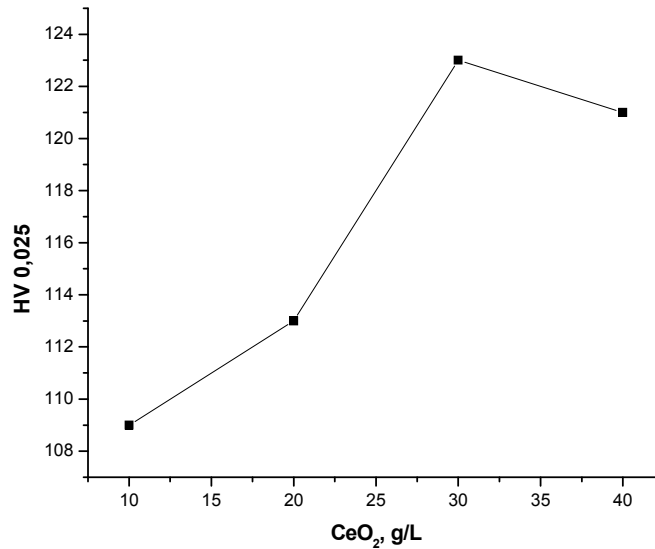


Fig.4. Microhardness variation of copper coatings with CeO<sub>2</sub> particles in electrolyte

### 3.2.2. Surface roughness

The roughness of samples obtained from electrolytes with and without particles was tested (Table 2). The roughness of composite coatings Cu/CeO<sub>2</sub> is smaller than of pure copper layers. The presence of CeO<sub>2</sub> in electrolyte by deposition got a growth a nucleation center. This phenomenon changes of layers structures through dimensions crystals diminution and the surfaces roughness.

Table 2. Roughness of copper layers with and without CeO<sub>2</sub> in electrolyte

CeO <sub>2</sub> g/L	R <sub>a</sub> , (μm)	R <sub>z</sub> , (μm)	R <sub>z max</sub> , (μm)	R <sub>z min</sub> , (μm)	S <sub>Rz</sub>
-	2,26	18,76	20,32	16,12	1,60
5	1,47	11,95	14,27	9,71	1,65
10	1,53	11,88	13,89	10,31	0,95

## 4. CONCLUSIONS

1. The experiments were performed to study the obtaining of copper coatings with and without CeO<sub>2</sub> from a copper sulphate electrolyte with formaldehyde as reducing agent.
2. The dispersed phase of CeO<sub>2</sub> was included in copper layers in very small amount.
3. The structure and the roughness of coatings obtained presented differences and this fact depended on the amount of CeO<sub>2</sub> in electrolyte.
4. It was observed decreases of layers roughness and an improving of microhardness compared with pure copper layers.

## REFERENCES

- /1/. E. J. O. Sullivan, *Fundamental and Practical Aspects of the Electroless Deposition Reaction, Advances in Electrochemical Science and Engineering*, vol.3, 1994, p.225-270.
- /2/. M. Paunovic, *Electroless Deposition of Copper*, Modern Electroplating, Fourth Edition, New York, 2000, p.127-235
- /3/. O. Mitoseriu, C. Iticescu, A. Preda, *Comparative Studies Concerning the Chemically and Electrochemically Obtaining of Cu-P Composite Coatings* The 10<sup>th</sup> Conference "Realization and Development in Metallurgy and the Science Materials", Galati, Romania, 3-5 October 2000. Published in vol. „Realizări și perspective în metalurgie și știința materialelor”, 2001, 85-92.
- /4/. C. Iticescu, G. Cârâc, O. Mitoseriu, *The Optimization of Parameters in Copper Coatings Obtained by Electroless Plating*, The 11<sup>th</sup> Conference on Physical Chemistry, Timișoara, Romania, 3-5 September, 2003, Annals of West University of Timisoara, Series Chemistry, vol.12, no.3, 2003, 569-575
- /5/. O. Mitoseriu, A. Preda, L. Mitoseriu, C. Iticescu, *Chemically Obtained Copper Matrix Composite Coatings*, Buletinul I.P. din Iasi, published by Technical Univ. "Gh. Asachi" Iasi, Tom XLVIII (LII), Fasc. 3-4, 2002, p.49-58
- /6/. C. Iticescu, O. Mitoseriu, G. Cârâc, *Preparation and Investigation of Cu-CeO<sub>2</sub> Composite Coatings*, The Annals of „Dunarea de Jos” University of Galati, fascicle IX, Metalurgy and Materials Science, no.1, 2003, p. 5-10

**INFLUENȚA PARTICULELOR DE OXID DE CERIU IN DEPUNERILE DE CUPRU OBTINUTE PRIN METODA CHIMICĂ**

**Rezumat:** Lucrarea prezintă studiul referitor la obținerea pe cale chimică a unor acoperiri de cupru. S-au folosit electroliți bazici de sulfat de cupru, iar reducătorul folosit a fost aldehida formică. În electroliți s-au introdus particule de CeO<sub>2</sub> cu dimensiuni micrometrice. Cantitatea de fază dispersă introdusă în electrolit a variat între 1-50 g/L. Particulele au fost menținute în soluție prin agitare mecanică (500 rotații/minut). S-au efectuat studii pentru a determina compoziția straturilor și structura acestora, prin teste de MO, SEM și EDXS. Particulele de oxid de ceriu s-au inclus în cantitate mică în matricea de cupru, dar suficientă pentru a modifica proprietățile acoperirilor obținute. S-au constatat modificări structurale și ale proprietăților. De asemenea, rugozitatea straturilor compozite Cu/CeO<sub>2</sub> scade mult comparativ cu acoperirile de cupru metalic. Cu creșterea cantității de CeO<sub>2</sub> incluse se remarcă o ușoară creștere a rugozității, dar nu va depăși, în nici un caz, valoarea determinată pentru stratul de cupru metalic obținut în aceleași condiții de lucru. Microdurețea acestor acoperiri este mai mare decât a cuprului metalic, însă ea scade cu creșterea cantității de oxid inclusă.

## TIG WELDING POOL CIRCUMSTANCES

BY

LAURENTIU DAN GHENGHEA, GABRIELA CIOBANU, BEIU BOGDAN

**Abstract.** *The work is focussed on specific conditions of TIG (Tungsten Inert Gas) welding pool formation, dealing with thermal field, movements in liquid pool formed by base and filler materials, pressure of particles that exist in electric arc over the liquid pool. Researchers contribution that studied TIG welding pool circumstances will be underlined and intended phases of a new research programm developed at Iasi Technical University will be put in specialists attention*

**Keywords:** *technological, parameters, characterisitcs, welded pool, thermal field*

### 1. TIG WELDING METHOD

Gas tungsten arc welding (GTAW, figure 1) uses a nonconsumable tungsten electrode (4) for one pole of electric arc (6) which is shielded with an inert gas (5). The arc fuses the base material (1) as well as filler material (3). The inert gas protects the electrode, the weld pool and has a contribution to required arc characteristics. The process could be done with a welding source (8) working cc<sup>-</sup> (direct polarity) or ac (alternative current). The last is used especially for welding aluminium, magnesium, their alloys and some types of stainless steels.

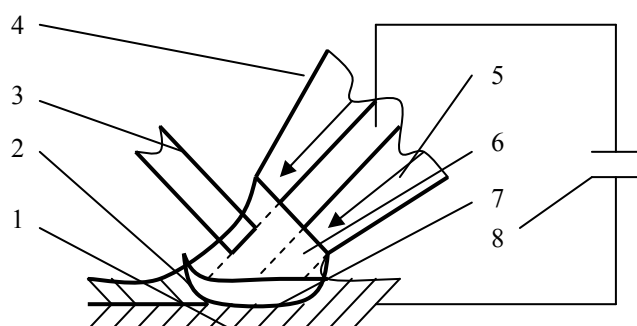


Figure 1 TIG welding method procedure:  
1 – base material; 2 – crystallised alloy; 3 – filler material; 4 – TIG pencil; 5 – inert gas; 6 – electric arc; 7 – melted alloy; 8 – welding source.

CC<sup>-</sup> (direct polarity) current, electrode negative, is preferred for welding most other materials, for automatic thick aluminium and thin magnesium welding. AC current is used with argon shielded gas and produces a cleaning action at base material surface in the half-positive part of electrode when contaminants are removed. A weld deposit without porosities is made in aluminium base materials welds in horizontal and overhead welding positions. Using cc current, helium inert gas could be used, the results are deeper arc penetration for welding pool but a preheating process is asked. Mixture gases could be used to get benefits of both gases. Most used for GTAW welding is argon 99,996% type A or 99,99% type B. Welding sources for GTAW (TIG) method need to have a constant current diagram (vertical volt-current

characteristic), a frequency oscillator is part of its, dealing with initiation of electric arc to eliminate touching of base material and tungsten electrode contaminations and possibilities to provide pulsating direct current at high or low frequency that offer conditions for penetration or weld deposit solidification control.

Electrode nonconsumable, with melting temperature around 3410 °C, is normally ground to a point or truncated in cone configuration. Could be in pure tungsten, but has poor electron emission features used when welding aluminium and magnesium. Most used electrodes are cover with thorium (1 – 2%) or zirconium (0,3 – 0,5%) assuring better electron emissions and a good versatility of TIG process, current density on electrode section has great values. To achieve welding deposit laterally, manual or automatically, a filler material, wire shaped, is introduced. The weld deposit could be made without filler material too, at edge or bended edge root in base materials. Parameters of welding technology for GTAW process are presented in table 1 and 2.

Table 1 Tungsten electrodes diameter for TIG process

Base material thickness [mm]	0 – 2	2 – 5	5 - 8	8 - 12	>12
Tungsten electrode diameter [mm]	2	3	4	4 - 5	5 - 6

Table 2 Welding current in GTAW welding process

Electrode diameter [mm]	CC		AC			
	Thoriated electrode		Series capacitors		Without capacitors	
	cc <sup>-</sup>	cc <sup>+</sup>	Pure W	Thoriated W	Pure W	Thoriated W
1	25 – 70	-	-	30 – 50	15 – 20	15 – 80
1,6	60 – 150	10 – 20	30 – 70	50 – 90	40 – 110	70 – 160
2,4	130 – 230	12 – 15	50 – 110	80 – 150	100 – 160	140 – 235
3,2	220 – 310	20 – 40	100 – 170	140 – 190	150 – 210	225 – 325
4	300 – 360	40 – 55	160 – 200	180 – 250	200 – 275	300 – 400
5	350 – 520	60 – 80	180 – 300	300 – 360	275 – 375	420 – 520
6,4	500 – 800	70 – 100	260 – 380	350 – 400	325 – 450	500- 630

Arc electric tension  $U_a$  could be calculate using (1):  $U_a = 10 + 0,04I_s$  [V] Values are under the value of 44 V.

The GTAW (TIG, 141) process allows welding of all types of grooves, joint geometries and positions in plate, sheet, pipe, tube and other shapes. It is particularly appropriate for welding base materials 1,6 to 10 mm thickness, for welding pipe with 25 to 150 mm diameter. The combination of GTAW for root pass welding with either SMAW (shielded metal arc welding, 111) or GMAW (gas metal arc welding 135,136) gives advantages for welding pipe because give a sure root welding and economic efficiency for next welding passes. Parameters for GTAW process used to weld plates are presented in table 3. This welding method could be used for different metallic materials joining and if we use numbers to appreciate welding assemblies characteristics, results are presented in table 4. Numbers represent 1 – very good welding characteristics; 2 –welding assembly not possible; 3 – welding assembly is possible but with some difficulties and is better to look for other method to manufacture proposed joint, table 4. For technologist welding engineer data presented in these tables are very important because give him all needed informations to design an welding technology that will be a guarantee for the best results of welded joint made in different materials using GTAW procedure.

Table 3 GTAW parameters for plates joining

Plate thickness [mm]	Tungsten electrode diameter [mm]	Filler material diameter [mm]	Welding current $I_s$ [A]	Inert gas consumption [l/min]	Welding speed [m/h]
1	1	1,6	40 – 160	2 – 3	18 – 21
1,5	1,6	1,6	60 – 100	2,5 – 3,5	18
2	1,6	2	70 – 120	3 – 4	16 – 18
3	1,6 – 2	2 – 3	90 – 140	3 – 4	15 – 18
5	3,15	3 – 4	130 – 170	3,5 – 4,5	12 – 15
7	3,15 – 4	4 – 5	150 – 260	4,5 – 5,5	9 – 13

Table 4 Possibilities for GTAW process at different materials

Metallic materials	CC		AC
	CC <sup>+</sup>	CC <sup>-</sup>	
Aluminium and its alloys	2	3	1
Magnesium and its alloys	2	3	1
Bronse with aluminium	2	3	1
Stainless steel under 0,7 mm	2	1	1
Low alloyed steel	2	1	2
Copper and its alloys	2	1	2
Nickel and its alloys	2	1	2

## 2. PARAMETERS OF GTAW WELDING POOL

The penetration in GTAW welding is attributed to arc force, this represents the inertia of a stream formed by metallic drops or the gas jet pressure impinging weld pool surface, also could be a combination of both phenomena. Penetration is the result of forming a cavity below the hemispheroidal weld pool. The force generating the cavity is the pressure of gas jet,  $p_G = \rho gh + 2\gamma R$  (1) where:  $p_G$  = jet gas pressure;  $\rho$  metal density;  $h$  = depth of penetration;  $\gamma$  = metal specific weight;  $R$  = radius of curvature at the root of penetration. Some results for axial force in GTAW welding are presented in table 5.

Table 5 Pressure on the weld pool in GTAW welding

Current [A]	Calculated axial velocity [m/s]	Axial pressure [N/m <sup>2</sup> ]			
		Calculated		Measured	
		Ar	He	Ar	He
200	200	800	116	820	240
300	450	4050		1800	
400	800	12800		2700	

Increasing current causes an increase in the arc force and the shape of weld pool is dependent on gas flow in the arc column. In low current GTAW welding the flow patterns in the welding pool could be observed and the molten pool has a hemispherical geometrical form. If we consider a distributed welding source that made a molten pool with 2,5 mm radius at an welding current of 100 A, the surface flow velocity is around 0,05 m/s (Atthey 1978). The weld pool shape is influencing by the circulation and has a toroidal form moving in opposite direction to that generated by electromagnetic forces. In GTAW automatic welding when parameters are constant

variations in depth of penetration occur. This is caused by base materials compositions and some researches (Bennet, Mills 1974; Metcalfe, Quigley 1976) presented influences of aluminium (less than 0,004%), sulphur and oxygen (Makara 1977). Chemical elements like: sulphur, selenium, tellurium, oxygen, cerium influence surface tension gradients, changing the magnitude and direction of toroidal flow in molten pool (Heiple, Roper 1982, Tinkler 1983). Conclusion could be that forces generating weld pool circulation would be as follow: (presented in figure 2)

1. Arc force due to current source acting in centre of the weld pool and generating a toroidal flow being the most important effect of electromagnetic forces.
2. Surface tension gradients that affect the shape of fused zone and giving width/depth ratio.
3. Drag forces due to plasma jet or gas generated by decomposition of electrode coatings responsible for instabilities in high-speed, high-current automatic GTAW welding
4. The pressure due to plasma jet or gas that causes a crater or depression in the weld pool surface and metal that is melted at the front above accelerated through the restricted cross-section around the crater.

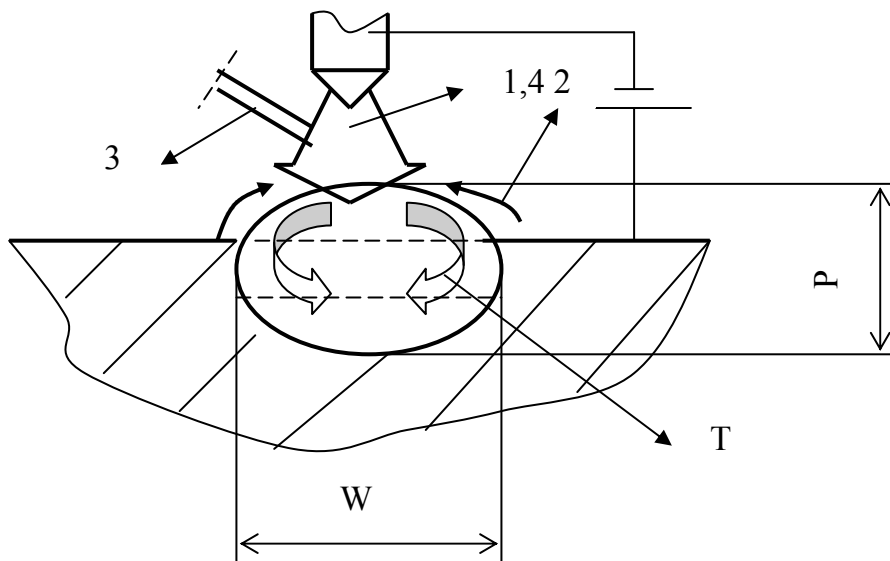


Fig. 2 Parameters of GTAW welding pool: 1 – arc force; 2 – surface tension; 3 – drag forces; 4 – plasma jet pressure; P – penetration; W – width of weld pool; T – toroidal flow in melted pool.

### 3. WELDING POOL TEMPERATURE

Lot of researches were done for weld pool temperature evaluation, Rabkin 1959 used thermocouples, Erohkin 1978 utilises infra-red pyrometer, calorimetry was investigated by Ando, Nishiguchi 1968, evaporation rate to measure surface temperature by Howden, 1969. Christiansen, 1965 presented the average weld pool temperature introducing a non-dimensional operating parameter  $n = qv/4\pi K\alpha T_m$  (2), symbols used represent:  $q$  = rate of heat flow;  $v$  = welding speed;  $K$  = absolute temperature;  $\alpha$  = diffusivity of heat;  $T_m$  = average temperature of molten pool based on thermal conductivity theory. Graphical representation of average temperature of molten pool, given by  $T_m/T_f$ , where  $T_f$  is fusion temperature, face to operating

parameter  $n$  is shown in figure 3. The surface temperature of the pool has been measured by a number of investigators and table 6 shows mean values.

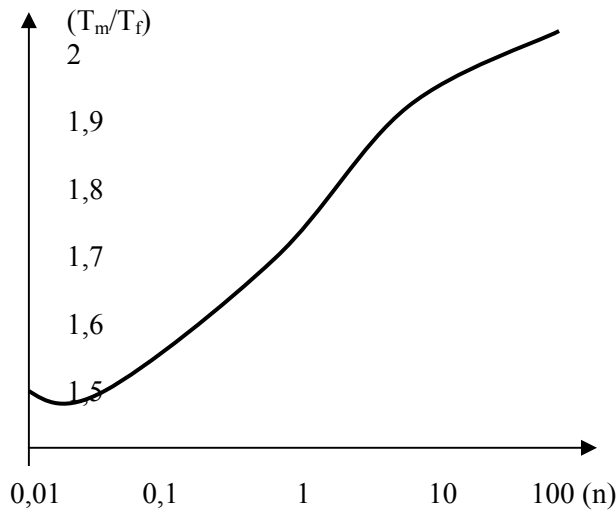


Figure 3 Average temperature  $T_m/T_f$  of the molten pool based on thermal conduction theory, Christensen 1965

Table 6 Mean surface temperature of arc molten pools

Metal	Process	Current	Shiel. gas	Temp.	Method, author
Al	GTAW SMAW GMAW	100	Argon	1900	H solubility, Howden 1963
				3100	Optical pyrometry Sparagen 1943
				>1600	Thermocuple Rabkin 1959
Cu	GTAW	150 100 240 170 450	Argon	1700	H solubility Vaporisation rate, Howden 1969
				1350	
				1550	
				1690	
				1890	
Fe	GTAW	150 120 140 80	Argon	2100	H solubility Vaporisation rate Optical pyrometry Lakticov 1978 OP
				1950	
				1880	
				1750	
Ni	GTAW SMAW	120	Argon	1900	HS
				2200	OP

The temperature field [ $^{\circ}\text{C}$ ] on surface of arc melted austenitic chromium-nickel steel (figure 4), welded with GTAW method usind argon shielding gas and current around 300 A, was presented by Erohin, 1978.

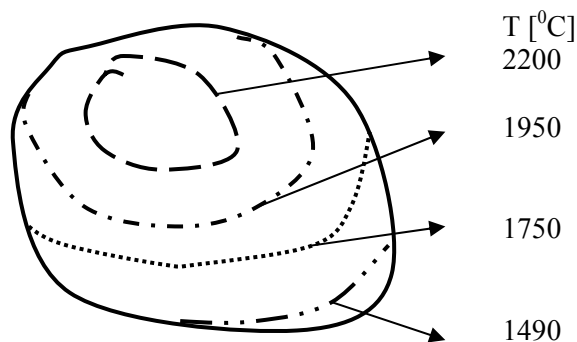


Figure 4 The temperature field on surface arc – melted austenitic chromium-nickel steel, argon shielded gas, 300 A, GTAW (Erokhin, 1978)

#### 4. OUR RESEARCH OBJECTIVES

Authors' proposed in 2005, to National Consil for Universities Research (CNCSIS), a research foccused on identifying influence of technological parameters on nanostructure of multifunctional materials. In their views was to use TIG welding technology for welded joint manufacture and to study epitaxial crystalisation at interface between base matrial and melted alloy formed. The general location for epitaxially crystalisation is the small zone where alloyed crystals grow directly on base material crystals. It is the cupling zone between base materials and welded joint and represents the most sensible part with great importance for mechanical characterisitics of joint. The GTAW method was chosen for research because all the parts involved could be modified and changed. Base materials could be all types of steels but especially stainless steels with thick between 0,2 mm and 6 mm. For small thicks no filler materials is needed and only distortion of internal grains structure will be investigated. Other materials like bronse, titanium, magnesium could be investigated. For thicker materials (2 – 6 mm) the filler materials get a big importance for melted bath composition. Here dillution coeficient will influence obtained alloy in welded joint and the composition could be evaluate using Schaeffler, De Long or WRC 1992 diagrams. In epitaxially crystalisation zone, complex atomic structures could be formed. Protection of melted bath could be made with argon or helium pure gases or with mixture like argon and 5 % of oxigen or carbon dyoxide. The volume of protection gas will be modifying to see how it influences the crystalisation phenomena. Heating energy use to melt filler and base materials could be different.

Welded joint used in experiments will be as simple as possible to achive needed informations. After cutting testing parts without internal deformations, the surface will be polished and lapped, hardness tests will be performed to be sure that welded metal deposition is under the value of 350 and using chemical reactions the specific regions in welded joint will be made visible for microscopy.

*Received April 19, 2005*

*Technical University "Gh.Asachi" Iasi*

#### REFERENCES

- /1/. Zgura G., s.a *Tehnologia sudarii prin topire*, Editura Didactica si Pedagogica, Bucuresti, 1983
- /2/. AWS, *Welding Handbook*, Seventh Edition, vol.I, Fundamentals of Welding, Editor Charlotte Weisman, USA 1981.
- /3/. Echim I., Lupescu I., *Tehnica sudarii prin topire a metalelor si aliajelor*, Editura Tehnica, Bucuresti, 1983.
- /4/. Ghenghea L.D., *Teoria proceselor de sudare*, Editura Tehnica Info, Republica Moldova, 2001.
- /5/. Lancaster J.F., Rykalin N.N., *Physics of Welding*, IIS/IIW, 1983.

#### CARACTERISTICI ALE BĂII DE SUDARE ÎN CAZUL METODEI TIG

**Rezumat:** Lucrarea prezinta caracteristicile tehnologice ale metodei de sudare cu protectie de gaz inert utilizand electrod din wolfram, nefuzibil (TIG, GTAW, 141). Sunt prezentate metodologii de alegere a parametrilor de sudare pentru diferite materiale, se accentueaza rezultatele unor cercetari asupra caracteristicilor geometrice ale barii de metal topit evidentiindu-se adancimea de penetrare si latimea cordonului realizat la utilizarea procedeului. Sunt descrise cercetari asupra campului termic realizat de sursa folosita pentru sudare si distributia temperaturii in baia de meatal topit care poate fi realizata cu sau fara material de adaos.

## A IOSIPESCU THIN SPECIMEN SETTING VARIANT FOR SHEAR STUDY

BY

BOGDAN LEIȚOIU, MAGDA ANTOHE AND MARIAN MAREȘ

**Abstract.** *The studied material is an additive acrylic resin, for stomatological use. On both faces, the specimens, type Iosipescu, was equipped with aluminum plates tabs, glued and rivetted. It was executed measurements on all four sample possible positions. The low dispersion of the experimental points plotted, in the  $\tau$ - $\gamma$  axis, proves the good precision of shear modulus evaluation method*

**Keywords:** *Iosipescu shear test, shear modulus, shear fixture, composite materials, acrylic resin*

### 1. MATERIALS AND SPECIMEN PROCESSING

Two sorts of materials designed for medical use and based on an additive acrylic resin were studied:

- mollosil-acrylic ( $\square_4$  specimen);
- mollosil-silicon-acrylic ( $\square_5$  specimen).

Because of the small sample thickness (Table 1) it was necessary to prevent the bending and twisting instability at great levels of load. In that spirit it was glued (cyan-acrylic) and gripped (with rivets) aluminum plates on the load sides. The measurement area was free, for applying the strain gages. After tabs applying, the loading sides of samples were machined, including the two symmetrical notches, as ASTM D 5379 requires.

Table 1. The specimen dimensions.

	$\square_4$	$\square_5$
h (mm)	11,2	11,4
w(mm)	1,6	3,3
$S_0$ (mm <sup>2</sup> )	17,92	37,62

The specimens machining was made by a milling machine, using a diamond wheel, the prismatic samples being mounted in a special dividing device, in order to ensure an accurate processing of parallel loading sides and of notches identity.

### 2. SHEAR STRAIN MEASUREMENTS

Strain gage rosettes *side-by-side*, produced by *Micro-Measurements Group*, type *N2A-06-C032A-500*, were used. Their technical parameters are:

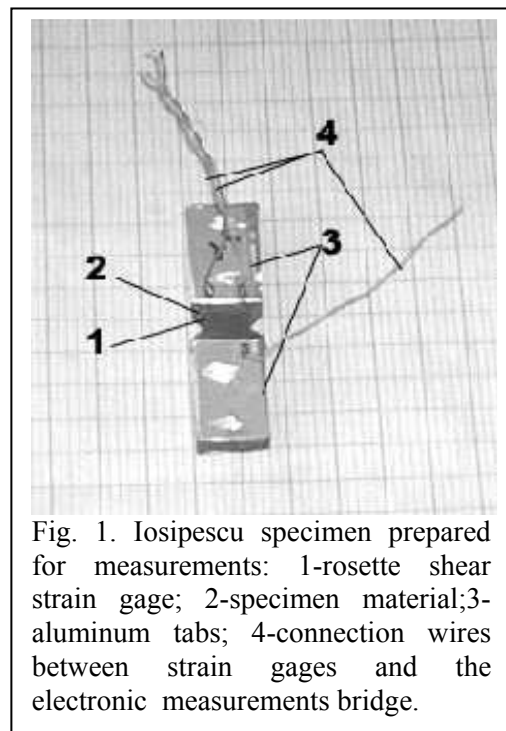


Fig. 1. Iosipescu specimen prepared for measurements: 1-rosette shear strain gage; 2-specimen material; 3-aluminum tabs; 4-connection wires between strain gages and the electronic measurements bridge.

- electrical resistance:  $R=500\Omega$ ;
- gauge factor:  $k_{TER}=2,01\pm 1,0\%$  (la  $24^{\circ}\text{C}$ );
- transverse sensibility:  $K_T=(+1,8\pm 0,2)\%$ .

The Wheatstone bridge was supplied by a 1V-tension voltage and was calibrated by a signal established from the following relation:

$$\varepsilon_{cal} = 10000 \frac{k_{bridge}}{k_{gauge}} \cdot \frac{U_{br.}}{U_{br.def.}} = 10000 \cdot \frac{2}{2,01} \cdot \frac{1}{4} (\mu\text{m} / \text{m}) = 2488 \mu\text{m} / \text{m} \quad (1)$$

The *shear strain* indicated by the bridge is:

$$\gamma_{1,2} = \varepsilon_1 - \varepsilon_2 \quad (2)$$

where  $\varepsilon_1$ ,  $\varepsilon_2$  are the extensional strains indicated by the two transducers of the shear rosette.

The bridge (type N 2314) indications were read using a digital voltmeter.

The reading correction takes into account (following manufacturer indications) the bridge supply and the transverse sensibility:

$$\gamma_{1,2} = (\varepsilon_1 - \varepsilon_2) = \frac{1 - \nu_0 K_t}{1 + K_t} (\varepsilon_{read.1} - \varepsilon_{read.2}) \quad (3)$$

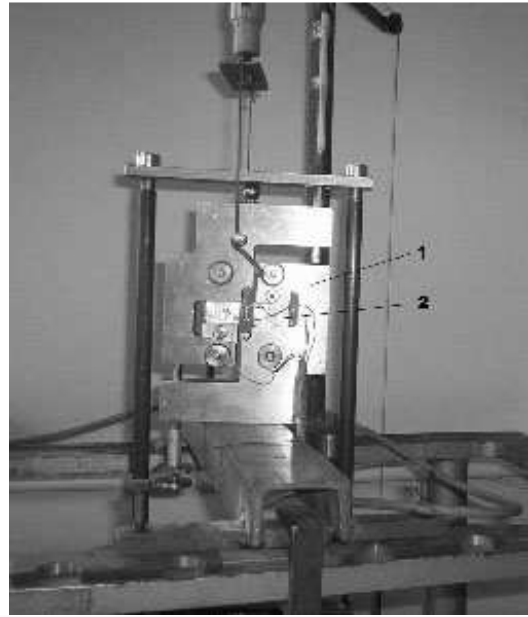


Fig. 2. The shear testing device (1) made at Technical Universit "Gh.Asachi"; the shear specimen (type Iosipescu) (2) with shear strain-gage connected to the bridge.

### 3. MATERIAL CHARACTERISTIC CURVES

The specimens were gripped in the shear fixture that is placed on a structure which allows the loading by marked masses (Fig.2).

The material characteristics are plotted, respectively, in  $\tau$ - $\gamma$  axis as following:

- *the shear stress*:

$$\tau = \tau_{1,2} = \frac{F}{S_0},$$

where (1,2) are the principal material directions (with 1 - direction of notches axis);

$F = m \cdot g$  is the load applied on the specimen,  $m$  = the sum of marked masses,  $g = 9,81\text{m/s}^2$ , the standard gravity acceleration, and

$S_0 = h \cdot w$  is the shear section area;

- *the shear strain* on the principal directions (1,2):

$$\gamma = \gamma_{1,2} = (\varepsilon_1 - \varepsilon_2)$$

The four positions that are indicated, from 1 to 4, in the diagrams and are all specimen's possible positions in the shear fixture:

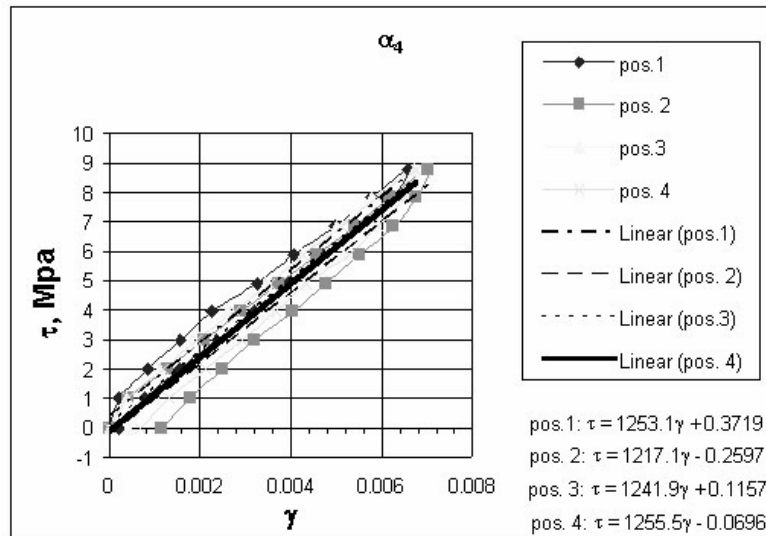


Fig. 4. The shear characteristic curves for  $\alpha_4$  specimen and the trend lines from which the shear modulus results.

-the second position results from the first, with an  $180^\circ$  rotation around the vertical specimen axis;

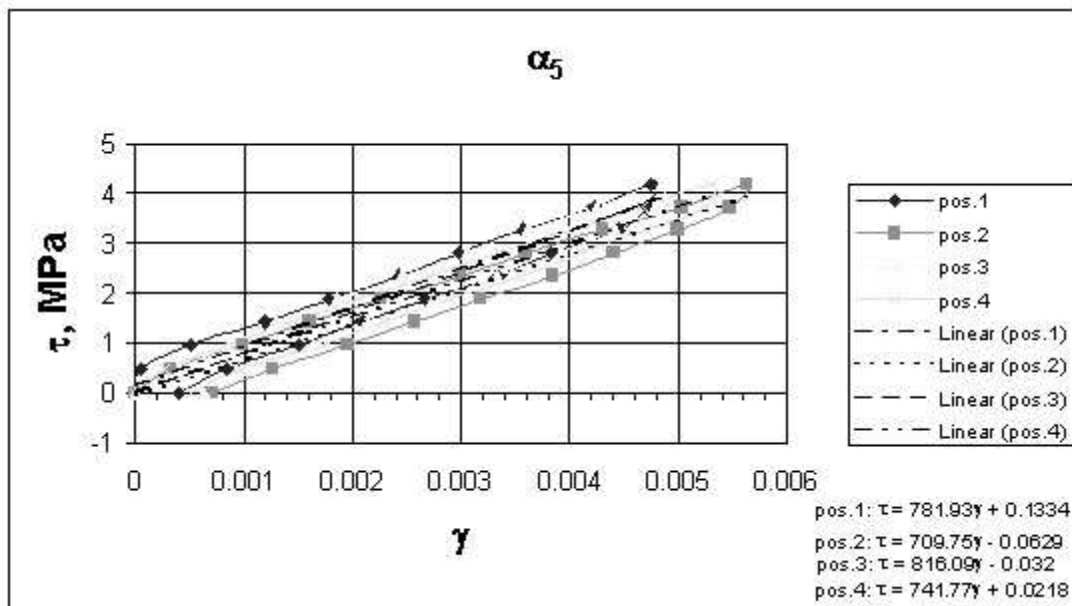


Fig. 5. The shear characteristic material curves for  $\alpha_{45}$  specimen and trend lines from which the shear modulus results.

-the 3-rd -from the 2-nd, after a  $180^\circ$  on the horizontal axis around rotation;

-the 4-th - from the 3-rd, after a  $180^\circ$  on the vertical axis around rotation.

That experimental strategy was assumed in order to increase the measurements accuracy and to control and remove the possible errors caused by specimen dimensional deviations and by the fixture's misalignments.

The shear modulus,  $G$ , is the trend line slope of the plotted characteristics:

$$\tau = G \cdot \gamma \quad (4)$$

from which:

$$G = \frac{\Delta\tau}{\Delta\gamma} \quad (5)$$

where  $\Delta\tau$  is the shear stress variation, and  $\Delta\gamma$  is the corresponding shear strain.

The entire estimation (for every complete loading cycle) is closer to the statistical material behavior.

The  $G$  modulus obtained it allows appreciating

Those results lead to the average shear modulus values:

$$G_{\square\square} = 1241,9 \text{ MPa} \quad \text{and} \quad G_{\square\square} = 762,39 \text{ MPa} \quad (\text{Table 2}).$$

Table 2. The in-plane shear modulus values.

Position	$\square_4$	$\square_5$
	MPa	MPa
1	1253.1	781.93
2	1217.1	709.75
3	1241.9	816.09
4	1255.5	741.77
$G_{\text{ave.}}$	1241.9	762.39

#### 4. Conclusions

The plotted points in the  $\tau$ - $\gamma$  axis, as material shear characteristics, for all four samples positions, show the low dispersion of the experimental data and proves the good accuracy of shear modulus evaluation method.

The  $\square_5$  material denotes a low stiffness that indicates it to be suitable for applications needing a large elastic deformability.

Received May 4, 2005

Technical University "Gh.Asachi" Iasi

#### REFERENCES

1. Mareș, M., Leițoiu, B., - *Iosipescu shear test as applied to some composite materials*, **Buletinul Institutului Politehnic din Iași**, publicat de Universitatea Tehnică „Gh. Asachi”, Iași, tomul I (liv), fasc. 6b, 2004, secția Construcția de Mașini, Conferința ACME 2004, Iași;
2. Leițoiu, B., Măcuța, S., Maței, C. - *On the Electrical Level Supply of the Strain Gauges Used for the Strain Measurements of the Insulator Material Samples*, The Annual Symposium of the Institute of Solid Mechanics-SISOM 2002, București, 16-17 mai 2002;
3. Mareș M., Leițoiu B., *Considerații cu privire la metodele de încercare la forfecare în plan aplicate materialelor compozite*, "Construcția de mașini", nr.10, București, 1999.

#### VARIANTA DE PRINDERE A EPRUVETELOR SUBTIRI TIP IOSIPESCU PENTRU STUDIUL FORFECARII

**Rezumat.** Materialul studiat este o rășină acrilică aditivată, de uz stomatologic. Epruvetele tip Iosipescu au fost echipate cu plăci de aluminiu pe ambele fețe, lipite și asigurate prin nituire. Au fost efectuate măsurări în cele patru poziții posibile ale epruvetelor. Imprăștierea extrem de redusă a punctelor în planul  $\tau$ - $\gamma$  subliniază precizia metodei de evaluare a modulului de forfecare

## THE APPLICATION OF IOSIPESCU SHEAR TEST FOR ACCURATE DETERMINATION OF IN-PLANE SHEAR MODULUS, FOR METAL MATRIX COMPOSITES

BY

MARIAN MAREȘ and BOGDAN LEIȚOIU

**Abstract.** *Some groups of scientists from Wyoming and Idaho Universities developed the present Iosipescu shear test fixture. On this base, a shear test fixture and a method for specimen processing were both designed and achieved at the Technical University Iași. They were validated by experimenting on some homogeneous materials. The specimens were instrumented with special designed strain gage rosettes. This paper presents some experimental results of Iosipescu shear test, as applied to some graphite and silicon carbide particulate reinforced aluminum matrix composites. The shear modulus was measured as the slope of the interpolation straight for experimental results in  $(\tau-\gamma)$  coordinates.*

**Keywords:** *shear modulus, Iosipescu test, metal matrix composites*

### 1. INTRODUCTION

The Iosipescu shear test was proved, by many series of results reported mainly by researchers from USA, as an ingenious and precise experimental method, especially for studying mechanical properties of composite materials. The test consists in a pure shear stress state, applied on a prismatic specimen, with two transversal 90-deg notches, on the top and bottom surfaces. The specimen is asymmetrically loaded by bending.

Professor Iosipescu demonstrated that, using notches with a depth of a quarter from specimen height, a quasi-uniform vertical shear stress distribution is obtained into the gage zone of the specimen. Consequently, one can accept that the experimental determinations are made studying a stress state of pure shear, so the results will depend only on the actual material properties.

### 2. EXPERIMENTAL METHOD

The method is widely accepted thanks firstly to Adams and Walrath: they implemented the test, by way of fixture and specimen design, for use on laminate composite materials, reinforced with high strength fibers. Their fixture design was developed at the University of Wyoming. It is referred to as “the modified Wyoming shear test fixture” and is included in ASTM Standard D 5379.

The fixture is presented as the main factor for correctly conducting the Iosipescu shear test, so its improvements were continuing to appear. At the Idaho University, Conant and Odom developed a new advanced design, based on a rigorous analysis of previously created variants. An important precise constituent is the special

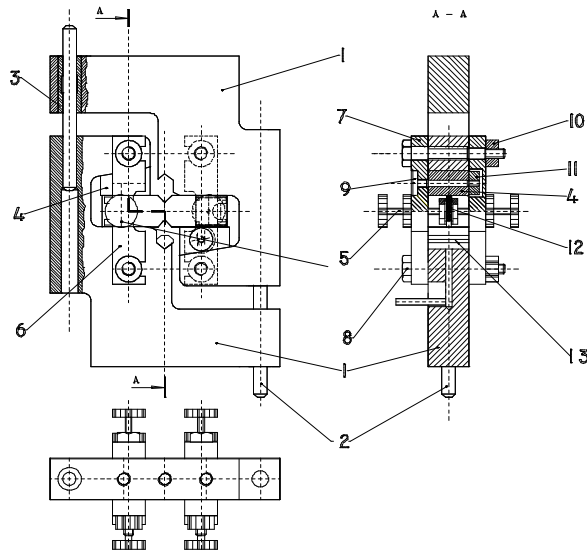


Fig.1. Idaho-type shear fixture, designed and realized at Technical University Iasi.

The Iosipescu specimen (Fig.2) is instrumented with shear strain gage rosettes (Micro-Measurement N2P-08-C032A-500, Fig.3) and placed into the above-cited fixture (see Fig.1). The fixture is loaded in compression, with marked masses, using a special experimental apparatus.

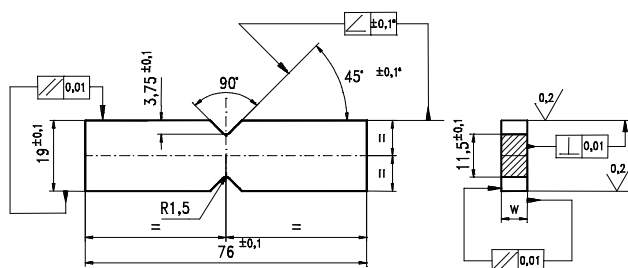


Fig.2. Iosipescu shear specimen geometry as indicated by ASTM Standard D 5379-93.

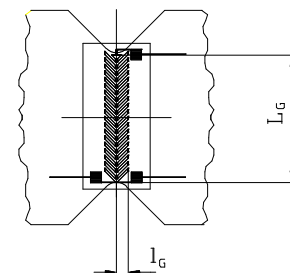


Fig.3. Special shear strain gage rosette.

The shear stress at the midpoint of the test section can be calculated as:

$$\tau_f = \frac{F}{A_f} \quad (1)$$

where  $F$  is the force that is applied on the fixture (the total weight of marked masses that are used as compression load) and  $A_f$  is the transverse area of the test section.

The strain gages are oriented on  $\pm 45^\circ$  to the shear stress direction and are placed both at the left and the right side of the test section. As a consequence, it can be used for separately measuring the normal shear strains  $\varepsilon_1$  and  $\varepsilon_2$ , in order to observe the possible difference between those values caused by specimen twisting.

The shear strain value can be calculated as

designed shear strain gage, created by Ifju and industrially produced by Micro-Measurements Group.

The results presented in this paper were obtained using an original Idaho-type fixture design (see Fig.1), together with cited-above type of shear strain gages.

The fixture was previously tested on some homogeneous materials and an extremely low scatter of experimental results (when measuring in-plane shear modulus  $G$ ) was observed.

The tests were developed in Technical University Iasi, at the Strength of Materials Dept. of the Mechanical Engineering Faculty.

$$\gamma = C_{st}(\varepsilon_1 - \varepsilon_2) \quad (2)$$

where  $C_{st}$  is a strain correction factor (indicated by Micro-Measurement Catalog) referring to transversal sensibility of strain gages.

The shear modulus value can be determined as the slope of  $\tau(\gamma)$  curve, or can be calculated as

$$G = \frac{\Delta\tau_f}{\Delta\gamma_{12}} \quad (3)$$

The tests were developed as loading and unloading cycles.

Using the above-cited fixture, the Iosipescu specimen can be loaded up to the failure (at  $F_{max}$  level of compression force), in order to determine the shear strength of the studied material, given by

$$\tau_{Rf} = \frac{F_{max}}{A_f} \quad (4)$$

### 3. MATERIALS AND SPECIMEN INSTRUMENTATION

The composites that are studied here are based on a commercial aluminum alloy of type ATSi7Cu3Mg, with a nominal composition of 2.9% Cu, 6.6% Si, 0.5% Fe, 0.36% Mg, 0.15% Ti and the balance aluminum. All the samples are made by Vortex casting, in laboratory conditions, at the Material Science and Engineering Faculty, in Technical University Iasi.

The study is focused on some hybrid-reinforced composites, with silicon carbide (SiC) (with an average size  $d \approx 40\mu\text{m}$  and 7% volume fraction) and graphite particles ( $d \approx 63\mu\text{m}$  and 3.5% volume content).

Each sample that was used in the present study was heat treated into the following stages:

- solutionizing for 4 hours, at 520°C;
- quenching in hot water;
- artificial aging, by mentioning 8 hours at 160°C;
- quenching in air.

All the heat treatments were also made in laboratory conditions, at the Material Science and Engineering Faculty, in Technical University Iasi.

The specimens were instrumented, on both faces, with Micro-Measurements N2P-08-C0032A-500 shear strain-gage rosettes. All the materials (adhesive M Bond 200, solution for surface preparation) and the entire methodology for that instrumentation were take over from Micro-Measurement Group.

### 4. PRELIMINARY RESULTS

Before determining the shear modulus, some preliminary tests were developed (on a Heckert 20 testing machine), in order to establish the shear strength of the studied materials. By these experiments one could determine:

- the maximums force that the specimen supports;

- the shear strength of the material;
- the extreme values of loading force, for shear modulus determining;
- the specific failure mode of the studied material, in shear test.

The shear strength, as the average value of experimental results, was  $R_{12}=42\text{MPa}$ , corresponding to a maximum loading force of about 3kN. The force-displacement dependence was linear (without any flow zone), as for the brittle materials.

Besides, the brittle fracture behavior of the composite was supplementary emphasized by the direction of first crack propagation, from the notch roots of the specimens. According to the literature (see Ref.5), the  $45^\circ$  off-axis crack-direction that was observed is striking characteristic for brittle materials.

## 5. SOME CHARACTERISTIC FEATURES OF IOSIPESCU SHEAR TEST

From the present authors' experience, there are few important aspects for taking into account when preparing and conducting an Iosipescu shear test:

- the specimens are to be rigorously machined, in order to respect the geometry recommended for standard test – mainly the parallelism of contact surfaces, together with the perpendicularity of gage surfaces onto the loading ones; (it is important to observe that the specimen has three planes of symmetry;)
- the fixture design imposes a strictly parallelism of the guidance columns and of the base surfaces; the specimen positioning are to be made respecting the coincidence of its longitudinal symmetry plane with that of the guidance columns; this plane must also include the loading forces resultant;
- the shear strain-gage rosettes are symmetrically positioned in relation with shear section and are placed back-to-back (with separately measurement), in order to emphasize the possible errors caused by specimen twisting and by loading imperfections;
- the calibration of measuring system configuration allows to establish the material characteristics ( $\tau$ - $\gamma$ ) during the loading-unloading process, for all the four strain-gages;
- an initial loading-unloading cycle is to be made, in order to eliminate the transition phenomena of the experimental procedure (including the settlement of loading surfaces of the specimen).

## 6. IN-PLANE SHEAR MODULUS DETERMINATION

The preliminary tests indicated the possibility of specimen loading with a maximum force of 1500N, without any appearance of irreversible phenomena (i.e. plastic deformation) into the volume of studied material. A loading method using marked masses was choose, in order to ensure the maximum loading force precision.

After a loading-unloading cycle one can obtain the ( $\tau$ - $\gamma$ ) dependence; a straight line is draw by interpolating those experimental data; its slope indicates the shear modulus of the studied material.

It must be observed that the loading and unloading curves are extremely close, indicating a “coherent response” (in keeping with the hypothesis of elasticity's theory) of the material to the applied load. As a consequence, a unique interpolation line can be draw and a single value of shear modulus is obtained.

Using the experimental data and basing on the effective curves of  $(\tau-\gamma)$  dependence (see Fig. 5), the average value of shear modulus of the studied material can be determined as  $G=0,24468 \cdot 10^5 \text{MPa}$ .

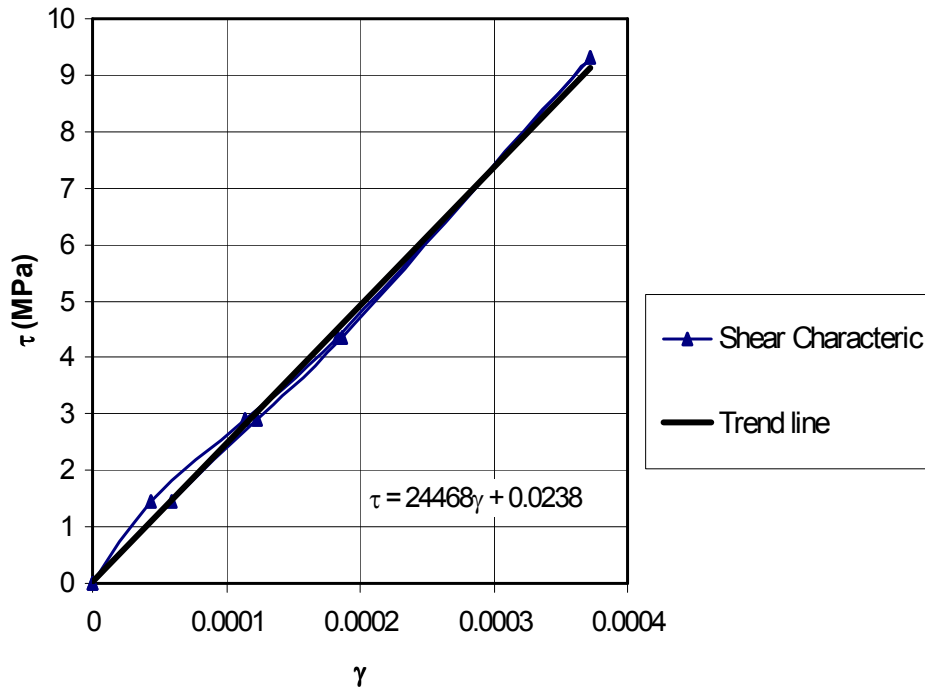


Fig.4. The shear characteristic plotted for one experiment.

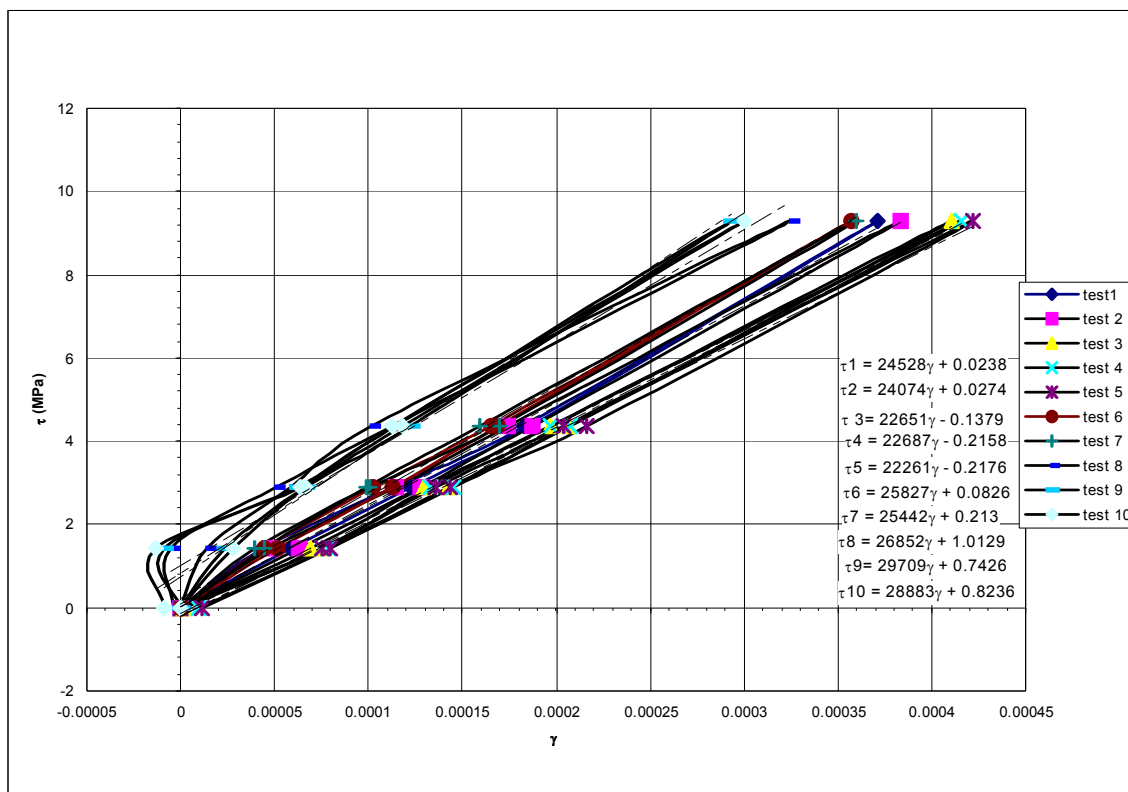


Fig.5. The experimental shear characteristics plotted for one specimen.

## 7. THE CHARACTERISTIC FEATURES OF STRAIN-GAGES ROSETTES

Two Micro-Measurements N2A-00-C032A-500 rosettes have been fixed back-to-back on each sample. The strain-gage parameters are:

- an electrical resistance  $R=500\Omega$ ;
- a strain-gage factor  $k_{TER}=2,03\pm 1,0\%$  (la  $24^{\circ}\text{C}$ );
- a transversal sensibility factor  $K_T=(+1,2\pm 0,2)\%$ .

The calculus of shear strain includes a correction, taking into account the transversal sensibility of the strain-gages (based on Micro-Measurements indications):

$$\gamma_{1,2} = (\varepsilon_1 - \varepsilon_2) = \frac{1 - \nu_0 K_T}{1 + K_T} (\varepsilon_{cit.1} - \varepsilon_{cit.2}) \quad (5)$$

where  $\square_1$ ,  $\square_2$  and  $\square_{cit.1}$ ,  $\square_{cit.2}$  are, respectively, the corrected and the effective of longitudinal strain values.

The correction fraction in the above-cited relation must be calculated from the above-presented strain-gages parameters, as:

$$\frac{1 - \nu_0 K_T}{1 + K_T} = \frac{1 - 0,285 \cdot 0,0019}{1 + 0,0019} = 0,997563 \quad (6)$$

## 8. CONCLUSIONS

In fig.6 is shown that the material is strengthened during the experiments. That's mean the material endures stiffness, according to the history of mechanical loading. The range of variations is about 30% from the average value, but predominant values are those from the last experiments (between  $0,25 \cdot 10^5$  MPa and  $0,30 \cdot 10^5$  MPa).

On can appreciate that the Iosipescu shear test allows an accurate determination of the in-plane shear modulus, but its accuracy is strongly influenced by a number of experimental factors:

- the fixture design have to ensure the precise and stable position of specimens;
- the specimen machining must lead to the geometrical precision exceeded by standard test;
- the special strain-gage rosettes are precisely positioned, taking into account the producer's recommendations, including the adequate preparation of gage surfaces of the specimens;
- the electronic equipment must be correctly connected and installed;
- a correction of experimental results must be made, according with the strain-gage parameters and following the recommendations of the strain-gages producer.

**Acknowledgements** – The authors would like to express their gratitude to Dr. Ioan Carcea and his colleagues from Materials Engineering and Science Dept. at Technical

University “Gh.Asachi” Iasi, for their full support in manufacturing the composites that were studied in this paper.

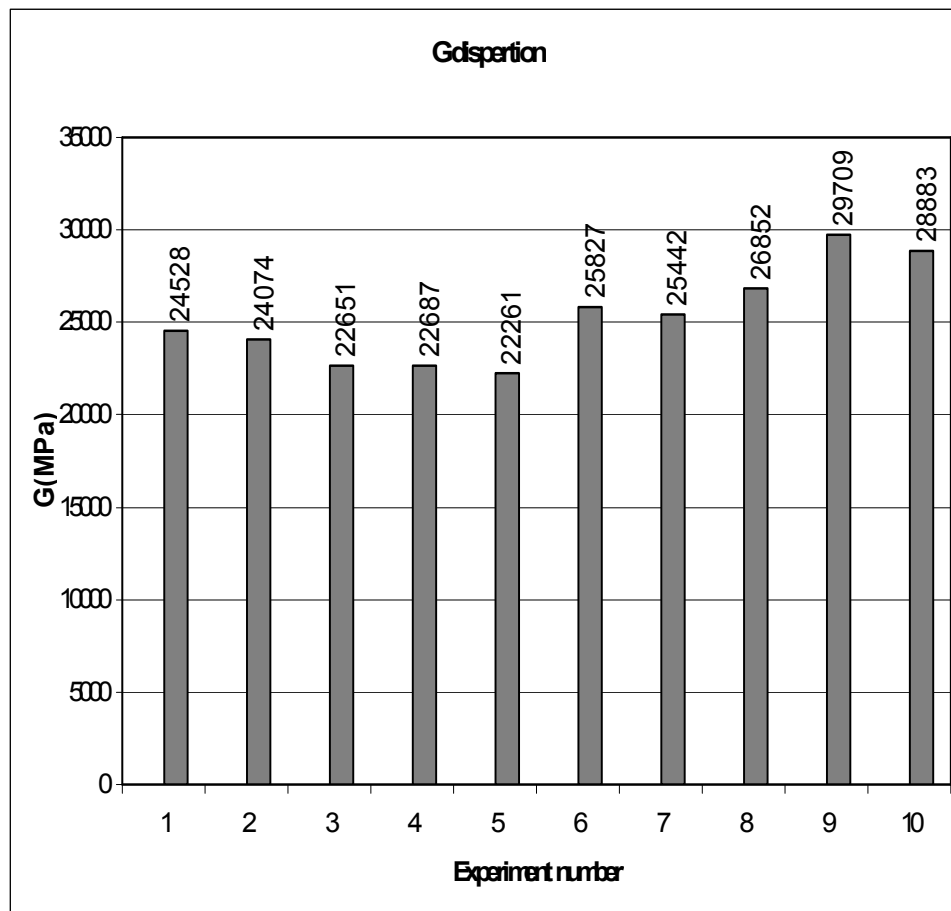


Fig. 6. Dispersion of shear modulus values

Received May 4, 2005

Technical University “Gh.Asachi” Iasi

#### REFERENCES

- /1/. M. Mares, I. Carcea, R. Chelariu, C. Roman,, *Mechanical and Tribological Properties of Some Aluminum Matrix Composites after Aging Treatments*, EUROMAT '97, vol. I, pp. 423÷426.
- /2/. R.N. Conant, E.M. Odom, *An Improved Iosipescu Shear Test Fixture*, Journal of Composites Technology & Research, vol. 17, no. 1, 1995, pp. 50÷55.
- /3/. P.G. Ifju, *The Shear Gage: Reliable Shear Modulus Measurements of Composite Materials*, Experimental Mechanics, vol. 34, no. 4, 1994, pp. 369÷378.
- /4/. M. Kumosa, D. Hull, *Mixed-mode Fracture of Composites using Iosipescu Shear Test*, International Journal of Fracture, vol. 35, 1987, pp. 83÷102.

#### CÂTEVA ASPECTE ALE APLICĂRII TESTULUI DE FORFECARE IOSIPESCU ÎN CAZUL UNOR MATERIALE COMPOZITE CU MATRICE METALICĂ

**Rezumat:** Forma actuală a dispozitivului de prindere pentru testul de forfecare Iosipescu a fost dezvoltată de cercetători de la universitățile americane Wyoming și Idaho.

Pe această bază, la Universitatea Tehnică din Iași au fost proiectate și realizate o variantă de dispozitiv de prindere și un procedeu de prelucrare a epruvetelor, care au fost validate pe materiale omogene. Tensiunile din epruvetă sunt măsurate folosind rozete tensometrice de construcție specială pentru acest test.

În lucrarea de față sunt prezentate rezultatele încercărilor efectuate asupra unor materiale compozite cu matrice dintr-un aliaj de aluminiu și armare cu particule de grafit și carbură de siliciu. Valorile modulului de forfecare au fost stabilite ca pantă a dreptei de interpolare a punctelor obținute prin reprezentarea rezultatelor experimentale în planul  $(\tau-\gamma)$ .

## RESEARCHES ABOUT THE STEEL SILICONIZING IN GAS MEDIUM AT LOW PRESSURE

BY

ZOLTAN MARKOS

**Abstract.** *The paper presents some results about steel siliconizing with  $\text{SiCl}_4$  at low pressure. The thermochemical treatment siliconizing with gas assure at saturation in silicon speed was made to obtain an uniform and compact layer and a sample surface that remains clean and without adherences. Because of the low pressure, the active substance ( $\text{SiCl}_4$ ) is evaporated at normal temperature and the vapor's debt can be maintained constant trough the constant temperature maintaining. For the dilution  $\text{SiCl}_4$  an active ( $\text{H}_2$ ) or an inert (Ar) gas was used. At siliconizing an increased saturation speed was obtained and the layer is compact and adherent. At treatments made in gas at low pressures, the sample's surfaces remain clean even for treatments made at high temperatures. The siliconizing in gas medium at low pressures assures the obtaining of very good results and a very easy control of work parameters. In the same time, the method reclaims very expensive and complex equipment..*

**Keywords:** *steel siliconizing, gas medium, low pressure*

### 1. GENERAL ASPECTS

The purpose of siliconizing thermochemical treatment is to obtain a diffusion layers enriched in silicon for pieces surface. This layers content about 8...12% Si and have a very good corrosion and oxidation resistance.

The siliconizing thermochemical treatment is a very complex process. The main factors which effect the compactness and the hardness in the diffusion layer could be, on the hand, the technological factors (silicon potential, temperature, work conditions etc.), and on the other hand, the percentage of carbon in the treated steel.

The siliconizing with gas assures saturation in silicon speed, obtains a uniform and compact layer and the sample surface remains clean and without adherences. For the dilution  $\text{SiCl}_4$  an active ( $\text{H}_2$ ) or an inert (Ar) gas is used.

For the treatment duration reducing, in the same time with the silicon corresponding potential it must be assured as high as possible the diffusion speed.

From the point de view of diffusion speed, we are tended to choose as high temperature as possible, and to obtain in this way a very high saturation speed.

### 2. EXPERIMENTAL EQUIPMENT

The siliconizing was achieved in an experimental furnace, realized at a quartz pipe (Fig.1). The heating was realized with radiant tube (silite rod).

For the treatment in gas medium, the purpose was realized at low pressure (1 ... 0.1 Torr) whit a Roots vacuum pump. The pressure was measured whit an electronic Penning-Pyrani Vacuumeter.

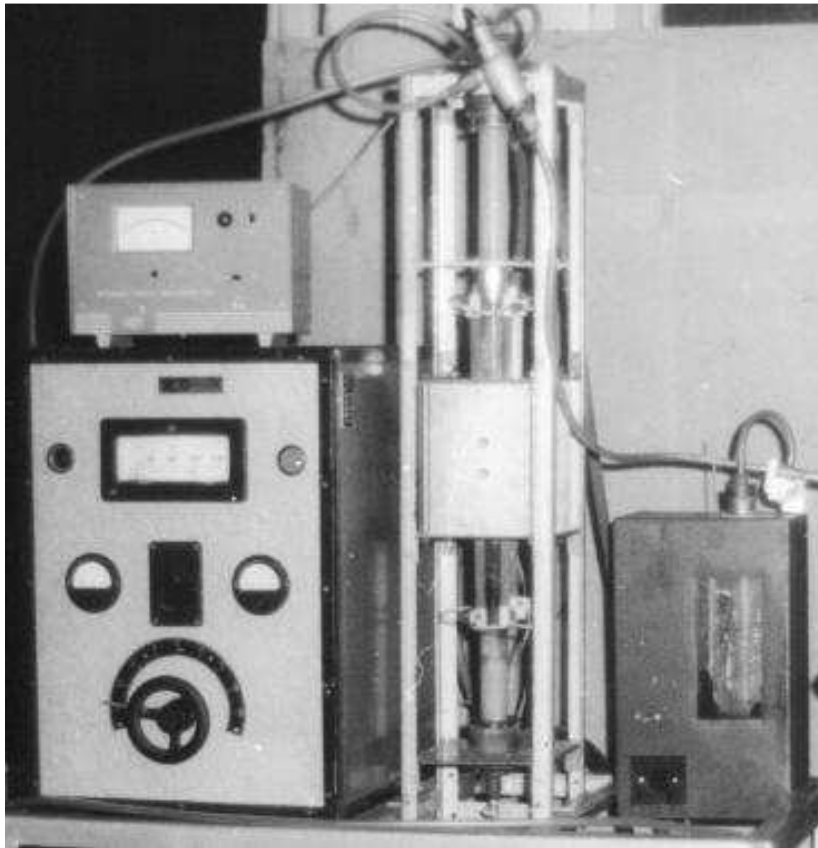


Fig.1. Siliconizing furnace

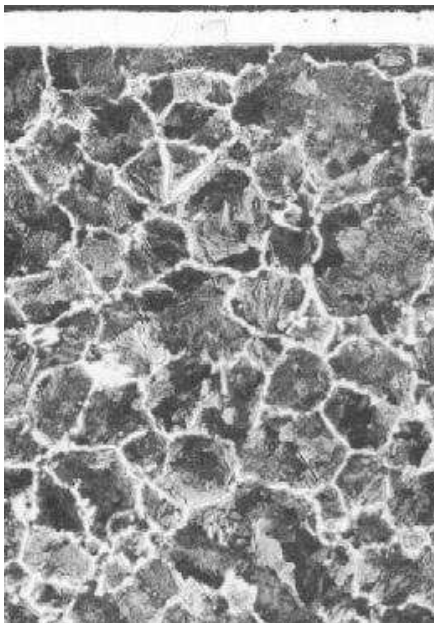


Fig.2. OLC 45 steel microstructure siliconized at low pressure, 1050°C, 0.5 hour with 70 ml/hour SiCl<sub>4</sub>. 100 X

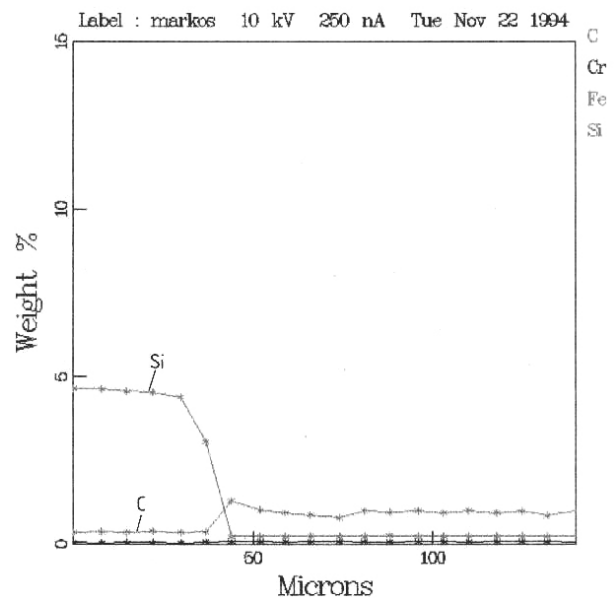


Fig.3. Carbon and silicon repartition for OLC 45 steel siliconized at low pressure, 1050°C, 0.5 hour with 70 ml/hour SiCl<sub>4</sub>

Because of the low pressure, the active substance ( $\text{SiCl}_4$ ) evaporates at normal temperature and the vapor's debt can be maintain constant trough the constant temperature maintaining.

### 3. SOME RESULTS OF EXPERIMENTAL TESTING:

The samples were obtained from carbon steel OLC 45 (STAS 880/80). The siliconizing was realized at 0.1 Torr pressure, 0.5 hour, whit a flow rate about 70....80 ml/hour  $\text{SiCl}_4$ .

The samples have been delaminated with optical microscope. The medium hardness in diffusion layer has been determined using Vickers method. The carbon and silicon repartition was studied on electron probe microanalyser type CAMECA 50 SX.

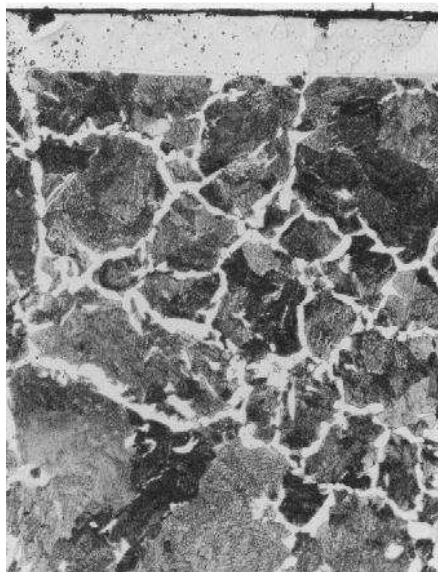


Fig.4. OLC 45 steel microstructure siliconized in powder medium with paste 1000°C, 2 hour **150 X**

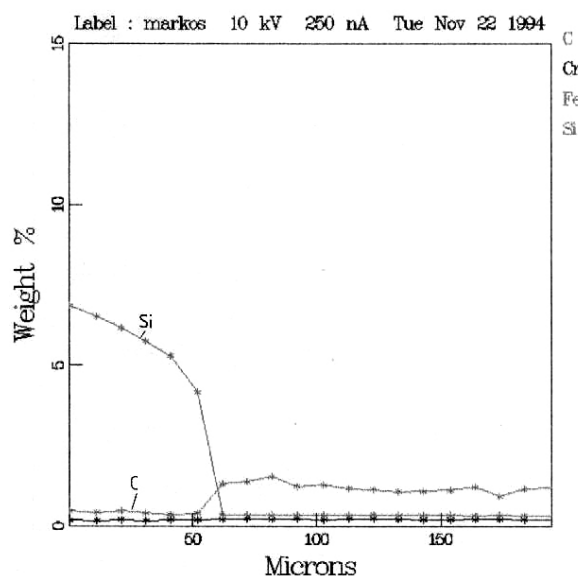


Fig.5. Carbon and silicon repartition for OLC 45 steel siliconized in powder medium with paste 1000°C, 2 hour

Watching the microstructures of two siliconized steels OLC 45 (at low pressure 1050°C, at 0.5 hour, whit 70 ml/hour  $\text{SiCl}_4$  – Fig.2. and siliconized in powder medium with paste at 1000°C, 2 hour – Fig.4.), we can observe that at siliconizing at low pressure in gas medium more compact layer was obtained, comparing with the case of powder medium with paste siliconizing. At powder medium siliconized, we can observe the presence of relative big porosities (Fig.4.).

At gas medium siliconized, the silicon percentage is approximately the same in the diffusion layer (Fig.3.). At pulverous medium siliconized, the silicon repatriation in the diffusion layer is not uniform (Fig.5.).

### 4. CONCLUSIONS:

At siliconizing in gas medium, an increased saturation speed was obtained and the layer is more compact and adherent. At treatments made in gas at low pressures, the sample's surfaces remain clean even for treatments made at high temperatures. Thanks to constant silicon potential during the treatment, the silicon repartition in diffusion layer is very uniform.

The siliconizing in gas medium at low pressures assures the obtaining of very good results and a very easy control of work parameters. In the same time, the method reclaims very expensive and complex equipment.

*Received April 26, 2005*

*University TRANSILVANIA of Brasov*

#### REFERENCES

- /1/. Bradley, B., Jellinek, M.: *Production of silicon metal from dichlorsilane*. Brevet no.3824121/16.08.1974. USA
- /2/. Markos, Z., Munteanu, Al., *Consideration sur la cinetique et mecanism de la diffusion du silicium dans les acieres*, 9e Congres International du Traitement Thermique 28-29.09.1994. NISA-France
- /3/. Markos, Z., Banciu, R.: *Research regarding the treatment temperature for steel siliconizing*. Romanian Journal of Engineering, University "Ovidius" of Constanta, 1999.

#### CERCETĂRI CU PRIVIRE LA SILICIZAREA OȚELURILOR ÎN MEDIU GAZOS LA PRESIUNI JOASE

**Rezumat:** Lucrarea prezintă rezultatele unor încercări de silicizare cu  $\text{SiCl}_4$  la presiuni joase. Tratatamentul termochimic de silicizare în mediu gazos asigură o viteză ridicată de difuzie a siliciului, straturi de difuzie compacte și aderente, precum și obținerea unor suprafețe curate la piesele tratate.

Deoarece la presiuni joase gazul activ ( $\text{SiCl}_4$ ) se evaporă la temperatura ambiantă, prin termostatarea lichidului putem asigura un debit uniform în timpul tratamentului. Pentru diluarea gazului activ s-a utilizat atât gaz inert (Ar) cât și gaz activ ( $\text{H}_2$ ). În cazul silicizării la presiuni joase, nu apar aderențe pe suprafața piesei nici în cazul tratamentelor executate la temperaturi ridicate.

Silicizarea în mediu gazos, la presiuni joase, asigură obținerea unor piese tratate de foarte bună calitate precum și un control facil și riguros ai parametrilor tratamentului termochimic. Procedul presupune utilizarea unei instalații destul de complexe și scumpe.

## STUDY CONCERNING THE PROPERTYS OF DIFFUSION LAYERS AT BRONZE SILICONIZING

BY

ZOLTAN MARKOS

**Abstract.** *The paper shows some test results about siliconized biphasic Sn bronzes. The main of thermochemical treatment siliconizing appliance for Cu-Sn alloys is to obtain some structure components in diffusion layer with higher mechanical characteristics and a better wear and corrosion resistance. The siliconizing process has been come out in sealed boxes, in a pulverous environment with paste. Within the interval 600...650°C, is possible to obtain a diffusion layer where the content of Si should approach the silicon solubility limit in a copper (5.3-5.4% Si). The layer is made by a solid solution  $\alpha$ , where silicon atoms replace the majority of Sn atoms. The experimental research tried to verify if the static friction coefficient could be an indicator for the appraisal of wears behavior. The obtained structures in the layer composed by Cu-Si-Sn solid solution and chemical compounds ( $Cu_3Si$ ,  $Cu_5Si$ , etc.) are ameliorating the friction coefficient.*

**Keywords:** *bronze siliconizing, diffusion layer properties*

### 1. INTRODUCTION

The special alloyed bronzes with Si, besides the high mechanical properties, show a very good corrosion resistance in different acids, alkali, seawater, etc. The main of thermochemical treatment siliconizing appliance for Cu-Sn alloys is to obtain same structure components in diffusion layer with higher mechanical characteristics and a better wear and corrosion resistance. Some examples of such components are: gears, buses, plain bearing, etc.

The siliconizing process has been come out in sealed boxes, in a pulverous environment with paste. To carry out the experimental tests, there have been utilized prismatic samples (10x10x12 mm), made of Cu-Sn14 STAS 197/1-80.

The active paste has been obtained at ferro-silicon (with 73% Si, having a granulation smaller than 0.2 mm) with soda waterglass ( $Na_2O.nSiO_2$ ). The activating agent employed was ammonium chloride. The experimental tests have been done in furnace at different temperatures during a four hours time length.

The experimental research tried to verify if the static friction coefficient could be an indicator for the appraisal of wears behavior. The tribometer used for the determination of these coefficients functions is in the principle of inclined plan.

### 2. EXPERIMENTAL RESEARCH RESULTS

After the thermochemical treatment at different temperatures (600°C, 650°C and 700°C), the diffusion layer have been checked in some microsections there have been created, in order to carry out the research of the optic microscope and electron probe microanalyser. Also, the microhardness of constituents had been measured.

The obtained structures in the layer, composed by Cu-Si-Sn solid solution and chemical compounds ( $\text{Cu}_3\text{Si}$ ,  $\text{Cu}_5\text{Si}$ , etc.), are ameliorating the friction coefficient. The Fig.1. is showing the microstructure of bronze siliconized at  $650^\circ\text{C}$  and the Fig.2. present the microstructure of sintered bronze siliconized.

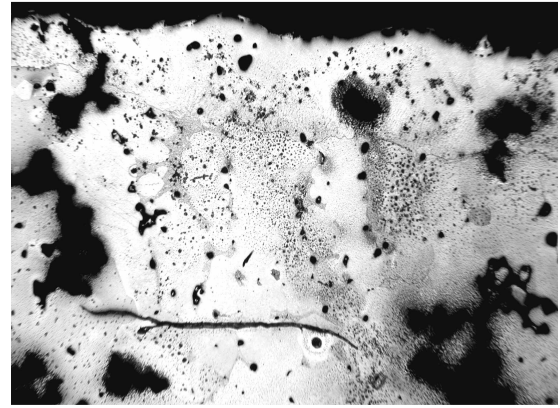
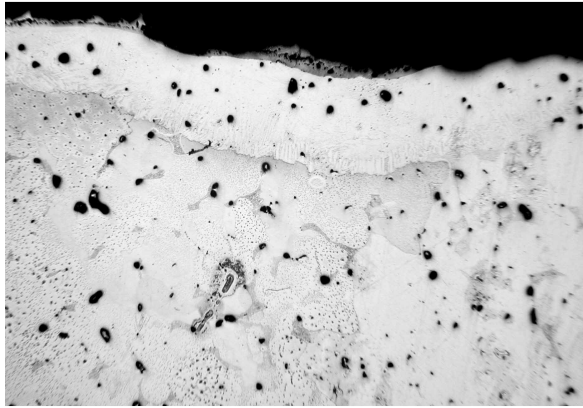


Fig.1. CuSn14 microstructure siliconized at  $650^\circ\text{C}$ , 4 hours, 150 X

Fig.2. Sintered bronze microstructure siliconized at  $650^\circ\text{C}$ , 4 hours, 150 X

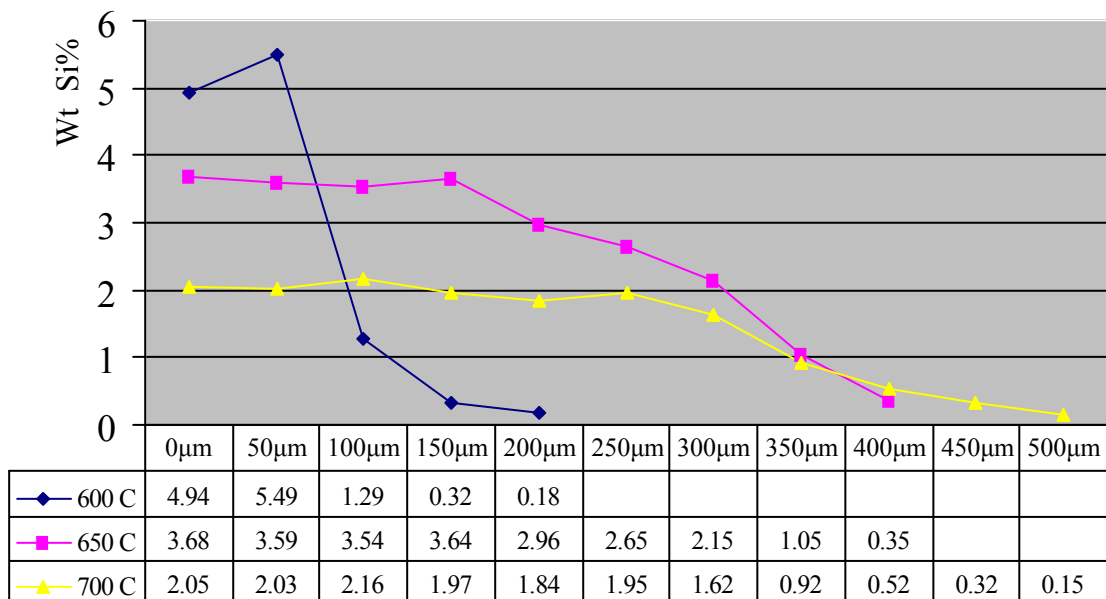


Fig.3. Si repartition in diffusion layers at different siliconized temperatures

The electron probe microanalysis results, for the samples siliconized at different temperatures, are presented in Fig.3.

Within the  $600^\circ\text{C}$  (Fig.4.), it is possible to obtain a diffusion layer of which the content of Si should approach the silicon solubility limit in a copper (5.3-5.4% Si). The layer is made by a solid solution  $\alpha$ , where silicon atoms replace the majority of tin atoms. The microhardness is within the interval 247...199  $\mu\text{HV}$ .

At  $700^\circ\text{C}$ , the silicon concentration in layer is smallest (Fig.5) and the microhardness is within the interval 157...133  $\mu\text{HV}$

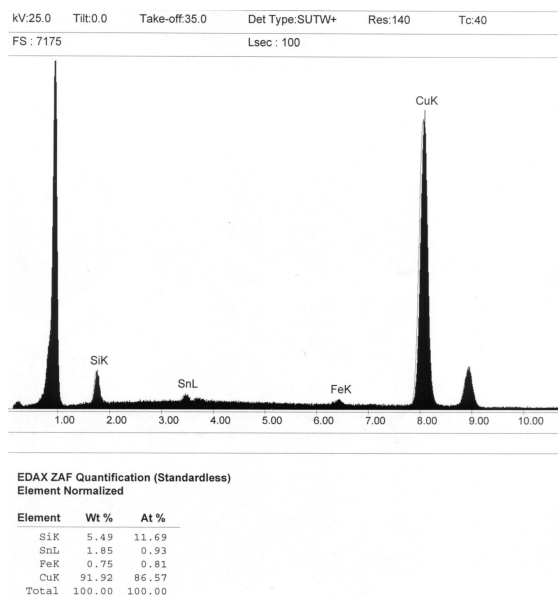


Fig.4. Microanalysis result at 600°C

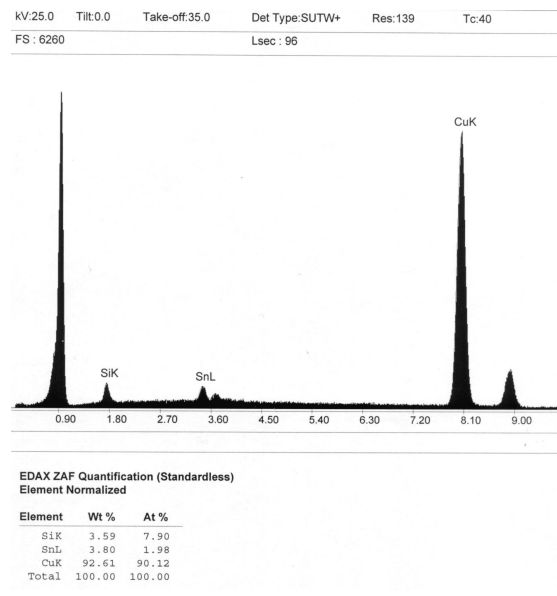


Fig.5. Microanalysis result at 700°C

At the determination of static friction coefficient, the tribosystem is composed of two material bodies, moving relatively, and submitted to given charges in a known environment. For the mobile semi-couple there were used siliconized and non-treated bronzes. The results of experimental tests are presented in Tab.1. Using treated semi-couple, the siliconizing of the CuSn14 alloy lead to the decrease of the friction coefficient.

Tab.1.

Characteristics of the fixed couple	Characteristics of the mobile couple	Values of the static friction coefficient		
		Min.	Max.	Average
OLC 45 Hardening and tempering at 560°C	Siliconizing CuSn 14	0.1824	0.1923	0.1879
	Molten CuSn 14	0.2782	0.2856	0.2820
OLC 45 Normalization 850°C/air	Siliconizing CuSn 14	0.1852	0.1936	0.1895
	Molten CuSn 14	0.2488	0.2672	0.2520

In conclusion, through siliconizing, there can be obtained adherent and compact diffusion layers. The temperature must be approximate at 600°C, in order to obtain a diffusion layer of which the content of Si should approach the silicon solubility limit in copper (5.3...5.4%) and a high hardness (247...199  $\mu$ HV). The layer is made of solid solution  $\alpha$ , where silicon atoms replace the majority of tin atoms. The obtained structures in the layer composed by Cu-Si-Sn solid solution and chemical compounds ( $\text{Cu}_3\text{Si}$ ,  $\text{Cu}_5\text{Si}$ , etc.) are ameliorating the friction coefficient.

Further more, it is imposed that the execution of some wear and corrosion tests, in order to establish the silicon optimum concentration within the diffusion layer.

*Received April 26, 2005*

*University TRANSILVANIA of Brasov*

#### REFERENCES

- /1/. Z. Markos, R.G. Florea, L. Balteş, R. Popescu, *Studii și cercetări privind silicizarea bronzurilor* Conferința Internațională BRAMAT 2001 –Brașov, Vol.II. pag.341-344 ISBN 973-8124-15-8/973-8124-17-4
- /2/. Massalski, T. B., *Binary Alloy Phase Diagrams* - Second Edition - ASM International - USA 1990
- /3/. Z. Markos, P.J. Szabo, *The influence of temperature on diffusion mechanism at bronze siliconizing*, International Conference on Materials Science and Engineering BRAMAT 2003 Brasov

#### STUDIUL PROPRIETĂȚILOR STRATURILOR DE DIFUZIE LA BRONZURILE SILICIZATE

**Rezumat:** Lucrarea prezintă rezultatele unor încercări cu privire la straturile de difuzie a pieselor silicizate. Tratatamentul termochimic de silicizare se aplică la bronzurile cu Sn în vederea obținerii unor straturi de difuzie cu proprietăți mecanice îmbunătățite, straturi care prezintă rezistențe ridicate la uzură și la coroziune. Tratatamentul de silicizare s-a realizat în cutii închise etanș, în mediu pulverulent cu pastă. La temperaturi relativ mici (600...650oC), este posibilă obținerea unor concentrații ridicate de Si în stratul de difuzie, valorile apropiindu-se de solubilitatea maximă a siliciului în cupru (5,3.....5,4%). Structura stratului de difuzie este formată dintr-o soluție solidă  $\alpha$ , unde atomii de Si înlocuiesc majoritatea atomilor de Sn. S-au determinat pe cale experimentală coeficienții de frecare statică, atât pentru bronzurile silicizate cât și pentru cele netratate, caracteristici care indică modul de comportare a pieselor la uzură. Structurile obținute în stratul de difuzie, cum ar fi soluția solidă ternară Cu-Si-Sn și compușii chimici ( $\text{Cu}_3\text{Si}$ ,  $\text{Cu}_5\text{Si}$ , etc.), conduc la creșterea rezistenței la uzare

## DETERMINATIONS OF MECHANICAL TESTING AND CORROSION TESTS OF THE TITANIUM ALLOYS TI GRADE 2 AND TI GRADE 12

BY

MIHAI BUZATU<sup>1</sup>, VALERIU GABRIEL GHICA<sup>1</sup>, IOANA PÂRVAN<sup>2</sup>, DANIELA DUMITRESCU<sup>3</sup>, STELIANA IVĂNESCU<sup>3</sup>

**Abstract.** *To ensure safety of final warehouse/yards of burnt fuel, are required many barriers. The material of which the storage container wall is made, interact with the environment where it is placed, through a number of processes of which a special attention is given to the corrosion one. Among container materials for final storage of burnt nuclear fuel in saline environment there are also considered titanium, due to their resistance to corrosion beside Hastelloy C4 a.o. In our paper, the materials tested on corrosion were titanium alloys: Ti Grade 2 and Ti Grade 12. The paper includes determinations of mechanical testing and corrosion tests (chemical tests speeded in boiling concentrated HNO<sub>3</sub>, according to ASTM A-262; chemical tests accelerated in 6 % FeCl<sub>3</sub> at 50 ± 2 °C, according to ASTM G 18) performed on delivery state-materials and welded joints. The titanium alloys selected, were smelted at the IMNR and welded joints were made within the Nuclear Research Branch-Pitesti, using different technological parameters during welding. The characterization of corrosion behavior of tested samples was based on determinations of mechanical tests (hardness, tensile strength), gravimetric determinations (corrosion rates) and metallographic microscopy determinations (microstructural characteristics, corroded sample appearance) The corrosion tests were performed on delivery state materials and welded joints. The welded joints on the two titanium alloys were made in SNC Pitesti. To achieve welded joints, the same welding technique was used, but the welding parameters were different. By interpretation and correlation of experimental results achieved, corrosion susceptibility of the two alloys (Ti Grade 2 and Ti Grade 12) in delivery – and welded states, was determined and data required for identifying corrosion mechanism were obtained, useful to estimate the corrosive process dynamics..*

**Keywords:** *titanium, titanium alloys, characterization, corrosion*

### 1. INTRODUCTION

Titanium is a passive material, which protects itself with an oxide film. The typical oxide constituted – TiO<sub>2</sub>, is very chemically resistant; it could be attacked just by HCl, H<sub>2</sub>SO<sub>4</sub>, NaOH and HF hot, concentrated solutions. Because this layer remains intact, the corrosion is uniform and slow. It varies between 0.1 ÷ 1 μm/year, depending on chlorine content and temperature.

The nature, the composition and the thickness of the oxide film formed on the titanium alloys depend on the environment conditions. Therefore, for the solutions assignation, even at a conceptual level, it must be known the material corrosion behavior in the storage medium in normal condition of practice and accident conditions. The interest is the trigger action mode of the uniform and local corrosion forms and particular, their evolution in time and the influence on the piece integrity.

Not just the material, appropriate sizes and wall thickness choosing is important but also the welded joints system choosing requires attention because of the corrosive process intensifications in the thermal influenced areas by welding.

The corrosion behaviour of the welded joints is influenced by the alloying elements and the alloy contaminants, by the microstructural modifications and by the technological proceedings used.

The weld area acts like a heterogeneous material in chemical, structural and behavior properties point of view, with residual tensions and deformations caused by the dilatations and compressions more or less connected with heating cycles and number of passes. In point of corrosion, a welding can be uniform or preferential corroded in the welded metal or in the thermal influenced area.

The welding area can corrode more or less than the basic metal, depending on composition area, or metallurgical conditions (for example: the secondary phase structure or precipitation, inclusions, etc).

Further, the thermal influenced area, heated during welding, can corrode as a result of metallurgical changes caused by welding heating cycles.

The influence factors of welding corrosion are:

- the basic metal and the addition metal composition and structure;
- the basic metal metallurgical conditions before and after the welding (thermal and mechanical process);
- the welding process in point of energy source (WIG, MIG, laser electron flux) and the equipment;
- the composition and the speed of the welding gases;
- the size and the geometry of the welded material.

## 2. EXPERIMENTAL RESULTS

The titanium alloys selected, were smelted at the Institute of Rare Non-Ferrous Metals (IMNR) Bucharest and welded joints were made within the Nuclear Research Branch-Pitesti, using different technological parameters during welding.

The studies make the object of a research contract concluded with CCEEM Bucharest.

The corrosion tested materials were titanium alloys: Ti gr.2 and Ti gr.12. The raw material for obtaining these alloys was titanium sponge TG100 with the following chemical composition: 0.02 % N; 0.03 % C; 0.07 % Fe; 0.02 % Si; 0.05 % Ni and 0.04 % O.

For Ti gr.12 alloy has been used nickel as an alloying element of 99.98 % purity as a small filing, degreased with perchloroethylene air dried.

The materials were delivered as milled plates at the size of 6x100x100 mm and as wire with a section of 2.5x2.5 mm. Ti gr.2 alloy was delivered in the initial state: plastic deformed, and Ti gr.12 alloy: annealed.

The chemical composition was determined by the producer using assays from titanium bar, and it is presented in Table 1.

Table 1. Chemical composition of titanium alloys tested.

Alloy type	Chemical composition (%)								
	C	N	O	H	Fe	Mo	Ni	Pd	Ti
Ti gr.2	0,034	0,009	0,068	-	0,043	-	-	-	rest
Ti gr.12	0,021	0,015	0,075	-	0,031	0,30	0,85	-	rest

The corrosion tests were performed on delivery state materials and welded joints. The welded joints on the two titanium alloys were made in SNC Pitești.

To achieve welded joints, the same welding technique was used, but the welding parameters were different.

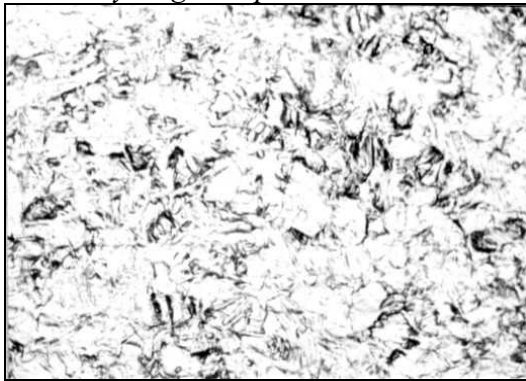
The welding method was arc V butt weld under inert gas – WIG (Wolfram Inert Gas) with filler material.

Thoriated tungsten electrodes of  $\phi = 2.5$  mm were used. The titanium reduced heat conductance favorable the obtainment of a narrow and the deep bead welding.

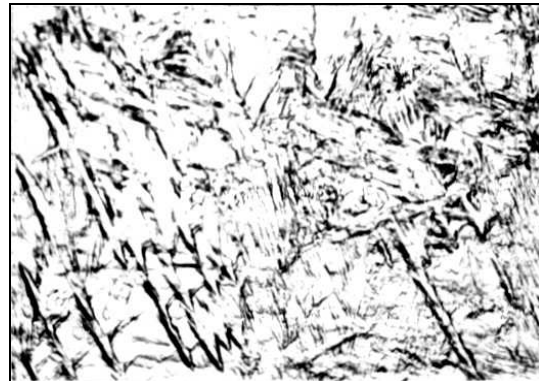
After welding the Ti Grade 2 plates 2, 3 and 5 were annealed. The annealing treatment for establishing the structure was made in vacuum furnace at the following parameters: 10–5 torr vacuum, annealing temperature – 650 0C, time of exposure in plateau – 15 minutes and free cooling for about 120 minutes.

The welded joints were examined by metallographic microscopy (fig.1 and fig.2).

*Alloy Ti gr.2 – plate 5*



a) basic material zone (x 200)



b) heat influenced zone (x 200)



c) welding zone (x 200)

Fig. 1. The aspect of structure on Titanium gr.2, plate 5 samples.

The structure is made on  $\alpha$  phase with polyhedral aspect in basic material zone (Fig. 1.a),  $\alpha$  phase with lamellar aspect in heat influenced zone (Fig.1 b), and  $\alpha$  phase with polyhedral aspect and macle tendency in welding zone (Fig.1 c).

The structure of basic material is made on  $\alpha$  phase with lamellar aspect, with small lamellas and tendency to seating in column forms (Fig. 2.a). Some local heterogeneity with precipitate shape is present. In the heat influenced zone the lamellas are bigger and heterogeneity more evident than in basic material (Fig.2.b). In

the welding zone the  $\alpha$  phase lamellas are greater and seating in column forms (Fig.2.c).

The results of hardness measurements are presented in Table 2.

*Alloy Ti gr.12 – plate 13*

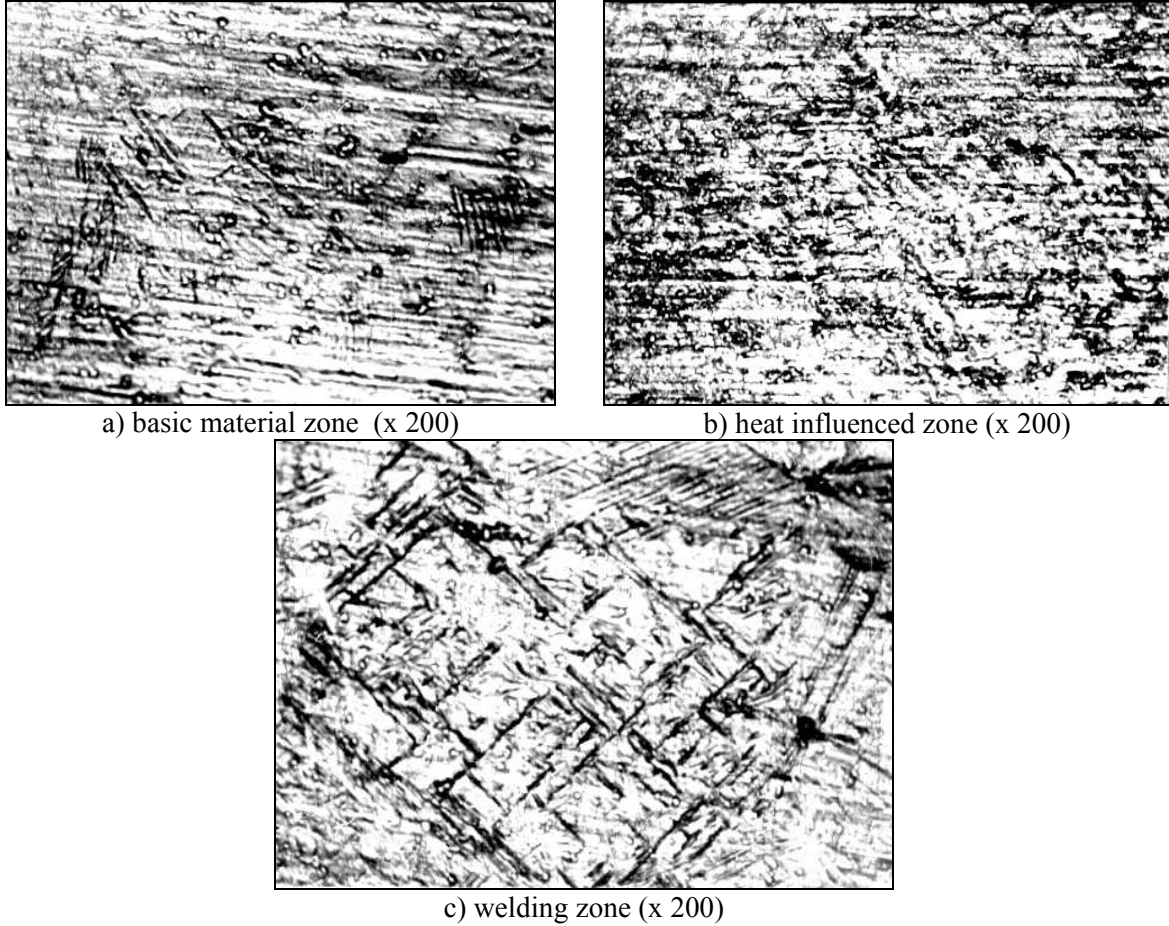


Figure 2. The aspect of structure on Titanium gr.12, plate 13 samples.

Table 2. Vickers hardness determinations values on alloys Ti Grade 2 and Ti Grade 12.

Zone	Print	Vickers hardness (HV)									
		Alloy Ti gr. 2								Alloy Ti gr. 12	
		Plate 5		Plate 6		Plate 7		Plate 8		Plate 16	
		A	B	A	B	A	B	A	B	A	B
Basic material	I	170	181	181	170	170	170	181	181	181	193
	VII	181	193	193	-	181	-	193	-	206	-
Welding zone	III	181	193	221	-	322	-	274	-	206	-
	IV	221	236	236	221	322	383	351	322	351	383
	V	181	181	206	-	274	-	221	-	206	-
Heat influenced zone	II	180	181	193	193	160	193	181	181	160	193
	VI	193	181	193	-	166	-	193	-	170	-

A – Values before corrosion testing

B – Values after corrosion testing

Mechanical breaking characteristics determined on titanium alloy welded samples are presented in Table 3.

Table 3. Mechanical breaking characteristics determined on titanium alloy welded samples.

Sample type	Breaking zone	F <sub>r</sub> (Kgf)	A <sub>med</sub> (mm <sup>2</sup> )	$\sigma_r = F_r / A_{med} \times 9,8$ (N/mm <sup>2</sup> )
Ti gr.2 plate 6	BM	1335	34,72	377
	BM	1322,5	34,77	373
Ti gr.2 plate 7	HIZ	1365	35,65	375
	HIZ	1255	33,11	371
Ti gr.2 plate 10	HIZ	1365	34,70	385
	BM	1345	33,43	394
Ti gr.2 plate 10	HIZ	1562,5	35,41	432
	HIZ	1725	35,15	476

BM – basic material; HIZ – heat influenced zone; S – welding zone;  $\sigma_{rmin} = 350$  N/mm<sup>2</sup> – Ti gr.2;  $\sigma_{rmin} = 480$  N/mm<sup>2</sup> – Ti gr.12;

Based on the chemical test performed in boiling concentrated HNO<sub>3</sub>, the average rates of generalized corrosion determined on welded samples were found to be generally a little higher than those determined on the samples taken from the delivery state material.

Regarding samples taken from the alloy Ti gr. 12 – plate 16, the corrosion rates determined on welded samples were however equal to those determined on the samples from delivery state material (Table 4a and 4b).

Table 4a. Average corrosion rates (mm/year) for samples tested in boiling HNO<sub>3</sub>

Tested sample type		Average corrosion rate by a different testing times (mm/year)	
		Cycle I (48 h)	Cycle II (96 h)
Titanium gr.2 Plate 5	Blank tests	0.122223	0.140951
	Welded samples	0.113867	0.209132
Titanium gr.2 Plate 6	Blank tests	0.113060	0.105910
	Welded samples	0.092523	0.115867
Titanium gr.2 Plate 7	Blank tests	0.097688	0.123948
	Welded samples	0.084933	0.107689
Titanium gr.2 Plate 10	Blank tests	0.100527	0.103092
	Welded samples	0.092157	0.106268
Titanium gr.12 Plate 16	Blank tests	0.157429	0.161127
	Welded samples	0.161117	0.193291

Table 4b. Average corrosion rates (mm/year) for samples tested in boiling HNO<sub>3</sub>

Tested sample type		Average corrosion rate by a different testing times (mm/year)		
		Cycle III (144 h)	Cycle IV (192 h)	Cycle V (240 h)
Titanium gr.2 Plate 5	Blank tests	0.155266	0.149302	0.130534
	Welded samples	0.243018	0.238977	0.205929
Titanium gr.2 Plate 6	Blank tests	0.099204	0.090759	0.074158
	Welded samples	0.148209	0.1504535	0.131952
Titanium gr.2 Plate 7	Blank tests	0.149537	0.119221	0.096028
	Welded samples	0.144119	0.123716	0.102542
Titanium gr.2 Plate 10	Blank tests	0.117024	0.092002	0.071804
	Welded samples	0.127511	0.100245	0.078971
Titanium gr.12 Plate 16	Blank tests	0.164336	0.130639	0.147447
	Welded samples	0.21388	0.172407	0.142590

Note: Blank tests correspond to the state material.

### 3. CONCLUSIONS

The hardness measurements made before corrosion testing revealed that welded joints of both alloys (Ti Grade 2 and Ti Grade 12) had the highest hardness values. Welded parameters: welding electricity (Is) = 170A, argon flow rate of the spraying gun (Q1) = 12l/min, argon flow rate of the device (Q2)= 14l/min,  $\phi$  addition material (dMA) = 3mm, number of passes (ntr) =2,  $\phi$  wolfram electrode (dw) = 2,5mm and V joint (b) = 0.

After corrosion testing, the hardness of basic material and heat influenced zone stayed almost constant, while hardness increased by about 20:60 units HV.

Breaking in the alloy Ti Grade 2 took place at a breaking stress higher than the one minimum accepted Ti Grade 12, breaking occurred in general, at stresses lower than the one minimum accepted (480 N/mm<sup>2</sup>).

Breaking occurred both in the basic metal and in the heat influenced zone.

Susceptibility to generalized corrosion in boiling concentrated HNO<sub>3</sub>, determined on welded joints was a little higher than one determined on the delivery state material.

The welded joints of the alloy Ti Grade 12 were more susceptible to generalized corrosion than the welded joints of alloy Ti Grade 2.

Received April 19, 2005

<sup>1</sup>"Polytechnic" University of Bucharest

<sup>2</sup>R.A.A.N. – S.C.N. Pitești,

<sup>3</sup>Non Ferrous and Rare Metals Institute, Pantelimon - Ilfov

### REFERENCES

- /1/. E. Smailos, R.Koster, *Corrosion Studies on Selected Packaging Materials for Disposal of High Level Wastes*, IAEA-TECDOC-421, Vienna, (1987);
- /2/. B.M.Ikeda, M.G.Bailey, *Crevice Corrosion of Titanium under Nuclear Fuel Waste Conditions* AECL – 9568, (1989);
- /3/. D.W.Shoesmith, *Corrosion of Nuclear Fuel Waste Containers Proceedings of a Workshop*, AECL – 10121, (1990);
- /4/. D.W.Shoesmith, B.M.Ikeda, M.J.Quinn, *Estimating the Lifetimes of Titanium Containers for Nuclear Fuel Waste: A.Damage Function for the Crevice Corrosion of Grade-2, Titanium*, AECL-11255, (1995);
- /5/. James J.Noël, M.Grant Baitey, *Hydrogen Absorption by Grade-2, Titanium*, AECL – 11608, (1996);
- /6/. D.W.Shoesmith, F.King, B.M.Ikeda *An Assessment of the Feasibility of Indefinite Containment of Canadian Nuclear Fuel Wastes*, AECL – 10972 (1995).

### CARACTERISTICI DETERMINATE PRIN TESTE MECANICE ȘI DE COROZIUNE ALE ALIAJELOR DE TITAN TI GRADE 2 ȘI TITAN GRADE 12

**Rezumat:** Lucrarea prezinta caracteristicile mecanice și de coroziune obținute prin testarea aliajelor de titan Ti Grade 2 și Ti Grade 12, obținute la IMNR. Sudarea acestora a avut loc prin diverse procedee, fiind executată la Filiala de cercetări nucleare de la Pitești.

## SOME ASPECTS CONCERNING THE DURABILITY OF ADHESIVE JOINTS

BY

FLORENTINA MOCANU, PAUL DORU BARSANESCU

**Abstract.** *In more recent years there has been a rapid development of adhesive bonding as an economic and effective method for the fabrication of various components and assemblies. The strength and toughness of adhesive bonded joints is known to be very sensitive to environmental exposure. Joint strength and toughness values can decrease significantly upon exposure to water and, as this represents the most common service environmental, techniques to assess the long term performance of joints in this environment, to assess the durability of the joint. The purpose of the current work is the study of adhesive joints durability in hostile environments. An accelerated durability test was performed using joints adhesives. The present paper discusses the results of some investigations, which had in view the establishment the adhesive joints durability. Both an epoxy and a cyanoacrilat adhesive were employed in this study. The variation of the static strength and the breaking energy under impact loading of the joints is study..*

**Keywords:** *adhesive joints, durability, relative humidity, polymeric resins, static strength, hostile environments, impact loading, dynamic strength, metallic substrates*

### 1. INTRODUCTION

The use of substances to bond materials together is well established. Egyptian carvings dating back more 3.000 years show the gluing of thin veneers to planks of sycamore. The gold leaf of illuminated manuscripts was bonded to paper by egg white and wooden objects were bonded with glues from fish, horn and cheese. The technology of animal and fish glues advanced during the 18<sup>th</sup> century. In the 19<sup>th</sup> century rubber and cellulose based adhesive were introduced. Decisive advances in adhesive technology waited the 20<sup>th</sup> century, during which time natural adhesives were improved and many synthetic polymers were developed.

In more recent years there has been a rapid development of adhesive bonding as an economic and effective method for the fabrication of various components and assemblies. With the development of new structural adhesives, adhesive joints of machine elements have been paid attention instead of conventional joints, such as bolted and riveted joints. Adhesive bonding of thin metallic plates is increasingly used as a substitute for brazing or welding. The use of adhesives offers advantages in comparison with conventional techniques such as brazing, welding, riveting, bolting, etc. Some of the advantages are:

1. the ability to join efficiently thin sheets, or dissimilar materials;
2. an increase in design flexibility;
3. an improved stress distribution in the joint, which leads to an increase in fatigue resistance of the bonded component;
4. enable the fabrication of complex shapes not feasible by other fastening means;

5. a convenient and cost effective technique [1].

## **2. GENERAL CONSIDERATIONS**

An adhesive is a substance capable of holding materials together by surface attachment. It defines the adhesive as a material which when applied to substrate surfaces can join them together and resist separation. The principal attribute of adhesive is their ability to form strong bonds with surfaces of a wide range of materials and to retain bond strength under expected use conditions.

The adhesion between adhesive and substrate is based on physical and chemical interactions at the interface. The demand for adhesives that had a high degree of structural strength and were resistant to both fatigue and environmental conditions led to the development of many high performance materials [2].

The strength and toughness of adhesive bonded joints is known to be very sensitive to environmental exposure. Joint strength and toughness values can decrease significantly upon exposure to water and, as this represents the most common service environmental, techniques to assess the long term performance of joints in this environment, to assess the durability of the joint. Such techniques should allow engineers to assess the level of deterioration of adhesive joint performance with respect to the service environment and to enable the optimization of an adhesive joint system (the combination of the substrate, adhesive and surface pre-treatment, to provide the best durability in a given environment).

The growing demands of high performance for structural applications and the use of relatively expensive specialty products in high technology components suggested a need for better understanding on the amount of adhesive required [3].

## **3. EXPERIMENTAL RESULTS**

### **3.1. Static Loads**

Fracture mechanics has proved to be a very valuable tool in the study of adhesive joint durability. Well defined toughness parameters may be measured before, during and after exposure to hostile environment. Any deterioration in joint toughness can thus be quantified and this information can be coupled with a detailed examination of the fracture surfaces after the test to identify the failure path and the likely mechanisms of environmental attack [4].

The residual toughness of the adhesive joints manufactured and then immersed in distilled water in an unstressed state was determined. Joints are then periodically removed from the immersion tank and tested using standard fracture mechanics tests and the residual toughness determined together with the locus of joint failure.

Such tests are frequently accelerated by increasing the temperature of the immersion tank to a value greater than would be expected in service, to increase the rate of water diffusion into the joint and thus accelerate the degradation. Some dangers are introduced by this temperature acceleration and it very important that the higher temperature that would not exist at the service temperature does not induce different failure mechanisms [5,6].

The epoxy adhesive and the cyanoacrilat adhesive used in this study have performed well under static and dynamic loads. Epoxy adhesive, which are strengthened at normal temperature, which is the case of the adhesive under study too,

are constituted of two components, after the mixing of which polymerization occurs. Strengthening agents of amine-type (which represents also the case of the example considered) produce an exothermal reaction, accompanied by a sufficient release of heat, capable to assure drying at room temperature.

The cyanoacrilat adhesive is one-part, heat curing adhesive witch is particularly suitable for steel-steel bonding. The adhesives were selected because of their suitability in civil engineering type applications. The material properties are shown in table 1 [2].

**Table 1.** Material constants of the adhesive and substrate used

Material	E [GPa]	$\nu$
Cyanoacrilat adhesive	11.3	0.22
Epoxy adhesive	14.5	0.25
Substrate	210	0.3

where: E - Young's modulus;

$\nu$  - Poisson's ratio.

The relation giving the static strength of the adhesive joints has the form:

$$\tau_r = \frac{F_{\max}}{l_s \cdot b} \quad (1)$$

where:  $F_{\max}$  – the maxim consumed for breaking the joint load;

$l_s$  - overlap length;

b – width substrate [1].

The static strengths are obtained in a testing machine (Hekert Eus, 200kN). Generally adhesive strengths are measured using a single lap-shear test specimen as shown in figure 1. The single lap joint is most commonly used for assessing the shear strength of adhesive-bonded joints in practice because of its simplicity. The most simple strength evaluation method of this test specimen is given by the average shearing stress at fracture. In this case the stress concentrates at the bonding edges and this concentration differs depending on the specimen's shape. Thus, this strength evaluation method cannot be applied to other shape adhesive structures.

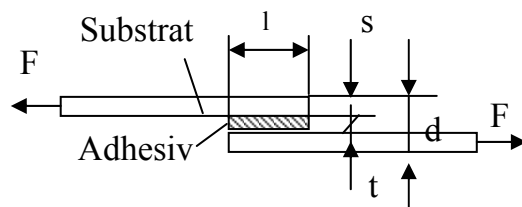


**Figure 1.** Schematic shape and dimension parameters of adhesive single-lap joints

In figure 1 dimension parameters represents: l - lap length; t - adhesive layer thickness; s - substrate thickness.

The supports have  $25 \pm 0.25$  mm width and for all joints. The overlap length was 12.5 mm, with a thickness of 0.5 mm. The thickness of the adherent was 8 mm. Plane strain conditions were assumed and creep in the adherents was considered to be negligible. A uniform load was applied at the end of the specimen. The tests employed

joints of single lap, as recommended by ISO 4588-89. Steel supports have been employed, the joints being realized with a Romanian adhesives, produced at the "P. Poni" Institute of macromolecular chemistry of Iassy. Setting of the samples in the testing machine should assure the axial orientation of the load's application. That is why, on the supports' ends some intermediary plates, with a thickness equal to that of the testing support, have been fixed.

The strength values have been determined through their test to traction up to the breaking, of some joints, as a result of the application of a longitudinal traction effort upon them, in parallels with the joining surface and with the sample's main axis.

All tests have been made on a universal test machine, the testing speed of which had been adjusted so that the joint should be broken over the  $65\pm 20$  sec. time interval as recommended by the norms.

For the tests a lot of 190 samples has been used, with supports made of steel. The supports' surfaces have been prepared prior to fixing according to ISO 4588-89. Good adhesion between adhesive and specimen can only be achieved after intensive pretreatment of the specimen surface. Therefore all specimen surfaces were pretreated by hand abrasion followed by cleaning with methyl ethyl ketone. In addition, some specimens were also stored in 55% concentration nitric acid for 8 minutes and afterwards rinsed intensively with water to reduce corrosion. All specimens were dried for 24 hours in an oven at room temperature before bonding. An accelerated durability test was performed using joints adhesives. Tests have been performed on single lap shear specimens in order to compare the performance of different adhesive joint. Overlap length and substrates thickness have been constant. Joints were submerged in distilled water at  $60^{\circ}\text{C}$  for periods of up to one year. Joints were periodically removed from the environment and tested to measure the value of shear stresses at break for the joint and to observe the locus of the joint failure

The values of shear stresses measured for these joints were then expressed as a % retention of the  $60^{\circ}\text{C}$  dry stress value. A number of unexposed dry joints had been post-cured at  $60^{\circ}\text{C}$  for periods of up to 18 days to determine the fully post-cured values of stress. These joints were then tested at  $23\pm 1^{\circ}\text{C}$  and 55% relative humidity.

### **3.2. Impact Loading**

The dynamic strength of the adhesive joints is also very important. Especially, as the adhesively bonded joints are widely used in aircraft and automobile structures, the crash worthiness of the products has been proved. Thus, the strength of the bonded joints subjected to high-rate load should be investigated.

The joint strength of structural adhesives under impact loading has recently attracted a great deal of attention with their widespread use in industrial applications. Adhesive bonding has become increasingly important as an almost indispensable structural joining technique in applications requiring lightweight designs such as in aeronautical and automotive industries.

The static and the dynamic strength was determined taking into account a series of working hypothesis such as:

- the thickness of the adhesive layer is constant;
- the adhesive layer thickness is small as compared with the supports;
- the adhesive is more flexible than the support material.

The experiments were conducted using a pendulum- type impact machine. The tests employed joints as recommended by ISO 9653-91. Steel supports have been employed, the joints being realised with the epoxy and cyanoacrilat adhesives. The adherents were made of the same carbon steel. For the tests a lot of 190 samples has been used. The thickness of the adhesive layer was approximately 200  $\mu\text{m}$ . The supports' surfaces have been prepared prior to fixing according to ISO 4588-89.

The specimens used for the research were configured as shown in figure 2.

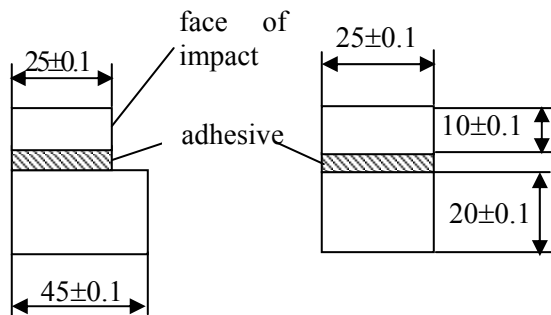


**Figure 2.** Schematic specimen of adhesive joints.

The relation giving the dynamic strength of the adhesive joints has the form:

$$R_n = \frac{W}{S} \quad (2)$$

where:  $W$  - the maxim energy consumed for breaking the joint;  $S$  - bonded area of the joint specimen [1].

#### 4. CONCLUSIONS

The results obtained are indicated the following conclusions:

- 1) The results clearly demonstrate the very deleterious effect of water immersion on the toughness of all joints studies. Is evident from this study that the durability was clearly different for the two adhesives employed;
- 2) for the joints exposed for periods for up to one year all failures remained cohesive in the adhesive layer and the retained toughness values after one year of exposure were 70% for the epoxy adhesive and 50% for the cyanoacrilat adhesive;
- 3) the joints with cyanoacrilat adhesive showed a much steeper decline in toughness values and this decline was accompanied by a change in the locus of failure from cohesive in the adhesive to interfacial along the adhesive-substrate interface;
- 4) after five months of exposure the retained toughness was 28% for these joints after which no further deterioration was seen and fully interfacial failure was then always subsequently observed;
- 5) effects such as adhesive plasticization, irreversible chemical ageing and the breaking down of the intrinsic adhesion forces across the adhesive/substrate interface may all contribute to the durability of the joint in a complex manner;
- 6) the epoxy adhesive is susceptible to moisture attack because it has hydrophilic groups that attract water molecules. The hydrophilicity of the epoxy resin can be caused by the hydroxyl groups, these can also form hydrogen bonds with water molecules. Moisture absorbed can act as a plasticiser, solvent or hydrolysis agent for

some adhesives. This contributes to the degradation of the adhesive mechanical properties (epoxide adhesive can absorb water up to a maximum of about 10% moisture by mass, depending on chemical nature and structure, stress state, exposure time, water concentration and temperature);

7) However, what is clear is that there is a strong needs to reduce the time required for durability testing, without introducing failure mechanisms that are not observed in service.

More detailed examination of this phenomenon follows.

*Received April 18, 2005*

*Technical University "Gh.Asachi" Iasi*

#### REFERENCES

- /1/. Mocanu F., *Contribuții la studiul proprietăților mecanice ale adezivilor*, Teză de doctorat, Universitatea Tehnică „Gh. Asachi”, Iași, 1997.
- /2/. Mocanu F., *Adezivi, îmbinări adezive*, Ed. „Gh. Asachi”, Iași, 2001.
- /3/. Reese R., Kawahara W., *Handbook on Structural Testing*, SEM, Fairmont Press, Lilburn, 1993, pg. 146-152.
- /4/. Lilleheden L., *Mechanical Properties of Adhesives "in situ" and in Bulk*, Journal of Adhesion and Adhesives, no. 13, 1995, pp.31÷37.
- /5/. Bigwood D. A., Crocombe A. D., *Elastic analyses and engineering design formulae for bonded joints*, Journal of Adhesion and Adhesives, no. 4, 1997, pp.229÷242.
- /6/. Groth H. L., *Viscoelastic and viscoplastic stress analysis of adhesive joints*, Int. J. Adhesion and Adhesives 10, 1998, pp. 207÷213.

#### UNELE ASPECTE PRIVIND DURABILITATEA ÎMBINĂRILOR ADEZIVE

**Rezumat:** Utilizarea îmbinărilor adezive este determinată, în primul rând, de comportarea acestora în timp. Comportarea îmbinărilor realizate cu adezivi este semnificativ influențată de condițiile de mediu în care acestea sunt expuse.

Rezistența îmbinărilor adezive structurale scade semnificativ în urma expunerii în cele mai uzuale condiții de exploatare, cum ar fi de exemplu temperaturile și umiditățile mai ridicate. Performanțele îmbinărilor realizate cu adezivi de-a lungul perioadei de exploatare trebuie neapărat cunoscute și în funcție de evoluția acestora poate fi apreciată durabilitatea îmbinărilor.

Scopul prezentei lucrări îl reprezintă studiul îmbinărilor realizate prin intermediul unui adeziv în condiții speciale de mediu. Încercările s-au efectuat pe epruvete care au suferit un proces accelerat de degradare. Se iau în discuție atât variația în timp a rezistenței de rupere a îmbinărilor adezive, solicitate static, cât și comportarea îmbinărilor în condiții de solicitare dinamică. Studiile s-au efectuat pe îmbinări realizate cu adezivi epoxidici și cianoacriilați. Rezultatele cercetărilor efectuate sunt sintetizate în prezenta lucrare.

## THERMAL CHARACTERISTICS OF SINGLE LAP JOINTS UNDER STATIC LOADS

BY

FLORENTINA MOCANU

**Abstract.** *In order to design and dimension a metal/metal adhesive bonded joint for a critical load application it is necessary to have a detailed knowledge of the strength behaviour of the joint. If we chose to use adhesive bonding, then we must be confident the joint can carry the applied loads. These loads may be static or impact. The purpose of the current work is to determine the variation mode of the strength of adhesive joints under static loading. The strength of adhesive bonded joints is known to be very sensitive to environmental exposure. When an adhesive joint is exposed to high environmental temperature the tensile load capability of the adhesive joint decrease. The purpose of the current work is the study of the thermal characteristics of single lap adhesive joints. In this paper the failure strength of adhesives as well as the tensile load capability of single lap joints was experimentally investigated with respect to the volume fraction of filler and the environmental temperature. An epoxy adhesive was employed in this study. The joints used in this study consist of metallic adherents.*

**Keywords:** *single lap adhesive joints, metallic substrates, polymeric resins, filler, high environmental temperature, thermal degradation, static strength*

### 1. INTRODUCTION

There are two kinds of joints: mechanical and adhesive. The mechanical joint is creating by fastening the substrates with bolts and rivets but the adhesive joint uses an adhesive interlayer between the adherends.

Adhesives are substances capable of bolding materials together in a useful manner by surface attachment. It defines the adhesive as a material which when applied to substrate surfaces can joint them together and resist separation. The principal attribute of adhesives is their ability to form strong bonds with surfaces of a wide range of materials and to retain bond strength under expected use conditions. An adhesive joint can distribute the load over a larger area that the mechanical joint (requires no holes, adds very little weight to the structure, has superior fatigue resistance).

Film adhesives occupy an important position among the class of structural adhesives. They are particularly efficient for bonding metallic and non-metallic substrates for the fabrication of lightweight and high-strength structures. Both thermoplastic and thermosetting adhesives are available in film form. Compared to the paste and other forms of adhesives film adhesives offer several advantages:

- control of adhesive layer thickness;
- easy handling and use;
- minimum waste and uniformity of product;
- supplied in carrier supported and unsupported forms [1, 2].

When the environmental temperature around adhesive joints approaches the glass transition temperature of the adhesive joint will fail load because of the degradation of the mechanical properties of the adhesive. Generally the structural epoxy adhesive has high toughness at low temperature, but degrades at high temperature because of its low glass transition temperature.

## 2. PROPERTIES OF THE EPOXY ADHESIVE.

The designer must therefore choose the geometry of the joint, the surface pre-treatment, the adhesive and its cure cycle and how to assemble the joint. The designer will also have considered the loads, which the joint expects to experience. Since it is almost impossible to design from first principles to predict the joint strength over a range of conditions, he must rely on previous experience to design efficiently. The design factors for an adhesive joint are following:

- the nonlinear mechanical properties of polymeric adhesive;
- the environmental temperature at which the adhesive joint is used;
- the dimensions of the adherend;
- the residual thermal stress generated due to the coefficient of thermal expansion difference between the adherend and adhesive;
- the glass transition temperature of the adhesive.

The epoxy adhesive mixtures could be used for bonding woods, metals, plastics, glass, ceramics, paper and leather.

Generally the structural epoxy adhesive has high mechanical properties at room temperature but its mechanical properties decrease faster than those of pure epoxy adhesive as environmental temperature increases. Since fillers in the adhesive improve the mechanical properties at high temperature the tensile properties of epoxy adhesive containing filler were rested with respect to environmental temperature and filler amount [3].

The mix ratio of resin and hardener of epoxy adhesive was 2:1. Table 1 shows the properties of the epoxy adhesive obtained from experiments and the properties of the filler.

**Table 1.** Properties of the epoxy adhesive and the filler

Properties	Filler	Adhesive
$\alpha$ ( $10^{-6}$ m/m °C)	6	55
$\nu$	0.3	0.25
$\rho$ (g/cm <sup>3</sup> )	3.4	1.2
E (Gpa)	350	10.5
$\tau$ (Mpa)	420	33

where:  $\alpha$  – coefficient of thermal expansion;

$\nu$  - Poisson's ratio;

$\rho$  – density;

E - Young's modulus;

$\tau$  – tensile strength.

### 3. TENSILE STRENGTH TESTING

#### 3.1. Experimental Results

The results of the tensile tests to which the adhesive joints with metallic supports, joints obtained by single lap do not represent an intrinsic characteristic of the adhesive. They depend on the adhesive's nature and application mode, on the film's thickness and polymerisation cycle, as well as on the support's material, mode of surfaces' preparation, thickness, mechanical characteristics and length of the supports. The adhesive thickness used was 0.3mm (at this value the joint failed in the bulk failure mode which yielded a much lower load capability of the joint than the joint failed in the interfacial failure mode) and the bond length used was 25mm. A steel plate 1.2mm thick was adopted for the adherend substrate. The assembled set was kept to 100°C for 24h to cure the epoxy adhesive layer. Bulk specimens made of homogeneous epoxy resin were also prepared under the same curing conditions for comparison.

The tensile tests on the single lap adhesive joint were performed at a static test speed of 1mm/min at 20, 40, 60 and 80°C. Specimens for the tensile testing were prepared in accordance with ASTM D2094-00. The testing itself was done in accordance with ASTM D2095-96. Tensile strength testing was conducted on samples prepared at Department of Strength of Materials of Technical University "Gh. Asachi" Iassy. All tests have been developed at normal conditions of the humidity, 50%±5% relative humidity, 7 days after the adhesive's strengthening in the joints. The supports' surfaces have been prepared prior to fixing according to ISO 4588-89. The bonding procedure for the joints is as follows: polishing by abrasive paper, degreasing of the surfaces of the adherents with acetone, bonding, curing for 24 hours at room temperature.

The tensile tests were performed three times under the environmental temperatures of 20, 40, 60 and 80°C. Table 2 shows the failure strength of the epoxy adhesive with respect to the environmental temperature and the volume fraction of filler [4].

**Table 2.** Tensile failure strength

Failure strength (MPa)		Temperature (°C)			
		20	40	60	80
	without filler	42	33	20	8
	filler 10%	48	37	25	8
	filler 20%	55	42	30	11
	filler 30%	64	49	38	18

It was assumed that the adhesive joint failed at the time of epoxy adhesive failure because the adhesive was much weaker than steel adherends. The failure strength was the engineering stress at the failure of the tensile specimen. The tensile properties of the epoxy adhesive increased as the volume fraction of the filler increased but decreased as the environmental temperature increased [5].

The failure strength of the epoxy adhesive containing 30% filler was 1.7 times higher than those the neat epoxy adhesive at 20°C. Also, the failure strength of the bonding joints with epoxy adhesive containing 30% filler was 2.4 times higher than those of the neat epoxy adhesive at 80°C. The increase ratio of the failure strength of the epoxy adhesive with respect to the volume fraction of filler at 20 and 80°C is shown in table 3.

**Table 3.** Increase ratio of the failure strength of epoxy adhesive at 20 and 80°C with respect to the volume fraction of filler.

Tensile properties	Test temperature (°C)	Volume fraction of filler (%)		
		10	20	30
Failure strength	20	1.3	1.5	1.7
	80	1.1	1.5	2.4

The tensile load capability of an adhesive joint decreases as the environmental temperature increases because of the thermal degradation of the adhesive. To reduce the degradation of the tensile load capability of the single lap adhesive joint whose adherends were made of steel, the adhesive joints joined by the epoxy adhesive containing filler were tested at several temperatures. Following curing the tensile strength was determined and the averages of the ten tests are reported in table 2. From the tensile tests on the epoxy adhesives it was found that the mechanical properties of the epoxy adhesives decreased sharply in the vicinity of glass transition temperature (65 °C) however, those of the filler containing epoxy adhesives did not.

In order to calculate the tensile load capability of the adhesive joint the adhesive layer was assumed to be isotropic and homogeneous. However, the adhesive layer is not homogeneous when the filler is added to the adhesive. The adhesive joint with filler has a higher load capability than the joint without one because the adhesive layer has a longer crack length when the adhesive joint fails. The average tensile strength of the single lap adhesive joint was defined as:  $\tau = \text{tensile load at failure} / \text{bond area}$ . The average tensile strength of the single lap adhesive joint increased as the volume fraction of the filler increased because the filler addition of the epoxy adhesive increased the tensile strength of the epoxy adhesive and decreased the coefficient of the thermal expansion of the epoxy adhesive which decreased the residual thermal stress in the single lap adhesive joint [6].

Although failure strength of the epoxy adhesive decreased much as shown in table 3 as the environmental temperature increased, the average tensile strength of the single lap adhesive joint did not decrease much compared to the adhesive properties due to the decrease of the tensile residual thermal stress.

The adhesive failure mode may be classified as:

- adhesive (adhesive failure occurs at the substrate/adhesive bond line). This is an indication that the bond between the adhesive and the substrate is weaker than either adhesive itself or the substrate material.
- cohesive (cohesive failure is usually seen as a failure within the body of the adhesive).

When both the adhesive and the bond between the adhesive and the substrate are very strong the substrate material may fail.

The failure mode of the adhesive joint was the cohesive in the adhesive layer rather than the interfacial failure between the adherend and the adhesive. The failure indices at the ends of the bond length are higher than those in the middle part due to the stress concentration.

### 3. CONCLUSIONS

From the present experimental investigation, the following conclusions can be drawn:

1. The results clearly demonstrate that the reaction generated at the interfaces between epoxy adhesive and steel substrate caused a decrease in tensile strength.
2. The reason for the failure of these adhesive bonding systems was due mainly to the thermal degradation of the adhesives themselves and their poor bonding behavior to metal side. In fact, the loss of adhesion after exposure was observed to take place in the adhesive layer and at the interfaces between the adhesive and adherend.
3. The average tensile strength of the single lap adhesive joint increased as the volume fraction of the filler increased because the filler addition to the epoxy adhesive increased the tensile strength of the epoxy adhesive and decreased the coefficient of thermal expansion of the epoxy adhesive, which decreased the residual thermal stress in the single lap adhesive joint.
4. From the tensile tests on the single lap adhesive joints it was found that the average tensile strength of the single lap adhesive joint did not decrease much compared to the adhesive properties because the tensile residual thermal stress in the joint decreased as the environmental temperature increased.

Received April 27, 2005

Technical University "Gh. Asachi" Iasi

### REFERENCES

- /1/. Mocanu F., *Contribuții la studiul proprietăților mecanice ale adezivilor*, Teză de doctorat, Universitatea Tehnică „Gh. Asachi”, Iași, 1997.
- /2/. Mocanu F., *Adezivi, îmbinări adezive*, Ed. „Gh. Asachi”, Iași, 2001.
- /3/. Lilleheden L., *Mechanical Properties of Adhesives "in situ" and in Bulk*, *Journal of Adhesion and Adhesives*, no. 13, 1995, pp.31÷37.
- /4/. Mocanu F., - *Influence of the filling material and of the crosslinking agents on the resistance of adhesive joints*, the Bulletin of Polytechnic Institute of Iasi, Tom. XLVII (LI), Fasc. 3-4, 2001, ISSN 1011-2855, pg. 75-83.
- /5/. Barsanescu P. D., Mocanu F., s.a. *Tensiuni remanente*, Ed. „Gh. Asachi”, Iasi, 2003.
- /6/. Yao, Q., Qu, J., *Effect of Thermal Residual Stresses on Polymer/Metal Interfacial Adhesion*// *J. Appl. Mech.*, 36, pag. 650-654, 2003.

### CARACTERISTICI TERMICE ALE ÎMBINĂRILOR ADEZIVE REALIZATE PRIN SIMPLĂ SUPRAPUNERE ÎN CONDIȚII DE SOLICITARE STATICĂ

**Rezumat:** Pentru proiectarea și dimensionarea optimă a îmbinărilor adezive metal/metal este absolut necesară cunoașterea, în primul rând, a modului de comportare a acestora. Dacă se preferă utilizarea îmbinărilor adezive trebuie avut grijă asupra modului de solicitare în condițiile exploatareii. Încercările pot fi statice sau dinamice. Prezenta lucrare își propune determinarea modului de variație a rezistenței îmbinărilor adezive în condiții de solicitare statică. Este cunoscut faptul că rezistența îmbinărilor adezive este influențată de condițiile de mediu în care acestea sunt exploatate. Atunci când îmbinarea este expusă în condiții de temperaturi ridicate încărcarea pe care aceasta o poate suporta scade. Lucrarea sintetizează rezultatele unor cercetări în vederea stabilirii

caracteristicilor unor îmbinări adezive realizare prin simplă suprapunere în diferite condiții de temperatură cu menținerea constantă a proporției materialului de umplutură. S-a stabilit pe cale experimentală comportarea îmbinărilor adezive cu suporturi metalici realizate prin intermediul unui adeziv epoxidic.

## FRACTURE BEHAVIOUR IN EPOXY ADHESIVE JOINT WITH VARIOUS BOND THICKNESSES

BY

FLORENTINA MOCANU

**Abstract.** . Mechanisms of fracture behaviour in the adhesive layer of an adhesive joint are important for understanding and thereafter improving the structural integrity. Bond thickness is one of the significant design parameters for adhesive joints. The purpose of the current work is the study on bond thickness dependence of the fracture toughness of adhesive joints. Adhesive joints between steel adherends with epoxy adhesive layer of various thickness (adhesive layer with 50mm, 12mm, 6mm, 3mm bond thickness) were investigated. Impact tests of the specimens were performed with a constant crosshead displacement rate at room temperature. An epoxy adhesive realized at the "Petru Poni" Institute of Macromolecular Chemistry Jassy was employed in this study. The joints used consist of metallic adherents.

**Keywords:** polymeric adhesives, adhesive joints, adhesive thickness, thickness effect, fracture energy, energy release rate, metallic substrates, fracture, loading rate.

### 1. INTRODUCTION

Polymeric adhesives are present almost everywhere as they can be conveniently used to join material of different properties to form specially structures otherwise cannot be made. The design of the joints of separate parts has become an important research area because the structural efficiency of a structure with joints is established with a few exceptions by its joints not by its basic structure. Adhesive joints have the following attractive features:

- joining of dissimilar materials is easier compared with the conventional joints;
- stress concentration does not appear because of the absence of the a hole unlike bolted or riveted joints;
- vibration absorption is feasible in an adhesive layer.

In many adhesive bonds extensive debonding would lead to adherend separation and no further interaction between the adhesive and the adherends. In some applications however significantly adhesive layers many remain in contact with the adherends. Our understanding of the phenomena requires that the following circumstances exist:

- the adhesive must be debonded over portion of its length;
- there must be the probability of friction at the interface between the adhesive and the adherend;
- the adhesive must be a viscoelastic material that is temperature dependent and must be confined by a channel like adherend cross-section [1, 2].

The effect of loading rate on the bond strength is important. An increased loading rate resulted in decreased bond strength probably due to the induction of a stiff

body response and elimination of the viscoelastic properties of the polymeric resin. Generally the results indicated a similar effect on both chemically cured and light-cured adhesives.

The adhesive bond strength is influenced by the bond thickness, its fracture energy dissipation for a given thickness and materials that an adhesive bonds together. Generally the adhesive is weaker and less stiff than the two adherends or substrate materials it joins.

As a result cohesive failure within adhesive often becomes the main concern for integrity of layered structures. Therefore a good understanding of adhesive joint fracture and associated thickness is critical for the design, construction and maintenance of joints bonded by adhesives. Because of the physical restriction in the thickness direction of adhesive joints and the influence of the two supports a complex behaviour is always expected [3].

## 2. ANALYSIS OF EXPERIMENTAL DATA

This study is a genuine one referring to an epoxy adhesive realized at the "Petru Poni" Institute of Macromolecular Chemistry Jassy. It is a new Romanian epoxy adhesive with higher mechanical properties in conditions of both static and dynamic stress. On propose a systematic study on the fracture behaviour of structural adhesives using adhesive joint specimens. The hypothesis tested in the present study was that the bond strength is altered under high-velocity debonding force relative to a low loading rate.

On studied the effect of adhesive thickness on the critical strain energy of an epoxy adhesive used to bond two steel substrates. Their experiments showed that for given temperature and loading rate the breaking energy depend on both specimen and adhesive thickness.

To avoid the complexity due to the combined effects of adhesive joint thickness temperature and loading rate a set of experimental data with fixed normal conditions of the temperature and humidity. All tests have been developed at  $23^{\circ}\text{C}\pm 3^{\circ}\text{C}$  and  $50\%\pm 5\%$  humidity relative. Crosshead displacement rate was 3.4m/s. Impact testing was conducted on samples prepared at Department of Strength of Materials of Technical University "Gh. Asachi" Iassy.

The results of the impact tests with the structural adhesive joints do not represent an intrinsic characteristic of the adhesive. They depend on the adhesive's nature and application mode, on the adhesive thickness and polymerisation cycle, as well as on the nature supports, mode of surfaces' preparation, thickness, mechanical characteristics and length of the supports.

Table 1 shows the breaking energy obtained on the adhesive joint specimens with some different thickness. Ten specimens were tested for each type. The specimen surfaces and adhesive/substrate interfaces influenced the adhesive fracture behaviour.

Surfaces of specimens for the impact testing were prepared in accordance with ASTM D2094-00 (polishing by a rotary sandpaper polisher, treating with hydrochloric acid, rinsing with water and drying).

The testing itself was done in accordance with ISO 9653-1991. After curing the energy was determined and the averages of the ten tests are reported in table 1.

Table 1. Fracture energy of the adhesive joint specimens

W (kJ/m <sup>2</sup> )		t (mm)				
		0.5	1	1.5	2	2.5
	b=50mm	19	45	21	16	16
	b=12mm	16	36	18	14	14
	b=6mm	14	28	16	12	12
	b=3mm	12	20	14	10	10

where: b - specimen thickness;  
t - adhesive thickness.

In comparison with other thickness values of 12, 6, 3mm the set of data (50mm) can be considered in pure strain condition and with least specimen-thickness influence. In table 1 two distinct monotonically increasing and decreasing regions are separated by the maximum energy rate. In the case b=3mm the plane stress conditions is assured. The failure mode of the adhesive joint was the cohesive in the adhesive layer rather than the interfacial failure between the adherend and the adhesive [4].

### 3. MODELLING OF BEHAVIOUR

The fracture energy is chosen to illustrate the size effect on concrete fracture because its solution can also be used to explain the adhesive thickness effect on adhesive joints. This energy is following expressed:

$$W = \frac{1}{b \cdot (l-s)} \cdot \int P \cdot d\delta \quad (1)$$

where: W – the average fracture energy;  
P – applied load;  
 $\delta$  – load-point displacement;  
b - specimen thickness;  
l – specimen width;  
s – crack length;  
b (l-s) – fracture area [5].

The fracture energy given by equation 1 can be related to the local fracture energy as:

$$W = \frac{1}{l-s} \cdot \int_0^{l-s} w \cdot dx \quad (2)$$

By dividing the specific work of fracture into the essential work of fracture ( $W_E$ ) and the plastic work or non -essential work of fracture ( $W_P$ ) the fracture energy is related to (l-s) by:

$$W = W_E + W_P = W_E + C (l-s) \quad (3)$$

where C is constant.

The last equation predicts the linear relationship for the fracture energy.

The critical energy is more often used to characterise the fracture of adhesive joints and bulk adhesives. Since this energy is related to the total crack it is reasonable to assume that the critical energy release rate is proportional to the local specific fracture energy.

In the case of an adhesive joint bonding two high modulus and non-yielding substrates, the critical energy of an adhesive joint increase initially with increasing adhesive thickness.

#### 4. CONCLUSIONS

The effects of adhesive thickness on the fracture energy of the adhesive joints made with epoxy adhesive were investigated. Table 1 shows the changes in fracture energy of the joint specimens as a function of adhesive and specimen thickness.

In general high loading rates eliminate the viscoelastic response of the polymeric adhesive to the applied load, inducing a stiff body response. This inelastic response does not allow for absorption of the energy through elastic deformation, as occurs during slow loading.

Most often the failure was large cohesive (failure within the body of the adhesive).

The average fracture energy of an adhesive joints increase with increasing bond thickness to a peak value and then gradually reduces to a plateau value corresponding to the bulk adhesive material.

More detailed examination of this phenomenon follows.

*Received April 27, 2005*

*Technical University "Gh.Asachi" Iasi*

#### REFERENCES

- /1/. Mocanu F., *Contribuții la studiul proprietăților mecanice ale adezivilor*, Teză de doctorat, Universitatea Tehnică „Gh. Asachi”, Iași, 1997.
- /2/. Mocanu F., *Adezivi, îmbinări adezive*, Ed. „Gh. Asachi”, Iași, 2001.
- /3/. Lilleheden L., *Mechanical Properties of Adhesives "in situ" and in Bulk*, Journal of Adhesion and Adhesives, no. 13, 1995, pp.31÷37.
- /4/. Barsanescu P. D., Mocanu F., s.a. *Tensiuni remanente*, , Ed. „Gh. Asachi”, Iasi, 2003.
- /5/. Mocanu F., - *The mathematical modelling of the epoxide adhesive behaviour at shear and shock*, the Bulletin of Polytechnic Institute of Iasi, Tom. XLV (XLIX), Fasc. 1-2, 1999, ISSN 1011-2855, pg. 111-114.

#### COMPORTAREA ÎMBINĂRILOR REALIZATE CU ADEZIVI EPOXIDICI ÎN FUNCȚIE DE GROSIMEA LIPITURII

**Rezumat:** Studiul mecanismului comportării stratului de adeziv din îmbinarea adezivă este important pentru cunoașterea și îmbunătățirea rezistenței îmbinărilor. Grosimea lipiturii este unul dintre cei mai importanți parametri care trebuie luați în considerație la proiectarea îmbinărilor. Lucrarea își propune studiul influenței grosimilor stratului de adeziv și a suptorilor asupra rezistenței la rupere a îmbinărilor adezive. Au fost studiate îmbinări adezive cu suptori de oțel realizate prin intermediul unui adeziv epoxidic de diferite grosimi (50mm, 12mm, 6mm respectiv 3mm). S-au luat în considerație încercări dinamice realizate la temperatura camerei cu o viteză de încercare constantă. Studiul s-a efectuat pe îmbinări cu suptori metalici realizate cu un adeziv epoxidic produs la Institutul de Chimie macromoleculară “Petru Poni” din Iași.

## VORTEX GAS DRYING

BY

IOAN RUSU. \*EMIL IACOB

**Abstract.** *The presence of humidity in the compressed air or in other gases made more difficult their transport as well as their utilization in technological aims by the occurring of the liquid and solid phase of water. The use of the vortex tubes it is dictated by their simple operation, low costs of achieving the equipment, by the missing of the freezing installations, ecological operation, etc. There are shown theoretical and some experimental aspects as well as some schemes of vortex equipment that can be used in metallurgical industry or in other fields of interest.*

**Keywords:** *vortex effect, gas drying*

### 1. INTRODUCTION

The vortex effect of energetical separation is a very complex gasodynamic process that appears in a spatial turbulent flow of a compressible viscous fluid. The apparatus that uses this effect is shown in Figure 1 (1-inlet nozzle, 2-diaphragm, 3-cold end, 4-the energetical separation room, 5-regulation valve, 6-hot end). The compressed gas flow rate  $\dot{m}_i$  with the initial parameters  $p_i^*$ ,  $T_i^*$  it is convergent introduced in (4), by means of the nozzle (1) and where it is accelerated to a speed close to the sound one. Inside the strongly turbionated gas flow it takes place a redistribution process of the initial energy, proces during which the gas from the axial zone becomes colder and that from the peripheral zone becomes warmer than the compressed one. From (4) the cold gas exits through (2) and the hot one – through the ring section between (5) and (6). The modification of the regulation valve section leads to the variation of the cold and hot gas flows ( $\dot{m}_r$ ,  $\dot{m}_c$ ), and finally to the modifications of the temperatures of these two flows.

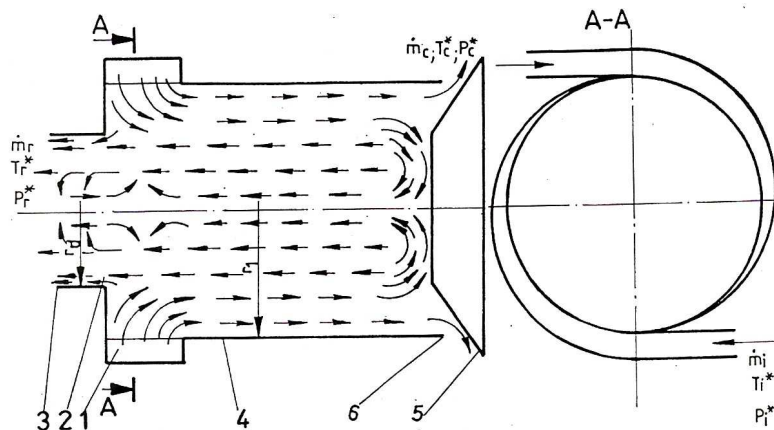


Figure 1. The scheme of a vortex tube and of the flows circulation inside it.

## 2. VORTEX GAS DRYERS

At the flowing of a two-phase mixture from the inlet nozzle (1), in the energetic separation chamber (4) will occur a vortex flow consisting in a liquid film disposed on the chamber walls and a gas flow with a lower or higher humidity level. A part of the liquid can sink over the diaphragm entering in the cold gas flow.

The formation and the maintaining of the liquid film on the chamber's wall is due to the powerful field of centrifugal forces, under the influence of what the condensate and the vapors introduced together with the compressed gas place themselves peripheral. Because of the fact that in the section of the nozzle is reached the maximum tangential speeds of the peripheral flow, we can suppose that the liquid film is being formed in this section. In the sections toward the valve (5) occur film breaking and the passing of the formed drops in the axial vortex.

A part of the slightly dispersed liquid exits from the orifice of the diaphragm together with the cold gas flow. The drops escaping the axial flow get into the peripheral flow where they vaporize totally or partially.

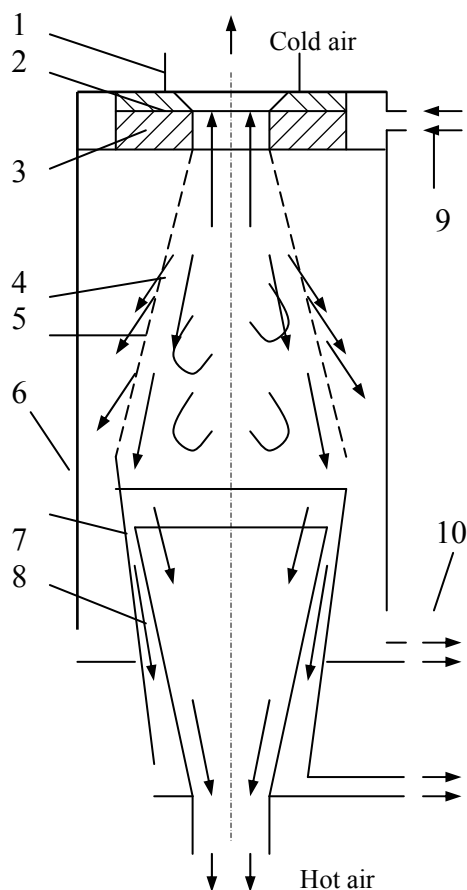


Figure 2. The scheme of a vortex separator

The scheme of a vortex separator is shown in Figure 2, in which: 1-cold air exit; 2-diaphragm; 3-inlet nozzle; 4-conical energetical separation chamber; 5-windows for condensate elimination; 6-body; 7-extra vortex chamber; 8-separation chamber; 9-compressed air; 10-condensed water.

The compressed wet air enters through (3) in chamber (4) where, thanks to the energetic separation effect, divides in two flows with different temperatures - the cold flow, axially disposed, exits through the diaphragm (2); the peripheral hot flow exits through the chamber (8). During the apparatus operation it takes place the condensation of the humidity from air, the drops formed and those existing at the apparatus inlet will form, because of the centrifugal forces, a liquid layer disposed on the interior walls of chamber (4). That, as well as the wet air layer in the neighborhood, is being vented through the windows (5) in the space between the body (6) and the chamber (4). The final separation of the humidity from air is being done after the formation of a stable layer of condensate on the walls of the chamber (7) (thanks to the it

conical shape and to the diminishing in the absolute speed of the vortex it takes place a stabilization and a growing of the thickness of the condensate layer, fact that enables it easy venting). The dry air exits the vortex separator through (8).

We can see that this vortex equipment combines two processes: the energetic separation in two flows (one cold and one hot) and that of the drying of the supplied compressed air. If one wants only the obtaining of a dry gas flow (nevermind its temperature) it is enough to close the orifice of diaphragm (2). Experimental results have confirmed the theoretical calculus, the diminishing of the compressed air humidity going up to 92%.

### 3. THE USAGE OF VORTEX TUBES IN DRYING INSTALLATIONS

The presence of humidity in the compressed air or in other gases made more difficult their transport as well as their utilization in technological aims by the occurring of the liquid and solid phase of water.

We present two possible industrial schemes of vortex dryers (Figure 2). In the first (Figure 2a) the compressed air enters in the oil separator (1) where takes place a condense separation after which it will cool in a heat exchanger (2),

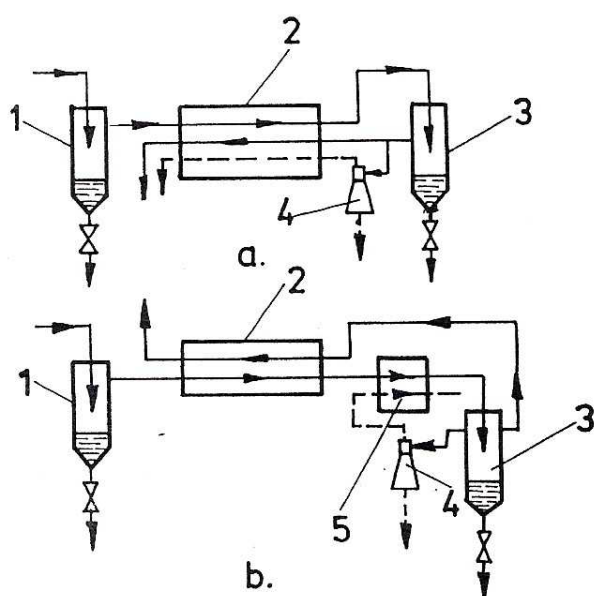


Figure 3. The schemes of the drying installations with vortex tubes cooling equipment; (a)-with triple flow heat recovery systems, (b)-with double flow.

reaching the second separator of water and oil (3). The most part of the compressed air returns in the recovery system (2) where it get warm and is sent to the user. The rest of the compressed air is being sent to the vortex cooler (4). The obtained cold flow enters the recovery system where it is heated and than exits in the environment. The hot flow is also eliminated in the atmosphere. In the gas drying case, after the detension from the cooler, the flows are being sent to a low-pressure duct for their further technological use. The second scheme (Figure 2b) is different because we use for rectifying cooling a heat exchanger with only two flows

(2); the heat of the inlet air flow is being sent only toward the reverse current of compressed air. The heat exchanger (5) is designated for a further cooling of the flow produced by the vortex tube.

In the shown schemes the minimum temperature of the gas that enters the separator (3) must be higher 273 K. For a reliable functioning of the installation it must be avoided the possibility of the ice occurring on the heat transfer surfaces. Concerning this, the circulation through the exchanger (5) enables the obtaining of a minimum heat transfer surface. If must be reached dew points lower than 273 K, the schemes will be changed: the separator (3) is being placed after the exchanger (2) in which the compressed air is being cooled to temperatures over 273 K. After the condense elimination, the compressed gas is cooled in one of the heat exchangers (refrigerators) at temperatures lower that 273 K. During the functioning of one refrigerator the other one is deiced for water elimination and so on.

Received April 19, 2005

Technical University "Gh.Asachi" Iasi

\*University of Medicine and Pharmacy "Gr.T.Popa" Iasi

#### REFERENCES

- /1/. Barsukov, S.M., *Vihrevoi efekt Ranka*, Izd.Irkusk.In-ta, Irkusk, 1983, 118 p;
- /2/. Suslov A.A. and others, *Vihrebye apparaty*, Masinostroenie, Moskva, 1985, 250 p.;
- /3/. Kosenko, V.N., *Vihrevaâ truba i eë premenenie v tehničeskom razdelenii gazovyh smesej*, Obzornaâ informaciâ, Centr. Inst. nauč. -tehnič. informacii, Moskva,1992,pp.12-13.

#### USCAREA GAZELOR PRIN METODA VORTEX

**Rezumat:** Prezența umidității în aerul comprimat sau în alte gaze face mai dificil transportul acestora, dar și utilizarea lor în scopuri tehnologice și aceasta datorită apariției fazelor solidă și lichidă de apă. Utilizarea tuburilor de vârtej în scopul uscării gazelor este determinată de modul simplu de operare a acestora, costurile mici de realizare a echipamentului tehnologic, de eliminarea necesității existenței unor instalații frigorifice, etc. Sunt prezentate câteva aspecte teoretice și experimentale precum și unele scheme de echipament turbionar ce poate fi utilizat în industria metalurgică sau în alte domenii de interes.

## THE VORTEX EFFECT OF ENERGETICAL SEPARATION USED FOR THE DUST-GAS MIXTURES SEPARATION

BY

IOAN RUSU

**Abstract.** *The paper presents the researches made by the authors concerning the possibility of applying the energetical separation effect at the dust-gas mixture separation. It is described the phenomena that occur during the separation process, finding theoretical relations that could lead to the designing of some specialised vortex installations. The constructive scheme of a vortex separation tube it is shown, concluding with the idea that this equipment combine the phase separation function with that of a energy separator, fact that made the biphasic mixture initial energy to be used better.*

**Keywords:** *vortex effect, dust-gas mixture separation*

### 1. INTRODUCTION

The vortex effect of energy separation consists in that through the relaxation of a vortical and compressed gas into a cylindrical or conical space the layers of gas situated in the close proximity of the axis's tube become cold and are evacuated through one side of the device (cold end) and the peripheral gas's layers become warm and are evacuated through the other side (warm end) of the tube /1, 2/. It is characterised by the occurrence of three simultaneously processes which take place in the vortex tube: the energetic transfer from the axial layers to the peripheral ones, heat transfer to the axial layers and the lowering of the total pressure of the peripheral gas stream, the main cause being the friction with the tube's walls.

The various applications of this effect led to the study of thermo-gaso-dynamic phenomena and than to the mathematical modelling of the processes occurring in the vortex tube. The theoretic research led to the conceiving of some calculus programs, which allows the optimisation of the tube's geometry and to some attempts for finding new fields of application of the energetical separation effect. So, the idea of its use in the dust-gas mixture separation has occurred.

### 2. THEORETICAL CONSIDERATIONS

The phasic separation of dust-gas mixtures inside a vortex tube is an example for a typical separation process of a fine dispersed phase (the sizes of the particles do not exceed a few micrometers) inside a field of big centrifugal forces.

In the case of the above mixtures, the main factors leading to a malfunctioning of the separation process are well known [1, 2, 3]: the turbulent pulsation from the gas vortex and the occurring of a concentration degree because of the diffusion (the dust particles transportation under the influence of centrifugal forces toward the limits of

the separation chamber leads at the accumulation of aerosols in the peripheral layers of the flow, near the walls, the occurring radial gradient of concentration being the driving force of the diffusive flow of the dust transport in the axial zone of the chamber [4].

We have observed that a negative influence upon separation process has the radial flow rate of solid particles made by means of the radial gradient of pressure. Also it must be remembered that upon a solid particle from the strongly turbionated flow of the free vortex can act an opposite force to the centrifugal one, force that is determined by the viscosity of the carrying medium and by the radial gradient of the tangential component of the carrying medium speed.

Thanks to the difference between the particle speeds measured in opposite points of the same diameter, it is also possible that immediately of its closest neighbourhood to occur a circulation of the carrying medium, that can lead to the occurring of a force that will push the particle in the direction of tangential speed growing, idea that is confirmed in [5].

Starting from the above aspects and from the analysis of the equilibrium of a cubic solid particle placed under the influence of a pressure field and of the centrifugal force, it was ascertained that for achieving a radial equilibrium of the particle it is necessary that its density be bigger than that of the one of the carrying medium, the minimum possible fraction being [4]:

$$\left(\frac{\rho_{md}}{\rho_{mp}}\right) = 1 + \left(\frac{R}{r}\right)^2 \left(\frac{12}{c_{pr} Re_t}\right)^{\frac{5}{3}} \left[ \frac{2 - \frac{12}{c_{pr} Re_t}}{1 - \frac{12}{(c_{pr} Re_t)^2}} \right]$$

where:  $\rho_{mp}$  and  $\rho_{md}$  – the density of the carrying medium, respectively of the dispersed medium;  $R$  – the separation chamber radius;  $r$  – the current radius;  $Re$  – the Reynolds criteria on the tangential direction;  $c_{pr} \approx 3$  – proportionality coefficient.

Neglecting the factors that obstruct the separation process of the biphasic mixtures and what have been previously mentioned, the vortex tubes can be used successfully in the above process. Another advantage would be the one that this apparatus combines the function of the phasic separator with that of energetical separator, fact that made the initial energy of the biphasic mixture to be better used

## 2. EXPERIMENTAL PROPOSALS

The constructive scheme of a separator vortex tube is shown in Fig. 1, in which: 1-inlet nozzle of the biphasic medium; 2-separation room; 3-dust storage; 4-regulating valve; 5-separator; 6-dust evacuation duct; 7-joint duct; 8-outlet cold pure air.

The biphasic gas-solid mixture is being strongly turbionated through the inlet nozzle 1, in the separation chamber 2 taking place both the energetical separation in two gas flows (cold and hot) and the cleaning of the axial layers from the dispersed solid phase. The cold cleaned flow exits toward the user through the diaphragm orifice. The hot flow of gas (the peripheral one) is being taken by the separator 5, passes through the space between valve and separation chamber wall and then it is being sent, for example, toward a local heating device.

The solid particles gather at the outskirts of the chamber 2, are collected by means of separator 5 to a dust storage 3 and than being transported by means of the evacuation duct 6 to dust storage tank. The joint duct 7 has the purpose of reintroduction of the carrying gas into the technological circuit.

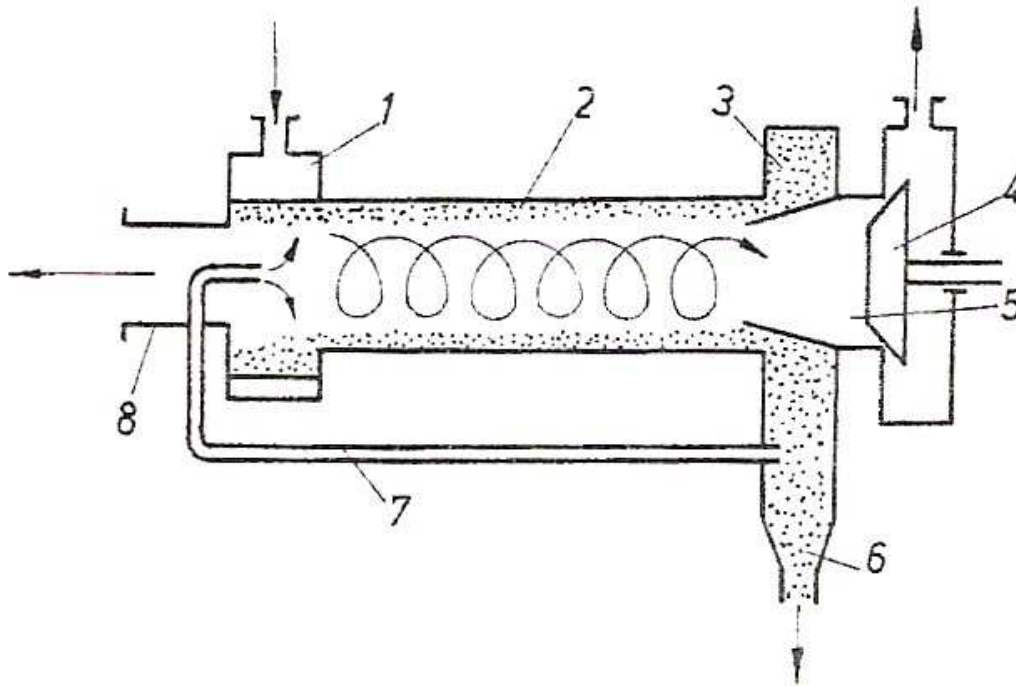


Figure 1. Constructive scheme of a dust-gas mixture separator vortex tube.

Received April 19, 2005

Technical University "Gh.Asachi" Iasi

#### REFERENCES

- /1/. Abramovici, G.N., *Prikladnaâ gazovaâ dinamika*, OGIZ, Moskva, 1952, 456 p;
- /2/. Barsukov, S.M., *Vihrevoi efekt Ranka*, Izd.Irkusk.In-ta, Irkusk, 1983, 118 p;
- /3/. Stefanescu, D., *Termogazodinamica tehnica*, Ed. tehnica, Bucuresti, 1986, 463 p;
- /4/. Suslov A.A., Ivanov S.V., Muraskin, A.V., Cizikov, U.V. - *Vihrevye apparaty*, Masinostroenie, Moskva, 1985;
- /5/. Epifanova, V.I., *Pribižennaâ metodika rasčetnogo opredeleniâ karakteristik vihrevogo ežektora*, Izvestiâ vuzov, Mašinstroenie, no. 10, 1975, pp. 42-44.
- /6/. Rusu, I., Munteanu, C., ș.a., *Researches Concerning Vortex Unconventional Cooling Equipments in Metallurgical Technology*, International Conference On Materials and Advanced Technologies – Materials, Functionally and Materials "EUROMAT'97", Maastricht, Olanda, 1997; vol. III, pp. 491 ÷ 494;
- /7/. Rusu, I., Munteanu, C., *The Optimum Characteristics of Vortex Microtubes*, Kontrol' i upravleniâ v tehničeskikh sistemah KUTS-97, noiembrie 1997, Vinița – Ucraina, vol. II, pp. 192 ÷ 198;
- /8/. Rusu, I., Dima, A., . *Transfer de căldură și instalații termice*, Editura Cermi, Iași, 1997, ISBN 973-97303-9-6, 178 p.

### UTILIZAREA EFECTULUI TURBIONAR DE SEPARARE ENERGETICĂ LA SEPARAREA AMESTECURILOR PRAF-GAZ

**Rezumat:** Lucrarea prezintă cercetările facute de autor privitoare la posibilitatea utilizării efectului turbionar de separare energetică la separarea amestecurilor de gaze și praf. Se descriu fenomenele care apar în timpul procesului de separare și care conduc la determinarea unor relații teoretice care să conducă la proiectarea unor instalații turbionare specializate. Este prezentată schema unui tub vortex destinat separării amestecurilor praf-gaz. S-a ajuns la concluzia ca acest echipament combină funcția de separator de praf cu cea de separator energetic, fapt ce face ca energia inițială a amestecului praf-gaz să fie utilizată mai eficient.

## RESEARCH REGARDING THE BEHAVIOUR OF HYSTERETIC STEEL BARS ENERGY DISSIPATORS

BY

V. V. MOLDOVEANU, C. BEJINARIU, L. DRAGOI, A. FLORESCU

**Abstract.** *The most simple energy dissipator based on bending deformation is the soft steel bar. Energy dissipation is obtained when the metal from the device is plastically deformed. The work researches the behaviour of the steel bars.*

**Keywords:** *hysteretic energy dissipator, plastically deformation, behaviour of steel bars*

Hysteretic dissipators are devices used for absorbing a part of the energy induced into a system by earthquakes or other exceptional phenomena like: explosions, dramatic shocks and powerful winds.

According to the worldwide research, a wide range of dissipators has appeared, especially designed to suit their purpose. These dissipators are successfully used for seismic isolation of buildings, bridges and for particular installations inside nuclear power plants, also for automobiles protection against shocks, as protection parapets on the highways, for reservoir's protection etc.

Hysteretic dissipators of great capacity are built based on plastic deformation of metals (usually steel or lead). The element of energy absorption from a device with metal plastic deformation can be conceived to function on one or more directions when it is bent, compressed, stretched, submitted to local yielding or to any other combination of these procedures. Energy dissipation is obtained when the metal from the device is plastically deformed, the energy being absorbed through internal friction.

The advantages of these types of dissipators are: stable behaviour, long reliability and great strength against environment conditions. These dissipators can offer rigidity to buildings, resistance and capacity to dissipate seismic energy.

The most simple energy dissipator based on bending deformation is the soft steel bar. This dissipator is a console type one, having one end fixed on the plate placed on the foundation and the other end free. The force actuates towards the free end through a spherical joint.

The soft steel is part of carbon steel class of general usage. The soft steel most frequently used for energy dissipators is OL37 steel. For the testing of hysteretic dissipators made by steel bars, were built 24 test pieces of rolled OL37 steel, having a diameter of 22 mm (12 pieces) and 30 mm (12 pieces).

From these 12 steel bars with the 22 mm diameter, 6 were thermally deformed by annealing and the other 6 of them remained in form in which they are delivered. The same process was applied to the other 12 steel bars of 30 mm diameter.

To eliminate the internal tensions which have appeared inside the steel bars as a consequence of modifying the delivery diameter and to increase plasticity for better energy dissipation, a thermal deformation of annealing was applied.

The annealing parameters, recommended for OL 37 are:

- slow heating at  $650 \div 700^{\circ}\text{C}$ ;
- one hour maintaining;
- cooling with the oven till  $200 \div 300^{\circ}\text{C}$  and then in the open air.

The steel bars have been rigidly fixed on the inferior part of the fixing device, figure 1, assembled on the rigid frame of the hydraulic testing stand. The stand was conceived in order to make possible testings in alternating cycles (from left to right) with one Hz frequency. The bilateral hydraulic cylinder used for testing ( $\varnothing 150/\varnothing 70/400$ ), actuates upon the free end of the testing device through a force dynamometrical trap and a spherical joint. The inductive moving translator assembled on the rod of the plunger, the force dynamometrical trap and the measure amplifier send to an acquisition plate then to a computer all the information gathered during the experiment.

Figure 2 represents hysteretic curves describing the evolution of degradation in alternating cycles of a bar with 22mm diameter in delivery state; the breaking of the bar has occurred after 168 charging cycles.

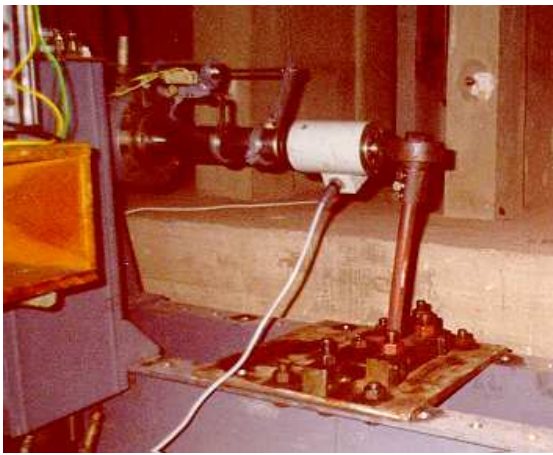


Figure 1. Testing the steel bar dissipator on the stand.

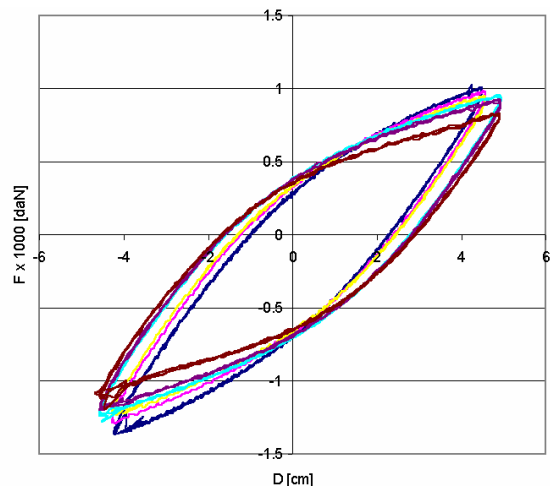


Figure 2. The evolution of degradation at alternating cycles of a 22 mm diameter bar in the delivery state (breaking at 168 cycles).

Figure 3 represents hysteretic curves which describe the first cycle and cycle 250, right before the breaking (breaking of the bar occurred after 264 charging cycle) of a 22mm diameter bar in annealing state.

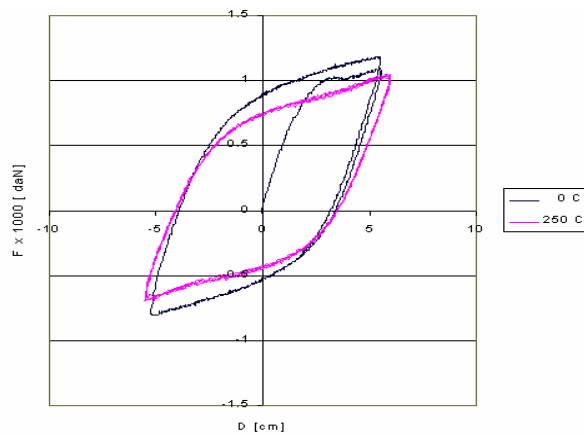


Figure 3. The evolution of degradation at alternating cycles of a 22 mm diameter bar in annealing state (breaking at 264 cycles).

In figure 4a and 4b appears the macroscopic image of a broken bar both in delivery and in an annealing state.



Figure 4. The breaking aspect for the delivery (a) and annealing (b) state bar.

Figure 5 represents the hysteretic superposed curves describing 4 bars with 22mm diameter; 2 bars made of steel in delivery state (I2, I5) and 2 made of annealed steel (I3, I4).

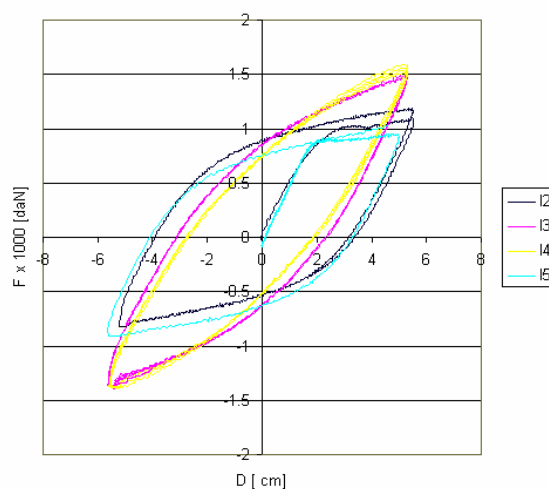


Figure 5. The evolution of the behaviour corresponding to the 250th cycle for four 22 mm diameter bars; (I2 and I5 annealed, I3 and I4 delivery state).

It can remark that the capacity of energy dissipation increases with 25% for annealed bars. At the same time the shape of the resulting curves for the same type of bars are almost alike, with a difference of maximum 3%.

As for the bars of 30 mm diameter it is to be mentioned that their behaviour is similar to 22 mm diameter bars. Their breaking occurred after a larger number of cycles ( $\approx 330 \div 350$  cycles).

Figure 6 and figure 7 shows the breaking distribution of the 12 bars of 22 respectively 30 mm diameter in comparison to the number of cycles.

Generally, it can note that the breaking, for the same type of bars, occurs at a close number of cycles.

Analyzing the behaviour of the two types of bars, submitted to alternating testing, it comes out that the capacity increases to resist for a larger number of cycles, by increasing the material share.

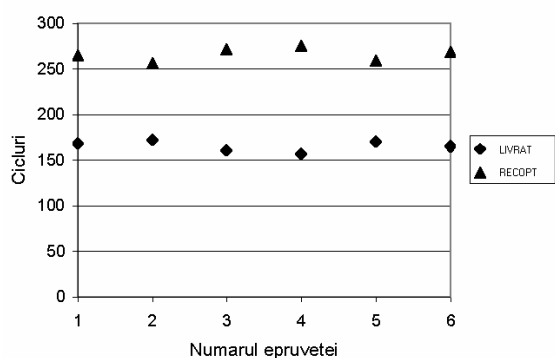


Figure 6. Distribution of 22 mm diameter bars breaking.

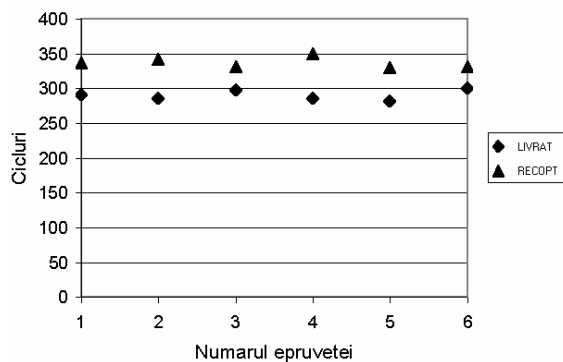


Figure 7. Distribution of 30 mm diameter bars breaking.

At the same time the difference between the numbers of cycles at breaking is reduced in the case of 30 mm diameter bars, both in delivery and annealing state. This phenomenon is explained by the increasing of the diameter and the effect of material processing for bringing it into delivery state.

Received May 6, 2005

Technical University "Gh.Asachi" Iasi

#### REFERENCES

- /1/. Moldoveanu, V.V., *Contribuții privind studiul disipatorilor histeretici de energie*, Teză de doctorat, Universitatea Tehnică Iași, 2001.
- /2/. Cousins, W.J., Robinson, W.H., Mc Verry, G.H., *Recent Developments in Device for Seismic Isolation*, Bulletin of the New Zealand National Society for Earthquake Engineering, vol.25, nr.3, September, 1992.
- /3/. Piccionne, Denise, *Principi costitutivi e tecnologia dei dispositivi per l'isolamento sismico delle strutture*, Tesi di laurea; Politecnico di Torino, 1995.

#### CERCETĂRI PRIVIND COMPORTAREA DISIPATORILOR HISTERETICI DIN BARE DE OȚEL

**Rezumat:** În lucrare se prezintă comportarea disipatorilor histeretici de energie confecționați din bare de oțel marca OL37, în stare de livrare și după recoacere. Barele de oțel au fost montate pe stand și încercate la îndoire în cicluri alternante. Se prezintă rezultatele obținute.

## RESEARCHES CONCERNING THE COOLING CHARACTERISTICS OF THE POWDER BACKING IN FLUIDIZED BED TIP SAND AND SALT MIXTURE BARBOTAGED WITH AIR

BY

CARMEN NEJNERU, MIHAI ADRIAN BERNEVIG, ION HOPULELE,  
ROXANA CARABET

**Abstract.** *The paper presents the researches on the cooling thermal transfer in fluidized beds. There were used for the experiments three sizes of the sand particles: 1)  $1400 < d_p < 3000 [\mu\text{m}]$ ; 2)  $1200 < d_p < 1400 [\mu\text{m}]$ ; 3)  $500 < d_p < 1200 [\mu\text{m}]$ . The cooling curves were drawn with a silver control cylinder within a chromel-alumel thermocouple connected to an y-t recording apparatus. By studying the variation graphics of the cooling curves it can be noticed that sand has the biggest cooling velocity and salt has the smallest. The others are between the two curves with closer medium values.*

**Keywords:** *fluidized bed, cooling velocity, cooling curve, heat transfer, sand particle*

### 1. INTRODUCTION

Fluidization is a technique in which a particle bed is brought into a condition where it behaves like a liquid, each particle being separated by the others through a gas stream.

The fluidized bed is a heterogeneous, non-adiabatic system where the solid particles are executing a continuous motion on the enclosure, under the influence of a turbulent beat of pulses of a fluid stream.

The fluid strains among the particle layer without moving them at small speed. As long as the loss of pressure is smaller than the weight of the layer, reported to the fluidization surface, the layer remains fixed.

At a certain speed the individual particles get a liberty degree which allows an easy vibration of the particles round about the primary position. In this condition the particles mass behaves like a viscous liquid, the solid and the fluidization agent forming one phase (the dense phase).

The agent velocity which is completing this condition is called the minimum fluidization velocity ( $v_{im}$ ) when appears the homogenous fluidization. Homogenous fluidization is characterized by uniform distribution of the particles and an uniform expansion of the layer, the distance between the particles increasing together with agent velocity.

Increasing continuously the speed of the fluid ( $v > v_{im}$ ) turns out that the layer explodes a lot and the movement of the particles became violent and chaotic.

A part of the fluid goes through the layer like some irregular bubbles which are breaking at the fluidized medium surface, throwing up a jet of particles, the whole

layer looking like boiling water. This is the non homogenous fluidization which is interested in applications with a view to heating in thermo-chemical and heat treatment.

During fluidization can appear secondary phenomena which produce the perturbation of the fluidized bed, specific to the non-homogenous fluidization such as: insistence and canalization.

The use field of the fluidized bed includes vast velocity intervals ( $v_1/v_{mf}=50\dots70$ ), because the nature of solid particles and the properties of the fluidization agent are different.

The nature, size and form of the solid particles belonging to the fluidized bed influence directly the structure and the characteristics of yield of fluidized bed.

The size of the particles is one of the most important parameters of the fluidization, both hydrodynamic and heat and mass change. For the achievement of an optimum fluidization it is necessary that the field scattering of the particles size must be as limited as it can.

If the fluidized bed is composed of particles whose size has a field scattering wide, the fluidization velocity grows so that it can lead to the appearance of the small particles entrainment phenomena.

The size of the particles influences directly the velocity of the fluidization (specially the minimum fluidization speed) which grows proportionally with  $d_p^2$ , and also influences the pressure loss and specific weight of the layer.

It has been experimentally determined that optimum density of the particles material is between 1280 – 1600 kg/m<sup>3</sup>. Dense materials produce low coefficients of heat transfer and need a bigger velocity of fluidization gas.

In fluidization are used materials such as: sand, corundum, graphite, aluminum oxide and other particles which are physical and chemical stable at the work temperature. The volume weight of the particles determines the specific weight of the fluidized bed and influences the minimum fluidization velocity and also the loss pressure in the layer.

## 2. OBJECTIVES

The fluidized beds can be used in heat and thermo-chemical treatments as active mediums, as heating mediums, soaking steps, and also as cooling mediums.

The cooling velocity is an important parameter of the heat and thermo-chemical treatments.

The paperwork is presenting an experimental study concerning the cooling capacity of the fluidized bed using different solid backing and as fluidization agent: air.

Advantages comparing to salt baths:

- it is favorable for an uniform cooling but slow, being used lesser in hardening and more in annealing.

- it is non-toxic comparing to salt baths.

- it is easy to handle and to get, and there are needed simple installations easy to be upkeep.

- it do not consume and damage like salt baths (it must always be added substances in order to be built-up the percentage).

- it is cheaper than the salt baths, and easier to be maintained constant as properties.

As a disadvantage is the fact that they cannot be used for pieces bigger than 100 mm, the fluidization could be badly bred, the specific convection of the fluidized bed being clogged.

Conclusion:

- the most important advantage is that in certain circumstances they can replace the salt baths.

It was experimentally analyzed the factors which influence thermic transfer in fluidized bed.

### 3. RESULTS

In order to determine the cooling medium like fluidized bed, it was used a control cylinder from silver within a chromel-alumel thermocouple which permits temperature measurement with a recording apparatus y-t. The control cylinder is heated up to the desired temperature (800°C) and cooled down in the fluidized bed.

The silver test bar has the following sizes and characteristics:

$$\text{Ø} = 13 \text{ [mm]}, h = 28 \text{ [mm]}, S = 1408 \text{ [mm}^2\text{]}, m = 39.9 \text{ [g]}, \rho_{\text{Ag}} = 10.5 \text{ g/cm}^3$$

$$\lambda_{\text{Ag}} = 418.5 \text{ W/m}\cdot\text{K}$$

The equipment used in experimental determination of the cooling curves is formed from:

- air fluidization system;
- heating system of the silver test bar (circular pipestill with electrical resistance);
- measurement system represented by an y-t recording apparatus (with modification apparatus of the shifting rate of the recording apparatus);
- Transformer of the filling variation of the ventilator for modification the air velocity.

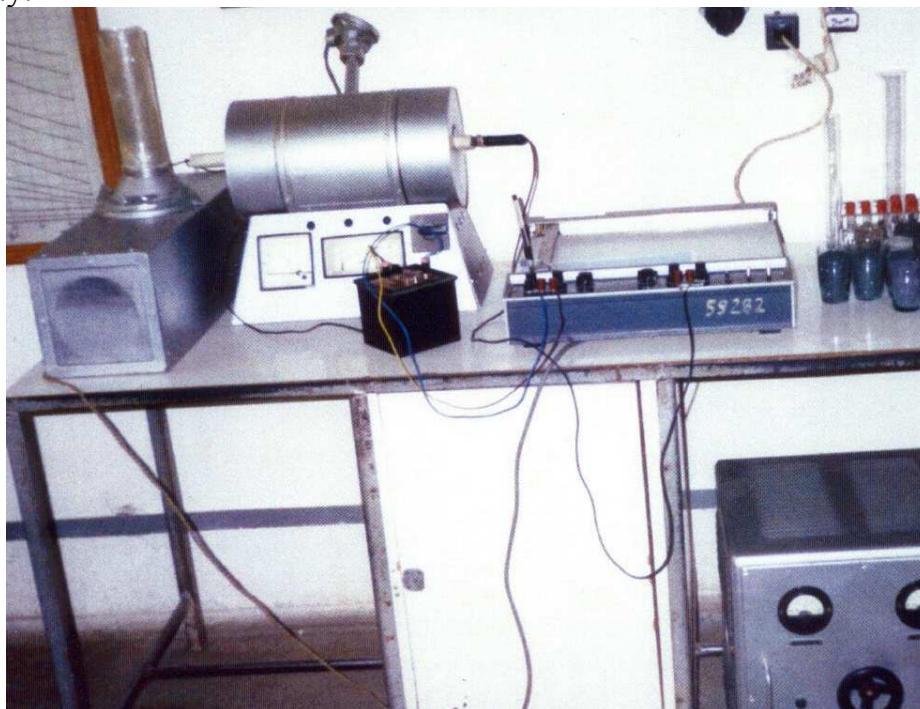


Fig.1 Equipment for the determination of fluidized beds cooling characteristics

There were used sand and salt mixture with the grain sizes:  $1400 < d_p < 3000$  (Fig.2); where : particle diameter (the eye sieve) - in  $\mu\text{m}$

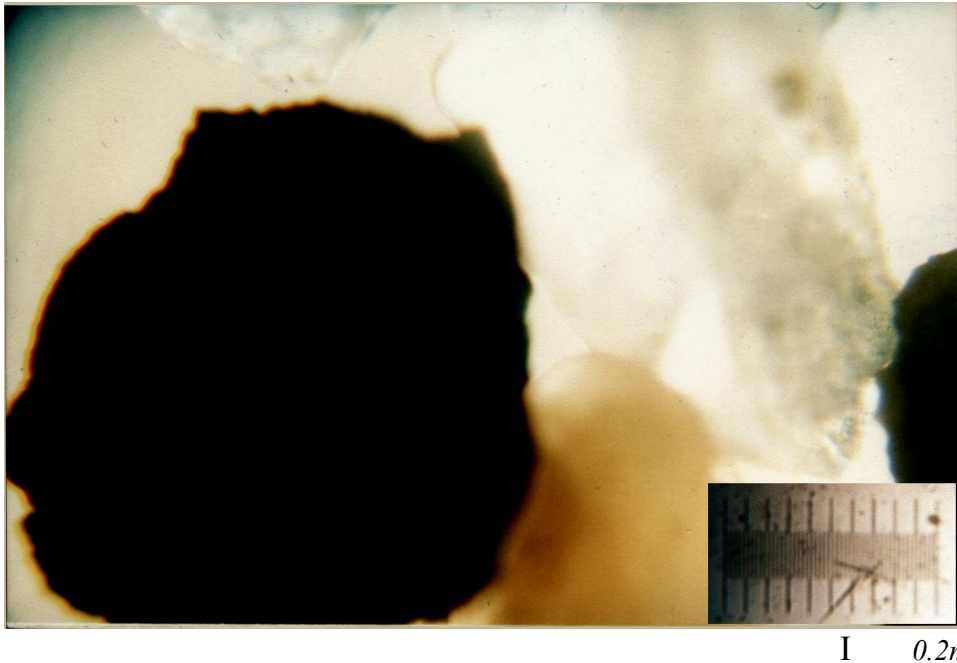


Fig.2 Sand and salt particles

The dusty environments mentioned before were fluidized with air.

The silver test bar was conducted in a circular pipestill until  $800^\circ\text{C}$  and then was introduced in the fluidized bed, the cooling curve being recorded by the y-t recording apparatus.

For each cooling environment was calculated:

- the maximum and medium cooling velocity;
- global factor of heat transfer;

$$\alpha_g = \frac{\alpha_1 \cdot \Delta t_1 + \dots + \alpha_s \cdot \Delta t_s}{t_{total}} ; \text{ where: } \alpha_i = \frac{3600 \cdot m \cdot c}{\Delta t_i \cdot S} \ln \frac{T_i - T_o}{T_f - T_o} \text{ [w/m}^2\text{k]}$$

where:

$m=0,0399$  Kg, the test bar weight;

$c=0,056$  Kcal/Kg, specific heat capacity at silver;

$S=0,001408$ , the test bar surface;

$\Delta t$ , sec= time interval;

$T_i, T_f, ^\circ\text{C}$  the initial and final temperature interval;

$T_o$  environment temperature;

- cooling intensity  $H = \frac{\alpha_g}{2\lambda} \text{ [m}^{-1}\text{]}$

$$\lambda_{Ag} = 418,5 \text{ w/mk}$$

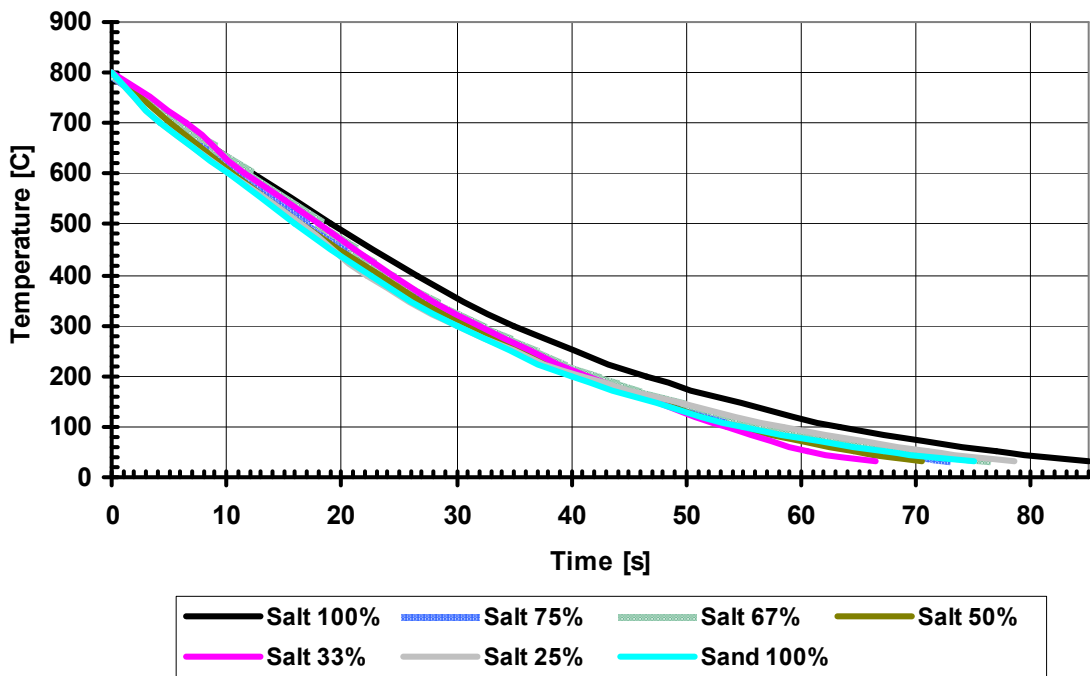
The results have been written in tables where we can find cooling intensities(H)

All the studied environments are for annealing (they cannot be used for hardening because of the small cooling velocities)

The cooling curves for salt and sand in diferents procents particles grains between 1400 - 3000  $\mu\text{m}$

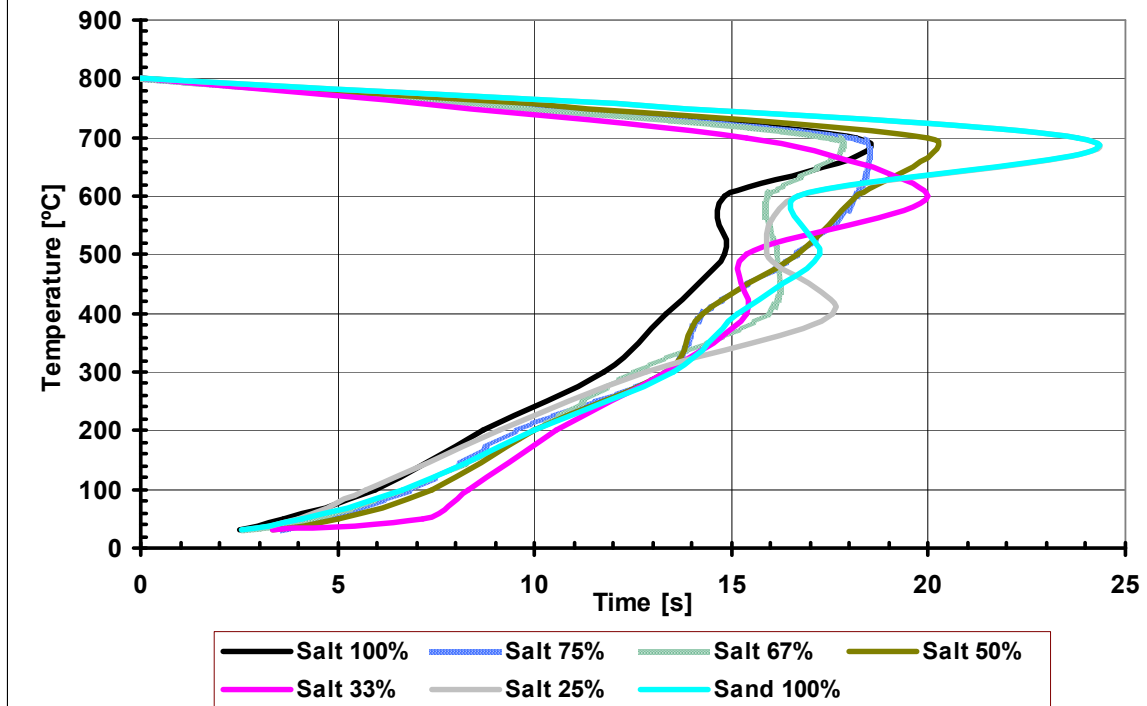
T[ $^{\circ}\text{C}$ ]	Salt 100%	Salt 75%	Salt 67%	Salt 50%	Salt 33%	Salt 25%	Sand 100%
800	0	0	0	0	0	0	0
700	5.5	5.5	5.7	5	6.5	4.2	4.2
600	12.25	11	12	10.5	11.5	10.2	10.2
500	19	17	18.2	16.5	18	16.5	16
400	26.5	24	24.5	23.5	24.5	22.2	22.6
300	35	31.5	32.5	31	32	30	30
200	46.5	42	42.5	41	41.5	41	40
100	63.25	56.5	57.5	54.5	53.5	58.5	55
50	77	67.5	69	64.5	60.5	71	67.2
30	85	73	76.5	70.5	66.5	78.5	75

The cooling curves for salt and sand in diferents procents particles grains between 1400 - 3000  $\mu\text{m}$



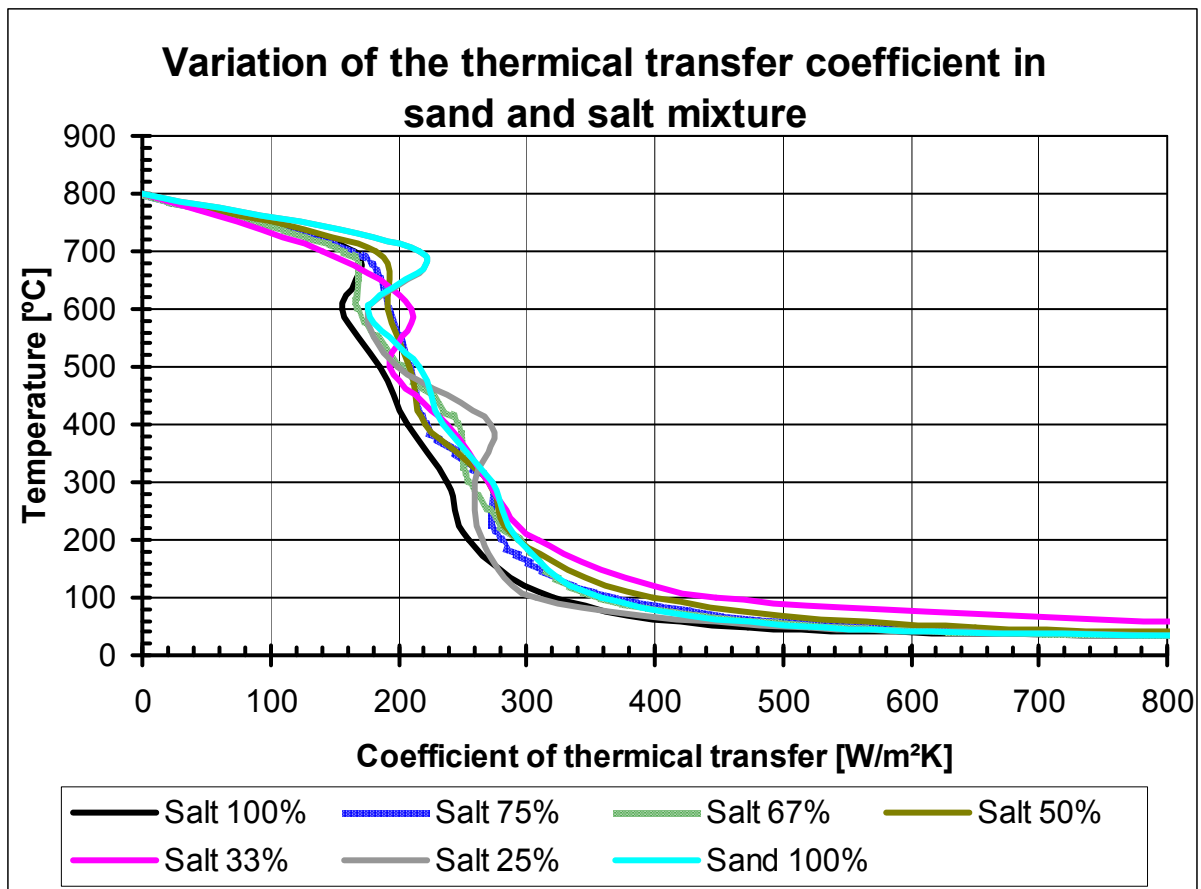
Velocities variation cooling for salt and sand particles grains between 1400 - 3000  $\mu\text{m}$ 

T[ $^{\circ}\text{C}$ ]	Salt 100%	Salt 75%	Salt 67%	Salt 50%	Salt 33%	Salt 25%	Sand 100%
800	0	0	0	0	0	0	0
700	18.18	18.18	17.54	20.00	15.38	23.81	23.81
600	14.81	18.18	15.87	18.18	20.00	16.67	16.67
500	14.81	16.67	16.13	16.67	15.38	15.87	17.24
400	13.33	14.29	15.87	14.29	15.38	17.54	15.15
300	11.76	13.33	12.50	13.33	13.33	12.82	13.51
200	8.70	9.52	10.00	10.00	10.53	9.09	10.00
100	5.97	6.90	6.67	7.41	8.33	5.71	6.67
50	3.64	4.55	4.35	5.00	7.14	4.00	4.10
30	2.50	3.64	2.67	3.33	3.33	2.67	2.56

Velocities variation cooling for salt and sand particles grains between 1400 - 3000  $\mu\text{m}$ 

Variation of the thermal transfercoefficient in sand and salt mixtures particles grains between 1400 - 3000 μm

T[°C]	Salt 100%	Salt 75%	Salt 67%	Salt 50%	Salt 33%	Salt 25%	Sand 100%
800	0	0	0	0	0	0	0
700	165.30	165.30	159.50	181.80	139.90	216.50	216.50
600	156.20	191.70	167.30	191.70	210.80	175.70	175.70
500	185.80	209.00	202.30	209.00	192.90	199.10	216.20
400	206.40	221.20	245.70	221.20	238.20	271.60	234.60
300	238.10	269.80	253.00	269.80	269.80	259.50	273.50
200	254.60	278.90	292.80	292.80	308.20	266.20	292.80
100	320.80	370.60	358.30	398.10	447.80	307.10	358.30
50	472.70	590.90	565.20	650.00	928.60	520.00	532.80
30	910.10	1323.70	970.70	1213.40	1213.40	970.70	933.40
H[m <sup>-1</sup> ]	0.41	0.47	0.45	0.49	0.52	0.44	0.46



#### 4. CONCLUSIONS

It can be noticed from graphics that sand and salt particles size influence the cooling velocity and the heat transfer coefficient in fluidized bed.

As a first step, the sand and the salt, being a good insulator, absorbs the heat from the test bar and yields it when the cooling velocity gets slower.

The form and the irregularity of the sand sands and salt grains has an important influence; the form of the sand grains are rounded and semi-elongation with amount of crown.

The velocity fluctuations between 700-400 C appear because of the form and irregularity of the sand and salt grains.

- due to the size of the particle (fluidization is very well made on larger size of the particle) it can be noticed an approaching of the cooling curves;

- it can also be noticed that sand has the biggest cooling velocity( 100%) and salt has the smallest cooling velocity (100%). The others are between the two curves with closer medium values.

- in mixtures  $V_{\max}$  lies between 18-21°C/s ;

- in sand  $V_{\max} = 25^{\circ}\text{C/s}$ , and in salt 100%  $V_{\max} = 18^{\circ}\text{C/s}$

*Received February 20, 2005*

*Technical University "Gh.Asachi" Iasi*

#### REFERENCES

/1/.C. Samoila, M.S. Ionescu, C. Druga, *Tehnologii si utilaje moderne de incalzire in metalurgie*, Editura Tehnica,Bucuresti, 1986

#### CERCETĂRI PRIVIND CARACTERISTICILE DE RĂCIRE ÎN PAT FLUIDIZAT A MEDIILOR PULVERULENTE TIP NISIP BARBOTAT CU AER

**Rezumat:** Lucrarea prezintă cercetările experimentale asupra transferului termic la răcire în medii pulverulente(nisip de turnătorie în amestec cu sare în diferite procente ) barbotate cu aer. Pentru experimente s-a folosit nisip și sare cu mărimea granulelor cuprinsă între  $d_p \in (1400 \div 3000) \mu\text{m}$ , unde  $d_p$  este diametrul mediu al particulei. Curbele de răcire au fost tratate cu ajutorul unei epruvete de argint cu termocuplu înglobat și conectat la un inductor y-t. Studiind graficele de variație ale curbelor de răcire se observă că viteza cea mai mare de răcire o are nisipul (100%) și cea mai mică sarea (100%). Celelalte fiind cuprinse între cele două curbe cu valori intermediare foarte apropiate.

**RESEARCHES CONCERNING THE COOLING CAPACITY OF THE  
HARDENING SYNTHETICALLY MEDIUMS: POLIALCHILENGLICOL  
(P.A.G. 15%)**

**BY**

**CARMEN NEJNERU, DAN-GELU GĂLUȘCĂ, VASILICĂ MIRON, ION HOPULELE**

**Abstract.** *The paper presents the experimental researches on the cooling capacity of the synthetical mediums like polialchilen glycol in water. It was used a silver control cylinder within a cromel –alumel thermocouple connected to an y-t recording apparatus. The measurements were made on barbotaged and non-barbotaged mediums by varying the initial temperature (20°C, 30 °C, 40 °C, 50 °C) and the results were tabled and graphically represented..*

**Keywords:** *hardening, cooling velocity, cooling curve, heat transfer, dynamic and kinematic viscosity*

## **1. INTRODUCTION**

The cooling has a great importance as a final operation of the thermic treatment because it determines the structure and the proprieties of the pieces thermically treated.

We analyze kinetic cooling curve of the alloy (the T.R.C. diagrams) for choosing the optimum cooling medium, and we compare the cooling curves.

If the cooling process in hardening properly made (the success of the operation guaranteed) and we can obtained structures in the sectioned view of the pieces (hardening martensite structures) without producing hardening defects such as: cracks, deformations or big residual stresses.

The cooling mediums used until our days do not satisfy totally the demands required by the modern thermal treatments that must assure a wide-open spectrum of the physico-mecanical properties of the thermal treated pieces. They must have a low price and to maintain constant their cooling properties. In order to satisfy the demands there were used synthetical hardening mediums such as residual substances obtained from petroleum industry, the paper chemical processing industry.

## **2. OBJECTIVES**

The oil has favorable cooling curve because it crosses quickly the minimum stability domain of the aftercooled austenite and has a slow cooling velocity in the martensite domain when tensions caused by the structural transformations are very big and the thermal tensions are smaller caused by the cooling velocity. The oil has the great disadvantage that it can burn. It also is a non-ecological medium because during the process there are toxic gas emissions. This is the reason that synthetic mediums replaced the mineral oil. The synthetic mediums are non-toxic and it does not exist to the danger of ignition. Such medium is polialchilenglicol, still it does not have the

same cooling properties in hardening as oil, and the tests make on different concentrations and different initial temperatures of the cooling medium in order to choose the optimum alternative.

P.A.G. has the following characteristics:

- great viscosity: for P.A.G.15% in water the dynamic viscosity  $\eta=75,97[\text{CP}]$ , kinematic viscosity  $\nu=75,2[\text{cSt}]$ ;
- great compatibleness in water;
- reverse solubility in water;
- instability at 50-100°C

The property of reverse solubility in water is interesting in cooling pieces because P.A.G. is soluble in cold water and insoluble in warm water meaning that when the hot piece immerse the glycol separates from water and surrounds the piece modifying cooling in high temperatures (also film boiling).

### 3. RESULTS

It was used a silver control cylinder for determining the cooling capacity of a medium like fluidized bed. Inside the control cylinder was assembled a chromel-alumel thermocouple which allows temperature measurement by a y-t recording apparatus. The test bar gets warm until the wanted temperature (800°C) and then cools in the analyzed medium.

The silver test bar has the following sizes and characteristics:

$$\begin{aligned} \text{Ø} &= 13 \text{ [mm]}, h = 28 \text{ [mm]}, S = 1408 \text{ [mm}^2\text{]}, m = 39.9 \text{ [g]}, \rho_{\text{Ag}} = 10.5 \text{ g/cm}^3 \\ \lambda_{\text{Ag}} &= 418.5 \text{ W/m}\cdot\text{K} \end{aligned}$$

The installation used in experiments includes:

- electrical pipe; y-t recording apparatus; triangular signal generator; thermostat tube; cooling tube; silver test bar with chromel-alumel thermocouple.

Table 1 Cooling curves for PAG 15% in non-barbotaged water

Cooling curves for PAG 15% in non-barbotaged water at T=20°C; 30°C; 40°C; 50°C				
T[°C]	20C	30C	40C	50C
800	0	0	0	0
700	3.4	3.2	3	2.8
600	7.4	6.6	6	6
500	11	10	9.4	9.2
400	13.8	13.8	13	12.6
300	16.2	15.2	15.6	15.4
200	18.8	18	17	16.8
100	29	21.8	22.2	22.2
50	44	35	39	41

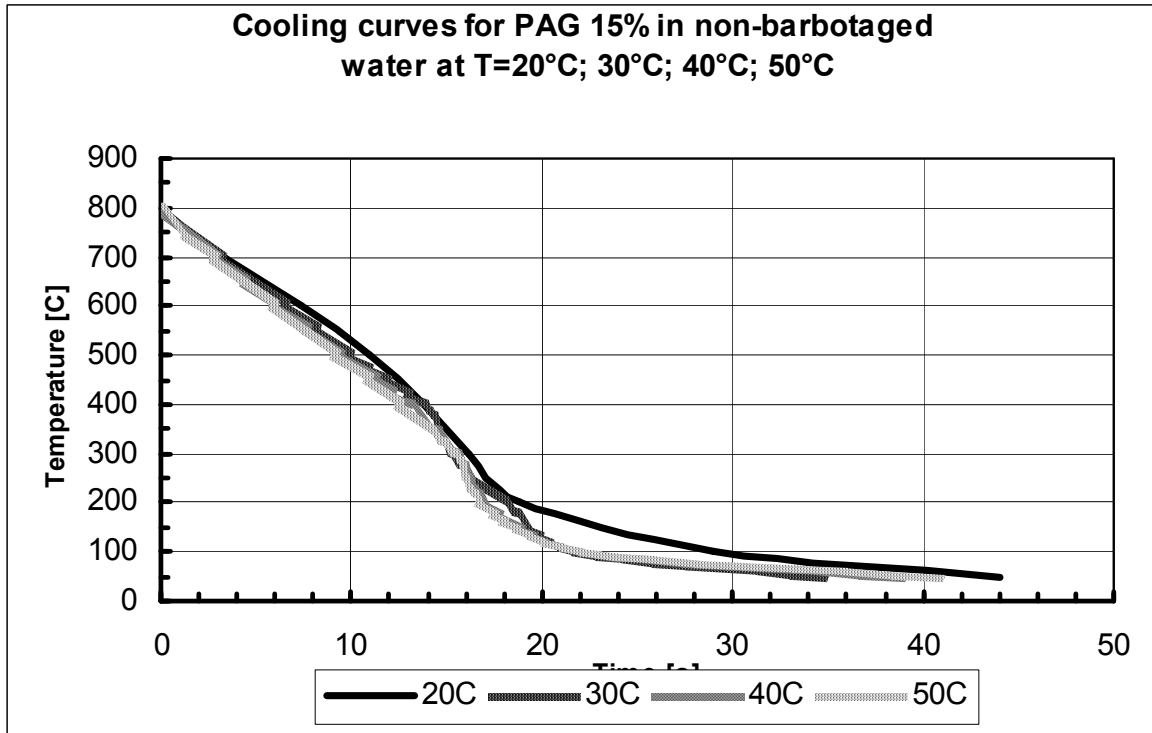


Figure 1 Cooling curve for PAG 15% in non-barbotaged water

Table 2 Cooling velocities variation for PAG 15% in non-barbotaged water

Cooling velocities variation for PAG 15% in non-barbotaged water at T=20°C; 30°C; 40°C; 50°C				
T[°C]	20C	30C	40C	50C
800	0	0	0	0
700	29.41	31.25	33.33	35.71
600	25	29.41	33.33	31.25
500	27.78	29.41	29.41	31.25
400	35.71	26.32	27.78	29.41
300	41.67	71.43	38.46	35.71
200	38.46	35.71	71.43	71.43
100	9.8	26.32	19.23	18.52
50	3.33	3.79	2.98	2.66

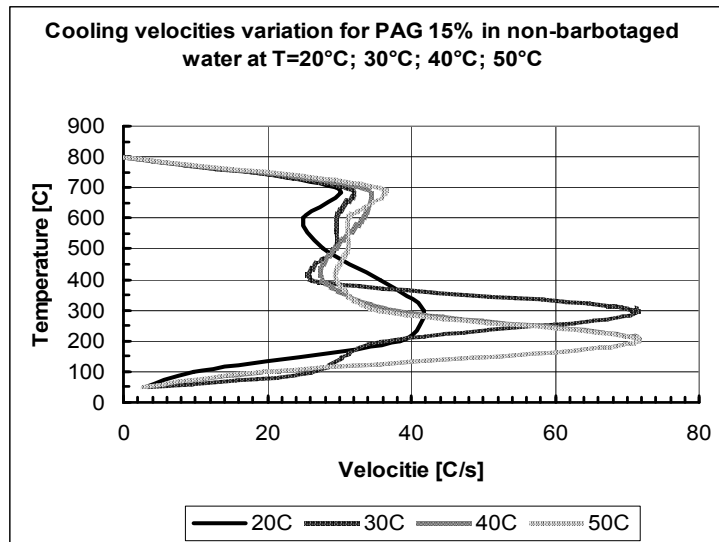


Figure 2 Cooling velocities variation for PAG 15% in non-barbotaged water

Table 3 Cooling curve for PAG 15% in barbotaged water

Cooling curves for PAG 15% in barbotaged water at T=20 <sup>0</sup> C; 30 <sup>0</sup> C; 40 <sup>0</sup> C; 50 <sup>0</sup> C				
T <sup>0</sup> [C]	20C	30C	40C	50C
800	0	0	0	0
700	3.2	3	2.6	2.6
600	6.8	6	5.6	5.6
500	10.6	9.6	8.8	8.4
400	14.6	13.2	12.6	12
300	17.6	15.6	15	15
200	19.4	17.6	16.4	16.8
100	23.2	21.6	19.8	20.6
50	36.2	32.6	33	35.2

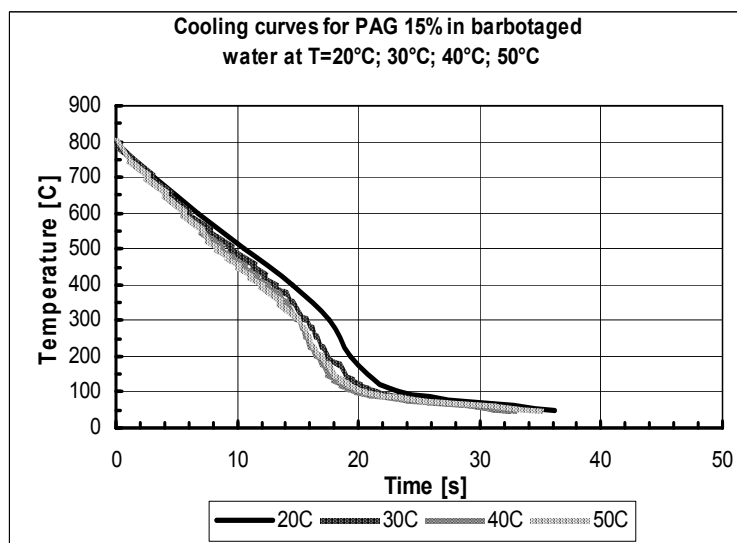


Figure 3 Cooling curve for PAG 15% in barbotaged water

Table 4 Cooling velocities variation for PAG 15% in barbotaged water

Cooling velocities variation for PAG 15% in barbotaged water at T=20°C; 30°C; 40°C; 50°C				
T[°C]	20C	30C	40C	50C
800	0	0	0	0
700	31.25	33.33	38.46	38.46
600	27.78	33.33	33.33	33.33
500	26.32	27.78	31.25	35.71
400	25	27.78	26.32	27.78
300	33.33	41.67	41.67	33.33
200	55.56	50	71.43	55.56
100	26.32	25	29.41	26.32
50	3.85	4.55	3.79	3.42

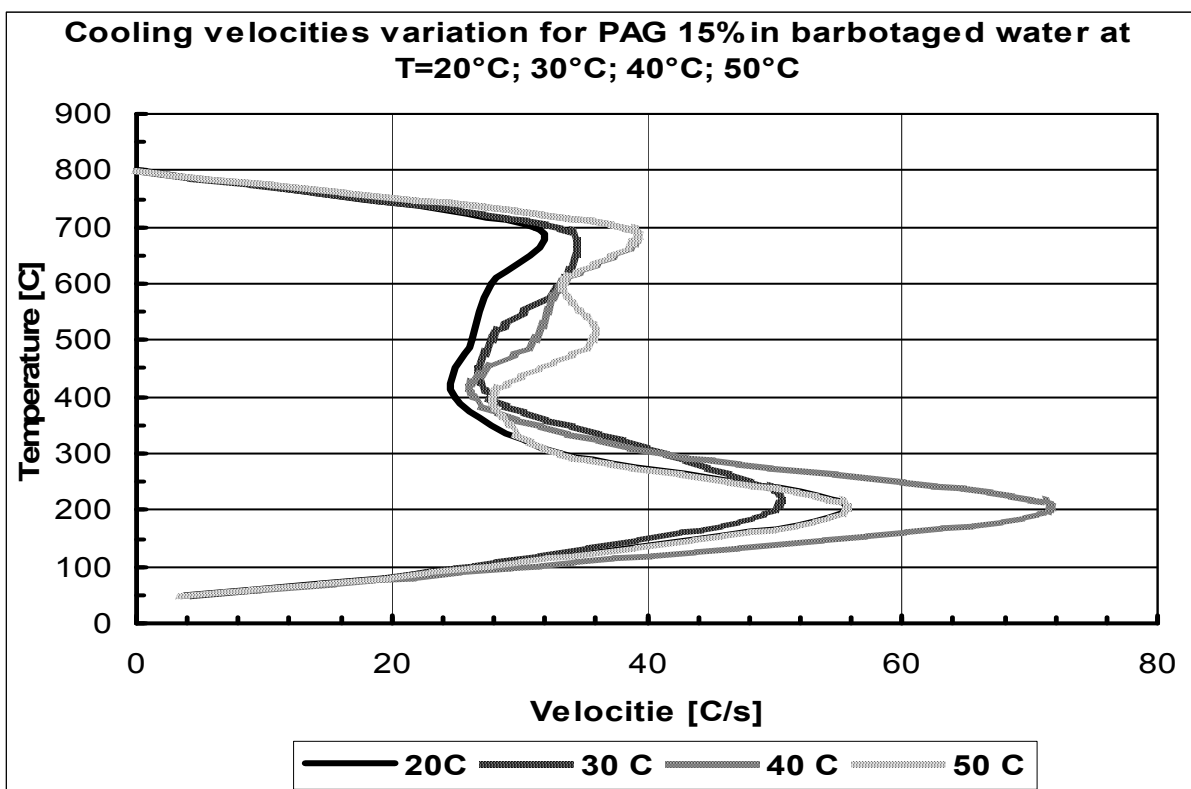


Figure 4 Cooling velocities variation for PAG 15% in barbotaged water

We made determinations on the cooling characteristics of P.A.G. 15% in water, the cooling medium got warm at 20°C, 30°C, 40°C, 50°C. P.A.G. is insoluble at 50-100°C so we choose the maximum temperature 50°C.

The tests were made in fluidized bed and calm bed.

The test bar got warm in the pipe until 800°C and then conducted in P.A.G., the cooling curve recorded by “y-t recording apparatus”.

The results appear in a table and based on them we can trace the cooling curve  $T = f(t)$ , and the cooling velocity variation depending on temperature  $v_r = f(T)$ .

#### 4. CONCLUSIONS

1. We notice from graphics that P.A.G. 15% in water the higher its initial temperature is the faster cools, reverse than water mostly because the property of reverse compatibleness.

2. P.A.G. has a small cooling velocity in the interval 700-350 about 30 °C/s and it makes it improper as a cooling medium for steel which are not capable of being hardened.

3. P.A.G. 15% in water, in the interval 300-150, has the cooling velocity is bigger then 50°C/s with the initial temperature of 40°C and 50°C and this might permit the appearance of the clefts.

P.A.G. 15% in water as a hardening cooling medium it uses only on steel capable of being hardened and it is better to have the initial temperature until 30°C.

*Received February 20, 2005*

*Technical University "Gh.Asachi" Iasi*

#### REFERENCES

- /1/. Hopulele, G. D. Gălușcă, I. Alexandru, *Tratamente termice și termochimice*, vol I și II, Rotaprint Iași, 1983
- /2/. R. Dudău, *Medii de răcire pentru călire*, referat pentru pregătirea la doctorat

#### CERCETĂRI PRIVIND CAPACITATEA DE RĂCIRE A MEDIILOR SINTETICE DE CĂLIRE TIP POLIALCHILENGLICOL (P.A.G. 15%)

**Rezumat:** Lucrarea prezintă cercetări experimentale asupra capacității de răcire a mediilor de răcire sintetice tip polialchilen glicol dizolvat în apă (15%). Curbele de racire au fost trasate experimental folosindu-se pentru înregistrarea racirii centrului unei probe cilindrice de argint de dimensiuni standardizate în centrul careia se găsește înglobat un termocuplu tip cromel-alumel. Incalzirea epruvetei s-a realizat într-un cuptor cilindric cu rezistența electrică, iar mediului de racire i s-a variat temperatura cu ajutorul unui calorimetru, barbotarea mediului fiind realizată cu aer. Experimentele s-au realizat pe mediu de răcire barbotat și nebarbotat și variind temperatura inițială (20°C, 30°C, 40°C, 50°C). După trasarea experimentală a curbelor de racire au fost calculate vitezele medii de racire pe intervale. Rezultatele au fost tabelate și reprezentate grafic. Din studiul graficelor se observă că polialchilen glicolul 15% în apă, are o viteză relativ mică de racire pe intervalul 700°C-300°C și aproape dubla în intervalul de temperatură 300°C- 50°C lucru datorat solubilității inverse în apă a polialchilen glicolului care este solubil în apă rece și insolubil în apă caldă.

## EXPERIMENTAL RESEARCHES OF TITANIUM THERMICAL LAYERS OBTAINED BY PLASMA SPRAYING

BY

PETRA MOȚOIU, MARIO ROSSO\*

**Abstract.** *The titanium powders are used in thermal spraying applications for layers which have a good behaviour in “metal on metal friction”, tenacity, shock and corrosion resistance.*

*Most of the industrial applications need very thin layers. As a consequence it is important as the adherence between the cover layer and the base one should be obtained without a middle coating layer. First of all the nature of the adherence is due to: the high temperatures of the materials used, the fine structure of the particles and the very high speed of spraying in oxygen or helium atmosphere, the result being an extremely high resistance of the layer adherence. The paper shows the characteristics of titanium powder and its plasma jet spray layers*

**Keywords:** *atomization, intermetallics, hardfacing, surface engineering, wear resistance, corrosion resistance*

### 1. INTRODUCTION

Thermal spraying technologies are an effective way to ensure surface protection against destructive effects of wear, corrosion and oxidising phenomena.

These technologies can be applied in majority of industrial sectors in order to improve properties of new parts or for reconditioning worn out parts technology.

Ideally, it would be comfortable to have a material able to resist to all type of wear, but the work condition intricacy combined with economic reason have lead to the development of a big number of powder materials that are used in thermal spraying technologies.

The main metal powders used in thermal spraying technology are usually classified according to the chemical composition, which can establish the properties of the new layer.

The titanium layers obtained by plasma spraying are used in different aerospace and non aeronautical applications due to the combination of low density, very good mechanical properties and high corrosion resistance.

The accomplishment of new titanium thermal layers is effectively used in order to increase the lifetime of different engine parts securing the thermal protection in use, (corrosion resistance) high corrosion and oxidising phenomenon.

The combination of these properties with a severe control of the thermal plasma spraying process of the titanium powders allows the accomplishment of layers whose hardness values are approximately 700HV. These hardness values are 1,5 times higher than those of the layers obtained by spraying classical powders (nickel and stellite powders).

## 2. EXPERIMENTS

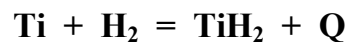
During the spraying process of the titanium powder on the metallic surface, due to the exothermic reaction which takes place between the basic constituents of the titanium powder and the metallic base, as well as due to the heat which the powder overtakes during its passing through the plasma flame, a pre-established properties layer is obtained. Each coating layer introduces an additional interphase, which participates into the thermodynamical transfer process between systems. These determinations point out discontinuities through the sample volume (the pores, the fissures, the heterogenous structural, chemical and mechanical), the present phases into the system as well as the metallographic constituents.

The experimentations will follow the influence of the technological parameters (argon and hydrogen flow, spraying angle, spraying distance, spraying speed, powder flow, physical powder properties) over the physical-mechanical properties of the obtained layers.

The study of the transformations induced into the material by the phase transition, plastic deformations, thermal treatments or by the system particles interaction will be accomplished using the electronic microscope.

The main phases of the titanium powder obtaining operation are:

The hydriding of the titanium sponge into an electrical resistant oven, at a temperature of 500 - 550 °C, when takes place the exothermic reaction:



The grinding of the titanium sponge in order to obtain TiH<sub>2</sub> with an appropriate granulation, in order to obtain titanium powder.

Vacuum dehydriding of the TiH<sub>2</sub> powder, into an identical oven with the one used for hydriding at the maximum temperature of 850 °C.

The grinding and sorting of the titanium powder. The grinding operation is optionally, in case that during the dehydriding begins the synthesis process. The grinding is executed into a titanium ball mill under normal or argon atmosphere.

The sorting is realised with the help of a set of sieves placed upon a vibrator.

The main characteristic of the process consists in the fact that the hydriding operation of the titanium sponge takes place simultaneously with the dehydriding operation in one single equipment, which is provided with two identical ovens.

Table 1. Titanium Sponge Chemical Composition

PROBE SYMBOL	Ti	Fe	SI	O <sub>2</sub>	N <sub>2</sub>	Mg	H <sub>2</sub>	Cl
	(% )							
BT - 1	99,5	0,1	0,05	0,1	0,02	0,08	0,005	0,10

Sponge granulation: 6 - 20 mm.

The pilot installation is composed of two hydriding - dehydriding ovens, vacuum equipment, measurement and control device of the process.

Oven power: 20 kW.

H<sub>2</sub> content : 0,029 - 0,021 % H<sub>2</sub>.

Table 2 shows chemical analysis results for the obtained powder.

Table 2. Chemical Composition of the Titanium Powder

Raw material	Granulometric class (mm)	Fe	Si	Ca	O <sub>2</sub>	N <sub>2</sub>	H <sub>2</sub>
		(%)					
Sponge of Ti IMNR	ϕ 0,1	0,10	0,05	-	0,17	0,037	0,021
Sponge of Ti IMNR	ϕ 0,1	0,10	0,055	-	0,25	0,06	0,027

Regarding the dimension and granulometric repartition of the powder, they have a very important influence upon physical-chemical properties of the layers obtained by plasma spraying. In order to achieve this goal a granulometric analysis of the titanium powder was made on a lab vibrator during 20 minutes, the obtained results being presented in Table 3.

Table 3. Granulometric Repartition of the Titanium Powder

Wight Charge	Granulometric repartition (%)									Diam med.
	+315	+200	+125	+80	+71	+63	+56	+40	-40	
	(μm)									
Powder Ti	4,66	0	10,36	23,83	11,92	3,62	4,14	6,22	35,25	40,25

Medium diameter of the particle ( $D_{med}$ ) has been calculated using the following formula:

$$D_{med} = 100 / \sum(a_i/d_{i med}) \quad (\text{mm}),$$

were:  $a_i$  = % content of the granulometric fractions

$d_{i med}$  = Medium diameter of the granulometric fractions

Figure 1 presents the curves of the granulometric distribution (powder load function of the particles sizes and the plurality of offices load function of the particles sizes) for the titanium powder, obtained by the hydruration – dehydruration proceeding.

The fluidity of the titanium powders or the flow speed depend on the granules surface quality, on the granulometric distribution and on the impurity content into the titanium powders. In order to determine the flow speed it was used a special mechanism composed of the funnel and the measure container. 50 g of powder are weighted, and then introduced into the funnel and the chronometre notates the flow time.

Figure 1 presents the morphology of the titanium powder obtained by the hydruration – dehydruration proceeding.

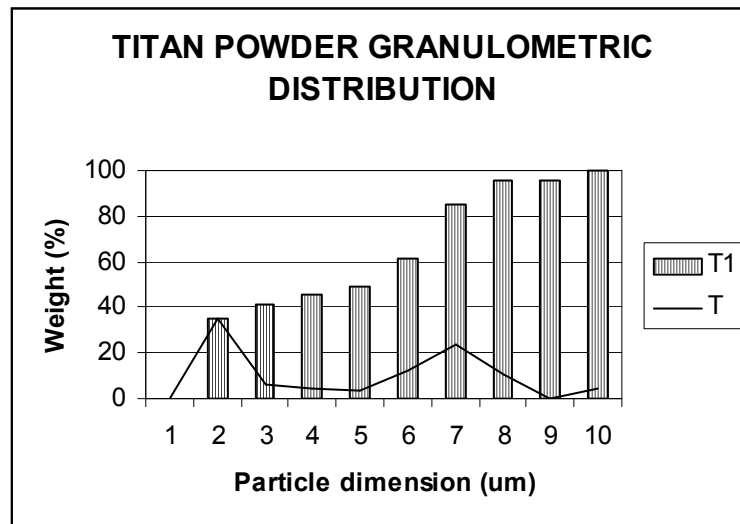


Figure 1 The morphology of the titanium powder

The granularity of the titanium powder is  $\approx 250 \mu\text{m}$ . The stereoscope analysis evidences the little spherical granules of the titanium powder and the visible spheroidale granules. The mettalographyc determination followed the achievement of a solidification structure study, taking into account the size and dimension of the crystals. The experimentations continued with the coating of an OL 37 mettalic surface (unalloyed steel) by plasma spraying of the titanium powder. The applied titanium coating will allow its usage into industrial processes where special materials are needed. The coating experimentations were made with the help of a METCO 7 M plasmatron, the obtained spraying parameters beeing presented in the next table.

Table 4 Optimum Coating Parameters

Argon and hydrogen flow [ $\text{m}^3 \cdot \text{h}^{-1}$ ]	Power plasma flame [kW]	Spraying distance [mm]	Spraying speed [ $\text{m} \cdot \text{s}^{-1}$ ]	Temperature of base material [ $^{\circ}\text{C}$ ]	Thickness of coating [mm]	Powder flow [ $\text{kg} \cdot \text{h}^{-1}$ ]
Ar+20 vol.%H <sub>2</sub> 37	80	60, 80, 120	0,3	$140 \pm 5$	0,5	0,7

The technological operations of the mettalic titanium powder plasma spraying process underlines its main steps. It must be taken into consideration the fact that respecting the operational parameters is determining for suitable coatings.

The preliminary thermal plasma coating experimentations were made upon numerous probes, taking into account a lot of factors which influence the final structural and physical-mechanical characteristics of the experimental samples.

There are two coating aspects which must be taken into consideration:

- The contact with the mettalic surface
- The internal interactions

Due to the fact that each separated particle strikes the surface and it is flattened by the powerful shock, the result is a local contraction of each particle which is somehow compensated by the material fluajul.

The correct choice of the plasma gas represents an important factor regarding the reactions type which can be generated at the metal-base interphase, finally a suitable surface resulting.

In order to achieve minimum expenses and a maximum heat transfer, argon is used with a 10 to 20 % H<sub>2</sub> addition.

For pure theoretical operations, in order to avoid any possible reaction with the plasma gas, pure argon is used.

Generally, the process must take place so that the plasma gas shouldn't react with the metallic base which has to be coated.

Macrostructural studies allow to examine the obtained surfaces. Samples with special prepared surfaces are used, in order to underline the present phases and the metallographic constituents.

Photo 1 presents the metallography (without chemical attack) of the coated titanium phase on the metallic base at 125 X.

Photo 2 presents the metallography (with chemical attack) of the coated titanium phase on the metallic base at 500 X.

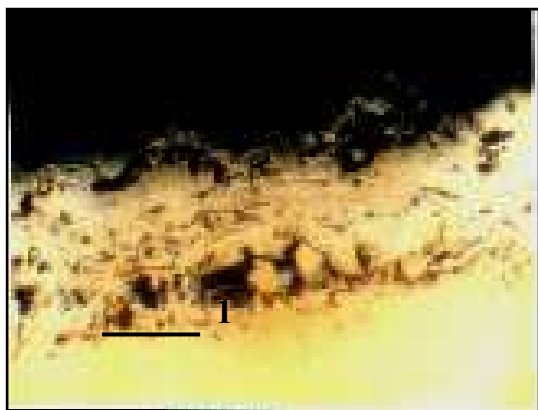


Photo 1 Ti powder microstructure (x125)



Photo 2 Ti powder microstructure (x500)

We can observe the multilayer character of the coating.



Photo 3 Ti powder and the base microstructure ( x500 )

For a better visualisation of the structure the base was attacked by a 1% HF solution.

For the new layer a special HF+HNO<sub>3</sub>+glicerinattack solution was used. Photo 3 shows structural modifications at the metal-base interphase, as well as a growth of the crystals dimensions.

The contact between components presents irregular surfaces. There are big contact surfaces between the Ni intermediary layer and the base one.

### CONCLUSIONS

The realised reaserches and studies allow to establish that the titanium mettalic powder may be used into the plasma spraying process for the thermal covering of the different mettalic surfaces.

The method of obtaining titanium powder by the hydruration – dehydruration process allows to achieve a powder whose phsycal-chemical characteristics are suitable due to its plasma spraying.

The fluidity of the titanium powders or the flow speed depend on the granules surface quality, on the granulometric distribution and on the impurity content into the titanium powders.

The coating experimentations were made with the help of a METCO 7 M plasmatron, the obtained spraying parameters beeing presented in the next table.

The experimentations were made with the coating of an OL 37 mettalic surface (unalloyed steel) by plasma spraying of the titanium powder. The applied titanium coating will allow its usage into industrial processes where special materials are needed.

*Received April 19, 2005*

*Research Institute For Nonferrous And Rare Metals– Bucharest  
\*Politehnico di Torino*

### REFERENCES

- /1/. E.Klar, J.Fesko, On the Particle Shape of Atomized Metal Powders, Prog.Powder Metal,vol.37.p 47 /66
- /2/. F.N.Longo, Microhardness of Some Flame Sprayed Coatings
- /3/. O.S.Nichipenko, Shaping of Powder Particles During the Atomization, vol.15 ( No.9 ), p 665/669
- /4/. S.Small, T.J. Bruce, The comparison of Water and Inert Gas Atomized Powders, Int.J.Powder Technol.,vol.4(No.3)

### CERCETĂRI EXPERIMENTALE DE OBȚINERE TERMICĂ A STRATURILOR DE TITAN ÎN JET DE PLASMĂ

**Rezumat:** Pulberea de titan este utilizată în aplicații de depunere termică a straturilor cu o bună rezistență la „frecare metal pe metal”, tenacitate, șoc și coroziune. În multe aplicații industriale sunt necesare straturi subțiri. În consecință este important ca aderența dintre materialul de bază și depunere să nu necesite un strat de acroș. Pentru a realiza o aderență de calitate superioară sunt necesare: temperatură ridicată a materialelor utilizate, structură fină a particulelor și o viteză ridicată a jetului de pulbere în atmosferă de oxigen sau heliu, rezultatul fiind o rezistență extrem de mare a aderenței stratului. Lucrarea prezintă caracteristicile pulberii de titan și a straturilor realizate în jet de plasmă.

## LABORATORY TECHNIQUE FOR ADVANCED REDUCING OF SOME POLLUTANTS FROM IRON AND STEEL WASTEWATERS

BY

CRISTIAN PREDESCU, \*ECATERINA MATEI, MIRELA GABRIELA SOHACIU,  
AVRAM NICOLAE

**Abstract.** *In this paper are presented the results obtained for wastewaters from blast furnace wet scrubbing treatment, after application of the coagulation method, this being a properly technique for suspended solids and/or unmiscible colloidal particles that are dispersed into liquid, with  $1\mu - 100\mu\text{m}$  diameters. The choosing of the coagulation technique has been made based on the source generating the waste water, the loading with the pollutants of the waters and local conditions of the site. The technique is worldwide applied for industrial wastewater treatment, being considered a BAT (best available technique), because of the high efficiency and the high flow rates of water. Also, in the paper are presented results from physical and chemical analysis and the calculus for removal rate of analyzed pollutants.*

**Keywords:** *pollutants, waste waters, best available techniques, coagulation process*

### 1. INTRODUCTION

The coagulation process takes place in two stages:

- In the initial step, the interparticulate forces responsible for the stability of the particulates are reduced or eliminated by addition of suitable chemicals;
- In the second step, particulate collisions occur due to transport by molecular motion or mechanical mixing and if these collisions are successful, aggregation occur.

Table 1 provides an overview of the coagulation process with the respect:

- 1) The principle phenomenon occurring;
- 2) The component actions associated with each phenomenon;
- 3) The standard terminology for those actions;
- 4) The facilities required to complete the process.

The chemicals used to destabilize particulates are known as *coagulants*. Chemical handling and feeding equipment must be designed for preparation of the chemical coagulant prior to addition. The coagulant is then injected into the process stream through a mixing device that should provide rapid and thorough dispersion of the coagulant in the water.

This rapid, flash or initial mixing stage, which occurs over a short time frame (usually less than 1 min.), serves to optimize the effectiveness of the coagulant for particulate destabilization.

Following destabilization, less intense mixing of the particulates must be provided to increase the rate of particulate encounters or collisions without breaking up or disrupting the aggregates being formed. Proper design of both mixing device and

the mixing basin is necessary to achieve optimum aggregation of the finely divided particulate contaminants prior to removal in the solid separation process.

Table 1 Overview of coagulation process

Phenomenon	Action	Facility involved
Formation of active coagulant species	<ul style="list-style-type: none"> <li>- Preparation of coagulant (dilution, dissolution);</li> <li>- Treatment dispersion of coagulant chemical reactions with ligands (<math>\text{OH}^-</math>, <math>\text{SO}_4^{2-}</math>) e.g., hydrolysis, polymerization, complex formation.</li> </ul>	Chemical handling and feeding equipment Mixing device for rapid and thorough dispersion of chemical.
Particulate destabilization	<ul style="list-style-type: none"> <li>- Compression of double layer by indifferent electrolytes;</li> <li>- Charge neutralization by specifically adsorbed charged species;</li> <li>- Surface precipitation and formation of interparticle “bridges”;</li> <li>- Coagulant precipitation and entrapment of particulates.</li> </ul>	Coagulation basins with devices for rapid mixing
Particulate transport	<ul style="list-style-type: none"> <li>- Random collisions due to thermal motion of water molecules (Brownian motion);</li> <li>- Ordered collisions due to differential relative particulate velocities achieved by mixing and differential settling.</li> </ul>	Basins with mixing devices for low-shear turbulence

Selection and of the type and dose of coagulant depends on the characteristics of the coagulant, the particulates and the water quality. However, prediction of the optimum coagulant combination from characteristics of the particulates and the water quality is not yet possible. As a consequence, each coagulation problem must be solved empirically.

The standard procedure for bench-scale testing of coagulant doses and types is the use of a “jar test”.

The most used coagulants are metals salts, such as: alum  $[\text{Al}_2(\text{SO}_4)_3 \cdot 18\text{H}_2\text{O}]$ , ferric sulfate  $[\text{Fe}_2(\text{SO}_4)_3 \cdot x\text{H}_2\text{O}]$ , ferric chloride  $[\text{FeCl}_3 \cdot 6\text{H}_2\text{O}]$ , ferrous sulfate  $[\text{FeSO}_4 \cdot 7\text{H}_2\text{O}]$ , magnesium carbonate  $[\text{MgCO}_3 \cdot 3\text{H}_2\text{O}]$ , sodium aluminate  $[\text{NaAlO}_2]$ . In water, these salts hydrolyze and lead to hydrolysis compounds, neutral or electrical charged.

Among these, iron salts are often used for waste water treatment, precipitation domain for  $\text{Fe}(\text{OH})_3$  being larger than for  $\text{Al}(\text{OH})_3$ . Thus, the formation of  $\text{Fe}(\text{OH})_3$  begins at  $\text{pH} = 3$ , but the optimum value of  $\text{pH}$  for coagulation is situated between 9.0 - 9.5.

In order to reach and maintain these values for  $\text{pH}$  is necessary to be added basis for alkali medium, such as: caustic soda or lime, etc. The advantage for using of caustic soda is the absence of calcium ions that are responsible for high values of hardness for reused water.

In the industry, for wastewaters treatment, the most used iron salts are: ferrous sulfate  $[\text{FeSO}_4 \cdot 7\text{H}_2\text{O}]$ , ferric sulfate:  $[\text{Fe}_2(\text{SO}_4)_3 \cdot 9\text{H}_2\text{O}]$ , ferric chloride  $[\text{FeCl}_3 \cdot 6\text{H}_2\text{O}]$ .

In literature, the  $\text{FeSO}_4 \cdot 7\text{H}_2\text{O}$  consumption, according to opalescence of water (suspended solids content) is: 0.2 mval/l for low content, 0.4 mval/l for medium content and 0.7 mval/l for high content, where: 1 mval  $\text{FeSO}_4 \cdot 7\text{H}_2\text{O}$  = 139 mg.

Although, the data from literature indicate the optimum contents for ferrous sulfate and caustic soda or lime, these values must be obtained by laboratory experiments.

The advantage for ferrous sulfate is its low cost, being a waste from pickling operations from iron and steel industry and a by-product resulted from chemical plants from coke manufacturing.

## 2. EXPERIMENTAL PROCEDURE

The experiments have as a goal the increasing of the wastewater treatment efficiency by application at laboratory scale of a Best Available Technique (BAT) for treatment of waste waters resulted at wet scrubbing of blast furnace gasses. These types of waters have in their composition, mainly suspended solids and also cyanides, phenols, chlorides, metallic ions, etc.

Based on literature information and actual data from national plants, it is observed that the application of this technique may lead to removal from these wastewaters of some major pollutants such as suspended solids and oils, the pollutants that formed the stable colloidal aqueous solutions.

For the experiment it was applied a procedure known as jar test. This procedure consisted of the following steps:

1. 10 Berzelius glasses had been filled with 500 ml wastewater, the first glass was the blank sample and in the next glasses had been added different quantities of coagulant ( $\text{FeSO}_4 \cdot 7\text{H}_2\text{O}$ ), from 5 to 50 mg/l, in ascending order; the concentration domain for coagulant had been chosen according to literature (optimum dose: 40 – 45 mg / l  $\text{FeSO}_4 \cdot 7\text{H}_2\text{O}$ ).
2. The content of each glass is stirring at about 100 rotations / min. during 1 hour for the dispersion of the coagulant into the entire volume of the samples.
3. The speed of the stirring is decreased at 25 – 30 rotations/minute during 15 – 20 minutes for settling of the sludge.
4. The stirring is stopped for about 30 – 45 minutes for settling and it is measured the final turbidity (content of suspended solids, mg / l) from the each glass by help of a nephelometer (turbidimeter).

The experimental results had showed the evolution of pH, suspended solids, chemical oxygen demand (COD) value and also sludge quantity as a function by coagulant dose.

## 3. EXPERIMENTAL RESULTS AND DISCUSSION

The samples for experiments had been chosen as follows:

- 5 wastewater samples from no. 1 and 2 Blast Furnace gas wet scrubbing, point of sampling: settling basin;
- 5 wastewater samples from no. 3, 4 and 5 Blast Furnace gas wet scrubbing, point of sampling: settling basin.

In order to reach the optimum value of pH it had been prepared an aqueous solution of caustic soda ( $\text{Na}_2\text{CO}_3$ , technical purity) at 36 % concentration. The value of the pH, after adding the caustic soda, into wastewaters samples, was 9, 5.

The necessary quantity of caustic soda was:

- 16 mg  $\text{Na}_2\text{CO}_3$  for 1 liter of wastewater from no. 1 and 2 Blast Furnace;
- 14,5 mg  $\text{Na}_2\text{CO}_3$  for 1 liter of wastewater from no. 3, 4 and 5 Blast Furnace.

The initial composition of wastewater samples is presented in table 2.

Table 2 Blast furnace water characteristics, settling basin sampling

No.	Parameters, mg / l	No. 1,2 Furnace			No. 3,4,5 Furnace		
		P 1	P 2	P 3	S 1	S 2	S 3
1	pH	6,8	6,7	6,8	7,6	7,5	7,2
2	Suspended solids	930	1015	870	650	600	639
3	Chlorides	500	515	510	955	1000	1010
4	Hardness	19	19	20	23	20	21
5	COD	60	65	51	38	40	40,5
6	Oils	46	50	43	40	45	38

The analysis methods for establishing the right quantity of these pollutants were made according to in force standards, thus: pH: SR ISO - 10523-97, suspended solids: STAS 6953 – 81, chlorides: STAS 8663 – 70, hardness: 3026 – 76, COD: SR ISO 6060 – 96, Oils: STAS 7877/1,2 – 95.

The obtained results and efficiency of this technique are presented in tables 3 -6 and fig. 1 -5.

Table 3 Obtained results from coagulation process of sampling from 1, 2 Blast furnaces, settling basin sampling

FeSO <sub>4</sub> .7H <sub>2</sub> O, mg/l	Suspended solids, mg/l			Oils, mg / l			COD, mg/l			Sludge average values, %
0	1010	930	875	50	46	43	65	60	51	0
5	995	879	815	46,5	40	37,5	59	57	50	5
10	810	725	695	41,5	35,3	30	52	43	41	10
15	729	639	539	36,8	31,6	25,4	49	32	37	25
20	610	500	473	27,5	26,8	22,8	34	25	23	30
25	535	465	415	23,6	22,0	20,5	28	22	20	40
30	530	461	400	21,0	20,6	19,8	23	21	18	45
35	530	460	390	20,5	20,0	19,5	22	20	18	55
40	535	462	390	20,6	20,0	19,5	23	22	20	60
45	540	483	410	20,5	20,2	19,6	23,5	22	20	65
50	550	512	415	20,5	20,2	19,5	23	23	21	70

Table 4 Obtained results after FeSO<sub>4</sub>.7H<sub>2</sub>O treatment of waters from 1, 2 Blast Furnaces, optimum dose: 35 mg / l

Parameter	Raw untreated water	Water treated with coagulant	Efficiency, %
pH	6,8	8,5	-
Suspended solids	935	460	50,53
Oils	48	20	58,33
COD	59	20	66,66

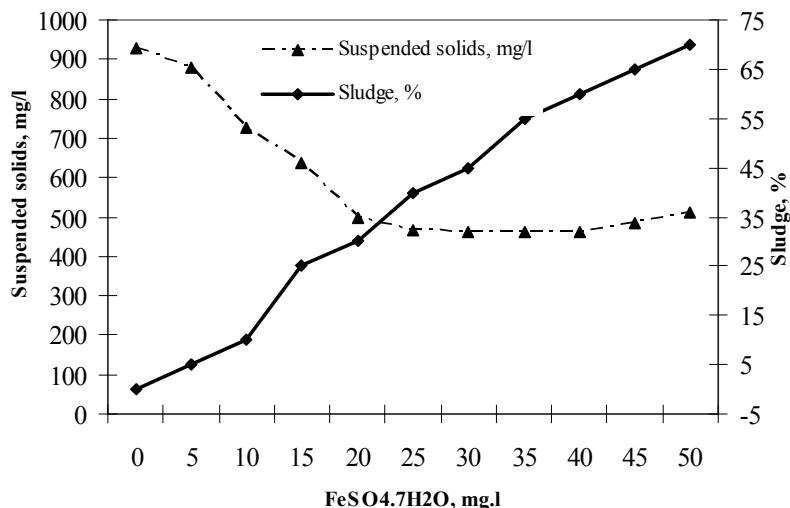


Fig. 1 Suspended solids and sludge content variation of wastewaters from wet scrubbing of 1, 2 Blast Furnaces, after FeSO<sub>4</sub>.7H<sub>2</sub>O treatment

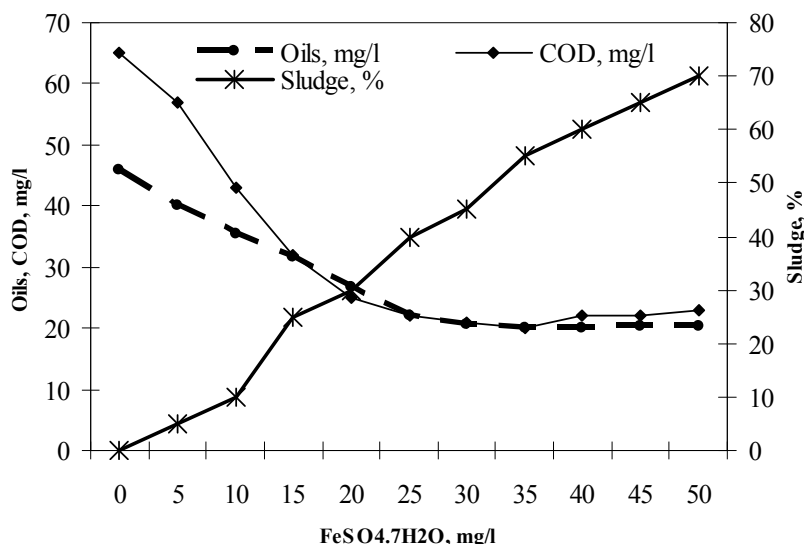


Fig. 2 Oil, COD (chemical oxygen demand) and sludge content variation of wastewaters from wet scrubbing of 1, 2 Blast Furnaces, after FeSO<sub>4</sub>.7H<sub>2</sub>O treatment

Table 5 Obtained results after coagulant treatment of samples from 3, 4, 5 Blast Furnaces, settling basin sampling

FeSO <sub>4</sub> .7H <sub>2</sub> O, mg/l	Suspended solids, mg/l			Oils, mg / l			COD, mg/l			Sludge average values, %
0	780	650	586	45,0	40,0	38,0	40,0	38,0	35,0	0
5	675	569	545	41,0	36,5	32,6	35,5	30,0	27,8	5
10	645	450	520	36,5	30,5	30,0	30,0	22,0	20,9	10
15	569	395	400	30,9	25,1	24,0	26,5	17,8	16,5	25
20	415	375	370	25,6	23,6	19,5	19,3	15,0	14,5	30
25	378	350	342	20,1	19,5	17,6	15,1	13,5	12,9	40
30	320	310	295	17,9	16,0	15,5	14,5	13,6	13,0	45
35	315	305	290	17,5	15,8	15,5	14,3	13,5	13,0	55
40	320	348	310	17,5	16,0	15,5	14,5	13,7	13,3	60
45	328	360	325	17,7	16,0	15,4	14,8	14,0	13,5	65
50	335	381	340	17,5	16,0	15,5	15,0	14,2	14,5	70

Table 6 Obtained results after  $\text{FeSO}_4 \cdot 7\text{H}_2\text{O}$  treatment of waters from 3, 4, 5 Blast Furnaces, optimum dose: 35 mg / l

Indicator	Raw untreated water	Water treated with coagulant	Efficiency, %
pH	7,6	8,6	-
Suspended solids	650	305	53,07
Oil	41	16,25	60,36
COD	38	14,2	62,63

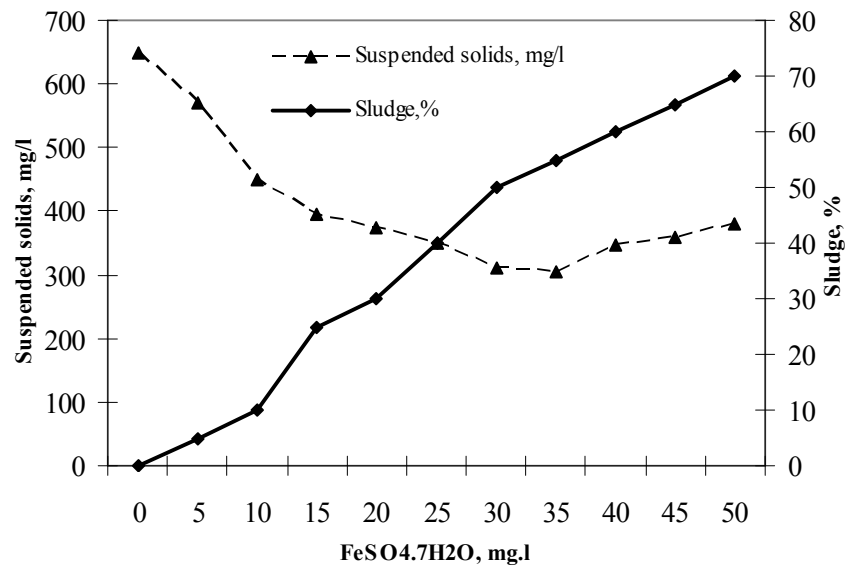


Fig. 3 Suspended solids and sludge content variation of wastewaters from wet scrubbing of 3, 4, 5 Blast Furnaces, after  $\text{FeSO}_4 \cdot 7\text{H}_2\text{O}$  treatment

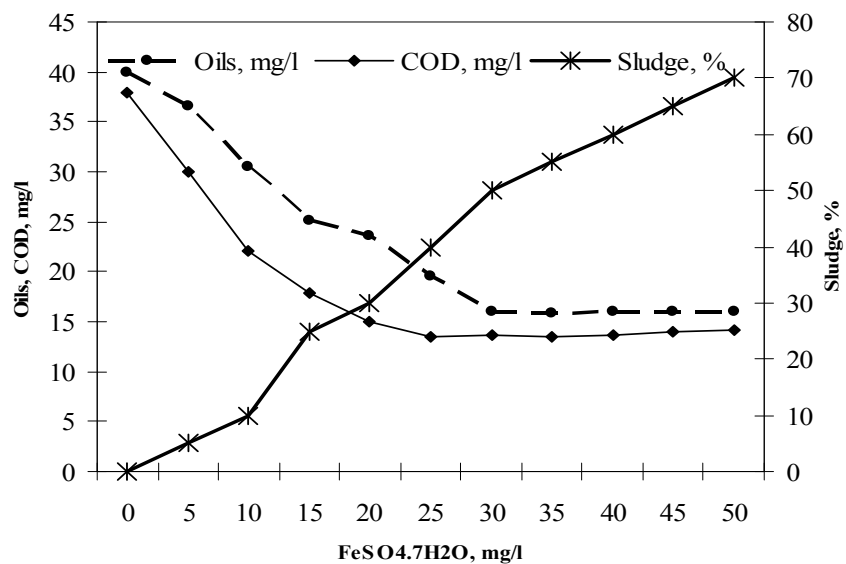


Fig. 4 Oil, COD (chemical oxygen demand) and sludge content variation of wastewaters from wet scrubbing of 3, 4, 5 Blast Furnaces, after  $\text{FeSO}_4 \cdot 7\text{H}_2\text{O}$  treatment

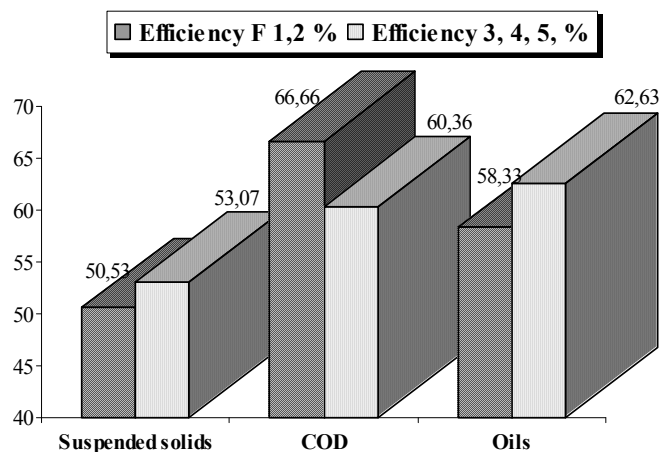


Fig. 5 Treatment efficiency with  $\text{FeSO}_4 \cdot 7\text{H}_2\text{O}$  for Blast Furnace wet scrubbing waste waters

#### 4. CONCLUSIONS

The use for iron salts (sulfate or chloride) in coagulation process is advantageous because:

- The hydrolysis products of iron have a low solubility than the ones of aluminum and for this reason iron ions will be found in settled sludge not in treated wastewater composition, thus being possible the recovery of this sludge;
- The hydrolysis products of iron have a high density, increasing in this way settling rate;
- Iron salts have a large domain for precipitation situated between 3 -13 than the aluminum salts situated between 4 - 8;
- Hydrolysis rate for iron salts, compared with aluminum salts, is not a function by temperature.

As it is observed from experimental data, the removal efficiency for suspended solids by help with coagulation technique is higher than 50%, using an optimum dose of  $\text{FeSO}_4 \cdot 7\text{H}_2\text{O}$  between 30 – 35 mg / l.

Also, it was observed a high efficiency for organic compounds from these types of waters as chemical oxygen demand (COD), higher than 60%. The same results had been obtained also for oil content, the removal efficiency being higher than 50%.

Received April 19, 2005

Politehnica University București

\*Metallurgical Research Institute ICEM SA București

#### REFERENCES

- /1/. X X X: - *Best available techniques reference document on the production of iron and steel - Integrated Pollution Prevention and Control (IPPC)*, July 2000
- /2/. J. A. Philipp ș.a - *Wastewaters management*, Thyssen Stahl A G, Germany, Iron & Steel Industry, 1997
- /3/. Matei, Ecaterina, ș.a - *Eficiențizarea proceselor de tratare a apelor uzate din sectorul siderurgic primar în vederea creșterii randamentului de epurare*, Contract Relansin 1814, 2003
- /4/. Nicolae, A., Matei, Ecaterina, ș.a - *Environmental management in the metallic materials industry*, Bucharest, Ed. Fair Partners, 2001

/5/. D. Robescu, Diana Robescu - *Procedee, instalații și echipamente pentru epurarea apelor*, Ed. UPB, curs litografiat, 1996, București

**TEHNICA DE LABORATOR PRIVIND REDUCEREA AVANSATĂ A UNOR POLUANȚI PREZENȚI ÎN APELE UZATE REZULTATE DIN SECTORUL SIDERURGIC**

**Rezumat:** În lucrare sunt prezentate rezultatele obținute în urma aplicării tehnicii de coagulare pentru apele uzate generate prin epurarea umedă a gazului de furnal, tehnică recomandată în special pentru separarea suspensiilor solide și/sau a substanțelor coloidale nemiscibile cu apa dispersate în soluție, cu diametre cuprinse între  $1\mu$  -  $100\mu$ m. Tehnica de coagulare a fost aleasă ținând cont de sursa de generare a apelor supuse epurării, de încărcarea cu poluanți a acestora și de condiții locale de mediu existente. Această tehnică este utilizată pe scară largă în străinătate la epurarea apelor industriale, fiind considerată în prezent BAT (best available technique), datorită eficienței de separare ridicată și posibilității aplicării în cazul unor debite de apă foarte mari. De asemenea, în lucrare mai sunt prezentate datele obținute în urma analizelor fizico-chimice a acestor tipuri de ape și calculul eficienței de îndepărtare a poluanților analizați.

## DEVELOPMENT OF ALTERNATIVE THERMAL BARRIER COATINGS FOR DIESEL ENGINES

BY

R. SOLTANI, H. SAMADI, AND T.W.COYLE

**Abstract.** *The use of thermal barrier coatings (TBCs) to increase the combustion temperature in diesel engines has been pursued for over 20 years. Increased combustion temperature can increase the efficiency of the engine, decrease the CO and (possibly) the NO<sub>x</sub> emission rate. However, TBCs have not yet met with wide success in diesel engine applications. The most common TBC system is Ytria Partially Stabilized Zirconia (Y-PSZ) which has shown good performance in turbine blade coatings where temperatures approach 1100°C. To reach the desirable temperature of 850-900°C in the combustion chamber from the current temperature of 350-400°C, a coating with a thickness of order 1mm is required, significantly thicker than turbine blade coatings which are on the order of 100μm thick. This results in different temperature and stress profiles in the coating during service than in the case of turbine coatings, and different failure mechanisms.*

*Recent advances in the control of coating structure have led to the development of new PSZ coating microstructures containing grains and pores with sizes in the range of 100-300 nm. Thermal-mechanical properties of such coatings have been characterized and compared with coatings exhibiting the traditional thermal spray structure to assess their suitability as thick TBC for diesel engine applications. Selected coatings have been subjected to engine testing in an instrumented single cylinder diesel test rig.*

*Among possible alternative materials, one of the most promising is mullite. Mullite has excellent thermo-mechanical behavior; however its low thermal expansion coefficient creates a large mismatch with the substrate. To address this problem, multilayer systems have been developed which minimize the thermal expansion mismatch stresses while maintaining chemical and phase stability. The design considerations for such multilayer systems are discussed.*

**Keywords:** *thermal barrier coating, diesel engine*

### 1. INTRODUCTION

Thermal Barrier Coatings (TBCs) in diesel engines offer advantages including higher power density, fuel efficiency, and multifuel capacity due to higher combustion chamber temperature (900°C vs. 650 °C) [1,2]. Using TBCs can increase engine power by 8%, decrease the specific fuel consumption by 15-20% and increase the exhaust gas temperature 200K [3]. Although several systems have been used as TBC for different purposes, yttria-stabilized zirconia with 7-8 wt% yttria has received the most attention. Plasma spray is the most common method of depositing TBCs for diesel applications. It creates a splat structure with 10-20 % volume fraction of voids and cracks [4] (figure 1). High porosity of this structure makes it an ideal choice for TBC.

Widespread application in diesel engines has been limited by insufficient reliability, short lifetimes and cost. Factors playing important roles in determining TBC lifetimes include thermal conductivity, thermal and chemical stability at the service temperature, and thermal expansion coefficient (TEC).

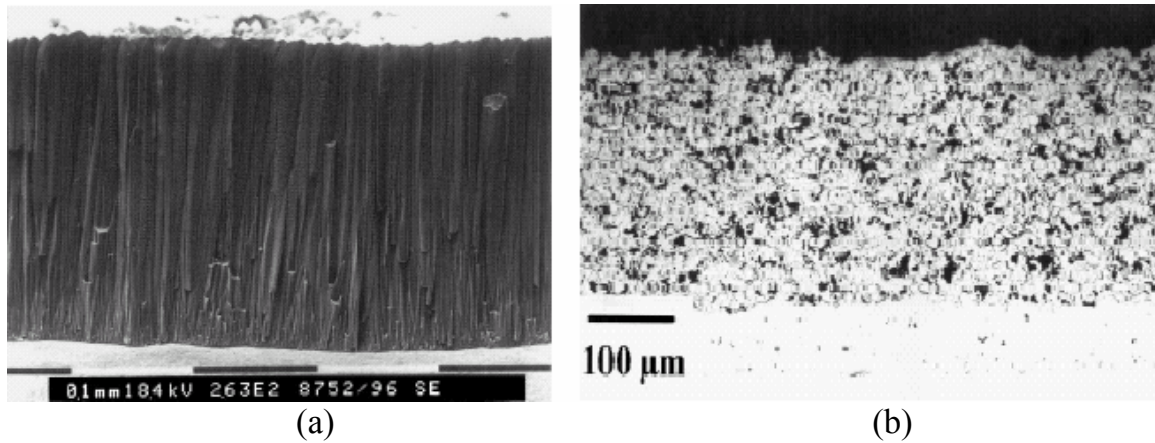


Figure 1. a) EB-PVD coating b) APS coating [5].

## 2. TBC IN DIESEL ENGINE VS. TURBINE BLADE

Recently, much attention has been focused on TBCs for turbine engines. However, the service environment of the coating in the turbine is markedly different than in the diesel engine. In the former, the service temperature is high (1000-1100°C). The superalloy substrate's maximum service temperature is about 800°C.

The thickness of the coating is a few hundred microns. Due to the high substrate temperature, oxidation of the bond coat plays a major role in coating failure. On the other hand, in the diesel engine the gas temperature, currently less than 650°C would ideally approach 900°C. The substrate temperature is limited to approximately 200°C, and therefore a thick coating (at least 1 mm) is required which leads to a high thermal gradient. In a thick thermal barrier coating (TTBC) the bond coat temperature is too low for severe oxidation and creep [6].

Recent work shows that the inelastic behavior of the TTBC ceramic material and the unique features of its microstructure determine the failure mechanism [7]. In a thick thermal barrier coating, when the surface of the YSZ coating is heated, a compressive stress is developed in the surface which will be relaxed after two hours of steady state heating. Upon cooling, the stress becomes tensile and initiates cracks [6].

Due to the mismatch in thermomechanical properties of the top coat and bond coat, this interface is a source for cracking and delamination [8].

## 3. ALTERNATIVES

As mentioned above, conventional YSZ coatings have not proven successful for TBCs in diesel engines. We have explored two approaches to developing alternatives. First, YSZ coatings were deposited using nanocrystalline starting powder to produce a new bimodal coating microstructure which may offer improved thermo-mechanical performance. Secondly, non-zirconia coatings have been investigated. The design of these coatings involves multiple layers of materials selected to minimize the stress in the coating during service.

There is a good thermal expansion coefficient match between YSZ, bond coat and substrate ( $10.7 \times 10^{-6} \text{ k}^{-1}$  vs.  $17.5 \times 10^{-6} \text{ k}^{-1}$  for NiCoCrAlY and  $16 \times 10^{-6} \text{ K}^{-1}$  for IN737) [9]. Good thermo-mechanical performance and fair oxidation protection are other properties of YSZ as a TBC. A number of materials have been proposed in the

literature as possible alternatives to YSZ for engine applications. Each has advantages and disadvantages when compared with the standard coating.

#### 4. NANOSTRUCTURED TBC

In recent years nanostructured materials have been considered as a new concept for increasing the performance of engineering components. Research efforts have demonstrated that many properties of nanostructured materials differ from conventional materials due to the large volume fraction of internal interfaces. Coatings often can provide the improved performance of an alternative material without the necessity of redesigning the entire component. There are several methods to produce nanoscale coatings, including thermal spray processes.

Researchers have shown that nanostructured coatings can exhibit better properties than conventional coatings of the same composition. Gell and coworkers [10-13] reported that nanostructured coatings of  $\text{Al}_2\text{O}_3\text{-TiO}_2$  showed superior mechanical properties, including indentation crack resistance, adhesion strength, spallation resistance, abrasive wear resistance, and sliding wear resistance. Lima et al. [14-16] and Ding and coworkers [17, 18] have investigated nanostructured partially stabilized zirconia (PSZ) coatings and report improved properties such as increased bond strength. Other investigators have suggested that nanostructured coatings would be expected to show better thermal resistance and reduced thermal conductivity compared to their coarse grained coatings. [19-21]

In the current work, PSZ coatings were deposited by air plasma spraying. Two different types of powder feed stocks were employed, a conventional micron particle size powder and a nanostructured particle powder, Fig.2. The influence of the powder type on the microstructure of the coatings was investigated.

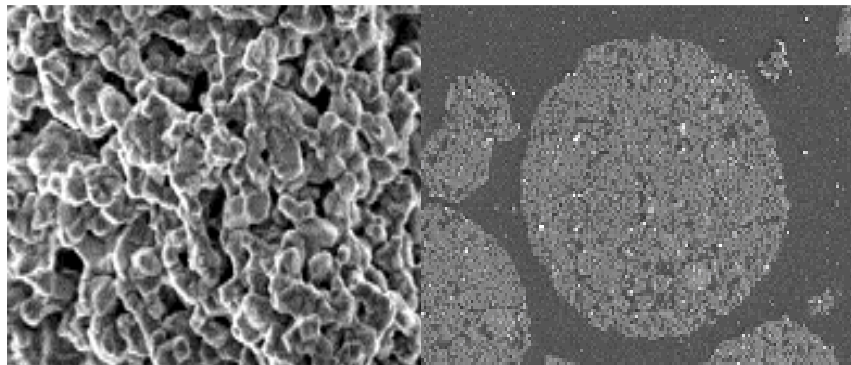


Figure 2. Morphology of nanostructured feedstock. Left: cross section, right agglomerated nano particles.

In the case of the nanostructured powder, the first major concern is to find process parameters which lead to retained non-melted submicron particles in the coating. The objective is to achieve a combination of particle temperature and velocity in the plasma jet which produces a molten skin on the agglomerated particles, but avoids complete melting. The spraying parameters employed are given in table 1.

The conventional powder, obtained from Sulzer Metco, was deposited with the same process parameters as used for the nanostructured powder.

In fig. 3 fracture surfaces of a coatings deposited using these parameters are shown. Compared with conventional splats having columnar grains, the non melted

nanoparticles are plainly seen as equiaxed grains with nano-scale porosity among them.

Table 1. The spraying parameters used for the Nanox S4007 feedstock

Parameters	
Power (kW)	32.5
Current (A)	740
Recorded Voltage (V)	44
Ar gas flow rate (slpm)	40
H <sub>2</sub> gas flow rate (slpm)	2
Ar carrier gas (slpm)	8
Distance (cm)	7
Feed rate (%)	57
Mean velocity ( m/sec)	226
Mean temperature ( °C )	2633

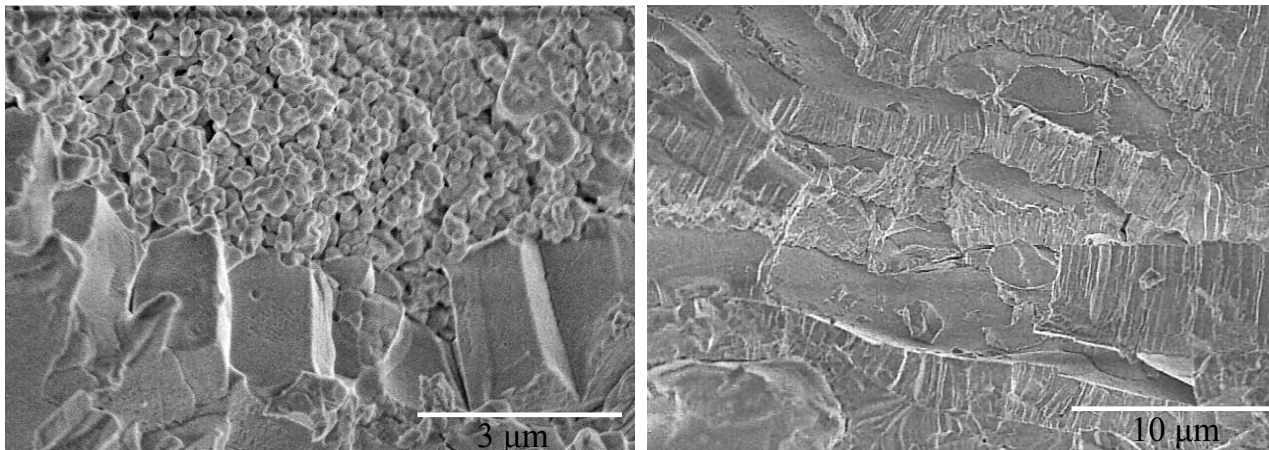


Figure 3. SEM images of fractured surfaces: Left: Non-melted nanoparticles could be easily distinguished Right: Conventional coating

The measured pore size distributions, indicating the diameter of the pores based on the incremental volume of intruded mercury are illustrated in fig 4. The maximum intrusions of mercury for the Nanox and 204B-NS samples are at the pore diameters of 0.2 and 0.43  $\mu\text{m}$ , respectively. It should be mentioned here that some apparent intrusion occurred at low pressures, corresponding to very large pore sizes. This is an artifact due to surface roughness and has been scaled out of the graphs shown. Also, during specimen preparation, especially in the case of the bimodal structured samples with weakly bonded and non-melted nanoparticles, material may be pulled out of the surface leaving relatively large voids which are not indicative of the true structure.

Employing a four-point bend test, creep testing of free standing samples was performed at 800° and 1000°C under a 30 N static load for 4-6 days, to make sure that the sample would enter the steady state creep region. The relative displacement of the center point and inner loading points was determined from the differential displacement of an LVDT.

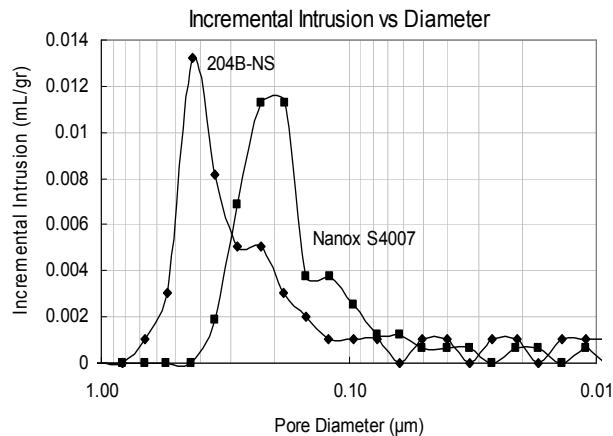


Figure 4. Pore size distribution versus intruded mercury volume for Nanox and 204B-NS.

A numerical method was used to calculate creep strain of samples; results are illustrated in fig. 5.

The coating with the bimodal structure containing pockets of retained nanoparticles shows significantly lower creep rates than the conventional coating at both test temperatures.

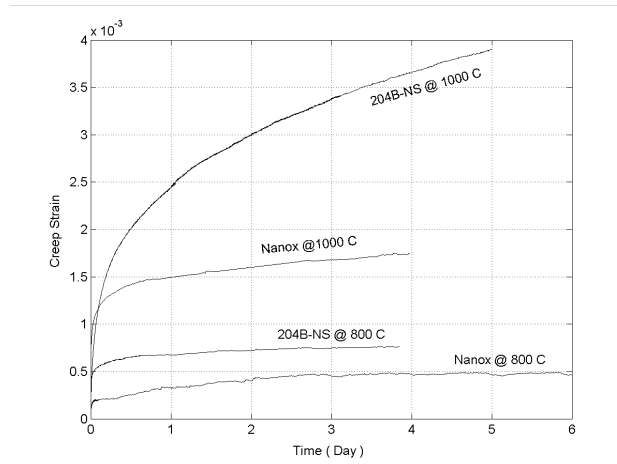


Figure 5. Creep strain of 204B-NS and Nanox samples (up to six days in 800 and 1000 °C under 30 N load); in both temperatures bimodal structure shows lower strain.

## 5. MULTILAYER SYSTEM

In a thick TBC, a low TEC is desirable for the hot surface to minimize thermally derived stresses and sensitivity to thermal shock. However, a large TEC mismatch with the metallic substrate limits coating adhesion. A multi layer system may permit these opposing requirements to be satisfied. Most traditional, high temperature refractory ceramic materials are found in the  $\text{Al}_2\text{O}_3\text{-SiO}_2\text{-MgO}$  system. Among these oxides, some have been considered as alternatives to YSZ in TBCs. The general advantage of materials in this system is their low prices relative YSZ TBCs.

Cordierite ( $2\text{MgO}\cdot 2\text{Al}_2\text{O}_3\cdot 5\text{SiO}_2$ ) has a very low TEC ( $1.67\times 10^{-6}\text{ K}^{-1}$  [22]). After plasma spraying, the cordierite composition is typically found to be amorphous. During subsequent heating, two phase transformations occur, at  $830^\circ\text{C}$  and  $1000^\circ\text{C}$ , which produce a volume change and cause cracking [23]. To deposit crystalline cordierite, the addition of 6 wt%  $\text{TiO}_2$  has been reported to be effective [24]. Increasing the temperature of the substrate to slow the cooling rate of the cordierite also increases the crystallinity; however the oxidation of metal substrates is a concern.

Finally, another way to increase the crystallinity of deposited cordierite is laser surface melting [24]. Zirconia-cordierite composites have also been studied [23]. There are two major problems with this system: the glassy nature of cordierite and its phase transformations remain as problems; and yttria diffuses gradually into the cordierite destabilizing the  $\text{ZrO}_2$  to allow the destructive tetragonal to monoclinic phase transformation to occur.

The high thermal expansion coefficient of forsterite ( $2\text{MgO}\cdot\text{SiO}_2$ ),  $11\times 10^{-6}\text{ K}^{-1}$  [22], permits a good match with the substrate. At thicknesses of some hundred microns, it shows a very good thermal shock resistance. Another advantage of forsterite is its crystallinity after spraying, which is higher than other oxides in this phase diagram [22]. This eliminates the amorphous to crystalline transformation which causes a volume expansion and coating delamination.

Although spinel ( $\text{MgO}\cdot\text{Al}_2\text{O}_3$ ) has very good high temperature and chemical properties, its TEC,  $7.68\times 10^{-6}\text{ K}^{-1}$ , is neither high enough to provide a good match with the substrate, nor low enough to provide good thermal shock resistance. There is only one reported study of spinel as a TBC, in which case it showed poor thermal cycling resistance [22].

Mullite is applied on SiC as an oxidation resistant layer to form an environmental barrier coating (EBC). Its low oxygen diffusivity, low creep rate at high temperatures, high thermo-mechanical fatigue resistance and close TEC match with SiC ( $4\text{-}5\times 10^{-6}\text{ K}^{-1}$  vs.  $5\text{-}6\times 10^{-6}\text{ K}^{-1}$  [22]) makes it the ideal choice for this application. In thin coatings (up to some hundred microns) on top of a metallic substrate, the durability of mullite has been reported to be better than that of zirconia [25]. The low TEC of mullite is an advantage relative to YSZ in high thermal gradients and under thermal shock conditions. Figure 5 compares surface stresses of 500  $\mu\text{m}$  thick coatings of yttria fully stabilized zirconia and mullite during cooling after heating to a steady state temperature distribution under a heat flux of  $270\text{ kWm}^2$ .

Two different values of heat transfer coefficient were used to vary the degree of the thermal shock experienced. Although both samples undergo a peak during cooling, the stress in mullite, unlike PSZ, remains compressive during the cooling process which prevents crack initiation in mullite [6].

However, the large mismatch in TEC with metallic substrates typically leads to poor adhesion. Also, as is the case for cordierite, mullite is amorphous as deposited. In service recrystallization occurs at  $750\text{ -}1000^\circ\text{C}$  which is accompanied by a volume contraction, cracking and top coat debonding [26].

There are two major points a multi layer coating system must address. First, the materials should be chemically and thermodynamically compatible. Second, the thickness of different layers should be optimized to minimize stress distribution among the layers during and after deposition and under service conditions. A set of

chemically compatible materials have been identified which offer a range of TECs and acceptable thermal conductivities. Coupled analysis of the temperature and stress distribution through the thickness of the multi layer coating is underway to evaluate stress levels in the coating with the objective of predicting optimal thicknesses for the individual layers.

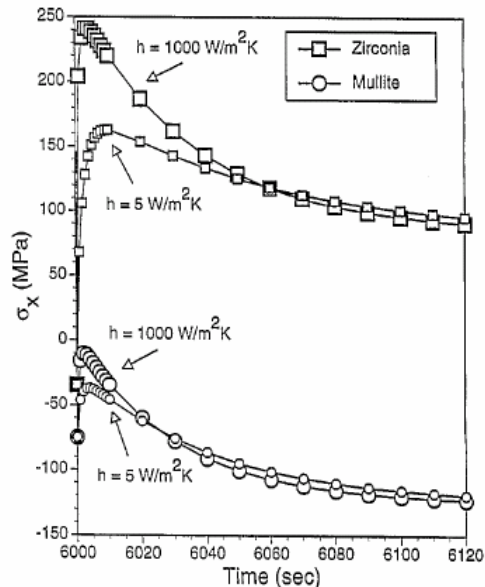


Figure 8. Surface stresses of zirconia and mullite during cooling ( $q=270 \text{ kWm}^{-2}$ ) [6].

## 6. SUMMARY

In this paper, two approaches to developing coatings for use as thick thermal barriers were discussed. The first involves modification of the structure of YSZ coatings, and has shown some improvement in creep resistance. The second approach is to replace zirconia with a combination of materials in a multilayer coating. Relatively low cost ceramic materials which are under consideration for the design of such a coating reviewed.

## 7. ACKNOWLEDGEMENT

Support for this research from Auto 21 and NRC (National Research of Canada, QC) is gratefully acknowledged.

Received April 26, 2005

Centre for Advanced Coating Technologies  
University of Toronto, Toronto, Ontario, Canada

## REFERENCES

- /1/. P. Ramaswamy, S. Seetharamu, K. B. R. Varma, N. Raman and K. J. Rao, *Thermomechanical fatigue characterization of zirconia (8% Y<sub>2</sub>O<sub>3</sub>-ZrO<sub>2</sub>) and mullite thermal barrier coatings on diesel engine components: effect of coatings on engine performance*, Proc. Instn. Mech Engrs., vol. 214, part.C (2000) 729-742.
- /2/. D. Zhu, R. A. Miller, *Thermal barrier coatings for advanced gas turbine and diesel engines*, NASA/TM—1999-209453.
- /3/. T.Hejwowski, A.Weronski, *The effect of thermal barrier coatings on diesel engine performance*, Vacuum, 65 (2002) 427-432.
- /4/. G.Qian, T.Nakamura, C.C.Berndt, *Effects of thermal gradient and residual stresses on thermal barrier coating fracture*, Mechanics of Mater., 27, (1998) 91-110.
- /5/. D. Stover, C. Funke, *Directions of the development of thermal barrier coatings in energy applications*, J. Mater. Process. Tech., 92-93 (1999) 195-202.

- /6/. K.Kokini, Y.R.Takeuchi, B.D.Choules, *Surface thermal cracking of thermal barrier coatings owing to stress relaxation: zirconia vs. mullite*, Surf. & Coat. Tech., 82(1996) 77-82.
- /7/. M.B.Beardsley, P.G.Happoldt and K.C.Kelley, E.F.Rejda and D.F.Socie, *Thermal barrier coatings for low emission, high efficiency diesel engine applications*, SAE paper, No 1999-01-2255.
- /8/. S.Rangaraji, K.Kokini, *Interface thermal fracture in functionally graded zirconia-mullite-bond coat alloy thermal barrier coating*, Acta Mater., 51(2003) 251-267.
- /9/. X.Q.Cao, R. Vassenb, D. Stoeverb, *Ceramic materials for thermal barrier coatings*, J. Europ. Ceram. Soc., 24 (2004), 1-10.
- /10/. L.Shaw, D.Goerman, R.Ren, M.Gell, *The dependency of microstructure and properties of nanostructured coatings on plasma spray conditions*, J. Surface and Coating Technology, 130 (2000)1-8.
- /11/. M. Gell, *The potential for nanostructured materials gas turbine engines*, J. NanoStructured Materials, 6 (1995)997-1000.
- /12/. M. Gell, *Application opportunities for nanostructured materials and coatings*, J. Materials Science & Engineering, A204 (1995)246-251.
- /13/. M. Gell, E.H. Jordan, Y.H. Sohn, D. Goberman, L. Shaw, and T.D.Xiao, *Development and implementation of plasma sprayed nanostructured ceramic coatings*, J. Surface and Coatings Technology, 146-147(2001)48-54.
- /14/. R.S. Lima, A. Kucuk, and C.C. Berndt, *Evaluation of microhardness and elastic modulus of thermally sprayed nanostructured zirconia coatings*, J. Surface and Coating Technology, 135 (2001)166-172.
- /15/. R.S. Lima, A. Kucuk, and C.C. Berndt, *Bimodal distribution of mechanical properties on plasma sprayed nanostructured partially stabilized zirconia*, J. Material Science and Technology, A327 (2002)224-232.
- /16/. R.S. Lima, A. Kucuk, and C.C. Berndt, *Integrity of nanostructured partially stabilized zirconia after plasma spray processing*, J. Material Science and Technology, A313(2001)75-82.
- /17/. Y. Zeng, S.W. Lee, L. Gao, and C.X. Ding, *Atmospheric plasma sprayed coatings of nanostructures zirconia*, J. the European Ceramic Society, 22(2002)347-351.
- /18/. H. Chen, and C.X. Ding, *Nanostructured zirconia coating prepared by atmospheric plasma spraying*, J. Surface and Coating Technology, 150 (2002)31-36.
- /19/. G. Skandan, R. Yao, B.H. Kear, Y. Qiao, L. Liu, T.E. Fischer, *Multimodal powders: a new class of feedstock material for thermal spraying of hard coatings*, J. Scripta Mater., 44, (2001)1699-1702.
- /20/. B.H. Kear, and G. Skandan, *Thermal spray processing of nanoscale materials*, J. NanoStructured Materials, 8(1995)765-769.
- /21/. E.H. Jordan, M. Gell, L. Shaw, and S. Jiang, *Fabrication and evaluation of plasma sprayed nanostructured alumina-titania coatings with superior properties*, J. Materials Science and Engineering, A 301(2001)80-89.
- /22/. H.G.Wang, H.Herman, *Thermomechanical properties of plasma-sprayed oxides in the MgO-Al<sub>2</sub>O<sub>3</sub>-SiO<sub>2</sub> system*, Surf. Coat. Tech., 42 (1990) 203-216.
- /23/. H.G.Wang, G.S.Fischman, H.Herman, *Plasma-sprayed cordierite: structure and transformations*, J. Mater. Sci., 24 (1989) 811-15.
- /24/. F.G.Razavy, D.C.Van Aken, J.D.Smith, *Effect of laser surface melting upon the devitrification of plasma sprayed cordierite*, Mat. Sci. & Eng., A362 (2003) 213-222.
- /25/. P.M.Pierz, *Thermal barrier coating development for diesel engine aluminum pistons*, Surf. & Coat. Tech., 61(1993) 60-66.
- /26/. P.Ramaswamy, S.Seetharamu, K.B.R.Varma, K.J.Rao, *Thermal shock characteristics of plasma sprayed mullite coatings*, J. Thermal Spray Tech., 7, 4 (1998) 497-5.

#### REALIZAREA UNEI BARIERE TERMICE ALTERNATIVE PENTRU MOTOARELE DIESEL

**Rezumat:** Utilizarea de bariere termice la motoarele diesel este absolut necesară pentru creșterea temperaturii de combustie. Autorii propun în acest scop mullit-ul, material alternativ, ce are o comportare termo-mecanică excelentă. S-a realizat un sistem multistrat care minimizează tensiunile termice, cu o menținere a stabilității chimice și a celei de fază.

## PRELIMINARY RESEARCHS ON METALURGICAL VALUE OF WASTES OF SECONDARY ALUMINIUM INDUSTRY

BY

MARIA ROMAN, VIOREL BADILITA, LUCIA FIRESCU, FLORIN STOICIU,  
IOAN MĂRGINEAN\*, C-TIN BRATU\*

**Abstract.** *IMNR and UPB-CEMS begin a research project in Relansin Program on Romania Aluminium Industry wastes recovery. The objective of the project is to identify the volume, chemical and physical characteristics of Romanian Aluminium Foundry by-products and to determine suitable process to use of secondary dross and fly ashes in concrete products. The paper presents some results of preliminary research on recycling Romanian secondary aluminium industry by-products*

**Keywords:** *aluminium, by-products, recycles, dross, ashes processing*

### 1. INTRODUCTION

Aluminium production is growing, as more and more applications are developing for this adaptable, durable and recyclable metal. One of the most important problems of aluminium industry is to find the proper way to process and recycle of aluminium by-products in useful products. Aluminium by-products shall consist in slag, dross, skimming and spilling from aluminium melting and ashes, which can contain from 20 to 90 % aluminium. World Aluminium Organization and International Aluminium Institute report that the remained waste can be use in different way:

- ✓ Source of minerals for cements. For example, slag is a source of aluminium oxide and magnesia;
- ✓ Component for asphalt, also known as bituminous concrete, consists of a mixture of aggregates bound together by asphalt cement;
- ✓ Soil mixtures used in agronomic applications;
- ✓ Raw material in foundry [1, 2, 3].

Although World Aluminium Organization has properly solution to process aluminium dross and ashes, which were sowed below, these methods are not utilized in Romania. We have to mention that there are huge quantities of dross and ashes stored near the aluminium companies like NEFRERAL, ALRO and ALPROM account of many years of aluminium processing. To take in consideration all this information and the necessity of ALMET SA and ALPROF SA to find new way to process their secondary dross, UPB-CEMS and IMNR propose one project in Relansin Program on Romania Aluminium Industry by-products reuse. The objective of this project is to identify the volume, chemical and physical characteristics of Romanian Aluminium Foundry by-products and at the end of our work, together with our partners ALMET

SA and ALPROF SA we have to establish some suitable method to process the new and the old aluminium dross and ashes. This project will be focused on understanding aluminium dross recovery, to establish a method of salt-free recovery of aluminium from aluminium dross. To develop a suitable process to use of secondary dross and fly ashes in concrete products.

Our work begins with ALMET and NEFERAL aluminium dross and ashes, which were preliminarily characterized. If the NEFERAL aluminium dross and ashes have been produced and stored about 20 years, the ALMET aluminium dross and ashes are new. Therefore, we suppose that the NEFERAL aluminium dross and ashes have a different composition and characteristics than the ALMET aluminium dross and ashes.

## 2. EXPERIMENTAL PROCEDURES

To characterize NEFERAL and ALMET wastes there were sampled 27 samples from different places and different casts. They were sorted into three size classes; sample 1 - big, sample 2 - medium and sample 3 - fine particle and there were notes like in table 1.

Table 1. Type and Size class of wastes samples

Name	Type	Size class of samples		
		1	2	3
Neferal	Stored dross	> 1.6 mm	1.6 ... 1 mm	< 1 mm
ALMET	New dross	> 0.8 mm	0.16 ÷ 0.8 mm	< 0.16
	New ash	> 0.8 mm	0.16 ÷ 0.8 mm	< 0.16

These samples were preliminarily characterized by chemical, diffraction and metallographic methods.

Chemical analyses were done by knowing specific standards of nonferrous metals.

Diffraction analysis was done by X-ray (DRX) and Bragg-Brentano method, coupling  $\Theta - 2*\Theta$ , on polycrystalline plane samples. Diffraction studies were made by DRON 2.0 apparatus with characteristic ray  $\text{CuK}\alpha_{1\&2}$ . Experimental data were digitally collected by systematic scanning method in angular space  $2*\Theta$ :  $4 \div 84$  grad. Phase qualitative analyses were done by methods of Hanawalt, in conformity with standards of A.S.T.M. The results show that there are diffraction maxima from more phases and there are diffraction maxima non-attributed. This means that there is one grade of uncertainty. To obtain certainty there were separate more fractions from integral material, which were named: white, very fine (in water suspension), magnetic, black, ochre, soluble fraction and heat at  $1000^{\circ}\text{C}$  NEFERAL ash. Phase analysis by DRX of these fractions had permitted to confirm identify phases and to determine new phases with some percent composition. The results are shown in table 2...8.

Metallographic analyses were done by Amplival Pol U microscope in sending and reflecting lights. There was studied integrated samples and magnetic separate samples.

## 3. RESULTS AND DISCUSSIONS

The samples average chemical composition is shown in table 2

Table 2. Samples average chemical composition

Elements	Chemical analysis, % mass		
	Dross from NEFERAL	Dross from ALMET	Ashes from ALMET
Aluminium	27.433	56.203	55.519
Cooper	0.937	1.892	0.809
Magnesium	1.020	1.360	1.308
Manganese	0.157	0.162	0.144
Nickel	0.210	0.033	0.073
Plumb	0.357	0.159	0.321
Zinc	0.540	0.473	0.664
Titan	0.670	0.340	0.648
Tin	0.870	0.030	0.052
Iron	5.383	2.521	1.772
Silicon	4.180	6.128	3.339
Boron	0.307	0.007	0.014
Sodium	1.317	1.688	2.816
Potassium	2.163	0.469	0.681
F <sup>-</sup>		1.322	1.069
Cl <sup>-</sup>	2.413	0.861	1.083
SO <sub>4</sub> <sup>2-</sup>	0.567	0.050	0.050
NO <sub>3</sub> <sup>-</sup>	1.383	1.912	2.848
CO <sub>3</sub> <sup>2-</sup>	1.330	2.122	2.197

Chemical results show that dross from NEFERAL have following average elements content 27.4% Al / 5.38 % Fe/ 4.18% Si / 1.31% Na / 2.16% K / 1.02 % Mg / 0.93% Cu / 0.54% Zn, 2.83% anther minor elements with content below 0.5% and a total content 5,7% ions; Cl<sup>-</sup>, SO<sub>4</sub><sup>2-</sup>, NO<sub>3</sub><sup>-</sup>, CO<sub>3</sub><sup>2-</sup>.

Chemical composition is varying slowly with sizes class of samples, figure 1, 2 and 3.

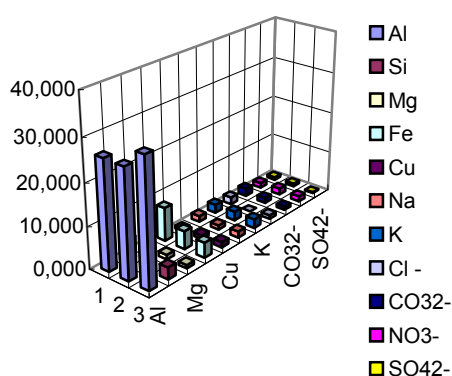


Figure 1. Dross from NEFERAL

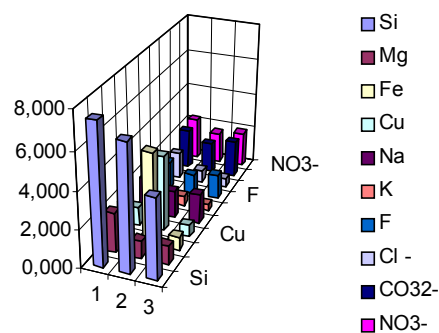


Figure 2. Dross from ALMET

The diffraction analysis show that dross from NEFERAL have following fazes: Al(OH)<sub>3</sub> – Nordstrandite (p ÷ z.p), α - Al<sub>2</sub>O<sub>3</sub> – Corundum (z.p), M<sup>+2</sup>O·(Al, M<sup>+3</sup>)<sub>2</sub>O<sub>3</sub> – Spinel (p), and in form of AlO(OH) – Boehmite (z.p). Silicon is present in form of free silicon (1 ÷ p) and SiO<sub>2</sub> – α Quartz (p ÷ z.p). Iron is present in form of α – Fe and M<sup>+2</sup>O·(Fe<sup>+3</sup>, M<sup>+3</sup>)<sub>2</sub>O<sub>3</sub> – Ferrites (p ÷ z.p).

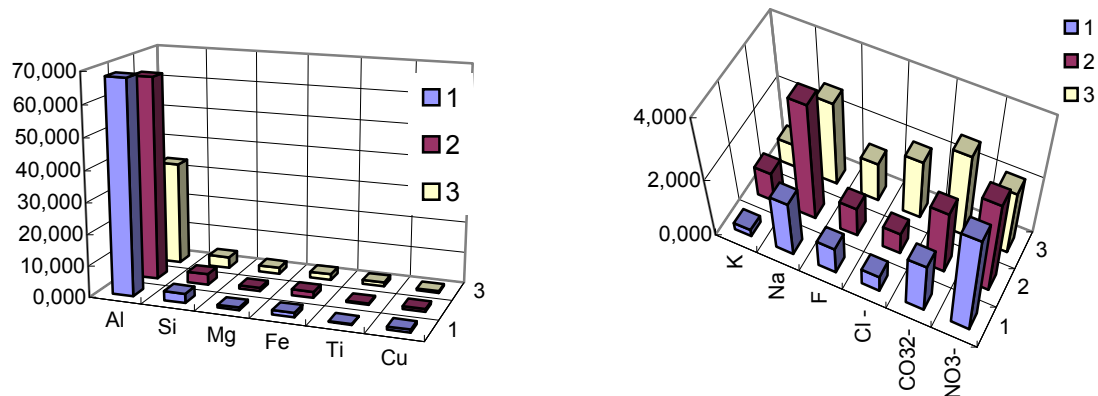


Figure 3. Ashes from ALMET

The phase analysis (DRX) and metallographic analyses show that compose of sample are; aluminium oxide and hydroxides -  $\text{Fe}_2\text{O}_3 \cdot n\text{H}_2\text{O}$ ; iron oxide like: magnetite -  $\text{Fe}_3\text{O}_4$ , hematite  $\text{Fe}_2\text{O}_3$  - goethite -  $\text{FeOOH}$ , ferrites -  $(\text{Fe}^{2+}\text{Mg}^{2+}\text{Mn}^{2+}\text{Ni}^{2+})(\text{Fe}^{3+}\text{Cr}^{3+}\text{Ti}^{3+})_2\text{O}_4$ , which have small crystal form gaped in glossy dross and other compounds with limonite characteristics. The oxides are around iron particle. Aluminium, which can be in fact different aluminium alloys (ATSi). Other components like;  $\alpha$  - Fe, NaCl - Halite,  $\text{SiO}_2$  -  $\alpha$  Quartz,  $\alpha$  -  $\text{Al}_2\text{O}_3$  - Corundum, KCl - Sylvite,  $\text{Al}(\text{OH})_3$  - Nordstrandite,  $\text{M}^{+2}\text{O} \cdot (\text{Al}, \text{M}^{+3})_2\text{O}_3$  - Spinel, or  $\text{AlO}(\text{OH})$  - Boehmite.

The dross from ALMET have following average elements content: 56.203% Al / 2.521% Fe/ 6.128% Si / 1.688% Na / 0.469% K / 1.360% Mg / 1.892% Cu / 0.473% Zn, 1,283% anther minor elements with content below 0.5% and a total content 6.267 % ions;  $\text{F}^-$ ,  $\text{Cl}^-$ ,  $\text{SO}_4^{2-}$ ,  $\text{NO}_3^-$ ,  $\text{CO}_3^{2-}$ .

The diffraction analysis show that in dross and ashes from ALMET, the elements are present in more fazes. These fazes differs from size class of samples. So, dross with dimensions above 0.16 mm size class are formed from free aluminium, alloys of aluminium (z.p) and free silicon (p). The samples with size class below 0.16 mm have complex fazes like:  $\alpha$  -  $\text{Al}_2\text{O}_3$  - Corundum (p),  $\text{M}^{+2}\text{O} \cdot (\text{Al}, \text{M}^{+3})_2\text{O}_3$  - Spinel (p ÷ z.p), and in form  $\text{AlO}(\text{OH})$  - Boehmite (p), Free silicon (1 ÷ p) and  $\text{SiO}_2$  -  $\alpha$  Quartz (p). The iron is present in form of  $\text{M}^{+2}\text{O} \cdot (\text{Fe}^{+3}, \text{M}^{+3})_2\text{O}_3$  - Ferrites (p). In this dross there were identify NaCl - Halite (p ÷ z.p), MgO - Periclase (p), and  $\text{CaCO}_3$  - Calcite (p). All, these fazes are friable and can be separate by grinding and screening.

The ashes from ALMET have following average elements content: 55.5% Al / 1.72% Fe/ 3.39% Si / 2.816% Na / 0.681% K / 1.308% Mg / 0.89% Cu / 0.664% Zn, 1.252% anther minor elements with content below 0.5% and a total content. 7.47 % ions;  $\text{F}^-$ ,  $\text{Cl}^-$ ,  $\text{SO}_4^{2-}$ ,  $\text{NO}_3^-$ ,  $\text{CO}_3^{2-}$ .

The phase analysis (DRX) and metallographic analyses show that compose of sample differs by their size class. All samples have a rich content of aluminium. Silicon content is growing with size class. Similar tendency show NaCl - Halite faze  $\text{M}^{+2}\text{O} \cdot (\text{Al}, \text{M}^{+3})_2\text{O}_3$  - Spinel,  $\alpha$  -  $\text{Fe}_2\text{O}_3$  - Haematite, KCl - Sylvite, MgO - Periclase,  $\text{CaCO}_3$  - Calcite,  $\text{Al}(\text{OH})_3$  - Nordstrandite,  $\text{AlOOH}$  - Diaspore. The sample with size class > 0.8 mm do not content the fazes  $\text{SiO}_2$  -  $\alpha$  Quartz, KCl - Sylvite,  $\alpha$  -  $\text{Fe}_2\text{O}_3$  -

Haematite,  $\text{CaCO}_3$  – Calcite,  $\text{Al}(\text{OH})_3$  – Nordstrandite,  $\text{AlOOH}$  – Diaspore. The content of metallic material is decreasing from 90% in sample with size class above 0.8 mm to 10 – 20% in sample with size class below 0.16 mm.

To illustrate the difference of phases content in the sample there are show some following diffraction pattern. Figure 4 shows diffraction pattern of NEFERAL dross size class < 1 mm , figure 5 shows diffraction pattern of ALMET dross size class <0,8, figure 6 shows diffraction pattern of ALMET dross size < 0.16. Figure 7 shows diffraction of ALMET ashes size > 0.8 mm and figure 8 shows Diffraction pattern of ALMET ashes size > 0.8 mm.0.16 ÷ 0.8 mm.

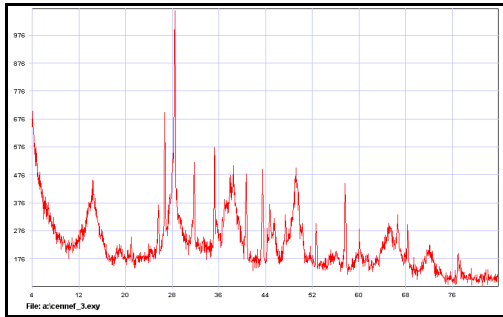


Figure 4. Diffraction pattern of NEFERAL dross size class < 1 mm.

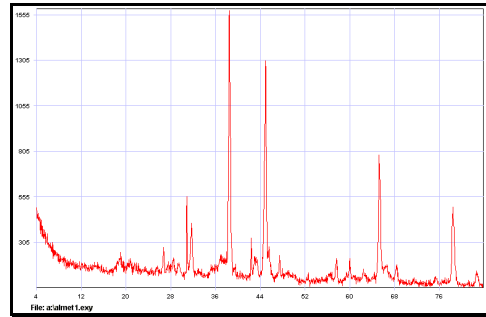


Figure 5. Diffraction pattern of ALMET dross size class <0.8.

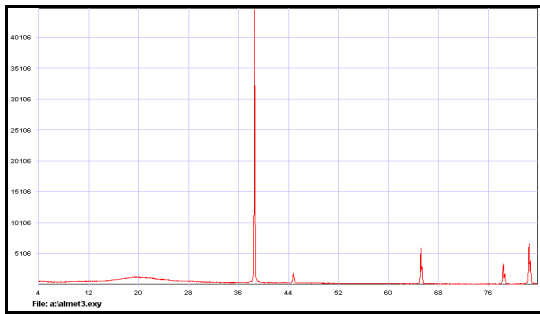


Figure 6. Diffraction pattern of ALMET dross size < 0.16.

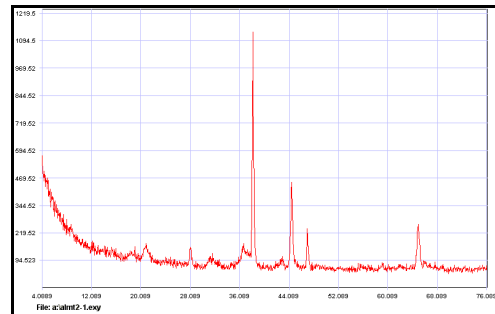


Figure 7. Diffraction pattern of ALMET ashes size > 0.8 mm.

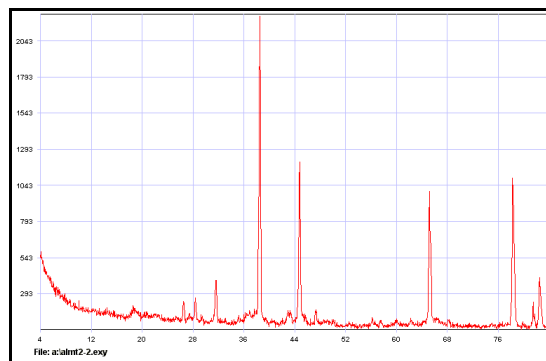


Figure. 8 Diffraction pattern of ALMET ashes size > 0.8 mm.0.16 ÷ 0.8 mm.

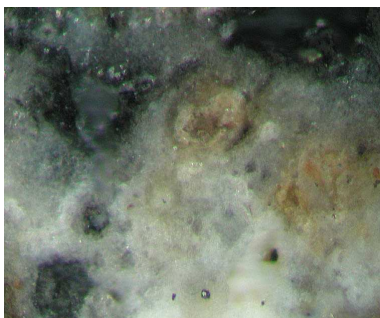


Figure 9. Aluminium oxides, X500, N+.

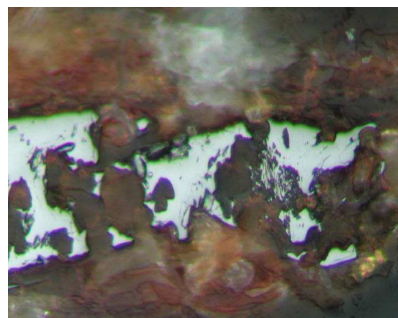


Figure 10. Iron and iron oxides, X500, N+.

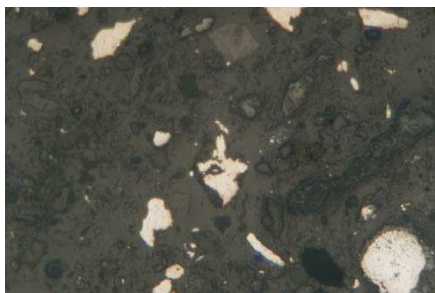


Figure 11. Aluminium alloy, oxides. X125, NII.

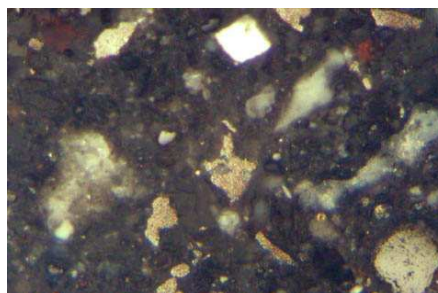


Figure 12. Aluminium alloy, oxides. X125, N+.

#### 4. CONCLUSION

All these preliminary results demonstrate that the dross and ash have complex composition. Our researches continue with experiments to establish which method is suitable to process them in concrete products.

Received April 19, 2005

National R&D Institute for Nonferrous and Rare Metals – IMNR  
\*Polytechnic University București

#### REFERENCES

- /1/. A. Ciocan, Valorificarea deșeurilor – Tehnici de procesare și valorificare a deșeurilor de aluminiu, Editura MatrixRom, București, (2003), p. 60
- /2/. European Aluminum Association 2001, [www.eaa.net](http://www.eaa.net)
- /3/. [www.eaa.net/material/recycled.htm](http://www.eaa.net/material/recycled.htm)
- /4/. "Environmental impact", [www.alcancom/sustainability/eulstep](http://www.alcancom/sustainability/eulstep)
- /5/. [www.green-networld.com/tips/aluminium.htm](http://www.green-networld.com/tips/aluminium.htm)
- /6/. International Aluminum Institute, The Global Aluminum Sustainable Development Initiative, [www.world-aluminum.org](http://www.world-aluminum.org) (2004), p.2;
- /7/. "Life cycle assessment of aluminium: inventory data for the worldwide primary aluminium industry" International Aluminum Institute March 2003 [www.world-aluminum.org](http://www.world-aluminum.org)

#### CERCETĂRI PRELIMINARE ASUPRA VALORII METALURGICE A DEȘEURILOR DIN INDUSTRIA ALUMINIULUI SECUNDAR

**Rezumat:** UPB-CEMS și IMNR a început un proiect de cercetare în cadrul Programului Relansin, care are ca obiectiv valorificarea integrală a zgurilor și cenușilor rezultate din procesarea deșeurilor de aluminiu. Lucrarea prezintă câteva rezultate preliminare privind caracterizarea zgurilor și cenușilor rezultate din industria românească a aluminiului secundar..

## MICROSTRUCTURAL ASPECTS CONCERNING THE THERMOMECHANICAL TREATMENT APPLIED OF CHROMIUM HIGH ALLOYED STEELS

BY

RODICA FLOREA

**Abstract.** *The paper addresses to the study of strengthening effect and stability achieved by thermomechanical treatments of chromium high alloyed steels. By means of investigation such as optical and electronic microscopy one can study the mechanism and kinetics of tempering processes concerning the ferrite matrix substructural changes and carbide phases precipitated at various temperatures. Based on theoretical conclusions from structural studies, one analyzes the efficiency and so the opportunity of some thermomechanical treatment experimental version applied for a 12% chromium steels. A particularly goal of this paper is to prove the better stability of this steel at tempering*

**Keywords:** *thermomechanical treatment, chromium high alloyed steels*

### 1. THEORETICAL CONSIDERATIONS

It is known that plastic deformation determines and stimulates phase transformation regardless whether this imply atoms diffusion or not. From the viewpoint of diffusion process stimulation, the plastic deformation (the deformation energy stored in the material), generates a fine structure which will accelerate any transformation. The stimulation of phase transformations will be also determined by imperfections of the crystal network (dislocations, vacancies, packing flows, limits, etc.) as preferred places of germination. These structural modifications are factors which could determine the increase of steels' stability at high temperatures.

Applying a thermomechanical treatment (martensite deformation), the martensite will become instable and the following tempering will determine the increase of dispersion degree of carbide phases in substructural ferrite matrix.

### 2. EXPERIMENTAL TESTS

The thermomechanical treatment was applied by means of a special equipment, designed and developed by the author and consists in:

- austenitizing furnace type tunnel, heated with silite bars and having automatically temperature setting;
- maintaining furnace, for obtaining the deformation temperature in samples;
- transfer equipment from the furnace to forming machine (multiple rolls mill)
- oil cooling device, with oil collecting basin;
- tempering furnace heated with electric resistance.

From the 10Cr130 steel, test pieces were manufactured of rectangular cross section, of various heights, in order to achieve degrees of deformation: 0%; 5%; 15%;

25%. Previous tests had established an optimum austenitisation temperature of 1050 C, for heating in silite furnace. The studied deformation temperature was 200 C. After hardening in oil, immediately after the forming, temperings at 200 C; 400 C; 500 C; 600 C were applied at 3 h maintaining times. At 500 C and 600 C, maintainings of 25 h and 100 h were realized.

### 3. EXPERIMENTAL RESULTS

In fig. 1 and 2 there are presented the electronic microstructures of 10Cr130 Steel classically hardened and tempered. The structure is composed by roughs martensite nails and precipitates in the form of fine lamellas (fig.1). At 600 C the quantity and the dimension of carbides phases increase (fig.2).

Electronic microstructures of 10Cr130 Steel hardened from 1050 C in oil and tempered at 200 and 600 C/3h

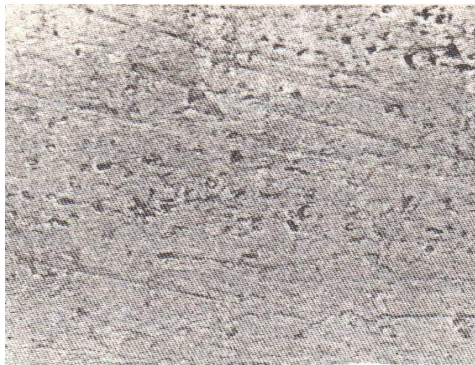


Fig. 1 Steel hardened and tempered 3 hours at 200 C 16000:1



Fig. 2 Steel hardened and tempered 3 hours at 600 C 16000:1

As a result of thermomechanical treatment, the structures obtained were studied at an optical and then at an electronic microscope and lead to the following conclusions.

After the plastic deformation of the martensite, some structural modifications appear determined by the cold deformation but also an ageing process at deformation. The plastic deformation, which stimulates the germination on existing dislocations, is the important mechanism which influences the precipitating processes. During the entire tempering, a segregational process of carbon and chromium on dislocations takes place and lead at the forming of germs of critical dimensions. Thus, at low degrees of deformation (<15%) the increase of the temperature at tempering leads at the distribution of the carbures on certain limits and sublimits, forming a very fragmented structure (fig. 7 and 8). At 25% deformation one can observe the appearing of some poliedric fields whose diameter is extending from 2000 Å to 3000 Å (fig. 6). At 500 C temperature and long exposure (100 h), the precipitates are suffering coagulation processes and loose their ability to stop the dislocations (fig. 9 and 10). A perfectly organized redistribution of carbides in multiple strings takes place.

Optical and electronic microstructures of 10Cr130 Steel thermomechanical treated (Maraging Variant) and then tempered between 200 C – 600 C and maintained between 3 and 100 hours

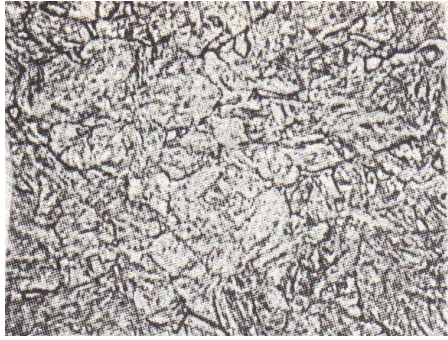


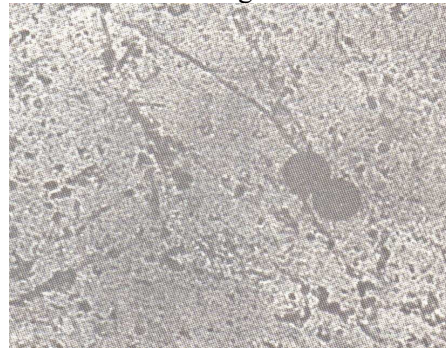
Fig. 3 Steel hardened and deformed with 5% degree. Vilella attack



400:1 Fig. 4 Steel hardened and deformed with 25% degree. Vilella attack



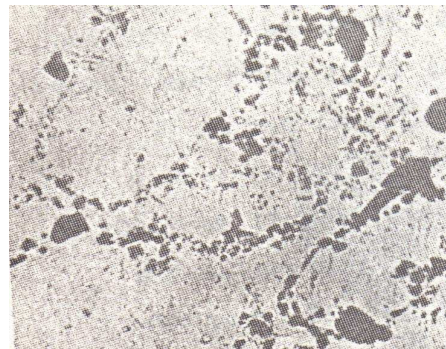
Fig. 5 Steel hardened and deformed with 25% degree and tempered 3 hours at 200 C



16000:1 Fig. 6 Steel hardened and deformed with 25% degree and tempered 3 hours at 500 C



Fig. 7 Steel hardened and deformed with 5% degree and tempered 3 hours at 400 C



16000:1 Fig. 8 Steel hardened and deformed with 5% degree and tempered 3 hours at 600 C

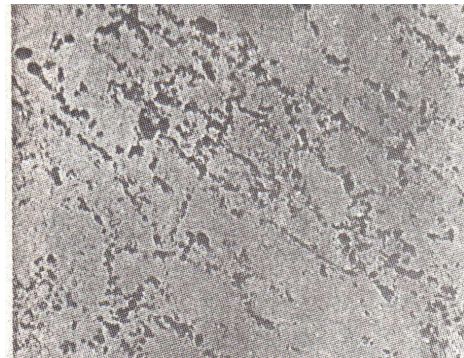
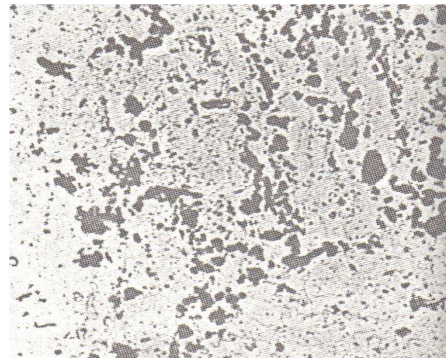


Fig. 9 Steel hardened and deformed with 15% degree and tempered 25 hours at 500 C



16000:1 Fig. 10 Steel hardened and deformed with 25% degree and tempered 100 hours at 500 C

#### 4. CONCLUSIONS

Although the thermomechanical treatment at 10Cr130 Steel was previously experimented, it could not be established a certain behavior at this steel at low degrees of deformation and neither the optimum fields of application. From our research related to the tempering processes of 10Cr130 steel under the influence of plastic deformation of martensite with 5-25% degrees of deformation, the following conclusions can be drawn:

- the increase of the dispersion and the increase of the quantity of carbide phases related to the dislocation density;
- the intensification of the decomposing process of martensite and the precipitation of chromium carbide phases;
- the acceleration of germinating processes on dislocations, macles, sliding planes, limits and sublimits and the localization of diffusion processes on certain poliedric microfields depending on the deformation degree;

All these structural modifications explain the hardening and the stability until 600 C. The improvement of refractoriness by the increase of stability at tempering imposes on the other hand to check the behavior at various temperatures depending on the strengths proprieties but also on the preservation of corrosion resistance.

*Received April 19, 2005*

*“Transilvania” University from Brasov*

#### REFERENCES

- /1/. R Florea, *The influence of austenite deformation on structure and properties of hardened structural steels*, Revue Prelucrari la cald, nr. 16 / 1999, INTEC SA
- /2/. R. Florea, R. Banciu, *Aspects regarding the transformations on tempering for thermomechanical treated steels*, Buletinul Institutului Politehnic din Iasi, tomul XLVI fasc. 1-2, 2000, sectia IX
- /3/. N. Popescu, C Gheorghe, *Tratamente neconventionale*, Editura tehnica, Bucuresti, 1990

#### ASPECTE MICROSTRUCTURALE PRIVIND APLICAREA TRATAMENTULUI TERMOMECHANIC OTELURILOR INALT ALIATE CU CROM

**Rezumat:** În lucrarea prezentată se efectuează un studiu asupra efectului de durificare și creștere a stabilității obținute ca urmare a aplicării tratamentului termomecanic oțelului cu 12% Cr și 0,1% C. Prin intermediul investigațiilor structurale la microscopul optic și electronic s-a putut studia mecanismul și cinetica transformărilor în timpul proceselor de revenire ulterioară, atât în ceea ce privește matricea feritică, cât și a precipitării carburilor la diferite temperaturi. Pe baza concluziilor teoretice asupra transformărilor structurale constatate în urma încercărilor experimentale s-a putut analiza eficiența și oportunitatea aplicării variantei de tratament termomecanic constând în deformarea prealabilă a martensitei la oțelul cu 12%Cr și în special creșterea stabilității martensitei deformate la revenire.

## RESEARCH AND STUDY REGARDING THE VARIATION OF SURFACE TENSION OF MOLTEN METALS AND ALLOYS WITH TEMPERATURE

BY

BEATRICE TUDOR, ADRIAN VASILIU

**Abstract.** *The paper presents the influence of the temperature on the surface tension metals and alloys, and several methods for the surface tension determination*

**Keywords:** *temperature, surface tension, aluminium alloys*

### 1. INTRODUCTION

To predict the surface tension of molten metal alloys, it is important to have a reliable reference data base for the surface tensions of the respective pure metal components of the system, and to this end, literature data pertaining to the surface tension of pure metals have been reviewed.

Surface tensions of molten metals are generally measured either in vacuum or in inert atmosphere.

### 2. RELATION BETWEEN SURFACE TENSION OF PURE METALS AND OTHER PHYSICAL PROPERTIES

The surface tension of a pure molten metal is dependent on the strength of the cohesive forces acting between neighbouring atoms, and intuitively, it would be expected that it could be related to other physico-chemical properties of the material. It must be emphasized that such considerations would only apply to pure materials which contain no highly surface active components whose presence at very low levels can exert a dramatic effect on the value of the surface tension, but have little influence on bulk properties.

There have been many attempts to correlate the surface tension of pure metals with material properties (heat of vaporization, compressibility, thermal expansion, shear viscosity), all of which have only met with limited success. From inspection of the experimental data it is immediately apparent that the surface tensions of molten metals tend to increase with increase in melting point. Figure 1 shows a plot of experimentally derived surface tension data against the absolute melting points.  $T_m$  of the respective pure metals.

Although the trend for  $\gamma$  to increase with increase in  $T_m$  is confirmed, the overall scatter shown in fig.1 is rather high, which suggests that if any relation between  $T_m$  and  $\gamma$  exists, then other parameters are probably involved.



- pendent drop;
- drop weight;
- detachment or maximum pull methods;
- levitating drop.

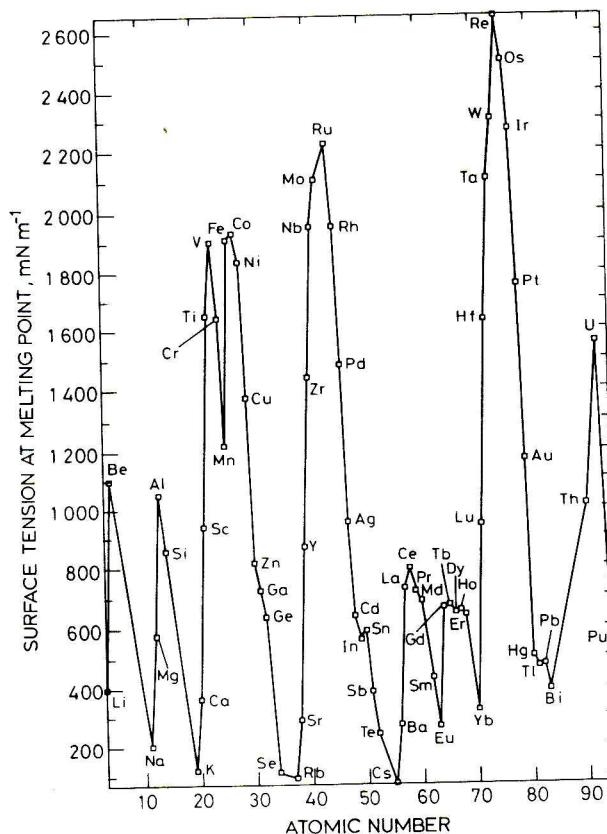


Fig.2. Variation of surface tension of molten metals at melting point with atomic number of element

### 3.EXPERIMENTAL RESULTS

The experimental system was so designed as to allow for the measurement of the liquid alloy drop sizes on images of the outline of a cross section sample taken at high temperatures it was made at the department of magnetic materials and Devices of the National Institute for development and Research in Iasi. The test bench consist of the sample enclosure, a camera, digital multimeter, vacuum device , a computer and monitor to take over and store the images and temperature values. Fig 3 illustrates the system described.

The inside part of the sample is made from stainless steel with water-cooled vacuum - tight walls and mounted on a horizontal orientation system. The alloy is melt and the drop heated in a horizontal electrical furnace having a tantal tape resistance . A system of concentric electrical thermal screens and circular screens of Mo provides a uniform temperature in the working area and prevents heat loss through radiations.

The sample holder allows for the sample to rotate and move freely. Temperature is measured by a thermocouple of Pt-Rh 6% vs Pt-Rh 30% which is in contact with the sample holder.

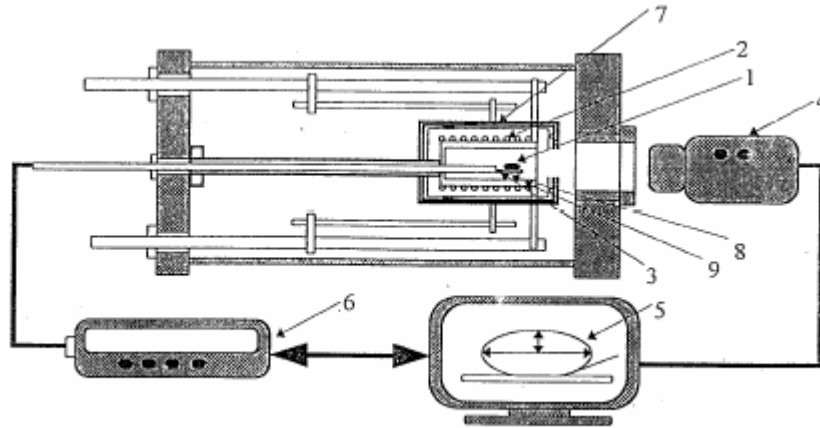


Fig 3 Test bench for the measurement of surface temperature of liquid alloys by the method of fixed drop.: 1.alloy drop; 2- resistive furnace, 3- thermocouple 4- camera CCD and microscope objective, 5 - image of the outline of the alloy drop on the computer monitor 6 – digital multimeter, 7 - thermal screen, 8 – item, 9 - alumina tube sustaining the furnace resistance

The drop image is taken by a CCD camera by a microscope objective. The video signal provided by the camera is introduced into an acquisition plate. By means of a special software the images are seen on the computer monitor, converted and saved into a standard graphic format in real time. At the same time the temperature is measured by a digital multimeter and recorded in the same file with the image by means of an interface RS 232. The saved images are subsequently processed to obtain the values of the surface tension from the drop geometry parameters. The vacuum device provides a pressure of. Inside the working area to reduce impurities sources. Another reason for vacuum operation is to avoid distortion of the drop image taken by the optical system. This distortion takes place under protection atmosphere due to the variation of the refraction index with the temperature at gas pressures close to the atmospheric pressure. The variation of the refraction index with the temperature along the system optical axis can be compensated for by recalculating the optical parameter with the help of a dimensional item located in the sample plan.

$$\gamma = \frac{g\rho b^2}{\beta} \quad (2)$$

where –  $g$  is gravity acceleration  $m/s^2$ ,  $\rho$ -alloy density,  $kg/m^3$ ,  $\beta$  - coefficient depending on the value  $\phi$  of the angle measured

$$\frac{1}{\left(\frac{R}{b}\right)} + \frac{\sin \phi}{\left(\frac{X}{b}\right)} = 2 + \frac{\rho g b^2}{\gamma} \cdot \left(\frac{Z}{b}\right) \quad (3)$$

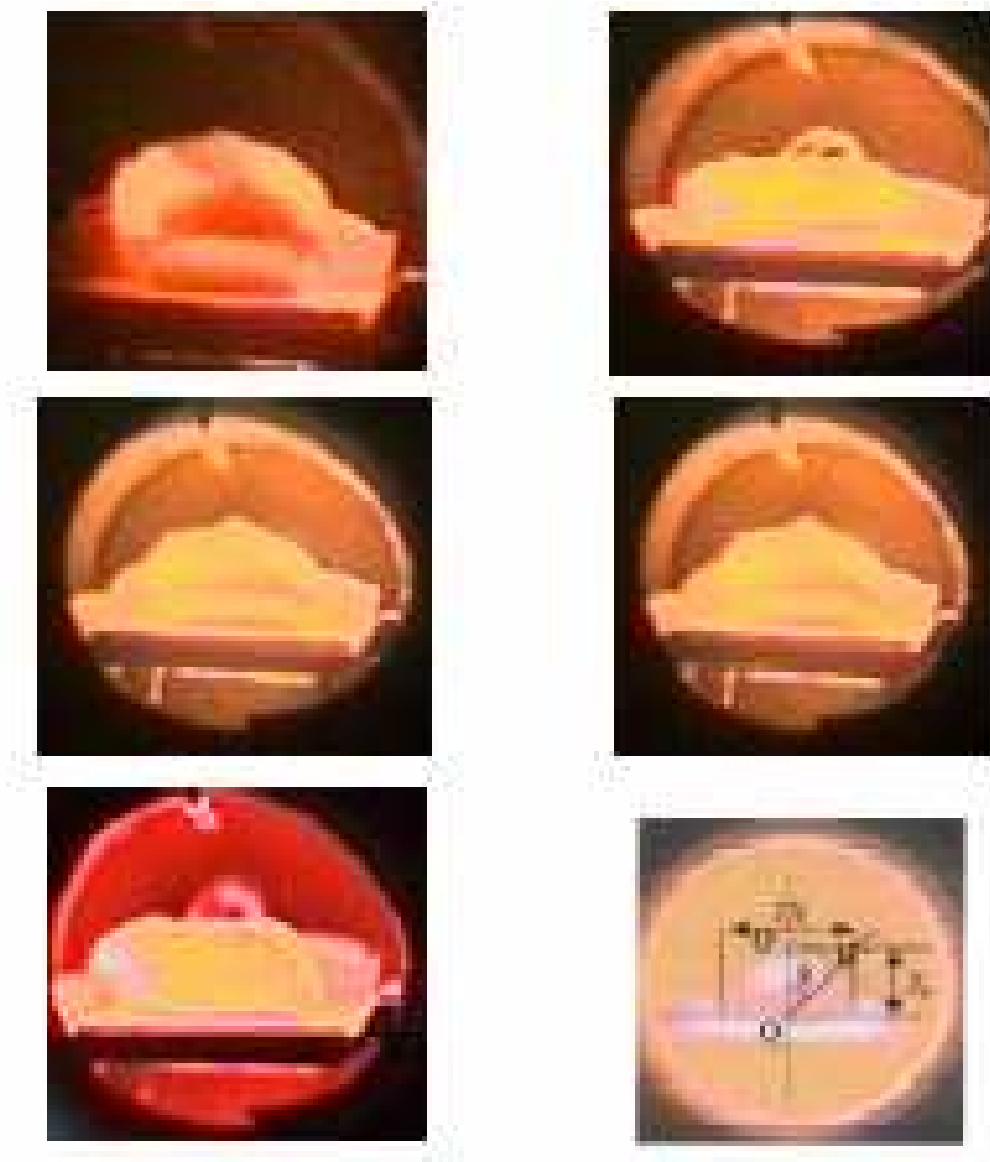
$$\beta = \frac{\rho g b^2}{\gamma} \quad (4)$$

$$\frac{1}{\left(\frac{R}{b}\right)} + \frac{\sin \phi}{\left(\frac{X}{b}\right)} = 2 + \beta \left(\frac{Z}{b}\right) \quad (5)$$

$$\gamma_{806^{\circ}\text{C}} = \frac{g\rho b^2}{\beta} = 0,859412 \text{ erg/cm} \quad (6)$$

$$\gamma_{893^{\circ}\text{C}} = \frac{g\rho b^2}{\beta} = 0,674246 \text{ erg/cm} \quad (7)$$

The drop image are presented in following photos:



### 3 CONCLUSIONS

Determining the surface tensions of the Al Cu alloy was achieved by means of a system based on the mobile drop method. This makes it possible for the liquid alloy drop size to be measured on the images of the cross section outline. The work is performed under vacuum of  $10^{-3}$  which ensures a pressure of inside the working area.

This is to reduce impurities and avoid distortion of the drop image as taken by the optical system.

With increasing temperature, the surface tension decreases due to lower forces of interaction between the alloy elements.

*Received May 5, 2005*

*“Dunărea de Jos” University Galati*

#### REFERENCES

- /1/. Keene B.J., *International Materials Reviews*, vol.38 nr. 4, 1993
- /2/. Gregson P.J., *Aluminium alloys : physical metallurgy, processing and properties – High Performance Materials in Aerospace*, Edited by Harvey M. Flower – London, U.K.,1995,Chapman & Hall
- /3/. Van Zytveld J.B., *Liquid metals – Inst.Phys.,Series 30,1977,p.212*

#### STUDII SI CERCETARI PRIVIND VARIATIA TENSIUNII SUPERFICIALE A METALELOR SI ALIAJELOR TOPITE CU TEMPERATURA

**Rezumat:** Lucrarea prezinta influenta temperaturii asupra tensiunii superficiale a metalelor si aliajelor, enumerarea metodelor de determinare a tensiunii superficiale si date privind determinarea tensiunii superficiale a aliajelor Al-Cu prin metoda picaturii imobile.procedeului. Sunt descrise cercetari asupra campului termic realizat de sursa folosita pentru sudare si distributia temperaturii in baia de meatal topit care poate fi realizata cu sau fara material de adaos.

## ON FORCE PARAMETERS AT EMPTY DRAWING OF THE TUBES WITH ULTRASONIC VIBRATIONS TRANSMITTED TO THE DIE ON THE DRAWING DIRECTION

BY

SUSAN MIHAI, ILIESCU VIOREL, DUMITRAS PETRU, MANTU MARIANA,  
GLIGOR-PITICARI OANA

**Abstract.** *The paper shows a calculus method of force parameters at empty drawing of the tubes with ultrasonic vibrations transmitted to the die, on the direction of the drawing “ultrasonic vibration drawing- U.V.D.” or U.V.D. technology, using the theorem of total consumed power, admitting the Coulomb type “friction and the existence of friction medium force reversion mechanism” at metal-tool contact. The experimental results that were obtained on tubes with thin walls made of 10 TiNiCr 180/ STAS3583 (AlSi321) stainless steel are in a good correlation with those obtained in the theoretical research. The efficiency of U.V.D. technology, that was determined using the  $\Delta F$  and  $\Delta C$  relative reductions recommends its use for empty drawing of the tubes made of cold hardly deformable metallic materials for sub-unity values of the drawing relative speed. ( $v_r/v_v \ll 1.0$ )*

**Keywords:** *empty drawing of tubes, ultrasonic fields, die, medium force friction reverse mechanism, Coulomb type friction, Bernoulli type laminated flow, relative drawing speed, oscillating system, technological efficiency*

### 1. INTRODUCTION

Empty processing of the tubes is usually performed at room temperature when the plastic deformation process are accompanied by superficial hardening or hardening under effort. As a consequence of the accumulated superficial hardening, the necessary force of plastic deformation increase along with the decrease of drawing safety. These processes take place with higher intensity when for the drawing of the tubes, hardly deformable metallic materials are used, by means of cold drawing. The continuous may lead to the exceeding of the critical value of drawing safety, with the destruction of the integrity of the metallic materials, along with the increase of the drawing force [1].

For the success of the obtaining of empty drawing tubes from hard cold deformable materials, in the present paper we propose their processing in an ultrasonic field, with ultrasonic vibrations that are transmitted to the die on the direction of the drawing, “ultrasonic drawing-U.V.D.” or U.V.D. technology, as an alternative to the classical technology –C.T.

The characterization of the U.V.D. technology, are compared to T.C. is accomplished on two main directions (objectives) of the paper: (i) the calculus of the force parameters; (ii) experiments on tubes having thin walls made of austenitic stainless steel; (iii) the efficiency of U.V.D. technology.

## 2. PARTICULARITIES OF THE PLASTIC DEFORMATION IN THE CASE OF U.V.D. TECHNOLOGY

The empty drawing of the tubes in an ultrasonic field, U.V.D. technology is accomplished with the die being situated at the maximum of wave oscillation and activated on the direction of the drawing.

The scheme of the ultrasonic activated die, situated in the maximum of the wave oscillation and activated on the drawing direction, U.V.D. technology is shown in fig.1

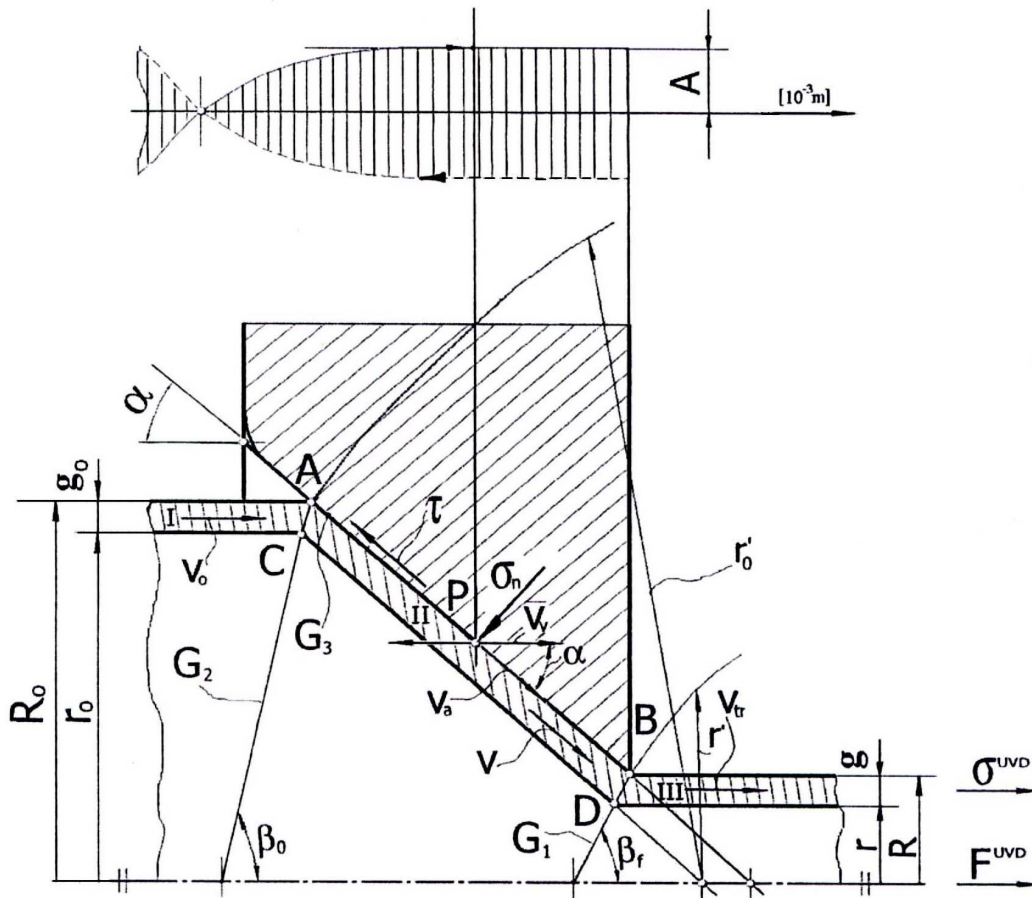


Figure 1. The scheme of the ultrasonic activated die in the case of empty drawing of the tubes, U.V.D. technology

The discussion of the plastic deformation process is accomplished according to three technological factors, of major importance, on which we can independently act, with special influences on the total drawing force: the rate of section decrease, the semi-angle of the conicity opening of the die and the friction force at tool-metal contact [2].

As a main particularity of the plastic deformation process, in the case of U.V.D. technology, we mention the decrease of the metal-tool contact friction, according to the "mechanism of average friction force reduction". In paper [3] are shown details and some contributions performed to die at the metal-tool contact, when the die is

situated in the maximum of the wave oscillation and activated on the drawing direction.

A certain P point, arbitrarily chosen in the area of deformation focus, takes part into two movements: of advance, on the generatrix of the cone-die, with  $v_a$  speed and of vibration, with  $v_v$  speed ( $v_0$ - maximum of speed vibration).

In the case of empty processing of the tubes, for which the semi-angle of cone opening of the die  $\alpha = 6 \dots 12^\circ$  ( $\cos \alpha \approx 1.0$ ), technologically  $v_{tr} \approx v_a$  ( $v_a \approx v_{tr} \cos \alpha$ ) is considered. Under these empty tube processing technological conditions in U.V.D. system, in paper [3] a calculus relation for the friction coefficient  $\mu^{U.V.D.}$  was measured:

$$\mu^{UVD} = \mu^{TC} \left( 1 - \frac{2}{\pi} \arccos \frac{v_{dr}}{v_v} \right) \quad (1)$$

in wich:  $\mu^{TC}$  is the size of friction coefficient in the case of classical processing (CT technology) and  $v_{tr}/v_0$  is the relative drawing speed ( $v_v = \max(d_u/d_i)$  for  $\mu = A \sin \omega t$  it follows  $v_v = 2\pi f A$ , with  $\omega = 2\pi f$ ,  $\cos \omega t = 1$ ;  $f$  is the frequency of ultrasonic wave oscillation at resonance, and  $A$ - the amplitude of oscillation.)

The analysis of relation (1) allows us conclude the fact that, for a given drawing process (U.V.D. technology), the metal-tool friction reduced according to  $v_{tr}/v_v \ll 1.0$  (for  $\mu^{T.C.} = ct.$ ) because  $\mu^{U.V.D.}$ , has lower values in these drawing conditions.

The diminution of metal-tool contact friction (U.V.D. technology), as compares to classical processing (T.C. technology), leads to the diminution of superficial hardening, with the reduction of the drawing force or of consumed power.

### 3. DETERMINATION OF FORCE PARAMETERS AT EMPTY TUBE-DRAWING WITH ULTRASONIC VIBRATION TRANSMITTED TO THE DIE ON THE DRAWING DIRECTION, U.V.D. TECHNOLOGY

The determination of force parameters, in the case of U.V.D. technology is based on the theorem of total consumed power, admitting in the process of plastic deformation the existence of the "reversion mechanism of the average friction force" at metal-tool contact, considering the geometry and kinematics of axial-symmetrical conical movement in the area of deformation focus shown in figure 1.

The hypothesis of plastic deformation through drawing are: the metal material is incompressible, the die is a rigid body, metal deformation is performed according to Von Mises's flowing condition, the kinematic speed field provides a Bernoulli type continuity, the metal-tool interface friction is of Coulomb type constant for a given drawing process, at the level of oscillating system only longitudinal elastic waves act, under stationary wave regime (with the formation of nodes and venters) the plastic deformation process is an isothermal one.[1,4,5,6]

The calculation relationship for the drawing force is of type [1,2,5]

$$F^{UVD} = \pi(R^2 - r^2)\sigma^{UVD}$$

In wich:  $R, r$  are radial sizes, and  $\sigma^{UVD}$  is the drawing tension. According to the geometry and kinematics of axial-symmetrical conical movement (see fig. 1), the following coefficients are used [7]:

$$\psi = \frac{g}{g_0}, \psi_1 = \frac{R}{R_0}, \psi_2 = \frac{r}{R}, \psi_3 = \frac{r_0}{R_0}, \psi_4 = \frac{1 - \psi_2}{1 - \psi_3}, \psi_5 = \frac{1 + \psi_2}{1 + \psi_3}$$

The tube has been divided into three areas which the speed field is uniform.

In area I and area III, the speed is uniform and has only axial component, because the drawing force direction coincides with the tube's symmetry axis.

In area II, of plastic deformation, the speed of the direction makes an  $\alpha$  angle with the symmetry axis. In this area, metal flow is parallel to the surface of the die.

The deformation zone is delimited by  $G_1$  and  $G_2$  surface, represented by the BD and AC segments, defined by the  $\beta_f$  and  $\beta_0$  angles. Using experimental tests, it was noticed that tube wall thickness modifies only when proper plastic deformation begins, which means that, considering the tube's geometry in the deformation area, for  $\beta_0$  and  $\beta_f$ , the relations [1,5] result:

$$\beta_0 = \frac{(\pi - \alpha)}{2}$$

$$\beta_f = \arctg\left(\frac{\psi \sin \alpha}{1 - \psi \cos \alpha}\right) = \arctg\left(\frac{\psi_1 \cdot \psi_4 \sin \alpha}{1 - \psi_1 \cdot \psi_4 \cos \alpha}\right)$$

From the continuity condition of metal flow for  $v_0$  and  $v_{tr}$ :

$$\frac{v_0}{v_{tr}} = \frac{R^2 - r^2}{R_0 - r^2} = \psi_1^2 \frac{1 - \psi_2^2}{1 - \psi_3^2}$$

Speed discontinuities at the level of  $G_1$ ,  $G_2$  and  $G_3$  surfaces are:

- on  $G_1$  surface:  $\Delta v_1 = v_{tr} \frac{\sin \alpha}{\sin(\alpha + \beta_f)}$ ;
- on  $G_2$  surface:  $\Delta v_2 = v_0 \cdot 2 \sin\left(\frac{\alpha}{2}\right)$ ;
- on  $G_3$  surface:  $\Delta v_3 = v = \frac{R^2 - r^2}{R_0^2 - (R_0 - g_0 \cos \alpha)^2} \cdot \cos^2 \alpha$

The consumed power in the process of drawing must compensate the losses produced through friction on  $G_3$  surface ( $W_f$ ), through shear due to speed discontinuities of  $G_1$  and  $G_2$  surface ( $WG_{1,2}$ ) and for proper plastic deformation ( $W_d$ ).

For the calculation of power losses, the following expression result:

❖ consumed power for deformation:

$$\dot{W}_d = \dot{V} \left( \frac{2}{\sqrt{3}} \right) \sigma_r \cdot \sqrt{(1/2) \varepsilon_{ij} \cdot \varepsilon_{ji}}$$

The  $\varepsilon_{ij}$  and  $\varepsilon_{ji}$  of the deformation tensor, in cylindrical components, are:

$$\varepsilon_{RR} = \ln \frac{R - r}{R_0 - r_0} = \ln(\psi_1 \cdot \psi_4);$$

$$\varepsilon_{\theta\theta} = \ln \frac{R + r}{R_0 + r_0} = \ln(\psi_1 \cdot \psi_5);$$

$$\varepsilon_{ZZ} = -(\varepsilon_{RR} + \varepsilon_{\theta\theta});$$

$$\varepsilon_{R\theta} = \varepsilon_{RZ} = \varepsilon_{\theta Z} = 0,$$

And volume speed  $\dot{V} = \pi v_{tr} (R^2 - r^2)$ . Therefore:

$$\dot{W}_d = \left( \frac{2}{\sqrt{3}} \right) \sigma_r \pi v_{tr} R^2 \left[ 1 - \left( \frac{r}{R} \right)^2 \right] \cdot \sqrt{\varepsilon_{RR}^2 + \varepsilon_{\theta\theta}^2 + \varepsilon_{RR} \cdot \varepsilon_{\theta\theta}}$$

❖ the power consumed during  $G_1$  surface crossing is:

$$\dot{W}_{G_1} = \int_{SG_1} \tau \Delta v_1 ds$$

where  $\tau = \left(\frac{1}{\sqrt{3}}\right) \sigma_r$ , and  $\Delta v_1$  with the expression given by [7] relation.

Therefore  $SG_1$  has the form:

$$SG_1 = \frac{\pi \cdot (R^2 - r^2)}{\sin \beta f},$$

so:

$$\dot{W}_{G_1} = \left(\frac{1}{\sqrt{3}}\right) \sigma_r \pi v_r R^2 \left[1 - \left(\frac{r}{R}\right)^2\right] \left[\frac{\sin \alpha}{\sin \beta f} \sin(\alpha + \beta f)\right]$$

❖ the power consumed during  $G_2$  surface crossing :

$$\dot{W}_{G_2} = \left(\frac{\sigma_r}{\sqrt{3}}\right) v_0 2 \sin\left(\frac{\alpha}{2}\right) \pi \left[\frac{(R_0^2 - r_0^2)}{\sin \beta_0}\right] = \left(\frac{2}{\sqrt{3}}\right) \sigma_r \pi v_r R^2 \left[1 - \left(\frac{r}{R}\right)^2\right] \operatorname{tg}\left(\frac{\alpha}{2}\right)$$

❖ the power consumed due to friction losses on  $G_3$  surface:

$$\dot{W}_f = \dot{W}_{G_3} = \int_{SG_3} \tau \Delta v_3 ds$$

where  $\tau$  -shear stress,  $\tau = \mu^{\text{UVD}} \sigma_r$ , coulomb type friction,  $\mu^{\text{UVD}}$  from (1).

The element surface  $ds$  has the expression:

$$ds = \frac{2\pi}{\sin \alpha} R dR \quad , R \in [R, R_0]$$

The normal stress can be determined using Sach's relationship [5]:

$$\sigma_r \approx \sigma_r \left[ \ln\left(\frac{R_0}{R}\right)^2 - 1 \right]$$

Therefore

$$\dot{W}_G = \int_{SG_3} \mu^{\text{UVD}} \sigma_r \left[ \ln\left(\frac{R_0}{R}\right)^2 - 1 \right] \Delta v_3 ds$$

so:

$$\begin{aligned} \dot{W}_{G_3} &= \mu^{\text{UVD}} \sigma_r \left[ \ln\left(\frac{R_0}{R}\right)^2 - 1 \right] v_r (R^2 - r^2) \frac{\cos \alpha}{g_0} \frac{\pi}{\sin \alpha} \int_R^{R_0} \frac{R dR}{R - \frac{g_0}{2} \cos \alpha} = \\ &= \mu^{\text{UVD}} \sigma_r \left[ \ln\left(\frac{R_0}{R}\right)^2 - 1 \right] v_r (R^2 - r^2) \frac{\pi \cos \beta}{g_0 \sin \alpha} \left[ R - \frac{g_0}{2} \cos \alpha \ln\left(R - \frac{g_0}{2} \cos \alpha\right) \right] = \\ &= \frac{\pi \mu^{\text{UVD}} \sigma_r}{g_0} v_r (R^2 - r^2) \left[ \ln\left(\frac{R_0}{R}\right)^2 - 1 \right] \frac{\cos \alpha}{\sin \alpha} \left[ (R_0 - R) - \frac{g_0}{2} \cos \alpha \ln \frac{R_0 - \frac{1}{2} \cos \alpha}{R_0 - \frac{1}{2} \cos \alpha} \right] = \\ &= \pi \mu^{\text{UVD}} \sigma_r v_r R^2 (1 - \psi_2)^2 K_2 \end{aligned}$$

In which  $K_2$  has the expression:

$$K_2 = (\ln \psi_1^{-2} - 1) \left[ \frac{1 - \psi_1}{1 - \psi_3} + \frac{\cos \alpha}{2} \ln \left( \frac{2 - (1 - \psi_3) \cos \alpha}{2\psi_1 - (1 - \psi_3) \cos \alpha} \right) \right] \operatorname{ctg} \alpha$$

From the balance of the total consumed power in the process of plastic deformation by drawing, for U.V.D. technology the following expression results:

$$\sigma^{UVD} = \frac{2\sigma_r}{\sqrt{3}} K_1 + \sigma_r \mu^{UVD} K_2$$

in which:

$$K_1 = \sqrt{\varepsilon_{RR}^2 + \varepsilon_{\theta\theta}^2 + \varepsilon_{RR} \cdot \varepsilon_{\theta\theta}} + \frac{\sin \alpha}{2 \sin \beta^f \sin(\alpha + \beta^f)} + \operatorname{tg} \frac{\alpha}{2}$$

These, with relation (2), the expression for  $F^{UVD}$  becomes :

$$F^{UVD} = \pi(R^2 - r^2) \left[ \left( \frac{2\sigma_r}{\sqrt{3}} K_1 + \sigma_r \mu^{UVD} K_2 \right) \right]$$

In the case of classical processing, CT technology, using (27) relationship, the drawing stress  $\sigma^{CT}$  has the expression:

$$\sigma^{CT} = \frac{2\sigma_r}{\sqrt{3}} K_1 + \frac{2\sigma_r}{\pi} \mu^{CT} K_2,$$

and the drawing force  $F^{CT}$  can be calculated using the relationship:

$$F^{CT} = \pi(R^2 - r^2) \sigma^{CT}$$

The magnitude of the drawing stress must not exceed the value of the tensile strength, with the accumulated superficial hardening in the process of plastically deformation, a condition that can be expressed by means of the so-called drawing safety coefficient (C) [1,2]:

$$C = \frac{S\sigma_r}{F}$$

where:  $\sigma_r$  is the tensile strength, S – cross section surface (at the exit of deformation focus zone); f- drawing force ( $F^{CT}$  or  $F^{UVD}$ ).

The effectiveness of U.V.D. technology, as compared to the classical processing, CT technology is determined considering the reduction of the drawing force and safety of the plastic deformation process, according to relationships [5] :

$$\Delta F = \frac{F^{CT} - F^{UVD}}{F^{CT}} 100 \quad [\%]$$

and

$$\Delta C = \frac{C^{UVD} - C^{CT}}{C^{UVD}} 100 \quad [\%]$$

#### 4. EXPERIMENTS ON TUBES WITH THIN WALLS MADE OF AUSTENITIC STEEL

The experiments have been performed on tube samples made of 10TiNiCr180/STAS 3583(AISI 321) stainless steel, with the initial sizes:  $D_0=4,85$  mm,  $g_0=0,70$  mm and the length of 1200 mm, with one of the ends being putrid and the thermally treated quenching in solution.



plastic deformation process, U.V.D. technology, it is recommended that the “z-z” vertical should be located at  $a_3$  distance, from the frontal surface of the guide for ultrasonic sounds.(7)

The chemical composition of 10TiNiCr180 steel spectrographically determined is, [%]: 0,10C; 2,0Mn; 1,0Si; 0,030S; 0,045P; 18,45Cr; 9Ni; 0,7Ti. The microscopic structure of the steel, analyzed in initial state is made of austenitic poliedrical crystals maclated .

Among the three technological factors, of major importance that influence directly the force parameters: the degree of section reduction

$$r [\%] = 100 \left[ 1 - \left( \frac{R}{R_0} \right)^2 \right],$$

the semi-angle of die conicity opening  $\alpha$  [ $^\circ$ ] and metal-tool contact friction-the first to are constantly maintained. The third one-metal-tool contact friction expressed by means of friction coefficient ( $\mu^{UVD}$ ) modifies according to the reverse mechanism of average friction force.

The experiments are accomplished at a constant drawing speed ( $v_{tr} = 0,33$  m/s) and five different values of oscillation amplitude of the die (A): 5, 10, 15, 20 and 25  $\mu\text{m}$ , witch, in fact, represent different vibration speed ( $v_v = 2\pi fA$ ;  $v_{v1} = 0,55$ ;  $v_{v2} = 1,09$ ;  $v_{v3} = 1,65$ ;  $v_{v4} = 2,20$  and  $v_{v5} = 2,74$  m/s).

Different value of the oscillation amplitude can be obtained by means of increasing the feeding voltage tension at the level of magnetostrective transducer and the premagnetization current. The section reduction (r) is of 23[%];  $D = 4,32$  mm,  $g = 0,65$  mm and the opening semi-angle of the die conicity  $\alpha = 8^\circ$  (reason for which  $v_{tr} \approx v_a$ ,  $\cos 8^\circ = 0,99$ ).

Dies with WCr, carbide middle are used, the lubrication being performed with 45% chlorided paraffin.

The processing of tube sample, U.V.D. and CT technologies is performed by means of singular drawing, on five sets of test-tubes A, B, C, D, E, according to the relative drawing speed ( $v_{tr}, v_v$ ) used in the experimental process.

## 5. EXPERIMENTAL RESULTS

The experimental results, that have been obtained in the case of the two tehnology-CT and U.V.D. are shown in table 1 and table 2, considering as discussion parameter the relative drawing speed. ( $v_{tr}/v_v$  ratio)

The size of the drawing force, for the two technology CT and U.V.D. are experimentally obtained, with force captors of DT 106000 type and tensiometric deck N 2314, being the result of five tests. At the same time, the drawing speed in the amplitude (A) of die vibration [7] are also experimentally measured.

For the calculation  $\sigma_{an}^{UVD}$ ,  $F_{an}^{UVD}$  there have been initially accomplished traction test, on test-tubes manufactured according to SR-EN 1002-1/95 using a MTS 810.24 type machine, having the 20 mm/min speed. At the same time, the safety coefficient of drawing ( $C^{CT}$  and  $C^{UVD}$ ) have been calculated. The size of  $\mu^{CT}$  friction coefficient was calculated considering  $\sigma^{CT}$  (see 30)

Using these obtained value, the  $\mu_{an}^{UVD}$  was measured according to (1).

Table 1 The results obtained by CT technology

Test tube set	Test tube dimensions initial and final ones				Technologies –CT					
	D <sub>0</sub> [mm]	g <sub>0</sub> [mm]	D [mm]	g [mm]	v <sub>tr</sub> [m/s]	r [%]	F <sub>ex</sub> <sup>CT</sup> [N]	σ <sup>CT</sup> [MPa]	μ <sup>CT</sup>	C <sup>CT</sup>
A	4,85	0,70	4,32	0,65	0,33	23	812	109	0.026	4.89
B	4,85	0,70	4,32	0,65	0,33	23	812	109	0.026	4.89
C	4,85	0,70	4,32	0,65	0,33	23	812	109	0.026	4.89
D	4,85	0,70	4,32	0,65	0,33	23	812	109	0.026	4.89
E	4,85	0,70	4,32	0,65	0,33	23	812	109	0.026	4.89

Table 2 The results obtained by U.V.D. technology

Test tube set	Technologies U.V.D.									Relative reduction	
	$\frac{v_{tr}}{v_r}$	r [%]	F <sub>an</sub> <sup>UVD</sup> [N]	σ <sub>an</sub> <sup>UVD</sup> [MPa]	F <sub>ex</sub> <sup>UVD</sup> [N]	σ <sub>ex</sub> <sup>UVD</sup> [MPa]	μ <sub>an</sub> <sup>UVD</sup>	μ <sub>ex</sub> <sup>UVD</sup>	C <sup>UVD</sup>	ΔC [%]	ΔF [%]
A	0,60	23	705	94	676	91	0,0065	0,0067	5,62	12,98	17,35
B	0,30	23	668	89	637	85	0,0052	0,0056	5,83	16,12	22,12
C	0,20	23	638	85	597	80	0,0044	0,0048	6,10	19,83	27,01
D	0,15	23	633	83	574	77	0,0030	0,0035	6,22	21,38	29,82
E	0,12	23	600	80	545	73	0,0020	0,0024	6,29	22,25	32,64

To estimate the efficiency of U.V.D. technology, as compared to the CT one, the relative reductions have been calculated ( $\Delta F$ ,  $\Delta C$ , [%])

The  $F_{ex}^{CT}$ ,  $F_{ex}^{UVD}$ ,  $\Delta F$ ,  $\Delta C$  variation is shown in figure 3.

## 6. CONCLUSIONS

1. The theoretical researches shows a calculation method of force parameters at the empty drawing of the tube, with ultrasonic vibrations transmitted to the die on the drawing direction or U.V.D. technology, using the theorem of total consumed power, admitting in the process of plastic deformation the existence of “reversion mechanism of the average friction force ” and the Coulomb-type friction at the metal-tool interface.
2. The experimental research, accomplished on tubes with thin wall made of 10TiNiCr180 stainless steel shows results that are in a good correlation with those obtained in the theoretical research.
3. The efficiency of U.V.D. technology, using the  $\Delta F$  and  $\Delta C$  relative reduction, recommends it for empty drawing tubes made of hard cold deformable metallic materials, for which the relative drawing speed ( $v_{tr}/v_v$ ) corresponds to the condition:  $v_{tr}/v_v < 1.0$

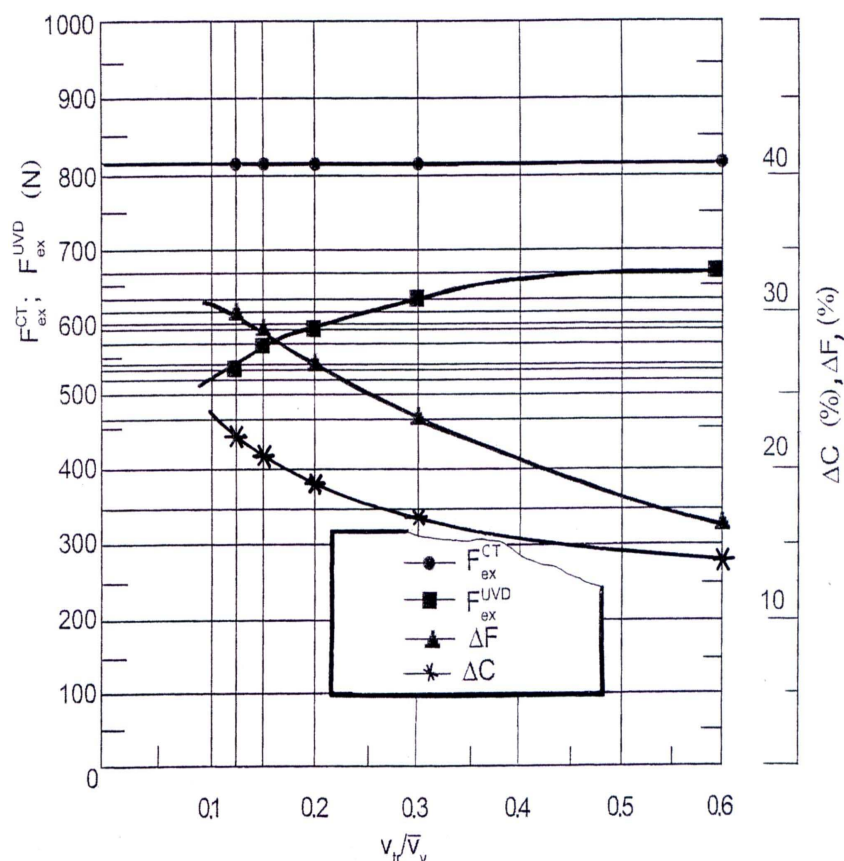


Figure 3 The variation of  $F_{ex}^{CT}$ ,  $F_{ex}^{UVD}$  forces and relative reduction, ( $\Delta C$ ,  $\Delta F$ ), according to  $v_{tr}/v_v$  ratio.

Received March 25, 2005

Technical University "Gh.Asachi" Iasi

#### REFERENCES

- /1/. Cazimirovici E. s.a. *Theory And Technology Of Drawing Deformation*, Technical Publishing House, Bucharest, 1990
- /2/. Susan M. *Metal Deformation Though Drawing*, Technopress Publishing House, Iasi, 2002
- /3/. Susan M., Bujoreanu L.G., *Rev. Metal. Madrid* 35 (1999), pp.379-383
- /4/. Avitzur B., *Metal Forming "Enciclopedia Of Physical Science And Technology"*, Vol. 9, Academia Press, 1992
- /5/. Susan M. s.a., - *Special Plastic Processing*, Gh. Asachi, Publishing House, Iasi, 2000
- /6/. Avitzur B. - *Study of Flow Through Cronical Conversing Dies*, Part I, Wire Industry, June 1982 p.449..453; Part II, Wire Industry, July 1982 p. 503..509; Part III, Wire Industry, Aug.1982 p. 613..649
- /7/. Susan M., Dima A., *Project nr. 905/2000. Final Raport*. RELANSIN National Programme, Ministry of Education and Research.
- /8/. Marapis N., *Ultrasonic Energy Applied to Metal*, Part I, Wire Industry, May 1991 p. 251..256, Part II, Wire Industry, June 1991 p. 327..333, Part III, Wire Industry, July 1991 p.371..373

#### CONSIDERAȚII PRIVIND TRAGEREA TUBURILOR ÎN PREZENȚA VIBRAȚIILOR ULTRASONICE TRANSMISE DORNULUI PE DIRECȚIA TRAGERII

**Rezumat:** Lucrarea prezinta o metodă de calcul a parametrilor de tragere a tuburilor în prezența vibrațiilor ultrasonice transmise dornului pe direcția de tragere. Rezultatele experimentale s-au efectuat pe oțel 10TiNiCr180.

## ON CONTACT FRICTION AT DRAWING OF WIRES OF CYLINDRICAL SYMMETRY WITH ULTRASONICALLY VIBRATED DRAW PLATE

BY

ILIESCU VIOREL, SUSAN MIHAI, MANTU MARIANA, MIRON VASILICA

**Abstract.** *The paper presents the possibility of reducing the metal tool contact friction at drawing of wires with draw plate situated at the maximum of wave oscillation and ultrasonically vibrated on the drawing direction. The reduction of contact friction is based on the "reversion mechanism of average friction force". A calculus relation was established for the average friction force reducing coefficient ( $\varphi$ ), with its graphical representation  $\varphi = g(v_r/v_w)$  using a calculus algorithm, in the case of RUL 1V wires drawing, in processing technological conditions at industrial level*

**Keywords:** *drawing, wire, ultrasounds, metal-tool contact friction, reversion mechanism of average friction force, technological efficiency*

### 1. INTRODUCTION

Generally, metallic wires are obtained through cold drawing, a technology which is also known as drawing. The plastic deformation through cold drawing is accompanied by superficial hardening or hardening under effort, with the increase of mechanical resistance characteristics and the diminution of plastic. Superficial hardening is to a great extent, determined by the metal-tool contact friction. The superficial hardening that was accumulated on the drawing brush, in classical drawing leads to the appearance of remnants tensions which generate certain defects such as micro fissures and fissures etc., with direct consequences on the quality of drawing products.

The drawing of wires with ultrasonically vibrated draw plate or the drawing in ultrasonic field leads to the diminution or even elimination of the defects generated by the elastically drawing [1]. The paper proposes the drawing of wires of cylindrical symmetry (round) with ultrasonically vibrated draw plate, when it is situated in the maximum (venter) of wave oscillation.

Under such drawing conditions, in ultrasonic field we obtain a substantial diminutions of metal-tool contact friction ( $F_6$ ) with diminution of superficial hardening and of course, with all the consequences that result from this. The reduction of metal-tool contact friction is explicated using the "reversion mechanism of average friction force". The measure of reduction of contact friction is given by the called "reduction coefficient of average friction force" ( $\varphi$ ).

The valuation of the new technology is performed in the case of drawing the wires of high mechanical resistance (RUL 1V/STAS 11250), and its efficiency is analyzed according to the relative reduction of drawing speed (DF).

## 2. THE REVERSION MECHANISM OF AVERAGE FRICTION FORCE

The drawing of metallic wires of cylindrical symmetry with the draw plate situated in the maximum of wave oscillation and ultrasonically vibrated is shown in fig. 1

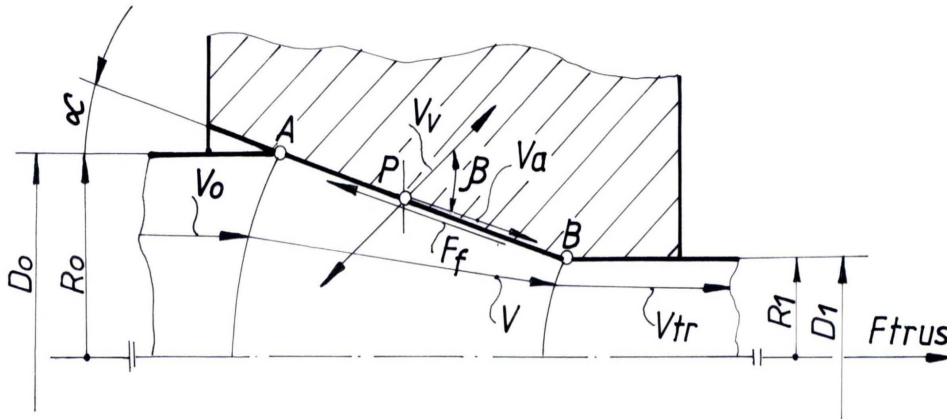


Figure 1 The scheme of drawing of wires with cylindrical symmetry with the ultrasonically vibrated draw plate ;  $R_0$ ,  $D_0$ - linear sizes of semi-finished wires;  $R_1$ ,  $D_1$  - linear wires of drawn wire ;  $V_n$ ;  $V_a$ ; and  $V_m$ - the speeds of draw plate vibration, of sliding of the metal on the generatrix of the cone of the draw plate and of the drawing;  $\alpha$  =the angle of draw plate conicity ;  $\beta$  = the angle between the vectors of vibration draw plate speeds ( $V_1$ ) , and of the sliding of the metal ( $V_a$ );  $F_f$ ,  $F_{rus}$  -friction and drawing forces.

To explicate the “reversion mechanism of the average friction force“ at the metal-tool contact, we analyse the movement of a certain P point, arbitrarily chosen, in the area of deformation forces, considering the kinematics of plastic deformation for this new drawing procedure.

The P point at the metal-tool contact surface takes part into two movements: an advanced one, on the generatrix of the draw plate cone, with  $v_a$  speed and a vibration one, with  $V$  speed. The resultant vector of the relative speed, the structure of the two vectors speed, will modify the movement direction of the P point, as it follows: on a certain period of time, from the period of the oscillation ( $T$ ),  $T/2 - 2t_1$  - the movement will coincide with that of the metal directions is bigger than that of the vector of advanced speed, on the same direction, and, in a contrary direction  $T/2 + 2t_1$  duration (when the size ratio of the projection of the two vectors, speeds on A-B direction is reversed), fig 2.

In other words, at  $T/2 - 2t_1$ , at the level of a complete oscillation period, the friction force is positive ( $F_f+$ ) and negative at  $T/2 + 2t_1$ .

Ratio [3]

$$\varphi = \frac{(T/2 + 2t_1) + (T/2 - 2t_1)}{(T/2 + 2t_1) - (T/2 - 2t_1)} \quad (1)$$

represents the reduction degree of friction average force, in a certain point, arbitrary chosen, in the area of deformation forces, when the draw plate is situated in the maximum of the wave oscillation (ventre) and ultrasonically vibrated. From the equation of the two speeds, of vibration ( $v_n$ ) and of advance ( $v_a$ ), we can determine  $t_1$

$$v_a = A\omega \cos\omega t_1 = v_n \cos\omega t_1 = v_n \cos\beta \cos\omega t_1 \quad (2)$$

from where, for  $t_1$ , we obtain the expression:

$$t_1 = \frac{1}{\omega} \arccos \frac{v_a}{v_v} = \frac{1}{\omega} \arccos \frac{v_a}{v_v \cos \beta} \quad (3)$$

A is the amplitude of wave oscillation and  $\omega$  is the pulsation ( $\omega=2\pi f$ , where f is the oscillation frequency;  $f=1/T$ ). At the same time,  $\mu$  is the wave oscillation:  $\mu = A \sin \omega t$ , from where  $v_v = d\mu/dt = A\omega \cos \omega t_1$  with  $v_v = A\omega = 2\pi fA$  for  $\cos \omega t = 1$ .

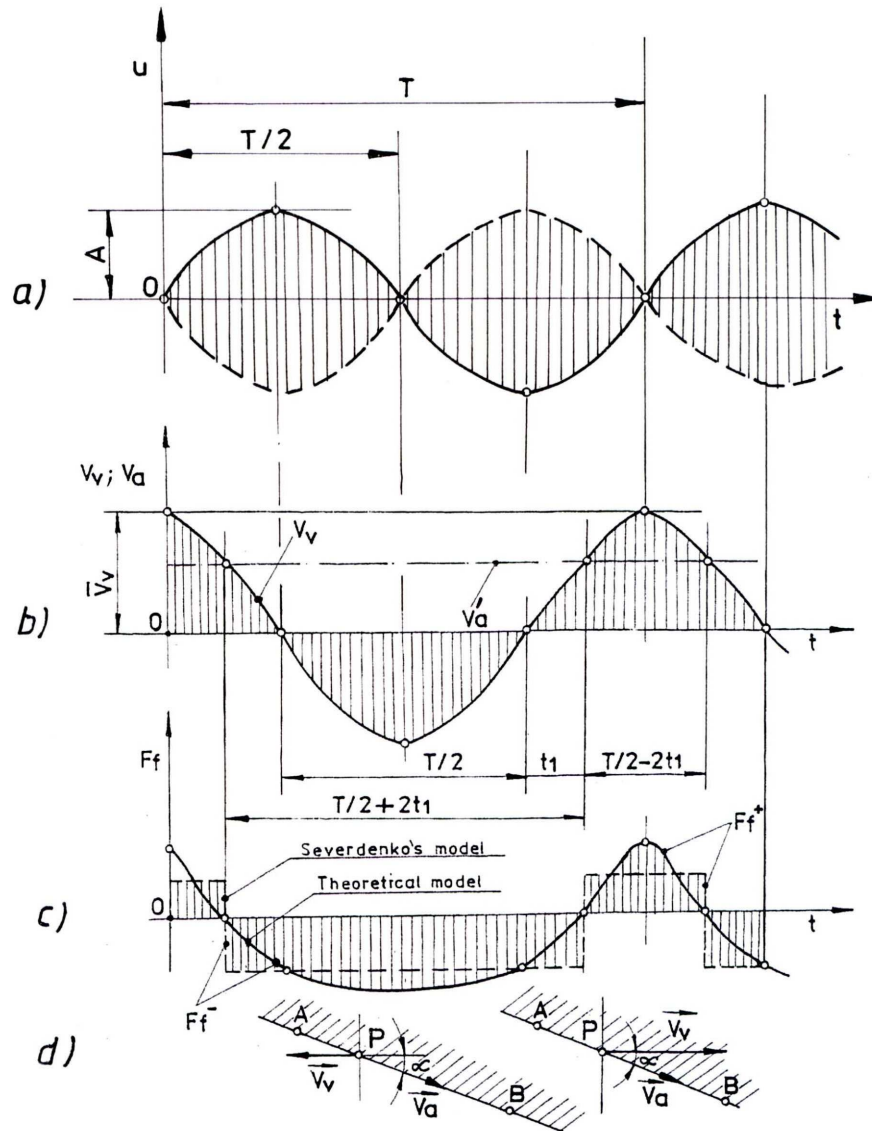


Figure 2 Explicitness of the " reversion mechanism of average friction force " at the metal-tool contact at an oscillation period: a -the wave movement ( with the formation of nodes and venders - stationary waves) b -variation of vibration ( $V_v$ ) speed and of the advanced one ( $V_a$ ); c -variation of friction force ( $F_f$ ); d -the vectorial representation of  $v_r$  and  $v_v$  speeds.

Replacing in relation(1) the  $t_1$  expression and respectively  $T(T=1/f)$ , for coefficient we obtain the relationship:

$$\varphi = \frac{\pi}{2} \cdot \frac{1}{\arccos \frac{v_a}{v_v \cos \beta}} \quad (4)$$

Replacing  $v_a$  with the average speed of metal movement ( entrance- exit in the

deformation zone) noted with  $v'_a$ , we obtain the reducing coefficient of average friction force on the whole metal-tool contact surface:

$$\varphi = \frac{\pi}{2} : \arccos \frac{v'_a \cdot \frac{\lambda \cos \alpha + 1}{2\lambda \cos \alpha}}{A\omega \cos \varphi} \quad [5]$$

or with proximally value:

$$\varphi = \frac{\pi}{2} \cdot \frac{A\omega}{v'_a} \cdot \frac{2\lambda \cos \alpha}{\lambda \cos \alpha + 1} \cos \beta \quad (6)$$

In the last two relations,  $\lambda$  is the wire elongation in the drawing process,

$$\lambda = \frac{S_0}{S_1} = \frac{D_0^2}{D_1^2} \quad (7)$$

The analysis of (4) relation leads to the conclusion that the reduction of the average friction force at the metal-tool contact is bigger, the smaller the angle between the oscillation direction and the metal movement direction ( $\beta$ ) and the bigger the ( $A$ ) amplitude and the frequency of the ultrasonic wave oscillation ( $f$ ).

### 3. APPLICATIONS IN THE CASE OF HIGH MECHANICAL RESISTANCE WIRES

The drawing of the wires with the draw plate situated in the maximum of the wave oscillation and ultrasonically vibrated is recommended in the case of drawing of the high mechanical resistance wires, especially considering the reduction of metal-tool contact, respectively of the superficial hardening that appears during drawing, according to the "reversion mechanism of average friction force"[4].

An important efficiency, in such drawing conditions is obtained when we use ultrasonic longitudinal waves with the draw plate vibrated on the direction of the drawing ( $\beta = \alpha$ ), a situation, when, from the technological point of view, we consider  $v_a \sim V_{tr}$  ( $v_a = v_{tr} \cos \alpha$ , with  $\cos \alpha \leq 1$ ). For a qualitative appreciation the effect of the reduction of metal-tool contact friction was on the drawing force ( $F_{tr}$ ) with Coulomb type friction, we can use the Gavrilenco's simplified relation, which, in the case of drawing without the ultrasonic intensification of the draw plate has the expression [5]:

$$F_{tr} = F_d + F_f = F_d(1 + \mu \operatorname{ctg} \alpha) \quad (8)$$

in which:  $F_d$  is the proper deformation force,  $F_f$  is friction force,  $\mu$  is friction coefficient and  $\alpha$  is the angle of conicity opening of the draw plate. In the case of drawing the wires with ultrasonically vibrated draw plate, the [8] relation becomes:

$$F_{trus} = F_d \left( 1 + \frac{\mu \operatorname{ctg} \alpha}{\varphi} \right) \quad (9)$$

in which  $\varphi$  is the reduction coefficient of friction average force. The efficiency of drawing the wires with the draw plate situated in the maximum of wire oscillation and ultrasonically vibrated, can be expressed through relative reduction (5)

$$\Delta F = \frac{F_{tr} - F_{trus}}{F_{tr}} \cdot 100 \quad [\%] \quad (10)$$

As an example, using the logical scheme shown in fig.3, at RUL1V/ STAS 11250 steel wires drawing, for which  $D_0 = 3,85$  mm;  $D_1 = 3.60$  mm;  $\lambda = 1,14$ ;  $\alpha = 8^\circ$  and

$v_v = 0,9; 2,0; \text{ and } 3,0 \text{ m/s}$ , in fig.4 is shown the shape of the graphic of  $\varphi = g(v_{tr}/v_v)$ .

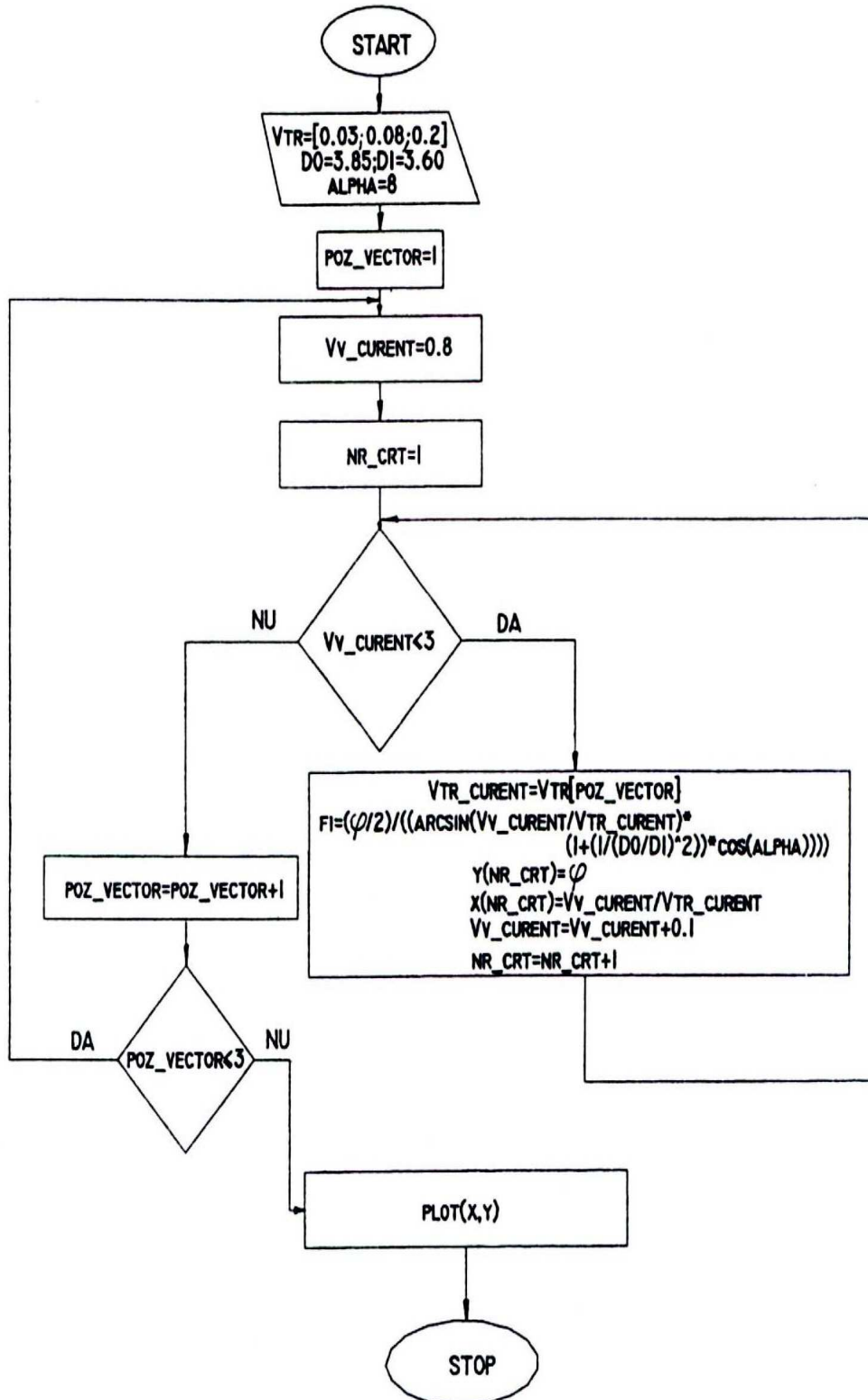


Figure 3 Calculus algorithm and graphical processing for the reduction coefficient of average friction force ( $\varphi$ )

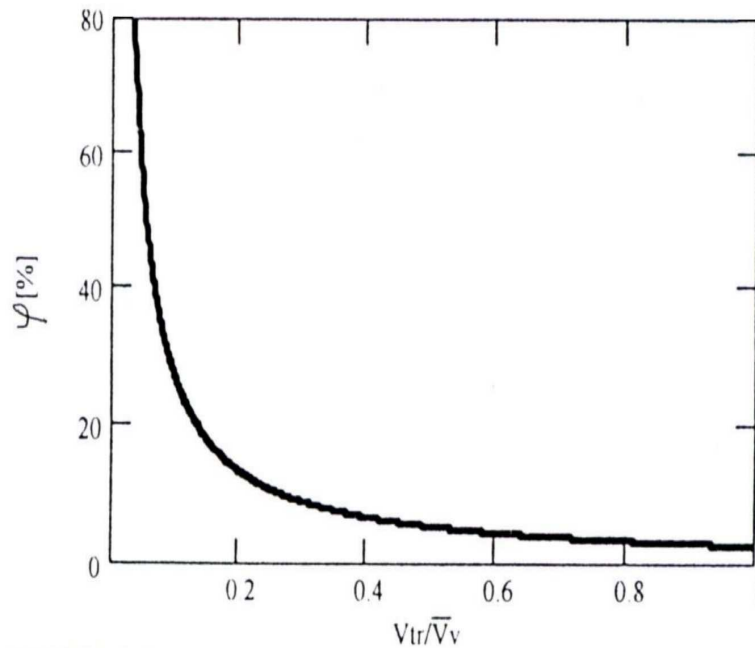


Figure 4 Variation of reduction coefficient of average friction force  $\varphi=g(v_{tr}/v_v)$

#### 4. CONCLUSIONS

The paper presents the explicitation of “reversion mechanism of average friction force”, at the metal-tool contact at drawing of wires with the draw plate situated in the maximum of wave oscillation and ultrasonically vibrated.

At the same time, a calculus relation was established for the reduction coefficient of average friction force ( $\varphi$ ); from which results that the reduction of metal-tool contact friction has important values when the intensification of the draw plate using ultrasound is made on the drawing direction, respectively  $\beta=\alpha$

Using a calculus algorithm the  $\varphi=g(v_{tr}/v_v)$  variation was presented. The efficiency of the new technology is expressed by the relative reduction of the drawing force ( $\Delta F$ ).

Received April 7, 2005

Technical University “Gh.Asachi” Iasi

#### REFERENCES

- /1/. Susan M., - *Metal Deformation Through Drawing*, Tehnopress Publishing House
- /2/. Susan M., Bujoreanu L. G., - *The Metal Tool Contact Friction at the Ultrasonic Vibration Drawing of Ball-bearing Steel Wires*, *Metalurgia*, Madrid 35(1999), pp. 379..383
- /3/. Severdenco V.P., - *Prokatka i vdocenie c ultrazvukam. Nauka i Tehnika* Minsk 1970
- /4/. Susan M., - *Doctorat thesis*, Science and Material Engineering Faculty, The “Gh. Asachi” Technical University, 1996
- /5/. Dragan Ov., *The Mechanism of Plastic Deformation of Tubes by Cold Drawing in Ultrasonic Field*, *Metalurgia* 23(1971), nr. 11, pp. 734..736

#### CONSIDERAȚII PRIVIND FRECAREA DE CONTACT LA TRAGEREA ÎN CÂMP ULTRASONOR A SĂRMELOR CU SIMETRIE CILINDRICĂ

**Rezumat:** Lucrarea prezinta posibilitățile reducerii frecării de contact la tragerea sârmelor în câmp ultrasonor, cu filiera aflată în vibrație iultrasonoră și situată în planul de oscilație maximă.

## THE TECHNOLOGY FOR HEAVY METALS FROM ELECTROPLATING SLUDGE VALORIFICATION, FOR ENVIRONMENT DEPOLLUTION

BY

ROMANITA TEODORESCU

**Abstract.** The paper presents the results of the researches performed into the RELANSIN program, for establish a new non-polluting technology, by total recovery of the some heavy metals from electroplating sludge resulted in the neutralization station of rinsing waters and spent solutions from the electroplating lines. This technology is non-producing of another noxious. The technology for recovery of the heavy metals from the sludge relies on chemical and hydro-metallurgical procedures, the final products being salts or pigments of the respective metals [ 1,2,3,4 ]. *The technology for the irreversible immobilization of the heavy metals contained in the sludge or in the technological residues consists of their solidification/stabilization in siliceous matrix , the final products obtained in the immobilization process being used as building materials [ 5 ]. This paper presents:*

1. *the technology for recovery of some metals which for the content in the sludge is very high 8-15%*
2. *the inertization of the technological residues resulted from the heavy metals recovery process by immobilization in different kinds of composites materials utilized like building materials.*

*The leaching tests have proved the irreversible binding capacity of metals in the composites materials structure[6].*

**Keywords:** *electroplating sludge, wastes, technologies, L:L extraction, cementation, precipitation.*

### 1. INTRODUCTION

Several industrial sectors especially those of surface treatment and electroplating lines, discharge waste solutions containing heavy metals such as zinc, copper, nickel, etc. These effluents are currently treated by conventional methods such as precipitation, ion exchange, evaporation, reverse osmosis, electro-dialysis , adsorption by activated carbon or clays, solvent extraction, cementation /1,2,3,4.../. The most popular is the neutralization/precipitation that generates sludge containing heavy metals. The resulting sludge, contain the metals like sparingly soluble hydroxides. Currently, these materials are stored in controlled waste disposals.

Nowadays we are facing an important decrease in natural raw materials. In the same time the concentration of useful non-ferrous metals in wastes is sometimes higher than that existing in ores.

Therefore, metals recovery from those polluting useless wastes, could be an important solution now and in the future. The use of wastes is also useful because of the necessity to eliminate the environmental pollution in the context of the integration of Romania in UE.

The available literature on this subject indicates that many specialists from all over the world are working to solve the pollution problems risen by the sludge containing toxic metal ions (Cr, Cu, Ni, Cd, Zn, Fe, Pb etc.). Chemical and hydro-metallurgical processes and the immobilisation of the metals in siliceous matrixes are

recommended for their recovery. These processes are based on metals leaching followed by their separation using different methods.

The immobilisation in siliceous matrix are realised by solidification/stabilisation of heavy metals from the sludge in hydraulic matrix with Portland cement, mixing with or without other supplements, or in ceramic matrix at the temp. over 1000°C /5,6./.

In the case of the immobilisation of heavy metals the most important is the study of the irreversible immobilisation capacity of the metals in siliceous matrix. These determinations were realised by the study of the heavy metals leaching in waters for long time in accordance with international norms by leaching tests / 7 /.

This work presents the experiments performed last years by our research group in the field of recovery of heavy metals from electroplating sludge with high content of the metals. These sludge resulted from collective neutralisation of washing waters and spent solutions arise from electroplating lines on two Romanian industrial platforms of machine building, and electro-techniques industry.

## 2. EXPERIMENTAL

### Materials and the methods

The work presents the researches which was carried out for a new technology non-polluting and non producing of another noxious, stabilisation for some heavy metals from EL-CO and HIDROJET industrial sludge valorification.

Two work methods was utilised:

- chemical or hydro-metallurgical processing of the sludge, in acid medium at normal or high pressure and temperature, for quantitative leaching of the metals with high content,
- recovery of the metals from the leaching solutions by various methods.

The influence of the various work parameters like temperature, pH, L:S ratio, number of the extraction steps on leaching and recovery of the metals efficiency was studied.

Table 1 shows the compositions of the sludge which were utilised in the works.

In order to the recovery of the heavy metals, the electroplating sludge was processed by washing, re-washing, filtration, drying and crushing.

The studies were conducted in three works variant (fig.nr.1), as follows:

In the first variant the processing of the sludge include the following steps:  
the acid leaching in counter-current at high temperature and pressure  
the processing of the finale solutions by cementation for copper recovery

The washed Cu-Zn-Ni sludge was introduced by continuous stirring in leaching reactor (autoclave), in the first step over intermediate solution, resulted in the second step of the leaching. In the reactor the enriching in copper and zinc of the solution, the advanced separation of the impurities and bring the pH in 2-3 interval., take place. After separation of the phases, siphon off the clear solution and filtration, a final solution and a thickened was resulted . The thickened was re-introduced together sulphuric concentrate acid and washing and fresh water in autoclave in the second leaching step. In that step take place the finish of the leaching of the metals reaction and the partial purification of the solutions by re-precipitation of some impurities.

After filtration results:

- an intermediate solution which is re-circulate in the first step of the leaching
- a residue which comport washing, drying, and inertization in siliceous matrix

Table 1. Spectral and chemical composition of the EL-CO and HIDROJET sludge

Metals (in dry sludge) %	Spectral analyse	chemical analyse, %			
		EL-CO		HIDROJET	
		Sample 1	Sample 2	Sample 1	Sample 2
Cu	p	18,56	17,1	<0,005	10,46
Zn		1	17	9,33	0,
Cr	0	1	0,	-	0,01
Fe			2,	22,62	0,54
Pb	0	0	0,	0,09	<0,01
Si	0	0	1,	0,25	0,016
Na				1,	26,4
Al	5	0	0,	-	0,009
Ni	0	1	4,	0,	0,007
Mg	0	0	0,	-	-
Ag	$5 \cdot 10^{-2}$	0,062	0,054	-	-
Sn	$5 \cdot 10^{-3}$	0,008	0,2	-	-
P	$5 \cdot 10^{-2}$	0,01	0,04	1	-
Anions: $\text{NH}_4^+$		absence	absence	absence	absence
$\text{NO}_3$		7,56	2,85	1,0	4,5
$\text{SO}_4$		9	1,	0,31	27,0
$\text{CO}_3$		8	10,97	0,84	30,07
Cl		0,76	0,22	0,01	14,87
$\text{H}_2\text{O}$		9,77	6,3	1,3	7,4
Lost of the burning:				1	2
P.C. $800^\circ\text{C}$		30,66	30,72	5,42	6,89
P.C. $1000^\circ\text{C}$		30,75	31,08	1	4
				5,45	2,33

The leaching efficiency of the sludge in that variant is about 85%.

In order to recover the copper from the final solutions the cementation technique with zinc metallic was applied. The Cu cement resulted was separated by filtration from Zn and Ni solutions, washed, dried and grind.

The total efficiency for cementation of the copper in that variant is over 97%.

In the second variant the processing of the sludge include the following steps:

- the acid leaching in counter-current at high temperature and pressure
- the processing of the finale solutions by L:L extraction for copper recovery
- the regeneration of organic phase
- alkaline precipitation in three steps
- the inertization of the residue in siliceous matrix

The recovery of the Cu from the final solutions was realised by extraction with organic solvents. Like extraction agent was utilised the agent ACORGA M 5640 in KEROSEN. The leaching solutions with 15 g/l Cu content - resulted by dilution with water - was introduced in extraction installation, in three steps, in counter-current. Cu was extracted in organic phase. The regeneration of organic phase and the recovery of the Cu after quantitative separation of the phases take place in stripping installation, in

three steps, in counter-current. Like stripping agent is utilise an acid solution of copper sulphate. Finally, after three re-circulation, a copper sulphate with 45 g/l concentration and a Zn and Ni sulphate solutions, resulted from this installation. The recovery of the copper from the sulphate solutions was realised in electrolytic installation.

The recovery of the metals from Zn and Ni sulphate solution was realised in three steps, in alkaline medium, by precipitation.

In the first stage, in the interval of the pH = 3-5,5, the metal impurities like Cr, Fe, residual Cu a.o. are take away from the solutions and accumulate in solid phase .

Under continuous stripping the solutions with Zn and Ni content resulted at the cementation or at the L:L extraction was introduced in precipitation reactor together the agent of precipitation (NaOH sau Na<sub>2</sub>CO<sub>3</sub>).

In the second stage of the precipitation , in the pH= 5,5-7,5 interval , take place the quantitative Zn precipitation. After washing, drying and burning of Zn precipitate a ZnO pigment possible to utilise in the tyre or construction industry, was obtained .

In the third stage of the precipitation, in the pH = 7,5-10,5 interval , take place the quantitative precipitation of the Ni and the complete release of metals from the solutions.

The salts of the nickel , carbonate or hydroxide, resulted from the precipitation ware separated by filtration from the suspension, washed and dried.

The washing waters, free of the heavy metals, ware sanded in the neutralisation station.

### Results and Discussions

In the following tables, the work parameters on the phases of the flow sheet , there are presented.

Table 1 shows that the sludge used for the experiments contain high quantities of heavy metals ions (Cu, Zn, Ni, Fe). In the experiments which were performed in the conditions presented in the table nr.2, 3... it was observed that :

Table nr.2 The work conditions utilised at the washing of the sludge

washing of the sludge	
washing agent	water
nr.of washing steps	4
work techniques	re-washing
temperature	20-30 <sup>0</sup> C
stirring times	30 min/ step
S:L ratio	1:4
The composition of the unwashed sludge: 3-8% SO <sub>4</sub> <sup>2-</sup> and 2 – 5 % Na	
The composition of the washed sludge: 0,5-1,3% SO <sub>4</sub> <sup>2-</sup> and 0,2 – 0,8 % Na	

Table nr.3 The work conditions utilised at the leaching of the sludge

Leaching <i>in open system</i> / autoclave	
washing agent	acid medium - H <sub>2</sub> SO <sub>4</sub>
acid concentration	20%
temperature	60 – 80 / 135-145 <sup>0</sup> C
pressure	Normal / 3-4 atm
consumption of the acid	Excess / stoichiometric
- S:L ratio	1 : 5 - 1 : 8
- reaction time	2h / 1h / step
- final pH	1,5 – 2 / 2,5 - 3
- technique of the work	counter-current
- density	1,1-1,2 / 1,2 – 1,3
Leaching efficiency	80% / 83-85%
The composition of the intermediate solution 11,55Cu, 10,82Zn, 1,44g/l Ni      pH = 0,89	
The composition of finale solution: 26,6 / 35 Cu, 24,57 Zn, 1,59 Ni, 0,7 Fe, 0,59 Cr, 0,43 g/l Si      pH = 2,6	

The composition of the sludge before and after washing shows that after 4 washing steps in counter-current in the optimum conditions presented in the table nr 2, the removal efficiency of the  $\text{SO}_4^{2-}$  is over 95%.

The analyse of the results obtained in the leaching experiments of the sludge in acid medium shows that :

- for the sludge with high content of Cu and Zn, working in open system, at 70 - 80°C S:L ratio 1 : 6, time 2 h , at pH=1,5 - 2, the leaching efficiency for the Zn is over 90% but for Cu is lower, about 50%
- for pH=0,5-1,5 the leaching efficiency is highest but, impurities pass in the solutions
- for the leaching of the sludge in autoclave, at high temperature 135-140°C and 3-4 atm pressure, pH between 2,1-2,6 the content of the impurities in the solutions is minimum and the leaching efficiency of the copper is over 85 %
- the composition of the final solutions resulted in the second step of the leaching, in autoclave, in two counter-current steps, shows that the Cu and Zn contents , between 35-45 g/l, are with 25-30% over the same content from the solutions resulted in open system and the content of the impurities is under the content from the same solutions
- the leaching efficiency is higher in the counter-current system
- the consumption of the reactive are lower by re-circulation of the solution

Table nr.4 The work conditions utilised at Cu cementation

<b>Copper cementation</b>	
Cementation agent	metallic Zn
Consumption of Zn	stoichiometric+excess 20-30 %
time	105 minute
temperature	45 <sup>0</sup> C
washing agent	water
Cementation efficiency	97%
Cu cement: Cu 92,3,Zn 0,28, Ni 0,006, Cr 0,14, Fe 0,01%	
sulphates solutions Zn 61,4, Ni 3,3 %	

Working in the conditions presented in the table nr.4 the results show that: the cementation of the Cu is quantitative and the Cu cement has good qualities.

Table nr.5 The work conditions utilised at the L:L extraction of the Cu

<b>L: L Extraction</b> in counter-current	
extraction agent	ACORGA M 5640 in KEROSEN
FO : FA Ratio	1:1
nr. of extraction steps	3
stirring time	5 minute / step
temperature <sup>0</sup> C	23
pH	about 2
extraction efficiency	99 %
Composition of the sulphate solution Zn , Ni 14 Zn, 2,7 Ni, 1,56 g/l Cu	

The analyse of results obtained in the extraction experiments show that : from the solutions with 14,3 Cu, 14 g/l Zn content, at pH=1,8-2, working in counter-current in 3 extraction steps, the rapport Cu/Zn is modified from 1,02 at 0,1-0,12 by removal of the Cu. The extraction efficiency of copper is over 95%. Therefore, from the solution where the content of the copper is under 14 g/l the extraction efficiency of copper is maximum.

Table nr.6 The work conditions utilised at the regeneration of the organic phase

<b>OF Regeneration in counter-current</b>	
stripping agent	copper sulphate solution
OF: SA Ratio	1:1
nr. of re-extraction steps	3
stirring time	5 minute / step
temperature °C	ambient
re-extraction efficiency	99,9 %
initial solution : copper sulphate solution 18 g/l Cu , acidity ~180g/l H <sub>2</sub> SO <sub>4</sub>	
finale solution: copper sulphate solution	

The experiments show that the Cu sulphate solution with 18 Cu, 180 g/l H<sub>2</sub>SO<sub>4</sub>, stripping agent , realised the quantitative retention of the copper from OF like Cu sulphate . After 3 re-extraction steps the content of the Cu in solution is 44-45 g/l . Cu is recovered from this solutions by electrolysis. The re-extraction efficiency of Cu is over 98%. The content of Cu and Zn in regenerated OF in 3 steps is under 0,1 g/l

Table nr.7 The work conditions utilised at precipitation Table nr.8 The work conditions utilised at burning

<b>Precipitation</b>	
medium	NaOH / Na <sub>2</sub> CO <sub>3</sub>
temperature	40-60°C
Nr.pp. steps	3
time	2h/ 1step, 3h/ 2 step 1h/ 3 step +1/2h at pH ct
pH	2,5 - 5,5 / 1step 5,5 - 7,5 / 2step 7,5 - 10,5 /3step

<i>Burning</i>	
Material	zinc precipitate (2 <sup>th</sup> step)
temperature	800 - 850°C
Time	2 h
harden / washing agent	water

The purification of the solutions was realised by precipitation with a solution of NaOH or Na<sub>2</sub>CO<sub>3</sub> 355 g/l , in the interval of the pH 2,5-5,5. The precipitate of the impurities after washing and dried is possible to utilise in construction materials.

After the impurities separation, under continue stirring, at the pH between 5,5-7,5 zinc was precipitated from the solutions like hydroxide or carbonate. The Zn precipitation efficiency is over 95%. Over pH 7,7 from the solution was precipitated the salt of the Ni with very good efficiency. The technique of precipitation allow the release of all the metals from the solutions resulted after recovery of copper .

After separation of zinc salts by filtration, washing with water in 4 steps, dried and burning at 800-850<sup>0</sup>C for 2 hours, resulted ZnO for rubber industry or substitution pigment in construction materials.

The immobilisation of the metals in the construction materials

From the technology which was presented in the fig.nr.1 resulted next to the final products:

- a precipitate of the impurities in the first step of the precipitation and
- the technological residues resulted at the leaching of the sludge.

Table nr.9 The medium composition of a finale residue

Metal / residue	Cu %	Fe %	Al% / P %	Cr %	Ni %	Na %	Si %	Zn %	Ca %	SO <sub>4</sub> <sup>2-</sup> %
EL-CO residue from autoclavization	2,08	7,16	0,44/	1,00	0,03 6	0,27	0,00 2	0,22	6,09	19,6
EL-CO residue from normale solubilisation	1,9	1,35	/0,02	0,03	0,05 6	0,08 6	3,47	0,16	5,24	3,6
HIDROJET rezidue normale solubilisation	0,004	29,0	/15,5	0,18	0,00 7	0,03 4	0,03 4	2,3	6,3	0,6

The ecological immobilisation in siliceous matrix was realised by solidification/stabilisation of heavy metals from the technological residues in hydraulic matrix, mixing Portland cement with 50% residue, or the immobilisation of heavy metals in a stable structure with 10-15% residue with or without other supplements, the resulted materials can be used like construction materials.

The study of the irreversible immobilisation capacity of the metals in siliceous matrix were realised by the study of the heavy metals leaching in waters for long time in accordance with international norms by leaching tests. The results show us that after 365 days the content of the metals in water was <0,001g/l, therefore all the metals was complete immobilised.

### 3. CONCLUSIONS

The researches which was carried out, allowed us to establish a complex technology which was patented and verified at pilot level.

The combinative process for the integral valorification of Cu, Zn, Ni, from the electroplating sludge consist in the leaching of the sludge in sulphuric acid, cementation or L:L extraction of the copper from the leaching solutions, the precipitation of the zinc and nickel from the solutions free of copper and the inertization of the technological residues in siliceous matrix.

Received April 19, 2005

Institute for Non-Ferrous and Rare Metals, București

### REFERENCES

- /1/. Zadiranov A.N. *Recycling technologies of nickel metal – containing wastes recovery in electroplating industry*, Recycling and Waste Treatment in Mineral Processing: Technical and Economic Aspects 16-20 June 2002, Lulea Sweden, Proceedings pg. 815-820.
- /2/. Serdar Aktaş, *Recovery of zinc from galvanized scraps*, Turkish Journal of Engineering & Environmental Science 2002, 26(5) 395-402.

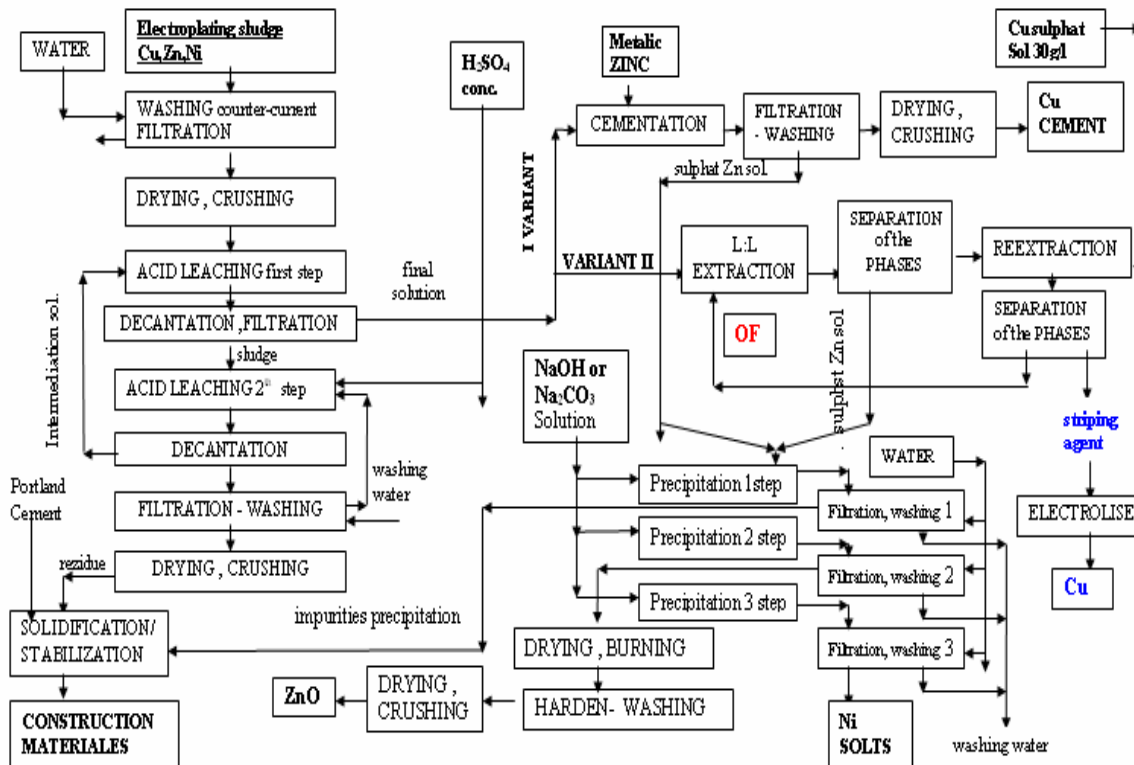
- /3/. Gunter Subklew , a.o. , *Separation of heavy metals from industrial waste waters by reactive liquid/liquid extraction*, Models in chemistry 134 (6), 28 apr. 1997, pp 853-864.
- /4/. Albinas Pigaga, a.o, *Waste treatment of two electroplating solutions of Cu and Zn by mixing and precipitation*, Separation Science and Technology, 37(13), 3155-3168 (2002)
- /5/. R. Teodorescu , S. Martinez , J. MaNoguez Carulla , R. Mateuca, *Stabilisation of heavy toxic metals from electroplating sludges in siliceous matrixes* ,3rd International Conference of Balkan Environmental Association on Transboundary Pollution 23 – 26 nov.2000, Bucharest, Romania
- /6/. M. Gheorghe, R. Teodorescu, *Some aspects regarding the influence of the type concrete matrix on the s/s process of some industrial electroplating sludge*; International Congress , Dundee University 2002 ,proc.
- /7/. German Standard: DIN 38414 Tail 4

## TEHNOLOGIE DE VALORIFICARE A UNOR METALE GRELE DIN NAMOLURI GALVANICE ÎN VEDEREA DEPOLUĂRII MEDIULUI

**Rezumat:** Lucrarea prezintă rezultatele cercetărilor efectuate în cadrul programului RELANSIN de stabilire a unei tehnologii noi, nepoluante și neproducătoare de alte noxe, prin recuperarea totală a unor metale grele din nămolurile galvanice rezultate în stațiile de neutralizare uzinale a apelor de spălare și a soluțiilor epuizate din liniile de acoperiri metalice. Tehnologiile pentru obținerea metalelor grele din nămoluri se bazează pe procedee chimice și hidro-metalurgice, produșii finiți fiind săruri sau pigmenți ai metalelor respective /1,2,3,4/. Tehnologiile de imobilizare ireversibilă a metalelor grele conținute în nămoluri sau în reziduurile tehnologice, constau în solidificarea/stabilizarea lor în matrice silicioase , produșii finiți obținuți în procesul de imobilizare fiind utilizați ca materiale de construcții /5,6/. Lucrarea prezintă :

1. tehnologia de recuperare a unor metale pentru care conținutul în nămol este de peste 8-15 %
  2. inertizarea reziduurilor tehnologice rezultate în procesul de recuperare a metalelor grele prin imobilizare în diverse tipuri de matrice silicioase cu obținere de materiale compozite cu utilizări în construcții .
- Testele de levigare ale acestor materiale evidențiază capacitatea blocării ireversibile a metalelor în structura matricei /7/..

Fig. 1. TEHNOLOGICAL FLOW SHEET



## CUTTING OF GLASS PLATES THROUGH THERMO SHOCK

BY

LUCIAN SCOROBETIU, VIRGIL CÂNDEA

**Abstract.** The paper presents a method of cutting tubes and thick plates of glass by heating the place for cutting with an electrical resistance having shape of a thread followed by sudden cooling with water flush.

**Keywords:** *glass tubes, plates cutting*

### 1. INTRODUCTION

The glass plates with reduced thickness (1-3 mm) may be easily cut by scratching them with diamond points, with hard roles, etc. The bigger the thickness of glass and older the material, the more difficult the cutting is done, and sometimes cutting at the required quota is impossible.

By the cutting method recommended in this paper, cutting of tubes and thick plates is possible, with enough dimensional precision, even if the material is aged or has heterogeneous areas.

### 2. CONTENT

The cutting method applied [1] is based on local heating and sudden cooling with water of the cutting area, which cracks under control after the direction of the heating element applied on plate.

The device for cutting glass tubes as in figure 1 is build up of two semi cylinder metallic support 1 and 2 and semi cylinder lids 3 and 4 foreseen with hinges between the glass tube 5 is caught. Inner components of the system are covered with rubber, which gives more safety at the danger of tube brooking. Heating component 11 is build up of a spire with the diameter of 1 mm from Cr-Ni alloy, which has the characteristic of compression on the circumference of the glass tube. The electric stream of 24 V-AC comes from transformer 6 in 0,5 s up to 5 s, controlled with the help of time relay 7. After turning off the electric stream an electro valve is opened which turns on the water stream pointed to the circumference of the tube through radial adjustments of cooling device 9.

The water for cooling is caught and evacuated from recipient 10 at the bottom of support device through the evacuation hole 8.

Data used for cutting glass tube with the diameter of 40 mm and with the width of 0,5 mm are: the electric tension of heating element  $U = 24V$ ; the electric force  $I = 1A$ ; heating time  $t = 5s$ ; quantity of water through the system used for cooling 0,1 liters; frequency: 3 cuts per minute

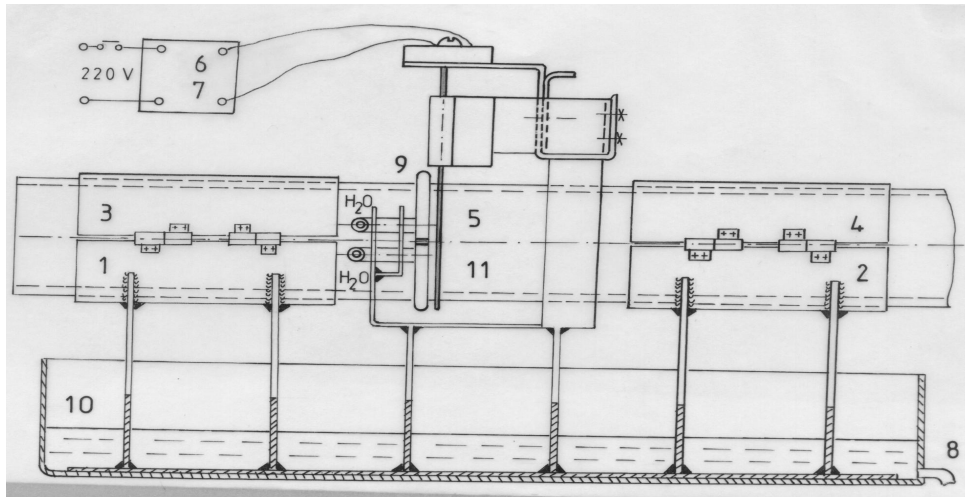


Figure 1. Cutting device for glass tubes

The cutting device acc. Fig.1 consists of a heating element 1, made of a thread with a diameter of 0.5 – 2 mm alloy Cr-Ni, which is applied on the surface of glass plate 2, by pressing with the help of the ceramic support 3. Thread supply is done with alternative electric power produced by a low tension transformer 4, with multiple secondary plugs, in time  $t=0.5 - 10s$ , checkable with time relay 5.

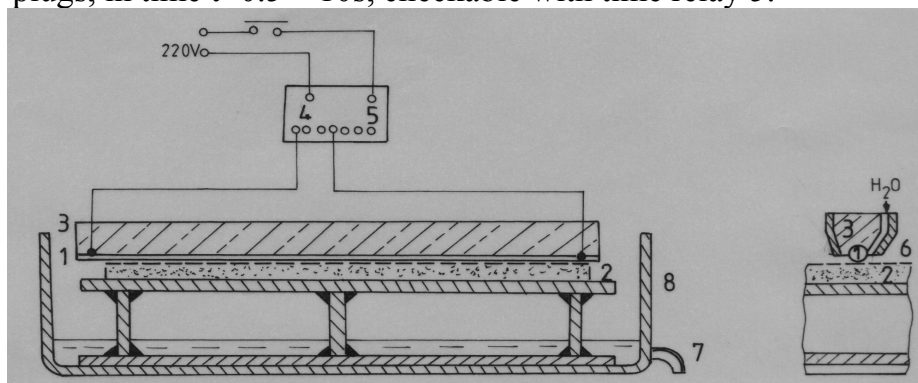


Figure 2 Device for cutting glass plates

When power supply is cut, it is ordered the opening of an electro valve that release water flush alongside the heating element, by radial nozzles of the cooling body 6. Cooling water is collected and may be evacuated through tray 8, in which is put the glass plate, through the draining orifice 7.

The parameters used at cutting, under acceptable conditions, of a glass plate with size  $60 \times 60 \times 5 \text{ mm}^3$ , on the symmetric axe of the surface: supply tension of heating element  $U=24V$ ; current intensity by resistance of Cr-Ni,  $I=5A$ ; heating time  $t=10s$ ; water quantity used at one cutting  $\approx 1l$ ; working time, 2 cutting/minute. There were also cutting parameters with liner energies smaller but the results were not satisfying.

Received March 16, 2005

“Transilvania” University Brasov

#### REFERENCES

/1/. Scorobetiu L., *Cutting Glass Tube Through Electrical Heating*, Conferința Internațională de Știința și Ingineria Materialelor, BRAMAT 2003, Universitatea Transilvania din Brașov

#### TĂIEREA PLĂCILOR DIN STICLĂ PRIN TERMOȘOC

**Rezumat:** Lucrarea prezintă o metodă de tăiere a tuburilor și plăcilor fine din sticlă prin încălzirea locului de tăiere prin intermediul unei rezistențe electrice, urmată de o răcire bruscă cu un jet de apă.

## EXPERIMENTATIONS REGARDING THE KINETICS OF HIGH TEMPERATURE OXIDATION OF THE ALUMINUM NITRIDE

BY

MIHAI COJOCARU, CECILIA TARCAN, FLAVIU GOSTIN

**Abstract.** *The aluminum nitride represents a very attractive material particularly due to its applications in electronics. It is a synthesis, ceramic and non-oxide compound. It generated a special interest, both theoretically and in practice, regarding its obtaining and complex of characteristics. The aluminum nitride is very unstable in basic media, relatively stable in acid media and in atmosphere it oxidize creating continuous films that have protective role. The oxidation reaction of the aluminum nitride is thermodynamically possible, the reaction free enthalpy having negative values regardless of temperature at which the oxidation process takes place in the range 273...1273K. The oxidation of the aluminum nitride frames in the typical redox process category, AlN being the reducing agent. It is necessary to rigorously control the apparition and the increase of the oxide films because its presence significantly modifies the level of the nitride matrix characteristics. The paper presents the results of the research regarding the kinetics of the aluminum nitride oxidation at temperature between 800 and 1000°C. The experiments was developed on samples obtained from the nitride powder through the HIP process. The powder was realized by direct synthesis, in the presence of  $(\text{NH}_4)_3\text{AlF}_6$ , in partially dissociated ammonia medium.*

**Keywords:** *mathematical modeling, oxidation kinetics, aluminum nitride*

### 1. INTRODUCTION

The world of materials is continually changing. As the technology advances the new and advanced materials get more competitive with respect to the traditional ones. The ceramics, composite and polymeric materials can be characterized by associated properties superior to those of the conventional materials – low density, high hardness, special thermal and electrical proprieties, etc. The industry of the advanced ceramics is obviously very different from that of the traditional ceramics. The main characteristic of the advanced ceramics industry is that it is based more on materials obtained by synthesis than on that from nature. The advanced ceramics materials are based on anionic and cationic elements and include oxides, carbides, nitrides and compound formed of mixed anions respectively. The using of the materials obtained by synthesis conducted to a new series of compositions with applications that revolutionized the materials science. The aluminum nitride represents a very attractive material particularly due to its applications in electronics. A special interest is with the methods of the aluminum nitride direct synthesis, from components, in solid state, in the presence of catalysts. The final properties of the compound are strictly dependent on the synthesis, formation and sintering conditions. The main properties that made the aluminum nitride a particularly attractively material are:

- the thermal conductivity is considerably lower than that of aluminum or of copper (16 W/m·°C at 20°C is compared to 207 W/m·°C for aluminum at the same temperature);
- the linear thermal coefficient of expansion is significantly lower than that of aluminum, too ( $4.03 \cdot 10^{-6} \text{grd}^{-1}$  in the interval 20...200°C, comparatively with  $23 \cdot 10^{-6} \text{grd}^{-1}$  for aluminum in the same interval);
- the electrical resistivity is extraordinarily large comparatively with that of the pure metals frequently used in electrotechnics ( $2.69 \cdot 10^{-6} \Omega \cdot \text{cm}$  for aluminum at 20°C and over  $10^{13} \Omega \cdot \text{cm}$  for its nitride at the same temperature).

To all these properties it can be added the extremely high hardness (9...10 on the Mohs scale), the elastic modulus close to that of tungsten carbide, and the last, but not the least, the high chemical stability in acid media.

## 2. SCOPE OF THE EXPERIMENTAL RESEARCH, WORKING METHODS, MATERIALS AND APPARATUS

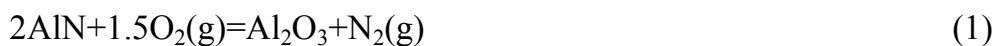
The aim of the experimental research was to estimate the oxidation kinetics of the aluminum nitride at high temperatures. The experiments programming method with a central compositionally orthogonal program of second order was used; this was necessary to simplify the research and to quantify the temperature respectively the holding time effects on the oxidation process kinetics.

The aluminum nitride powder was used. This was obtained by direct synthesis from components (aluminum and nitrogen obtained by the dissociation of ammonia), in presence of  $(\text{NH}_4) \text{AlF}_6$ . The oxidation kinetics has been studied on cylindrical assays (total surface of  $1.4 \text{cm}^2$ ). These were obtained by HIP (hot isostatic pressing) at 1950°C for 3min, in vacuum, under a pressure of 25MPa: the maximum residual porosity in these conditions was of 1.5%.

The interaction effects of the aluminum nitride with air have been estimated in the interval 800...1000°C, for time periods of 60...180min. The specific weight variation and the calculated dimension of the oxide film were used as indicators.

## 3. RESULTS. COMMENTS

The thermodynamically assessment of the AlN oxidation reaction (reaction 1, fig.1) indicates that this reaction is possible, regardless of temperature ( $\Delta G_T^0 < 0$ ) and it is strongly exothermic:



The independent parameters were that describing the oxidation kinetics, respectively the temperature ( $Z_1$ ) and holding time on constant temperature ( $Z_2$ ). The specific weight variation,  $\Delta m/S$ ,  $\text{mg}/\text{cm}^2$  and the dimension of the oxide film  $\delta$ ,  $\mu\text{m}$  are symbolized as  $Y_1$ , respectively  $Y_2$ .

Remark: the medium conditions expressed through the value of the oxygen potential were maintained at constant values in all experiments.

The base levels and the variation range of the independent parameters are presented in table 1. The certain experimental conditions imposed by the programming method are shown in table 2.

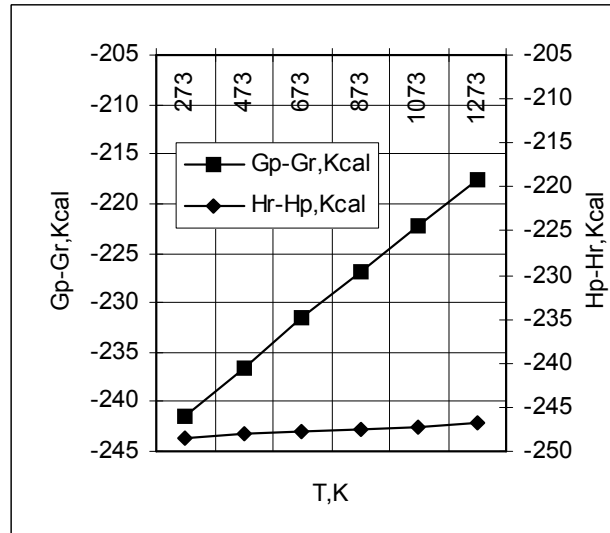


Fig. 1- The thermodynamical characterization of the aluminum nitride oxidation reaction

Factors	Z <sub>1</sub>	Z <sub>2</sub>
Code	X <sub>1</sub>	X <sub>2</sub>
Base level, Z <sub>i0</sub>	900°C	120min
Variation range, ΔZ <sub>i</sub>	100°C	60min
Upper level, Z <sub>i0</sub> + ΔZ <sub>i</sub>	1000°C	180min
Down level, Z <sub>i0</sub> - ΔZ <sub>i</sub>	800°C	60min

Table 1- Base level and the variation ranges of the independent parameters

Table 2- The central compositionally orthogonal programming matrix of second order

No. exp.	X <sub>0</sub>	X <sub>1</sub>	X <sub>2</sub>	X <sub>1</sub> X <sub>2</sub>	X <sub>1</sub> <sup>1/3</sup> X <sub>1</sub> <sup>2</sup> -2/3	X <sub>2</sub> <sup>1/3</sup> X <sub>2</sub> <sup>2</sup> -2/3	Y	
							Y <sub>1</sub> Δm/S [mg/cm <sup>2</sup> ]	Y <sub>2</sub> δ [μm]
1	+1	-1	-1	+1	+1/3	+1/3	0.0375	0.104
2	+1	-1	+1	-1	+1/3	+1/3	0.1500	0.417
3	+1	+1	+1	+1	+1/3	+1/3	0.3375	0.938
4	+1	+1	-1	-1	+1/3	+1/3	0.1656	0.460
5	+1	+1	0	0	+1/3	-2/3	0.2187	0.608
6	+1	-1	0	0	+1/3	-2/3	0.0625	0.174
7	+1	0	+1	0	-2/3	+1/3	0.2593	0.720
8	+1	0	-1	0	-2/3	+1/3	0.1093	0.3036
9	+1	0	0	0	-2/3	-2/3	0.1718	0.477

Remark: the dimension of the oxide film, δ, was estimated from the specific weight variation, using the following relation (rel.2):

$$\delta = \frac{\Delta m}{S} \cdot \frac{1}{\gamma_{Al_2O_3}} \tag{2}$$

where:  $\gamma_{Al_2O_3} = 3.6 \text{ g/cm}^3$ ;

$\frac{\Delta m}{S}$  represents experimental values of the specific weight variation.

The particular forms of the regression equations (eq. 3-4) were obtained by statistics processing of the data obtained from the experiments (tab.3).

Table 3-The results obtained from the statistics processing of the experimental data.

Y	$b_0 \cdot 10^2$	$b_1 \cdot 10^2$	$b_2 \cdot 10^2$	$b_{12} \cdot 10^2$	$b_{11} \cdot 10^2$	$b_{22} \cdot 10^2$	$S_0^2$	$S_{bi}$	$S_{bii}$
Y1	15.1	7.86	7.24	1.48	-1.81	2.55	0.000147	0.00495	0.00857
Y2	45.44	21.85	20.12	4.12	-5.0	7.0	0.0025	0.00203	0.00353

Y	$S_{bij}$	$S_{b0}$	$t_{0.005;9;2}$	$\Delta b_i$	$\Delta b_{ii}$	$\Delta b_{ij}$	$\Delta b_0$	$F_{tab}$	$F_{calc}$
Y1	0.00606	0.00699	2.26	0.01118	0.0193	0.01369	0.01579	19.25	1.45
Y2	0.0025	0.00287		0.0046	0.00799	0.00565	0.00648	19.16	16.49

$$Y_{\Delta m/S} = 10^{-2} [15.1 + 7.86X_1 + 7.24X_2 + 1.48X_1X_2 + 2.55X_2^2] \quad (3)$$

$$Y_{\delta} = 10^{-2} [45.44 + 21.85X_1 + 20.12X_2 + 4.12X_1X_2 - 5X_1^2 + 7X_2^2] \quad (4)$$

The response surfaces corresponding to the curvilinear models (eq. 3-4) together with the isoproperty diagrams related to these (fig.2) create a very suggestive image on the oxidation kinetics of the aluminum nitride.

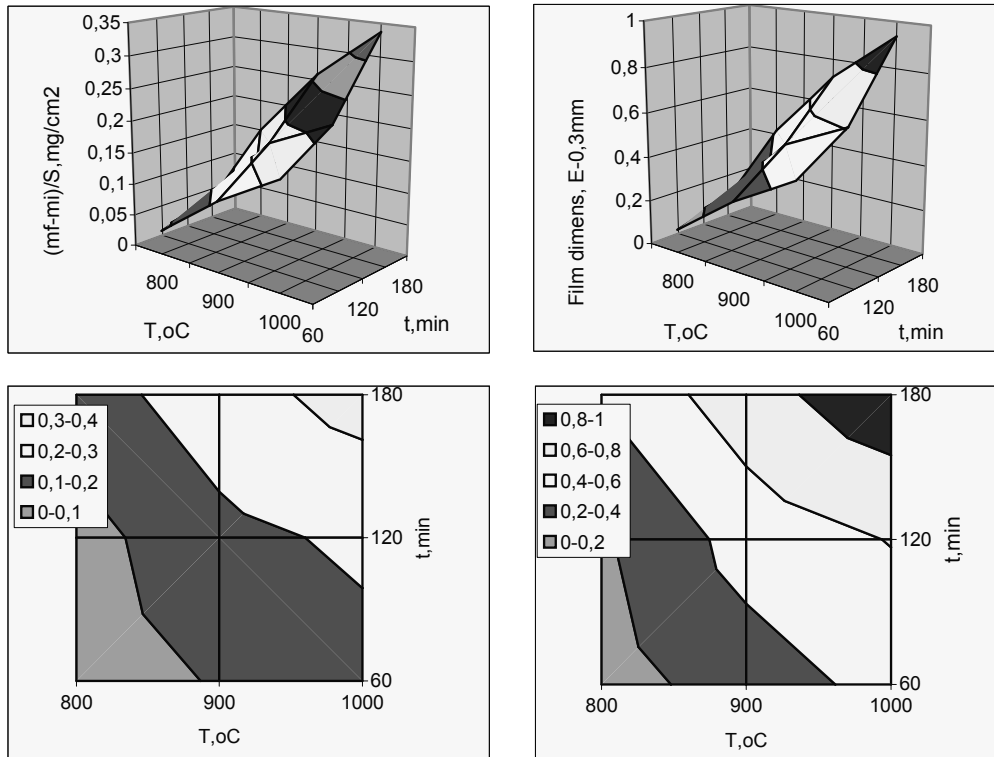


Fig. 2-The response surfaces of the calculated mathematical models and the domains of isoproperty

It can be seen that the main factors taken into account, the temperature and the isothermal holding time strongly influence the kinetics of the AlN oxidations. The effects of these factors taken individually, on specific weight variation ( $\frac{\Delta m}{S}$ ), respectively on dimension of the oxide film ( $\delta$ ) are extremely close one to each other. The maximum value of the oxide film dimension, realized in extreme conditions, 1000°C /180min, doesn't exceed 1 $\mu$ m (0.938  $\mu$ m), being considerably lower than the value corresponding to the oxidation of pure aluminum at room temperature, in

alkaline media ( $\sim 5.8\mu\text{m}$ ), or in superheated steam at  $155^\circ\text{C}$  ( $\sim 1\mu\text{m}$ ). The oxide films formed through the oxidation of aluminum nitride have a protective role, being continuous and perfectly adherent, due to the insignificant change in the density of the superficial layers through its apparition ( $\gamma_{\text{Al}_2\text{O}_3} = 3.6\text{g/cm}^3$ ;  $\gamma_{\text{AlN}} = 3.24\dots 3.26\text{g/cm}^3$ ), and the coefficient of expansion in the case of forming a  $\text{Al}_2\text{O}_3$  film on Al differs from that on AlN with hundredths of unit: 1.21 respectively 1.25, so the difference is insignificantly.

The oxidation of the aluminum nitride frames in the category of the typical redox processes (reaction 5), AlN being the reducing agent, and oxygen being the oxidizing agent.



The aluminum maintains its oxidation number (+3) and the proper oxidation-reduction takes place between the two non-metals, oxygen and nitrogen. The electronegativity, higher for nitrogen than for oxygen, allows the realization of the substitution; this fact is confirmed also by the thermodynamics calculations (fig.1).

The rate of the oxidation process should be higher in the initial stages than that in the late stages, the oxide film acting as a barrier for the diffusion process, its growing also being accomplished through a redox process, but with a slower kinetics. The results confirm these assumptions. In time the rate is decreasing, and as the temperature increases the differences between the rates of oxidation tend to diminish reaching a limit rate dependent on the intensity with which the electric-thermal phenomena take place, i.e. the dynamics of apparition and disappearance of the penetration canals for oxygen in the oxide film.

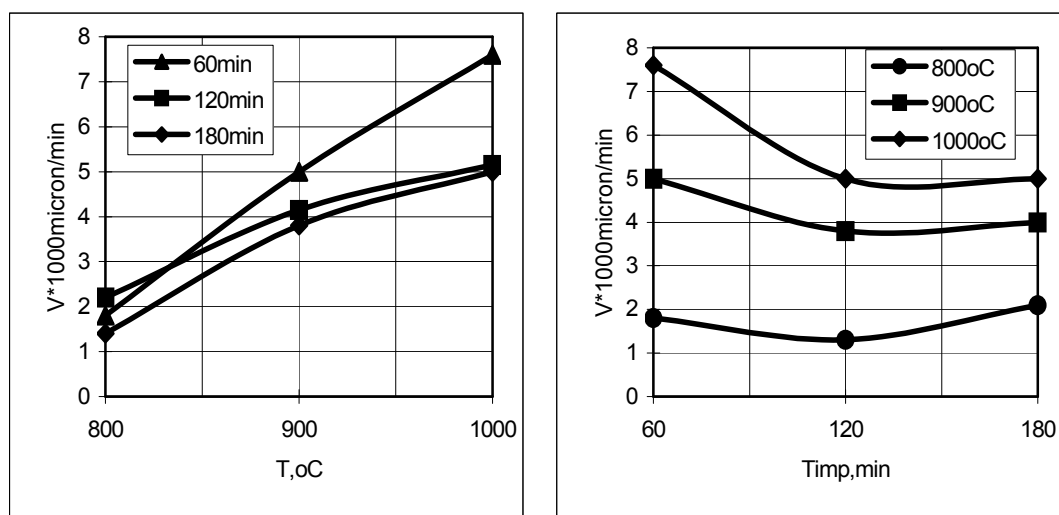


Fig. 3-The rate evolution of the oxide film formation on the aluminum nitride surface

The presence of the oxide films on the surface of the powder particles or of the products made from this represents a certainty. For the case of highly densified aluminum nitride products (residual porosity under 1.5%), the dimensions of the oxide

films can be estimated with the following relations (determined through statistical processing of the experimental data) (eq.6...8):

$$\delta_{60\text{min}} = -1.31 + 1.78 \cdot 10^{-3} T \quad r=0.99 \quad (6)$$

$$\delta_{120\text{min}} = -12.88 + 1.95 \ln T \quad r=0.98 \quad (7)$$

$$\delta_{180\text{min}} = -1.65 + 2.60 \cdot 10^{-3} T \quad r=0.99 \quad (8)$$

Remark: the temperature is expressed in Celsius centigrade degree and the  $\delta$  results in microns.

#### 4. CONCLUSIONS

The presence of the continuous and perfectly adherent oxide films, on the surface of aluminum nitride powder particles or on that of the products realized from it, represents a certainty. Although the oxide films have hardness close to that of the nitride, it certainly changes the tribological behavior of the products.

Received April 26, 2005

“Politehnica” University București

#### REFERENCES

- /1/. Samsonov G.Vș.a., *Tugoplavkie soedinenia*, Moskov, Metallurghia, 1976
- /2/. Wagner C.J. *Electrochem., Soc.* 99, 396, 1952
- /3/. Kauffe K., Pfeiffer H. Z. *Electrochem.*, 56, 390, 1952
- /4/. Taloi D., Florian E,ș.a., *Optimizarea proceselor metalurgice*, Ed. Didactica și Pedagogică, București, 1983
- /5/. Sreider A.V., *Oxidirovanie aliuminia i ego splavov*, Moskov, 1960
- /6/. \* \* \* ,Chemical Reaction and Echilibrium Software with extensive Thermochemical Database Outokumpu HCS Chemistry for Windows ver. 2.03 Finland
- /7/. Drăgușin Ion Eugen, Teză de doctorat, București, 2001

#### EXPERIMENTĂRI PRIVIND CINETICA OXIDĂRII LA TEMPERATURI ÎNALTE A NITRURII ALUMINIULUI

**Rezumat:** nitrura aluminiului reprezintă un material deosebit de atractiv, în special datorită aplicațiilor din domeniul electronicii. Compus de sinteză, ceramic, neoxidic, a generat un interes deosebit atât din punct de vedere teoretic, legat de obținerea sa, cât și din punct de vedere practic prin complexul de caracteristici asociate. Din punct de vedere chimic nitrura aluminiului este deosebit de instabilă în medii cu caracter bazic, relativ stabilă în medii acide, iar în aerul atmosferic se oxidează creând pelicule continue cu rol protector. Reacția de oxidare a nitrurii aluminiului este termodinamic posibilă, entalpia liberă de reacție fiind negativă indiferent de temperatura la care are loc procesul de oxidare în intervalul 273...1273K. Oxidarea nitrurii aluminiului se încadrează în categoria proceselor redox tipice, AlN jucând rol de agent reducător. Apariția și dezvoltarea peliculelor de oxid este necesar să fie riguros controlate deoarece prezența acestora modifică semnificativ nivelul caracteristicilor matricii de nitrură. În lucrare sunt prezentate rezultatele cercetărilor privind cinetica oxidării nitrurii de aluminiu în domeniul de temperaturi 800...1000°C. Cercetările au fost desfășurate pe probe de nitrură obținute prin comprimarea la cald a pulberii realizate prin sinteză directă, în prezența activizatorului  $(\text{NH}_4)_3\text{AlF}_6$ , în mediu de amoniac parțial disociat